CHARACTERIZATION OF MOLYBDENUM BLACK COATINGS WITH REFERENCE TO PHOTOTHERMAL CONVERSION OF SOLAR ENERGY

A thesis submitted for the degree of
Doctor of Philosophy

by

FERDOUSE JAHAN
B.Sc.(Hons), M.Sc.

December, 1987

Department of Mechanical Engineering
Brunel University
Uxbridge, Middlesex,
England.

PAGE NUMBERING AS ORIGINAL

MISSING PAGES ARE UNAVAILABLE

ABSTRACT

A study of thermal, structural, electrical and optical characteristics of molybdenum black surface coatings on various substrates has been made. The suitability of these coatings for use as selective absorbers for solar collector applications has been assessed.

Molybdenum black (Mo black) coatings were prepared by electrodeposition (on aluminium) and a chemcial conversion method (on zinc and electroplated cobalt on nickel plated copper substrates). The solar absorptance (α_s) and thermal emittances (ϵ_{th}) of the coatings were determined from room temperature spectral reflectance measurements in the solar (0.3 to 2.5μm) and infrared regions (2.5 to 50 μm) respectively. The effect of different preparation parameters and substrate pretreatments on the spectral selectivity has been investigated in order to optimize the thermal performance. The spectral selectivity is related to the Mo-black coating thickness and surface roughness together with the microstructure of the substrate and the intermediate layer.

Dip coatings on polished zinc have significant selectivity (α_s/ϵ_{th} = 8.4 when α_s = 0.76). The absorptance of the dip coatings is increased to 0.87 with ϵ_{th} = 0.13 by chemical etching of zinc prior to coating deposition. For coatings on electroplated cobalt on nickel plated copper (cobalt (NC) substrate), an absorptance as high as 0.94 has been obtained with an emittance value 0.3. By using an addition agent in the plating solution of cobalt the high emittance can be reduced to 0.1 with α_s = 0.91 giving a coating with a relatively high efficiency (82.5%) for photo-thermal energy conversion.

A study of the surface composition and microstructure of the coatings has been made using scanning and transmission electron microscopy together with electron diffraction, X-ray diffraction and X-ray photoelectron spectroscopy. The structural investigations indicate that Mo-black coatings contain polycrystals of orthorhombic Mo_4O_{11} with a small proportion of $Ni(OH)_2$. Presence of water and also Mo_4O_{11} in the coatings are evident from IR spectroscopy study.

The bandgap of the coating has been determined from optical transmission spectra (1.66 eV) and also from reflectance spectra (0.85 eV). The discrepancy between these two values has been discussed. The refractive indices of the coatings have also been estimated. The band gaps and refractive indices are found to be related to the spectral selectivity of the coatings.

The durability test of the coatings shows that the coatings on etched zinc are more resistant to heat treatment than the coatings on unetched zinc. The coatings on cobalt (NC) substrates also show good stability for relatively short periods at temperatures ~400^{o}C.

A study of the electrical properties of Mo-black coatings suggests that at electrical field strengths (greater than 10^6V/m) the dominant conduction process is of the Poole-Frenkel type. The activation energy of the conduction process has been estimated to be ~0.56 eV at higher temperatures. The effect of heat treatment on the electrical properties of the coatings has been examined. The dielectric constant of Mo-black has been estimated from A.C. measurements. At high frequency (20 kHz) the value of the dielectric constant is about 4.0.

To my parents
my dearest husband
and
our lovely daughter

'FARIHA'

ACKNOWLEDGEMENTS

I would like to express my sincere appreciation and deep gratitude to my supervisor Dr B.E. Smith for his guidance, advice, constant encouragements and kind help, in many ways, throughout this study.

I wish to thank Professor A.J. Reynolds, Head of the Mechanical Engineering Department, for his permission to use the research facilities within the Department.

I am especially indebted to Dr M.G. Hutchins, of the Department of Geology and Physical Sciences at Oxford Polytechnic, for his kind permission to use an integrating sphere spectrophotometer and for useful discussions.

I am grateful to Dr J.K. Critchley of the Chemistry Department for providing laboratory facilities in the Chemistry Department and for helpful advice. Thanks also to Dr J. Beynon, Physics Department, for valuable discussions and the use of a vacuum coating unit. Thanks are due to Dr D.N. Waters (Chemistry Department) and Dr B.R. Orton (Physics Department) for helpful discussions in relation to IR and XPS studies.

I wish to acknowledge Dr K.A. Hodd, Department of Materials Technology and Dr B.J. Griffiths, Department of Manufacturing and Engineering Systems, for use of the infrared spectrophotometer and the Talystep equipment.

I also wish to express my sincere appreciation to Mr R. Bulpett and his colleagues of the E.T.C. Department for the experimental assistance with

the SEM and XPS studies and to Mr. T. Purser (Physics Department) for providing additional TEM facilities.

I am obliged to the Mechanical Engineering Departments' technical staff for their kind co-operation and assistance throughout this study.

I am indebted to the Association of Commonwealth Universities for awarding me a Commonwealth Scholarship and to the Department of Mechanical Engineering (Brunel University) for granting me a six months studentship.

I am most grateful to my husband, Dr. M.H. Islam, for his good understanding, constant encouragement, helpful suggestions and co-operation during the course of this work. I am grateful to my parents, brothers and sisters for their constant encouragement throughout the long path of this study.

Finally, my thanks are due to Miss Ruth Sterland for skilfully typing this thesis.

CONTENTS

CHAPTER I

INTRODUCTION AND THEORETICAL BACKGROUND

1.1 Introduction

Potentially useful applications of solar energy have attracted the attention of many researchers. In recent years, direct transformation of solar energy into electricity or heat has been successfully used in various countries for domestic and industrial applications (Duffie and Beckman, 1980; Dickinson and Cheremisinoff, 1980; McNelis, 1982; Sauer, 1985; Dunkui, 1986).

Solar energy is a potentially useful alternative energy source because of its widespread availability and effectively inexhaustible supply. An enormous amount of solar energy reaches the earth's surface (about 7 X 10^{17} kWh per year). Taking current annual world energy consumption at about 7.3 X 10^{13} kWh, the solar energy incidence is about 10,000 times the current use (Tabor, 1984). However, the two greatest problems in utilizing solar energy are (i) its low energy density and (ii) its irregular availability due to the daily cycle as well as to seasonal and climatic variations. Efficient collection and conversion of solar energy into other forms of energy is therefore needed if applications are to be successful. Some form of energy storage may also be needed.

Solar energy can be converted directly into thermal, chemical or electrical energy. From the technical viewpoint, solar systems can be divided into two broad classes as illustrated in Fig.1.1; (i) those in which the primary interaction is a selected quantum process and (ii) those

in which the primary process is production of heat. The present work is concerned with the latter case i.e., photothermal conversion of solar energy.

1.2 Photothermal conversion of solar energy

The fundamental principles of photothermal conversion of solar energy are shown schematically in Fig.1.2. The incident solar energy is converted to thermal energy. This can be used for domestic, commercial and industrial processes such as heating of swimming pools, domestic water heating, space heating, crop and timber drying, desalination of water together with generation of electrical power.

1.2.1 Solar collector

A solar collector is a special kind of heat exchanger that transforms solar radiant energy into heat. It is designed to collect incident solar radiation and convert it into heat which is then transferred to a working fluid. A schematic cross-section of a flat plate solar water heater is shown in Fig.1.3(a). It has a solar energy absorbing surface on a heat conducting substrate which incorporates tubes. The water passes through these tubes. The back and sides of the collector are well insulated and the absorber plate is covered by one or more glass or plastic plates transparent to solar radiation.

Only part of the incident energy is transferred to the heat transfer fluid in contact with the absorber. Part of the incident radiation is lost by reflection at various interfaces leading to optical losses. Part of the thermal energy produced by photon absorption is lost by convection, conduction and radiation to the collector exterior. These constitute the

thermal losses. The remainder of the solar input is passed on as heat to the water or other heat transfer fluid. (The various losses associated with a typical collector are illustrated schematically in Fig.1.2).

In the steady state, the performance of a solar collector is described by an energy balance that indicates the distribution of incident solar energy into useful energy gain, thermal losses and optical losses. The useful rate of energy gain Q_u of a flat plate solar collector may be expressed as (Duffie and Beckman, 1980):

$$Q_u = A_c \{ \alpha_s \tau_c I - (\frac{1}{\varepsilon_{th}} + \frac{1}{\varepsilon_c} - 1)^{-1} \sigma (T_p^4 - T_c^4) - h (T_p - T_c) \} \quad (1.1)$$

where α_s is the solar absorptance of the receiver surface, τ_c the transmittance of the cover, I (W/m^2) the solar irradiance, ε_{th} the thermal emittance of the receiver surface, ε_c the thermal emittance of the cover, A_c(m^2) the collector area, σ(=5.67X10^8 W/m^2K^4) the Stefan-Bolztmann constant, T_p(K) the temperature of the receiver surface, T_c(K) the temperature of the cover and h (W/m^2K) is a combined heat transfer co-efficient for conduction and convection losses. The collector efficiency, η is given by

$$\frac{\text{rate of useful energy transfer to collector fluid}}{\text{rate of solar energy incidence on collector}} = \frac{Q_u}{IA_c} \quad (1.2)$$

The relative performances of different collectors at a given site depend essentially on their geometry and the optical and thermal properties of the materials of which they are constructed together with the flow rate of the working fluid. Two major modes of heat loss from the collector system are convection and radiation losses. Both increase with increase of operating temperature. The conventional way of minimizing convective

losses is to employ one or more glass cover plates. A single glass cover permits the solar energy (~83%) to reach the absorber surface. On the other hand, it absorbs most of the long wavelength radiant energy emitted by the absorber and reradiates (~50%) back to the absorber surface. The net loss of energy is therefore reduced significantly. According to equation 1.1. the radiation heat losses also depend upon the emissivity of the absorber, ε_{th}. Different heat losses calculated for four different flat plate collectors are shown in Fig.1.3(b) (after Duffie and Beckman, 1980). This figure demonstrates that for the absorber surface of low emittance (0.10) the radiative loss is reduced significantly. The efficiency of a solar collector at a given operating temperature can, therefore, be increased (1) by increasing the absorptance of the absorber surface and (ii) by reducing the thermal emittance, while maintaining high solar absorptance.

The seemingly contradictory requirement of having a good absorber that is simultaneously a poor emitter (according to Kirchoff's law, Appendix A) can be met by spectral selectivity of a surface. Such a surface is referred to as a selective surface. The fabrication of surfaces with wavelength selective properties is possible due to a distinct separation between the spectral distribution of solar radiation (which is similar to that of a blackbody at 6000K) and the thermal radiation emitted by the absorber at the operating temperature (which will not exceed 1000K for most of the applications envisaged) as shown in Fig.1.4. The spectral ranges of solar radiation and reradiation loss are generally well separated on the wavelength scale. Thus a surface or material can be synthesised so that it has high absorption in the solar range (below 2.5 μ m) and low absorption in the thermal range, (above 2.5 μ m) resulting in low emittance. The present research is related to such selective surfaces. Typical thermal performance curves for single-glazed flat plate

collector employing selective and non-selective absorber surfaces are shown in Fig.1.5. An increased efficiency can be observed at higher temperatures for selectively coated collectors due to a reduction in radiative heat losses to the surroundings.

1.2.2 Selective surfaces

1.2.2.1 General description

A selective surface is a surface whose radiative characteristics vary with wavelength. Generally, optically selective surfaces can be classified into two categories:

1) The reflection-absorption type (solar selective absorber) is applied directly to the absorber surface.

2) The reflection transmission type (transparent heat mirror) is applied to the cover plates of the converter system. The present work is concerned with the former type.

The variation of absorptance as a function of wavelength for an ideal selective absorber surface is shown in Fig.1.6. Such a surface totally absorbs solar radiation and totally reflects infrared radiation. In practice, this ideal performance will not be achieved. However, surfaces with high absorptance through the solar region ($<2.5\,\mu m$) and high reflectance in the thermal region ($>2.5\,\mu m$) can be produced.

A selective surface should not only exhibit high solar absorptance and low thermal emittance, but should also be stable under working conditions throughout the lifetime of the solar collector. The absorber surfaces

should satisfy the following criteria:

1) High absorptance in the solar region.
2) Low emittance in the infrared region.
3) Long term stability under operating conditions at desired temperatures.
4) Stability against ageing at stagnation temperature.
5) Long term compatability with substrate materials.
6) Resistance to atmospheric corrosion.
7) Good reproducibility of optical characteristics.
8) Reasonable production cost.

1.2.2.2 Physical processes leading to solar selectivity

The spectral selectivity of an absorber surface can be based on selections from a range of different physical processes and types of material. These include:

a) Intrinsic solar selective surfaces.
b) Absorbing semiconductor/reflecting metal tandems.
c) Interference stacks.
d) Optical trapping by surface cavities or physical wavelength discrimination.
e) Particulate coatings and composite films.

None of the above can individually generate a desirable spectral profile. In practice, many selective surfaces exhibit a combination of these properties. The selectivity of the Mo-black coatings studied in the present investigation is also influenced by different mechanisms. These are discussed below.

a) Intrinsic selective absorbers

Intrinsic materials are those which exhibit desired spectral selectivity naturally, without the need for any other material to augment the reflectance behaviour. There is no intrinsic material in nature which exhibits ideal solar selectivity as illustrated in Fig.1.6. There are, however, a very few materials which possess a pronounced degree of intrinsic spectral selectivity, e.g., hafnium carbide (HfC) has a low emittance in the thermal infrared (ε_{th} ~ 0.10) and high solar absorptance of about 0.70 (Meinel and Meinel, 1976).

b) Semiconductor/metal tandems

Absorbing semiconductor and reflective metal tandems are one of the most common types of selective absorber. These tandems generally consist of a combination of two optically active materials to provide two basic functions of the converter, absorption and reflection. A schematic cross section of a tandem absorber is shown in Fig.1.7. Metals naturally provide high infrared reflectance. Unfortunately, these are also reflective in the solar region. If a metal is coated with a semiconductor layer, which has high absorptance in the solar region and high transmittance in the infrared region, then the desired spectral profile can be obtained from the tandem. For semiconductors, solar absorptance is a result of the absorption of photons having energies greater than the bandgap of the semiconductor. The coating absorbs the photons which raises the valence electrons into the conduction band. For longer wavelength photons, whose energy is insufficient to excite the valence electrons (i.e., less than the bandgap energy) the materials appear transparent. This region of transparency permits the metal base to 'see through' the absorber and suppress the emittance by its high reflectance.

Since most of the semiconductors have high refractive indices resulting in large reflection losses, antireflection coatings must be used or the refractive index of the semiconductor layer should be lowered by structural or textural effects, in order to minimize the front-surface reflection. Therefore, if the absorber-reflector tandem is to be effective, the absorbing semiconducting layer must have the absorption edge in the proper spectral range (~2 μm) and a low refractive index, possibly a value of 2 or less (Seraphin, 1979).

The semiconductor coating may be an intrinsic element such as Si, Ge or oxides of metals such as nickel oxide, copper oxide, chromium oxide . There are, however, numerous successful candidates of semiconductor/ metal tandems. Most well known examples are black nickel coatings (Ni-Zn-S alloy) on highly reflecting metals (Tabor, 1956, 1961), black chrome on nickel plated steel or copper (Lampert, 1979, Mattox and Sowell, 1974). The simplest tandem stack is oxidized metal/metal combination, as most of the metal oxides are semiconducting in nature. The oxidation can be accomplished by heating, dipping in baths or other methods of chemical conversion. Mo-black coatings studied in the present work also act as tandem absorbers.

c) Interference stacks

The interference stack consists of a combination of dielectric and metal layers. It is also known as a multilayer thin film which acts like a selective filter for solar energy absorption by optical interference.

If a metal is covered with a thin dielectric layer, which need not have any intrinsic absorption, then the reflectance of the metal in the solar region can be reduced by destructive interference. The condition of zero

reflectance of the tandem is determined by the refractive index and thickness of the individual layer (Park, 1963). Interference effects are sometimes used in metal oxide/metal tandems to increase solar absorption, e.g., the oxide films of Fe_2O_3 and Cr_2O_3 on stainless steel studied by Karlsson and Ribbing (1982).

A single dielectric layer on a metal has a very narrow absorption band, as the reflectivity of the dielectric is weak at its air interface, and this results in weak interference effect. In practice multilayers of alternate dielectric and metals have been used in the interference stack to broaden the absorption band. The basic concept of a four-layer interference stack is shown in Fig.1.8. The second reflective layer is a very thin metal layer of thickness about 50Å and is partially transparent. The absorption in this coating is enhanced by multiple reflection between the semitransparent, dielectric and metal alternating layers. One successful interference stack is an Al_2O_3-Mo-Al_2O_3 coating (Peterson and Ramsey, 1975). For Mo-black coatings on mechanically polished zinc, interference effects may have some influence on the absorption process.

d) Optical trapping and wavefront discrimination

Selectivity by wavefront discrimination is an important mechanism for the generation of spectrally selective surfaces. The textural profile of a surface can discriminate between the highly directional solar radiation and the hemispherical wavefront of the thermal radiation. Surface irregularities such as grooves and pores with dimensions large compared with the wavelengths of the incident radiation increase the solar absorptance by multiple reflections as shown schematically in Fig.1.9(a). They may also increase the thermal emittance to a lesser extent, (Bogaerts and Lampert, 1983).

By reducing the size of the surface roughness to the order of the cut-off wavelength (maximum wavelength to be absorbed) the solar absorptance can be increased without affecting thermal emittance significantly. The different optical behaviour of a surface in the visible and infrared region is explained in Fig.1.9(b). As the visible wavelengths are similar to the actual surface irregularities, the surface appears rough or cavity-type to the incoming radiation and increases absorption through multiple reflections and partial absorption in the micro-cavities. For the thermal infrared, the wavelength is larger than the magnitude of the surface roughness. The surface therefore appears smooth and mirror-like and reflects and radiates like a flat surface.

Many solar selective surfaces owe their absorptance to the topography of the surface. Metals (which may not exhibit a high intrinsic absorption coefficient in the visible) can also be a good absorbers if roughened by appropriate techniques. A review of experimental methods for the preparation of selectively absorbing textured surfaces has been published by Pellegrini (1980). Nearly ideal textured surfaces have been produced by chemical vapour deposition of rhenium (Seraphin, 1974) and of tungsten (Cuomo et al, 1975).

The most successful selective absorber semiconductor/metal tandem would also be inferior if textural effects did not reduce the refractive index of the semiconductor layer. An example is the PbS on aluminium investigated by Williams et al (1963). If the PbS is applied as solid material, the tandem should have a solar absorptance of only 0.36. When it is deposited as a porous structure with sufficient void density, the effective refractive index is lowered to 1.8 resulting in high absorptance (0.90). There are many tandem type selective surfaces reported in the literature where surface roughness is responsible for high absorptance,

such as black cobalt (Smith et al, 1980), black chrome (Lampert, 1978), black molybdenum (Carver et al, 1982).

In the present work on Mo-black coatings, surface roughness also plays an important role in increasing the selectivity.

e) Particulate coatings

Particulate coatings consist of dispersions of metallic or semiconductor particles in dielectric or conductive matrices. In these coatings the absorptance is enhanced by reflective scattering where absorption is obtained by multiple reflections within the geometry of the surface and by resonant scattering which is characterized by a dependence not only upon the geometry but on the physical properties of the material. One good example of a particulate coating is the well-known black chrome, in which small particles of metallic chromium in the size range of 150A^{o} are embedded in a chromium oxide host matrix (Lampert, 1979). Other interesting surfaces of a particulate nature are 'black molybdenum' produced by chemical vapour deposition (Chain et al, 1981), and semiconducting PbS imbedded in a silicon paint (Williams et al, 1963).

No attempt has been made to present a complete review on solar selective surfaces, as a number of reviews on selective surfaces (Meinel and Meinel, 1976; Peterson and Ramsey, 1975; Lampert, 1979; Mattox and Sowell, 1980; Koltun, 1980; Agnihotri and Gupta, 1981) have been published. An excellent review by Niklasson and Granqvist (1983) includes a comprehensive list of annotated references on selective absorber surfaces covering the period 1955 to 1981.

1.3 Review of molybdenum oxides

Molybdenum is a transition element (atomic number 42 and atomic weight 95.94) located in the Periodic Table in Group VI between chromium and tungsten. It falls horizontally between niobium and technetium. The outstanding feature of molybdenum is its extraordinary chemical versatility. It has oxidation states from (-II) to (VI) and co-ordination numbers from 4 to 8 (Cotton and Wilkinson, 1972).

Molybdenum forms a wide range of oxides, such as MoO_3 (Andersson and Magneli, 1950), Mo_9O_{26}, Mo_8O_{23} (Magneli, 1948), Mo_4O_{11} (Magneli, 1948), $Mo_{17}O_{47}$ (Kihlborg, 1959) and MoO_2 (Magneli, 1946, Brandt and Skapski, 1967). Among all of these oxides, MoO_2 and MoO_3 are the most well known and researched. The intermediate oxides are formed by heating MoO_3 and Mo metal in vacuo at temperatures between 550 to 800^{o}C for various times (Kihlborg, 1959). They have been characterized by means of X-ray powder photographs and most of their structures have been determined from single crystal X-ray data.

1.3.1 Comparison of structures of MoO_3, MoO_2 and Mo_4O_{11}

The crystal structures of different phases of molybdenum-oxygen system (MoO_2, MoO_3 and intermediate oxides between these two) have been studied by Hagg and Magneli (1944), Magneli (1948) and Kihlborg (1963). According to them all the Mo-oxides are composed of polyhedra connected by the sharing of corners or edges. The MoO_6 octahedron (Fig.1.10.a) is the most frequently occurring type of polyhedron but MoO_4 tetrahedra and MoO_7 pentagonal bipyramids (Fig.1.10.a) are also found.

The structure of Mo_4O_{11} is rather different from those of the other Mo-oxides. The occurrence of MoO_4 tetrahedra in Mo_4O_{11} totally lacks analogy with other oxides which are exclusively built-up by MoO_6 octahedra. The orthorhombic Mo_4O_{11} structure projected parallel to (010) plane is given in Fig.1.10.b. The orthorhombic unit cell contains four molecules of Mo_4O_{11}. Compared to MoO_2 and MoO_3 it has large lattice parameters (Table 1.1).

MoO_2 has a distorted rutile structure (Figl.11). It has monoclinic symmetry. There are four molecules in a unit cell of dimensions,

$$a = 5.611\text{Å};\ b = 4.856\text{Å};\ c = 5.628\text{Å};\ \beta = 120^\circ$$

MoO_3 has a unique layer structure (Fig.1.12). In an orthorhombic unit cell, there are four molecules of MoO_3. The unit cell dimensions are given in Table 1.1.

The structure of Mo_4O_{11} is a very spacious one compared with those of the other Mo-oxides. This is illustrated by the quotient between the volume of the unit cell and the number of the bulky O atoms per unit cell (Table 1.1). Thus Mo_4O_{11} has a very open oxygen packing while MoO_2 is fairly closely packed. It was reported by Hagg and Magneli (1944) that the stoichiometry of Mo_4O_{11} may vary between $MoO_{2.85}$ to $MoO_{2.72}$.

1.3.2 Optical and electrical properties

There has been considerable interest in the optical and electrical properties of the transition metal oxides due to their wide range of physical properties. The incomplete d-shell of the metal ion, which is the common feature of this group is responsible for a wide range of

optical and other properties. The electrical and optical properties of MoO_2 and MoO_3 both in single crystal and amorphous structures have been studied by several investigators.

MoO_2 is a dark brown solid. Its melting point is 2200K (Samsonov, 1973). The specular reflectance of single crystal MoO_2 has been measured by Chase (1974) in the wavelength range 0.2 to 12.0 μm. According to his data, the computed solar absorptance of crystalline MoO_2 is about 70% (Carver et al, 1982). In addition, infra red (IR) measurements in the range 2-50 μm of MoO_2 powder have shown that it has very weak absorption peaks in the region 10.2 - 11.2 μm (Hanafi et al, 1975). Due to weak absorption in the IR region it should be a poor emitter. The optical band gap of MoO_2 is 1.72 eV (0.72 μm) (Hanafi et al, 1981). This indicates the possibility of high absorption in the visible region due to band-to-band transitions. (However, a higher value (3eV) for the bandgap of single crystal MoO_2 has been reported by Chase (1974)).

Electrical measurements have shown that MoO_2 is a metallic conductor (Ben-dor and Shimony, 1974, Roger et al, 1969). The room temperature specific resistivity is of the order of 10^{-6} Ω-m and increases with the increase of temperature as is expected for metals. It has been reported by Bendor and Shimony (1974) that doping by NiO in pure MoO_2 lowers the conductivity.

MoO_3 in contrast to MoO_2 is a non-conductor. It is an almost colourless solid with greenish tinge. Its melting point is 1068K (Samsonov, 1973). The electrical and dielectric properties of vacuum evaporated MoO_3 thin films have been studied by Simmons and Nadkarni (1969, 1970, 1972), Nadkarni and Simmons (1972), and Nadkarni et al (1982), for use as a capacitor. According to them, evaporated films of MoO_3 contain an excess

of Mo-metal. These act as donor centres and control the electrical properties of the film. The donor density in MoO_3 is estimated to be about $10^{24}/m^3$. Some data on electrical properties of MoO_3 thin films are given in Table 1.3.

The optical and photoelectric properties of single crystal and thin film MoO_3 have been studied by Deb (1968), Deb and Chopoorian (1966) and Rablais et al (1974). According to them 'as deposited' thin films of MoO_3 are transparent but they can be coloured by the application of electric fields or by irradiating with UV light. Sufficient application of either of these colouration techniques results in deep blue films. Optical absorption spectra of MoO_3 thin films in the visible and near infrared region obtained by Colton et al (1978) are shown in Fig.1.13 before and after colouration. It can be seen that in the blue films, the absorption spectra have maxima near 0.6 μm and 0.77 μm and continuous absorption throughout the NIR region with maxima near 1.4 μm and 2.4 μm. Deb and Chopoorian (1966) reported that the same type of colour centres can also be formed on heating the film in oxygen in inert atmosphere. According to them the formation of colour centres in MoO_3 is closely related to the presence of Mo^{+5} state and the oxygen ion vacancies in the lattice. During the evaporation in vacuum, MoO_3 undergoes some thermal decomposition and thereby incorporates some lower valence Mo^{+5} state in the lattice which is confirmed by electron-spin-resonance (ESR) measurements. There is considerable spread of data for the absorption edge of MoO_3 in the literature. Hanafi et al (1981) obtained a value of 2.74 eV for the band gap of MoO_3 from diffuse reflectance measurements. A value of about 2.92 eV has been obtained by Comanion and Mackin (1965) on powdered MoO_3. The absorption edge of single crystal MoO_3 has been given as 2.8 eV by Deb (1968). Considerably higher values for the band gap 3.2 eV and 3.7 eV have been obtained by Rablais et al (1974) and Deb and

Chopoorian (1966) respectively for vacuum evaporated MoO_3 thin films.

The optical properties of MoO_2, MoO_3 and the intermediate oxides $Mo_{13}O_{38}$, Mo_9O_{26}, Mo_8O_{23}, $Mo_{17}O_{47}$ and Mo_4O_{11} have been studied by Hanafi et al (1981) in the range 0.3 to 0.9 μ m. The absorption spectra of all these samples showed strong resemblances except for Mo_4O_{11} and MoO_2 which were of an entirely different character. They found that the energy gap increased gradually from 2.74 eV for MoO_3 with increase of oxygen deficiency to 3.1 eV for Mo_9O_{26} and Mo_8O_{23} and then decreased to 1.72 eV for MoO_2. They explained this variation of bandgap in relation to changes in crystal structure. They could not explain the great similarity in the absorption curves and the values of bandgap between MoO_2 and Mo_4O_{11}. Table 1.2. shows the bandgap of the different oxides of Mo according to the work of Hanafi et al (1981).

Hanafi et al (1975) have also measured the IR absorption spectra of all of these oxides except Mo_4O_{11}. They have reported that most of the absorption bands of MoO_3 are still present in the spectra of the non-stoichiometric oxides. This is thought to be due to the most frequently occurring MoO_6 octahedra. The behaviour of the intermediate oxides deviates gradually from that of MoO_3 towards that of MoO_2.

Porter et al (1972) have measured the optical absorption spectra of some intermediate oxides of Mo (MoO_2, Mo_4O_{11}, Mo_9O_{26}) in the visible and NIR region. They found that both MoO_2 and Mo_9O_{26} have one main absorption peak while the absorption peak of Mo_4O_{11} was split, having maxima at about 0.51, 0.58 and 0.95 μ m. According to their investigation the absorption band shifts linearly with changing metal-oxygen ratio. The intermediate

oxides, Mo_4O_{11}, $Mo_{17}O_{47}$, Mo_8O_{23}, Mo_9O_{26} are thermally unstable at higher temperatures and decompose above 973K with formation of MoO_2 and MoO_3 (Samsonov, 1973).

1.3.3 Molybdenum oxides for use as a solar selective surface

Molybdenum oxides for use as a solar selective surface, termed as 'Mo-black' (or 'black-Mo') has been investigated by several research groups. Mo-black can be prepared by different methods on different substrates.

The previous work at Brunel University (Hosseini, 1981) has shown that Mo-black coatings for use as solar selective absorbers can be prepared by the electrodeposition and simple chemical dip methods from an aqueous solution, which is one of the easiest and most cost-effective methods of producing solar selective absorbers.

Mo-black coatings known as 'Moly black' were first prepared by Hoffman and Hull in 1939 by an electrodeposition method. They used an aqueous solution of nickel sulphate ($NiSO_4$) ammonium molybdate [$(NH_4)_6Mo_7O_{24}$] and boric acid (H_3BO_3). The substrates used were aluminium, electroplated zinc, electroplated cadmium and die-cast zinc. The purpose of their work was to produce decorative coatings. According to their analysis, this highly lustrous, deep black coating contains about 45% Mo, 10% Ni with the balance chiefly oxygen. They also mentioned that very thin Mo-black coatings can be deposited simply by immersion of zinc plated substrates in the solution.

The electrodeposited Mo-black coating on copper substrateshas been studied by INCRA (1977), but the resulting coating was not satisfactory as a solar

selective absorber. Smith et al (1981) and Hosseini (1981) have studied Mo-black coatings prepared by the electrodeposition method on aluminium substrates and the chemical dip method on zinc and galvanized steel substrates. Hosseini used an aqueous solution of ammonium molybdate and nickel sulphate with concentration of 30 g/dm^3 and 150 g/dm^3 respectively. He suggests that the electrodeposited coating is composed of $MoO_2.2H_2O$ together with $Ni(OH)_2$ whereas the dip coating might be in the form of Mo_2O_3 oxide. According to his investigation, the electrodeposited coating is effectively non-selective due to continuous absorption in the IR region resulting in high emittance. The mechanism of the absorption in this coating was said to be unknown. Dip coatings on zinc and galvanized steel showed significant selectivity, e.g., $\alpha_v / \varepsilon_{th} = 4.3$ when α_v (absorptance in the visible range) = 0.84 for a coating on zinc substrates. The absorptance in these coatings was thought to be due to interference effects (Hosseini et al 1983). It was concluded that the dip coating might form a basis for selective coatings but the durability needed to be improved. In the present research, attempts have been made to improve the selectivity as well as durability of Mo-black coatings by changing preparation conditions and substrate conditions.

During the progress of the present work, some more work has appeared in the literature on Mo-black coatings for use as a selective solar absorber surfaces. Potdar et al (1982) have studied Mo-black coatings on nickel plated copper substrates prepared by cathodic electrodeposition method. These films have a solar absorptance of $\alpha_s \sim 0.85$ and thermal emittance of $\varepsilon_{th} \sim 0.11$. It has been reported that these films are adherent and non-crystalline and consist of essentially MoO_3 with some metallic nickel. Agnihotri et al (1983) have studied black molybdenum coatings prepared by chemical conversion method on galvanized steel and zinc plated mild steel. The best value of solar absorptance is 0.88 with $\varepsilon_{th} = 0.20$. These

coatings have been reported to contain MoO_3 and to be amorphous in nature. It has been reported (Gupta et al, 1983) that Mo-black coatings on galvanized steel do not degrade on annealing at 250°C in air up to 800 hours. The selective properties remain almost constant on thermal cycling (600 times at 150°C) and 98% humidity.

Black molybdenum films prepared by chemical vapour deposition (CVD) method from molybdenum carbonyl has been studied by Carver (1979) and Chain et al (1980, 1981). The CVD Mo-black exhibits a solar absorptance of $\alpha_s = 0.77$ and a thermal emittance of $\varepsilon_{th} = 0.44$. After annealing and then overcoating these films with an antireflection layer of Si_3N_4, the absorptance increases to 0.82 with $\varepsilon_{th} = 0.08$ (Carver, 1979). A higher value of absorptance of $\alpha_s = 0.91$ with $\varepsilon_{th} = 0.11$ has been reported by Chain et al (1980, 1981) for CVD Mo-black. These films are stable at 500°C for 1000 hours in a rotary pump vacuum. CVD Mo-black is a cermet type absorber. It consists of MoO_2 with Mo-inclusions and thus exhibits an absorptance close to that of MoO_2 and an emittance approaching that of Mo.

Recently Smith and Teytz (1984) have prepared a Co-Mo coating by chemical dip method from a solution of cobalt sulphate and sodium molybdate on electroplated cobalt film on nickel plated copper. Its optimum α_s and ε_{th} combination is $\alpha_s = 0.89 \pm 0.01$, $\varepsilon_{th} = 0.16$ to 0.20. The composition of this coating is thought to be either $MoCoO_2$ or $MoCo(OH)_2$ or a compound containing Co_2O_3 mixed with a molybdenum oxide in low valence states. Table 1.4 summarizes the radiative properties of some coatings referred to as Molybdenum-black in the literature.

1.4 Aim of the study

The purpose of this research is to investigate Mo-black coatings in relation to their use as selective absorbers for photothermal conversion of solar energy and to understand the physical processes responsible for selective absorption in these coatings. One aim is to study the relationship between the microstructural and optical properties under various conditions. A previous study (Hosseini, 1981) showed that Mo-black dip coatings had some potential for use as a solar selective absorbers, but durability needed to be improved. The aim of the present study is to concentrate on dip coatings.

It is known that the interfacial layer or the condition of the substrate has great influence on the radiative properties of solar selective surfaces and also on the durability of the coatings. Therefore to improve the selectivity and durability of Mo-black coatings different types of substrates, such as chemically etched zinc, electroplated cobalt (plated with and without addition agent) on nickel plated copper need to be studied. However, for comparison with the previous work and to see the effect of etching of the zinc substrates on the radiative properties and microstructures of the coatings, another aim is to study Mo-black on unetched zinc and aluminium substrates. To characterize these coatings, it is intended to make detailed studies on radiative properties ($\alpha_s, \varepsilon_{th}$), microstructures and compositions of the coatings.

(i) The radiative properties, e.g., solar absorptance α_s and thermal emittance ε_{th} of the coatings will be determined from the reflectance measurements in the solar (0.3 to 2.5 μm) and infrared

regions (2.5 to 50 μm).

(ii) The surface morphology of the coatings and the substrates will be studied in the scanning electron microscope (SEM) and their relationship to the optical properties of the coatings will be investigated. Some optical microscopy will also be performed.

(iii) The effects of deposition parameters (such as, solution temperature, deposition time) of Mo-black and substrate pretreatment on the radiative properties and microstructure of the coatings will be investigated. The effect of various deposition conditions of an intermediate cobalt layer will also be studied. Thus the preparation conditions for the optimum properties will be determined.

(iv) The compositional analysis of the coatings will be done by using X-ray diffraction, electron diffraction, X-ray Photoelectron Spectroscopy (XPS), together with infrared spectroscopy.

(v) The stability of the dip coatings will be tested by short term heat treatment at different temperatures together with atmospheric ageing.

(vi) Transmission measurements in the UV and visible region will be done to determine the bandgap of the coating material and its relation to the optical properties of the coating.

(vii) Some electrical measurements (both A.C. and D.C.) will also be performed to yield ideas about the band structure, conduction process and dielectric nature of the coatings.

Table 1.1. X-ray structural data and the average volume per oxygen atom for different oxides of molybdenum

Oxides	Number of Formula Units per cell	Average Volume per O atom $Å^3$	Structure Symmetry and Unit cell dimensions/Å	References
MoO_2	4	16.4	Monoclinic a=5.611, b=4.856, c=5.628 $\beta = 120^o$	Rogers et al, 1969
$Mo_{17}O_{47}$	2	16.8	Orthorhombic a=21.61, b=19.63, c=3.95	Kihlborg, 1959
Mo_4O_{11}	4	20.2	Orthorhombic a=24.4, b=5.45, c=6.7	Magneli, 1948
Mo_8O_{23}	2	18.9	Monoclinic a=16.88, b=4.052, c=14.45 $\beta = 106.19^o$	Magneli, 1948
Mo_9O_{26}	2	18.7	Monoclinic a=16.75, b=4.03, c=14.45 $\beta = 96^o$	Magneli, 1948
MoO_3	4	16.9	Orthorhombic a=3.962, b=13.85, c=3.69	Andersson and Magneli, 1950

Table 1.2. The values of optical bandgap for different oxides of Mo (Hanafi et al, 1981)

Oxide	Band gap eV
MoO_3	2.74
$Mo_{13}O_{38}$	3.00
Mo_9O_{26}	3.10
Mo_8O_{23}	3.10
Mo_4O_{11}	1.75
$Mo_{17}O_{47}$	2.88
MoO_2	1.72

Table 1.3 Some properties of Mo-oxides

Sample	Resistivity Ω–m	Thermal Activation Energy of Conduction (eV)	Work Function (eV)	Dielectric Constant	Refractive Index	References
Single crystal of MoO_2	10^{-6} to 10^{-7}	---	---	---	---	Bendor & Shimony, 1974
Single Crystal of MoO_3	---	0.29 to 0.70 (extrinsic) 1.83 (intrinsic)	---	5.7 (high frequency)	2.24	Deb, 1968
Thin film of MoO_3 (vacuum evaporated)	---	---	---	5.7 (high frequency) 18.0 (low frequency)	2.38	Deb and Chopoorian, 1966
Thin film of MoO_3 (vacuum evaporated)	---	0.27	---	15.8	---	Nadkarni and Simmons 1972; Simmons et al 1980
Electrodeposited Mo-black	---	---	0.46	---	1.9 (Visible) 2.6 (IR)	Hosseini, 1981

Table 1.4 Previous Studies of solar selective properties of Mo-black coatings

Substrate	Fabrication Technique	Absorptance α_s	Emittance ε_{th}	Composition	References
Quartz	Chemical Vapour Deposition (CVD)	0.82	0.08	Mixture of Mo and MoO_2 (polycrystalline)	Carver, 1979
Quartz	CVD	0.91	0.11	Same	Chain et al, 1981
Incoloy 800	CVD	0.93	0.17	Same	Chain et al, 1981
Nickel Plated Copper	Electrodeposition	0.85	0.11	MoO_3 (amorphous)	Potdar et al, 1982
Zinc and Galvanized Steel	Chemical Dip	0.75 (α_v = 0.84)	0.19	Mo_2O_3 (estimated)	Hosseini, 1981
Aluminium	Electrodeposition	0.90	0.83	$MoO_2.2H_2O$	Smith et al, 1981
Galvanized Steel	Chemical Dip	0.88	0.20	MoO_3	Agnihotri et al, 1983
Electroplated cobalt on Nickel Plated Copper	Chemical Dip	0.89	0.16 to 0.20	$MoCoO_2$ or $MoCo(OH)_2$	Smith and Teytz, 1984

CHAPTER II

PREPARATION OF MO-BLACK COATINGS AND EXPERIMENTAL TECHNIQUES

2.1 Techniques for preparation of Mo-black coatings

2.1.1 Electrodeposition of Mo-black coatings

Mo-black coatings were prepared by a cathodic electrodeposition method on an aluminium substrate from an aqueous solution of ammonium paramolybdate [$(NH_4)_6Mo_7O_{24}.4H_2O$], nickel sulphate [$NiSO_4.6H_2O$] and boric acid [H_3BO_3] (Hoffman and Hull, 1939). A schematic diagram of the electrodeposition equipment is shown in Fig.2.1. The apparatus consisted of a hot water bath with temperature control unit to provide the desired solution temperature, a regulated power supply unit, ammeter, plating tank and thermometer to measure the temperature of the solution. A pH meter (Data Scientific, PTI-15) was used to measure the pH of the solution. The density of the coatings was obtained from the difference of the mass of the substrate before and after coating deposition. The coating thickness was also measured by surface profile stylus equipment (Rank Taylor Hobson Talystep).

2.1.1.1 Aluminium substrate preparation

To obtain good quality, uniform and adherent coatings, the substrate pretreatment was extremely important. In this experiment the pretreatment of aluminium substrates was in two stages. Firstly, the oxide layer was

removed by grinding with emery paper of grade 320 and 600 in one direction. The substrates were then chemically etched with concentrated NaOH (150 g/dm^3) solution at a temperature of 25-30^{o}C for a few seconds and immediately immersed in boiling distilled water for a further few seconds with constant stirring. This was followed by washing with more distilled water and drying with compressed air.

The use of emery paper to remove the oxide layer made the surface rougher which gave good adhesion. However, surface roughness affected the thermal radiative properties of the coatings. An attempt was made to avoid the use of emery paper by dissolving the oxide layer with a chemical solution. In this process, (Lowenheim, 1963) the aluminium substrates were first degreased with choloroform and rinsed with alcohol. This was followed by a mild etching with NaOH solution and washing in boiling distilled water. These were then immersed in a zincate solution (which consisted of 200 g/dm^3 of NaOH and 80 g/dm^3 of ZnO) for a few seconds at a temperature of 25^{o}C. The oxide layer present on the surface of aluminium dissolved in the zincate solution and a very thin layer of zinc was deposited on the aluminium surface. The substrates were then immersed and agitated in distilled water in two successive stages to remove all of the zincate solution. The zinc layer formed on the aluminium was then dissolved by dipping in a 30% (by volume) solution of HNO_3. Washing of the substrates with distilled water was followed by their rapid transfer to the plating bath.

2.1.1.2 Bath composition and plating conditions

In the present investigation the concentration of Mo-black electroplating bath was

$(NH_4)_6Mo_7O_{24}.4H_2O$ - 30 g/dm^3

$NiSO_4.6H_2O$ - 150 g/dm^3

H_3BO_3 - 22 g/dm^3

Here boric acid was used to buffer the solution during plating. The required bath temperature was in the range of 55–70^{o}C and the current density used from 1.5 to 3.0 mA/cm^2. The coatings were prepared for various lengths of time from 20 to 60 minutes on rough aluminium substrates. On smooth aluminium substrates, the plating time varied from 5 to 20 minutes. The coating thickness expressed as the coating mass per unit area was found to increase with plating time and current density. Table 2.1 gives plating conditions of some coatings on aluminium substrates.

2.1.2 Mo-black coatings by chemical conversion

Mo-black coatings were prepared on zinc and electroplated cobalt on nickel plated copper substrates by immersion and agitation for a few minutes in a solution of ammonium paramolybdate and nickel sulphate. Boric acid (used in the electroplating bath) was not required in the dipping process.

2.1.2.1 Bath composition

Different concentrations of ammonium paramolybdate and nickel sulphate (Table 2.2) were used in preparation of the Mo-black coatings by the dipping process. Solution 1 was suggested by Agnihotri et al (1983); but tended to be unstable at room temperature. The solution was soluble only at a temperature above 60^{o}C. Below 60^{o}C a light bluish-white precipitate formed. However, the precipitates could be dissolved at lower temperatures by decreasing the pH of the solution. In this case the rate

of deposition was very high. It was difficult to control the thickness of the coating (which was found to be critical for optimized selectivity). Lower concentrations of ammonium paramolybdate were, therefore, tried (solution 2,3 and 4 in Table 2.2). These were soluble even at room temperature. Solution 2 (without nickel sulphate) gave no black coating even for long times of immersion (the effect of the concentration of nickel sulphate on the optical properties of the coatings is described in section 3.1.1). Solution 3 gave the most reproducible results and was used throughout this investigation.

2.1.2.2 Zinc substrate preparation

Commercially available zinc sheet of thickness 1mm was used in this study. To obtain uniform and adherent coatings, the thin surface layer of oxide was removed from the zinc substrates by using emery paper of grades 600 and 1200 under a flow of water to avoid deep scratches. The substrates were then washed with distilled water, rinsed with alcohol and dried with compressed air. The second step was chemical etching. Various concentrations of HNO_3 were used to etch the zinc substrates ranging from 5% to 50% by volume. (The concentration of HNO_3 had some effect on the surface topography of the coatings (Section 3.2.2)). The zinc substrates were etched in HNO_3 at a temperature of $20^{o}C$ for a few seconds with constant stirring, followed by washing with distilled water, rinsing with alcohol and drying.

2.1.2.3 Plating conditions for zinc substrates

Following the pretreatment, zinc substrates were immersed in the plating solution for various lengths of time. During the deposition process, the solution was gently stirred in order to avoid non-uniformity and the

formation of air bubbles. After deposition of the coatings, they were washed with distilled water and dried with compressed air. The colour of the coating depended on the time of immersion and hence on the coating thickness. An observable colour was found just after immersion in the solution. Up until 20 seconds the coating was very thin and non-uniform. As the time of immersion increased, the coating became darker and more uniform. After 60-70 seconds of immersion, no visible interference colours were observed in the coatings on etched substrates and the colour of the coating was dark grey. For unetched substrates, interference colours were not observed after 3 minutes immersion. Fig.2.2 shows the variation of coating mass per unit area with deposition time for both etched and unetched zinc substrates. The coating mass increased rapidly for the first 3 minutes and then much less rapidly. The rate of deposition was higher for etched zinc than the unetched zinc (Fig.2.2) indicating that the acid etched substrate was more reactive. The difference between the measured surface area and the true surface area of the coating on etched zinc might also account for the observed higher deposition rate (as the etched zinc had rough topography).

The temperature of the solution influenced the coating thickness. Though the coating could be formed at room temperature, the rate of deposition was low. Fig.2.3 shows the effect of solution temperature on the coating thickness. At high temperatures it was difficult to control the coating thickness due to the high deposition rate and the coating adhesion was poor. The best results were obtained in the temperature range 35 - 45^{o}C.

2.1.2.4 Preparation of electroplated cobalt on nickel plated copper substrates (Cobalt (NC) substrates)

These substrates were prepared by electroplating a cobalt film onto dull

nickel which had been plated onto copper sheet. The following procedures were used:

a) The copper sheet was mechanically polished with 1200 grade of emery paper to remove the oxide layer and washed with distilled water.

b) The copper sheet was then chemically cleaned in a solution of ammonium persulphate (10 g/dm^3) at a temperature of 40 - 45^{o}C for 1 minute with constant stirring. It was then immersed in dilute H_2SO_4 at room temperature and finally washed with distilled water and alcohol and dried.

c) Dull nickel was electroplated onto these cleaned copper substrates from a solution of nickel sulphate, nickel chloride and boric acid in the respective amounts of about 200, 40 and 20 g/dm^3. The operating conditions were as follows:

Temperature of the solution	30 - 40^{o}C
pH of the solution	3.5 - 3.8
Cathode current density	20 - 25 mA/cm^2
Plating time	10 - 15 minutes
Anode used	Nickel sheet

d) The final step was the electrodeposition of cobalt. The cobalt films were prepared by the cathodic electrodeposition method on nickel plated copper substrates. The composition of the cobalt plating bath used in this study was as follows:

$CoSO_4 \cdot 7H_2O$	100 g/dm^3
H_3BO_3	40 g/dm^3
$CoCl_2$	20 g/dm^3

Plating was done under the following conditions:

Temperature of solution	45 - 60^{o}C
Cathode current density	25 - 45 mA/cm^2
Plating time	4 - 10 minutes

The major problem experienced with cobalt plating was pitting. The pits were due to large numbers of gas bubbles [either air or hydrogen (Ollard, 1969)]. Compressed air agitation was used in an unsuccessful attempt to prevent pitting. Finally, these pits were completely removed by using sodium-lauryl-sulphate (40 mg/dm^3) in the plating solution as an addition agent. This reduced the surface tension at the interface between the solution and the work and allowed small gas bubbles to detach, thus preventing the formation of pits. In the following sections, the electroplated cobalt on nickel-plated copper substrates will be referred to as "cobalt (NC)" substrates.

2.1.2.5 Plating conditions for cobalt (NC) substrates

For the preparation of Mo-black dip coatings on cobalt (NC) substrates, the molybdate solution composition was as described in section 2.1.2.1. However, in this case the required solution temperature was in the range 60 - 80^{o}C. At lower temperatures, the chemical reaction was very slow and the coating was non-uniform. The solution pH, to obtain an optimized coating, was in the range 2 to 3.5. If the pH was below or above this critical range a blue film was formed. To obtain uniform coatings the

solution was stirred continuously during deposition. After deposition, the coatings were cleaned with distilled water and dried with compressed air. There was a threshold time of immersion to yield an observable conversion coating. This was of the order of 60 - 70 seconds. Partial corrosion of the cobalt occurred during this time. It was not possible to determine the mass per unit area or the thickness of the Mo-black coating on cobalt (NC) substrate by weighing; as the weight of the cobalt substrate decreased after immersion in the solution due to the initial corrosion. The properties of the coatings were therefore compared with reference to their immersion time in the Mo-black plating solution.

2.2 Measurement of thermal radiative properties

Two parameters of the solar selective surface which are most relevant to the performance of the surface in solar thermal conversion are the solar absorptance α_s and thermal emittance ε_{th}. Methods of measuring the solar absorptance and thermal emittance of a surface can be classified into two main categories (Fussell et al 1963):

a) Optical methods: in which α_s or ε_{th} are measured by the radiation reflected from or emitted by the surfaces; this radiation may be either spectrally resolved or integrated.

b) Thermal methods: in which α_s or ε_{th} are measured by the temperature or rate of change of temperature of the surfaces.

In the present investigation, measurement of spectral reflectance ρ_λ was used to determine the solar absorptance α_s and thermal emittance ε_{th} of the coatings.

2.2.1 Measurement of solar absorptance(α_s)

All the specimens studied in the present work were coatings on metal substrates and therefore, effectively opaque. The solar absorptance of these coatings α_s was determined from spectral reflectance (ρ_λ) measurements (for wavelengths throughout the solar spectrum) using an integrating sphere reflectance spectrophotometer. α_s was then calculated by applying Kirchoff's law for an opaque material (Appendix A) and the use of selective ordinates for air mass 2 calculated by Wiebelt and Handerson (1979). In the selected ordinates method, the solar spectrum is divided into a finite number of intervals which correspond to uniform increments of solar energy. The spectral reflectance ρ_λ of the specimen is thus weighted equally in each such interval and no further weighting is necessary. Table 2.3 shows the terrestrial spectrum for air mass 2 divided into twenty equal increments of energy, with a mean wavelength for each increment that divides the increments into two equal parts (Wiebelt and Henderson, 1979). Reflectances at these mid points λ were used in the present investigation to calculate α_s.

The total spectral reflectance ρ_λ of the coatings was measured by using a Beckman 5240 integrating sphere spectrophotometer for the wavelength range 0.3 to 2.5 μm. The integrating sphere (Fig.2.4(a)) was designed to perform total or diffuse reflectance measurements with monochromatic illumination. It consisted of a 6 inch internal diameter sphere coated inside with an excellent diffuse reflector (white barium sulphate paint). A barium sulphate plate was used as a reference standard. Monochromatic radiation was focused onto and reflected from the sample at all angles inside the integrating sphere (the exact nature depends upon the specularity of the sample). The scattered radiation underwent multiple reflections from the inside surface of the sphere. It is the nature of

the integrating sphere to be uniformly illuminated by the reflected sample radiation (Longhurst, 1957). The reflected energy flux reaching the detector in the integrating sphere is therefore directly proportional to the total reflectance of the specimen. Direct reflections from the sample surface are prevented from reaching the detector.

An optical block diagram of the spectrophotometer is shown in Fig.2.4(b). It is a digital direct reading, ratio recording spectrophotometer capable of either double or single beam operation. The major components of the instrument are a power supply, single monochromator, UV-visible sources (deuterium and tungsten) with automatic source changer, NIR source (tungsten) electronics, recorder, sample compartment, UV-visible detector (photomultiplier) and NIR detector (PbS cell).

Before recording the spectral reflectance of a specimen, the spectrophotometer recorder and the digital display were calibrated at 100% reflectance using $BaSO_4$ plates in both reference and test specimen holders (through the NIR wavelength range 0.7 - 2.5 μ m). Then the specimen under investigation was placed in position and its spectral reflectance was recorded for the same wavelength range. The spectrophotometer recorder was again calibrated for the UV-visible region (0.3 - 0.8 μ m) as above. The spectral reflectance for the same specimen was then recorded for the UV-visible region. The reflectance data were input to a microcomputer, and stored on a disc. The solar absorptance α_s was calculated by the computer using the selected ordinate method. The estimated random error in the measurement of α_s was $\pm$ 0.001 (Appendix B).

2.2.2 Measurement of thermal emittance (ε_{th})

In the present investigation, the thermal emittance (ε_{th}) of the coatings

was determined by measuring the specular reflectance (ρ_λ) of the surface in the infrared region for the wavelength range from 2.5 to 50 μm. The overall thermal emittance was calculated by applying Kirchoff's law (Appendix A) and weighting with the blackbody spectrum at a notional solar collector operating temperature of 35^{o}C (Duffie and Beckman, 1980).

The IR reflectance was measured by using a Perkin-Elmer (model 683) double beam ratio recording spectrophotometer with reflectance attachment. The optical diagram and a photograph of the actual specular reflectance attachment are shown in Fig.2.5. It consists of two front-surfaced mirrors installed on a mounting block. The mirrors are set up in such a way that a single reflection of the radiation from the surface of the sample at the same angle as the angle of incidence is obtained. The area of illumination is 1.5 X 3.5 cm^2 and the angle of incidence of the radiation is about 26.5^{o} from the normal. The reflectance of the sample was compared with the reflectance of a standard aluminium mirror. Examples of the emittance and standard error calculations for this measurement are given in Appendix B.

The thermal emittance of some specimens was measured by using a thermopile to detect radiation emitted by the sample fixed to a vertical flat plate heater (Walter, 1978). The heater was constructed with a resistance wire element, which was wound on a mica sheet, sandwiched between two aluminium sheets. The assembly was then mounted on a wooden block. The specimen was clipped to the heater and heated to a temperature (~70^{o}C). The surface temperature of the specimen was determined by an electronic thermometer using a spring-loaded surface temperature thermocouple. The thermopile was located 1cm apart from the specimen, so that the thermopile essentially detected only the radiation from the heated sample. It has been verified that the thermopile output is approximately proportional to

the emissive power of the sample (Walter, 1978).

To obtain the emittance of an unknown surface, the variation of the thermopile output with the surface temperature for two standard specimens of known emittance was obtained together with that for the unknown sample. These two standard specimens were polished aluminium with an emittance of 0.04 and nextel black paint with emittance of 0.97. The emittance was then calculated using the following empirical relation:

$$\varepsilon = \frac{x - x_o}{x_1 - x_o} (\varepsilon_1 - \varepsilon_0) + \varepsilon_0 \qquad (2.1)$$

where ε_1 and ε_2 are the emittances of nextel paint and polished aluminium respectively and x_1, x_0, and x are the thermopile outputs at the same temperature for nextel, aluminium and the specimen respectively. Fig.2.6 shows plots of thermopile output voltage as a function of surface temperatures of the specimens, and defines the quantities x, x_o and x_1. The emittance of the standard specimens were determined by calorimetric method using the equipment developed by Hosseini (1981) (Appendix C).

2.3 Structural study of Mo-black coatings

To explain the physical processes responsible for selective absorption of a surface, compositional and microstructural data are most important. These can be obtained from a range of surface analytical techniques, such as scanning electron microscopy, X-ray microanalysis, X-ray diffraction, electron diffraction and X-ray photoelectron spectroscopy. The various techniques used in the present investigation are described in this section.

2.3.1 Scanning Electron Microscopy (SEM) and Electron Probe Micro-Analysis (EPMA)

Analyses of surface microstructure and compositional variations of the coatings were carried out using a Cambridge Stereoscan 250 MK-2 scanning electron microscope (SEM) equipped with a solid state detector. The instrument was also equipped with a link system 860, fully quantitative energy dispersive X-ray analyser (EDX) for chemical compositional analysis.

A schematic block diagram of the electron and X-ray optics of an SEM is shown in Fig.2.7. The electron optical column of the SEM focusses electrons generated by the electron gun into a fine probe of electrons which strikes a point on the specimen surface. The interaction between the electrons and the specimen produces a variety of different signals: high energy backscattered electrons, low energy secondary electrons, absorbed electrons, X-rays and cathodo luminescent radiation (Fig.2.8) (Goldstein et al 1981). Each of these signals can be collected and amplified. The resulting signal is utilized to control the brightness of the cathode-ray-tube (CRT). To obtain signals from a particular area, the electron beam is scanned in a TV raster fashion across the specimen surface by two pairs of electromagnetic coils. As the CRT scan is synchronized with the beam scan, the signals from the specimen are transferred from point to point and a signal map of the scanned area is displayed. In principle, all of the signals resulting from the interaction of the electron beam with the specimen can be used to derive information about the topography, composition, crystal structure, electronic structure, electrical and magnetic character of the specimen (Goldstein et al., 1981).

In the scanning electron microscope (SEM), the signals of greatest interest are those due to the secondary and backscattered electrons, since they vary as a result of differences in surface topography as the electron beam is swept across the specimen. In the present study, secondary electron imaging was used to study the surface topography of the surface coating and substrate materials. The secondary electron co-efficient increases as the angle between the specimen surface and the incident beam decreases. This means that areas of the specimen with high angles of tilt will appear bright.

In the electron probe microanalyzer (EPMA), frequently referred to as the electron microprobe, the radiation of interest is the characteristic X-rays which are emitted as a result of electron bombardment. The analysis of the characteristic X-radiation can yield both qualitative and quantitative compositional information.

Specimen preparation for SEM examination was straight forward. The specimen was carefully cut to the required size and then firmly attached to the mount using adhesive or double sided tape. For good electrical contact, the specimen was earthed to the stub by using silver paint or DAG. The whole specimen was coated with a thin layer of gold or carbon to prevent charging effects. The same specimens were examined in the SEM before and after heat treatment to determine the effect on the surface topography. By using the electron probe microanalyzer, information related to the concentration of different elements present in the coating was obtained.

2.3.2 X-ray Photoelectron Spectroscopy (XPS)

X-ray photoelectron spectroscopy (XPS) was used to analyse the elemental

composition of the Mo-black coatings and also to determine the oxidation state of the molybdenum in the coatings. XPS is a technique for establishing the composition of the outer atomic layers of a surface, for all elements (except hydrogen and helium) to a sensitivity in the range of 0.1 - 1% (Riggs and Parker, 1975, Briggs, 1977). The spectra contain information about the chemical state of the surface atoms. In X-ray photoelectron spectroscopy, the sample is irradiated by a monochromatic beam of X-rays under high vacuum. Usually Al K_α(1487.6eV) or Mg K_α(1253.6 eV) is used as the source. The X-rays of frequency ν and energy, $h\nu$ eject photoelectrons directly from the core level of the atoms with a fixed kinetic energy given by

$$E_K = h\nu - E_B - \phi_s \text{ (conservation law of energy)} \qquad (2.2)$$

Here E_B is the binding energy of the electrons in the material, E_K is the kinetic energy with which the electron is ejected by the incident photon energy $h\nu$ and ϕ_s is the spectrometer work function which can be defined as the energy required to raise an electron from Fermi level to the free electron state (vacuum level) outside the spectrometer. An energy level diagram of a conducting material in electrical equilibrium with the spectrometer is shown in Fig.2.9. The kinetic energy of the ejected electrons (which depends on the energy of the exciting radiation and the energy with which the electron is bound to its nucleus) is measured in the high resolution electron spectrometer. Then the binding energy can be determined using equation (2.2), which is unique to a particular atom, thus making identification of an element possible. Changes in the chemical bonding around an atom in a molecule produce shifts in binding energy which can also be measured. The oxidation states of the atoms can therefore be determined from the measured binding energy shifts.

In the present work, the Mo-black coatings on different substrates were investigated in a vacuum of ~ 1.3 X 10^{-5} Pa, with a spectrometer (Kratos Analytical Instruments Ltd, Model ES300) employing monochromatized Al K_α radiation. The resolution of this instrument is $\pm$ 0.95 ev.

The coatings were cut to the required size and mounted on the end of the sample probe on a removable tip using double-sided tape or special type of metal clips. The sample probe also had provision for heating. The study was carried out for both 'as prepared' and heat treated samples. An attempt was also made to determine the depth profile of the coatings using Argon ion beam etching. For comparison, standard MoO_3 and MoO_2 powder and Mo-metal foil were also studied.

2.3.3 X-ray diffraction

Attempts were made to study the structure of the coatings by using X-ray diffraction. Several specimens were examined in the diffractometer, type PW1050, controlled by a PW1710 diffractometer control unit. In this investigation Co K_α radiation (λ = 0.179 nm) (50 kV, 10 mA) was used between Bragg angles of 4^o and $50^o\theta$. The same specimen was studied before and after heat treatment. The diffraction patterns for uncoated substrates were also obtained.

2.3.4 Electron diffraction

Electron diffraction examination was performed to study the structure of the deposited coatings on various substrates using a transmission electron microscope (model JEM7). Both transmission and reflection electron microscopy were used.

For high resolution reflection electron diffraction (RED) study, no special technique for sample preparation was needed. The sample was cut into the required size (1 square cm) and directly attached on the sample holder and investigated. Both uncoated substrates and coated area were observed.

For transmission electron diffraction (TED) studies thin Mo-black films were deposited by an electrodeposition method on aluminium coated glass slides. The aluminium layer was etched away from the glass by using a solution of approximately 5% NaOH. After washing to remove NaOH, a drop of water was added to the oxide film and the test film made to go into the drop by carefully scratching from the glass using a needle. Then the drop of water containing fragments of oxide film was collected onto a carbon coated grid. After drying, the grid was inserted into the specimen holder and examined in the microscope. The microscope was provided with a heating and cooling specimen attachment capable of varying the sample temperature from -93 to 1000^{o}C.

Various areas of the film were viewed and representative micrographs and diffraction patterns were taken at different fixed temperatures. Using the diameter D of the hkl diffraction ring the hkl interplanar spacing d could be determined using Bragg's law. The calculations required a knowledge of the electron microscope camera length L which is related to D and d by

$$2\lambda L = Dd \qquad (2.3)$$

λ the wavelength of the incident electrons was 0.0042 nm at 80 kV. Values of $2\lambda L$ the camera constant for both heating, cooling and standard stages were calculated by using a gold film as standard; D was determined

experimentally and d values were obtained from the ASTM index.

2.4 Study of electrical properties of Mo-black coatings

An attempt was made to study the electrical properties of the Mo-black coatings to get information about the conduction mechanism through the coatings and find out the value of activation energy of the conduction process, dielectric constant and conductivity of the coatings.

2.4.1 Electrical measuring systems

All the electrical measurements were carried out inside the water-cooled high vacuum vapour diffusion pump (Edward model 12E7/114) at a pressure of about 10^{-3} Pa. A glass belljar 37cm high and 30 cm diameter was positioned above a thick aluminium base plate and the topside of the belljar was covered with a 2cm thick aluminium plate. The experimental arrangement is shown in Fig.2.10. The electrical measurements were taken on a metal-insulator-metal sandwich structure. The aluminium substrate was the bottom electrode. Spring loaded pressure contacts were obtained from the top surface of the coating using highly polished flat metal buttons. Aluminium, copper and brass buttons were used in the measurements. The spring loaded metal buttons were supported on an insulating pyrophillite rod placed at one edge of the heater assembly. A schematic diagram of the specimen holder in the vacuum chamber is shown in Fig.2.11. The electrical connecting wires from the contacts, heater and thermocouple were terminated on a lead-through which was fixed on the top of the vacuum chamber. All connecting wires inside the vacuum chamber were insulated by alumina beads. Outside the vacuum chamber, connections were taken from the lead-through to the various measuring equipments.

The measurements were carried out in the temperature range 20 - 250°C. The specimen holder and its heater assembly was constructed on a single unit as shown in Fig.2.12. The heater was made up with nichrome wire wound on an insulated mica sheet, which was sandwiched between another pair of mica sheets. Two flat Al-sheets were then used as cover plates of the heater. The heating power was provided by a Farnell Stabilized power supply. The device temperature was monitored by a Comark electronic thermometer (type 1601 Cr /Al).

2.4.2 Electrical circuitry for DC measurements

The schematic diagram of the DC circuitry for measuring the I-V characteristics of the coatings is displayed in Fig.2.13. A Farnell stabilized power supply (Model-L30A) was used to pass a constant DC current through the coatings. To measure the current flowing through the coating a Hewlett-Packard DC micro-volt-ammeter (Model-425A) was used. A digital multimeter (Farnell, Model-FO876 007) was used to measure the potential difference across each sample.

2.4.3 Electrical circuitry for capacitance measurements

The capacitances of the coatings were measured by using a Marconi Universal Bridge TF1313A. By using an external source and detector, the measurements were carried out in the frequency range 500Hz to 25,000 Hz. The measurement circuit is shown in Fig.2.14. A low frequency oscillator (model J2E, frequency range 15Hz - 50 kHz) was used as the source which was connected to the bridge and the detector was a Farnell oscilloscope (DTV 12-14).

2.5 Optical measurements

Transmittance measurements in the UV and visible region (0.3 - 0.9 μ m) were made on thin electrodeposited Mo-black films prepared on semi-transparent aluminium coated glass substrate. Corning 7059 glass slides were used as substrates for preparing the film for transmission measurements. Before preparing the film, the glass substrates were cleaned adequately. They were washed in water and then boiled in a 3% solution of Decon 90 detergent in distilled water for 15 minutes. They were then rinsed in distilled water for a further 10 minutes. Finally they were dried by compressed air. The glass substrates were then coated with a semi-transparent conducting aluminium layer produced by vacuum evaporation method in a Balzers BA510 coating unit under a pressure of about 5×10^{-4} Pa. This conducting semi- transparent aluminium layer is used to make the glass substrate the cathode for electroplating the Mo-black film on aluminium. To prevent the oxidation of the aluminium the Mo-black films were electrodeposited immediately after aluminium film deposition.

Transmission measurements of the films were made using a Perkin Elmer (model λ -3) double beam spectrophotometer. To compensate for the absorption by the aluminium film underneath the Mo-black film, a glass substrate coated with equal thickness of aluminium, which was prepared in the same evaporation, was used in the reference beam. The measurements were made as a function of current density and thickness of the films.

Table 2.1 Plating conditions of some Mo-black coatings on aluminium substrates

Substrate condition	Solution Temperature (^{o}C)	Deposition time (Minute)	Current density mA/cm^2	Coating mass per unit area (mg/cm^2)
Roughened aluminium	69	30	1.45	1.72
	69	45	1.45	2.42
	69	60	1.60	3.33
	65	15	3.03	1.80
	65	20	2.66	2.13
	65	30	2.69	3.07
	65	45	2.05	2.18
	65	45	3.03	3.76
Shiny aluminium	65	5	2.40	0.70
	65	10	2.38	1.18
	65	20	2.45	2.17
	65	10	1.44	0.72
	65	15	1.49	1.10
	65	25	1.43	1.64

Table 2.2 Bath compositions for the preparation of Mo-black coatings by the chemical dip method.

Solution number	Quantity of solute in 0.150 dm^3 of distilled water / g	
	Nickel Sulphate	Ammonium Molybdate
1	1	9
2	0	3
3	1	3
4	3	3

Table 2.3 Spectral distribution of terrestrial beam radiation at air mass 2 and 2.3 km visibility, in twenty equal increments of energy (Wiebelt and Henderson, 1979).

Energy band number	Wavelength range μm	Midpoint Wavelength μm
1	0.300 - 0.434	0.402
2	0.434 - 0.479	0.458
3	0.479 - 0.517	0.498
4	0.517 - 0.557	0.537
5	0.557 - 0.595	0.576
6	0.595 - 0.633	0.614
7	0.633 - 0.670	0.652
8	0.670 - 0.710	0.690
9	0.710 - 0.752	0.730
10	0.752 - 0.799	0.775
11	0.799 - 0.845	0.820
12	0.845 - 0.894	0.869
13	0.894 - 0.975	0.923
14	0.975 - 1.035	1.003
15	1.035 - 1.101	1.064
16	1.101 - 1.212	1.170
17	1.212 - 1.310	1.258
18	1.310 - 1.603	1.532
19	1.603 - 2.049	1.689
20	2.049 - 5.000	2.292

CHAPTER III

EXPERIMENTAL RESULTS AND INTRODUCTORY ANALYSIS

The experimental techniques used in the present work have been described in Chapter II. For the sake of clarity, in this chapter, the results of these experiments are presented separately with only a brief analysis. A complete discussion of the results will be presented in Chapter V.

3.1 Spectral reflectance, solar absorptance (α_s) and thermal emittance (ϵ_{th}) of coatings and substrates

Spectral reflectance measurements of Mo-black coatings have been carried out on different substrates and the effects of variables controlling the preparation of the coatings on the absorptance and emittance have been examined. The coatings on zinc and cobalt substrates have been studied in detail unlike those on aluminium which are effectively non-selective.

Solar absorptance has been determined from measurements of the total spectral reflectance (Section 2.2.1) for the solar region 0.3 to 2.5 μm. Generally the thermal emittance of the coating has been determined from specular reflectance measurements (Section 2.2.2) in the range 2.5 to 50 μm. The thermal emittance of some coatings has also been determined by using a thermopile (Section 2.2.2).

3.1.1 Mo-black dip coatings on zinc substrates

A number of factors relating to the preparation of Mo-black dip coatings on zinc substrates have been studied with reference to their effects on solar absorptance and thermal emittance. The factors are as follows: solution concentration, solution temperature, substrate pretreatment and coating mass per unit area (i.e., thickness).

Table 3.1.1 shows the effects of variation of nickel sulphate concentration on absorptance and emittance of the coatings. All coatings were prepared at a temperature of 45°C on mechanically polished substrates. The addition of a small amount of nickel sulphate enhanced the solar absorptance with only a small increase in thermal emittance. The solution having 1 g nickel sulphate (in 0.15 dm^3 of distilled water) gives better selective properties than the other solutions i.e., led to reasonable absorptance values with a good selectivity factor $\alpha_s / \varepsilon_{th}$ (Table 3.1.1).

The total reflectance spectra in the range 0.3 to 2.5 μm for three Mo-black coatings (of different thicknesss) on mechanically polished zinc are shown in Fig.3.1.1. Interference peaks are present throughout the solar region except in the UV region (below about 0.4 μm). The height of the interference peaks reduces as the coating thickness increases. For the thickest coating no peaks can be seen in the region below 0.7 μm.

Figs.3.1.2(a) and (b) show the spectral total reflectance spectra of Mo-black coatings on chemically etched zinc substrates for different thicknesses (i.e., different coating mass per unit area). No interference peaks are present in the region below 0.7 μm except for the thinner coatings (~0.10 - 0.15 μm), where one peak can be seen having a maximum at

about 0.7 μm. The coatings have their lowest reflectance ordinarily in the UV and visible region. For all coatings an interference minimum is present in the region from 0.8 to 1.1 μm. This minimum does not shift much towards the higher wavelengths as the coating thickness increases. After this minimum, the transition takes place between low and high reflectance. In the near infrared, the reflectance decreases as coating thickness increases and optical interference peaks are observed in the reflectance spectra of thicker coatings (Fig.3.1.2 (b)). The values of computed solar absorptance α_s of dip coatings on both type of substrates (etched and unetched) zinc are given in Table 3.1.2 for different coating massper unit area.

The thermal emittances of the coatings were determined from the IR specular reflectance in the region 2.5 - 50 μ m and are given in Table 3.1.2. The IR specular reflectance spectra of the coatings on unetched and etched zinc substrates for different coating thicknesses are shown in Figs.3.1.3 and 3.1.4 respectively. In both cases, as the coating thickness increases, the IR reflectance decreases i.e., the emittance increases which is also evident from Table 3.1.2. The thinner coatings (thickness below ~ 0.2 μm) appear to be transparent to the IR radiation, i.e., thermal radiation is reflected from the substrate resulting in high reflectance throughout the IR region. As the coating thickness increases, the films become opaque to infrared radiation and the emittance increases. For the thickest coating strong and broad absorption bands from 10.5 to 22.0 μm can be seen in Fig.3.1.4(b). The absorption peaks at 2.9 - 3.1 μm and at about 6.2 μm indicate the presence of water in the coatings (Nakamoto, 1970).

Comparison between thermal emittances obtained by using thermopile (Section 2.2.2) and from the IR specular reflectances can be seen in Table

3.1.3(a). The emittances determined using the thermopile are somewhat lower than those obtained from IR reflectance measurements. This discrepancy may be due to the exclusion of diffuse component of the IR reflectance as the instrument used was designed for measurement of specular reflectance only. The emittance of some samples determined from IR reflectance spectra is compared to that determined by a calorimetric method (Appendix C) by Yousif (1987). The results are given in Table 3.1.3(b) and show better agreement. However, emittances of the coatings determined by calorimetric method are lower than those obtained from IR reflectance.

The variations of solar absorptance and thermal emittance of the dip coatings with coating mass per unit area are shown in Figs.3.1.5 (a) and (b) for etched and non-etched zinc substrates respectively. The emittance and absorptance values are thickness dependent for coatings on both type of substrates but the emittance is more thickness dependent than the absorptance. On etched zinc substrates, the absorptance first increases from 0.79 to 0.87 with the increase of coating mass per unit area, while the increase in emittance is smaller. After that the emittance increases more rapidly with coating mass and the absorptance decreases slightly and then goes to the maximum value. (Data for the thickest coating is not included in Fig.3.1.5 (a), see Table 3.1.2 (a)).

The highest selectivity factor ($\alpha_s/\varepsilon_{th}$ = 8.78) is obtained for the thinnest coatings on etched zinc although the absorptance for this coating is the lowest (0.79) (Table 3.1.2(a)). On unetched substrates, the highest value of absorptance is 0.78. The highest selectivity factor obtained is 9.86 (Table 3.1.2 (b)) for the thinnest coating. Fig.3.1.5(c) shows the variation of selectivity factor $\alpha_s/\varepsilon_{th}$ of the coating with

coating mass per unit area. The values of $\alpha_s / \varepsilon_{th}$ are slightly higher for coatings on unetched substrates (especially at low coating mass). As the coating mass increases, the selectivity factors approach the same value for both type of substrates (Fig.3.1.5(c). In both cases the selectivity factor decreases with the coating mass per unit area, as the emittance gradually increases with the coating mass but the absorptance does not change so much.

The effect of substrate pretreatment on the spectral reflectance spectra of Mo-black dip coatings is illustrated in Fig.3.1.6. The corresponding values of α_s and ε_{th} are tabulated in Table 3.1.4. Chemical etching of the zinc substrate enhances the absorptance of the coatings considerably with only a small increase in emittance. Table 3.1.4 also shows that etching of zinc substrates with 50% HNO_3 acid gives the highest value of absorptance (0.89) but the emittance is also high (0.30). However, best values of α_s and ε_{th} are obtained after etching with 30% HNO_3, though $\alpha_s / \varepsilon_{th}$ has a value of 5.7 which is somewhat lower than the value (7.6) for coatings on highly polished zinc (1 μ m finish). It is shown in section (5.3) that the selectivity factor is not the primary factor to characterize a selective surface (unless $\alpha_s \geqslant 0.90$).

The effect of solution temperature on α_s and ε_{th} of the coatings was examined and the results are shown in Table 3.1.5. The solution temperature has no significant effect on the radiative properties of the coating in the range 35° - 45°C. At 55°C, however, the absorptance is lower and emittance is higher than for the coatings prepared at lower temperature. This may be due to the change in thickness of the coatings, as the rate of deposition increases with the solution temperature (Fig.2.3). As described earlier, the absorptance decreases slightly after a certain critical thickness but the emittance increases continuously with

thickness.

3.1.2 Mo-black dip coatings on cobalt (NC) substrates

A range of Mo-black coatings on electroplated cobalt on nickel plated copper substrates has been studied. Both the plating conditions of cobalt and preparation of the Mo-black coatings influence the absorptance and emittance of these coatings. Several parameters have been varied to yield an absorber with the best optical properties. Table 3.1.6 shows some plating conditions of cobalt substrates as well as Mo-black coatings. The values of α_s, ε_{th} and $\alpha_s/\varepsilon_{th}$ are also listed in Table 3.1.6. This shows that the highest absorptance value obtained from these coatings is 0.94 with an emittance of 0.28 - 0.33. These coatings have high absorptance but due to the high emittances (Table 3.1.6) the selectivity factor $\alpha_s/\varepsilon_{th}$ is not high enough. (The highest selectivity factor obtained is 4.1 with α_s = 0.90). The emittance of the coatings increases with the plating time of cobalt and also deposition time of Mo-black. Use of an addition agent (Na-lauryl sulphate) in the plating solution of cobalt was found to influence the values of α_s, and ε_{th} of the coatings (Table 3.1.7). The emittance values obtained with use of the addition agent (Table 3.1.7) are significantly lower than those in Table 3.1.6, while the absorptance drops slightly to (0.90 - 0.91). The highest selectivity factor obtained for these coatings is 11.0 for 3 minutes dipping time in Mo-black plating solution. The spectral reflectance spectra in the range (0.3 - 2.5 μm) for Mo-black coatings on cobalt (NC) substrates plated with and without addition agent are shown in Fig.3.1.7. Throughout the solar region, no interference peak can be seen except a low broad hump in the 1.1. to 1.5 μm region. Fig.3.1.7 also shows that the coatings on cobalt (NC) without addition agent have lower reflectances than those prepared with an addition agent. The IR specular reflectance

spectra in the range 2.5 - 50 μm of the same two coatings are displayed in Fig.3.1.8.

The effect of dipping time and solution temperature on α_s, and ε_{th} has been studied for Mo-black coatings on cobalt substrates plated with addition agent (Table 3.1.8). The table shows that better values of α_s, and $\alpha_s/\varepsilon_{th}$ are obtained at a paramolybdate solution temperature of 60°C, rather than 80°C. The absorptance and emittance of the coatings (formed at 60°C) plotted as a function of dipping time are shown in Figure 3.1.9. The absorptance α_s varies only slightly with dipping time while the emittance varies significantly. The best values of α_s and ε_{th} are obtained for a deposition time of 5 minutes with selectivity factor $\alpha_s/\varepsilon_{th}$ = 9.1 (Table 3.1.8). If the deposition time is below 5 minutes, the coating is not sufficiently absorbing. When the deposition time is higher than 5 minutes, the absorptance α_s decreases slightly and the emittance ε_{th} increases significantly. The rise of emittance with the dipping time may be due to the increase of thickness.

Figs.3.1.10(a) and (b) show the IR specular reflectance spectra in the range 2.5 - 50 μm for Mo-black coatings prepared at 60°C and 80°C respectively. It can be seen from the figures that as the time of deposition increases, the IR reflectance decreases i.e., the emittance increases. The thickness of the coatings (which increases with the deposition time) is affecting the transmittance in the IR region resulting in an increase in emittance. The IR reflectance also decreases with the rise of solution temperature for the same time of deposition (Fig.3.1.11).

The two sets of total reflectance spectra in the range of 0.3 - 2.5 μm of Mo-black coatings on cobalt (NC) substrates prepared at 60°C and 80°C are shown in Figs.3.1.12 and 3.1.13 respectively. Interference peaks appear

in the region above 0.7 μm and these are more prominent for the coatings prepared at 80°C. The number and height of the maxima tend to increase with the increase of dipping time and temperature of the solution except for the thinnest coating (deposition time 3 minutes) prepared at 60°C. This behaviour accounts for the slight decrease of solar absorptance with the increase of dipping time above 5 minutes and also with the rise of solution temperature. The spectral reflectance of plated cobalt substrate (with addition agent) on nickel plated copper has also been studied and is given in Fig.3.1.14. The value of solar absorptance obtained from the cobalt substrate is 0.56.

Fig.3.1.15 shows another set of spectral reflectance spectra in the solar region for Mo-black dip coatings on plated cobalt (NC) prepared under different conditions. The results obtained from these coatings are tabulated in Table 3.1.9 with their preparation conditions. The spectral reflectance spectra show that these coatings behave as a grey surface in the solar region, i.e., the reflectance does not change significantly throughout the solar region and it is low resulting in high absorptance. These coatings have high IR reflectance (Fig.3.1.16) resulting in low emittance. The highest selectivity factor obtained from these coatings is 10.1 with solar absorptance of 0.91 (Table 3.1.9). Long deposition time of Mo-black does not affect the emittance of the coatings. These coatings were prepared at a relatively high pH value (3.2), which may reduce the deposition rate of Mo-black coatings (low deposition rate was also evident from the conversion colour of molybdate solution during preparation). These cobalt substrates were prepared at relatively low temperatures, with low current density for short times (Table 3.1.9).

3.1.3 Electrodeposited Mo-black coatings on aluminium substrates

The total reflectance spectra in the range 0.3 to 2.5 μm for four coatings on aluminium substrates of different thicknesses are shown in Fig.3.1.17. As the thickness of the coatings increases, the reflectance decreases (especially in the near infrared region) and the transition shifts towards longer wavelengths. As a result the absorptance α_s increases with coating thickness. No interference peaks have been observed in the reflectance spectra of the coatings (Fig.3.1.17). Fig.3.1.18 shows the variation of absorptance and emittance of the coating with coating mass per unit area. Both the absorptance and emittance of the coating increase with coating mass but the emittance is more thickness dependent than the absorptance. The absorptance appears to reach a limiting value in the range of 0.86 - 0.87, whereas, the emittance is still increasing with thickness but appears to be less dependent at higher thicknesses. Fig.3.1.19 shows specular reflectance spectra of the coatings and the aluminium substrate in the range 2.5 to 50 μm. Though the substrate has a relatively high reflectance, there is strong absorption in the coating material. Absorption bands for water around 2.9 - 3.1 μm and at about 6.2 μm (Nakamoto, 1970) are also present. The values of α_s, ε_{th} and $\alpha_s/\varepsilon_{th}$ are given in Table 3.1.10 with corresponding coating masses per unit area. This table shows that electrodeposited Mo-black coatings on aluminium substrates are not significantly selective ($\alpha_s/\varepsilon_{th} < 2$). The observed non-selectivity of the coatings may be due to the strong absorption in the infrared region resulting in high emittance.

3.1.4 Mo-black coatings on various additional substrates

Mo-black coatings prepared on vacuum evaporated aluminium (on rough glass), galvanized steel and cobalt plated aluminium have also been

studied. Results obtained from these coatings are given in Table 3.1.11.

A. Aluminized glass

Mo-black coatings were prepared by the electrodeposition method on aluminium coated glass. Before deposition of aluminium, the glass substrates were ground with silica carbide powder (without grinding, aluminium film diffused into the Mo-black coatings) and cleaned properly as described in section 2.5. The ground glass substrates were then coated with a conducting aluminium layer produced by vacuum evaporation in a Balzers BA510 coating unit under a pressure of about 10^{-4} Pa using aluminium wire on a tungsten spiral as a source. The spectral reflectance spectra of these coatings (Fig. 3.1.20) are quite similar to those obtained from coatings on aluminium sheet (Fig. 3.1.17). The highest absorptance obtained from these coatings is 0.88 (Table 3.1.11). Due to the roughness of the substrate and also the high thickness of the Mo-black coatings, the emittance is very high. Fig. 3.1.23 shows the specular IR reflectance of one coating which is rather low, resulting in high emittance. No further study, therefore has been done on these coatings.

B. Galvanized steel

On galvanized steel substrates, Mo-black coatings were prepared by a chemical dip method (similar to the case of zinc substrates). The spectral reflectance spectra of these coatings are shown in Fig.3.1.21. The reflectance decreases with the time of deposition giving higher absorptance. However, these coatings also have low specular reflectance in IR region (Fig.3.1.23). The values of solar absorptance obtained in these coatings are consistent with those obtained by Hosseini (1981) and Agnihotri et al (1983).

Table 3.1.1. Absorptance α_s and emittance ϵ_{th} of Mo-black dip coatings on mechanically polished zinc substrates for different concentrations of nickel sulphate.

Quantity of solute in 0.15 dm^3 of distilled water/g		Deposition Time	Solar Absorptance	Thermal Emittance	Selectivity Factor
Nickel Sulphate	Ammonium Molybdate	Seconds	α_s	ϵ_{th}	α_s/ϵ_{th}
0	3	40	0.65	0.06	10.8
		80	0.63	0.05	12.6
		240	0.67	0.06	11.1
1	3	40	0.69	0.07	9.8
		80	0.70	0.10	7.0
		180	0.75	0.19	3.9
3	3	40	0.66	0.10	6.6
		80	0.67	0.14	4.8
		180	0.72	0.30	2.4

Table 3.1.2 Absorptance α_s, emittance ε_{th} and selectivity factor $\alpha_s/\varepsilon_{th}$ for Mo-black dip coatings on zinc substrates; (a) etched zinc, (b) unetched zinc.

(a)

Coating Mass Per Unit Area mg/cm^2	α_s	ε_{th}	$\alpha_s/\varepsilon_{th}$
0.000	0.74	0.09	8.22
0.039	0.79	0.09	8.78
0.046	0.80	0.10	8.00
0.059	0.83	0.13	6.38
0.065	0.84	0.13	6.46
0.077	0.86	0.14	6.14
0.085	0.87	0.17	5.12
0.102	0.86	0.21	4.10
0.140	0.85	0.34	2.50
0.190	0.86	0.46	1.87
0.230	0.87	0.55	1.58
0.350	0.87	0.65	1.34

(b)

Coating Mass Per Unit Area mg/cm^2	α_s	ε_{th}	$\alpha_s/\varepsilon_{th}$
0.000	0.45	0.05	9.00
0.046	0.69	0.07	9.86
0.065	0.70	0.10	7.00
0.120	0.75	0.19	3.95
0.180	0.77	0.40	1.93
0.210	0.78	0.48	1.63

Table 3.1.3(a) Comparison between the results of two methods of the emittance measurement

Sample	Mo-black coatings on etched zince substrates		
	Emittances determined by using a thermopile	Emittances determined from IR reflectance spectra	% Difference
a	0.10	0.13	23
b	0.13	0.15	13
c	0.15	0.17	11
d	0.17	0.20	15
e	0.22	0.25	12
f	0.33	0.40	17

Table 3.1.3(b) Comparison of emittances of Mo-black coatings measured by calorimetric and radiometric methods.

Sample	Emittances determined from IR reflectance method	Emittances determined by calorimetric method	% difference
Copper substrate	0.091	0.115	4.5
Mo-black dip coating on cobalt (NC) substrate	0.175	0.161	8.0
Mo-black dip coating on mild steel substrate	0.480	0.423	11.9
Electrodeposited Mo-black on aluminium substrate	0.624	0.485	22.0

Table 3.1.4 Solar absorptance α_s, thermal emittance ε_{th} and selectivity factor $\alpha_s/\varepsilon_{th}$ for Mo-black dip coatings on zinc substrates for different substrate pretreatments.

Substrate Pretreatment	α_s	ε_{th}	$\alpha_s/\varepsilon_{th}$
Highly Polished	0.76	0.09	8.4
Etched with 20% HNO_3	0.84	0.12	7.0
Etched with 30% HNO_3	0.87	0.13	6.7
Etched with 50% HNO_3	0.89	0.30	2.9

Table 3.1.5 Absorptance α_s and emittance ε_{th} of Mo-black dip coatings on etched zinc (30%HNO_3) substrate prepared at different paramolybdate solution temperatures

Temperature of Solution ^oC	Deposition Time 60 Seconds		Deposition Time 120 Seconds	
	Solar Absorptance α_s	Thermal Emittance ε_{th}	Solar Absorptance α_s	Thermal Emittance ε_{th}
35	0.86	0.20	0.85	0.28
45	0.86	0.17	0.85	0.30
55	0.84	0.27	0.85	0.37

Table 3.1.6 Absorptance α_s, emittance ε_{th} and selectivity factor $\alpha_s/\varepsilon_{th}$ of Mo-black coatings on cobalt (NC) substrates for various plating conditions (without addition agent).

Cobalt Plating			Mo-black Plating		Thermal Radiative Properties		
Solution Temperature (^oC)	Current Density (mA/cm^2)	Plating Time (Minutes)	Solution Temperature (^oC)	Deposition Time (Minutes)	α_s	ε_{th}	$\alpha_s/\varepsilon_{th}$
60	36.8	5	60	5	0.90	0.22	4.09
56	32.1	5	60	5	0.91	0.25	3.64
60	35.0	5	60	10	0.92	0.30	3.06
56	30.6	5	60	15	0.90	0.29	3.60
56	31.7	5	80	5	0.90	0.25	3.60
56	25.0	10	60	10	0.94	0.28	3.36
56	25.0	8	60	10	0.94	0.33	2.85
60	34.1	12	60	10	0.92	0.37	2.49

Table 3.1.7 Absorptance α_s emittance, ε_{th} and selectivity ($\alpha_s/\varepsilon_{th}$) factor of Mo-black coatings on cobalt (NC) substrates for various plating conditions (with addition agent).

Cobalt Plating			Mo-black Plating		Thermal Radiative Properties		
Solution Temperature ^{o}C	Current Density mA/cm^2	Plating Time minutes	Solution Temperature ^{o}C	Deposition Time minutes	α_s	ε_{th}	$\alpha_s/\varepsilon_{th}$
58	35.7	4	60	3	0.88	0.08	11.0
58	40.0	5	60	5	0.91	0.10	9.1
60	49.0	5	60	10	0.90	0.13	6.9
60	44.0	5	60	15	0.89	0.17	5.24
60	47.8	5	75	8	0.89	0.13	6.85
58	42.6	5	80	5	0.89	0.13	6.85
58	42.6	5	80	10	0.87	0.21	4.14

Table 3.1.8 The values of α_s, ε_{th} and $\alpha_s/\varepsilon_{th}$ of Mo-black coatings on cobalt (NC) substrate at two different molybdate solution temperatures

Time of Deposition (Minutes)	Solution Temperature 60°C			Solution Temperature 80°C		
	α_s	ε_{th}	$\alpha_s/\varepsilon_{th}$	α_s	ε_{th}	$\alpha_s/\varepsilon_{th}$
5	0.91	0.10	9.1	0.89	0.13	6.8
10	0.90	0.13	6.9	0.87	0.21	4.1
15	0.88	0.18	4.9	0.88	0.26	3.4

Table 3.1.9 Absorptance α_s, emittance ε_{th} and selectivity factor $\alpha_s/\varepsilon_{th}$ of Mo-black coatings on cobalt (NC) substrates (without addition agent)

Cobalt Plating			Mo-black Plating		Thermal Radiative Properties		
Current Density mA/cm^2	Temperature of the Solution ^oC	Plating Time Minutes	Temperature of the Solution ^oC	Deposition Time Minutes	α_s	ε_{th}	$\alpha_s/\varepsilon_{th}$
25.1	45	4	60	5	0.91	0.09	10.1
24.9	45	4	60	8	0.89	0.10	8.9
25.2	45	4	60	12	0.88	0.09	9.7

Table 3.1.10. Absorptance, emittance and selectivity factors for electrodeposited Mo-black coatings on Al-substrates

Coating Mass per unit area (mg/cm^2)	Solar Absorptance α_s	Emittance, ε_{th} Determined by using a Thermopile	Selectivity factor $\alpha_s/\varepsilon_{th}$
0.70	0.78	0.40	1.95
1.18	0.81	0.53	1.53
1.64	0.83	-	-
2.17	0.86	0.60	1.43
2.50	0.87	0.62	1.34
3.84	0.87	0.72	1.20

Table 3.1.11 Results obtained from Mo-black coatings on various substrates.
a) Electrodeposited coatings, b) Dip Coatings

(a)

Substrate	Thickness μm	Solar Absorptance α_s	Thermal Emittance ε_{th}
Vacuum evaporated aluminium on ground glass	1.5 2.0 2.8 3.6	0.78 0.83 0.86 0.88	0.70 - - -

(b)

Substrate	Deposition Time Minutes	Solar Absorptance α_s	Thermal Emittance ε_{th}
Galvanized steel	2 5 10	0.82 0.86 0.88	0.40 - -
Cobalt plated aluminium	10	0.89	0.17

C. Cobalt plated aluminium

The results obtained from Mo-black coatings on cobalt plated aluminium are quite satisfactory (Table 3.1.11). A thin cobalt layer was plated on aluminium sheet using the procedure of section 2.1.2.4. Mo-black coatings was prepared by chemical dip method (section 2.1.2.5). The coating has low reflectance in the solar region (Fig.3.1.22) giving high absorptance (0.89). In the IR region, the reflectance increases with wavelength (Fig.3.1.23) resulting in a low emittance (0.17). The selectivity factor of this coating is 5.2.

3.2 Scanning Electron Microscopy (SEM) and Electron Probe Microanalysis (EPMA)

Scanning electron microscopy (SEM) and electron probe microanalysis (EPMA) techniques have been used to study the microstructure and elemental compositions of the coatings. In SEM, the secondary electron image (SEI) has been used for the microstructural examination, while in EPMA the SEI and characteristic X-ray images have been employed for spot analysis and X-ray line scan studies.

A metallographic technique has been employed for cross-sectional observations using SEM. Some optical microscopic studies of Mo-black coatings on zinc substrate have also been performed.

3.2.1 Electrodeposited Mo-black coatings on aluminium

The electrodeposited Mo-black coatings on an aluminium substrate generally have a microstructure of relatively flat irregular platelets, separated by prominent fissures. A similar surface texture has also been observed by

(Smith et al, 1981) and (Safi, 1985). Several coatings were observed in the SEM. The resultant micrographs showed that there are some differences in the surface topography of the coatings with different thicknesses. A typical SEM micrograph of a thick electroplated Mo-black coating (coating mass per unit area ~ 3.85 mg/cm^2) is shown in Fig.3.2.1. The surface consists of rather smooth and flat platelets with sharp clearly defined edges. The individual platelets are separated by wide cracks. Fig.3.2.2 shows a secondary electron micrograph of a thin electroplated coating (coating mass per unit area ~ 1.58mg/cm^2). It can be seen that the surface of the coating consists of quasi-hemispheres of different sizes with relatively narrow cracks. The width of the hemispheres varies from 3 to 20 μm. Safi (1985) also reported two types of surface topography as in Figs. 3.2.1 and 3.2.2.

These features required a more extensive study. Further work has therefore been carried out using four different coating thicknesses and at different current densities. The surface topography of Mo-black coatings of four different thicknesses are shown in Figs.3.2.3 - 3.2.6. By comparing these figures, the following features can be observed:

(i) As the thickness of the coating increases, the surface topography appears more smooth and flat.

(ii) The coating becomes more uniform as the thickness increases. It can be observed that a few hemispheres are still present in some areas of the coating of intermediate thickness (Fig.3.2.4.b), which may be due to non-uniformity of the coating thickness.

(iii) The width of the cracks, which arise from stresses in the growing film, increases with the coating thickness.

(iv) As the thickness of the coating increases, the size of the fragments increases.

No significant change in the surface topography of the coating has been observed with the plating current density. The secondary electron image of two coatings of almost equal thicknesses prepared with different current densities are shown in Figs.3.2.7 and 3.2.8. There is no noticeable difference between these two micrographs. The elemental analysis of the coatings has been performed by an energy dispersive X-ray analyser (EDX). The resultant EDX patterns of these two surfaces (Figs.3.2.7 and 3.2.8) are shown in Figs.3.2.9 and 3.1.10 respectively and the corresponding compositional data in terms of mass percentage are given in Table 3.2.1. The EDX spectrum shows that the coating consists mainly of molybdenum and a small proportion of nickel. The percentage of nickel decreases as the plating current density increases. Table 3.2.1 also shows a small amount of aluminium which may come from the aluminium substrate through the cracks.

The SEM micrograph of the underside : Mo-black coating (removed from an aluminium substrate) is shown in Fig.3.2.11 and the corresponding EDX spectrum is shown in Fig.3.2.12. The spectrum shows the presence of molybdenum and nickel. However, a small amount of aluminium (and iron) transferred from the substrate can also be seen in the EDX spectra.

3.2.2 Mo-black dip coatings on zinc

A typical surface microstructure of a Mo-black dip coating on mechanically polished zinc is shown in Fig.3.2.13. The surface consists of a large number of smooth irregularly shaped platelets separated by prominent fissures (i.e., similar to the electroplated coatings on aluminium). A

similar surface structure was also observed by Agnihotri et al (1983) and Hosseini (1981). Optical microscopy was used to study cracking and growth of Mo-black coatings on zinc substrates. Fig.3.2.14 - 3.2.24 show the surfaces of four Mo-black coatings of different deposition time from 6 to 60 seconds under different conditions. After deposition of Mo-black coatings for the required time, they were washed with distilled water and observed in the optical microscope in the wet condition. The resulting photographs are shown in Figs.3.2.14-17. It can be seen that the surface of the coatings is rather smooth and continuous. There are no visible cracks in the coating surface. Some slightly circular and irregularly shaped pits and voids can be seen on the surface of each coating. The size of these pits increases with increase of deposition time. Some polishing scratch marks can also be seen in the thinner coatings. The coatings were left to dry naturally and dried coatings were again observed in the microscope (Figs.3.2.18-21). There is no significant difference between the photographs relating to wet and dry conditions, except that the photographs for the latter condition are sharper. The surface of the thickest film (deposition time 60 seconds) is the roughest (Fig.3.2.21); but there are no cracks. However, when hot air was applied to the coatings, (approximate temperature 55 - 70^{o}C) the surface cracked into irregularly shaped flat platelets as shown in Figs.3.2.22-24. No cracks were observed in the thinnest coating (deposition time 6 seconds) after this treatment. In the cracked coatings, it can be seen that size of the individual fragments increases with increase of deposition time, i.e., with thickness. There is evidence that cracks are more likely to be nucleated from the pits on the surface (Fig.3.2.24). The above study indicates that the formation of the cracks in the coating surface may be due to the loss of some water from the coating or due to the thermal expansion mismatch between the coating material and the substrate. However, when coatings are very thin compared with the substrate, all the

mismatch may be taken up in the coating (Kramer, 1983).

The SEM study of Mo-black dip coatings on zinc substrate also shows that the surface of the thinner coating is continuous, e.g., there are no cracks in a coating of deposition time 5 seconds (Fig.3.2.25). However, some voids can be seen in the surface. Fig.3.2.26 shows the surface topography of a coating of deposition time 8 seconds. Very few cracks can be seen in this coating. The cracks are generally formed in rough areas or from the voids in the surface (Fig.3.2.26.b). Some cracks were seen to be formed when a particular area was focussed. This may be due to the heating due to bombardment of the high energy electron beam. Figs.3.2.27-29 show the surface topography of Mo-black coatings of three different deposition times. By comparing these figures it can be seen that the width of the cracks and size of the fragments increases with the increase of deposition time as observed in the optical microscopy studies. The underneath surface of a Mo-black coating has also been studied. The interface of the coating platelets appears as a smooth surface (Fig.3.2.30). Two flower-like structures can be seen in the micrograph of the interface. Some of these structures breakdown with the fragments. After peeling some fragments off the coating, it was again observed in the SEM. Some damaged areas can be seen in the zinc substrate (Fig.3.2.31). The elemental analysis of the coatings have been done by electron probe microanalysis (EPMA). A typical EDX spectrum of a Mo-black coating on zinc is shown in Fig.3.2.32. The zinc signal may come from the zinc substrate through the coatings and also through the cracks as the electron beam in EPMA can penetrate to a depth of 1 μm (Bulpett, 1984) and the thickness of the dip coating was below 1 μm. Coating composition (at %) is given in Table 3.2.2. This shows the decrease of the apparent at% of zinc with increase of deposition time. The EDX spectrum of the Mo-black coating underside (Fig.3.2.33) indicates the presence of a small amount of

zinc, presumably from the zinc substrate.

The maximum value of solar absorptance α_s obtained from smooth flat Mo-black dip coatings was 0.76 (Section 3.1.1). Surface pretreatment of zinc substrates was therefore investigated as a possible means of enhancing the solar absorptance of the coatings, i.e., use of a textured surface. Different concentrations of HNO_3 from 5% to 50% were used to etch the zinc substrates prior to coating deposition (Section 2.1.2.2) and the surface of the coatings was studied in the SEM. The resultant micrographs are shown in Figs.3.2.34-38. All of these coatings were prepared under the same conditions except for the surface pretreatment. From these micrographs it can be seen that the surface texture of the coating depends on the concentration of the etchant and etching time. For a zinc substrate etched with HNO_3 of concentration below 20%, some nodules can be seen but they are few in number (Fig.3.2.34) and also not spherical and prominent (Fig.3.2.35). Etching with 20-30% HNO_3 leads to a more uniform distribution of coatings nodules (Figs.3.2.36-39). The number of nodules increases with the etching time and concentration of HNO_3. More optimal values of solar absorptance and thermal emittance are obtained after etching the zinc substrates with 30% HNO_3 (Jahan & Smith, 1986). The surface of these coatings consist of a large number of rounded nodules with typical dimensions ranging from 0.5 to 2 μm. (Fig.3.2.39). Some very fine cracks can also be seen in the coating surface. After etching the zinc substrate with 50% HNO_3, the coating surface appeared to be rougher (Fig.3.2.40). Agglomeration of nodules or large ridges of the coating material can be seen in a particular direction. The microstructures of the zinc substrate after etching with HNO_3 have also been studied (Figs.3.2.41-42). By comparison of the topography of the zinc substrates with those of the coating, it seems that they are related, i.e., the coating is an outgrowth of the substrate itself. The coatings

may start to grow as a large number of nodular structures on the substrate surface. As the coating thickness increases, the nodules gradually disappear and finally flat platelets with wider cracks can be seen (Figs.3.2.43-44). This is probably due to the 'geometric leveling' of the rough topography of etched zinc (Lowenheim, 1978).

The composition of the coatings on etched zinc has also been studied by EDX technique. The EDX spectrum of three coatings of different thickness are shown in Fig.3.2.45-47 and the corresponding compositional data are given in Table 3.2.3. These spectra show the presence of molybdenum, nickel and zinc in the coatings. Table 3.2.3 shows that the percentage of zinc decreases with the coating mass per unit area which is consistent with the zinc signal from the substrate penetrating through the coating (as the coating thickness was below 1 μm). This table also shows that the percentage of nickel in the coatings increases with increase of nickel sulphate concentration in the plating solution. Figure 3.2.45 shows the presence of copper and titanium in the coating. These are not present in the EDX spectrum of Mo-black coating on unetched zinc (Fig.3.2.33). The copper and titanium signals are probably from the etched zinc substrate. This is shown by EPMA study of etched zinc (Fig.3.2.48). When the coating thickness increases, these signals disappear (Fig.3.2.46-47). However, the presence of these impurities (Cu, Ti) could not be detected in the EDX spectrum of an unetched zinc substrate (Fig.3.2.49).

The metallographic cross-section of a Mo-black dip coating on an etched zinc substrate was prepared and studied by SEM and EPMA. The SEM cross-sectional view (with Mo and Zn X-ray line scans of the coatings) is shown in Fig.3.2.50, while Fig.3.2.51 shows the cross-section at higher magnification. It can be seen that the zinc line starts to rise when the Mo-black signal decreases consistent with the limited presence of zinc in

the coatings near its interface with the substrate. These figures show the rough and porous structure of the coatings which are outgrowths of the substrate. The EDX spectrum obtained from the cross section of the coating of Fig.3.2.51 shows Mo and Zn signals (Fig.3.2.52).

3.2.3 Mo-black dip coatings on cobalt (NC) substrates

SEM studies of Mo-black dip coatings on electroplated cobalt substrate show a quite different type of surface morphology. Several coatings have been studied in SEM. The resultant micrographs show that the surface topography of the coatings depends upon the plating conditions of cobalt. These are current density, temperature of solution, deposition time and also the plating conditions of the Mo-black coatings.

The micromorphology of three different coatings is shown in Figs.3.2.53-55 with corresponding values of solar absorptance α_s and thermal emittance ε_{th}. Widespread cracking of the Mo-black coatings is observed in every sample. The surface of the coating of Fig.3.2.53 consists of large numbers of limb-like protruberances with a few nodules. They are uniformly distributed and oriented in different directions parallel to the substrate. For this coating, cobalt was plated at a temperature of $50^{o}C$ with $25mA/cm^2$ current density for 10 minutes. The deposition time for Mo-black was 10 minutes. The high proportion of surface voids and the surface roughness may be responsible for the high solar absorptance (0.94). The surface of the coating of Fig.3.2.54 consists of elongated oval type structures. Due to this coarse surface texture, the emittance of the coating increases to 0.35. The absorptance decreases to 0.92. The Mo-black was prepared under the same condition in both samples, but in the sample of Fig.3.2.54 cobalt was plated at a temperature of $60^{o}C$ with $34mA/cm^2$ current density for 12 minutes.

Fig.3.2.55 shows the surface topography of another Mo-black coating. The surface shows the same features as in Fig.3.2.54 but they are relatively less prominent. (This may be due to the thickness of Mo-black coating). The Mo-black coating was prepared at 80°C for 5 minutes. The comparatively smooth surface gives α_s = 0.90, when ε_{th} = 0.25. Cobalt for this coating was plated under the same condition as in Fig.3.2.54 for 5 minutes. The surface topography of this plated cobalt is shown in Fig.3.2.56. By comparison the textures of the cobalt and the Mo-black coating, it can be seen that the surface texture of Mo-black coating is dependent on the surface texture of cobalt.

The surface topography of the Mo-black coating changed significantly when an addition agent (Na-lauryl sulphate) was used in the plating solution of cobalt. A typical SEM micrograph of a Mo-black coating on electroplated cobalt, (with addition agent) is shown in Fig.3.2.57. It can be seen that the coating surface is rather smooth and has large numbers of nodules of 1-2 μm in size. Cracks are also observed in the coating. The deposition time of this Mo-black coating was 10 minutes at a temperature of 60°C. The cobalt was plated at a temperature of 60°C with 49 mA/cm^2 current density for 5 minutes, from a solution containing addition agent. The surface structure of the cobalt is shown in Fig.3.2.58. The surface of the coating becomes smoother as the deposition time of Mo-black coating increases (Fig.3.2.59). For this sample Mo-black was plated for 15 minutes. Fig.3.2.60 shows the SEM micrograph of another coating prepared at 80°C for 10 minutes. The surface is quite smooth and flat. No surface features were observed. This is probably due to the thickness of the coating. A similar surface texture has also been observed by Smith et al (1984) for coatings prepared at a temperature of 80°C. The values of absorptance α_s and emittance ε_{th} obtained from this surface are 0.87 and 0.20 respectively.

Fig.3.2.61 shows the surface morphology of a cobalt surface plated with a low current density of about 27mA/cm^2 at a temperature of 45^{o}C for 4 minutes. The surface shows large numbers of flakelike protruberences, rather small in size. They are generally oriented with their broad face nearly vertical. The surface texture of Mo-black coatings on this type of cobalt surface (Fig.3.2.61) is shown in Fig.3.2.62. The surface consists of submicron sized nodules. The values of solar absorptance α_s and the thermal emittance ε_{th} obtained from this coating are 0.91 and 0.09 respectively.

Energy dispersive X-ray analysis (EDX) has been carried out using the SEM instrument for selected coatings. Figs.3.2.63-65 show EDX spectra of some coatings and the corresponding compositions are given in Table 3.2.4. The EDX spectra indicate the presence of Mo and Co in the coatings. A very small shoulder for Ni is also observed. Table 3.2.4 shows that the percentage of cobalt decreases with the increase of deposition time of Mo-black coating whereas percentage of Mo increases. It may be possible that the coating contains a significant amount of metallic cobalt or the cobalt signal may come from the plated cobalt substrate through the coating materials and cracks.

A metallographic cross-section of a Mo-black coating on cobalt (NC) substrate was prepared and studied by SEM and EPMA. The SEM micrograph of the metallographic section of the coating of Fig.3.2.54 is shown in Fig.3.2.66, where the individual layersof Mo, Co, and Ni on copper substrate can be identified. The figure also shows the rough surface structure of plated cobalt. Fig.3.2.67 shows the X-ray line scans for Mo, Co and Ni superimposed on the metallographic cross-section. This figure clearly shows the presence of Mo at the top surface layer. The X-ray line scan for Co rises somewhat earlier than expected, perhaps because the

Table 3.2.1 Apparent composition of electrodeposited Mo-black coatings (on aluminium) determined by electron probe microanalysis.

Plating Current Density mA/cm^2	Mass %		
	Mo	Ni	Al
3.15	90.2	6.6	3.1
1.50	86.7	10.2	3.2

Table 3.2.2 Apparent composition of Mo-black dip coatings on unetched zinc substrates determined by electron probe microanalysis

Deposition Time / Seconds	Atomic %		
	Mo	Ni	Zn
60	58.3	1.4	40.2
80	62.1	1.3	36.5
120	70.3	1.8	27.3

Table 3.2.3 Apparent composition of Mo-black dip coatings on etched zinc substrates determined by electron probe microanalysis.

Mass % of $NiSO_4$ in the plating solution	Coating Mass per unit area g/cm^2	Mass %		
		Mo	Ni	Zn
50	2.01×10^{-4}	59.3	6.1	34.6
25	4.50×10^{-5}	46.6	1.4	52.0
14	2.90×10^{-4}	83.9	1.1	15.0

Table 3.2.4 Apparent composition of Mo-black dip coatings on cobalt (NC) substrate determined by electron probe microanalysis.

Deposition Time of Mo-black (Minute)	Mass%	
	Molybdenum	Cobalt
5	31.9	68.1
10	35.1	64.9
15	42.1	57.9

surface of the cobalt layer is highly textured. Fig.3.2.68 shows the EDX spectrum obtained from the cross-section of the coating indicating the presence of Mo and Co in the coating.

3.3 Electron diffraction

3.3.1 Reflection Electron Diffraction (RED)

Evidence for the presence of orthorhombic Mo_4O_{11} in some of the coatings was provided by RED. Fig.3.3.1 shows a typical electron diffraction pattern of a Mo-black coating on an etched zinc substrate. In Table 3.3.1 the corresponding interplanar spacing (d-values) calculated using equation (2.3) (Section 2.3.4) are compared with the d-values listed in the A.S.T.M index for MoO_3 MoO_2 and Mo_4O_{11}. It can be seen that the best match (for the most intense lines) is shown by orthorhombic Mo_4O_{11}. The 1.505Å ring corresponds roughly to ZnO (ASTM data 1.48Å), probably from the etched zinc substrate. However, some Mo_4O_{11} reflection lines are missing possibly due to buckling of the coating. The RED pattern of one dip coating (previously heating in air at 400°C for 4 hours) shows a spot pattern (Fig.3.3.2), i.e., single crystal pattern.

An RED pattern from a Mo-black coating on a cobalt (NC) substrate is shown in Fig.3.3.3. The corresponding data (Table 3.3.2) includes lines for both CoO and metallic Co. Diffraction ringsfor Mo-black coating could not be found.

3.3.2 Transmission Electron Diffraction (TED)

TED provided further evidence for the presence of Mo_4O_{11} in Mo-black coatings. As it is difficult to detach Mo-black dip coatings from the

etched zinc and cobalt (NC) substrates, only the electrodeposited coating has been studied in TED. Both electron micrographs and corresponding diffraction patterns have been obtained at different temperatures, ranging from -160°C to 320°C. Fig.3.3.4 shows an electron diffraction pattern of a Mo-black coating prepared on aluminium. The specimen was prepared by etching away the aluminium substrate with NaOH (Section 2.3.4). The micrograph shows block like isolated features possibly artifacts due to etching process while the diffraction pattern is a densely populated spot pattern. A transmission electron diffraction pattern of an electrodeposited coating on a copper substrate shows spotty rings (Fig.3.3.5) (the coating is less adherent to copper so it can easily be stripped off from the copper substrate). The calculated d-values are given in Table 3.3.3. These correspond to orthorhombic Mo_4O_{11}. The electron micrograph of the coating (Fig.3.3.5.a) shows rounded and some irregular shaped microcrystals in a net like arrangement of voids. After holding the sample at -160°C for 2 hours, most of these crystals appeared to be needle-like as shown in Fig.3.3.6 with its selected area diffraction (S.A.D.) pattern. The calculated d-values are similar to those for Mo_4O_{11} (Table 3.3.3). The reason for changing the shape of the microcrystals is not clearly understood. The effect may be due to sharper imaging of existing crystals at lower temperature. Needle-shaped microcrystals of orthorhombic Mo_4O_{11} were also found by Lavina et al (1980). Fig.3.3.7 shows a rather similar room temperature image (obtained after warming the specimen from -160°C) to that obtained before cooling (Fig.3.3.5).

Another sample stripped from the same copper substrate was studied in a hot stage from room temperature to 320°C. Figs.3.3.8 - 10 show the micrographs and corresponding S.A.D. patterns of the sample at a temperatures of 23, 200 and 320°C. The sample was kept at each temperature for 65 minutes and then the micrographs were taken. The

Table 3.3.1 Interplanar spacing (d) of Mo-black dip coating on etched zinc substrate determined by RED.

Mo-black dip coating on etched zinc			Data from A.S.T.M. index for								
			Mo_4O_{11}			MoO_3			MoO_2		
Pattern Intensity	D/cm	d/Å	d/Å	I/I_mX100	hkl	d/Å	I/I_mX100	hkl	d/Å	I/I_mX100	hkl
S	0.60	4.07	4.00	100	211	9.12	80	100	-	-	-
-	-	-	3.75	95	311	3.45	100	210	3.42	100	011 111
-	-	-	3.48	85	411	3.04	40	300	-	-	-
M	0.94	2.59	2.59	30	602	2.53	30	310	2.43	69	211
W	1.08	2.25	2.23	40	521 103	2.15	5	224	2.18	6	210
M	1.50	1.68	1.71	40	331 221	1.72	20	420	1.71	41	312
M	1.60	1.52	1.58	45	232	1.59	10	334	1.52	9	013
W	1.90	1.28	1.33	25	16.2.0	1.30	2	700	1.29	5	413

Table 3.3.2 Reflection electron diffraction results of Mo-black coating on cobalt (NC) substrate.

Mo-black dip coating on Cobalt (NC) substrate			Data from A.S.T.M. index for					
			CoO			Co		
Pattern Intensity	D/cm Measured	d/Å Calculated	d/Å	$I/I_m X100$	hkl	d/Å	$I/I_m X100$	hkl
-	-	-	2.46	75	111	-	-	-
S	1.15	2.12	2.13	100	200	2.16	20	100
-	-	-	-	-	-	2.02	60	002
M	1.30	1.88	1.50	50	220	1.91	100	101
M	1.90	1.28	1.28	20	311	1.25	80	110
-	-	-	1.22	15	222	1.14	80	103
M	2.25	0.98	0.98	13	331	1.06	80	112
-	-	-	-	-	-	1.04	60	201
W	2.2	0.74	0.96	30	420	1.01	20	004

Table 3.3.3 Interplanar spacing (d) of electrodeposited Mo-black coating at different conditions determined by TED.

d-spacing values for Mo-black coating/Å					Data for Mo_4O_{11} From A.S.T.M. index		
Pattern	Sample 1 (at room temperature)		Sample 2				
Intensity	Before Annealing	After Annealing	At room temperature	at -160°C	d/Å	I/ImX100	hkl
-	-	-	-	-	12.3	30	200
W	-	4.55	-	-	4.53	25	401
S	4.00	4.00	-	4.00	4.00	100	211
-	-	-	-	-	3.95	65	501
M	-	-	3.76	3.76	3.75	95	311
-	-	-	-	-	3.48	85	411, 601
W	-	3.33	-	-	3.33	10	102
S	2.85	2.86	-	-	2.79	50	212
-	-	-	-	-	2.72	60	020
W	-	-	2.67	2.67	2.66	70	810, 220
W	2.53	2.53	-	-	2.59	30	602
M	-	-	2.46	2.46	2.47	10	221, 512
S	2.0	2.0(M)	-	2.10	1.98	30	10.0.2
-	-	-	-	-	1.94	45	522
W	-	1.90	1.88	-	1.88	40	622
W	1.77	-	-	-	1.78	35	713
W	-	1.72	-	1.68	1.72	40	123
W	1.63	-	-	-	1.65	70	913
VW	-	-	1.60	-	1.61	30	232
VW	1.40	1.40	-	-	1.40	15	424

micrograph at room temperature shows very small precipitates with random network of voids. As the temperature increases, the voids grow in size as shown in Fig.3.3.9 and 10 and the grain size also increases. The increase of grain size is also revealed by the spotty diffraction rings (Cullity, 1967). The calculated d-values closely matched with those in the A.S.T.M. index for Mo_4O_{11} (Table 3.3.3). Fig.3.3.11 shows the electron micrograph and S.A.D. pattern of the sample at room temperature after annealing. Comparison of the micrograph of Fig.3.3.11 with Fig.3.3.8 provides additional evidence for grain growth during annealing if the darker regions are taken to be crystalline.

3.4 X-ray diffraction

Several specimens prepared on different substrates have been examined by X-ray diffraction using Co K_α radiation (λ = 0.179 nm). Without any exception, a very broad diffraction peak has been observed with maximum intensity between 4 and $5^\circ\theta$. No other peaks except those corresponding to the substrate were observed up to $50^\circ\theta$. Fig.3.4.1 shows the X-ray diffraction pattern of a Mo-black coating on an aluminium substrate, with a broad peak at about $\theta = 4.7^\circ$. The corresponding lattice spacing is 10.9Å. Fig.3.4.2 shows the X-ray diffraction pattern of the aluminium substrate for the same region as in Fig.3.4.1. No peak can be seen between 4 and 5°_θ. This indicates that the low angle peak is due to coating. In case of dip-coatings on zinc and cobalt (NC) substrate, the low angle peaks are very broad as shown in Figs.3.4.3 and 4. The maximum intensity is at about 4.4° and $5.0^\circ\theta$ for coatings on zinc and cobalt (NC) respectively. The corresponding lattice spacings are 11.7 and 10.3 Å respectively. These lattice spacing values are in only fair agreement with the value (12.3 Å) for the 200 plane in orthorhombic Mo_4O_{11} (Table 3.4.2). The absence of other diffraction peaks may be due to the preferred orientation

Table 3.4.1 X-ray diffraction peak positions (θ^{o}) and interplanar spacings (d) for a Mo-black dip coating on etched zinc substrate (estimated thickness ~0.6 μm).

Intensity	Mo-black coating		Data for Zn from A.S.T.M Index		
	θ^{o}	d/(Å)	d/(Å)	$I/I_m X100$	hkl
S	21.29	2.465	2.473	53	002
W	22.85	2.305	2.308	40	100
S	25.36	2.089	2.091	100	101
W	32.06	1.686	1.687	28	102
M	41.89	1.340	1.342	25	103
W	42.00	1.337	1.332	21	110
W	46.45	1.235	1.237	2	004
W	49.70	1.173	1.172	23	112

Table 3.4.2 X-ray diffraction peak positions (θ^{o}) and interplanar spacings (d) for an electrodeposited Mo-black coating as an aluminium substrate after heating in air for 8 hours at 400°C.

Mo-black Coating			Data from A.S.T.M. Index for MoO_3			Data from A.S.T.M. Index for Mo_4O_{11}		
Pattern Intensity	θ^{o}	d/(Å)	hkl	d/(Å)	$I/I_m X100$	hkl	d/(Å)	$I/I_m X100$
S	4.7	10.92	100	9.12	80	200	12.3	100
W	7.45	6.91	020	6.93	34	301	5.19	10
M	13.63	3.80	-	-	-	311	3.75	95
M	14.98	3.47	210	3.45	100	411	3.48	85
M	15.95	3.25	-	-	-	610	3.26	20
W	19.73	2.61	220	2.63	10	602	2.59	30
W	23.6	2.23	-	-	-	103	2.22	30
W	29.05	1.84	008	1.86	15	11.02	1.85	35

of the crystalline material. For coatings on etched zinc substrate, this low angle peak could not be identified. Fig.3.4.5 shows the X-ray diffraction pattern of a coating on an etched zinc substrate and the calculated d-spacing values are tabulated in Table 3.4.1. The table shows that the d-spacing values of the peaks in Fig.3.4.5 closely match with those of zinc metal listed in the A.S.T.M. index.

Fig.3.4.6 shows the X-ray diffraction pattern obtained from a coating on cobalt (NC) substrate. Only three peaks of Co appeared in the diffraction pattern, possibly due to the texture of the cobalt coating. Peaks for Ni and Cu are also present. Fig.3.4.7 shows the X-ray diffraction pattern of a Mo-black coating on an aluminium substrate after heat treatment at 400°C for 8 hours in air. The calculated d-spacing values are tabulated in Table 3.4.2. These indicate that a mixture of MoO_3 and Mo_4O_{11} is present. No change has been observed in the diffraction pattern of the coatings on zinc and cobalt (NC) substrates after heat treatment under the same conditions.

3.5 X-ray Photoelectron Spectroscopy (XPS)

XPS measurements on Mo-black coatings on different substrates have been carried out in order to analyse the chemical elemental compositions of the coatings and the oxidation state of molybdenum in the deposited coatings. The XPS spectra obtained from the coatings have been compared with some standard samples i.e., molybdenum metal foil, molybdenum dioxide (MoO_2) and molybdenum trioxide (MoO_3) powders. The depth profile composition of the coatings has been determined by using argon ions (Ar^+) bombardment and measuring the main photoelectron peak areas of the individual constituent elements and then dividing by their corresponding sensitivity factors (see Appendix D). The coatings have also been studied in XPS after various

heat treatments. The relative positions of peaks due to Mo $3d_{3/2}$ electrons for Mo-metal, MoO_2 and MoO_3 and Mo-black coatings under different conditions are schematically shown in Fig.3.5.0.

3.5.1 Standard materials

In the XPS spectrum of Mo, the doublet due to Mo($3d_{3/2}$-$3d_{5/2}$) electrons gives the most intense peaks and their binding energy is dependent mainly upon the oxidation state (Cimino and Angelis, 1975). It is therefore possible to analyse the oxidation state of Mo in the samples by following the displacement of the 3d doublet. As shown in Fig.3.5.0, the binding energy of Mo 3d electrons increases with the increase of oxidation state. The binding energy data of the Mo 3d doublet and the Mo $3p_{3/2}$ singlet in different oxidation states are given in Table 3.5.1. with their standard deviation of error. The binding energy of O 1s and full width at half maximum (FWHM) of the Mo 3d doublet are also reported in Table 3.5.1.

A. <u>MoO_3 powder and Mo-metal</u>

MoO_3 powder used in the present investigation was supplied by BDH Chemicals Ltd (purity 99.5%). A representative spectrum for the Mo($3d_{3/2}$ - $3d_{5/2}$) doublet in MoO_3 is shown in Fig.3.5.1. The separation between the two peaks of the doublet is 3.1 eV, and they are almost completely resolved. The average binding energies for Mo $3d_{3/2}$, $3d_{5/2}$ and $3p_{3/2}$ peaks are 236.1 eV, 233.0 eV and 398.1 eV respectively. These values are in close agreement with the published data (Patterson et al, 1976, Apetkar et al, 1974). Fig.3.5.2 shows the Mo ($3d_{3/2}$ - $3d_{5/2}$) peaks of Mo-metal including the C 1s peak. The binding energy of the Mo ($3d_{5/2}$) peak in Mo-metal is at about 227 eV which is 6 eV lower than that of Mo ($3d_{5/2}$) peak in MoO_3 (Table 3.5.1). The metal foil was cleaned by emery paper just before recording the spectrum, to remove oxide from the

surface.

B. $\underline{MoO_2 \text{ powder}}$

Commercially available MoO_2 powder (supplied by Alfa-Ventron, purity 99%) has also been studied. A representative spectrum of the Mo 3d doublet of MoO_2 is shown in Fig.3.5.3. It appears that surface oxidation to MoO_3 has occurred. As can be seen in Fig.3.5.3, the spectrum contains three distinct Mo 3d peaks. The lower binding energy peak at about 229.3 eV is assigned to the Mo($3d_{5/2}$) peak of MoO_2. The higher binding energy peak at about 236.0 eV is assigned to the Mo($3d_{3/2}$) electrons of MoO_3. The central peak is a combination of the Mo($3d_{3/2}$) peak of MoO_2 (232.4 eV) and the Mo($3d_{5/2}$) peak of MoO_3 (233.0 eV). This peak is somewhat broader than the Mo ($3d_{5/2}$) peak of MoO_3. The binding energy of Mo $3d_{3/2}$ peak in MoO_2 has been determined by adding 3.1 eV to that of the Mo ($3d_{5/2}$) peak, as in general, the separation between the two peaks of the Mo 3d doublet is 3.1 $\pm$ 0.1 eV. The same method has also been used by Kim et al (1974) and Swartz and Hercules (1971). However, on etching with Ar^+ ions, the 3d doublet for MoO_3 gradually disappears (Fig.3.5.4). There is a marked decrease in the intensity of the low kinetic energy peak due to Mo ($3d_{3/2}$) electrons in MoO_3 and the central peak due to the combination of Mo($3d_{3/2}$) peak of MoO_2 and Mo($3d_{5/2}$) peak of MoO_3. The intensity of the Mo($3d_{5/2}$) peak of MoO_2 has also increased after Ar^+ bombardment. According to Kim et al (1974), on Ar^+ bombardment, most of the MoO_3 is sputtered off or reduced to MoO_x and MoO_2 where $2 < x < 3$. Fig.3.5.4 also shows that after 30 minutes etching, the shoulder for Mo ($3d_{3/2}$) due to MoO_3 disappears but the Mo($3d_{5/2}$) peak for MoO_2 does not reduce i.e., it has the same binding energy as before exposure to Ar^+ bombardment. Kim et al (1974) also reported that it is not possible to reduce the MoO_2 further to metallic Mo. However, the ratio of the intensity of Mo ($3d_{5/2}$) and Mo ($3d_{3/2}$) peaks and the flatness of the 3d doublet indicates that it is a mixture of

two oxides. Bombardment of MoO_3 with Ar^+ also produces a mixture of two oxides: MoO_2 and MoO_x where $2 < x < 3$ as shown in Fig.3.5.5. The effect of Ar^+ bombardment on the binding energy of Mo ($3d_{5/2}$) of MoO_2 and MoO_3 is shown in Table 3.5.5.

3.5.2 Electrodeposited Mo-black coatings on aluminium

The binding energies of Mo 3d electrons of electrodeposited Mo-black coating are found to be higher than those for MoO_2 and lower than MoO_3 (Fig.3.5.0). The position of Mo 3d doublet shifts after various heat treatments and Ar^+ ion etching.

A. As-prepared coatings

A typical survey scan XPS spectrum of a Mo-black coating on an aluminium substrate is given in Fig.3.5.6. It shows that the coating consists mainly of molybdenum oxide and a very small amount of nickel, (the nickel peak is barely above the noise level). The appearance of the C 1s peak in the XPS spectra originates from the spectrometer rotary pump oil that inevitably contaminates the samples at the working pressure (1.3×10^{-5} Pa). It may also come from mishandling of the specimen before location in the spectrometer. In the present investigation the C 1s peak has been used as a reference peak for the determination of binding energies. The binding energy of C 1s peak was found to be 284.9 eV, by calibration of the spectrometer according to Anthony and Seah (1984). Other values for the C 1s level have been reported in the literature (Cimino and Angelis, 1975). A different choice would change the absolute values of electrons binding energies but not the relative values. The O 1s peak is almost symmetrical, as shown in Fig.3.5.7(a), with a binding energy of about 529.9 eV. This peak, therefore, corresponds to the oxygen of a molybdenum oxide. It is suggested by Robert et al (1972) that the O 1s peak at about

530 eV is assigned to the oxide O^{2-} while peaks at higher binding energies (> 531 eV) should be assigned to surface hydroxide ions (OH^-) or strongly chemisorbed oxygen (O^-). A typical narrow scan spectrum of the Mo 3d doublet for a Mo-black coating is shown in Fig.3.5.7(b). The results obtained from electrodeposited Mo-black coating on aluminium are given in Table 3.5.2 with calculated standard deviations. The average binding energies for the Mo $3p_{3/2}$, $3d_{3/2}$ and $3d_{5/2}$ peaks are 395.6 eV, 234.5 eV and 231.3 eV respectively. The binding energies of the Mo ($3d_{3/2}$ - $3d_{5/2}$) peaks for the Mo-black coating are (1.6 - 1.7) eV lower than those for MoO_3 (Fig.3.5.8) and (2.1 - 2.0) eV higher than the corresponding MoO_2 peaks. The shift in binding energy of the $3d_{5/2}$ peak from that of Mo-metal is 4.3 eV where as for MoO_2 and MoO_3, the shifts in binding energies are 2.3 eV and 6 eV respectively (Table 3.5.1). By considering the above results it can be argued that the oxidation state of Mo in the coating is between +4 and +6. However, Swartz and Herculus (1971) reported that the binding energies of the Mo($3d_{3/2}$ - $3d_{5/2}$) peaks for oxidation state +5 are 234.5 and 231.0 eV respectively, which agree closely with the values given above for Mo-black coatings.

B. Heat treated coatings

When the Mo-black coatings are heated in air, the 3d doublet shifts towards the higher binding energy (Fig.3.5.0). Fig.3.5.9 shows the shift of the 3d doublet of Mo after heating the coating in air at a temperature of 400°C for 2 hours. The Mo($3d_{3/2}$ - $3d_{5/2}$) peaks are well resolved like those of MoO_3 (Fig.3.2.5). The average binding energies of the Mo $3p_{3/2}$, Mo $3d_{3/2}$ and Mo $3d_{5/2}$ lines are shifted to 397.8 eV, 235.9 eV and 232.5 eV respectively (Table 3.5.2). These values are very close to those for MoO_3. There is a very small shift in binding energy (0.1 - 0.3 eV) of the 3d doublet towards the lower binding energy after heating the coating inside the spectrometer chamber at 450°C for 2 hours. The intensity of Mo

($3d_{3/2}$) peak has increased compared to that of Mo($3d_{5/2}$) peak after heat treatment in vacuum (Fig.3.5.10). The 3d doublet is less resolved (Table 3.5.2) and there is an obvious broadening of the peaks. These features suggest the presence of a mixture of two oxides (Miller et al, 1971).

C. Effect of Ar+ ions etching

The effect of Ar^+ bombardment on a Mo-black coating is shown in Fig.3.5.11. The Mo 3d doublet shifts towards the higher kinetic energy region after ion bombardment. The binding energy of Mo($3d_{5/2}$) peak is 229.8 eV (Table 3.5.5) which is only 0.5 eV higher than that of MoO_2. However, the peak shape indicates that it may consist of two oxides: MoO_2 and MoO_x where $2 < x < 3$, as previously discussed for MoO_2 (Section 3.5.1). This shift in binding energy of the 3d doublet after ion bombardment may be due to artefacts produced by the Ar^+ ion. (This is an unavoidable disadvantage of Ar^+ ion etching according to Briggs (1978). Fig.3.5.11 also shows the decrease of the intensity of C 1s peak after etching, which indicates that the carbon originates from surface contamination. The Mo-black to metal interface has also been studied in ESCA (Fig.3.5.12). The calculated binding energy of the Mo 3d doublet is 0.6 eV higher than that of the coating surface (Table 3.5.2). The effect of Ar^+ ion etching on the Mo-black interface is the same as observed for the Mo-black surface. The values of binding energy of Mo-black interface before and after etching are given in Table 3.5.5.

3.5.3 Mo-black dip coatings on zinc

The XPS results obtained for Mo-black coatings on zinc substrates are similar to those obtained for electrodeposited coatings on aluminium substrates, except the results for vacuum heat treated coatings. The Mo 3d doublet in vacuum heat treated coatings is found to be shifted to lower

oxidation state (Fig.3.5.0).

A. As-prepared coatings

A typical survey scan spectrum of a Mo-black dip coating on a zinc substrate is shown in Fig.3.5.13. Like electrodeposited coatings on aluminium substrates, dip coatings also consist of oxides of molybdenum and a small amount of nickel. Fig.3.5.13 shows that the nickel 2p peak is barely above the noise level. The survey scan spectrum also shows an O ls, a C ls peak and photoelectron and Auger peaks for zinc. The survey scan spectra obtained at two different take-off angles (70^{o} and 20^{o} measured relative to the surface) are shown in Figs.3.5.13(a) and (b) respectively. These indicate that the ratio of C ls peak to Mo 3d peak height increased (from 0.88 to 1.22) when the take off angle decreased. This is consistent with the presence of carbon being associated with the surface contamination of the specimen. The O ls peak is almost symmetrical (Fig.3.5.14) indicating the presence of one kind of oxygen species. This peak can be assigned to oxide oxygen as the binding energy is about 529.9 eV (Robert et al, 1972). Fig.3.5.15 shows the narrow scan spectrum of the Ni 2p peak. The presence of strong broad satellite bands consistently at about 5.5 and 6.8 eV above the main peak of Ni $2p_{3/2}$ may indicate the presence of $Ni(OH)_2$ in the coatings (McIntyre and Ceok, 1975). The binding energy of $Ni2p_{3/2}$ is estimated to be 855.0 eV. After etching with Ar^{+} ions for 30 minutes, the satellites disappear, but the binding energy of Ni $2p_{3/2}$ peak does not shift significantly. This result also suggests the presence of $Ni(OH)_2$ in the coatings (Kim and Winograd, 1974). Narrow scan spectra of the Mo 3d doublet of Mo-black dip coatings on etched and unetched zinc substrates are shown in Fig.3.5.16. The calculated binding energies of Mo $3p_{3/2}$, Mo $3d_{3/2}$ and Mo $3d_{5/2}$ electrons are given in Table 3.5.3. The binding energy values of the Mo ($3d_{3/2}$ - $3d_{5/2}$) peaks for Mo-black dip coatings suggest that the oxidation state of

Mo is +5 (Swartz and Hercules 1971). A similar results were obtained for the electrodeposited coatings (3.5.2).

B. Heat treated coatings

Mo-black dip coatings on zinc substrates have been studied in ESCA after different heat treatments. The effectsof heat treatment on the XPS results obtained for the Mo-black dip coatings are summarised in Table 3.5.3. No significant change in the binding energy of O 1s has been observed after heat treatment. There is a comparatively large shift (1.9 - 2.2 eV) in the binding energies of the Mo($3d_{3/2}$ - $3d_{5/2}$) peaks of the dip coatings after heat treatment in vacuum in contrast with the results for the electrodeposited coatings. No significant change in the binding energy of the 3d doublet was observed after heating at 100°C (Table 3.5.3). As the temperature increases to 200°C and 300°C, the Mo 3d doublet shifts towards the higher kinetic energy region. Fig.3.5.17 shows the Mo 3d spectrum of a Mo-black coating on unetched zinc before and after heating inside the spectrometer chamber at 300°C for 90 minutes. The binding energies of Mo ($3d_{3/2}$ - $3d_{5/2}$) electrons are 232.2 and 229.2 eV respectively after heat treatment (as for MoO_2). Fig.3.5.17 also shows that the intensity of the Mo ($3d_{3/2}$) increases comparedto Mo($3d_{5/2}$) peak after heat treatment. The shape of the Mo 3d doublet indicates that it may consist of two oxides: MoO_2 and MoO_x where $2 < x < 3$. The same result was obtained after heating the Mo-black coating on etched zinc at 300°C for 3 hours (Fig.3.5.18). The binding energy values of the $3p_{3/2}$ and 3d doublet indicate +4 oxidation state for Mo after heat treatment in vacuum.

After the coating was heated in air, the binding energies of the Mo($3p_{3/2}$) and 3d doublet increased (Table 3.5.3) suggesting that the coating oxidized to a higher oxidation state. Fig.3.5.19 shows a survey scan spectrum of a Mo-black dip coating after heating in air at 390°C for 2

hours. The Mo 3d spectrum of a Mo-black coating on etched zinc, before and after heat treatment in air at 200^{o}C for 2 hours is shown in Fig.3.5.20 whereas Fig.3.5.21 shows the results after the same treatment for a coating on an unetched zinc substrate. Under the same heat treatment conditions, the binding energies of the Mo ($3d_{3/2}$- $3d_{3/2}$) peaks of coatings on unetched zinc increase more than those for coatings on etched zinc (Table 3.5.3). This indicates that the coatings on etched zinc may be more stable at higher temperatures than the coatings on unetched zinc. Fig.3.5.22 shows the Mo 3d spectrum of a coating after heating at a temperature of 390^{o}C for 2 hours. The figure shows a well resolved 3d doublet similar to that of MoO_3. The calculated binding energies of Mo ($3d_{3/2}$ - $3d_{5/2}$) electron are (235.6 - 232.6) eV which is only 0.4 eV lower than that of MoO_3.

C. Depth profile of the coating using Ar+ ions etching

In the XPS study Ar^+ ions bombardment has been used in an attempt to study any depth variation in coating compositions. The etching rate was roughly 1A^{o}/minute with 5 KeV, Ar^+ ion and a beam current of 5mA. Alternating cycles of Ar^+ ion etching and XPS scans were used to obtain the depth profile data. The atomic percentage of the chemical elements of the coating was calculated by measuring the individual main peak areas and dividing with their corresponding sensitivity factors (Appendix D). It was observed that the intensity of the C 1s peak decreased as the time of etching increased. Fig.3.5.23 shows a survey scan spectrum of Mo-black dip coating after 200 minutes etching. It can be seen that the C 1s peak had completely disappeared, giving further confirmation that the C 1s peak originated from surface contamination. The shift in binding energies of the Mo.$3d_{5/2}$ peak are given in Table 3.5.5, with corresponding etching time. Fig.3.5.24 shows the Mo 3d spectra before etching and at two different etching times. It can be seen that after 10 minutes etching, the binding

energy of Mo $3d_{5/2}$ peak shifts from 231.4 to 229.9eV. The peak shape also changed after etching. The intensity of Mo $3d_{3/2}$ peak increased compared to that of the Mo $3d_{5/2}$ peak and also the 3d doublet became broader. This indicates a mixture of two oxides (Fig.3.5.24). All these above effects may be due to the artefacts produced by Ar^+ ion etching (Briggs, 1978). After 10 minutes, the shape and also the binding energy of Mo 3d doublet did not change significantly with the increasing time of Ar^+ bombardment. No shift in the binding energy of the Mo 3d doublet of vacuum heat treated Mo-black dip coatings was observed after Ar^+ ion bombardment for prolonged times (Table 3.5.5). The table also shows that in any sample, the final product after prolonged bombardment is MoO_2. The atomic percentages of Mo, Zn and O_2 of a Mo-black dip coating on etched zinc at different etching times are given in Table 3.5.6. The ratio of elements Mo/Zn/O is 1/0.44/2.56 at the surface of the coating. After 60 minutes etching the ratio of Mo/Zn/O becomes 1/0.23/1.33. After that the ratio of the elements remains nearly the same (Table 3.5.6). A complete XPS depth profile of a thin Mo-black dip coating on zinc is shown in Fig.3.5.25.

3.5.4 Mo-black dip coatings on cobalt (NC) substrates

For coatings on cobalt (NC) substrates, the binding energies of Mo 3d electrons are somewhat higher than those for coatings on Al and Zn substrates and does not shift much after heat treatments.

A. As-prepared coating

A typical survey scan spectrum of a Mo-black dip coating on a cobalt (NC) substrate (electroplated cobalt on nickel plated copper) is shown in Fig.3.5.26. The figure shows that the main element of the coating is Mo. It also shows O 1s, C 1s peaks and very small peaks for Co 2s and 2p. The narrow scan spectra for Co 2p, O 1s and Mo 3d are shown in Figs.3.5.27-28.

Fig.3.5.27 shows that Co 2p peaks are very broad. It is difficult to measure corresponding binding energies accurately. However, the estimated binding energy of Co ($2p_{3/2}$) peak is about 780.0 eV. A strong satellite for the Co ($2p_{3/2}$) peak can be seen at about 6 eV higher binding energy than the main peak. These features indicate the presence of cobalt oxide (CoO) (McIntyre and Cook, 1975, Smith et al, 1980). Fig.3.5.28(a) shows the symmetric peak of O 1s of binding energy 530.1 eV which is due to the metal oxides (Robert et al, 1972).

The narrow scan spectrum of the Mo 3d doublet is shown in Fig.3.5.28(b). Compared to the 3d doublet for coatings on Al and Zn substrates, it is well resolved and sharper. The average binding energies of Mo ($3p_{3/2}$), Mo ($3d_{3/2}$) and Mo ($3d_{5/2}$) are given in Table 3.5.4. In these coatings, the binding energy of the Mo 3d doublet is 0.5 eV higher than that for coatings on Al and Zn. However comparing the binding energy of Mo ($3d_{5/2}$) peak with that of the standard material, it seems that the oxidation state of Mo in the coating is between +4 and +6.

B. Effect of heat treatment and Ar^+ ions etching

For coatings on cobalt substrates the shift in binding energy of the Mo ($3d_{3/2}$ - $3d_{5/2}$) peaks was only 0.3 eV after heating in air at 400°C for 2 hours (Table 3.5.4). After heat treatment the Mo 3d doublet is more resolved and sharper (Fig.3.5.29) and the binding energy of the Mo $3p_{3/2}$ peak increased from 396.4 to 398.1 eV (i.e., close to the value for MoO_3). When the coating was heated inside the spectrometer chamber at a temperature of 300°C for 2 hours the binding energy of the 3d doublet decreased by 0.3 eV towards the lower oxidation state of Mo (Table 3.5.4).

Argon ion bombardment was used to profile the coatings. Fig.3.5.30 shows the survey scan spectrum of the coating referred to in Fig.3.5.26 after 70

Table 3.5.1. XPS data for standard samples including shift in binding energy of Mo $3d_{5/2}$ electrons with respect to that of Mo $3d_{5/2}$ electrons in Mo metal.

Oxidation State	Sample	Electrons Binding Energy / eV				FWHM of Mo 3d doublet	Shift in B.E.
		Mo $3p_{3/2}$	Mo $3d_{3/2}$	Mo $3d_{5/2}$	O 1s	eV	eV
0	Mo-metal	-	230.2 ± 0.2	227.0 ± 0.1	-	-	0
+4	MoO_2	395.6	232.4 ± 0.2	229.3 ± 0.2	529.9	-	2.3
+5	$MoCl_5$*	-	234.5 ± 0.2	231.0 ± 0.1	-	-	4.0
+6	MoO_3	398.1	236.1 ± 0.1	233.0 ± 0.1	529.9	4.4	6.0

* Data taken from Swartz and Hercules (1971)

(FWHM = Full Width at Half Maximum)

Table 3.5.2 XPS data for electrodeposited Mo-black coatings on aluminium substrates including a shift in binding energy of Mo $3d_{5/2}$ peak with respect to that of Mo-metal.

Sample	Electron Binding Energy eV				FWHM of Mo 3d doublet eV	Shift in B.E. eV
	Mo $3p_{3/2}$	Mo $3d_{3/2}$	Mo $3d_{5/2}$	O 1s		
As-prepared coating	395.6	234.5 ± 0.1	231.3 ± 0.2	530.1 ± 0.2	5.5	4.3
After heating in air at 400°C for 2 hours	397.8	235.9 ± 0.1	232.8 ± 0.1	529.6 ± 0.2	4.6	5.8
After heating in vacuum at 450°C for 2 hours	-	234.2 ± 0.3	231.2 ± 0.2	-	6.0	4.2
Substrate-coating interface (as-prepared)	397.0	235.0 ± 0.3	231.9 ± 0.3	530.6 ± 0.2	6.0	4.9

(FWHM = Full Width at Half Maximum)

Table 3.5.3 XPS data for Mo-black dip coatings on zinc substrates including shift in binding energy of Mo $3d_{5/2}$ peak with respect to that of Mo-metal.

Substrate	Treatment	Electron Binding Energy / eV				FWHM of Mo 3d doublet eV	Shift in B.E. eV
		Mo $3p_{3/2}$	Mo $3d_{3/2}$	Mo $3d_{5/2}$	O 1s		
Unetched zinc	As-prepared	395.6	234.1 ± 0.3	231.1 ± 0.2	529.6	6.0	4.1
Etched zinc	As-prepared	395.6	234.4 ± 0.2	231.4 ± 0.1	529.9	5.6	4.4
Unetched zinc	Heated for 2h at 200°C in air	-	235.6	232.7	-	5.6	5.7
Unetched zinc	Heated for 1.5h in vacuum at 100°C	-	233.8	230.6	-	5.6	3.6
	at 200°C	-	232.8	229.6	-	5.6	2.6
	at 300°C	-	232.2	229.2	-	5.6	2.2
Etched zinc	Heated for 3 h in vacuum at 300°C	394.6	232.2 ± 0.2	229.2 ± 0.1	529.9	5.6	2.2
Etched zinc	Heated for 2 h in air at 200°C	397.02	235.0	232.1	-	5.6	5.1
	at 300°C	397.0	235.2	232.4	-	4.8	5.4
	at 390°C	397.0	235.6 + 0.1	232.6 + 0.1	529.6	4.4	5.6

(FWHM = Full Width at Half Maximum)

Table 3.5.4 XPS data for Mo-black dip coatings on cobalt (NC) substrates including shift in B.E. of Mo $3d_{5/2}$ with respect to that of Mo-metal.

Sample	Electron Binding Energy/eV				FWHM of Mo 3d doublet	Shift in B.E.
	Mo $3p_{3/2}$	Mo $3d_{3/2}$	Mo $3d_{5/2}$	O 1s	eV	eV
As-prepared	396.4	235.0 ± 0.1	231.9 ± 0.1	530.1 ± 0.2	5.2	4.9
Heated in air at 400°C for 2 hours	398.1	235.3 ± 0.1	232.2 ± 0.1	530.6 ± 0.1	4.6	5.2
Heated in vacuum at 300°C for 2 hours	397.0	234.7 ± 0.2	231.5 ± 0.1	530.6 ± 0.2	5.6	4.5

(FWHM = Full Width at Half Maximum)

Table 3.5.5 Shift in binding energy of Mo $3d_{5/2}$ electrons due to etching by Ar^+ ion bombardment for various samples.

Sample	Etching Time Minutes	Electron B.E. eV		Decrease in B.E. eV
		Before Etching	After Etching	
MoO_2	30	229.3	229.2	0.1
MoO_3	30	233.0	229.2	3.8
Mo-black film (electroplated)	30	231.3	229.8	1.5
Mo-black to metal interface	30	231.9	229.9	2.0
Mo-black dip coating on zinc (as-prepared)	10	231.4	229.9	1.5
	60	-	229.1	2.3
	160	-	229.3	2.1
Mo-black dip coating (heated at 290°C for 3 hours in vacuum)	10	229.2	229.0	0.2
	60	-	228.9	0.3
	160	0	229.2	-
Mo-black dip coating on cobalt (NC) substrate	10	231.9	229.4	2.5
	70	-	229.0	2.9
	220	-	229.0	2.9

Table 3.5.6. Atomic percentage of chemical elements Mo, Zn and O_2 for a Mo-black dip coating on etched zinc substrate after Ar^+ ion etching for various times.

Ar+ ions Etching Time / Minutes	Zn	Mo	O_2
0	11	25	64
10	10	33	57
60	9	39	52
165	10	37	53
270	11	35	53
375	10	35	55
480	10	34	55

minutes etching. The spectrum clearly shows a marked reduction of the intensity of the C 1s peak where as the intensities of Mo 3p, 3d and Co 2s, 2p have increased suggesting that carbon is the surface contamination. The binding energy of the Mo 3d doublet shifted towards a lower oxidation state after etching with Ar^+, (Table 3.5.5). The effectsof Ar^+ ion etching on the Mo 3d doublet of the coating are displayed in Fig.3.5.31. As the same effect has been observed in the Mo-black coatings on different substrates (Al, Zn and Co) as well as in the standard Mo-oxide (MoO_2 and MoO_3) after Ar^+ bombardment, it can be concluded that the observed lower oxidation state of the Mo below the coating surface is mainly due to the Ar^+ ion etching effect. Using the XPS elemental sensitivity factors (Appendix D) the atomic ratios of Co, Mo and O have been calculated. At the surface of the coating, the ratio of the elements Mo/Co/O is 1/0.22/2.31. After 10 minutes etching, the ratio becomes 1/0.21/1.84. The reduction of O to Mo ratio may be due to the Ar^+ ion etching as it reduces the Mo-oxide to the lower oxidation state. However, the ratio of the elements after 10 minutes of etching remains almost constant up to 370 minutes of etching as shown in Fig.3.5.32. In the present investigation, the ratio of Co to Mo is somewhat less than that obtained by Smith and Keytz (1984). They report that in an outer layer of about 80 nm thick the ratio of Mo/Co/O is 1/0.5/1.8 and after that the ratio becomes 1/0.85/1.72.

3.6 Electrical properties of Mo-black coatings

Electrical measurements on Mo-black coating have been carried out to determine the values of (i) the thermal activation energy of the conduction process (ii) the dielectric constant (iii) and the conductivity of the coatings. Investigation of the conduction mechanism in the coatings has also been an aim of this part of the work. The measurements

have been made on a metal-insulator-metal sandwich structure. The metal substrate acts as the bottom electrode. A pressure contact has been made on the top surface of the coating using highly polished flat metal buttons. Both copper and aluminium button electrodes have been used in the present investigation. The measurements of current-voltage (I-V) characteristics have been carried out in the temperature range 20 to 240^{o}C. The capacitance of the coatings has been measured in the temperature range 20 to 150^{o}C and over a frequency range 5 X 10^{2} to 2 X 10^{4} Hz. All the measurements have been done on electrodeposited Mo-black coatings and in vacuum at a pressure of about 1.3 X 10^{-3} Pa.

Structural instabilities adversely affect the electrical characteristics being examined (Chan and Loh, 1970). In order to obtain reliable and reproducible electrical characteristics, the samples have been heat treated to minimise the number of structural defects. The annealing temperature (245^{o}C) and time (2 hours) was the same for all the samples.

3.6.1 Current-voltage (I-V) characteristics at room temperature

The I-V characteristics of Mo-black coatings for four different thicknesses are shown in Fig.3.6.1. It can be observed that the current decreases with increasing coating thickness. The main feature of the I-V graphs is that they are non-linear and the slope of I-V curves is greater than 1. Fig.3.6.2 shows the plots of logI as a function of $V^{1/2}$. It can be seen that these are linear plots above an applied voltage of about 12V. This relation is indicative of either Schottky emission (Schottky, 1914) or Poole-Frenkel emission (Frenkel, 1938). Both phenomena are described by

$$I \propto \exp \frac{\beta E^{1/2}}{kT} \qquad (3.6.1)$$

where I is the current, k the Boltzmann constant, T the absolute temperature and E is the applied electric field (i.e., V/d). Here V is the applied voltage and d is the sample thickness. β is the field lowering coefficient and is given by

$$\beta = \left[\frac{e^3}{n\pi\varepsilon_o \varepsilon_r}\right]^{1/2} \qquad (3.6.2)$$

where ε_o is the dielectric constant of free space (8.854×10^{-12} F/m) and ε_r is the relative dielectric constant of the dielectric while e is the electronic charge. The difference between the Schottky and Poole-Frenkel effect is expressed by n = 1 for Poole-Frenkel and n = 4 for Schottky emission.

According to relation (3.6.1), the slope of the plots of logI vs $V^{1/2}$ is given by

$$m = \frac{\log e\ \beta}{kT\ d^{1/2}} = \frac{0.434\beta}{kTd^{1/2}} \qquad (3.6.3)$$

The experimental values of β_{exp} have been calculated using equation (3.6.3) and compared with the theoretical values of β_s (Schottky field lowering coefficient) and β_{PF} (Poole-Frenkel field lowering coefficient). Theoretical values of β has been calculated by using the high frequency dielectric constant (2×10^4 Hz) from capacitance measurements. The values of β_{exp}, β_s and β_{PF} for four Mo-black coatings are given in Table 3.6.1. It can be seen from Table 3.6.1 that the experimental values of

β_{exp} agree better with the values of β_{PF} rather than those of β_s. The relative dielectric constants ε_r have been calculated from d.c. measurements using equation (3.6.2) for both n=4 and n=1 and compared with the dielectric constant calculated from a.c. measurements. The values of ε_r, $(\varepsilon_r)_s$ (n=4) and $(\varepsilon_r)_{PF}$ (n=1) are also included in Table 3.6.1. The results shown in Table 3.6.1 are in favour of the Poole-Frenkel mechanism which gives a more reliable value of dielectric constant than the assumption of the Schottky effect and yields values of ε_r comparable with those obtained from a.c. measurements. The results therefore suggest that the dominant conduction mechanism in the high field region may be of the Poole-Frenkel type.

In order to investigate the effect of electrode material on the I-V characteristics of the coating, coatings of same thicknesses prepared under same conditions have been studied with two different electrodes (Cu and Al). The resultant I-V characteristics of one pair of coatings measured at $20^{o}C$ are shown in Fig.3.6.3. This figure shows that the electrical characteristics of the coatings with two different electrodes are rather similar. Thus it may be stated that for the Mo-black coatings, the conduction mechanism is independent of electrode material. However Figs.3.6.1 and 2 show that the conductivity of the coatings is thickness dependent which gives further evidence for bulk limited conduction, i.e., Poole-Frenkel type (Maissel and Glang, 1983).

In order to study the effect of annealing on the I-V characteristics of the coating a few samples have been studied at room temperature before and after annealing. It has been found that the conductivity of the coating increases more than one order of magnitude after annealing. A typical I-V characteristic of a coating of thickness 3.5μm before and after annealing is shown in Fig.3.6.4.

3.6.2 I-V characteristics at different temperatures

The I-V characteristics of Mo-black coatings of four different thicknesses at various temperatures are shown in Figs.3.6.5(a-d). It is evident from these figures that both the electric field and temperature have a profound influence on the magnitude of the electrical conductivity. The temperature dependence of the current at constant bias voltages is shown in Figs.3.6.6(a-d) for different thicknesses. It can be observed that these curves are nonlinear in the lower temperature region. The nonlinearity of the curves in the lower temperature region may be due to the transition from hopping conduction to free band conduction as observed experimentally in different oxide thin films (Ramadan et al, 1984; Al-Ismail and Hogarth, 1983; Islam, 1987). It has also been reported that the transi-tion between these two processes was gradual.

The thermal activation energy of the conduction process has been calculated using the following relation:

$$I = I_o \exp(-\Delta E/kT) \qquad (3.6.4)$$

where ΔE is the activation energy, k is the Botlzmann constant, T is the absolute temperature and I_o is given by:

$$I_o = e\mu N_d (V/d)A \qquad (3.6.5)$$

where e is the electronic charge, μ is the mobility, N_d is the trap or impurity centre density, V is the applied voltage, d is the thickness of the sample and A is the effective area. The calculated values of activation energies at the higher and lower temperature regions (~23^oC) for different thicknesses of the coatings are given in Table 3.6.2. No

systematic change in the activation energy has been observed with the thickness of the coatings or the applied voltage.

Figs.3.6.7(a-b) show the plots of LogI versus $V^{1/2}$ for Mo-black coatings of two different thicknesses at various temperatures. These figures show the linear dependence of I on $V^{1/2}$ at high electric fields and at different temperatures. The values of coefficient β have been calculated at different temperatures and are given in Table 3.6.3. This shows that the β-value increases with increase of temperature. Values of the relative dielectric constant ε_r of the coatings at different temperatures have also been determined using equation 3.6.2. and are given in Table 3.6.3.

Values of the conductivity σ of the Mo-black coatings has been determined at room temperature for four different thicknesses and are given in Table 3.6.1. The conductivity of the coatings increases slightly with the increase of coating thickness as shown in Table 3.6.1. It has been observed that the conductivity of the coating increases with the increase of deposition rate (increase of plating current density). The variation of conductivity with temperature for coatings prepared at two different current densities is shown in Fig.3.6.8. The room temperature, conductivity of a coating increased by a factor of 2.6 when the plating current density increased from 1.45 to 2.65 mA/cm^2.

3.6.3 A.C. measurements

The aim in performing a.c. measurements on Mo-black coatings was to obtain information about the dielectric properties. The capacitance and loss factor have been measured simultaneously at different temperatures (20 to 150°C) over a frequency range 5×10^2 to 2×10^4 Hz using the bridge

mentioned in section 2.4.3.

The variation of capacitance with frequency at room temperature for four different thicknesses of Mo-black coatings is shown in Fig.3.6.9. From this figure it can be seen that at room temperature the capacitance increases with decrease of frequency and the variation is more pronounced at lower frequencies. Fig.3.6.9 also shows that the capacitance decreases with increase of film thickness.

The relative dielectric constant ε_r of the Mo-black coatings has been calculated at different frequencies using the relation:

$$C = \varepsilon_o \varepsilon_r (A/d) \qquad (3.6.6)$$

where ε_o is the dielectric constant of free space, A is the effective area and d is the coating thickness. The values of ε_r at different frequencies for four different coating thicknesses are given in Table 3.6.4. It can be seen that although the capacitance decreases with the increase of coating thickness (Fig.3.6.9), no systematic change in the dielectric constant has been observed with the coating thickness. The values of dielectric constant ε_r calculated for different coatings are in the range 3.5 to 4.8 and decrease slightly with the increase of frequency.

The variations of capacitance with temperature at different frequencies for two Mo-black coatings of thickness 4 and 7 μm are shown in Figs.3.6.10 (a-b). It may be seen that the capacitance of the coatings increases with increase of temperature for all frequencies and after attaining a maximum value at about 100°C, the capacitance decreases with further increase of temperature. (The samples were kept at various fixed temperatures for about 20-30 minutes and then the measurements were taken at those

Table 3.6.1 Some electrical parameters for Mo-black coatings.

Sample Thickness (μm)	Experimental Values		For Schottky Mechanism, n = 4		For Poole-Frenkel Mechanism, n = 1		Conductivity σ
	β_{exp} / $10^{-5}eV^{-\frac{1}{2}}m^{\frac{1}{2}}$	Relative Dielectric Constant, ε_r	β_s / $10^{-5}eV^{-\frac{1}{2}}m^{\frac{1}{2}}$	$(\varepsilon_r)_s$	β_{PF} / $10^{-5}eV^{-\frac{1}{2}}m^{\frac{1}{2}}$	$(\varepsilon_r)_{PF}$	/ $(\Omega - m)^{-1}$
3.5	3.6	2.8	2.2	0.9	4.3	3.7	6.1×10^{-13}
4.0	3.6	3.22	1.9	0.9	3.8	3.7	6.5×10^{-13}
5.5	3.7	-	1.8	0.9	3.5	3.6	6.9×10^{-13}
8.0	4.0	3.5	2.0	0.8	4.1	3.3	7.7×10^{-13}

Table 3.6.2 Activation energy of Mo-black coatings for electrical conduction process at two different ranges of temperature.

Sample Thickness μm	Different Bias Voltages V	Activation Energy ΔE/(eV) (150-240°C)	Activation Energy ΔE/(eV) (20 - 60°C)
3.5	2	0.58	0.12
	4	0.55	0.13
	6	0.58	0.14
4.0	2	0.60	0.11
	4	0.58	0.13
	6	0.60	0.14
5.5	2	0.45	0.11
	4	0.47	0.13
	6	0.49	0.15
8.0	2	0.58	0.17
	4	0.60	0.15
	6	0.61	0.14

Table 3.6.3 The values of β and ε_r at different temperatures

Temperature (^{o}C)	Sample thickness 4.0 um		Sample thickness 5.5 μm	
	β $(10^{-5} eV V^{\frac{1}{2}} m^{\frac{1}{2}})$	ε_r	β $(10^{-5} eV V^{\frac{1}{2}} m^{\frac{1}{2}})$	ε_r
22	3.6	3.7	3.7	3.5
60	4.0	3.3	4.8	2.8
100	4.9	2.7	5.7	2.3
150	5.5	2.4	6.8	2.0
200	5.9	2.2	7.8	1.71

Table 3.6.4. Relative dielectric constant ε_r of Mo-black coatings for various frequencies

Frequency / kHz	Relative Dielectric Constant for Various Thickness / µm		
	5.0	6.0	8.0
0.5	4.67	4.77	4.08
1.0	4.52	4.63	3.87
5.0	4.23	4.35	3.66
10.0	4.11	4.16	3.58
15.0	4.05	4.11	3.56
20.0	4.01	4.07	3.52

particular temperatures).

The variation of dielectric constant ε_r with temperature at various frequencies is shown in Figs.3.6.11(a-b). As the dielectric constant ε_r is directly proportional to the capacitance for fixed coating thickness, the variation of ε_r with temperature and frequency is the same as that of capacitance in Fig.3.6.10. Fig.3.6.12 shows the typical variation of dielectric loss $\tan\delta$ with frequency at different temperatures for a coating of thickness 4 μm. It can be seen that the dielectric loss decreases with the increase of frequency and the variation is more pronounced at low frequencies. Fig.3.6.12 also shows that the dielectric loss increases with the increase of temperature.

The capacitance measurements have also been performed before and after annealing of the coatings. It has been observed that the capacitance increases in all the samples after annealing of the coatings. Fig.3.6.13 shows a typical variation of capacitance measured at room temperature with frequency before and after annealing of a coating of thickness 4μm. The dielectric constant at 20 kHz increased by 5.7% after annealing the coating at 240^{o}C for 2 hours.

3.7 Optical measurements

Optical measurements in the UV and visible region have been made on thin Mo-black coatings prepared by an electrodeposition method on semitransparent aluminized glass substrates as described in section 2.5. The objective of this study is to obtain an estimate of the valence-conduction bandgap and the extent of any band tailing (Appendix F).

The absorbance spectra for coatings of different thicknesses are shown in Figs.3.7.1 and 2 prepared at two different plating current densities. These figures show that the fundamental absorption edge is exponential in nature.

The absorption coefficient $\alpha(\omega)$ has been calculated from the absorbance A and film thickness d using the following relation (Longhurst, 1957):

$$\alpha(\omega) = 2.303 \frac{A}{d} \qquad (3.7.1)$$

The plots of $(\alpha \hbar\omega)^{1/2}$ as a function of $\hbar\omega$ are shown in Figs.3.7.3 and 4. These figures show a well defined linear region for the higher values of absorption and thus satisfy the relation:

$$\alpha\hbar\omega = B(\hbar\omega - E_{opt})^2 \qquad (3.7.2)$$

given by Tauc et al (1966) and Davis and Mott (1970). Here E_{opt} is the optical energy gap and B is a constant. The values of E_{opt} and B estimated from Figs.3.7.3 and 4 are given in Table 3.7.1. The values of optical band gap, E_{opt}, are obtained by extrapolating the linear region of the curve to $(\alpha \hbar\omega)^{1/2} = 0$ and the square of the slope of these lines give the value of the constant B.

The values of band tails E_e are estimated from the Urbach (1953) relation:

$$\alpha(\omega) = \alpha_o \exp(\hbar\omega/E_e) \qquad (3.7.3)$$

where α_o is a constant. Figs.3.7.5 and 6 show the exponential behaviour of the absorption edges, which are replotted from the experimental data of

Figs.3.7.1 and 2 according to relation (3.7.3). The values of band tail E_e estimated from Figs.3.7.5 and 6 are also included in Table 3.7.1.

Within this limited study, no systematic change of the optical band gap with coating thickness has been observed. The main feature observed in this study is the variation of E_{opt} with the rate of deposition i.e. with the plating current density. The mean values of E_{opt} for the coatings are 1.89 eV for slow deposition rate and 1.67 eV for rapid deposition rate. The values of E_{opt} are in fair agreement with the published value (1.75 eV) for Mo_4O_{11} (Hanafi et al, 1981). It is evident from Table 3.7.1 that the E_{opt} decreases and E_e increases with the increase of rate of deposition. This effect may be due to an increase of overall disorder with the rapid rate of deposition. This supports the theory of Mott and David (1971) which suggests that the extent of the localised states near the mobility edge increases with the increase of disorder in the material. Additionally, as the rate of deposition increases, deeper band tails of the localised states extend to the gap and cause an increase in the value of E_e and a decrease in the value of E_{opt}. Similar effects have also been observed in other oxide thin films by Shabalov and Feldmann (1983) and Al-Ani et al (1984, 1985). The values of the constant B from equation (3.7.2) are of the order of $10^5 cm^{-1}eV^{-1}$ which is in reasonable agreement with the theoretical value 10^5 to 10^6 $cm^{-1}eV^{-1}$ (Mott and Davis, 1979).

The refractive index n has been estimated from the relation (Moss et al., 1973)

$$2nd = \frac{\lambda_1 . \lambda_2}{\lambda_1 - \lambda_2} \qquad (3.7.4)$$

where λ_1 and λ_2 are the wavelengths of adjacent transmission maxima in the absorbance vs wavelength curve (Figs.3.7.1 and 2), d is the coating thickness and n is the refractive index of the coating. The calculated values of refractive index n for three coatings are listed in Table 3.7.1.

Table 3.7.1 Some optical parameters of Mo-black coatings

Plating current density mA/cm^2	Sample thickness (nm)	Optical band gap E_{opt} (eV)	Band tail, E_e eV	B / $10^5 eV^{-1} cm^{-1}$	Refractive index
1.4	210	1.92	0.30	4.49	-----
1.4	230	1.96	0.50	4.35	4.0 at λ = 0.49 μm
1.4	530	1.80	0.70	1.00	2.6 at λ = 0.77 μm
2.8	300	1.67	0.77	4.00	-----
2.8	370	1.67	0.83	3.36	-----
2.8	400	1.66	0.77	3.25	2.8 at λ = 0.55μm

CHAPTER IV

STABILITY OF MO-BLACK COATINGS

Stability of selective surface properties is one of the most important factors in selection of surfaces for solar thermal conversion. The coatings for solar energy collectors must not only exhibit high solar absorptance α_s and low thermal emittance ε_{th} but should also be thermally and mechanically stable. They should ideally retain effective α_s and ε_{th} values within the operating temperature range of a solar collector throughout its useful life time. The surface should be thermally, chemically and mechanically stable under different environmental conditions. It is difficult to assess actual lifetimes of the collectors. However, the durability of the surfaces can be tested under the following conditions: high humidity, condensation, thermal ageing at elevated temperatures, temperature cycling, outdoor ageing, mechanical adhesion testing.

In the present investigation, the influence of short term heat treatment at elevated temperatures (up to 400^{o}C) in both air and in vacuum on optical properties and microstructures of Mo-black coatings has been examined. A few coatings have also been tested after natural outdoor ageing. As described in the previous chapter (Section 3.1.3) the electrodeposited coatings are effectively non-selective, the stability tests have therefore been performed on dip coatings.

Adhesion measurements have been performed on Mo-black coatings

electroplated on aluminium and attempted for dip coatings on zinc.

4.1 Mo-black coatings on zinc

4.1.1 Spectral reflectance

A number of Mo-black coatings on etched zinc substrates have been heat treated in air at atmospheric pressure and in a vacuum of about 10^{-3} Pa at temperatures of 100, 150, 200 and 300°C for periods up to 4 to 24 hours. Three to five samples have been tested at each temperature. Generally no significant changes in the solar absorptance α_s and the thermal emittance ε_{th} of the coatings have been observed in these short-term heat-treatment tests (apart from in air at a temperature of 200°C when the absorptance of some coatings decreased by 2-5%). The values of α_s and ε_{th} for various heat treatments in air are given in Table 4.1. Figs.4.1(a,b) show the spectral reflectance as a function of wavelength for two coatings after heat treatment in air at 100 and 150°C respectively. It can be seen that the reflectance in the short wavelength region increases slightly after heat treatment whereas in the NIR region it decreases. As a result the solar absorptance α_s does not change significantly. On the other hand, coatings on unetched zinc deteriorate even after heat treatment for 8 hours at 150°C. Fig.4.2 shows the effect of heat treatment on the spectral reflectance spectra of a coating on unetched zinc. The reflectance increases throughout the solar region resulting in a decrease in absorptance from 0.75 to 0.70. Hosseini (1981) also reported that these coatings degrade after heat treatment in air at 280°C for 3 hours. Therefore, no further heat treatment at higher temperature has been done on the coatings on unetched zinc. All the results given below are of the coatings on etched zinc. The specular reflectance spectra in the IR region (2.5 - 50 μm) before and after heat treatment in air at 100°C for

24 hours is shown in Fig.4.3. This figure shows that the absorption band (due to water) at 6.2 μm has almost disappeared after heat treatment and the band at about 2.9 μm is drastically reduced. The slight decrease in the emittance value after heat treatment may be due to the loss of water. The effect of heat treatment at 200°C in air on the spectral reflectance of a coating is shown in Fig.4.4. For this sample, it can be seen that after the first 8 hours of heat treatment, the reflectance decreases in the NIR region and increases slightly in the short wavelength region. After 16 hours of heat treatment, the reflectance increases also in the NIR region resulting in a slight decrease in the solar absorptance from 0.86 to 0.85. Fig.4.5 shows the effect of heat treatment at 300°C for 4 hours on the spectral reflectance spectra. In the short wavelengh region the reflectance increases considerably after heat treatment, but in the NIR region the reflectance decreases drastically. No significant change has therefore been observed in the values of α_s after heat treatment at 300°C. In some coatings the absorptance increases slightly after heat treatment, as shown in Table 4.2. Fig.4.6 shows the reflectance spectra of a coating after heat treatment at different temperatures and the values of α_s and ε_{th} are tabulated in table 4.2. The corresponding specular reflectance spectra in the IR region is shown in Fig.4.7. The figure shows that after heat treatment at 200°C and 300°C the water peak disappears.

The Mo-black coatings when heat treated in vacuum show no degradation at all in this short term heat treatment test and in some cases α_s increased slightly and ε_{th} decreased. The effects of heat treatment in vacuum at different temperatures on the values of α_s and ε_{th} are displayed in Table 4.3. The spectral reflectance curve of the coatings after different heat treatments are shown in Figs.4.8-11. In most cases the reflectance increases slightly in the short wavelength region and decreases in the NIR

region. The changes in the reflectance are more pronounced after heat treatment at 325°C (Fig.4.11). However, it has been observed that for coatings on a zinc substrate etched with 50% HNO_3 the reflectance increases slightly throughout the solar region. Fig.4.9. shows the effect of heat treatment on the spectral reflectance spectrum for one of these coatings (corresponding to a solar absorptance α_s decrease from 0.89 to 0.88). The thermal emittance ε_{th} also decreases as shown in Table 4.3. Fig.4.12 shows the spectral reflectance spectra of a coating after heat treatment in vacuum at different temperatures and the values of α_s and ε_{th} are given in Table 4.4. It can be seen that after these successive heat treatments, the value of α_s increases by 2.3% where as ε_{th} decreases by 5.8%. Fig.4.13 shows the effect of heat treatment on the IR reflectance of the same sample. No absorption band for water can be seen in the IR spectra after heat treatment at 300°C.

4.1.2 Microstructure

The effect of heat treatment on the microstructure of the coatings has been examined by scanning electron microscope (SEM). Figs.4.14 to 4.17 show typical surface microstructures before and after heat treatment at different temperatures. No significant change in the surface structure can be seen after heat treatment at 100°C for 24 hours (Fig.4.15). By comparing the as prepared structure (Fig.4.14) with the structure after heat treatment at 200 and 300°C (Figs.4.16-17), it seems that heat treatment causes a flattening of nodules i.e., they are still present, but some are less prominent. This may be the reason for the slight increase in the reflectance in the short wavelength region. The fine cracks in the as prepared coating becomes more prominent and wider after heat treatment at higher temperature. Some damaged areas have been observed in the surface structure after heat treatment at higher temperatures as shown in

Fig.4.18. Fig.4.19 shows the surface structure of a coating prepared on etched zinc with 50% HNO_3 for 8 hours. By comparing the as prepared surface with the heat treated surface, a decrease of surface roughness can be seen after heat treatment. This may account for a slight increase in the reflectance (Fig.4.9) of the coating.

4.2 Mo-black coatings on cobalt (NC) substrates

4.2.1 Spectral reflectance

Thermal stability testing of Mo-black coatings on cobalt (NC) substrates has been performed in air at temperatures of 200, 300 and 400°C for short periods (2 - 5 hours). Two samples have been tested at each temperature. Coatings on cobalt substrates plated with and without addition agent have been examined. The results obtained for various heat treatments are tabulated in Table 4.5 and 4.6. The effects of heat treatment on spectral reflectances of the coatings are shown in Figs.4.20 - 22. It can be seen that the reflectance of the coating generally increases slightly after heat treatment. However, the very broad reflectance peak at about 1.1 μm flattens somewhat. It may also be noticed that the changes in the reflectance after heat treatment at 300 and 400°C are less than that at 200°C. The solar absorptance α_s decreases only 0 - 1.1% after heat treatment at 300 and 400°C but it decreases about 2.2% after heat treatment at 200°C. It is evident from Table 4.5 that the emittance decreases after all heat treatments for coatings prepared on cobalt (NC) substrate plated without addition agent. Fig.4.23 shows an example of an IR reflectance increase after heat treatment. For coatings on cobalt (NC) plated with addition agent, the emittance increases after heat treatment (Table 4.6). Fig.4.24 shows the IR reflectance spectra of a coating on cobalt substrate plated with addition agent before and after heat

treatment in air at 300°C for 4 hours.

4.2.2 Microstructure

The surface structure of the coatings has been examined in SEM after heat treatment. Fig.4.25 shows a typical surface structure of a coating prepared on cobalt plated without addition agent, before and after heat treatment at 300°C for 5 hours. After heat treatment, the crack width increases and the limb-like features seem to be less compact. Fig.4.26 shows the microstructure of a coating prepared on cobalt substrate plated with addition agent, before and after heat treatment at 300°C for 5 hours. No significant changes have been observed except that the surface cracks are somewhat wider after heat treatment.

4.3 Outdoor testing

A few Mo-black coatings on etched zinc and cobalt (NC) substrates were left in outside ambient air facing southward (with shelter from direct rainfall ..) for five months. Their solar absorptance and thermal emittance have been remeasured. The values of the absorptance and emittance of the coatings before and after outdoor testing are given in Table 4.7. The coatings on etched zinc seem to be unchanged after outdoor exposure. The spectral reflectance spectra in the solar region of one of these coatings is shown in Fig.4.27 before and after outdoor ageing. The coatings on cobalt (NC) substrates, however, appear to be affected by the external atmosphere. The absorptance of the coating on cobalt (NC) plated without addition agent remains unchanged but it decreases for coatings on cobalt plated with addition agent from 0.87 to 0.85 after outdoor ageing. The IR reflectance of the coatings in both cases decreases giving an increase of emittance (Table 4.7). Compared with the as prepared coating,

the surface appeared rougher and spotty. However, more samples should be tested and the structural and compositional changes of the coatings (if any) should be examined.

4.4 Adhesion measurement

It is well known that adhesion of a film to its substrate strongly depends on the chemical nature, cleanliness and the microstructure of the substrate (Chopra, 1969). The Mo-black coatings are quite adherent to the substrates (aluminium, zinc and plated cobalt), when prepared under appropriate conditions as described in section 2.1.

The adhesion of the Mo-black coatings prepared by electrodeposition on aluminium substrate has been examined by using a Hounsfield Tensometer. A schematic diagram of the testing arrangement is shown in Fig.4.28. The coatings have been prepared on a flanged cylinder or 'dolly' (made of aluminium) following the same procedure as described in section 2.1.1. They have been specially designed to fit into the adapting collets on the Hounsfield Tensometer and also into the electrodeposition bath (Block, 1985). The coated aluminium dolly was then stuck to another test dolly using a two component adhesive (araldite) as shown in Fig.4.28.b. The araldite was left to cure for 24 hours under ambient conditions to reach maximum strength. Then, using the Hounsfield Tensometer, the load was applied to the adhered samples (Fig.4.28) until the molybdenum coating parted from the aluminium substrate. Readings have been taken continuously during tests and recorded in the chart. The adhesion of these coatings was in the range of 40 to 65 kg/cm^2 (depending on plating current density). The adhesion of the coating decreased with the increase of plating current density (Block, 1985).

An attempt was made to test the adhesion of Mo-black dip coatings on etched zinc and cobalt (NC) substrates by using an Elcometer 106 Adhesion Tester. The photograph of this instrument is given in Fig.4.29. The instrument employs the pull-off method to measure the lift off force required to pull a test dolly of a small area of coating away from the substrate. The test dolly was attached to the coating using the same method as described above (Fig.4.28). After curing, the coating was cut through around the base of the test dolly, the instrument claw was engaged and then the pull-off force was applied until the dolly was removed from the surface. The maximum pull off force achieved was recorded by observing the position of the dragging indicator on the engraved scale.

Unfortunately, this adhesion measurement test was not satisfactory on coatings on etched zinc or cobalt (NC) substrates. Only a very small portion of the coatings was removed from the substrate in some cases, and in other cases, the failure between the adhesive and the dolly occurred in the range 30 - 40 kg/cm^2.

Despite the microcracks in the coatings, they were mechanically stable. The coatings did not peel or flake off even after heat treatment (apart from very thick coatings on highly polished zinc).

Table 4.1. Solar absorptance α_s and thermal emittance ε_{th} of Mo-black dip coatings on etched zinc substrates after various heat treatment in air.

Temperature of heat treatment/(^{o}C)	As prepared		Period of Heat Treatment					
			8 hours		16 hours		24 hours	
	α_s	ε_{th}	α_s	ε_{th}	α_s	ε_{th}	α_s	ε_{th}
100	0.87	0.14	0.87	0.14	0.87	0.15	0.86	0.13
150	0.85	0.13	0.85	0.12	0.85	0.12	0.85	0.12
200	0.86	0.17	0.86	0.15	0.85	0.14		
300	0.87	0.14	0.87*	0.15*				

* Heat treated for 4 hours.

Table 4.2. Solar absorptance α_s and thermal emittance ε_{th} of an air heat treated Mo-black coating on etched zinc.

Run no.	Heat Treatment	α_s	ε_{th}
1	As prepared	0.86	0.15
2	8 hours at 200^{o}C	0.86	0.14
3	4 hours at 300^{o}C	0.88	0.14

Table 4.3 Solar absorptance α_s and thermal emittance ε_{th} of Mo-black dip coatings on etched zinc after heat treatment in vacuum.

Temperature of heat treatment/(°C)	As prepared		Period of Heat Treatment					
			8 hours		16 hours		24 hours	
	α_s	ε_{th}	α_s	ε_{th}	α_s	ε_{th}	α_s	ε_{th}
100	0.85	0.13	0.86	0.12	0.86	0.12	0.85	0.13
100**	0.89	0.30	0.88	0.25	0.88	0.23	0.88	0.24
200	0.86	0.14	0.86	0.14	0.86	0.13	--	--
325	0.87	0.14	0.87*	0.13*	--	--	--	--

* Heat treated for 4 hours.

** The zinc substrate of this coating was etched with 50% HNO_3.

Table 4.4 Solar absorptance α_s and thermal emittance ε_{th} of a vacuum heat treated Mo-black dip coating on etched zinc.

Run no.	Heat Treatment	α_s	ε_{th}
1	As prepared	0.86	0.17
2	8 hours at 150°C	0.86	0.15
3	4 hours at 200°C	0.87	0.15
4	4 hours at 325°C	0.88	0.16

Table 4.5 Solar Absorptance α_s, and thermal emittance ε_{th} of heat treated Mo-black dip coatings on cobalt (NC) substrates (without addition agent).

Heat Treatment	As Prepared		After Heat Treatment	
	α_s	ε_{th}	α_s	ε_{th}
5 hours at 200°C	0.91	0.25	0.89	0.25
	0.92	0.30	0.90	0.28
5 hours at 300°C	0.94	0.29	0.94	0.24
	0.90	0.26	0.89	0.21
2 hours at 400°C	0.94	0.33	0.94	0.29
	0.90	0.25	0.89	0.23

Table 4.6. Solar absorptance α_s and thermal emittance ε_{th} of heat treated Mo-black coatings on cobalt (NC) substrates (with addition agent).

Heat Treatment	As Prepared		After Heat Treatment	
	α_s	ε_{th}	α_s	ε_{th}
5 hours at 200°C	0.88	0.19	0.86	0.21
	0.89	0.13	0.88	0.17
5 hours at 300°C	0.91	0.10	0.89	0.11
	0.90	0.13	0.89	0.16
2 hours at 400°C	0.89	0.13	0.89	0.16
	0.88	0.20	0.88	0.20

Table 4.7. Effect of 5 months outdoor exposure on solar absorptance α_s and thermal emittance ε_{th} of Mo-black dip coatings.

Substrate	As Prepared		After 5 Months	
	α_s	ε_{th}	α_s	ε_{th}
Etched zinc	0.86 0.85 0.84	0.18 0.15 0.14	0.86 0.85 0.84	0.17 0.16 0.14
Cobalt (NC) plated without addition agent	0.90	0.22	0.90	0.31
Cobalt (NC) plated with addition agent	0.87	0.13	0.85	0.16

CHAPTER V

DISCUSSION

5.1 Characterization of Mo-black coatings

5.1.1 Electrodeposited coatings on aluminium

5.1.1.1 Mo-oxide present in the coatings

The present work on electron diffraction, X-ray diffraction and X-ray photoelectron spectroscopy (XPS) together with the absorption peaks in the IR spectra has given consistent results and reveals that the coatings consist mainly of a molybdenum oxide, Mo_4O_{11} with a small amount of nickel hydroxide (Table 5.1). The detailed study of the electrodeposited coating in the transmission electron microscope (TEM) shows that the interplanar spacing values calculated from the electron diffraction patterns are in good agreement with those given in the A.S.T.M. index for Mo_4O_{11} (Table 3.3.3). X-ray diffraction studies of the as-prepared coatings yield only the broad low angle (200) peak of Mo_4O_{11} at about $4.7^{o}\theta$ (Co K_{α} radiation). The absence of other peaks (Section 3.4) may be due to preferred orientation of Mo_4O_{11} in the coating relative to the substrates. However, after heat treatment of the coating in air at a temperature of $400^{o}C$ for 8 hours, X-ray diffraction peaks for both Mo_4O_{11} and MoO_3 are obtained (Fig.3.4.7). Recently, Potdar et al (1987) reported that electrodeposited Mo-black coatings on nickel plated copper substrates crystallize after heat treatment at $390^{o}C$ and consist of the Mo_4O_{11} phase (as-prepared coatings were reported to be

amorphous). The SEM study of the electrodeposited coatings in this work shows that they consist of rather smooth flat platelets with widely spaced cracks.

5.1.1.2 XPS study

Evidence for the presence of Mo_4O_{11} in the coating is also available from the XPS study (Section 3.5.2). This reveals that the oxidation state of Mo in the coating is between +4 and +6. The basis of the chemical shift of a core photoelectron peak is the change in the electrostatic potential of the core electron when valence electron charge density is accepted or withdrawn from the atom (Briggs and Seah, 1983). There is, therefore, a relationship between the binding energy and the chemical state of the element. Fig.5.1 shows the plots of binding energy (B.E.) for both $Mo(3d_{3/2})$ and $Mo(3d_{5/2})$ peaks as a function of oxidation state of Mo. This figure also includes the results obtained by Swartz and Hercules (1971) and Cimino and Angelis (1975). In the present investigation, (in contrast to the results of Swartz and Hercules), the variation of B.E. with oxidation state is not linear. It is similar to that obtained by Cimino and Angelis i.e., the binding energy values of MoO_2 are closer to those of the metal than those of MoO_3. (However Fig.5.1 shows that the binding energy values obtained in the present study are different from those obtained by Cimino and Angelis (1975). This discrepancy may be due to use of a reference value (284.9 eV) for the C1s peak in the present study while they used a value of 283.8 eV) Fig.5.1 also shows that the general trend in B.E. as a function of oxidation state is identical for both $Mo(3d_{3/2})$ and $Mo(3d_{5/2})$ levels. Using the binding energy value of $Mo(3d_{5/2})$ for a Mo-black coating from Table 3.5.2, the estimated oxidation state of Mo from Fig.5.1 is +5.1. This oxidation state is fairly close to the oxidation state of Mo_4O_{11} (+5.5) (Kennedy, 1972). It has been reported by Hosseini (1981) that the oxidation state of Mo in the

electrodeposited Mo-black coatings is +4. According to his data, the Mo ($3d_{3/2}$) peak of the coating has been shifted by 4.4 eV from the corresponding peak of Mo-metal, which is close to the present data. Comparing the B.E. of the Mo 3d doublet of standard MoO_2 (+4) and its shift from Mo-metal (from published data and the present investigation) it can be argued that the oxidation state of Mo in the coating is higher than +4. The presence of strong absorption bands other than those for water in the IR region (Fig.3.1.19) also rules out the possibility of the presence of MoO_2 in the coatings (Section 5.1.2.2). Potdar et al (1982) reported that the electrodeposited Mo-black coatings on nickel plated copper substrates consist of the MoO_3 phase. This is not supported by the present investigation. None of the X-ray diffraction, electron diffraction or XPS results show evidence of MoO_3 in the as prepared coatings. After heat treatment of the coatings in air at high temperatures (400°C) the shift of the Mo $3d_{5/2}$ peak from the corresponding peak of Mo-metal is 5.8 eV (Section 3.5.2). The shift in B.E. and also the shape of the Mo 3d doublet of the air heated coating (Fig.3.5.9) is quite similar to that of MoO_3. This indicates that after heating in air, the surface of the coating oxidizes to MoO_3.

The vacuum heated coatings do not show a significant change in the B.E. of the Mo 3d doublet, but the peak is comparatively less resolved which may indicate the presence of more than one valency state of molybdenum. It may be possible that after heat treatment in vacuum, some Mo (+5) in the coating reduces to +4, via dehydroxylation (Patterson et al, 1976):

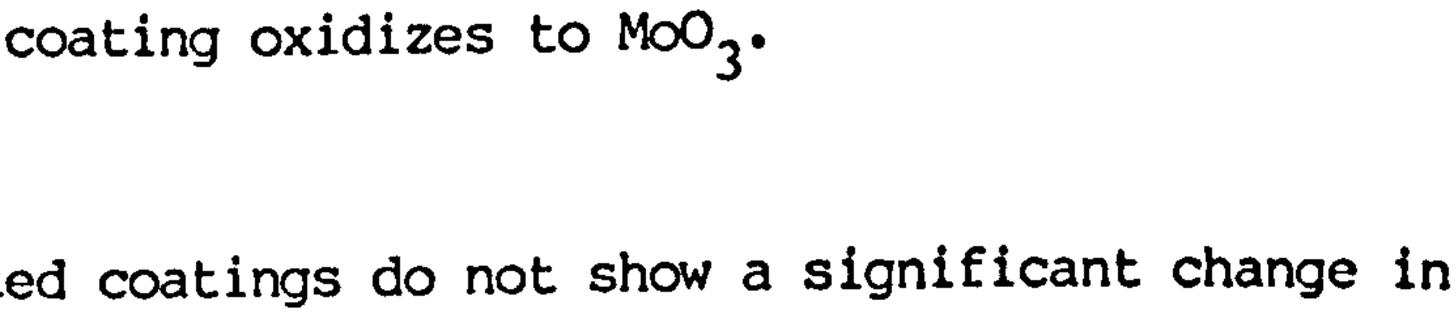

The depth profile of the coating has been studied by bombarding with Ar+ions. However, the results are not fruitful. After bombardment of

the coating surface, it has been observed that Mo 3d doublet shifts towards a low binding energy, which corresponds to MoO_2 (Table 3.5.5). Sputtering off of water molecules by Ar^+ may account for this change in B.E. However, reduction of the oxide to the lower oxidation state by Ar^+ etching is very common for most of the metal oxides (Briggs, 1978). Some oxides even reduce to the metal (Kim and Winograd, 1974). However, it has been reported by Kim et al (1974) that in the case of MoO_3, after prolonged bombardment with Ar^+ ions, the final product is MoO_2. A similar effect has also been observed in the present investigation. It is therefore unlikely that the observed shift in the binding energy of the Mo 3d doublet is due to an actual variation in the oxidation state of Mo with depth in the coatings.

5.1.2 Dip coatings on zinc

5.1.2.1 Structure and compositional analysis

The structure and composition of the Mo-black dip coatings on zinc substrates have been studied by XPS, SEM, X-ray and electron diffraction. The results of these investigations are given in Chapter III in detail. Because of the strong adhesion of the coatings to the zinc substrates, it is not possible to do any transmission electron microscopy. The reflection electron diffraction (RED) study of the coatings indicates their polycrystalline nature. However, the rings are spotty, possibly due to the presence of a small number of large crystallites (Cullity, 1967). The interplanar spacing values deduced from RED give evidence for the presence of Mo_4O_{11} (Table 3.3.1) in the coatings.

XPS studies of the as prepared dip coatings give results similar to those obtained for the electrodeposited coatings, i.e., the oxidation state of

Mo in the coatings is between +4 and +6. There is no significant difference between the B.E. of the Mo 3d doublet for coatings on etched and unetched zinc. The estimated oxidation state of Mo in the coating is about +5 from Fig.5.1, which is consistent with the presence of Mo_4O_{11}. The coatings on zinc substrates are more sensitive to heat treatment in air as well as in vacuum. The coating oxidizes to +6 oxidation state (MoO_3) when heated in air. The shifts in B.E. of Mo 3d doublet after heat treatment under various conditions are given in Table 3.5.3. This shows that coatings on etched zinc substrates are more resistant to oxidation than the coatings on unetched zinc substrates. The shift in the B.E. of Mo 3d doublet depends upon the temperature of heat treatment. The B.E. of Mo $3d_{5/2}$ electrons of the coatings on etched zinc has been shifted from 231.4 eV to 235.6 eV when heated at 390°C in air for 2 hours. The same amount of shift in the B.E. of Mo $3d_{5/2}$ electrons has been observed for coatings on unetched zinc substrate when heated at lower temperature (200°C) for the same time. The dip coatings reduce readily to the lower oxidation state (+4) when heated in vacuum, unlike the electrodeposited coatings. No significant change in the oxidation state of Mo has been seen after heat treatment in vacuum at a temperature of 100°C. However when the coating is heated above 200°C in vacuum, the shift in B.E. of Mo $3d_{5/2}$ peak of the coating is 2.2 eV from the corresponding peak of Mo-metal. The same amount of shift in B.E. has been observed for MoO_2 (Table 3.5.1). As zinc is a low melting point metal, heating of the coating may lead to diffusion of zinc through the coating. The coating might then be reduced to a lower oxidation state by zinc according to the following reaction (Verchere and Fluery, 1973):

$$Mo(V)\ oxide + Zn = Mo(IV) + ZnO$$

The reduction of Mo(VI) to Mo(IV) using Zn metal has also been reported by

Haight (1953).

Argon (Ar^+) ion bombardment has been used to study the depth profile of the coatings. After etching, the B.E. of the Mo 3d doublet is shifted towards that of MoO_2 (Table 3.5.5) as in the electrodeposited coatings. No shift in B.E. beyond MoO_2 (+4) has been observed after a prolonged time of bombardment. It has also been observed that the B.E. of Mo 3d doublet of a vacuum heated coating, which is already in +4 oxidation state (MoO_2 phase), does not shift after Ar^+ bombardment. These results are in agreement with the results reported by Kim et al (1974). According to them, MoO_2 cannot be decomposed by Ar^+ bombardment. The above results reveal that the as-prepared Mo-black coating is not in the MoO_2 phase.

The elemental composition of the Mo-black dip coatings has been determined from the XPS measurements. The atomic percentage of oxygen in the coating is about 72% (Table 3.5.6). This is also consistent with the presence of Mo_4O_{11} in the coatings. After etching with Ar^+ ions, the percentage of oxygen reduces to 57%. The atomic percentages of Mo, Zn and O_2 in a thin coating are shown in Fig.3.5.25 as a function of etching time. The reduction of oxygen content in the first few minutes of etching may be due to the reduction of the coating material to the lower oxidation state by the ion bombardment. In the present investigation, it has been observed that the percentage of zinc decreases slightly for the first few minutes of etching and then remains the same until the substrate is exposed by thinning of the coating (Fig.3.5.25). The reason for the initial decrease of zinc signal may be due to healing up of the cracks by Ar^+ bombardment. Briggs and Seah (1983) also reported that argon ion bombardment can induce changes in surface topography.

5.1.2.2 Infrared spectra

The IR spectra of a thick Mo-black dip coating on zinc shows strong absorption bands in the region 10 to 23 μm (Fig.3.1.8). These absorption bands are also observed in the IR spectra of electrodeposited Mo-black coatings.

To identify these absorption peaks, IR absorption spectra of standard MoO_3 and MoO_2 powder have been examined after compression into a disc formed with a KBr binder. Fig.5.2 compares the IR spectra of standard MoO_3 powder with those of Mo-black coatings. The position of the absorption peaks are tabulated in Table 5.2. Those for MoO_3 are very close to the published data (Hanafi et al, 1975; Barraclough and Stals, 1966). No significant absorption peaks were identified in the IR spectra of MoO_2. It has been reported by Hanafi et al (1975) that MoO_2 has weak absorption bands at 10.2, 10.5 and 11.2 μm only. In Mo-black coatings the absorption bands are at about 10.5, 11.7, 14.5, 20.3 and 21.5 μm (Table 5.2). Not all of these vibrational frequencies correspond to those of MoO_3. Unfortunately, no information is available concerning the IR absorption spectrum of Mo_4O_{11} (which is thought to be present in the Mo-black coatings). However, Hanafi et al (1975) studied the IR absorption of MoO_3 and its suboxides including MoO_2 (except Mo_4O_{11}). According to them most of the bands of MoO_3 still occur in the intermediate oxides. The behaviour of intermediate oxides changes gradually from that of MoO_3 towards that of MoO_2. The band at 10.5 μm in the suboxides may be an indication for the presence of an oxidation state of Mo lower than that of MoO_3. The absorption peaks at about 10.5, 11.7 and 21.5 μm of Mo-black coatings appear in the intermediate oxides between MoO_2 and MoO_3 (Hanafi et al, 1975). The strong absorption peak at 10.5 μm is attributed to the Mo=O stretching frequency. The bands at longer wavelengths are assigned

to stretching vibrations of Mo-O-Mo-O-Mo chains (Barraclough and Stals, 1966). The strong absorption peak at about 14.3 μm, which is not found in the spectra of other oxides of Mo (as reported in literature), may be related to the crystal structure of Mo_4O_{11} (Section 1.3.1).

5.1.2.3 Micromorphology

The surface topography of Mo-black dip coatings depends upon the pretreatment of zinc substrate. A detailed study of the surface microstructures of the coating in the SEM and optical microscopy reveals the following factors:

(a) The surface topography of the dip coatings on mechanically polished zinc substrates is quite similar to that of electrodeposited coatings, i.e., smooth platelet structure with widely spaced cracks (Fig.3.2.13).

(b) The as-deposited naturally dried coating does not show any cracks in the surface, when viewed in the optical microscope (Fig.3.2.18-21). Cracks develop after applying hot air on the coating surface (approximate temperature 55-65^{o}C). It has also been observed that the cracks are more likely to be nucleated from the surface defects such as pits (Fig.3.2.24).

(c) Very thin coatings do not show any cracks in the surface even after applying hot air and/or when viewed in the SEM (Fig.3.2.25).

(d) Except for very thin coatings, all coatings show a cracked surface in the SEM. These may be due to the heating produced by electron bombardment.

Cracks in the Mo-black coatings may, therefore, be due to thermal

expansion mismatch between the coating and the substrate (Kramer, 1983) or due to loss of some water from the coatings.

(e) The surface of the coatings prepared on etched zinc substrates shows a nodular structure (Jahan and Smith, 1986). The size and distribution of the nodules depend upon the concentration of the etchant and etching time and also the thickness of the Mo-black coating as described in section 3.2.2. By comparing the microstructure of the etched zinc substrate, it seems that the morphology of the coatings is related to the topography of the etched zinc susbtrates.

The compositional analysis of the coatings by electron probe microanalysis shows that the coating consists mainly of molybdenum with small amounts of nickel (Table 3.2.2). However, EDX spectra also show zinc signals which may originate from the zinc substrate through the coatings and also through cracks. The decrease of zinc signal with the increase of (coating mass/area), i.e., thickness (Table 3.2.3) also reveals that the zinc is coming from the substrate.

Information concerning the surface topography has been obtained using the Talysurf surface measuring instrument which was also used to estimate the thickness of the coatings. The surface profiles obtained across the centres of the Mo-black dip coatings on etched and unetched zinc substrates are shown in Fig.5.3. From the Talysurf scan, the centre line average roughness values have obtained and are given in Table 5.3. It should be mentioned here that the surface profiling stylus used in the measurements had a tip of radius 2.5 μm and hence only features coarser than this would be observed. Table 5.3. shows that the roughness value is higher for coatings prepared on etched zinc substrates.

5.1.3 Mo-black dip coatings on cobalt (NC) substrates

5.1.3.1 Structural and compositional analysis

Due to strong adhesion of the coatings to the cobalt substrates, it was not possible to do any transmission electron microscopy studies. The reflection electron diffraction patterns of these coatings show rings for the cobalt layer only. The interplanar spacing values calculated from the ring diameter correspond to metallic cobalt and cobalt oxide (Table 3.3.2). X-ray diffraction peaks from these coatings are due to the substrate, cobalt and nickel, i.e., both are in the metallic state. A broad low angle peak has also been observed in the X-ray diffraction pattern at about $5^{o}\theta$ (with Co K_{α} radiation) (Fig.3.4.4).

RED patterns show the presence of cobalt oxide with metallic cobalt, whereas, the X-ray study reveals the presence of metallic cobalt only. It is not unusual to have some oxide on the surface of metallic cobalt and (in comparison to X-rays) the electrons penetrate only a relatively short distance into the material (Kittel, 1968).

The results of the XPS study of the coatings on cobalt (NC) substrates have been given in Section 3.5.4. The B.E. of Mo 3d doublet of this coating is 0.5 eV higher than that for coatings on aluminium and zinc. The doublet is also sharper than for coatings on other substrates. From Fig.5.1, the estimated oxidation state of molybdenum is +5.4, which is close to the oxidation state of Mo_4O_{11} (Kennedy, 1972). The coatings on cobalt seem to be more resistant to heat treatment. A small increase in B.E. (0.3 eV) of Mo 3d doublet has been observed after heat treatment in air at $400^{o}C$ for 2 hours. (The Mo 3d peaks are sharper and better resolved (Fig.3.5.29)). After heat treatment inside the spectrometer at

300°C for 2 hours, the Mo 3d doublet shifts by 0.3 eV towards the lower oxidation state. The doublet is somewhat broader which may indicate that some Mo (V) reduces to the lower oxidation state via dehydroxylation (as for coatings on aluminium substrates). Ar^+ bombardment has the same effect on the B.E. of Mo 3d doublet, i.e., it shifts towards the lower binding energy (+4 oxidation state). This is thought to be an etching effect. The marked reduction of the intensity of the Cls level after etching indicates that the carbon is only surface contamination (Fig.3.5.26 and 30). The XPS study of these coatings shows the presence of a small amount of cobalt in the coatings. However, it is not clear whether the cobalt signal is coming from the cobalt underlayer through the cracks in the coatings or is already present in the Mo-black coatings. The ratio of Mo to Co in the coating was found to be 4.55. The ratio of Mo to Co in the present coating is higher than that obtained by Smith and Teytz (1984). They reported that in an outer layer of about 80 nm, the ratio of Mo to Co is 2.0 and after that it becomes 1.18. The higher percentage of Co in their coatings may be due to use of a different plating solution for Mo-black. Instead of nickel sulphate (used in present investigation), they used cobalt sulphate. So it is more likely that cobalt is deposited with molybdenum oxide. They suggested the composition of the coatings is close to $MoCoO_2$ or $MoCo(OH_2)$. It might also be a compound containing Co_2O_3 mixed with a molybdenum oxide. In the present investigation the ratio of Mo/Co/O is found to 1/0.23/2.73 on the surface. The ratio of Mo to O is similar to that in Mo_4O_{11}. After etching 10 minutes by Ar^+ ions the ratio becomes 1/0.21/1.84. After that the ratio of the elements remain approximately constant up to 370 minutes etching (thickness ~ 370Å).

The infrared spectra of the coatings on cobalt (Fig.3.1.10) show the main absorption peaks more or less in the same position (10.5, 11.7 and

14.3 μm) as for coatings on zinc and aluminium. This may indicate that the coatings on cobalt also contain Mo_4O_{11}.

5.1.3.2 Micromorphology

The Mo-black dip coatings on cobalt (NC) substrates have been prepared from the same solution of ammonium molybdate and nickel sulphate as used for the preparation of coatings on zinc. However, the solution temperature is comparatively high (60-80°C) as described in Section 2.1.2.5. A wide range of surface microstructures of such coatings have been observed by varying the preparation conditions of Mo-black as well as initial cobalt layer (Section 3.2.3). This leads to a corresponding variation in the thermal radiative properties of the coatings. The morphology of the coatings seems to replicate the structure of the plated cobalt layer which changes with the plating current density and solution temperature. In the present investigation three different types of surface structure have been observed:

(a) After plating at a solution temperature of 50-60°C the surface of the cobalt layer has platelet structures of different sizes orientated in different directions (Fig.3.2.56) and almost perpendicular to the substrate. The Mo-black coatings on this cobalt surface consist of limb like structures oriented randomly, forming microcavities on the surface (Fig.3.2.53). These features become thicker when the cobalt plating current density deposition time are increased.

(b) By using an addition agent (Na-lauryl sulphate) in the plating solution of cobalt, the surface structure of the cobalt can be modified into a rather smooth surface. (This has a brighter appearance). An SEM micrograph shows that the platelets are less densely distributed and also

shows small flake-like protruberences (Fig.3.2.58). Mo-black coatings on this type of cobalt have a nodular structure (Fig.3.2.57). However, the surface of the coating changes to a rather smooth platelet structure (Fig.3.2.60) when prepared at a high temperature (80^{o}C) and/or for longer times of deposition. This smooth surface is probably due to the high thickness of the coatings.

(c) The cobalt layer prepared at a comparatively low temperature (45^{o}C) and with low current density (~25mA/cm^{2}) consists of a large number of small flake like protruberences. The Mo-black coatings prepared on this type of substrate have nodules of submicron size (Fig.3.2.62).

The surface profiles were obtained from the Talysurf instrument for Mo-black coatings on two types of cobalt (NC) substrate, i.e., plated with and without addition agent. These are shown in Fig.5.4. The CLA roughness values of the coatings are given in Table 5.3. It can be seen that the roughness value of the coating decreases from 0.3 μm to 0.13 μm after using the addition agent in the plating solution of cobalt.

5.2 Thermal radiative properties of Mo-black coatings and their relation to other properties

5.2.1 Electrodeposited coatings on aluminium

The electrodeposited coatings are effectively non-selective. Although these coatings exhibit moderate absorptance (0.86 - 0.87), the attainable selectivity is 1.4 - 1.9 (Section 3.1.3). As the coating mass per unit area (i.e., thickness) increases, both the solar absorptance α_s and thermal emittance ε_{th} increase. The emittance is more strongly influenced by coating thickness than is absorptance (Fig.3.1.18).

The spectral reflectance spectra (Fig.3.1.17) show that the coating has strong absorption (0.90 - 0.91) in the visible region and in this region the reflectance does not change significantly with thickness or wavelength. In the near-infrared (NIR) region the reflectance increases with wavelength and also becomes thickness dependent. It can be seen that the transition between low reflectance and high reflectance takes place around 0.9 - 1.1 μm. This cut off wavelength slightly shifts towards higher wavelengths with increase of coating thickness. According to Fosch (1956) and Christie (1970), the onset of linear increase of the reflectance can be taken as a measure of the forbidden energy gap E_g. For coating of the optimum properties the abrupt transition has been observed at about 1.1 μm which corresponds to an energy gap of 1.13 eV. High absorption occurs when the incident photon energy is sufficient to excite the valence electrons into the conduction band. Photons containing less energy than the gap energy will not be absorbed. This accounts for the abrupt transition in absorption in the near infrared region.

The forbidden energy gap E_g of the coating material has also been estimated according to Kubelka-Munk (K-M) theory (1938, 1948). According to K-M theory, the total diffuse reflectance from a semi-infinite layer of material R_∞ will be related to the ratio α/s as follows:

$$\alpha/s = F(R_\infty) = \frac{(1 - R_\infty)^2}{2 R_\infty} \qquad (5.1)$$

where α and s are the absorption and scattering coefficients respectively. $F(R_\infty)$ for any reflectance is called the Kubelka-Munk function.

K-M theory has been successfully used to estimate the absorption edge of

powder and polycrystalline samples (Nozik, 1972; Hanafi et al, 1981; Golestani-Fard et al, 1983). Waring and Hzu (1983) have used the diffuse reflectance technique to study the absorption edge in pigments. A few reports have also been found on use of diffuse reflectance of thin films to study the absorption edge (De Chelle et al, 1984; Al-Ani, 1984; Tandon and Gupta, 1970).

Fig.5.5 shows plots of the K-M function $F(R_\infty)$ as a function of of a thick Mo-black coating (~8 μm) prepared on a rough aluminium substrate. According to Tandon and Gupta (1970) the energy co-ordinate of the point on low energy side of the curve at which the linear increase in $F(R_\infty)$ starts is the value of the forbidden energy gap of the material. The point at which the linear variation in $F(R_\infty)$ (i.e., increase of α) starts gives the value of E_g (as the absorption starts when the incident photon energy $h\nu$ is sufficient to excite the valence electrons into the conduction band i.e., $E_g = h\nu$). For Mo-black coatings (Fig.5.5), the estimated value of E_g is about 0.85 eV. The wavelength corresponding to this bandgap energy is 1.46 μm. Therefore the incident photons with energy higher than 0.85 eV should be highly absorbed in the coatings and the photons with energy less than 0.85 eV should not be absorbed. The reflectance spectra of the coatings (Fig.3.1.17) show an abrupt transition at a lower wavelength (~ 1.1 μm). The absorptance of the coating can be increased if by some means, the absorption edge can be shifted to a higher wavelength (~ 2.5 μm) (Lampert 1979).

The nonselectivity of the electrodeposited Mo-black coatings is mainly due to their high emittance value (0.4 - 0.7). It has been suggested by Smith et al (1983) that to get high selectivity values, the absorbing film thickness should not be greater than 1-2 μm, unless the films are very porous. In the present investigation, the thickness of the Mo-black

coatings on aluminium substrates is greater than 2 μm. Due to the high thickness, strong absorption bands in the infrared region have been observed in the reflectance spectra of the coating (Fig.3.1.19). The absorption bands around 2.9 - 3.1 μm and at 6.2 μm give evidence for the presence of water (Nakamoto, 1970). A very broad and strong absorption band in the region 10.1 - 22 μm (975-450 cm^{-1}) is due to the absorption in the coating material. (These peaks are absent in the IR spectra of thin Mo-black coatings on zinc and cobalt substrates (Section 3.1.1 and 3.1.2).

The results obtained from electrodeposited Mo-black coatings are consistent with the results obtained by Hosseini (1981). The Mo-black coatings prepared on copper substrates studied by INCRA (1977) exhibited less selectivity. The absorptance of these coatings varied between 40 - 60% and thermal emittance in the range 30 - 70%. Potdar et al (1982) prepared Mo-black coatings on nickel plated copper substrate by the electrodeposition method and reported moderate absorptance (85%) and a low thermal emittance (11%). The low emittance of this coating was said to be due to the low thickness ~ 0.1 μm.

The radiative properties of Mo-black film prepared by the chemical vapour deposition (CVD) method (Carver, 1979, Chain et al, 1980, 1981) are quite different from those of the electrodeposited coatings. The CVD Mo-black film exhibits a solar absorptance of 0.77 and a thermal emittance of 0.44. Post deposition annealing in a reducing atmosphere and overcoating with Si_3N_4 increases the absorptance to 0.82 and also reduces the emittance to 0.08 (Carver, 1979). The abrupt changes in the thermal emittance during annealing are explained by Carver (1979) as being due to a large increase of electrical conductivity together with structural changes. The composition of the Mo-black film prepared by the CVD method is quite different from that prepared by electrodeposition methods. Films prepared

by CVD consist of an MoO_2 matrix with smaller Mo-inclusions, i.e., a cermet. Coatings prepared by electrodeposition are mainly oxides of molybdenum. According to Potdar et al (1982) Mo-black consists of MoO_3. Smith et al (1981) suggested that the coatings consist of $MoO_2.2H_2O$. From the present investigation it is concluded that the coatings may contain Mo_4O_{11} (Section 5.1.1) together with water. The non metallic portion of MoO_2 in the CVD film is a conducting oxide but the Mo-oxide in the present study is found to be a high resistance semiconductor (Section 3.6). However, the radiative properties of the present coatings are comparable with those of as-deposited CVD films ($\alpha_s/\ \varepsilon_{th}$ = 0.87/0.6 and 0.77/0.44 respectively). During annealing in the reducing atmosphere, the oxide MoO_2 of CVD films partially reduces to Mo-metal which can suppress thermal emittance drastically. In the present coatings, there is no evidence of the presence of metallic Mo or any other metal, which could enhance the IR reflectance. The coatings therefore exhibit a high emittance due to high thickness. The presence of a large amount of water, (Fig.3.1.19), is also another reason for high emittances.

The surface topography of the electrodeposited Mo-black coatings (Section 3.2.1) corresponds to a rather smooth platelet structure. No surface features exist on the scale of the wavelengths of interest which would enhance absorption by multiple reflection. As these coatings are relatively thick compared to the wavelength of solar radiation, no interference peaks have been observed in the reflectance spectra which could enhance the absorption. However, the wavelength dependence of the optical constants of the coating might contribute to the wavelength selectivity of reflectance. According to Williams et al (1963) for a thick homogeneous coating (when the interference effect is absent), the reflectance is given by:

$$R_\lambda = \frac{R_{c\lambda} + R_{m\lambda}(1-2R_{c\lambda})e^{-2a_{c\lambda}d}}{1 - R_{m\lambda}R_{c\lambda}e^{-2a_{c\lambda}d}} \qquad (5.2)$$

where $a_{c\lambda}$ = absorption coefficient of the coating

d = coating thickness

$R_{c\lambda}$ = normal spectral reflectance at the air coating interface

R_λ = normal spectral reflectance of the coated surface.

$R_{m\lambda}$ = normal spectral reflectance at the coating-metal interface

The reflectances $R_{c\lambda}$ and $R_{m\lambda}$ at normal incidence are related to the coating and metal optical constants as follows:

$$R_{c\lambda} = \frac{(n_{c\lambda} - 1)^2 + k_{c\lambda}^2}{(n_{c\lambda} + 1)^2 + k_{c\lambda}^2} \qquad (5.3)$$

$$R_{m\lambda} = \frac{(n_{c\lambda} - n_{m\lambda})^2 + (k_{m\lambda} - k_{c\lambda})^2}{(n_{c\lambda} + n_{m\lambda})^2 + (k_{m\lambda} + k_{c\lambda})^2} \qquad (5.4)$$

where $n_{c\lambda}$, $n_{m\lambda}$ = the refractive index (real part) of the coating and the metal respectively.

$k_{c\lambda}$, $k_{m\lambda}$ = the extinction coefficient of the coating and metal respectively.

Since for a thick film $R_\lambda = R_{c\lambda}$, the value of refractive index $n_{c\lambda}$ of the coating can be estimated from the reflectance data using equation (5.3). For semiconductors, in most cases $n_{c\lambda} > k_{c\lambda}$. Hence $n_{c\lambda}^2 >> k_{c\lambda}^2$ (Moss et al, 1973). Therefore, to calculate $n_{c\lambda}$ from equation (5.3), the contribution of $k_{c\lambda}$ to the reflectance $R_{c\lambda}$ was assumed to be negligible.

Fig.5.6 shows the variation of $n_{c\lambda}$ with the wavelength of a Mo-black coating of thickness of about 6 μm. It may be observed that the value of $n_{c\lambda}$ is constant up to about 1 μm and is equal to 1.85. According to Williams et al, (1963) one requirement for low reflectance in the solar region is a low coating refractive index (n<2). However, for this coating, it can be seen that the value of $n_{c\lambda}$ rises rapidly from 2.0 at 1.2 μm up to 5.88 at 2.5 μm. This rapid rise of $n_{c\lambda}$ in the NIR region may be responsible for limited absorptance (0.87) of this coating. An increase of $n_{c\lambda}$ with the increase of wavelength in the solar region has also been found by Fan (1978) in MgO-Au selective absorber.

5.2.2 Dip coatings on zinc substrates

Mo-black dip coatings on mechanically polished zinc substrates exhibit a low thermal emittance of about 0.1. The thickness of the Mo-black dip coatings is estimated to be in the range 0.1 to 0.6 μm. Such a thin coating is almost transparent to longer wavelengths. The thinner coating, therefore, may have an emittance value close to the emittance of the polished metal substrate. By using highly polished zinc substrates (1 μm finish), emittances as low as 0.06 to 0.09 have been achieved (Section 3.1.1). However, the emittance increases with increase of coating thickness (as shown in Fig.3.1.6(b)), due to the decrease of transmittance in the IR region. The absorption peaks in the region 10.5 to 22 μm due to the coating material can be seen in the reflectance spectra of a thicker coating (Fig.3.1.4). These do not appear in the spectra of a thin coating (Fig.3.1.4). Such IR absorption bands together with the absorption band due to water increase the emittance of thicker coatings.

The results obtained from coatings on polished zinc substrates (Table

3.1.2.b) show that although these coatings exhibit a high selectivity factor (in the range 7 - 9) the absorptance of the coatings is comparatively low (0.70 - 0.78). Interference peaks can be seen in the reflectance spectra of the coating in the solar region (Fig.3.1.1), especially for thinner coatings. The refractive index n has been calculated from the interference fringes by using the formula

$$2nd = \frac{\lambda_1 . \lambda_2}{\lambda_1 - \lambda_2} \qquad (5.5)$$

where d is the coating thickness and λ_1 and λ_2 are the wavelength of two adjacent maxima (Moss et al, 1973). The values of n estimated using equation (5.5) are tabulated in Table 5.4(a). From this table it seems that the refractive index decreases as the coating thickness increases. Except for the thinnest coating, the values of n are found to be 3.5 and 4.5 at wavelength ~ 0.95μm. Such a high refractive index would cause high reflection losses in the front surface, resulting in low absorptance.

The reflectance spectra of the dip coatings (Fig.3.1.1)show an abrupt transition around 0.9 - 1.1 μm. As in the case of electrodeposited coatings, this is possibly related to the bandgap of coating materials (Section 5.2.1). These coatings also have high absorption (0.80 to 0.90) in the visible region. These results are comparable with the results obtained by Hosseini (1981).

For a coating of high thickness, (where no interference peaks are observed in the short wavelength region (below 0.7 μm)), the equation (5.2) has been used to obtain a theoretically calculated value of reflectance. In equation (5.2), $R_{C\lambda}$ - the reflectance at the air-coating interface has

been assumed to be equal to the reflectance from a thick coating. The value of absorption coefficient $a_{c\lambda}$ has been taken from the transmission measurements. The reflectance $R_{m\lambda}$ of the metal substrate has been calculated by using equation (5.4). (The values of the extinction coefficient $k_{m\lambda}$ and refractive index $n_{m\lambda}$ of the zinc substrate were taken from Gray (1972)). The experimental and predicted value of reflectances at two different wavelengths 0.4 and 0.7 μm for two coatings are given in Table 5.4(b). The detailed calculation is given in Appendix G. It can be seen that the calculated values are in good agreement with the experimental values. This may indicate that the influence of the substrate on the absorptance of the coating is negligible.

Several schemes have been used to enhance the solar absorptance of selective surfaces: (1) surface roughening (Gilbert et al, 1978); (ii) porous surface (Williams et al, 1963); (iii) antireflection top coatings (Seraphin, 1976); (iv) cermet type coatings (Fan, 1978) and combinations of these. In the present work an attempt has been made to reduce the reflectance of the Mo-black dip coatings by etching the zinc substrate prior to coating deposition. It has been observed that by using etched zinc substrates the absorptance of the coating can be increased by 14% without increasing the emittance significantly. The reduction of the surface reflectance may be attributed to the surface morphology of the coatings which develops after deposition on etched zinc substrate. The spectral reflectance spectra of these coatings are displayed in Fig.3.1.2. The results are given in Table 3.1.2(a). The solar absorptance of these coatings is 0.86 - 0.87 with a selectivity factor 6.1 to 6.7. As described in section 3.2.2 the surface of the coatings prepared on etched zinc substrates consists of a large number of nodules of different sizes ranging from 0.5 to 2 μm. This surface structure may reduce the front surface reflection and also may cause multiple reflection of incident

light resulting in high absorptance in the coating. No interference peak appears in the reflectance spectra except for the thicker coatings where interference peaks appear in the NIR region. The absence of an interference peak in these coatings may be due to the surface morphology as explained by McMahon and Jasperson (1974). They reported that due to surface morphology, the reflection from the front surface of a PbS film does not obey the Fresnel equation and consequently the interference is not complete.

The thickness of the coating has been found to be critical to get maximum solar absorptance. As shown in Fig.3.1.6.(a) the absorptance first increases sharply with coating thickness and attains a maximum value (0.87), at this point the thickness of the coating is estimated to be in the range 0.15 - 0.25 μm. After this the absorptance decreases slightly and then again goes back to the maximum value (0.87) and remains constant. SEM studies reveal that as the coatings get thicker, the surface becomes smoother. The disappearance of the textured surface may be responsible for the slight decrease in absorptance after a critical coating thickness is reached. When the coating gets thicker, then the absorptance again increases slightly due to the thickness of the coatings.

As the surface roughness of the coating is of the order of solar radiation wavelengths, it does not affect the emittance value significantly. The thinner coatings seem to be transparent in the IR region and as the coating thickness increases, emittance increases due to IR absorption as explained in previous section.

The radiative properties of the coatings on etched zinc appear to be very sensitive to the etching conditions, e.g., time of etching, agitation, concentration of etchant (HNO_3). The effect of concentration of HNO_3 on

the radiative properties is shown in Fig.3.1.3. An SEM micrograph (Fig.3.2.41) shows that when zinc was etched with 50% HNO_3, nodules agglomerate to form large ridges in a definite direction, which increases the surface roughness. The resulting coating exhibits a high absorptance (0.89) as well as high emittance (0.3).

The use of surface roughness to provide partial solar selectivity has been previously discussed by Tabor (1956). This technique can be used to enhance the solar selective properties of almost any selective surface (Petit and Sowell, 1976; Sikkens et al, 1983).

The reflectance of a surface is a sensitive function of its roughness. The reflection of normally incident radiation from a rough surface consists of two components; one is specular reflection and the other is diffuse reflection or scattering. Thus the radiative properties of a rough surface differ from those of a smooth surface predicted by the electromagnetic theory. The relation between reflectance and root mean square (rms) roughness was derived by Davies (1954) from the statistical treatment of the reflection of electromagnetic radiation from a rough conducting surface. According to Davies, for a perfect conductor, the specular component of reflectance from a rough surface reduces, for the case of normal incidence, by a factor of exp $(-4\pi\sigma^2/\lambda^2)$. Since no material is perfectly conducting, this is modified by Bennett and Porteus (1961), so that for an actual metal surface, the specular reflectance at normal incidence is given by

$$R_s = R_o \exp\ (-4\pi\sigma^2/\lambda^2) \qquad (5.6)$$

where R_s is the specular reflectance of the rough surface, R_o that of a perfectly smooth surface of the same material, σ the rms roughness of the

surface and λ the wavelength.

The value of R_s for a Mo-black coating (thickness ~ 0.2 μm) on etched zinc substrate has been calculated using the value of CLA roughness (Table 5.3) by applying the equation (5.6). The calculated value of R_s is compared to the experimental value (Table 5.4(c)). Although the Davies theory is strictly applicable to electrical conductors, the calculated and experimental values of R_s show fair agreement. Torrance and Sparrow (1965) successfully applied the Davies theory to specular reflectance of a non-conductor (polycrystalline magnesium oxide). The observed discrepancy between the calculated and experimental values of R_s (Table 5.4(c)) could be attributed to the following reasons: (i) the surface profiling stylus used in the measurement for roughness had a tip of radius 2.5 μm, and hence only features coarser than this would be observed. (ii) instead of rms roughness value, CLA roughness value was used in the present work and usually rms roughness value is higher than the CLA value (Dagnall, 1980).

The Davies theory could not be applied to longer wavelengths due to the presence of IR absorption bands. It is evident from equation (5.6) that as the wavelength increases, the exponential term increases and R_s/R_o tends to unity. This indicates that at higher wavelengths, the surface roughness of Mo-black coating does not affect its specular reflectance and thus the emittance of the coating does not increase significantly after using an etched zinc substrate, which increases the absorptances.

The bandgap E_g of Mo-black dip coatings on etched zinc has been estimated from the reflectance data using the Kubelka-Munk (K-M) theory. Fig.5.7 shows plots of K-M function $F(R_\infty)$ as a function of wavelength for Mo-black dip coatings on etched zinc substrates of two different thicknesses. The

estimated values of E_g obtained are 0.89 and 0.91 eV for coating thicknesss 0.18 and 0.84 μm respectively. The values of E_g do not change significantly with coating thickness and are nearly the same as for electrodeposited Mo-black coatings.

It may be concluded therefore that the high absorption in these coatings is due to the band gap of this semiconducting oxide coupled with surface morphology which reduces the front surface reflections.

5.2.3 Mo-black dip coatings on cobalt (NC) substrates

Mo-black coatings on electroplated cobalt (NC) substrates have higher selectivities than the coatings on zinc or aluminium substrate. These coatings exhibit a high solar absorptance (0.90 - 0.94) with low thermal emittance. Table 3.1.6 - 9 show results obtained from the coatings on cobalt substrates. The radiative properties (α_s, ε_{th}) of these coatings are sensitive to the parameters used in the initial cobalt plating and also in the deposition of Mo-black. With the variation of deposition conditions, the surface structure of the coatings changes as described in section 3.2.3, which in turn changes the optical response of the coatings. The spectral reflectance spectra (Figs.3.1.7 and 3.1.15) of the optimum coatings show that the coatings are very good intrinsic absorbers. The coatings exhibit low reflectance throughout the solar region. No interference peaks involving the substrate have been observed, especially in the visible region (Fig.3.1.7 and Fig.3.1.12). The high absorptance of the coatings are mainly due to surface morphology. The presence of front surface relief and high porosity of the coatings and underlying cobalt layer reduces drastically the front surface reflections giving high absorptance. Assuming that the coatings have negligible k (imaginary part of refractive index; Moss et al, 1973) the real part of refractive index n

can be calculated using equation (5.3). The estimated value of n is 1.5 to 1.8. The values of n of these coatings are comparable with the values obtained by Smith and Teytz (1984) for Mo-Co coatings. They estimated the porosity level of the coatings to be ~ 30% by volume. However, in the present study, the results (α_s, ε_{th}) obtained from the coatings prepared at a solution temperature of 80°C are comparable with the results reported by Smith and Teytz (1984). It has been observed that the coatings prepared at a solution temperature of 60°C give better selectivity (Table 3.1.8). With the increase of solution temperature, the absorptance of the coatings decreases; this may be due to the increase of coating thickness, which diminishes the substrate effect. The increase of thickness as well as smoothness of the coating with the rise of solution temperature is also revealed by SEM micrograph (Fig.3.2.60). It is also observed that as the coatings become smoother (owing to their comparatively high thickness), interference peaks appear in the NIR region (Fig.3.1.13), similar to the spectra obtained by Smith and Teytz (1984). With the increase of thickness the emittances of the coatings also increases (Table 3.1.8). A similar effect is also observed with increase of deposition time at a constant solution temperature, which can be explained in the same manner.

With high absorptance these coatings also exhibit low thermal emittance (~0.10). The substrate metallic cobalt may lead to an increase of IR reflectance. The actual thickness of the coating is not known. However, the IR reflectance spectra (Fig.3.1.10.(a)) reveals that the coatings are thin enough to be transparent in the IR region. Thus the emittance of the optimum coatings (0.1 - 0.13) are close to the emittance of the plated cobalt substrate (0.09). However, for thicker coatings (prepared at 80°C), small IR absorption peaks at about 10.5, 11.6 and 14.3 μm can be seen in the IR reflectance spectra (Fig.3.1.13.(b)). These absorption peaks together with the absorption peaks of water (~2.9 and 6.2 μm) reduce

the IR-reflectance of the coating. As a result emittance increases. Similar effects were observed for coatings on zinc substrates (5.2.2).

Higher emittance values (0.22 - 0.30) have been obtained for the coatings prepared on cobalt plated without addition agent and at a higher temperature 56 to 60^{o}C (Table 3.1.6). These high emittance values are mainly due to the surface microroughness (Fig.3.2.53-54). As mentioned in Section 5.1.3, the average roughness value for these coatings is higher than for coatings prepared on cobalt plated with addition agent (Table 5.3). However, this microroughness enhances the solar absorptance of the coating to 0.94, possibly due to multiple reflection.

5.3 Efficiency of Mo-black coatings when used as solar selective absorbers

The efficiency η of a solar selective surface can be defined (Neal and Musa, 1982) as

$$\eta = \frac{\text{absorbed flux - emitted flux}}{\text{solar insolation}}$$

For a surface of absorptance α_s and thermal emittance ε_{th},

$$\text{the absorbed flux} = \alpha_s I$$

$$\text{and the emitted flux} = \varepsilon_{th} \sigma \ (T_s^4 - T_\omega^4)$$

where I is the solar insolation, T_s is the surface temperature, T_ω is the temperature of the enclosure wall and σ is the Stephan-Boltzmann constant. The efficiency of Mo-black coatings on different substrates has been calculated at a temperature of 100^{o}C with an insolation of 800 watt/m^2.

The calculated values of η are tabulated in Table 5.5. From this table it can be seen that the Mo-black coating on cobalt (NC) (plated with addition agent) has the highest efficiency (82.5%). Table 5.5 also shows that although the selectivity factor ($\alpha_s / \varepsilon_{th}$) is higher for Mo-black coatings on highly polished zinc substrates than the coatings on an etched zinc (30% HNO_3) substrate, the latter hasahigher efficiency (76%) than the former (68.2%). It indicates that the selectivity factor is not the only primary factor to identify a good selective surface. Seraphin (1979) also reported that under nearly all conditions, a surface with $\alpha_s = 0.5$ and $\varepsilon_{th} = 0.05$ will, in overall efficiency, be inferior to a surface with $\alpha_s = 1.0$ and $\varepsilon_{th} = 0.10$, although both are characterized by the same selectivity factor $\alpha_s / \varepsilon_{th}$. Electrodeposited Mo-black coatings on aluminium substrates have the lowest efficiency (34%). The efficiency of Mo-black films prepared by different methods as reported in the literature has been calculated and included in table 5.5 for comparis-on with the efficiency of the Mo-black coatings in the present investigation. By comparing the efficiency of all types of Mo-black coatings, it is observed that the coatings on cobalt (NC) substrates in the present study have the highest efficiencies and the efficiency of the coatings on etched zinc substrates is also comparable to that in the literature. However, it should be mentioned that a comparison between the different Mo-blacks described in the literature is difficult. The calculation method of α_s and ε_{th} varies from one author to another. This can lead to discrepancies in the values of α_s and ε_{th} and as a result in the values of efficiency η .

5.4 Stability of Mo-black coating properties at elevated temperatures

5.4.1 Coatings on zinc substrates

The stability of Mo-black dip coatings on etched zinc substrates has been

examined by thermal ageing test and outdoor ageing test. Data for solar absorptance α_s and thermal emittance ε_{th} of the coatings after different heat treatment are given in Table 4.1 - 4.4. In general no significant change in the reflectance spectra has been observed after heat treatment at 100 and 150°C. For most coatings the absorptance decreases after heat treatment at 200°C in air (especially for thinner coatings). There are slight increase in reflectance in the visible region, which is compensated by the slight decrease in reflectance in the NIR region (Figs.4.1 - 4.4). As a result the values of α_s remain effectively unchanged. The emittance of the coatings also remains effectively unchanged after heat treatment and in some cases decreases. The decrease in emittance may be due to loss of water. The water absorption peak reduces significantly after heat treatment (Fig.4.3). At a higher temperature (300°C), the water absorption peak completely disappears (Fig.4.7). No change has been identified by visual inspection. The SEM micrographs also show no noticeable difference after heat treatment at 100 and 200°C except that cracks are much wider (Figs.4.15 and 4.16). Heat treatment at 300°C leads to dramatic changes in the reflectance spectra of the coatings (Figs.4.5 and 4.6) i.e., the reflectance increases significantly in the UV and visible region. Reduction in the reflectance occurs simultaneously in the NIR region, resulting in no change in the solar absorptance. In some cases the value of α_s increases (Table 4.2) and the coatings have a darker appearance. The SEM micrograph (4.17) does not show significant difference in the surface morphology except that the cracks become wider. It also seems that the nodules are less densely distributed and become flattened which may explain the increase of reflectance in the short wavelength region. The decrease of reflectance in the NIR region is not clearly understood.

The same characteristic reflectance has been observed when coatings are

heat treated in vacuum. The results for the vacuum heat treated coatings have been given in Table 4.3-4. No degradation of the radiative properties (α_s, ϵ_{th}) of the coatings has been observed apart from those of coatings prepared on 50% HNO_3 etched zinc. For this coating, the solar absorptance first decreases slightly and then remains constant after further heat treatment. This is thought to be due to reduction of surface roughness (Fig.4.19). The emittance of the coating also decreases. In fact, the emittance of the coating decreased in all cases, for heat treatment in vac-uum at temperatures 200 to 300°C. The presence of nickel in the coating (shown by XPS and EPMA studies) could be responsible for this reduction of emittance (Section 3.5.3 and 3.2.2). It has been reported by Kim and Winograd (1974) that after annealing in vacuum at a temperature of 200-300°C, $Ni(OH)_2$ changes to NiO via dehydration and finally reduces to metallic Ni. This metallic nickel together with the loss of water could enhance the IR reflectance resulting in a decrease in emittance after annealing.

5.4.2 Mo-black coatings on cobalt (NC) substrates

The Mo-black coatings on cobalt (NC) substrates have been heat treated in air up to a temperature of 400°C. The results are given in section 4.2. There is very little change in the radiative properties of the coatings. The solar absorptance decreases only 1.1% at temperatures of 300 and 400°C respectively. At 200°C, there is a decrease of 2.2% in solar absorptance. No change in the physical appearance has been observed. The coatings on cobalt plated without addition agent seem to be more stable to heat treatment. The emittance of these coatings decreases at all temperatures. This may be due to the decrease of surface roughness as revealed from SEM micrograph (Fig.4.25) and also due to dehydration. The coatings on cobalt plated with addition agent show increases in emittance

after heat treatment. No significant change in the morphology has been observed apart from the cracks are somewhat wider. The IR reflectance spectrum (Fig.4.24) shows that, although the reflectance increases slightly in the short wavelength region due to loss of water, in the longer wavelength region, the reflectance decreases, resulting in an increase in emittance.

5.5 Electrical properties of Mo-black coatings

The current-voltage (I-V) characteristics of electrodeposited Mo-black coatings shown in Fig.3.6.1 reveal non-ohmic behaviour in the high field region (above 10^6V/m). Non-ohmic behaviour in metal-insulator-metal devices is usually explained by the following mechanisms: (i) Tunnelling; (ii) Space-charge limited conduction (SCLC); (iii) Schottky emission and (iv) Poole-Frenkel emission. The description of these mechanisms are given briefly in Appendix E. It is possible for more than one conduction mechanism to be operating at one particular voltage but generally one mechanism dominates.

In the present coating, the possibility of tunnelling can be ruled out due to the high thickness of the coatings (> 3 μm). The SCLC has been rejected as the slopes of the LogI vs logV curves (Fig.3.6.1) for all samples are less than two. It is known that for SCLC, the current is proportional to V^2 (Simmons, 1971).

The analysis of the I-V data of the coatings as presented in section 3.6.1 closely agrees with the Poole-Frenkel conduction mechanism. The results obtained in the present investigation are different from the results obtained by Hosseini (1981). He suggested that the conduction mechanism in the electrodeposited Mo-black coatings is of Schottky emission type.

In the present analysis Schottky emission has been ruled out for the following reasons: (1) For the Schottky effect the linear part of lnI vs $V^{1/2}$ plots for the same electrode material of different sample thickness should pass through a single point but this is not found in the present case (Fig.3.6.2). (ii) The I-V characteristics at room temperature using two different types of electrode material (Al and Cu) are identical (Fig.3.6.3) which indicates that the conduction mechanism is independent of electrode material. (iii) The calculated value of relative dielectric constant with the assumption of Schottky emission is rather low and not comparable with the value obtained from the a.c. measurements. However, the high frequency dielectric constant is comparable with the relative dielectric constant calculated with the assumption of Poole-Frenkel emission (Table 3.6.1). (iv) The experimental values of β_{exp} calculated using equation (3.6.3) agree better with the values of β_{PF} rather than β_s (Table 3.6.1). Considering the above features, it seems that the conduction mechanism of the electrodeposited Mo-black coating is dominated by Poole-Frenkel emission. The electrical properties of vacuum deposited MoO_3 film have been studied by Nadkarni and Simmons (1972) in the thickness range 0.22 to 1.1 μm. They reported that the conduction process of MoO_3 film is Schottky type below 0.6V and is bulk limited for V > 0.6V.

The I-V characteristics at different temperatures (Fig.3.6.5) show that the conductivity of the coating increases with temperature indicating semiconducting properties. At higher temperature, the current is an exponential function of temperature and the thermal activation energy associated with this process is about 0.56 eV. In the room temperature region the activation energy is found to be low (~0.13 eV). According to the model of the density of states for disordered material (Appendix F) hopping conduction and free band conduction occur in a disordered material depending upon the operating temperature, (Mott and Davis, 1979). At low

temperatures, there will be insufficient energy to excite electrons into the conduction band and the dominating mechanism will be hopping of electrons from one site to another within the localized states. As the temperature is increased, there will be a transition from hopping to free band conduction over some temperature range. As the band edges for disordered materials are not sharp, this transition is gradual, which accounts for the curvature in the logI vs 1/T plots (Fig.3.6.6). If the measurements could be extended below the room temperature region, another linear region in the logI vs 1/T plots is expected which would probably be associated with a very low activation energy indicating hopping conduction.

The conductivity of the coating increases after annealing at high temperatures in vacuum. It is known from XPS and EPMA studies that the coating contains nickel hydroxide. Annealing in vacuum at high temperature changes nickel hydroxide to nickel oxide via dehydration. It may finally reduce to metallic nickel (Kim and Winograd, 1974). The metallic nickel may produce excess donor centres in the matrix and increase the carrier concentration resulting in an increase of electrical conductivity. The removal of water molecules during heat treatment may also account for the increase of conductivity.

The relative dielectric constant ε_r of the coating has been calculated from capacitance measurements at different temperatures (20 to 150^{o}C) in the frequency range $5X10^{2}$ to $2X10^{4}$ Hz. The values of ε_r decreasesslightly with the increase of frequency and attain a nearly constant value in the range 3.5 to 4 at higher frequencies (Table 3.6.3). The presence of water may influence the capacitance of the coating. It has been observed that the capacitance increases with the rise of temperature up to 100^{o}C and then decreases on further increase in temperature. The decrease of

capacitance could be due to the removal of water molecules. Similar results have been found by Chandrashekar and Hari Babu (1984) for a vacuum evaporated CeO_2 film and Morley and Campbell (1968) for a silicon oxide film. According to them, the capacitance decreases at certain temperature because of the removal of absorbed gas molecules and defects.

5.6 Presence of water in Mo-black coatings

The IR spectra of Mo-black coatings (Figs.3.1.3 and 3.1.4) show that the coatings contain water. The evidence for the presence of water in the coatings is also obtained from capacitance measurements at higher temperatures (Section 5.5). The presence of H_2 in the coatings was confirmed by Butterworth Laboratories Ltd. According to their analysis, the presence of H_2 in the coatings is 2.12% (by mass) (Report 1).

Water in the coatings may be present as lattice water (physisorbed) or co-ordinated water (chemisorbed). There is no definite border line between the two. However, for Mo-black coatings, the shape and position of the IR absorption bands suggests that the water contained in the coatings is most probably lattice water. The IR spectra show strong broad absorption bands in the 2.8 to 3.1 μm region. These are assigned to the OH stretching vibration of lattice water and at about 6.2 μm for HOH bending vibrations (Nakamoto, 1970). The hydroxyl ion (OH) is characterized by a sharp band at a lower wavelength (2.7 to 2.8 μm) than the OH stretching bands of water (Nakamoto, 1970). This is not found in the IR spectra of Mo-black coatings.

The IR spectra of the heat treated coatings also suggest that most of the water in the coatings is physisorbed. After heat treatment of the coatings at 100 and 200°C the absorption band at 6.2 μm completely

disappears and the band at 2.8 to 3.1 μm is significantly reduced (Figs.4.3 and 4.7). Both of these absorption bands disappear after heat treatment at 300°C (Fig.4.7 and 4.13). Gregg and Sing (1982) reported that physisorbed water is removed by prolonged outgassing at a temperature below 100°C, ligand water is progressively removed at temperatures ranging between 100 and 300°C whilst hydroxyl groups are driven off between 300 and 500°C. For Mo-black coatings all water absorption bands disappear after heat treatment at 300°C and it can therefore be concluded that water in the coatings is not chemically bonded. The presence of water in the coatings was also reported by Hosseini (1981) on the basis of a thermogravimetric test. Most of the weight loss of the coating was found in the temperature below 300°C and this also suggests that the water is physisorbed.

5.7 Band gap and optical constants of Mo-black coatings

The absorption spectra of electrodeposited Mo-black coatings of thickness in the range 0.23 to 0.50 μm are shown in Figs.3.7.1 and 3.7.2 in the wavelength range 0.3 to 0.8 μm. The absorption edges in these spectra are exponential in nature indicating the presence of localized states in the mobility gap of the coating material. This could be due to the lack of long range order or defects in the structure. The absorption coefficient α calculated using equation 3.7.1 is in the range 10^4 to $10^5 cm^{-1}$.

The plots of $(\alpha \hbar\omega)^{1/2}$ vs $\hbar\omega$ (Fig.3.7.3 and 3.7.4) show good straight lines in the high absorption region and thus satisfy equation (3.7.2) for indirect transitions (Mott and Davis, 1970) (Section 3.7). The values of the optical band gap E_{opt} determined from the extrapolation of the linear portions to $(\alpha \hbar\omega)^{1/2} = 0$ are given in Table 3.7.1

Table 5.6 compares the value of band gaps of the coatings determined by different methods. It can be seen that there is large discrepancy between the values of band gap determined from transmission and reflectance measurements. This discrepancy could be attributed to the different preparation conditions and large thickness difference. The coatings for transmission measurements were prepared at a comparatively low temperature ($50^{o}C$) on thin semitransparent vacuum evaporated Al-film. The thickness of these coatings was in the range 0.23 to 0.5 μm and the colour yellow to light green. In contrast, the coatings used in the reflectance measurement were almost black and of high thickness (6 to 8 μm). (These coatings were prepared on rough Al-sheetat a temperature of about $65^{o}C$). The different solution temperatures could change the rate of deposition (Hosseini, 1981), resulting in a shift in the optical band gap. It was shown earlier (section 3.7) that the band gap decreases with the increase of deposition rate. Very thin vacuum evaporated silicon and germanium film also show a shift in the absorption edges to shorter wavelength compared to that found in thick evaporated films or bulk material (Mattox and Kominiak, 1975). Melsheimer and Ziegler (1985) also reported that the band gap energy of tin oxide film varies between 2.25 to 4.45 eV depending upon the preparation conditions and evaluation techniques. In Table 5.6, the values of the band gap energy for MoO_3, MoO_2 and Mo_4O_{11} obtained by Hanafi et al, (1981) have been included. By comparison with the published data, it may be seen that the value of E_{opt} obtained from transmission measurements in this work agrees well with the band gap of Mo_4O_{11}. However, the values of band gap of Mo_4O_{11} and MoO_2 are quite similar (Hanafi et al, 1981), (Table 5.6).

The values of refractive index n calculated from the interference fringes of the transmission spectra of electrodeposited Mo-black are given in Table 3.7.1. Due to limited numbers of fringes, the wavelength dependence

of n could not be established. However, assuming that the effect of thickness on the value of n is negligible, it seems that n decreases with the increase of wavelength. Deb and Chopoorian (1966) reported that the refractive index of MoO_3 thin films decreases with increase of wavelength and approaches a constant value of 2.38 which is close to the value obtained in the present investigation at 0.77 μm, n = 2.6.

The high frequency dielectric constant obtained from the relation $\varepsilon = n^2$ is about 6.7 which is in rather poor agreement with the measured dielectric constant of 4. Table 5.7 compares the value of the refractive index of Mo-black coating obtained by different methods. The value of n varies from 1.85 to 3.5 in the solar region. It is known that the surface condition has a great influence on the value of refractive index. Its value could also vary due to evaluation techniques and corresponding errors. However, the higher value of refractive index for Mo-black dip coatings on polished zinc indicates low absorption, which is found in the present measurement. Electrodeposited Mo-black coatingshave comparatively low refractive indices corresponding to high absorption, but the small difference in the refractive indices for the solar and long wavelength region could explain the small selectivity of this coating. For coatings on etched zinc and cobalt (NC) substrates, the surface texture reduces the refractive index ($\leqslant$ 2) and thus front surface reflection is reduced, resulting in high absorptance. High transparency in the IR region of these coatings is due to low thickness and leads to low emittance. Hence these coatings are significantly selective.

Table 5.1. Summary of the compositional analysis of Mo-black coatings on different substrates.

Coating preparation technique	Substrate	Phase present in the coatings			Oxidation state of Mo in the as-prepared coatings
		As-prepared	After heating in air	After heating in vacuum	
Electrode-position	Al	Mo_4O_{11} (TED, X-ray diffraction and IR study)	MoO_3/Mo_4O_{11} (X-ray and XPS study)	Mo_4O_{11} (TED)	+5.1
Dip	Zn	Mo_4O_{11} (RED, X-ray and IR study)	MoO_3 (XPS study)	MoO_2 (XPS study)	+5.0
Dip	Cobalt (NC)	Mo_4O_{11} (X-ray and IR) study)	MoO_3 (XPS study)	Possibly mixture of two phases (XPS study)	+5.4

Table 5.2 Infrared absorption peaks of Mo-black coatings and standard sample of Mo-oxides.

IR absorption peaks/(μm)			
Mo-black coatings	MoO_3	MoO_2*	MoO_3*
2.9 - 3.1 (Water absorption peak)	-	-	-
6.2 (Water absorption peak)	-	-	-
-	10.1	10.2	10.3
10.5	-	10.5	-
11.7	11.6	11.2	11.4
-	12.2	-	12.1
14.5	-	-	-
-	16.9	-	17.2
20.3	20.4	-	20.6
21.5	-	-	-
-	23.8	-	23.5

* From Hanafi et al (1975)

Table 5.3 Central Line Average Roughness (CLA) values of Mo-black dip coatings on different substrates.

Substrates	CLA Roughness (µm)
Unetched zinc (0.5 µ finish)	0.04
Unetched zinc (6.0 µ finish)	0.14
Etched zinc (30% HNO_3)	0.40
Etched zinc (50% HNO_3)	0.46
Cobalt (NC) plated without addition agent	0.30
Cobalt (NC) plated with addition agent	0.15

Table 5.4(a) Values of refractive index n for Mo-black dip coatings on polished zinc substrates

Coating Thickness (µm)	Refractive index n for various wavelengths λ / µm	
	n	λ / µm
0.19	7.2	0.69
0.30	4.5	0.94
0.49	3.5	0.96

Table 5.4(b) Experimental and calculated values of reflectance of a thick Mo-black dip coating on polished zinc substrate.

Coating thickness (μ m)	Wavelength (μ m)	R_λ experimental	R_λ Calculated
0.30	0.40	0.08	0.09
	0.70	0.15	0.13
0.49	0.40	0.08	0.085
	0.70	0.12	0.11

Table 5.4(c) Calculated and experimental values of reflectance (specular) for a Mo-black dip coating on an etched zinc substrates

Wavelength μ m	CLA roughness μm	Calculated R_s	Experimental R_s
2.5	0.4	0.59	0.46

Table 5.5 Efficiency and thermal radiative properties of Mo-black coatings studied in the present investigation and of those reported in the literature.

Sample	Absorptance α_s	Emittance ϵ_{th}	Selectivity factor α_s / ϵ_{th}	Efficiency η(%)	Reference
Electrodeposited Mo-black coating on aluminium	0.87	0.02	1.34	34.0	Present work
Mo-black dip coating on					
i) Polished zinc	0.76	0.09	8.4	68.2	Present work
ii) Etched zinc with 30% HNO_3	0.87	0.13	6.7	76.0	Present work
iii) Etched zinc with 50% HNO_3	0.89	0.30	2.96	63.0	Present work
Mo-black dip coating on cobalt (NC) substrate					
i) With addition agent	0.91	0.10	9.1	82.5	Present work
ii) Without addition agent	0.94	0.28	3.36	70.0	Present work
Electrodeposited Mo-black coating on nickel plated copper	0.85	0.11	7.72	75.6	Potdar et al. 1982
Cobalt-Molybdenum immersion coating	0.89	0.2	4.45	71.8	Smith and Teytz, 1984
Mo-black film prepared by chemical vapour deposition method.					
i) As-prepared	0.77	0.31	2.48	50.4	Chain et al, 1981
ii) After annealing and overcoating with Si_3N_4	0.91	0.11	8.27	81.5	

Table 5.6 Optical band gap of Mo-black coatings and standard samples of Mo-oxides.

Sample	Band gap (eV)	Determination techniques
Thin electro-deposited Mo-black coating on vacuum evaporated Al-film	1.66	Transmission spectra Plots of $(\alpha\hbar\omega)^{1/2}$ vs $\hbar\omega$ (Section 3.7)
Thick electro-deposited Mo-black coating on Al-sheet	1.13 0.85	Reflectance spectra Plots of R_λ vs λ Plots of α/s vs λ (Section 5.2.1)
Mo-black dip coating on zinc	1.24 0.91	Reflectance spectra Plots of R_λ vs λ Plots of α/s vs λ (Section 5.2.2)
Powder sample of i) MoO_2 ii) Mo_4O_{11} iii) MoO_3	 1.72 1.75 2.74	Diffuse reflectance spectra Plots of ln α/s vs λ (Hanafi et al, 1981)

Table 5.7 Refractive index of Mo-black coatings determined by different methods.

Sample	Thickness (μm)	Refractive index, n	Evaluation Technique
Electrodeposited Mo-black on a vacuum evaporated Al-film	0.50	2.6 at = 0.77 μm	Using interference fringes from the transmission spectra (Section 3.7)
Electrodeposited Mo-black on Al-sheet	6.0	1.85 in the wavelenth region 0.4 to 1.0 μm	From reflectance spectra using Fresnel's equation (Section 5.2.1)
		2.0 in the high wavelength region	From A.C. measurement using the relation $\varepsilon = n^2$ (Section 3.6)
Mo-black dip coating on polished zinc	0.49	3.5 at = 0.94 μm	Using interference fringes from the reflectance spectra (Section 5.2.2)

Report no. 1.

Butterworth Laboratories Ltd.

TEDDINGTON MIDDLESEX U.K. TW11 8ET. Tel. 01-977 0750

APPLICATION FORM FOR MICROANALYSIS

BL Ref. No. 2499

Applicants Name Dr B.E. SMITH

Address: DEPT. MECH. ENGINEERING, BRUNEL UNIVERSITY, UXBRIDGE, MIDDX. UB83PH

Tel. No. UXB.(0895)37188 Extn. 708

Order No. 113/201/015532

Sample No. 1

Type and/or Structure MOLYBDENUM BLACK ELECTRODEPOSITED COATING.

Carcinogenic/Toxic (Not known)

Elements present Mo, N?, O, H? M.Pt. or B.Pt. ?

Solvent ? Drying Req. No

Moisture/Air/Oxygen Sensitive [ ] N_2/He Dry Box /

Other Comments

Urgent Service [ ] Normal Service [✓]

Cable/Telephone service or Discussion required [ ]

DATE RECEIVED 18/2/85

DATE REPORTED 11.3.85

ANALYSIS REQUIRED

	Single	Duplicate	Expected	% Found
C.				
H.	✓			2.12
N.				
O.	✓			Not determined
F.				
Cl.				
Br.				
I.				
S.				
P.				
B.				
Si.				
Metal				
Mol. Wt.				
Infra Red				
N.M.R.				
Mass Spec.				
X.R.F./ X.R.D.				
Other				

COMMENTS:

Regret we cannot determine oxygen.

SIGNED: David Butterworth

CHAPTER VI

CONCLUSIONS AND SUGGESTIONS FOR FURTHER WORK

6.1 Conclusions

1. Mo-black coatings prepared by electrodeposition on aluminium substrates have moderate absorptance (~0.87). Due to their high emittances the coatings are effectively non-selective (Section 3.1.3). The high absorptance of these coatings may be related to the bandgap of the coating material (which is found to be about 0.85 eV using the Kubelka-Munk theory) and the porosity of the coating (Section 5.2.1). The high emittance of these coatings is probably due to their relatively large thickness and presence of water in the coatings.

2. Mo-black dip coatings on polished zinc substrates have comparatively low absorptance (0.70 - 0.78) with high selectivity factor (7 to 9.8). The low absorptance of these coatings may be due to high reflection losses related to a high refractive index (Section 5.2.2). The low emittance of the dip coatings is due to their low thickness (below 1 μm). Thinner coatings appear to be almost transparent in the IR region. Both absorptance and emittance of these coatings increase with increase of thickness but emittance is more thickness dependent than the absorptance (Section 3.1.1).

3. By using chemically etched zinc substrates, the absorptance of the dip coatings can be increased by 14% without any significant change in the emittance (Section 3.1.1). The enhanced absorption is thought to be due to reduction of surface reflection loss. The thickness of the coatings is found to be

critical for optimum properties. Thick Mo-black coatings exhibit less selectivity for both etched and unetched zinc substrates.

4. On electroplated cobalt (NC) (cobalt on nickel plated copper) substrates, Mo-black dip coatings give more promising results. These coatings exhibit high solar absorptance (0.92 - 0.94) mainly due to the surface morphology of the coatings together with the structure of the plated cobalt layer. These coatings have a rather high emittance (0.25 - 0.33) probably due to surface roughness.

5. It has been observed that the properties of these coatings are sensitive to the preparation conditions of both Mo-black and the initial cobalt layer. By using an addition agent in the cobalt plating solution, the emittance of the Mo-black coatings can be reduced to 0.1 to 0.13 with a slight decrease in solar absorptance. Mo-black coatings prepared at a solution temperature of $60^{o}C$ give better results than those prepared at $80^{o}C$.

6. In the present investigation, maximum efficiency (82.5%) has been obtained from the Mo-black coating on cobalt (NC) substrate plated with addition agent (Section 5.3). The coatings on etched zinc substrates have an efficiency of 76%. It has also been observed that although the coatings on highly polished zinc have a higher selectivity factor than those on etched zinc, their efficiency is lower.

7. The SEM studies have shown that both electrodeposited coatings on aluminium and dip coatings on polished zinc consist of flat smooth, platelets with widely spaced cracks. This suggests that absorptance in these coatings is due to intrinsic absorption by the coatings and not due to surface morphology. Mo-black coatings on chemically etched zinc

substrates show a nodular structure (Section 3.2.2), which may enhance the solar absorptance without affecting the thermal emittance significantly.

8. The morphology of Mo-black coatings on cobalt (NC) substrates depends on the preparation conditions. The coatings have a nodular structure and comparatively smooth surface when prepared on cobalt plated with addition agent. On cobalt plated without addition agent, the surface of Mo-black coatings consists of a large number of limb like structures with few nodules. When cobalt is plated with a comparatively low current density and at low temperature, the surface of Mo-Black coating consists of submicron sized nodules (Section 3.2.3).

9. The electron diffraction studies of the Mo-black coatings on aluminium and zinc substrates suggest that the coatings are polycrystalline in nature. The interplanar spacing values indicate the presence of orthorhombic Mo_4O_{11} (Section 3.3). X-ray diffraction patterns from the coating contain only one very broad low angle ($\theta \sim 4.5$) peak together with peaks from the substrates. The difference in the electron and X-ray diffraction results is probably due to the differences in atomic scattering factors for electrons and X-rays (e.g., for lighter atoms such as O_2).

10. The X-ray photoelectron spectroscopy study indicates that the oxidation state of molybdenum in the Mo-black coatings is about +5, which is close to that in Mo_4O_{11}. The oxidation state of molybdenum remains almost the same for coatings on different substrates (Al, Zn and Co). It has been observed that the coatings reduce to a lower oxidation state (+4) after bombarding with Ar^+ ions which is most probably the etching effect.

11. The XPS study shows that the coatings mainly consist of molybdenum with a small percentage of nickel. The EPMA also shows the same results. However, the percentage of nickel in the coating increases with increase of $NiSO_4$ concentration in the plating solution. Peaks from the substrates (Al, Zn, or Co) also appear in the XPS and EPMA spectra. (These possibly due to cracks in the coatings). The atomic percentage of oxygen at the surface of coatings is about 71%. After etching with Ar^+ ions it reduces to 57 - 61%, due to the reduction of molybdenum to a lower oxidation state.

12. XPS studies reveal that the coating oxidizes to MoO_3 (+6) after heat treatment in air at high temperature. The coatings on cobalt seem to be less affected by heat treatment.

Mo-black coating on zinc substrate reduce to a lower oxidation state (+4) after heating in vacuum, (zinc probably acts as a reducing agent). No significant shift in the binding energy of Mo 3d peaks has been observed for coatings on aluminium and cobalt substrates after heat treatment in vacuum.

13. IR absorption peak positions provide further evidence that the Mo-black coating does not consist of MoO_2 or MoO_3 (Section 5.1.2.2). But contains an intermediate oxide, e.g., Mo_4O_{11}), as suggested by the electron diffraction study.

14. No significant changes in the reflectance spectra of Mo-black coatings on etched zinc have been observed after heat treatment at 100°C and 200°C for a period of 24 and 16 hours respectively. No degradation has been observed even after heat treatment at 300°C for 4 hours. Same characteristic reflectance has been observed whether the coatings are

heat treated in air or vacuum. Coatings on cobalt (NC) substrates have been tested up to 400°C. The coatings on cobalt plated without addition agent seem to be more stable than the coatings with addition agent, i.e., the emittance increases in the latter case whereas it decreases in the former case. The solar absorptance remains unchanged after heat treatment in both cases.

15. The coatings are semiconducting. Annealing at elevated temperature increases the electrical conductivity of the coating. The I-V characteristics of the coating are ohmic at low applied fields but they are non-ohmic at higher applied field. Analysis of the I-V characteristics suggest that in the high field region the dominant conduction mechanism is of the Poole-Frenkel emission type. It has also been observed that the activation energy of the coating varies with temperature.

AC measurements show that the capacitance of the coating decreases with the increase of frequency. The relative dielectric constant decreases from about 4.6 to 4.0 when frequency increases from 5×10^2 Hz to 2×10^4 Hz. At higher frequencies it is less frequency dependent. Capacitance measurements as a function of temperature give evidence for the presence of water in the coating.

16. Transmission measurements in the UV and visible region suggest that the optical band gap E_{opt} decreases and the band tail increases with increase of coating deposition rate. This may be due to an increase of structure disorder in the system with increasing deposition rate. (The value of E_{opt} decreases from 1.89 eV to 1.66 eV with the increase of current density from about 1.4 mA/cm^2 to 2.8 mA/cm^2 (Section 3.7)).

17. It is concluded that for the production of selective surface for a solar collector, a Mo-black coatings on electroplated cobalt on a nickel plated copper substrate is the most suitable of the materials studied in the present work. This is recommended on the basis of its performance, durability and reproducibility of optical characteristics.

6.2 Suggestions for further work

i) Longer term thermal stability testing for Mo-black coatings on etched zinc is needed, as the short term heat treatment up to temperatures of 300^{o}C gives no significant degradation in the optical properties of these coatings.

ii)A more systematic study should be done on the effect of addition agents in the cobalt plating solution together with the effect of solution temperature and plating conditions on the thermal radiative properties and microstructure of the Mo-black coatings on cobalt (NC) substrates.

iii) The long term thermal stability at elevated temperature of coatings on cobalt (NC) substrates should be examined.

iv) The effects of humidity, ultraviolet exposure and temperature cycling in degradation of coatings on both zinc and cobalt substrates should be examined.

v) Further study of IR absorption spectra might provide information on chemical bonding in the coatings.

vi) Neutron diffraction studies might be appropriate for this material (due to the presence of lighter elements such as oxygen and hydrogen).

vii) Mo-black coatings on other substrates, such as, aluminium, and mild steel, with an intermediate cobalt layer could be studied.

viii)A flat plate solar collector could be constructed using a Mo-black coating as a selective surface and its thermal performance under operating conditions could be investigated.

REFERENCES

Agnihotry, O.P. and Gupta, B.K. (1981), "Solar Selective Surfaces", (Wiley Interscience).

Agnihotri, O.P., Gupta, B.K., Agarwal, A.K. and Bhatnagar, V.P. (1983), Thin Solid Films, 109,193.

Al-Ani, S.K.J., Arshak, K.I. and Hogarth, C.A. (1984), J.Mat.Sci., 19 , 1737.

Al-Ani, S.K.J., Sarkar, M.A.R., Beynon, J. and Hogarth, C.A. (1985), J.Mat.Sci., 20,1637.

Al-Ani, S.K.J., (1984) Ph.D. Thesis, Brunel University, U.K.

Al-Ramadhan, F.A.S., Arshak, K.I. and Hogarth, C.A. (1984), J.Mat.Sci., 19, 3687.

Andersson, G. and Magneli, A. (1950), Acta.Chem.Scand., 4,793.

Anthony, M.T. and Seah, M.P. (1984), Surf.Interface.Anal. 6,107.

Apetkar, E.L., Chadinov, M.G., Alkeseev, A.M. and Krylov, O.V. (1974) React.Kinet.Catal.Lett. 1,493.

Barraclough, C.G. and Stals, J. (1966), Aust.J.Chem., 19,741.

Ben-dor, L. and Shimony, Y. (1974), Mat.Res.Bull. 9,837.

Bennett, H.E., and Porteus, J.O., (1961), J.Opt.Soc.Am., 51, 2, 123.

Block, G.R. (1985), Final Project Report, Brunel University, U.K.

Bogaerts, W.F. and Lampert, C.M. (1983). J.Mat.Sci., 18,2847.

Booth, D.C., Allred, D.D. and Seraphin, B.O. (1979). Sol. Energy Mater. 2, 107.

Brandt, B.B. and Skapski, A.G. (1967) Acta Chem. Scand., t, 21,661.

Briggs, D. (1978) "Handbook of X-ray and ultra-violet photoelectron spectroscopy". (Heyden: London).

Briggs, D. and Seah, M.P. (1983) "Practical surface analysis by Auger and X-ray photoelectron spectroscopy". (John-Wiley and Sons: New York).

Bulpett, R. (1984) Vacuum, 34, 481.

Carver, G.E. (1979) Sol. Energy. Mater., 1,357.

Carver, G.E. and Seraphin, B.O. (1979), App. Phys. Lett. 34, 279.

Carver, G.E., Divrechy, A., Karbal, S., Robin, J. and Donnadien, A. (1982) Thin Solid Films, 94, 1269.

Chan, W.S. and Loh, C.K. (1970), Thin Solid Films, 6, 91.

Chandrashekar, M. and HariBabu, V. (1984) J.Mat.Sci.Lett., 3, 600.

Chain, E.E., Carver, G.E. and Seraphin, B.O. (1980), Thin solid Films, 72, 59.

Chain E.E., Seshan, K. and Seraphin, B.O. (1981) J.Appl.Phys., 52, 3, 1356.

Chase, L.L. (1974) Phys. Rev. B, 10, 2226.

Chopra, K.L. (1969) "Thin Film Phenomena", (Mc-Graw Hill Book Co, New York).

Christie, E.A. (1970) Intern. Solar Energy Conf., Melbourne, Australia, paper 7/81.

Cimino, A. and De Angelis, B.A. (1975) J. Catal., 22 140.

Colton, R.J., Guzman, A.M. and Rablais, J.W. (1978) J.Appl. Phys. 49, 1, 409.

Companion, A.M. and Mackin, M. (1965) J.Chem.Phys. t.42, 4219.

Cotton, F.A. and Wilkinson, G.J. (1972), "Advanced Inorganic Chemistry", 3rd Ed., Wiley, Interscience, New York, London.

Cullity, B.D. (1978) "Elements of X-ray diffraction". (Addison-Wesley publishing Co. Inc.).

Cuomo, J.J., Ziefler, J.F. and Woodale, J.M. (1975), App.Phys.Lett., 26, 557.

Dagnall, H. (1980), "Exploring Surface Texture", Rank Taylor Hobson, Leicester, England.

Davis, H. (1954), Proc.Inst.Electr.Engn. 101, 4, 209.

Davis, E.A. and Mott, N.E. (1970), Phil.Mag., 22, 903.

DeChelle, F., Berger, J.M., Ance, C., Coulibaly, S.P. Ferraton, J.P., Donnadieu, A., Zellama, K., Germain, P. and Squelard, S. (1983), Thin Solid Films, 103 243.

Deb, S.K. and Chopoorian, J.A. (1966), J.App.Phys. 37, 4818.

Deb, S.K. (1968), Proc. Royal Soc., A304, 211.

Dickinson, W.C. and Cheremisinoff, P.N. (1980), "Solar energy technology handbook", (Part B), Marcel Dekker, Inc. Butterworths, London.

Duffie, J.A. and Beckman, W.A. (1980), "Solar Engineering of Thermal Processes," Wiley, New York.

Dunkui, M. (1986), Sun World, 10, 2, 46.

Fan, J.C.C. (1978), Thin Solid Films, 39, 87.

Fan, J.C.C. and Spura, S.A. (1977), Appl. Phys. Lett. 30, 511.

Fosch, P.D. (1956) Proc. Phys. Soc. B69, 70.

Frenkel, J. (1938), Phys. Rev. 54, 647.

Fussell, W.B., Triolo, J.J. and Henniger, J.H. (1963), Measurement of

Thermal Radiative Properties of Solid, NASA-SP31, 83.

Gesheva, K.A., Chain, E.E. and Seraphin, B.O. (1980), Sol. Energy Mater., 3, 415.

Gilbert, L.R., Messier, R. and Roy, R. (1978), Thin Solid Films, 54, 149.

Golestani-Fard, F., Hogarth, C.A. and Waters, D.N. (1983), J.Mat.Sci.Lett. 2, 505.

Goldstein, J.I., Newbury, D.E., Echlin, P. Joy, D.C., Fiori, C., Lifshin, E. (1981), "Scanning Electorn Microscopy and X-ray Microanalysis" Plenum Press, New York and London).

Gray, D.E. (1972) "American Institute of Physics Handbook", 3rd Edition, Mc-Graw Hill Book Co. New York.

Gregg, S.J. and Sing, K.S.W. (1982), "Absorption, Surface Area and Porosity", Academic Press, London.

Grim, S.O. and Matienzo, L.J. (1975), Inorg.Chem. 14, 1975.

Gupta, B.K., Agarwal, A.K. and Bhatnagar, V.P. (1983), Proc. of SPIE, "Optical and Process Technology for Energy Efficiency and Solar Applications", San Diego, California, 428, 182.

Hagg, G., and Magneli, A. (1944), Arkiv Kemi. Mineral.Geol. A.19, 2.

Haight, G.P., Jr. (1953), Anal.Chem. 25, 4.642.

Hanafi, Z.M., Khilla, M.A. and Abu-el-Saud,A. (1975), Rev.Chim.Min. t.12, 546.

Hanafi, Z.M., Khilla, M.A. and Abu-el-Saud,A. (1981), Rev.Chim.Min. t.18, 133.

Hoffman, R.A. and Hull, R.O. (1939), Proc.Am.Electroplat.Soc., 45.

Hosseini, R. (1981), Ph.D Thesis, Brunel University, U.K.

Hosseini, R., Smith, B.E. and Critchley, J.K. (1983), Surface Tech. 20, 321.

International Copper Research Association (INCRA) (1977), Final Project Report No 250.

Islam, M.H. (1987), Ph.D. Thesis, Brunel University, U.K.

Jahan, F., and Smith, B.E. (1986), J.Mat.Sci.Lett. 5, 905.

Karlsson, B and Ribbing, C.G. (1982), J.Appl.Phys. 53, 9, 6340.

Kennedy, M.J. (1972), Ph.D Thesis, Brunel University, U.K.

Kihlborg, L. (1959), Acta. Chem. Scand. t,13, 954.

Kihlborg, L. (1963), Advanc. Chem. Set, t,39, 37.

Kihlborg, L. (1963), Arkiv. Kemi. t,21, 443.

Kim, K.S., Baitinger, W.E., Amy, J.W. and Winograd, N. (1974), J.Electron Spectrosc. Relat. Phenom., 5, 351.

Kim, K.S. and Winograd, N. (1974), Surf.Sci. 43, 2, 625.

Kittel, C. (1968), "Introduction to Solid State Physics, (John Wiley & Sons, Inc., New York).

Koltun, M.M. (1981), "Selective Optical Surfaces for Solar Energy Converters", Allerton Press, New York.

Kramer, B.M. (1983), Thin Solid Films, 108, 117.

KRATOS Instruction Manual for the ES300, Barton Dock Road, Urmston, Manchester

Kubelka, P. and Munk, F (1931), Z.Tech.Phys. 12, 593.

Kubelka, P. (1948), J.Opt.Am. 38, 448.

Lamb, D.R. (1967), "Electrical Conduction Mechanisms in Thin Insulating Films", (Methuen Monograph, London).

Lampert, C.L. (1979), Ph.D Thesis, University of California, USA.

Lampert, C.L. (1979), Solar Energy Mater. 1, 81.

Lampert, C.L. (1979), Solar Energy Mater. 1, 319.

Lavina, A., Aznarez, J.A. and Ortiz, C. (1980) J.Crys.Growth, 48, 100.

Longhurst, R.S. (1957), "Geometrical and Physical Optics", Longmans, Green and Co Ltd., London.

Lowenheim, F.A. (1963) "Modern Electroplating", 2nd Edition. Wiley, New York.

Lowenheim, F.A. (1978), "Electroplating", McGraw-Hill, New York.

Lubis, A., Witono and Budiono, C. (1985) Sun World, 9, 2, 36.

Magneli, A. (1946) Arkiv, Kem. Mineral Geol. A24, 2.

Magneli, A. (1948) Acta Chem. Scand. 2, 501.

Magneli, A. (1948) Acta Chem. Scand. 2, 861.

Magneli, A. (1957), Acta Chem. Scand. t,11, 1587.

Maissel, L.I. and Glang, R. (1983) "Handbook of Thin Film Technology". (McGraw-Hill Book Co., New York).

Mattox, D.M. and Kominiak, G.J. (1975) J.Vac.Sci.Tech. 12, 1, 182.

Mattox, D.M. and Sowell, R.R. (1980) "A Survey of Selective Solar Absorber Surface and their limitations", US-DOE Report DE-AC04-76-DP00789.

McMahon, T.J. and Jasperson, S.N. (1974) App.Opt. 13, 12, 2750.

McIntyre, N.S. and Cook, M.G. (1975) Anal.Chem. 47, 2208.

McNelis, B. (1982) Sun at Work in Britain, 15, 30.

Mead, C.A. (1962), Phys.Rev. 128, 2088.

Meinel, A.B. and Meinel, M.P. (1976) "Applied Solar Energy", (Addison-Wesley Publishing Co., Reading, Massachusetts).

Millard, J.P. and Streed, E.R. (1969), App.Opt. 8, 7, 1485.

Miller, A.W., Atkinson, W., Barber, M. and Swift, P. (1971) J.Catal. 22, 140.

Morley, A.R. and Campbell, D.S. (1968) Thin Solid Films, 2, 403.

Moss, T.S., Burell, G.J. and Ellis, B. (1973), "Semiconductor Opto-Electronics", (Butterworths, London).

Mott, N.F. and Davis, E.A. (1971), "Electronic Process in Non-Crystalline Materials". Clarendon, Oxford.

Mott, N.F. (1969), Phil.Mag., 19, 835.

Nadkarni, G.S. and Simmons, J.G. (1972), J.Appl.Phys. 43, 3741.

Nadkarni, G.S., Shirodkar, V.S. and Simmons, J.G. (1982), Thin SOlid Films, 94, 101.

Nakamoto, K. (1970), "Infrared Spectra of Inorganic and Co-ordination Compounds".

Neal, W.E.J. and Musa, A.H. (1982), Surf.Tech. 14, 345.

Niklasson, G.A. and Geranqvist, C.G. (1983) J.Mat.Sci. 18, 3475.

Nozik, A.J. (1972), Phys.Rev. B6, 453.

Park, C.K. (1964), App.Opt. 3, 877.

Patterson, T.A., Carver, J.C., Leydon, D.E. and Hercules, D.M. (1976). J.Phys.Chem. 80, 1700.

Pellegrini, G. (1980). Sol.Energy Mater. 3, 391.

Peterson, R.E. and Ramsey, J.W. (1975) J.Vac.SCi.Technol. 12, 174.

Petit, R.B. and Sowell, R.R. (1976) J.Vac.Sci. Technol. 13, 2, 596.

Porter, V.R., White, W.B. and Roy, R. (1972) J. Solid State Chem. 4, 250.

Potdar, H.S., Hedge, R.I., Badrinarayon, S. and Pavaskar, N. (1982) Sol. Energy Mater. 6, 183.

Rablais, J.W., Colton, R.J. and Guzman, A.M. (1974) Chem.Phys.Lett. 29, 1, 131.

Riggs, W.M. and Parker, M.J. (1975) "Methods of Surface Analysis (Ed" Czandernal, A.W.) Elsevier, New York.

Robert, T., Bartel, M. and Offergeld, G. (1972), Surf.Sci., 33, 123.

Rogers, D.B., Shanon, R.D., Sleight, A.W. and Gilson, G.L. (1969), Inorg.Chem. t.8, 476.

Safi, I. (1986), M.Phil. Thesis, Brunel University, UK.

Sauer, H.D. (1985) Sun World, 10, 2, 46.

Samsonov, G.V. (1973), "The Oxide Handbook". IFI/Plenum, New York.

Schofield, J.H. (1973), Laurence Livermore Laboratory Report, CRL-51326.

Schottky, W. (1914), Physik, Z. 15, 862.

Seraphin, B.O. (1974), Proc. Symp. on the Materials Science Aspects of Thin Film Systems for Solar Energy Conversion, Tucson, AS (July, 1974).

Seraphin, B.O. (1976), Thin Solid Films, 39, 87.

Seraphin, B.O. (1979), "Topics in App. Phsics," (Ed. Seraphin, B.O.) Springer-Verlag, Berlin, Germany.

Shabalov, A.L. and Feldman, M.S. (1983) Thin Solid Films, 110, 215.

Siegel, R. and Howell, J.R. (1972), "Thermal Radiation Heat Transfer", (McGraw-Hill Book Co., New York).

Sikken, M., VanHeereveld, A.A.M.T. and Vogelzang, E. (1983), Thin Solid Films, 108, 229.

Simmons, J.G. and Nadkarni, G.S. (1969), J.Vac.Sci.Tech. 6, 12.

Simmons, J.G. and Nadkarni, G.S. (1970), J.Appl.Phys. 41, 545.

Simmons, J.G. and Nadkarni, G.S. (1972), J.Appl.Phys. 43, 3650.

Simmons, J.G. (1971), "DC Conduction in Thin Films", Mills and Boon Ltd. London.

Simmons, J.G. and Verderber, R.R. (1967), Proc.Roy.Soc., 77, A301.

Smith, B.E., Hosseini, R., Farmakis, C. and Critchley, J.E. (1981) "Proceeding of Solar World Forum", ISES, Brighton, 1, (Pergamon, Oxford).

Smith, G.B., Ignatiev, A. and Zajac, G. (1980), J.Appl.Phys. 51, 8, 4186.

Smith, G.B. and Teytz, K. (1984), Sol. Energy Mater. 9, 449.

Swartz, W.E. and Hercules, D.M. (1971), Anal.Chem. 43, 1774.

Tabor, H. (1956), Bull.Res.Counc. of Israel, 5A, 119.

Tabor, H. (1977), "Application of Solar Energy for Heating and Cooling of Buildings", ASHRAE GRP 170, Ed. Jordon, R.C. and Lin, Y.H.

Tabor, H. (1984), Sun World, 8, 1, 5.

Takyu, K. (1984) Sun World, 8, 1, 16.

Tandon, S.P. and Gupta, J.P. (1970), Phys.Stat.Sol. 38, 363.

Tauc, J., Grigorovici, R. and Vancu, A. (1966), Phys.Stat.Solidi. 15, 627.

Urbach, G. (1953), Phys.Rev. 92, 1324.

Verchere, J.A. and Fleury, M.B. (1973), Proc. of the 1st Intern. Conf. on the Chemistry and Uses of Molybdenum, Ed. P.C.H.Mitchel, Climax Molybdenum Co. London (1975), 59.

Walter, D.J. (1978), Final Project Report, Brunel University, U.K.

Waring, Jr. R.K. and Hzu, W.Y. (1983), J.Appl.Phys. 54, 7, 4093.

Wiebelt, J.A. and Henderson, J.B. (1979), J. Heat Transfer, 101, 101.

Williams, D.A., Lappin, T.A. and Duffie, J.A. (1963) Trans. A.S.M.E. J.Eng.Power, July 1983, 213.

Yousif, K.M (1987), Private Communication.

APPENDIX A

RADIATION LAWS

Thermal radiation is electromagnetic energy that is propagated through space at the speed of light. In the spectrum of electromagnetic radiation, the wavelength range of thermal radiation is approximately 0.2 to 1000 μm (Duffie and Beckman, 1980). It is emitted by all substances by virtue of their temperature; the atoms molecules or electrons are raised to excited states, return spontaneously to lower energy states, and in doing so, emit energy in the form of electromagnetic radiation. There are four physical laws concerned with the radiation spectra from a substance. These are Kirchoff's law, the Stephan-Boltzmann law, Plank's law and Wien's law. The basic principles of selective surface are based on these laws.

A.1.1 Stefan-Boltzmann law

Josef-Stefan and Ludwig Boltzmann independently derived this law. it states that the total rate of emission of thermal radiation from unit area of a black body at absolute temperature T is given by

$$E_b = \sigma T^4 \qquad (A.1)$$

where σ is the Stefan-Boltzmann constant and is equal to 5.6697×10^{-8} W/m^2K^4.

No surface can emit more energy at temperature T than this amount. Most

surfaces radiate less as they are not perfect or ideal black bodies. (A perfect blackbody is defined as one which absorbs all incident radiation of all wavelength from all directions). Therefore, for real bodies the equation (A.1) can be written as

$$E = \varepsilon\sigma T^4 \qquad (A.2)$$

where ε is the emissivity of the material and has a value less than unity. The value of ε depends on the nature of the surface and temperature of the surface.

A.1.2 Kirchoff's law

Kirchoff's law is concerned with the relation between the emitting and absorbing abilities of a material. It may be stated as follows. In thermal equilibrium the ratio of the monochromatic emittance to monochromatic absorptance of a body at a given wavelength must be a constant. Thus for a condition of thermal equilibrium

$$\varepsilon_\lambda = \alpha_\lambda \qquad (A.3)$$

where α_λ is the monochromatic absorptance at wavelength λ and ε_λ is the monochromatic emittance at the same wavelength (if the incident radiation is independent of angle), (Siegel and Howell,1972).

From the law of conservation of energy, for any surface, the sum of absorptance α_λ, transmittance τ_λ and reflectance ρ_λ must be unity. Thus for an opaque material,

$$\alpha_\lambda + \rho_\lambda = 1 \ (\text{as} \ \tau_\lambda = 0) \qquad (A.4)$$

Hence using equation (A.3) and (A.4)

$$\varepsilon_\lambda = \alpha_\lambda = 1 - \rho_\lambda \qquad \text{(A.5)}$$

Thus it is possible to determine α_λ or ε_λ from the reflectance measurement which has also been used in the present work.

A.1.3 Planck's Law

The Stefan-Boltzmann equation (A.1) represents the black body emission over the entire wavelength range of spectrum. It does not reveal the distribution of energy with wavelength in the spectrum. The wavelength distribution of radiation emitted by a black body is given by Max-Planck, which can be expressed as

$$E_{b\lambda} = C_1 \lambda^{-5} [\exp C_2/\lambda T - 1]^{-1} \qquad \text{(A.6)}$$

where $E_{b\lambda}$ is the monochromatic emissive power at wavelength λ from the black body at a temperature T. C_1 is the first radiation constant = $3.7415 \ 10^{-16}$ W.m^2. C_2 is the second radiation constant = 1.43879×10^{-2} mK. For real bodies, the equation (A.6) becomes

$$E_{b\lambda} = \varepsilon_\lambda C_1 \lambda^{-5} [\exp C_2/\lambda T - 1]^{-1} \qquad \text{(A.7)}$$

where ε_λ is the emissivity of the body at temperature T. The Stefan-Boltzmann equation (A.1) can be obtained by integrating equation (A.6) over all wavelength ranges. That is

$$E_b = \int_0^\infty E_{b\lambda} \, d\lambda = \sigma T^4 \qquad \text{(A.8)}$$

A.1.4 Wien's Law

Wilhelm Wien determined the wavelength at which the intensity of black body radiation at a given temperature has its maximum value. According to Wien's law, the wavelength corresponding to the peak intensity of the black body radiation is inversly proportional to the temperature i.e.,

$$\lambda_{max} = 2898/T \qquad (A.9)$$

where λ is in μm and T is in K.

About 25% of the emitted energy is at wavelengths below λ_{max} and 75% above. Only 1% of the energy is emitted at wavelengths below 0.5 λ_{max} (Tabor, 1977).

Planck's law and Wien's law are illustrated in Fig.A.1 which shows the spectral radiation distribution for blackbody radiation at 6000, 1000 and 400K. The shape of the energy distribution curve and the displacement of the wavelength of its maximum intensity with temperature is clearly shown in this figure. (Wiens law is sometimes referred to as Wien's displacement law due to this displacement of λ_{max}). The distribution of the black body radiation at temperature of 6000K is an approximation of the distribution of solar radiation outside the earth's atmosphere and thus 6000K represents an approximation of the surface temperature of the sun. The peak intensity of solar radiation i.e., of black body radiation at 6000K is at a wavelength of about 0.5 μm. At a temperature of 400K, the peak wavelength is about 7.2 μm.

APPENDIX B

CALCULATIONS OF SOLAR ABSORPTANCE (α_s), THERMAL EMITTANCE (ϵ_{th}) AND RANDOM ERROR FOR THESE MEASUREMENTS

B.1. Calculation of solar absorptance (α_s)

Solar absorptances (α_s) of the coatings were calculated from total reflectance data in the solar region (0.3 - 2.5 μm) using selected ordinates for air mass 2 given by Weibelt and Henderson (1979), and by applying Kirchoff's law (Section 2.2.1). The values of α_s were calculated by a microcomputer attached to the spectrophotometer. An example print out from the computer is given below.

```
REFERENCE....CNC10
SAMPLE TYPE..MO ON CO NI CU
DATE.........24/10/85

MICRONS     REFLECTANCE

0.402           0.050
0.458           0.050
0.498           0.050
0.537           0.046
0.576           0.046
0.614           0.048
0.652           0.044
0.690           0.046
0.730           0.046
0.775           0.048
0.820           0.056
0.868           0.060
0.924           0.064
1.004           0.070
1.064           0.074
1.168           0.078
1.256           0.078
1.532           0.068
1.688           0.056
2.292           0.044
SOLAR ABSORPTANCE =.9439
~~~~~~~~~~~~~~~~~~~~~~~~
```

B.2. Calculation of random error for solar absorptance measurements

The total reflectance of a Mo-black coating was taken four times. The solar absorptance (α_s) was calculated using each spectrum and the values are

$$\alpha_1 = 0.924 \qquad \alpha_2 = 0.927$$

$$\alpha_3 = 0.926 \qquad \alpha_4 = 0.922$$

The mean value for these measurements is $\alpha = 0.925$

The deviations of each absorptance value from the mean value are

$$d_1 = [1.0] \times 10^{-3} \qquad d_2 = [2.0] \times 10^{-3}$$

$$d_3 = [1.0] \times 10^{-3} \qquad d_4 = [3.0] \times 10^{-3}$$

The standard deviation is

$$S = [1/4 \{ (1)^2 + (2)^2 + (1)^2 + (3)^2 \}]^{1/2} \times 10^{-3}$$

$$= 1.936 \times 10^{-3}$$

Therefore, the standard error on the mean is

$$S / \sqrt{3} \simeq 1.11 \times 10^{-3}$$

$$\simeq 0.001$$

Thus the absorptance is 0.925 ± 0.001

B.3 Calculation of thermal emittance (ε_{th})

The thermal emittances of the coatings were calculated from specular reflectance data in the wavelength range 2.5 to 50 μm by using Kirchoff's law, after first computing the weighting function using the spectral distribution of a blackbody radiator at the notional temperature of a solar collector.

Reflectance factor (as defined by the ratio of the flux reflected by a specimen to that reflected by an ideally reflecting surface (Al-mirror) located at the same position and irradiated under identical conditions) was weighted using a compact table of fraction of blackbody radiant energy between zero and λT for even fractional increments (Duffie and Beckman, 1980). One example calculation is shown below for Mo-black coating on cobalt (NC) substrate.

Wavelength, at energy midpoint at 35°C	Reflectance from reference mirror, R_λ	Reflectance from specimen R_s	Reflectance factor R_s/R_λ
5.39	62.0	37.0	0.60
6.66	65.0	50.0	0.77
7.53	66.3	56.0	0.84
8.31	66.0	57.0	0.86
9.06	67.0	60.0	0.90
9.77	67.5	60.5	0.90
10.49	67.3	59.5	0.88
11.23	71.0	64.0	0.90
12.05	75.5	68.5	0.91
12.89	77.0	70.0	0.91
13.80	78.0	71.0	0.91
14.84	78.5	74.0	0.94
16.00	77.0	71.0	0.92
17.37	76.0	72.0	0.95
19.00	71.0	67.5	0.95
21.04	75.0	72.0	0.96
23.73	77.5	75.0	0.97
27.63	75.0	73.0	0.97
34.41	74.0	73.0	0.99
50.00	74.5	73.0	0.98

$$\varepsilon_{th} = 1 - \frac{\Sigma R_s/R_\lambda}{20} = 0.0995 \sim 0.1 \qquad \text{A.7}$$

B.4 Calculation of the random error for emittance measurements.

The IR specular reflectance spectra of one Mo-black coating was taken four times. The emittance was calculated using each spectrum and the values are:

$\varepsilon_1 = 0.10$ $\varepsilon_2 = 0.096$

$\varepsilon_3 = 0.096$ $\varepsilon_4 = 0.105$

The mean value for these measurements is $\varepsilon = 0.099 \sim 0.1$

The deviations of each emittance value from the mean value are

$d_1 = [1.0] \times 10^{-3}$ $d_2 = [3.0] \times 10^{-3}$

$d_3 = [3.0] \times 10^{-3}$ $d_4 = [6.0] \times 10^{-3}$

The standard deviation is

$$S = [1/4\ ((1.0)^2 + (3.0)^2 + (3.0)^2 + (6.0)^2)]^{1/2} \times 10^{-3}$$
$$= 3.7 \times 10^{-3}$$

Therefore, the standard error on the mean is

$$S/\sqrt{3} \simeq 2.1 \times 10^{-3}$$

Thus the emittance is

$$0.1 \pm 2.1 \times 10^{-3}$$
$$\simeq 0.1 \pm 0.002$$

APPENDIX C

COMPARISON OF EMITTANCE MEASUREMENTS BY IR REFLECTANCE METHOD AND CALORIMETRIC METHOD

To compare the emittance measured by IR reflectance method to that measured by calorimetric method, emittance of a shiny aluminium sample was determined by the above two methods.

In the calorimetric method, emittance was determined by recording the specimen cooling rate in vacuum ($\sim 10^{-3}$ Pa), using the equipment developed by Hosseini (1981). (The experiments have been described by Hosseini, 1981). Fig.C.1 shows the cooling curve for shiny aluminium. The rate of change of sample temperature with time dT/dt was obtained from the recorded curve of temperature as a function of time. Then dT/dt was plotted as a function of T^4 (Fig.C.2). The slope of this curve is given by (Hosseini 1981)

$$S = \frac{A\sigma}{mc}\,\varepsilon_{th} \qquad (C.1)$$

where A = specimen surface area

σ = Stephan-Boltzmann constant

m = mass of the specimen

c = specific heat capacity of specimen

ε_{th} = emittance of the specimen.

The slope for the shiny aluminium specimen as obtained from Fig.C.2. was $2.5 \times 10^{-12} s^{-1} K^{-3}$.

The emittance was calculated using equation (C.1) and is equal to 0.036.

The emittance of the same specimen was calculated from the IR specular reflectance spectrum and the value was found to be 0.032. The percentage discrepancy is 11%. It should be mentioned that the emittance measured in the calorimetric method is the hemispherical value (at ~100°C) whereas, in IR reflectance method, the emittance is near normal and measured at room temperature.

A comparison of infrared emittance measurements and measurement techniques has been reported by Millard and Streed (1969). The measurements were made by two calorimetric and four reflectance techniques and with two portable devices. According to them, for gemoetrically plane and smooth surfaces the percent deviation of emittance value determined by specular IR reflectance method is +(2-3)% from the steady state calorimetric value. Large deviation (+25%) were observed for rough surface as not all the reflected energy was collected using specular reflectance attachment.

APPENDIX D

QUANTIFICATION OF XPS DATA

Quantification of the XPS data for compositional analysis may be achieved to an estimated accuracy of $\pm$ 20% (Briggs, 1978) by the use of sensitivity factors, which are used to modify the ratios of intensities calculated by measurement of peak areas. The sensitivity factors are based on photoionisation cross-section data and instrumental effects. The former are tabulated values based on derived theoretical photoionisation cross-sections (Schofield, 1973), whilst the later effects are described as a transmission function which may be measured for each spectrometer. The KRATOS ES 300 spectrometer operated under FRR (Fixed Retarding Ratio) conditions is assumed to have a transmission function proportional to energy as follows (KRATOS):

$$T \propto E^{1.0}$$

The sensitivity factors for oxygen, zinc, cobalt and molybdenum used in the present study are given below:

Elements	Sensitivity Factor
Mo 3d	3.73
O 1s	0.86
Zn 2p	2.63
Co 2p	3.31

APPENDIX E

D.C. CONDUCTION MECHANISMS IN THIN INSULATING FILMS

The various current transport mechanisms in dielectric thin films have been extensively reviewed by many authors (Lamb, 1967; Simmons, 1971). The possible mechanisms of conduction processes occurring in metal-insulator-metal (MIM) structure are illustrated schematically in the energy band diagram shown in Fig.E.1 in the presence of an electric field. The electrons can be injected from the metal into the conducton band of the insulator by a field-assisted thermal excitation over the potential barrier at the metal insulator interface (process A). This process is referred to as 'Schottky emission'. The electrons may also be thermally excited into the conduction band from trapping levels in the forbidden band of the insulator and this is referred to as the 'Poole-Frenkel' effect (Process B). Electrons may tunnel into the conduction band of the insulator directly from the metal cathode (Process C) or from the trapping levels within the insulator (Process D). If the insulator thickness is very thin (less than 50 Å) electrons can tunnel directly between the electrodes. Charge injection into the conduction band, tunnelling or impurity conduction in some cases, results in a build up of space-charge within the bulk which modulates the transfer process. The effect is referred to as a space-charge-limited conduction.

A number of above mechanisms may operate simultaneously at one particular applied voltage, but generally one mechanism dominates the observed current.

E.1 Schottky emission

The Schottky effect (Schottky, 1914) is the emission of electrons into the conduction band of the insulator from the metal-contact electrode by thermal activation over the field-lowered metal-insulator interfacial barrier. The barrier height (ϕ_s) is reduced due to the interaction of the electron image force with the applied field E and is given by

$$\Delta\phi_s = \left[\frac{e^3 E}{4\pi\varepsilon_o \varepsilon_r}\right]^{1/2} = \beta_s E^{1/2} \qquad \text{(E.1)}$$

where $\beta_s = \left[\frac{e^3}{4\pi\varepsilon_o \varepsilon_r}\right]^{1/2}$ is the Schottky field barrier coefficient, ε_r is the high frequency dielectric constant, ε_o is the permittivity of free space (equal to 8.854×10^{-12} F/m) and e is the electronic charge.

The resultant barrier height is now ($\phi_s - \Delta\phi_s$). Considering the reduction of the potential barrier the current density obeys the following equation.

$$J = AT^2 \exp\left(-\frac{\phi_s - \beta_s E^{1/2}}{kT}\right) \qquad \text{(E.2)}$$

where A is the Richardson Dushman constant and T is the absolute temperature.

E.2. The Poole-Frenkel Effect

The Poole-Frenkel effect (field-assisted thermal ionization) involves the lowering of a coulombic potential barrier when it interacts with an applied field. It is a bulk-limited conduction process. In this process,

the emission of electrons occurs from trapping centres in dielectrics into the conduction band by joint effect of temperature and electric field. In a uniform electric field the reduction of a coulombic barrier, $\Delta\phi_{PF}$, is given by

$$\Delta\phi_{PF} = \left[\frac{e^3 E}{\pi \epsilon_o \epsilon_r}\right]^{1/2} = \beta_{PF}\, E^{1/2} \qquad \text{(E.3)}$$

where $\beta_{PF} = \left[\frac{e^3}{\pi \epsilon_o \epsilon_r}\right]^{1/2}$ is the Poole-Frenkel coefficient which is analytically equal to twice the value of β_s, i.e., $\beta_{PF} = 2\beta_s$.

Frenkel (1938) suggested that the ionization potential ϕ_{PF} of the atoms in a solid is lowered by an amount $\Delta\phi_{PF}$ as in equation (E.3) in the presence of a uniform electric field. The resultant barrier is now $(\phi_{PF} - \Delta\phi_{PF})$.

The current density in thin film insulators containing shallow traps is given by (Mead, 1962).

$$J = J_o \exp\left(\frac{\beta_{PF} E^{1/2}}{kT}\right) \qquad \text{(E.4)}$$

where $J_o = N_c e\, \mu E \exp(-\phi_{PF} / kT)$ (E.5)
is the low field current density.

In equation (E.5) μ is the mobility of the charge carriers and N_c is the effective density of states in the conduction band of the insulator.

APPENDIX F

CONCEPTS OF AN ENERGY BAND STRUCTURE

A crystalline material is characterized by the presence of a definite long range order of the atomic constituents of the material. The main characteristics of the energy distributions, of the density of states of crystalline materials are the sharp band edges in the valence and conduction bands. The forbidden energy gaps which separate the valence and conduction bands are well defined as shown in Fig.F.1(a).

Non-crystalline or amorphous materials do not have a well ordered array of atomic constituents and there is virtually no long range order in the material (although short range order will generally be present (Mott, 1969)). It is believed that the lack of long range order in non-crystalline materials leads to tails of states extending from the valence and conduction bands (Fig.F.1(b)). The existence of these localised states, termed as 'band tails', causes smearing of the valence and conduction band edges, so that the optical energy gap is no longer well defined (Simmons and Verderber, 1967). Furthermore, non-crystalline materials are thought to contain imperfections, such as impurities or dangling bonds or microvoids and these may lead to levels within the forbidden energy gap which are called 'impurity bands' as shown in Fig.F.1(b) (Davis and Mott, 1970). The energies E_c and E_v (Fig.F.1(b)) separate the ranges of energy where the states are localised and nonlocalised. The energy intervals E_c-E_A and E_B - E_v are the width of localised states. According to Davis and Mott (1970) the optical band gap, E_{opt}, is equal to E_A - E_v or E_c - E_B which ever is smaller.

APPENDIX G

CALCULATION OF REFLECTANCE R_λ USING THE VALUES OF OPTICAL CONSTANTS

For a thick homogenous coating when the interference effect is absent, the reflectance R_λ is given by (Williams et al, 1963)

$$R_\lambda = \frac{R_{c\lambda} + R_{m\lambda}\,(1-2\,R_{c\lambda})\,e^{-2a_{c\lambda}d}}{1 - R_{m\lambda}\,R_{c\lambda}\,e^{-2a_{c\lambda}d}} \qquad (G.1)$$

The meaning of the symbols has been given in section 5.2.1. To apply this equation to a thick Mo-black dip coating in the shortwavelength region (below 0.7 μm) where no significant interference peak has been observed, it was assumed that $R_{c\lambda}$ - the reflectance at the air coating interface is equal to the reflectance from a thick coating. The values of R_λ has been calculated at two different wavelengths 0.4 μm and 0.8 μm.

$$\begin{aligned} &\text{At } 0.4\ \mu m \quad R_{c\lambda} = 0.08 \\ &\text{At } 0.7\ \mu m \quad R_{c\lambda} = 0.11 \end{aligned} \qquad (G.2)$$

From the transmission measurements

$$a_{c\lambda} = 5.7 \times 10^4 \ \ cm^{-1}$$

$$k_{c\lambda} = \frac{a_{c\lambda}\lambda}{4\pi} = 0.18$$

From equation (5.4)

$$R_{m\lambda} = \frac{(n_{c\lambda} - n_{m\lambda})^2 + (k_{m\lambda} - k_{c\lambda})^2}{(n_{c\lambda} + N_{m\lambda})^2 + (k_{m\lambda} - k_{c\lambda})^2} \qquad (G.3)$$

At $\lambda = 0.4$ μm, $n_{m\lambda} = 0.846$

$k_{m\lambda} = 2.917$

The values of $n_{m\lambda}$ and $k_{m\lambda}$ has been taken from American Institute of Physics Handbook (Gray, 1972). The value of $n_{c\lambda}$ has been taken from the transmission measurement (Table 3.7.1).

$$n_{c\lambda} = 4 \text{ at } \lambda \simeq 0.49 \text{ μm}$$

From (G.3) at $\lambda = 0.4$ μm

$$R_{m\lambda} = \frac{(4 - 0.846)^2 + (2.917 - 0.18)^2}{(4 + 0.846)^2 + (2.917 + 0.18)^2}$$

$$\simeq 0.52$$

For a coating of thickness 0.3 μm, the term $e^{-2a_{c\lambda}d} \simeq 0.03$.

Using the values of $R_{m\lambda}$, $R_{c\lambda}$ and the term $e^{-2a_{c\lambda}d}$ in equation (G.1)

$$R_{\lambda}\,(\text{cal}) \simeq 0.09$$

Similarly, using the values $n_{m\lambda}$ and $k_{m\lambda}$ at wavelength 0.7 μm and also the value of $n_{c\lambda}$ at about 0.77 μm (as obtained from table 3.7.1), $R_{m\lambda}$ has been calculated and is equal to 0.33. Then the reflectance R_{λ} at 0.7 μm has been calculated for the same coating and compared with the experimental value of R_{λ}. The calculated and experimental values of R_{λ} are given in Table 5.4(b).

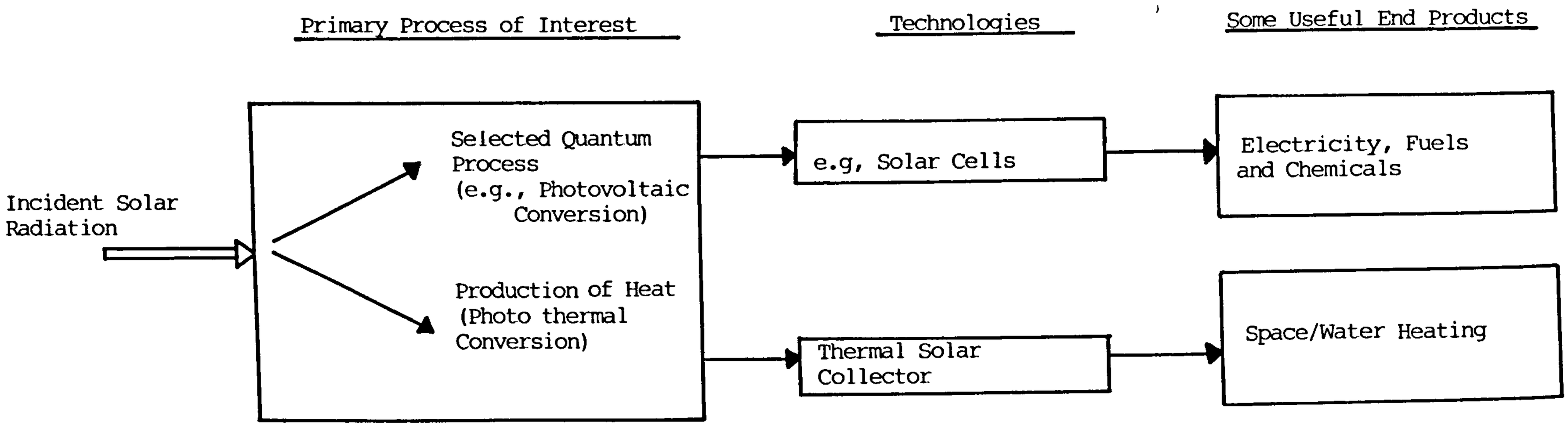

Fig.1.1 Solar energy conversion processes

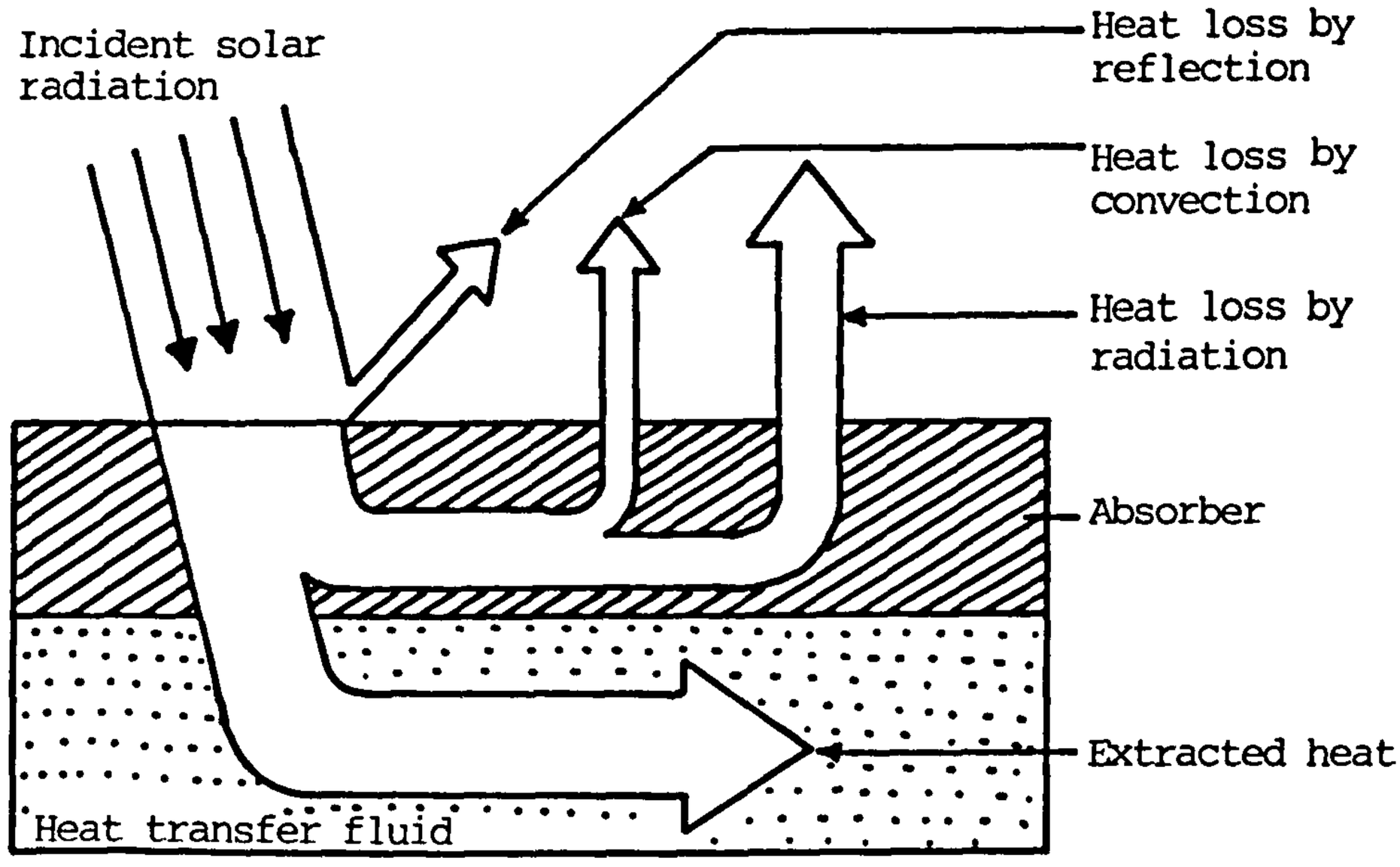

Fig.1.2 Basic principle of solar photothermal conversion

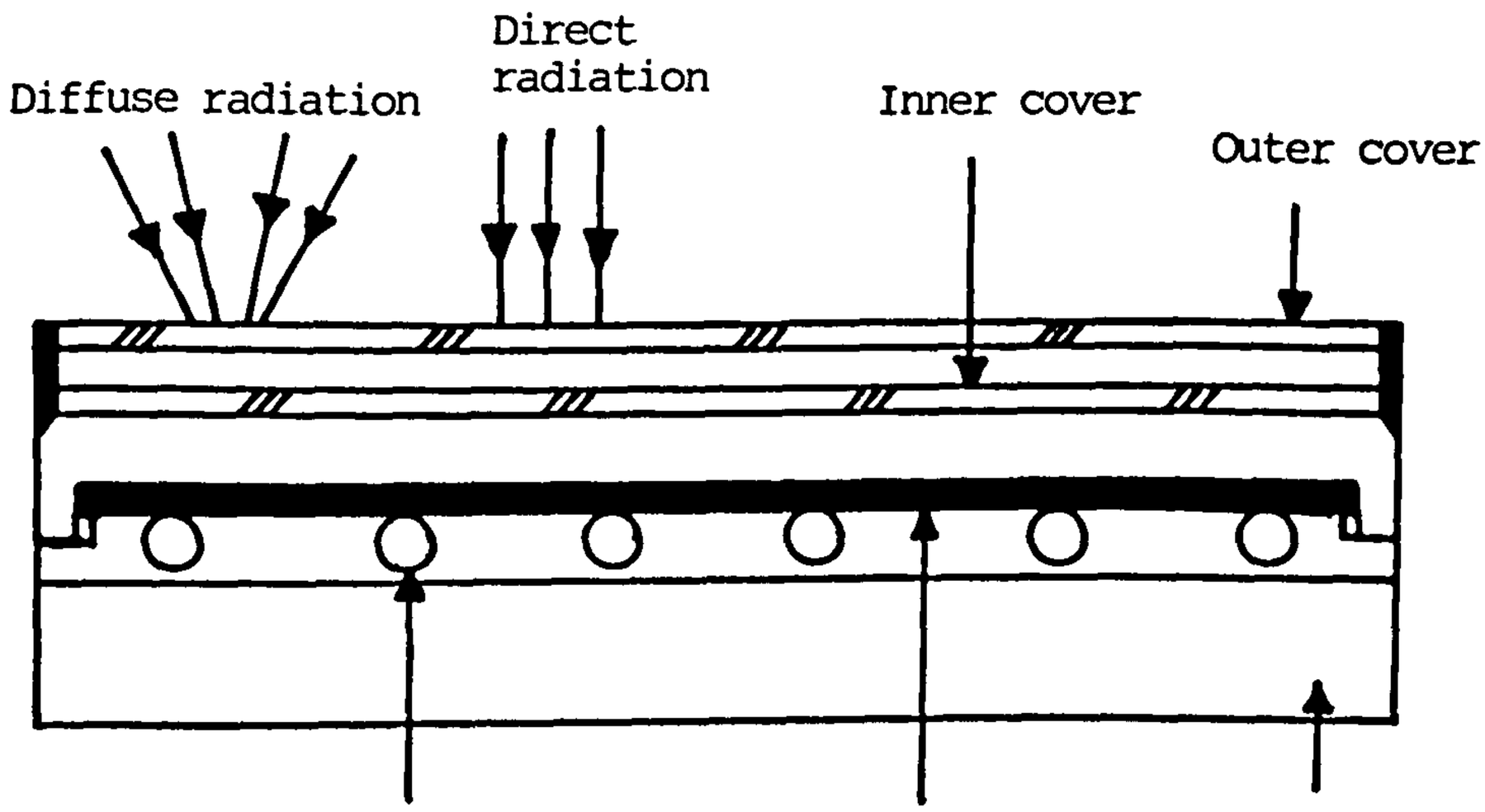

Fig.1.3(a) Schematic cross section of a flat plate solar collector.

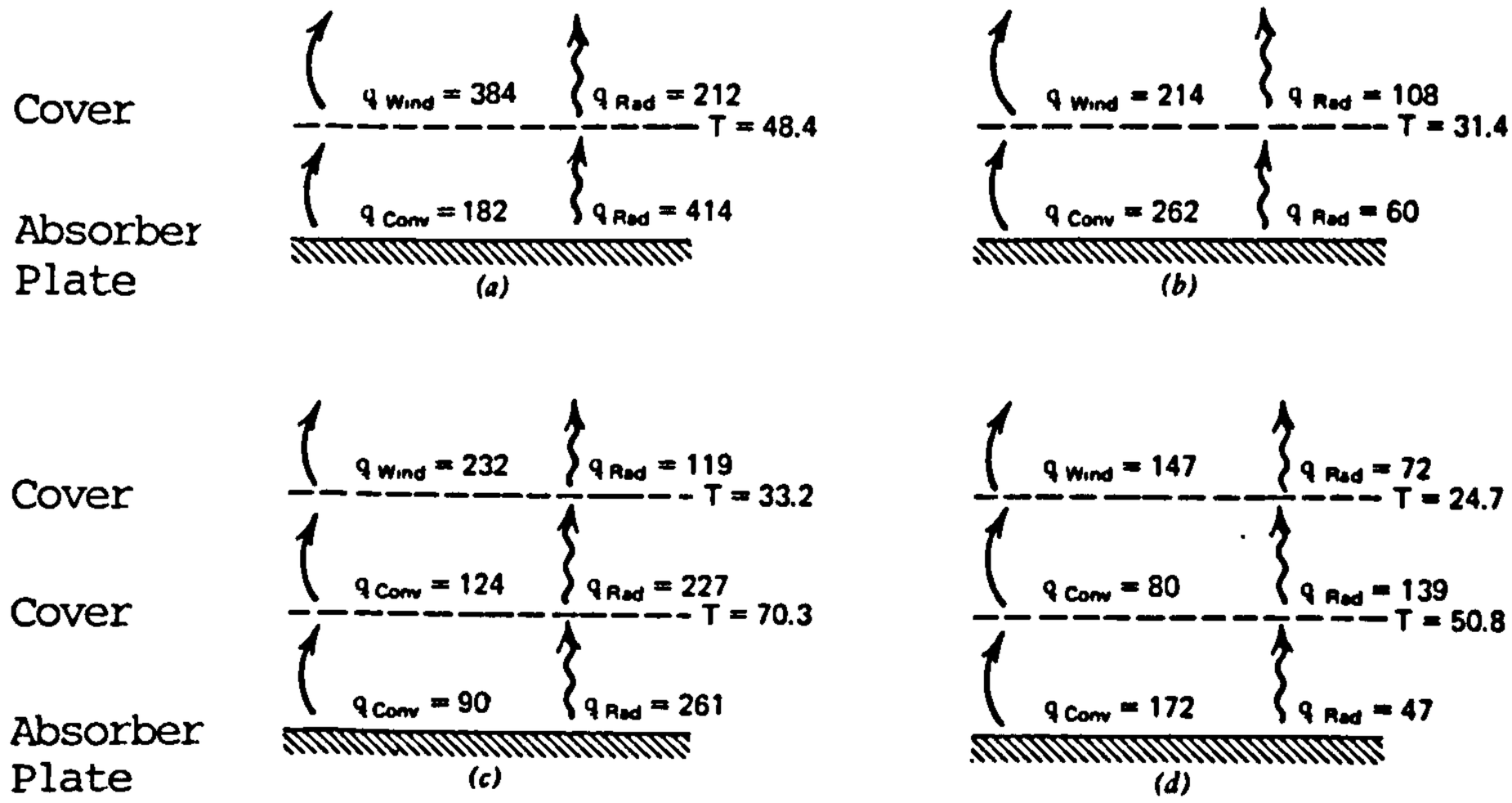

Fig.1.3.(b) Various heat loss calculations for four different solar collectors operating at 100°C with ambient temperature of 10°C; (a) one cover, plate emittance = 0.95; (b) one cover, plate emittance = 0.10; (c) two covers, plate emittance = 0.95; (d) two covers, plate emittance = 0.10; (after Duffie and Beckman, 1980).

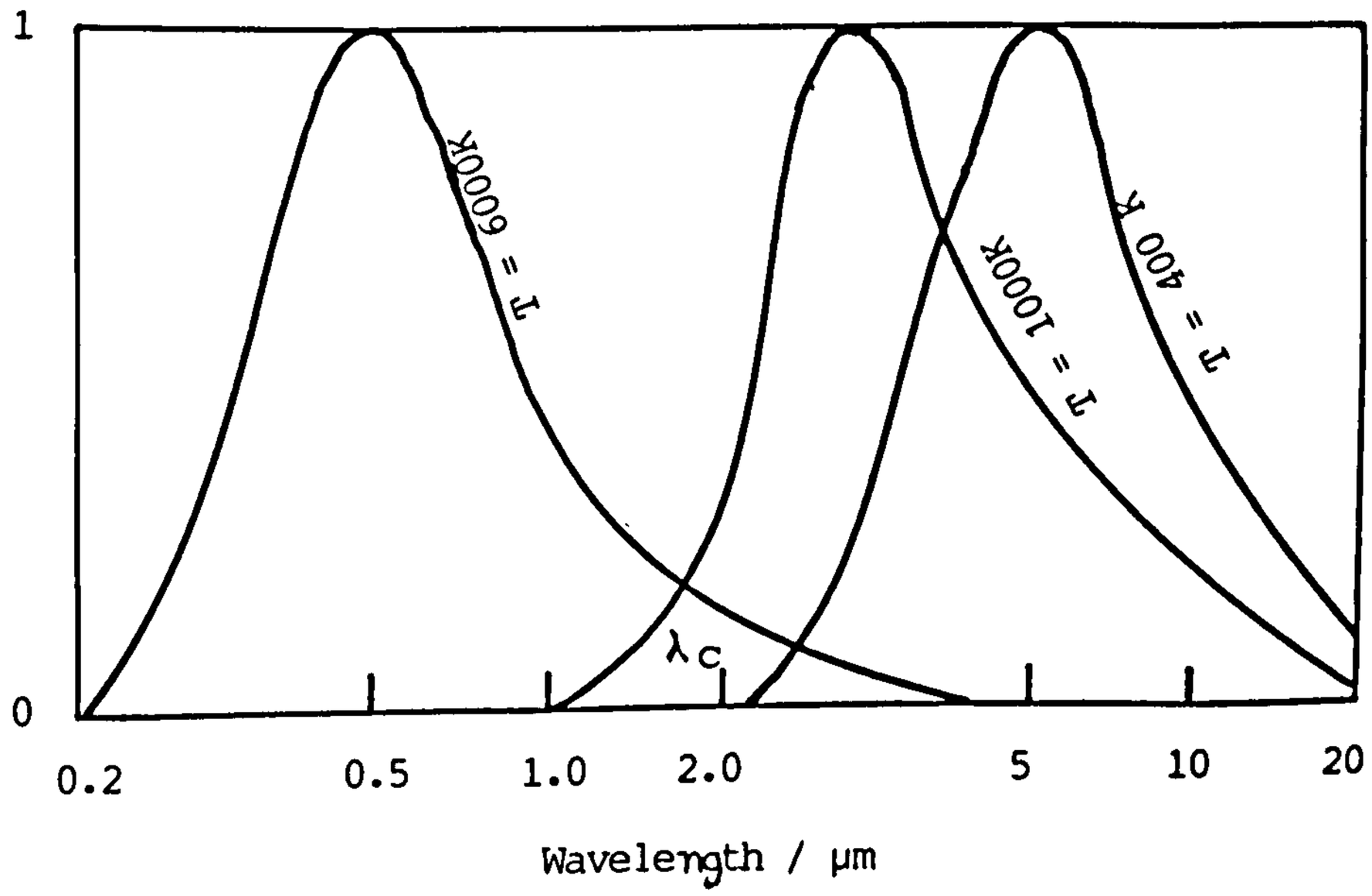

Fig.1.4. Normalised spectral distribution of solar energy and blackbody radiation.

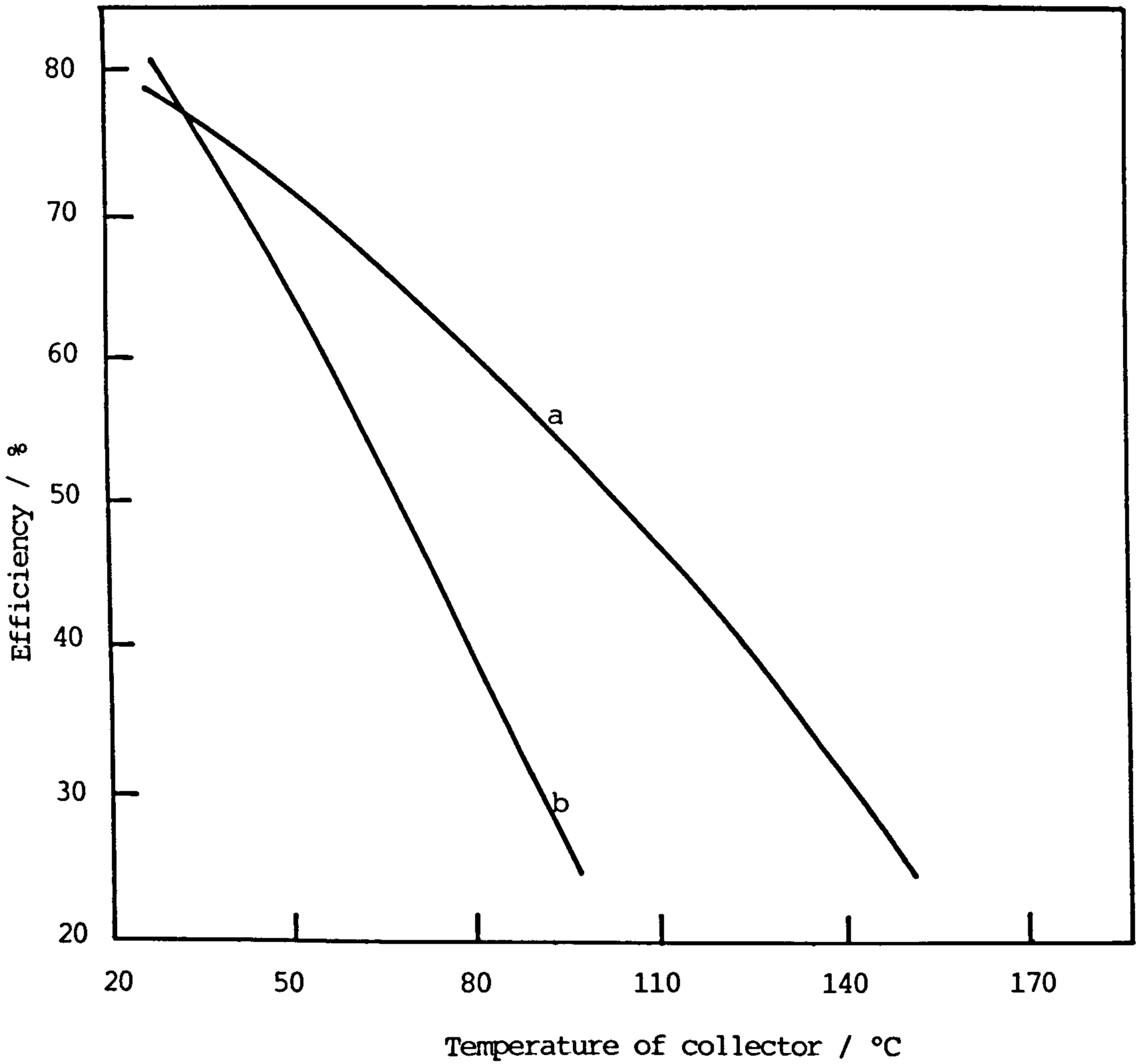

Fig.1.5 The efficiency of a solar energy collector as a function of temperature of the absorber plate: (a) single-glazed selective absorber ($\alpha_s = 0.92$, $\varepsilon_{th} = 0.10$), (b) single-glazed non-selective absorber ($\alpha_s = \varepsilon_{th} = 0.95$)

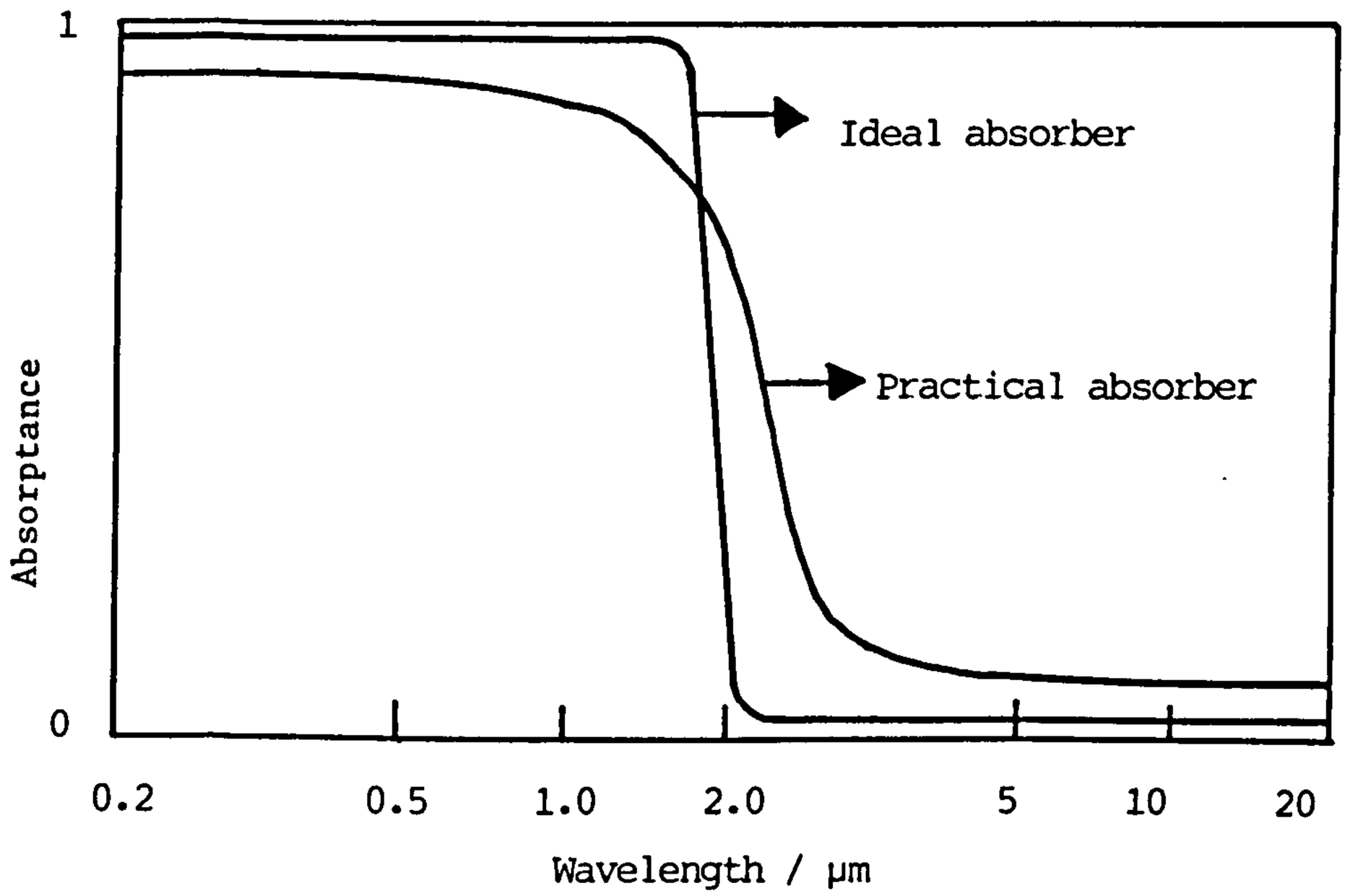

Fig.1.6 Spectral profile of the absorptance for an ideal and practical solar selective surface.

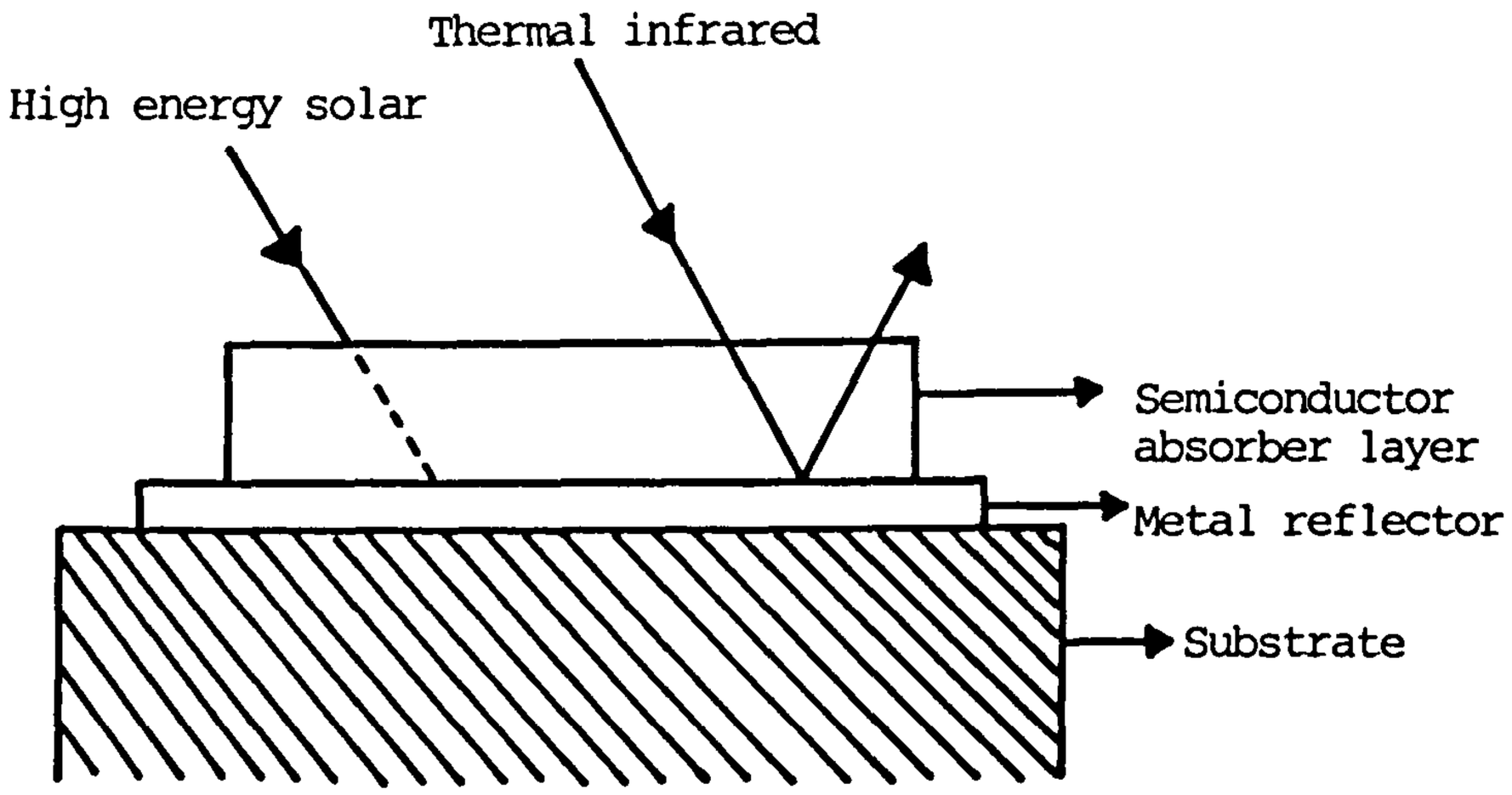

Fig.1.7 Schematic cross-section of a semiconductor-metal tandem selective absorber.

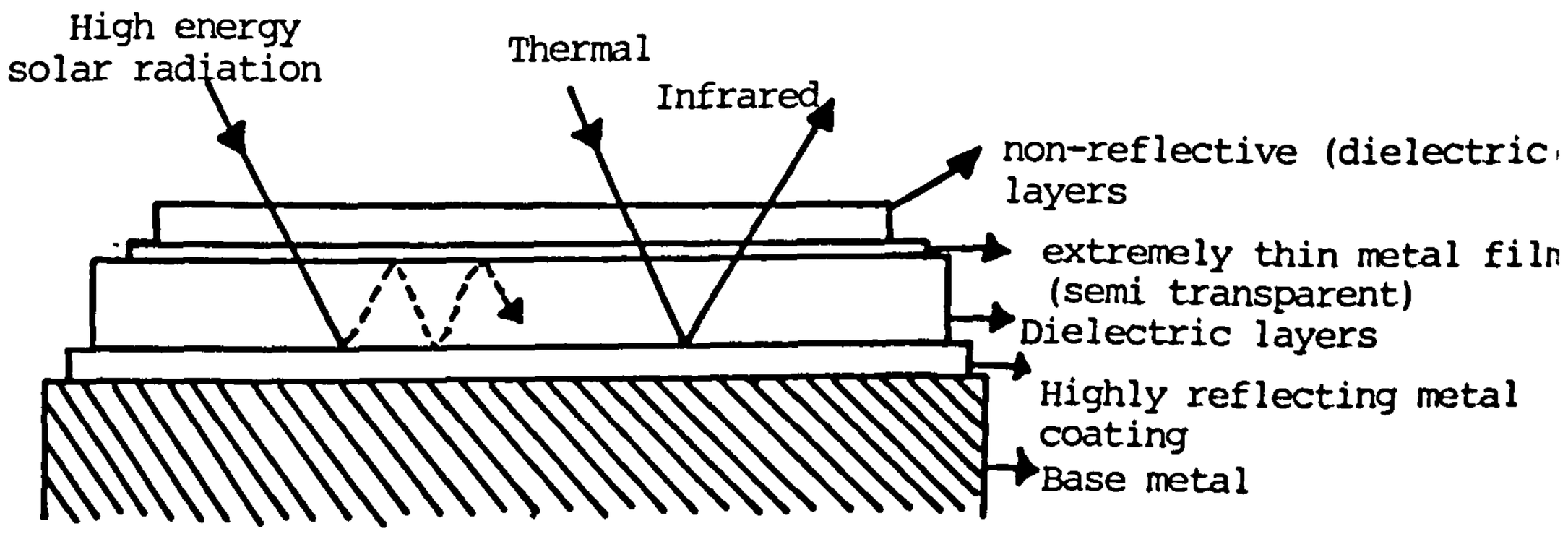

Fig.1.8 Schematic cross section of a four-layer interference stack consisting of two dielectric layers separated by a thin semi-transparent metal film.

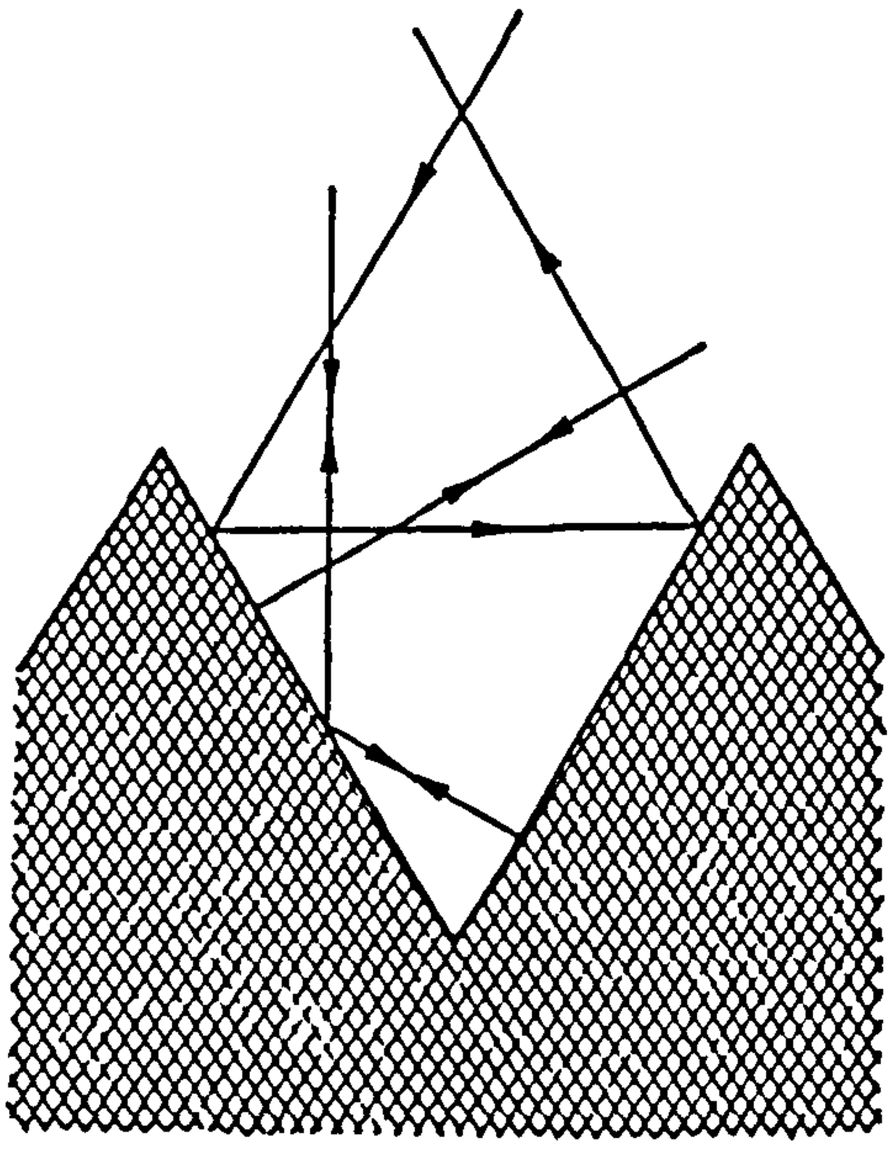

Fig.1.9(a) V-corrugated selective surface showing multiple reflection of the incident solar radiation.

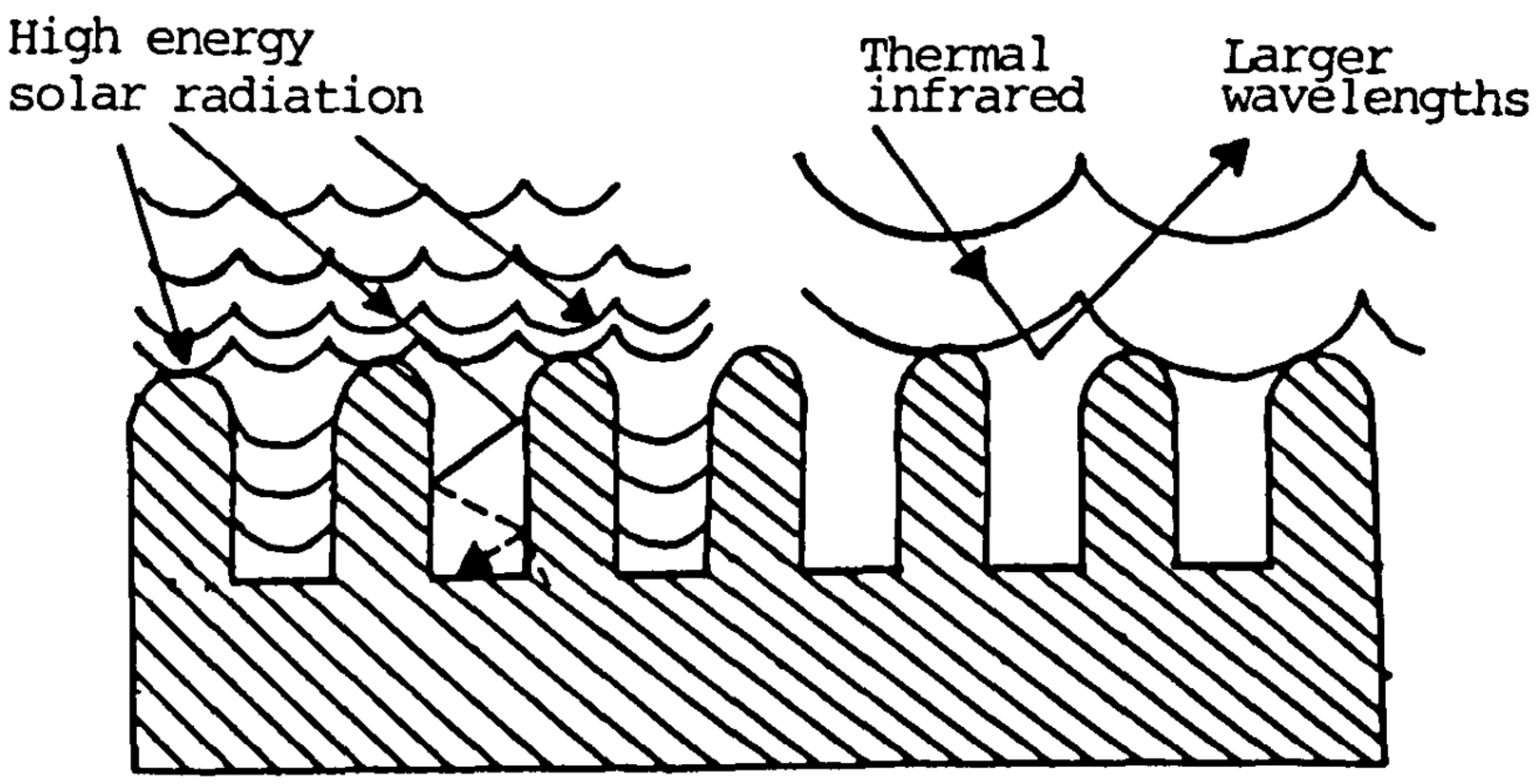

Fig.1.9(b) Wavefront discrimination effect on texturised surface (schematically).

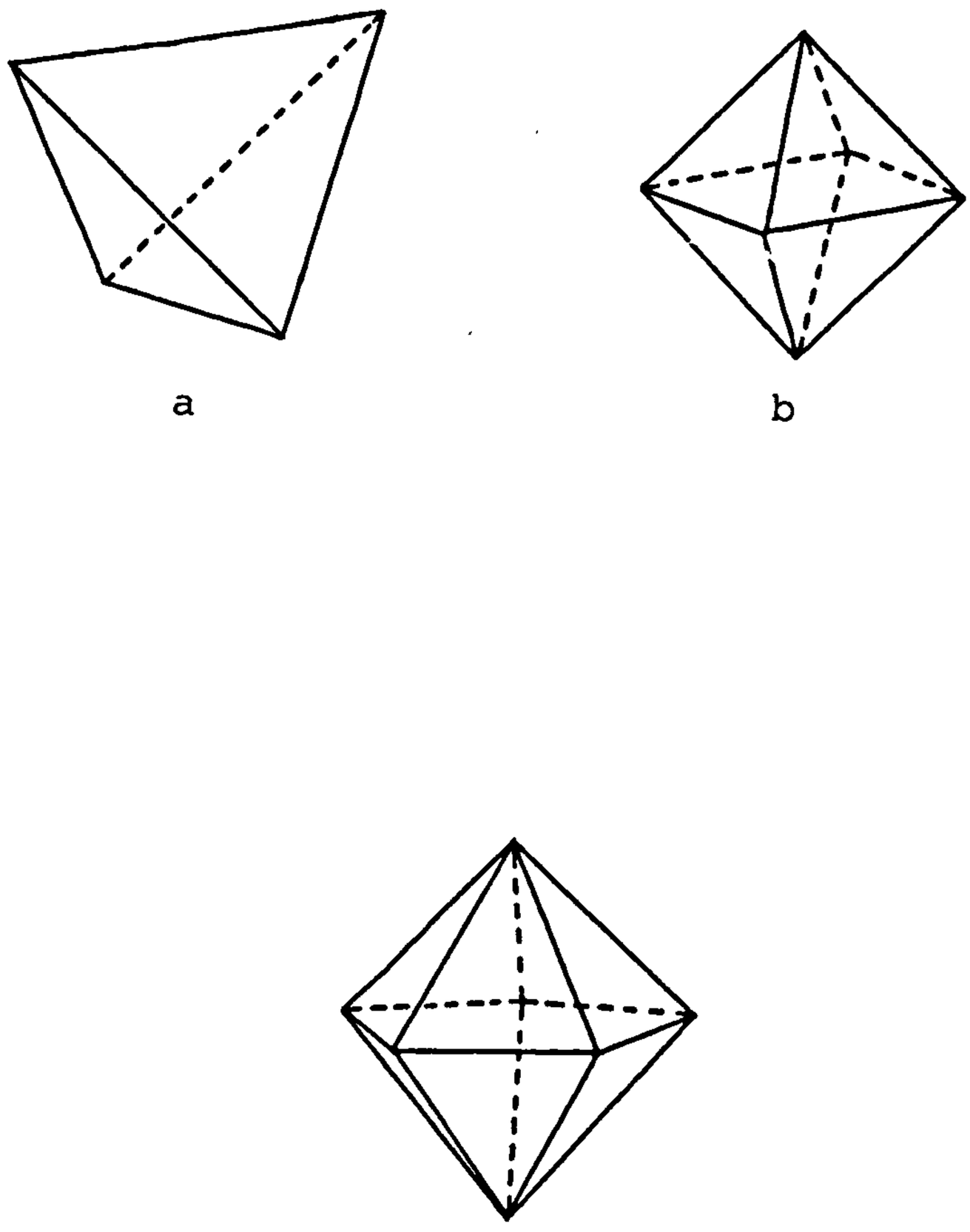

Fig.1.10(a) Diagram of (a) Tetrahedron, (b) Octahedron and (c) Pentagonal bipyramid.

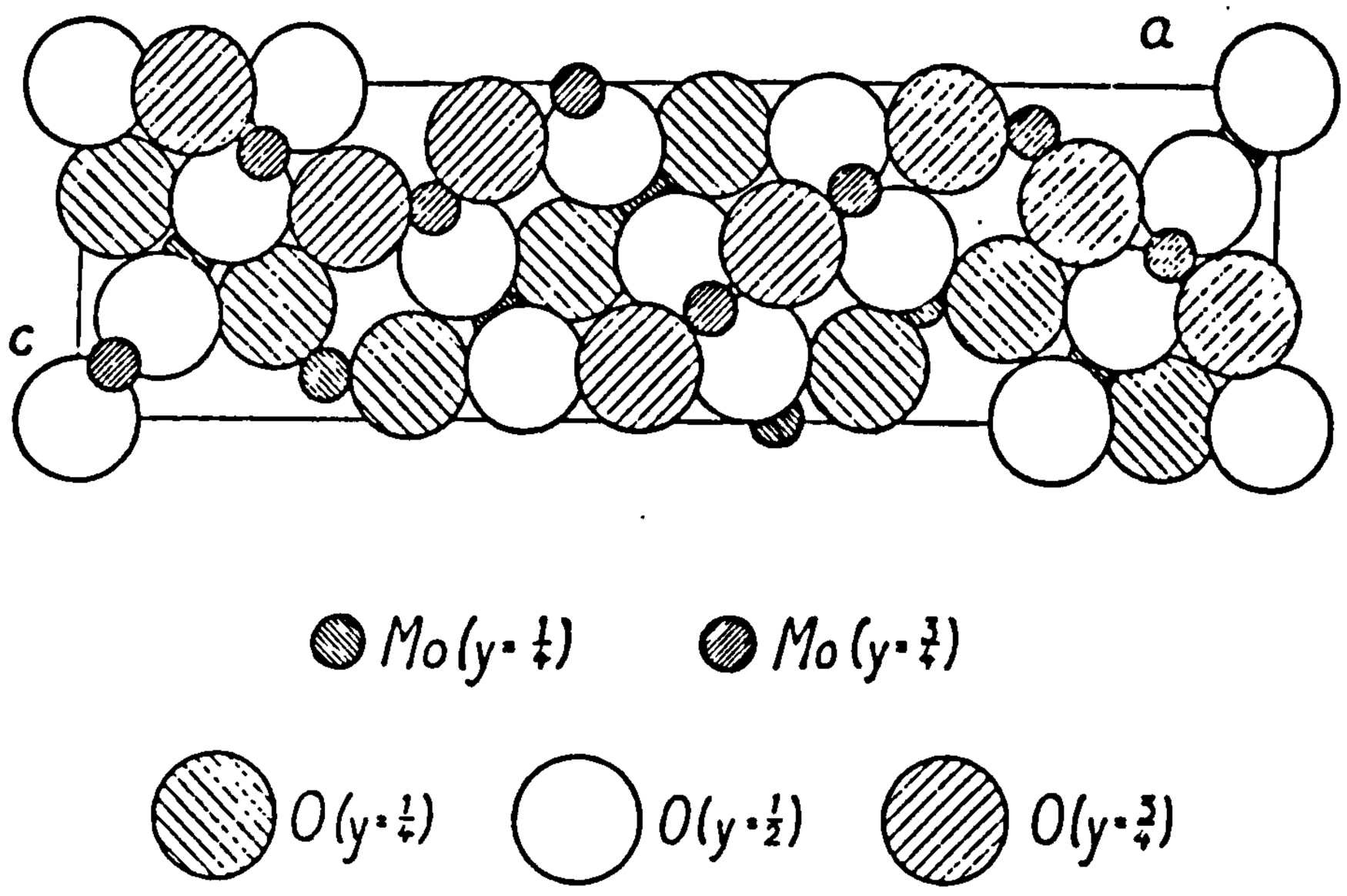

Fig.1.10.(b) Projection of the unit cell of Mo_4O_{11} parallel to [0 1 0] (after Magneli, 1948).

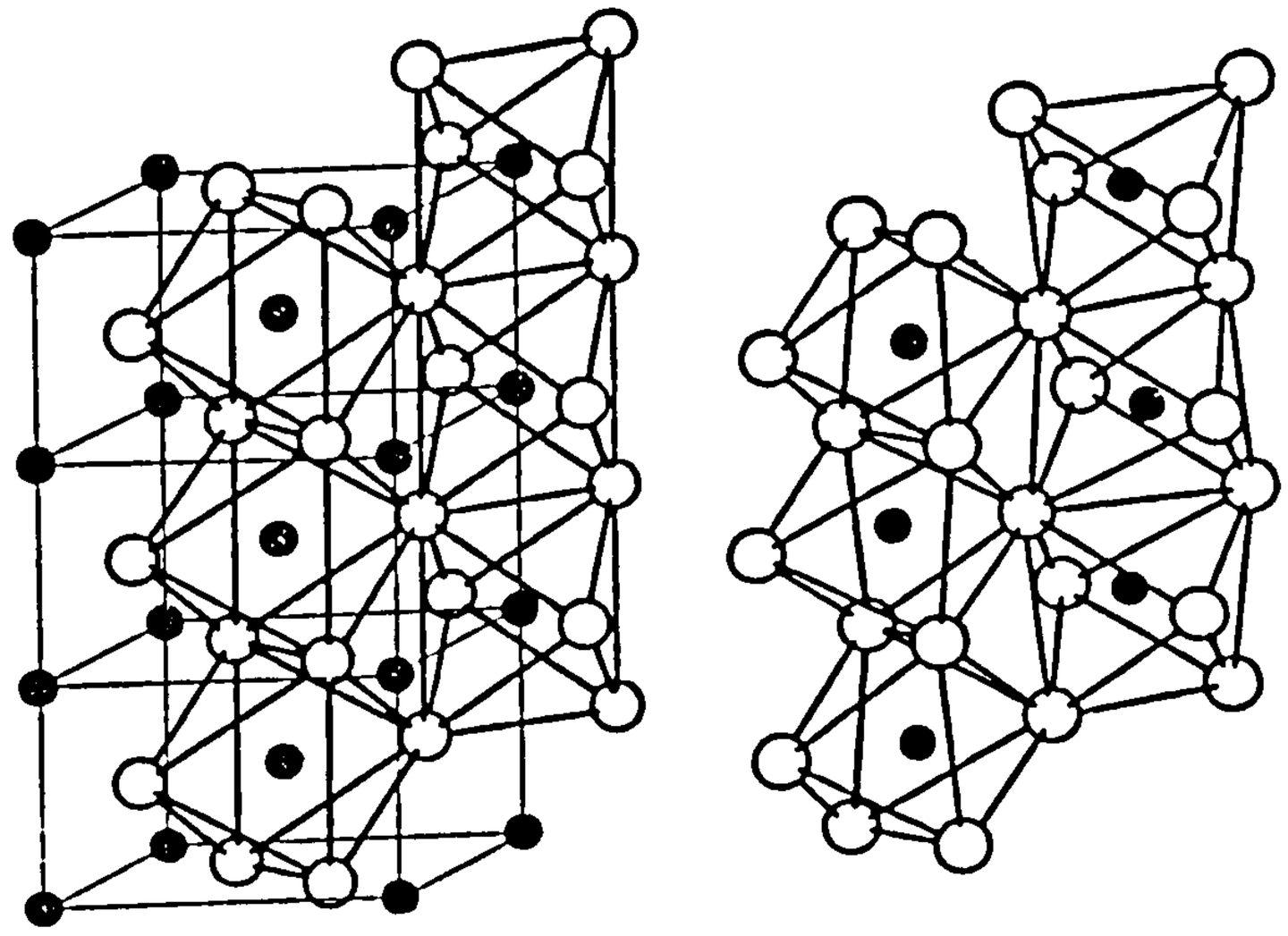

(a) (b)

Fig.1.11. (a) The rutile structure type. Three unit cells are indicated.

(b) The MoO_2 structure type. The black circles represent Mo-atoms.
(after Magneli and Andersson, 1955).

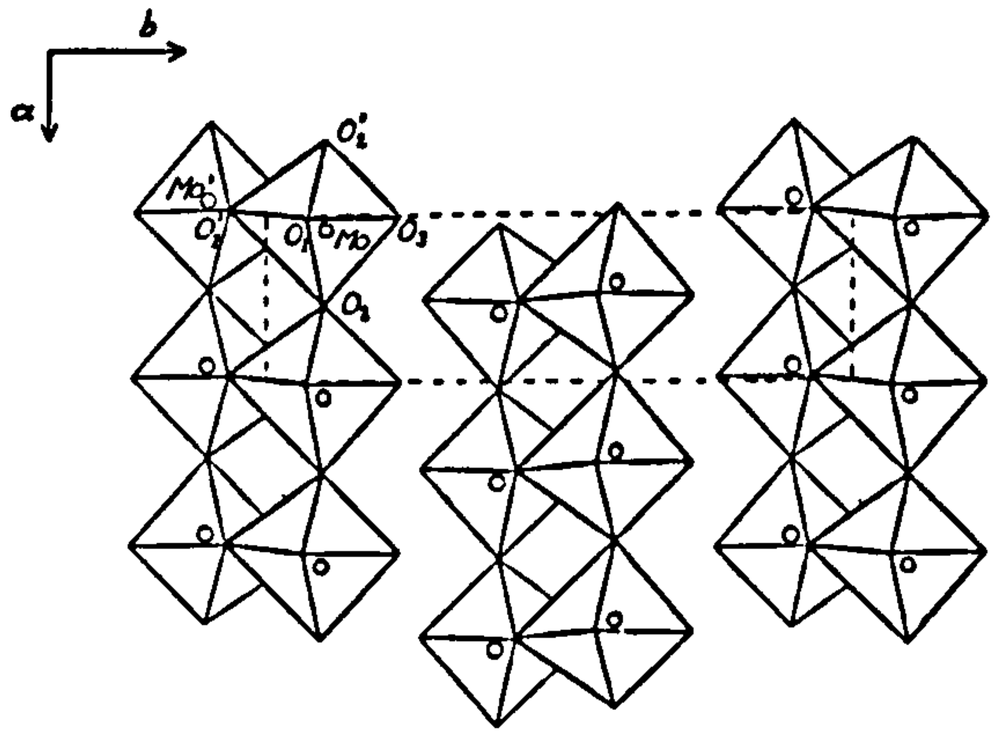

Fig.1.12. Crystal structure of MoO_3 viewed along (001). The extension of one unit cell is indicated by dashed lines; (after Andersson and Magneli, 1950).

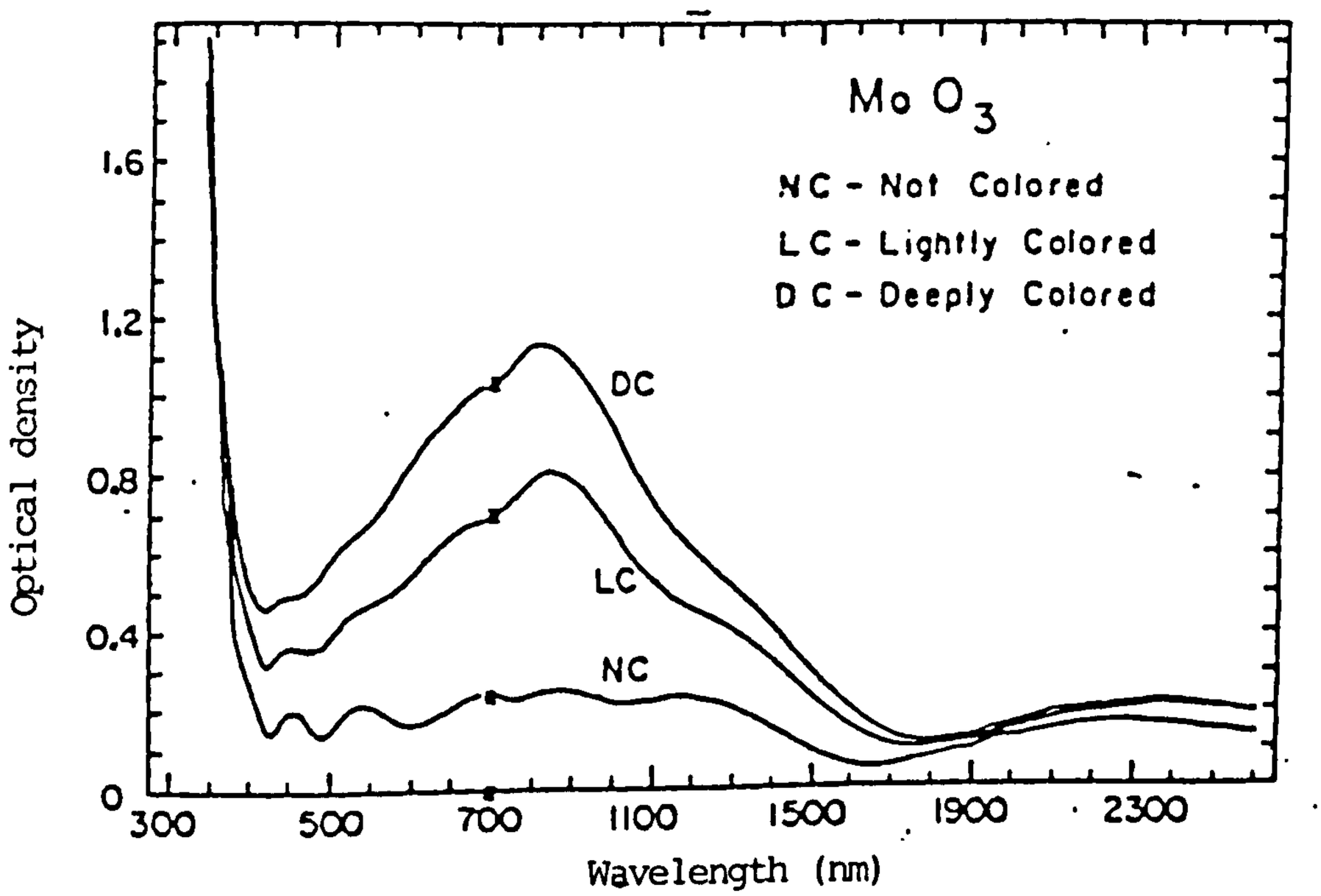

Fig.1.13. Optical absorption spectra of MoO_3 before and after electrolytic colouration. (after Colton et al, 1978).

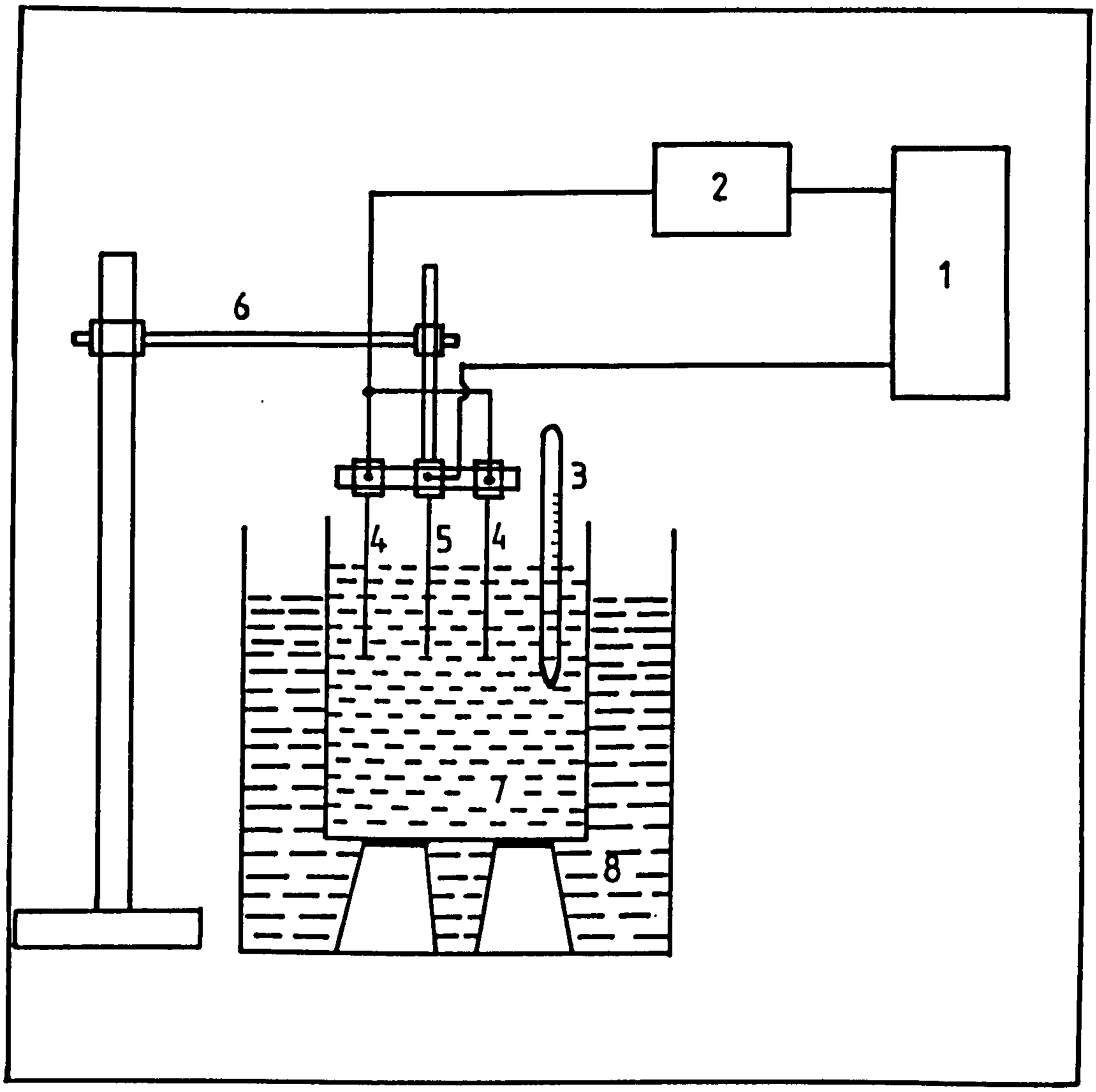

Fig. 2.1. Schematic diagram of electrodeposition apparatus.

1. Low voltage stabilized power supply.
2. Ammeter
3. Thermometer
4. Anodes
5. Substrate
6. Specimen holder
7. Solution tank
8. Hot water bath

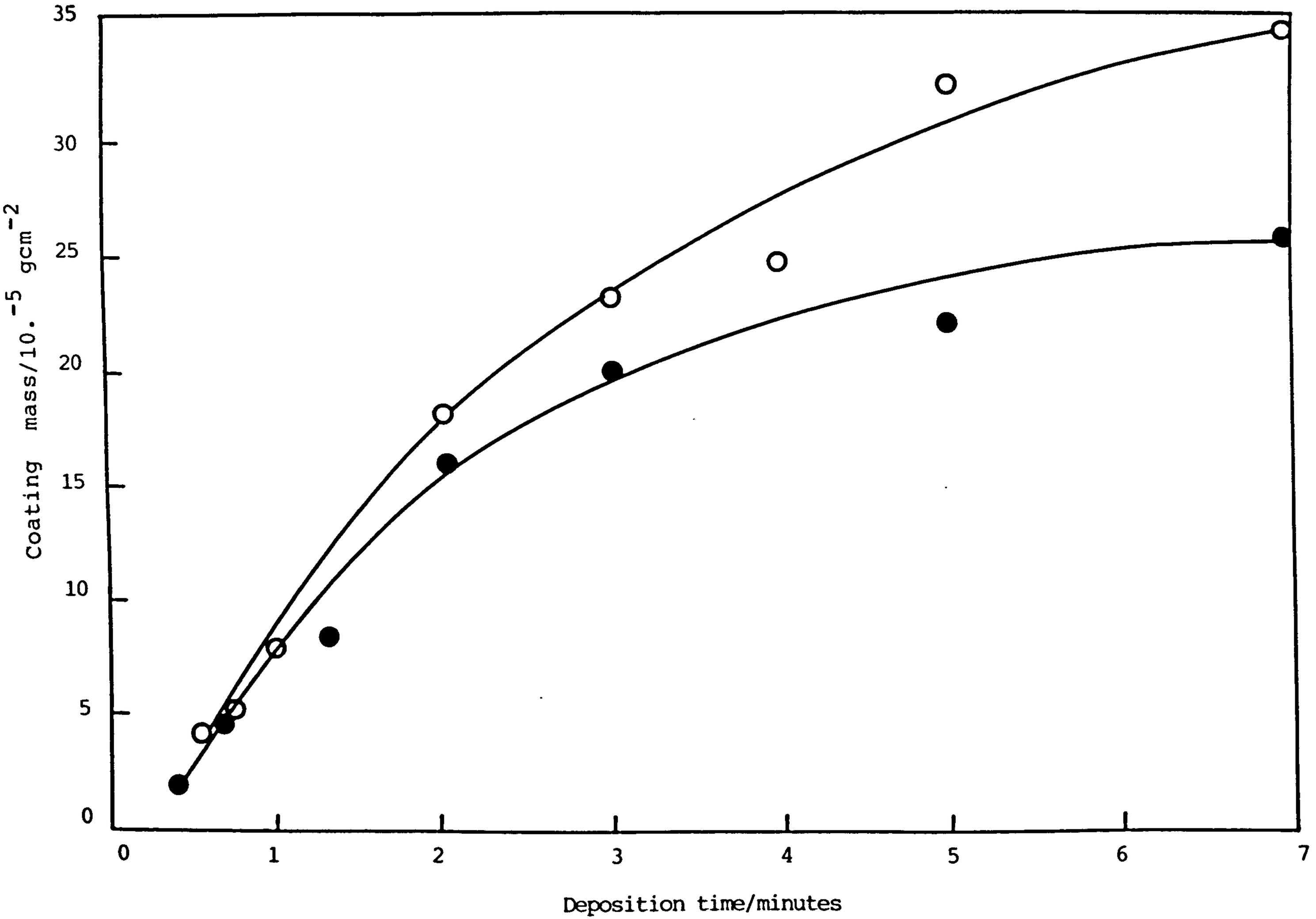

Fig. 2.2 Variation of coating mass per unit area with deposition time for Mo-black dip coatings on Zn substrates; O Etched Zinc
● Unetched Zinc

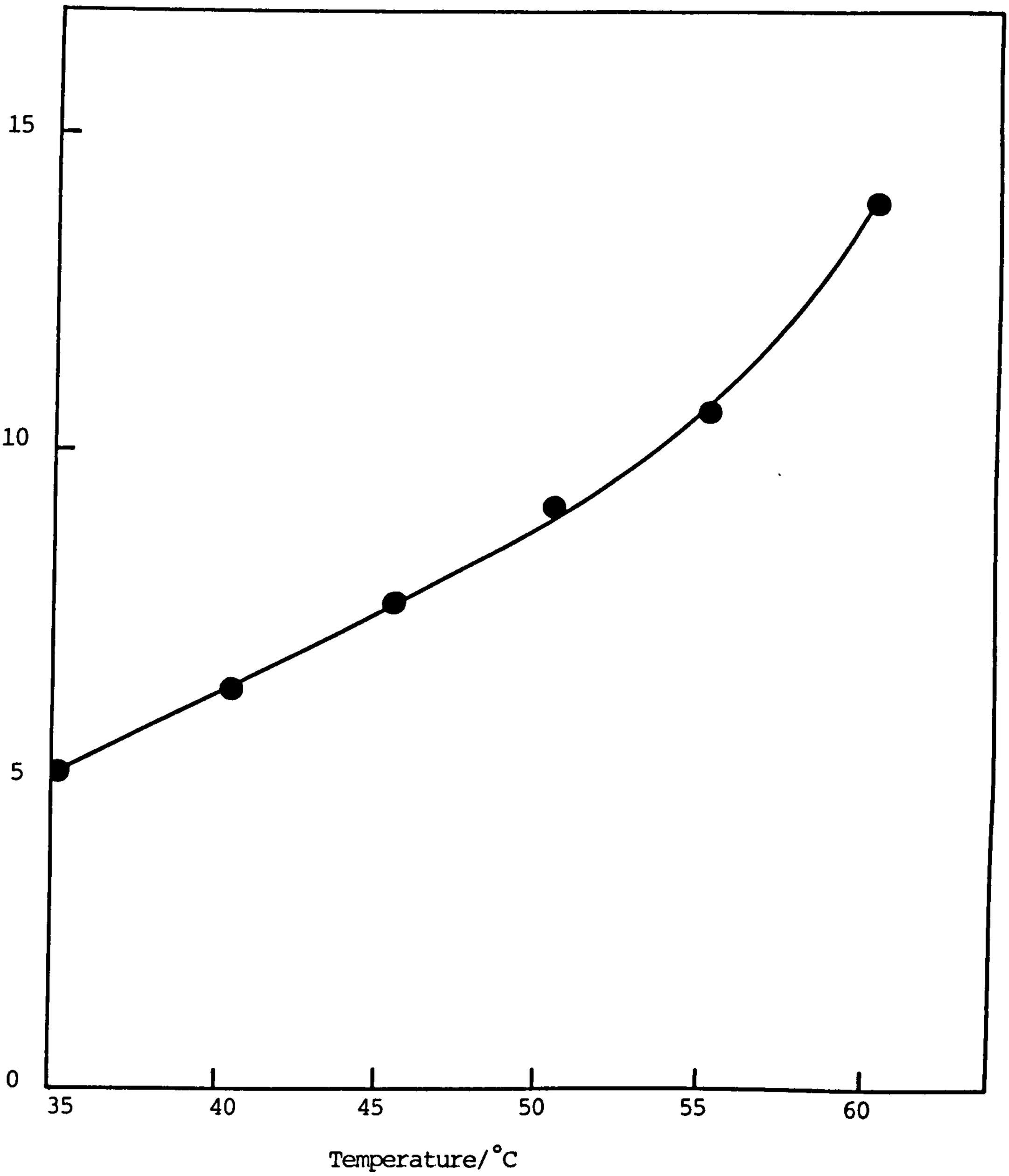

Fig. 2.3. Variation of coating mass per unit area with temperature of the plating solution for Mo-black dip coatings on etched Zn substrates at fixed deposition time (60 seconds).

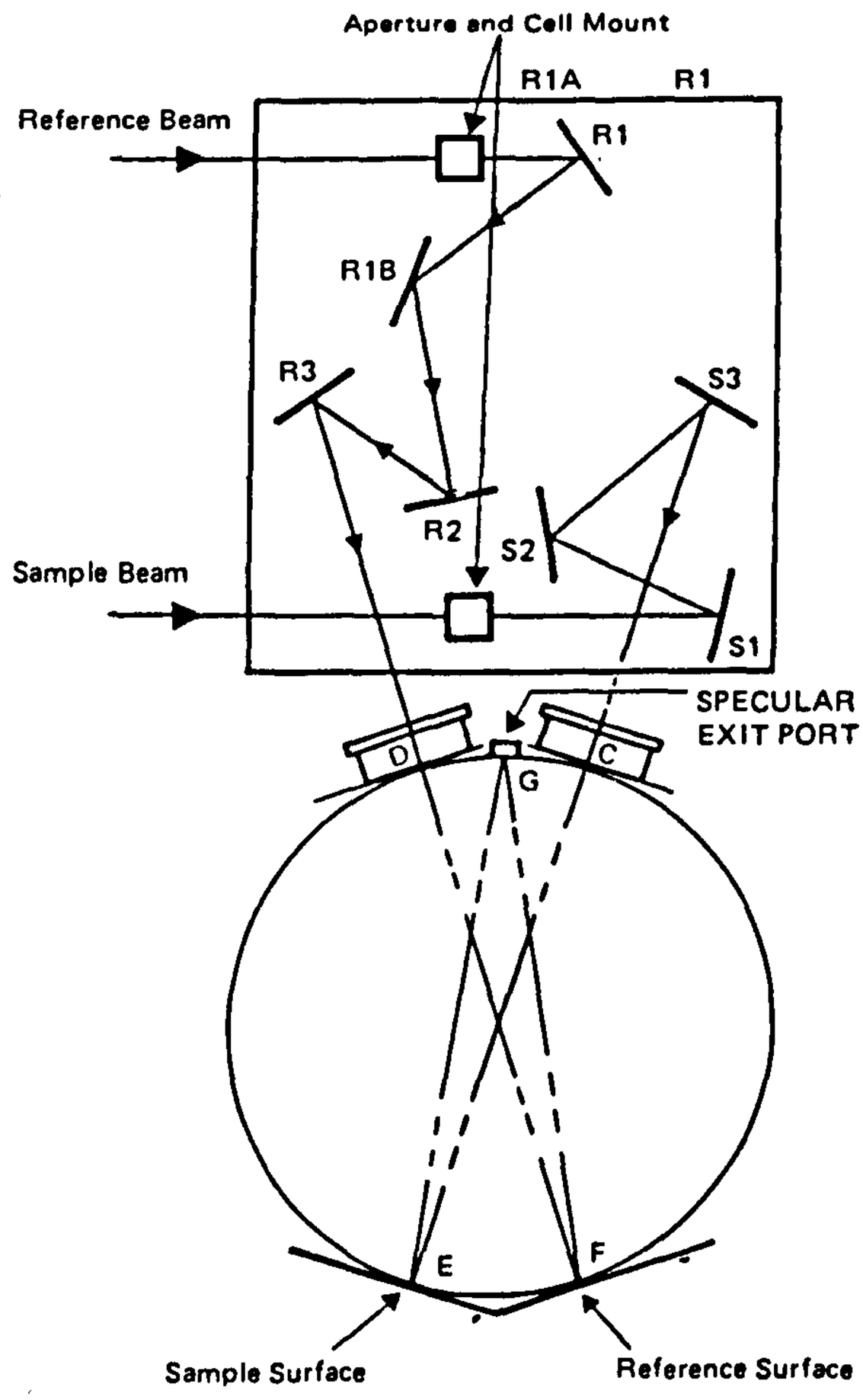

Fig.2.4(a) Optical diagram of an integrating sphere.

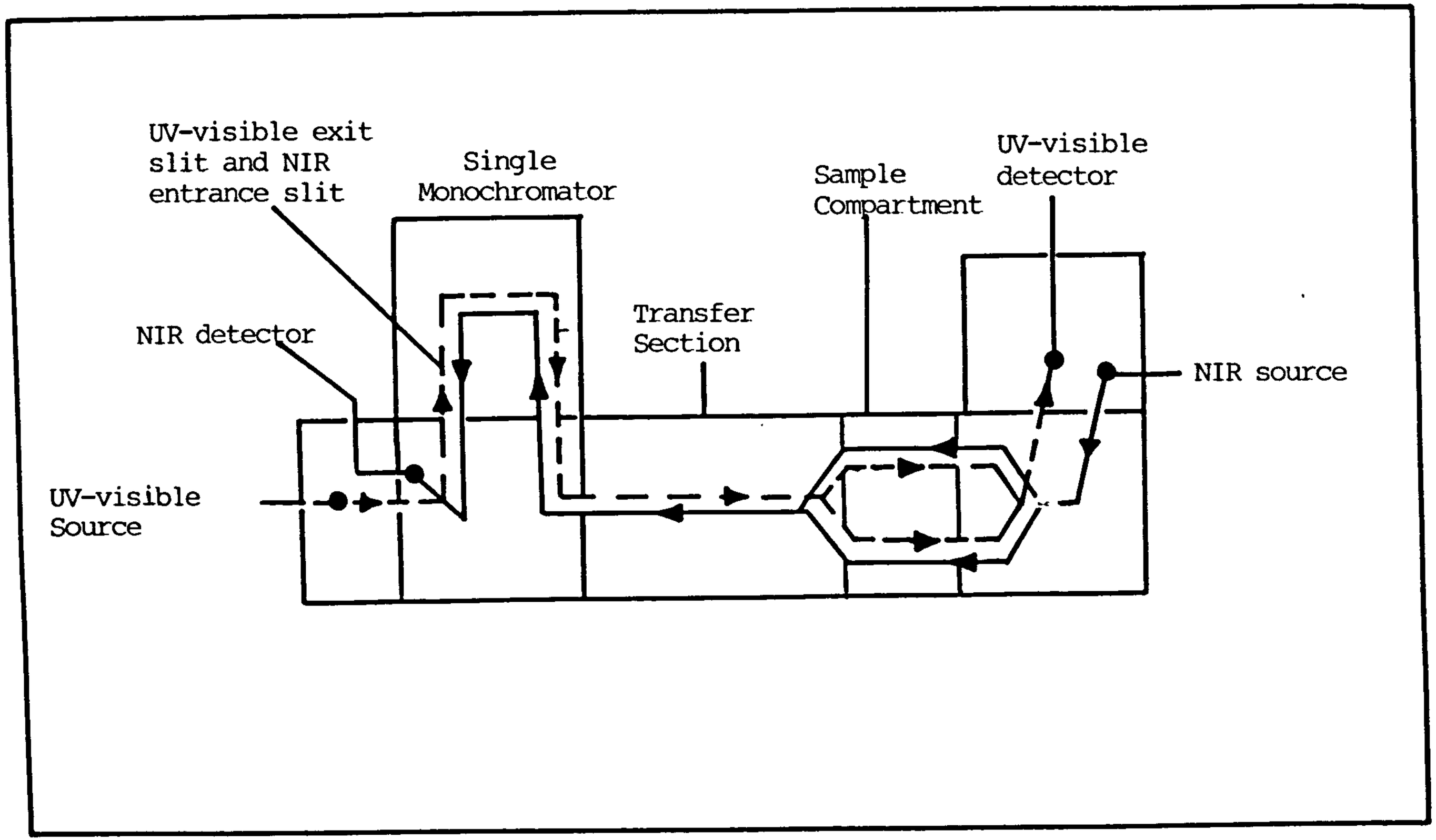

Fig. 2.4(b) Optical block diagram of Beckman 5240 UV-visible-NIR Spectrophotometer: (------) NIR light path, (————) UV-visible light path.

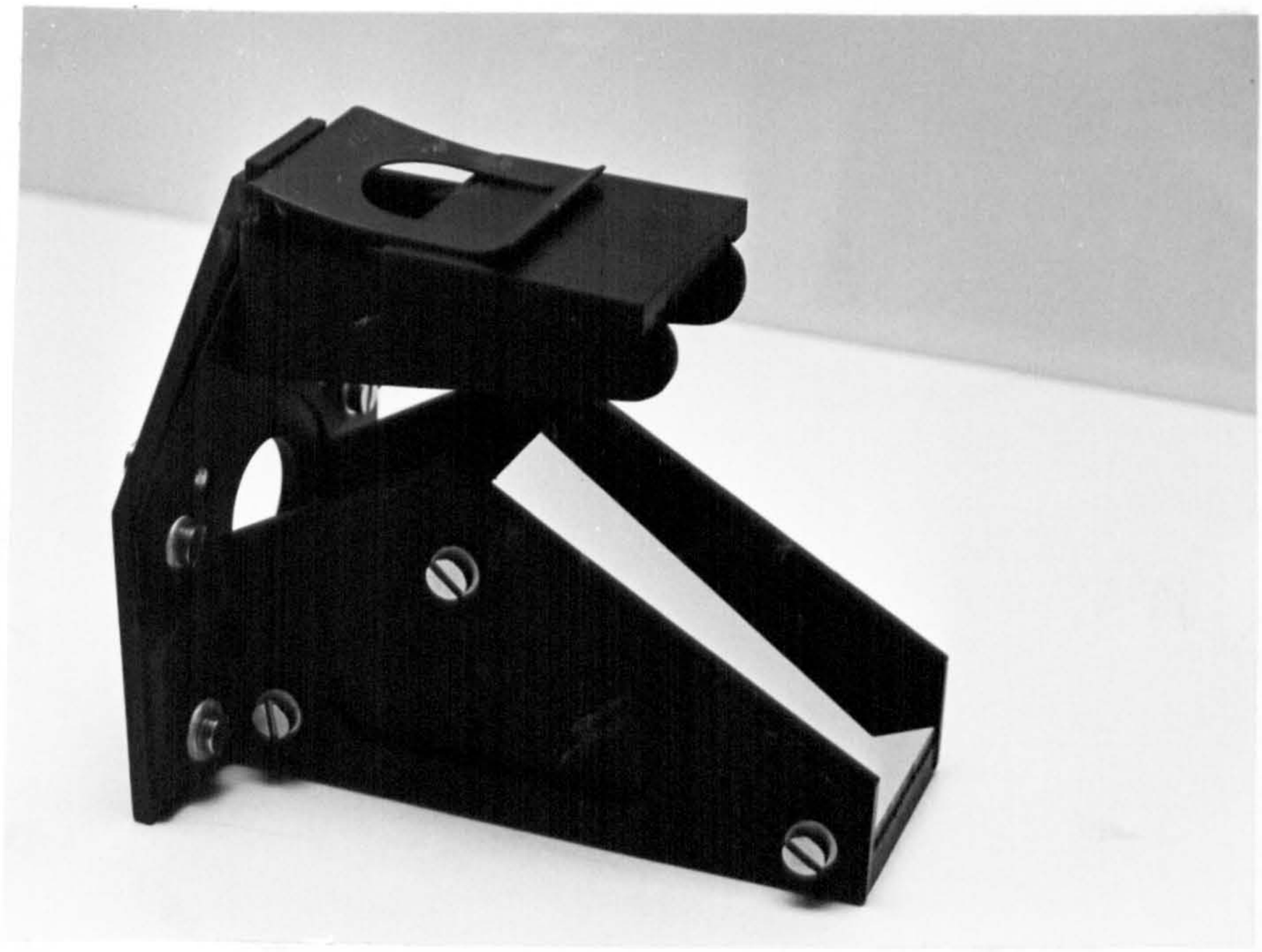

(a) Photograph

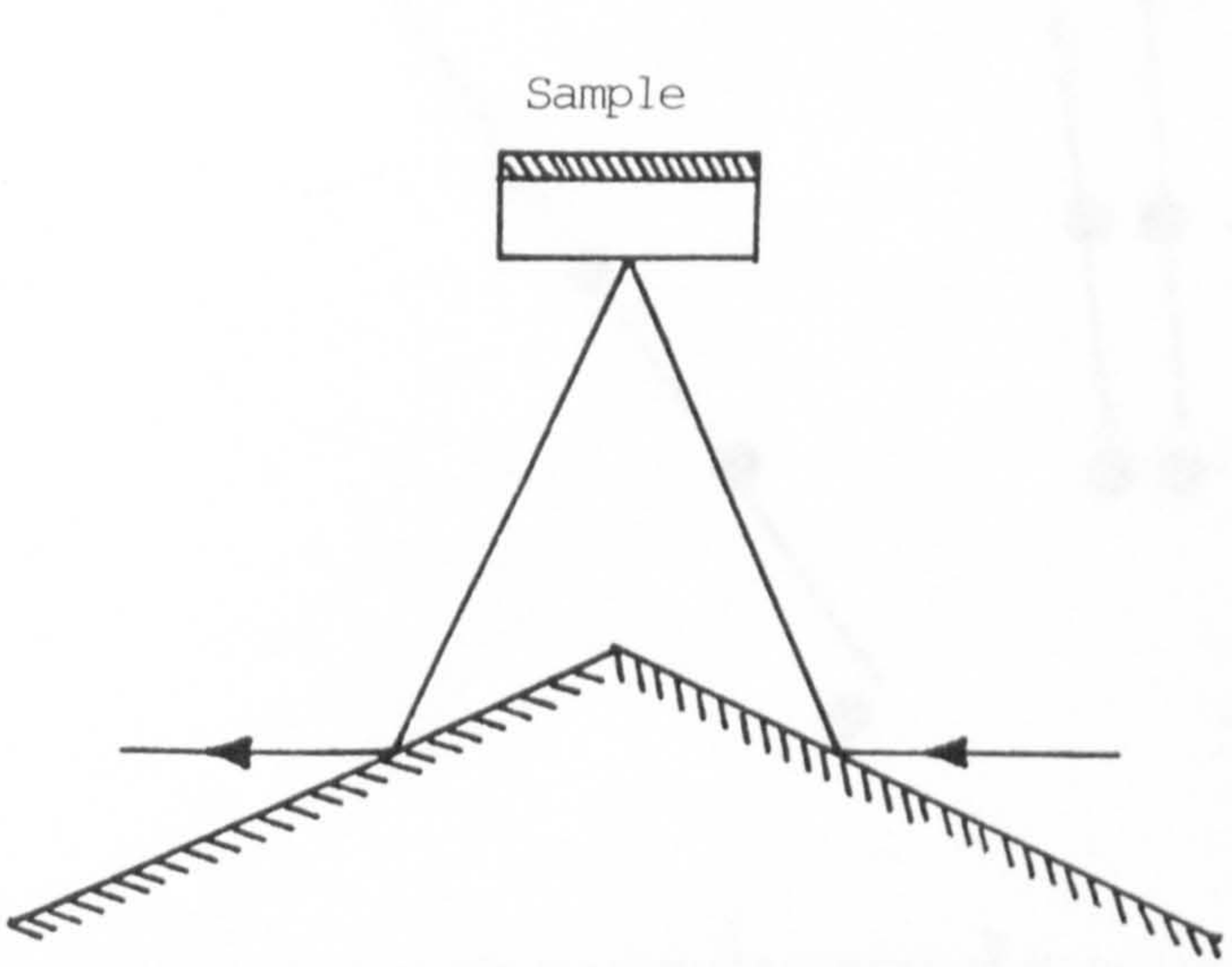

(b) Optical diagram

Fig. 2.5. Photograph and optical diagram of specular reflectance attachment for Perkin Elmer 683 IR spectrometer.

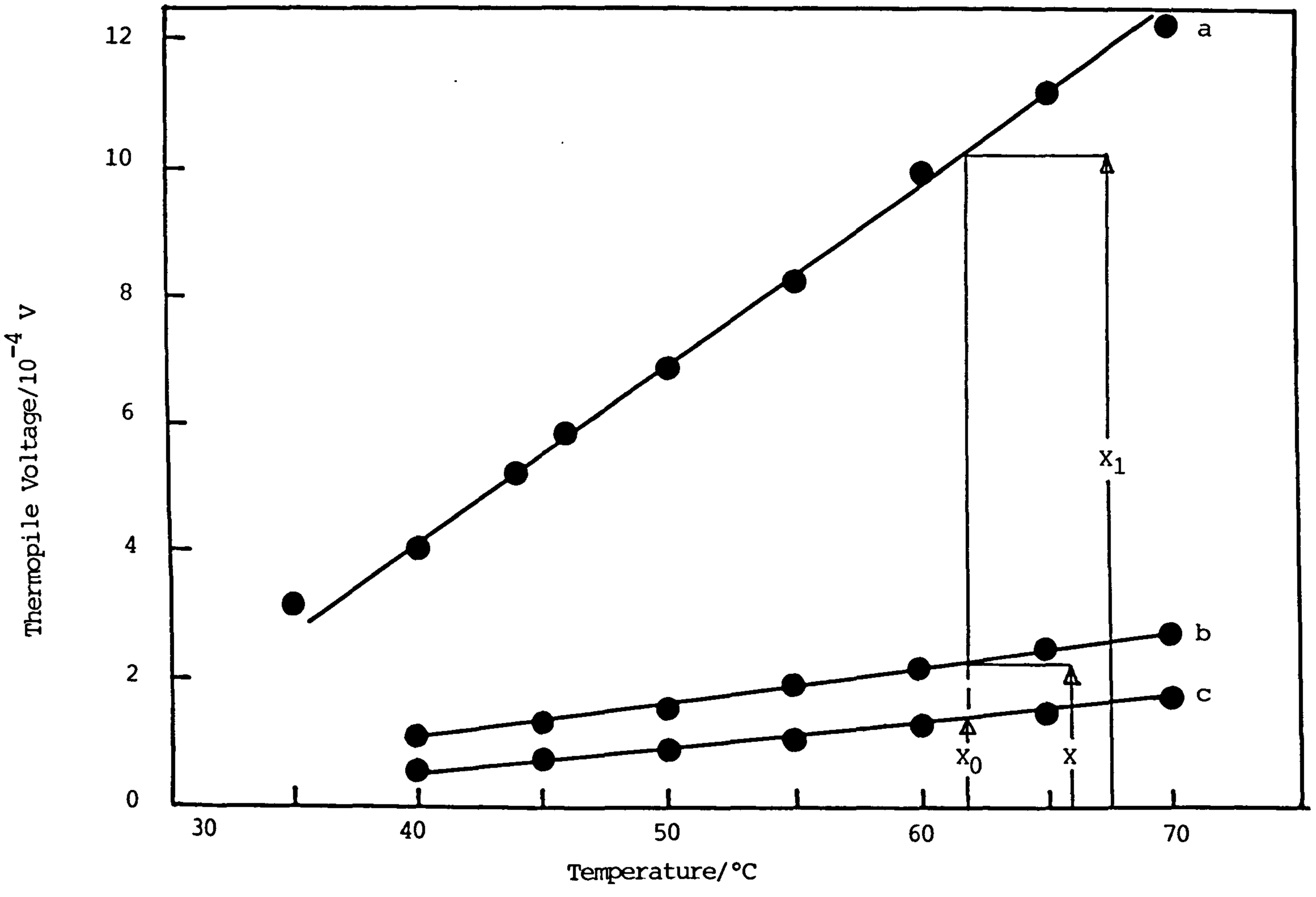

Fig. 2.6. Thermopile output as a function of the temperature of the specimen.
a) Nextel paint b) Mo-black dip coatings on etched zinc
c) Bright aluminium

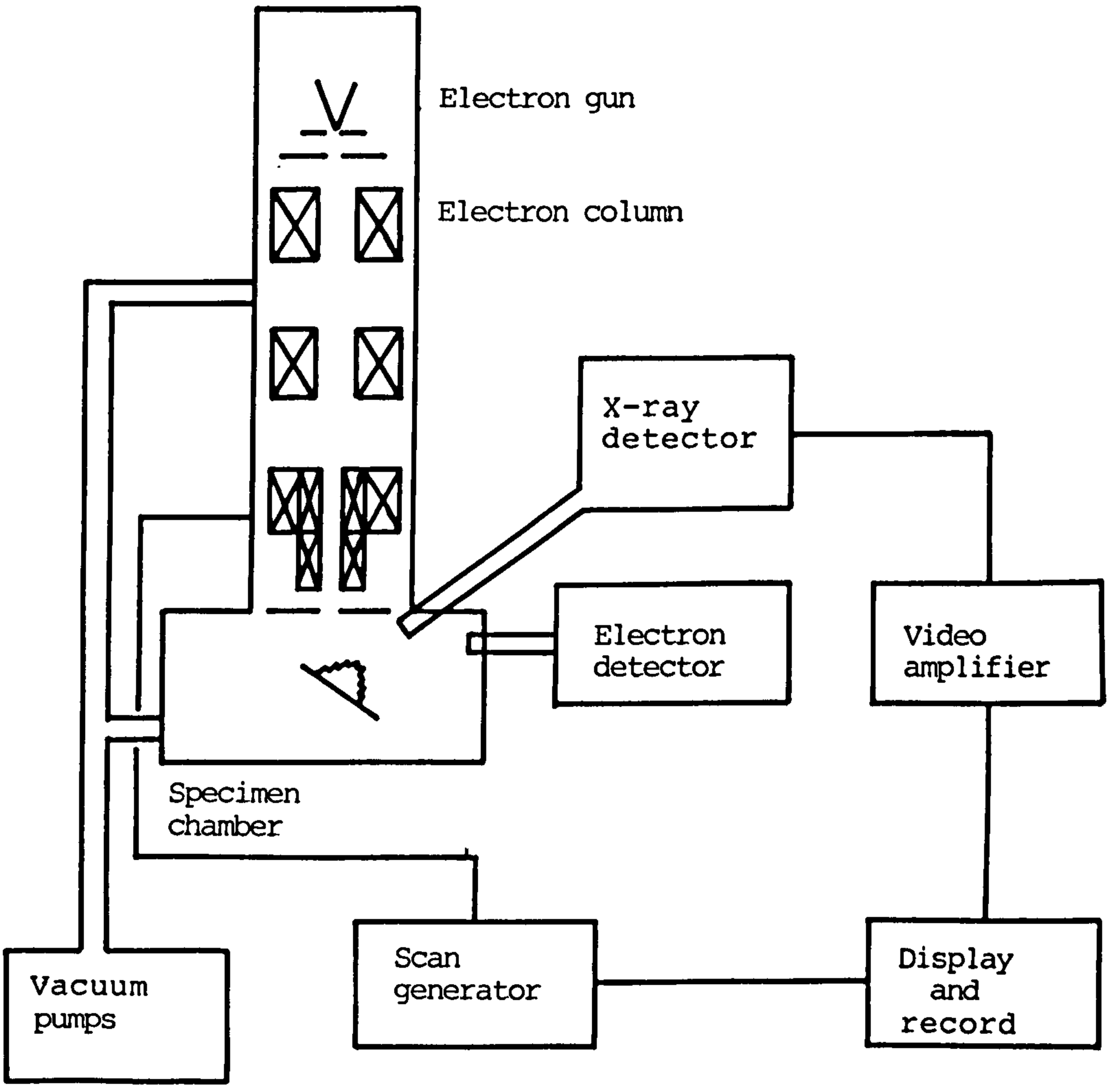

Fig. 2.7. Block diagram of scanning electron microscope.

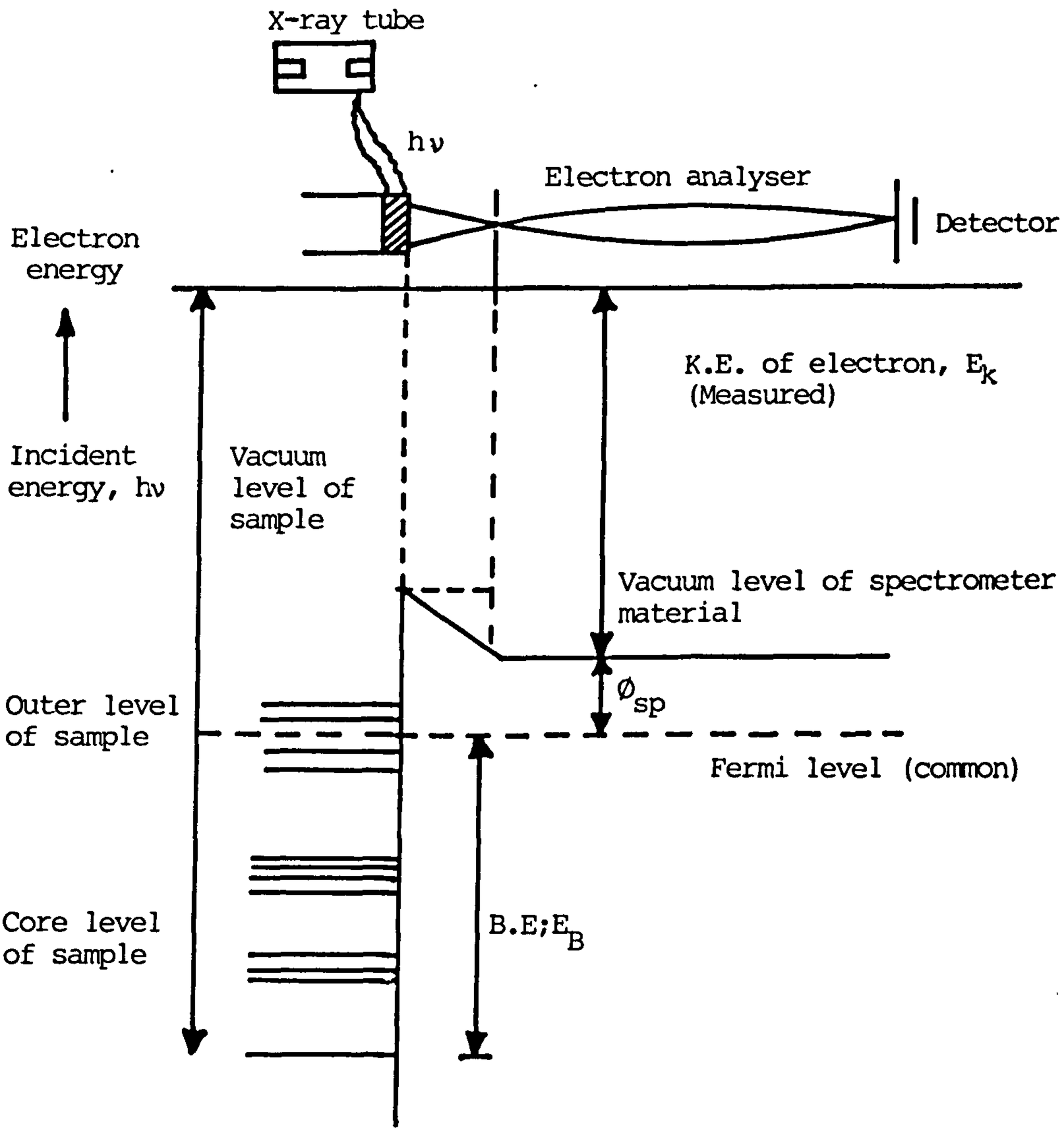

Fig. 2.9. Energy level scheme for a conducting sample in electric equilibrium with the spectrometer (XPS). The upper part of the figure shows experimental arrangements schematically. (after Briggs, 1978)

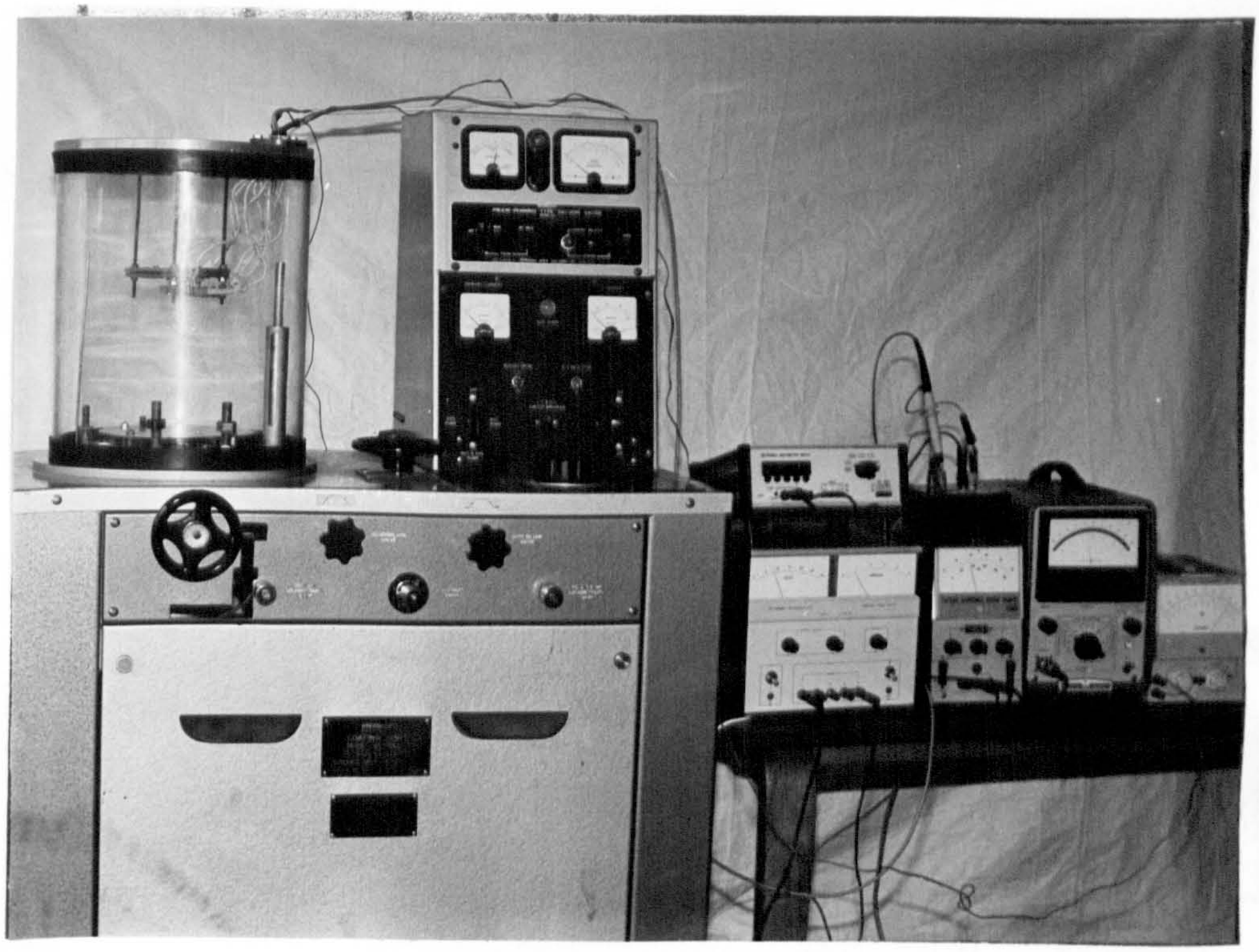

Fig. 2.10 Experimental arrangement for electrical measurements.

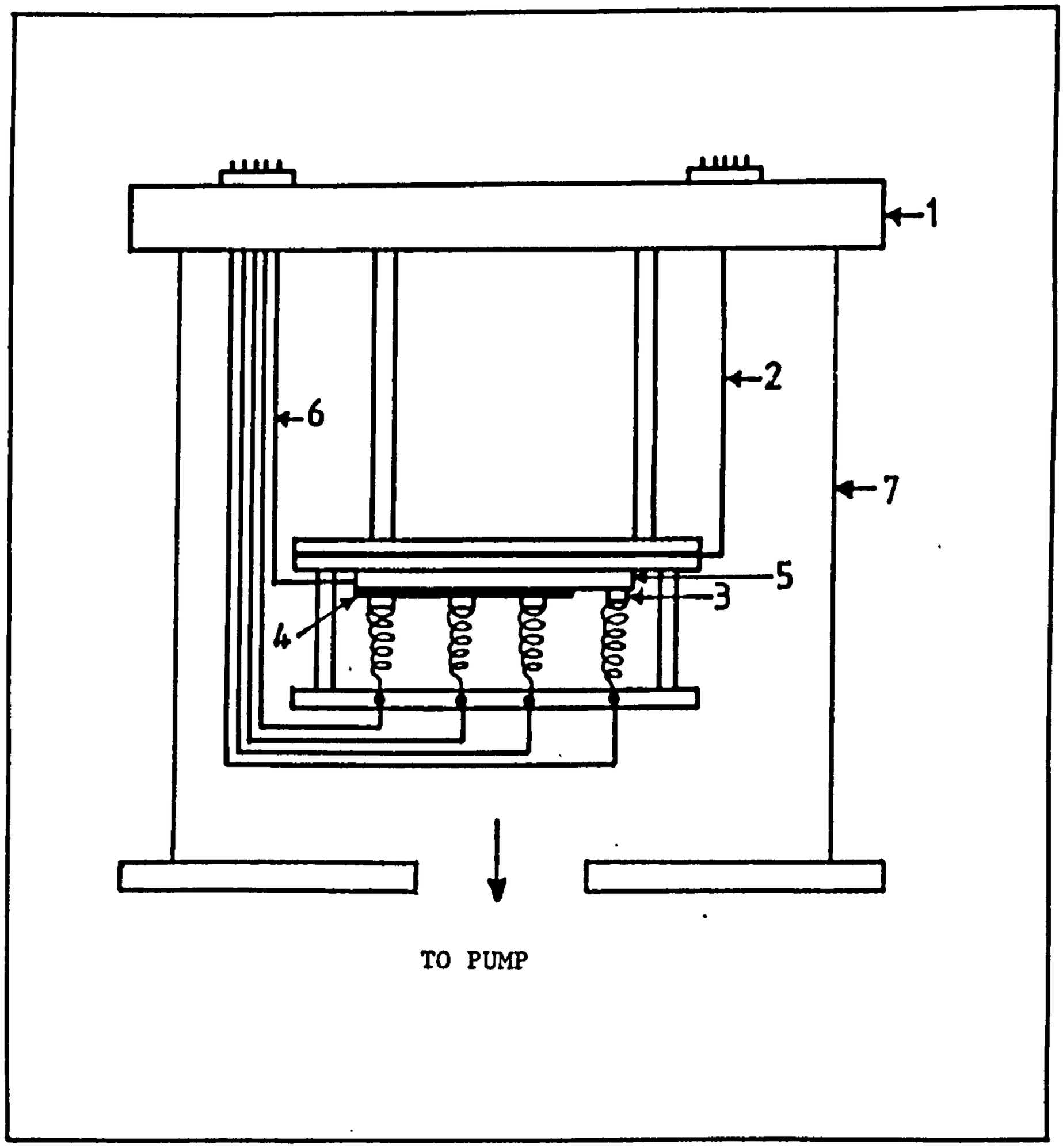

Fig. 2.11. Schematic diagram of the specimen holder in the vacuum chamber.

1. Top cover
2. Heater
3. Contact
4. Coating
5. Substrate
6. Thermocouple
7. Glass bell jar

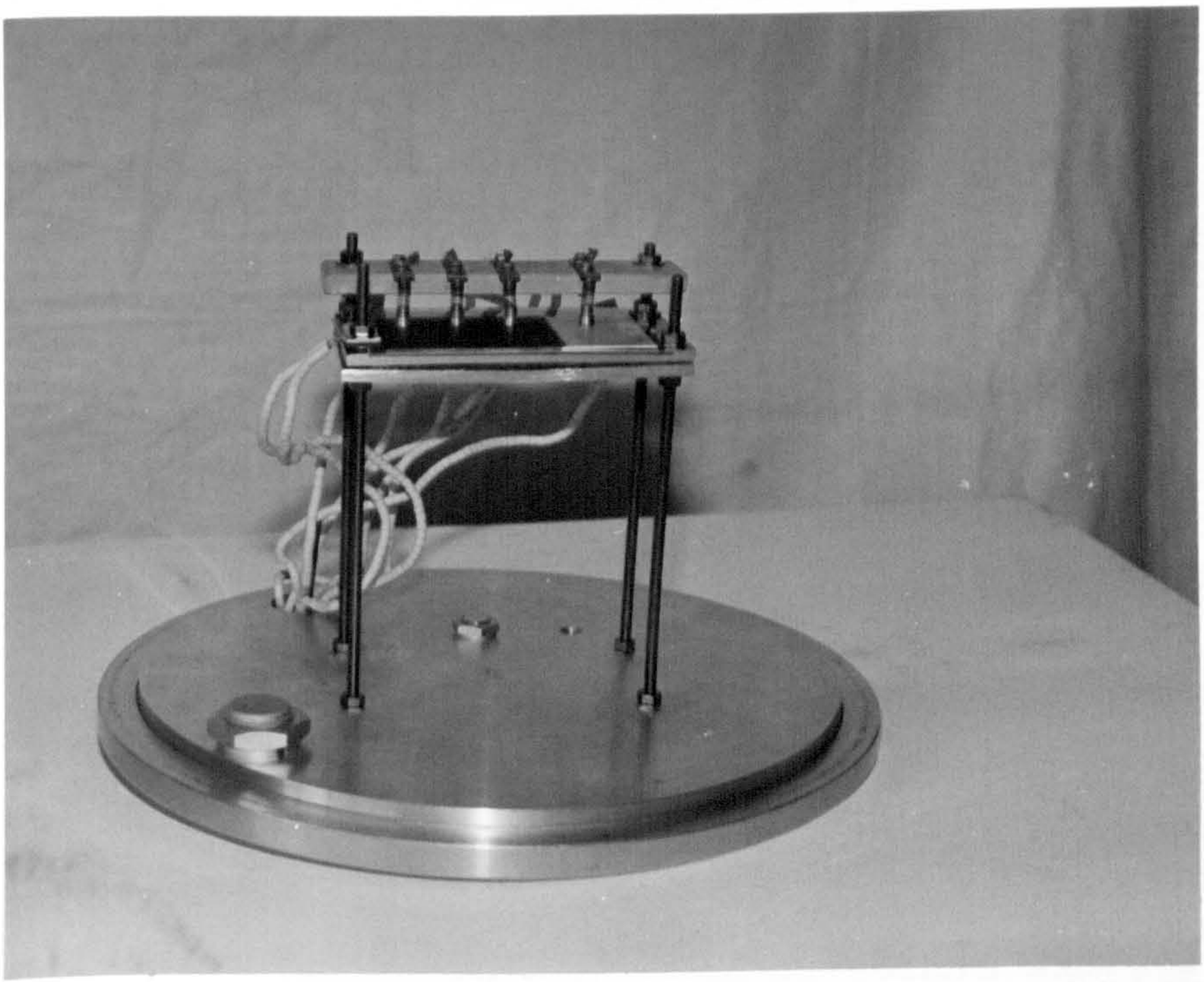

Fig. 2.12. Specimen holder with heating system.

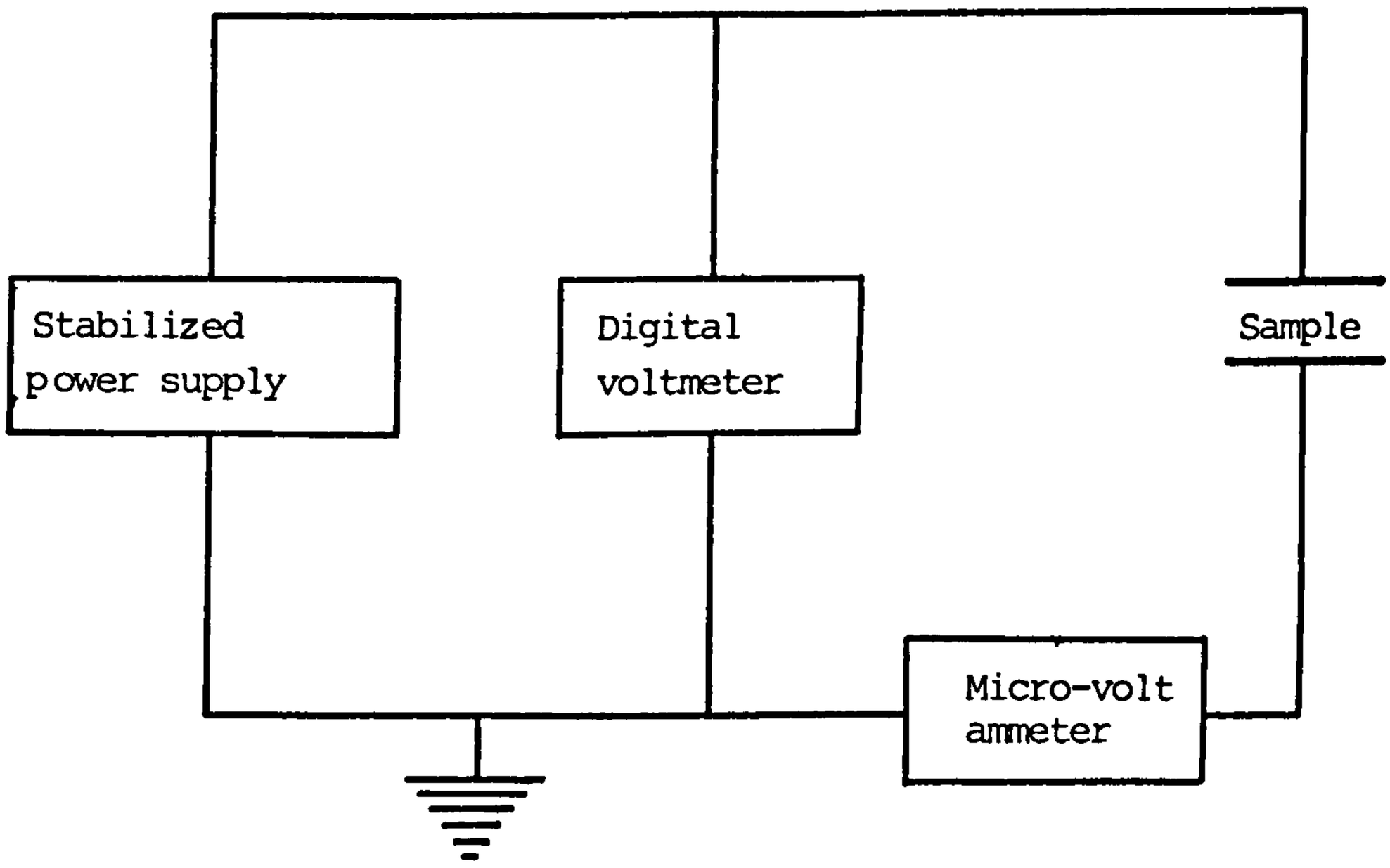

Fig. 2.13. Schematic diagram of electrical circuitry for D.C. measurements.

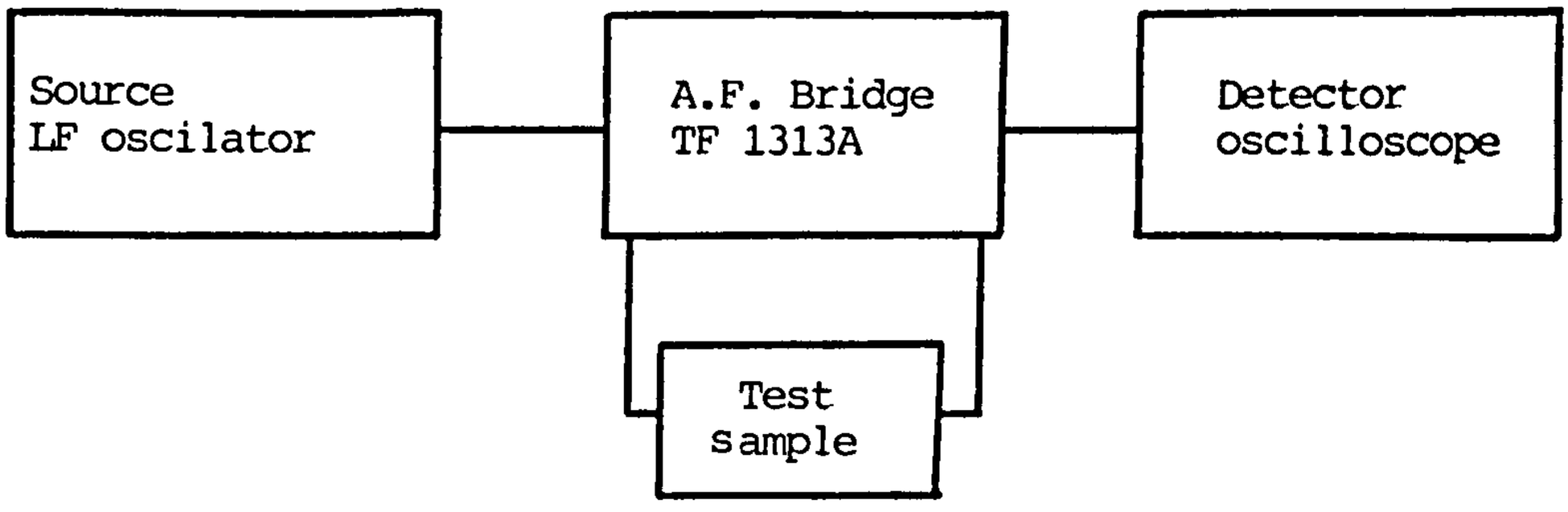

Fig. 2.14 Schematic diagram of equipments for measuring capacitance.

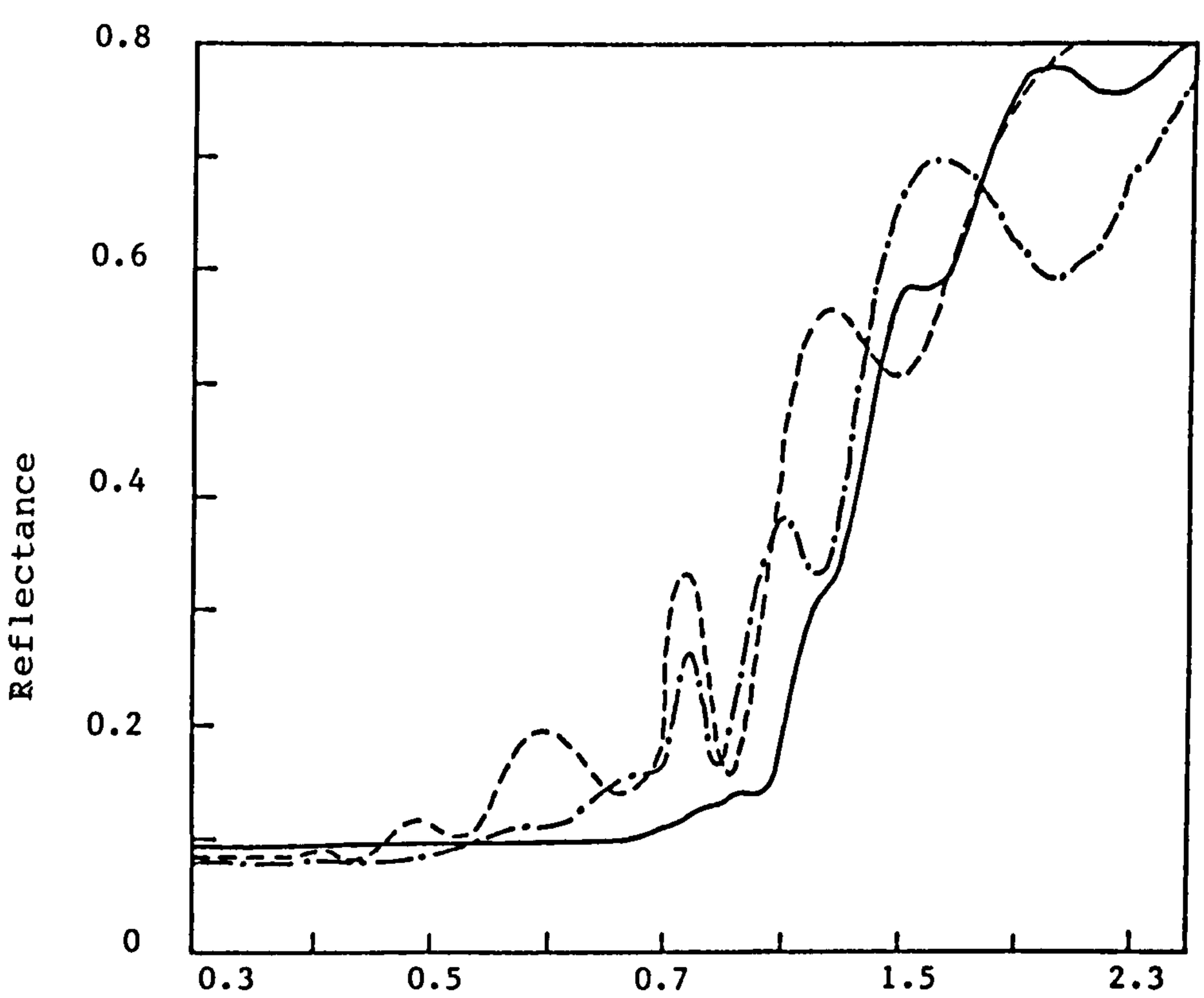

Fig. 3.1.1 Spectral total reflectance of Mo-black dip coatings on mechanically polished zinc substrates for various coating mass per unit area : (---) 0.065 mg/cm^2 (-·-·-) 0.12 mg/cm^2, (——) 0.21 mg/cm^2.

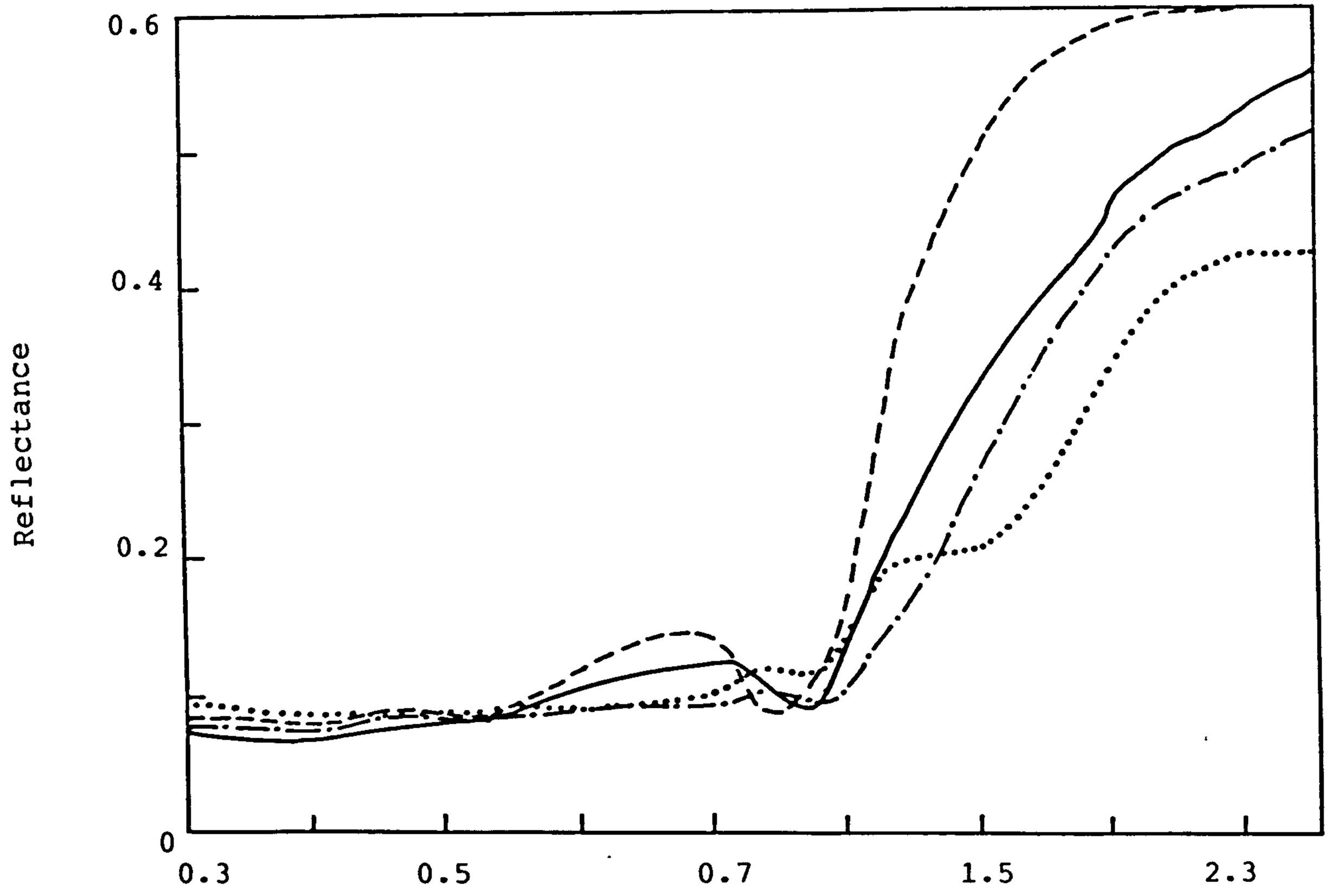

Fig. 3.1.2(a) Spectral total reflectance of Mo-black dip coatings on etched zinc substrates for various coating mass per unit area.
(----) 0.039 mg/cm^2, (——) 0.065 mg/cm^2, (-·-·-) 0.077 mg/cm^2
(.....) 0.085 mg/cm^2.

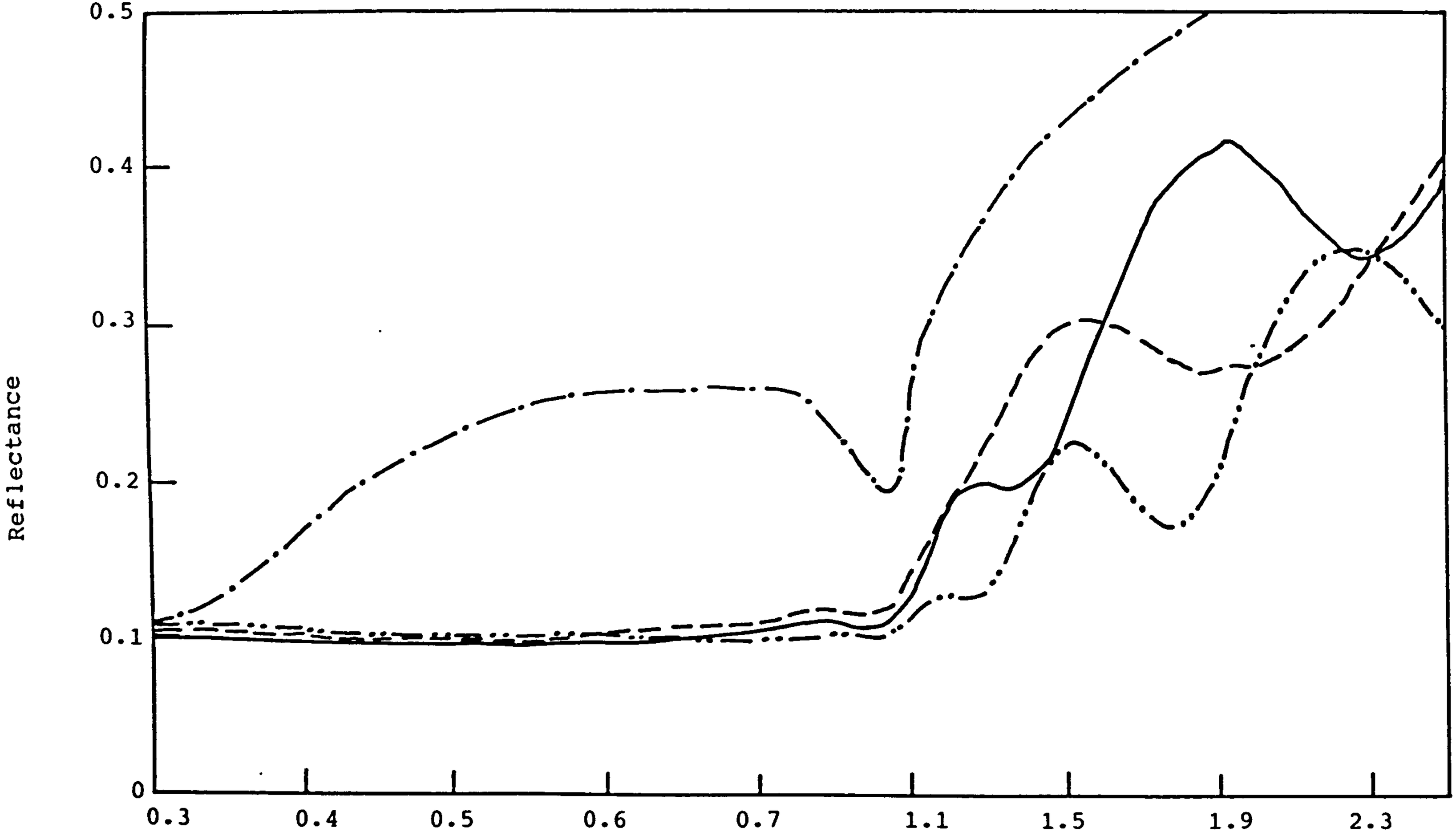

Fig. 3.1.2 (b) Spectral total reflectance of Mo-black dip coatings on etched zinc substrates for various coating mass per unit area. (——) 0.14 mg/cm², (---) 0.16 mg/cm², (-·-·-·-) 0.23 mg/cm², (-·-·-) etched zinc substrate.

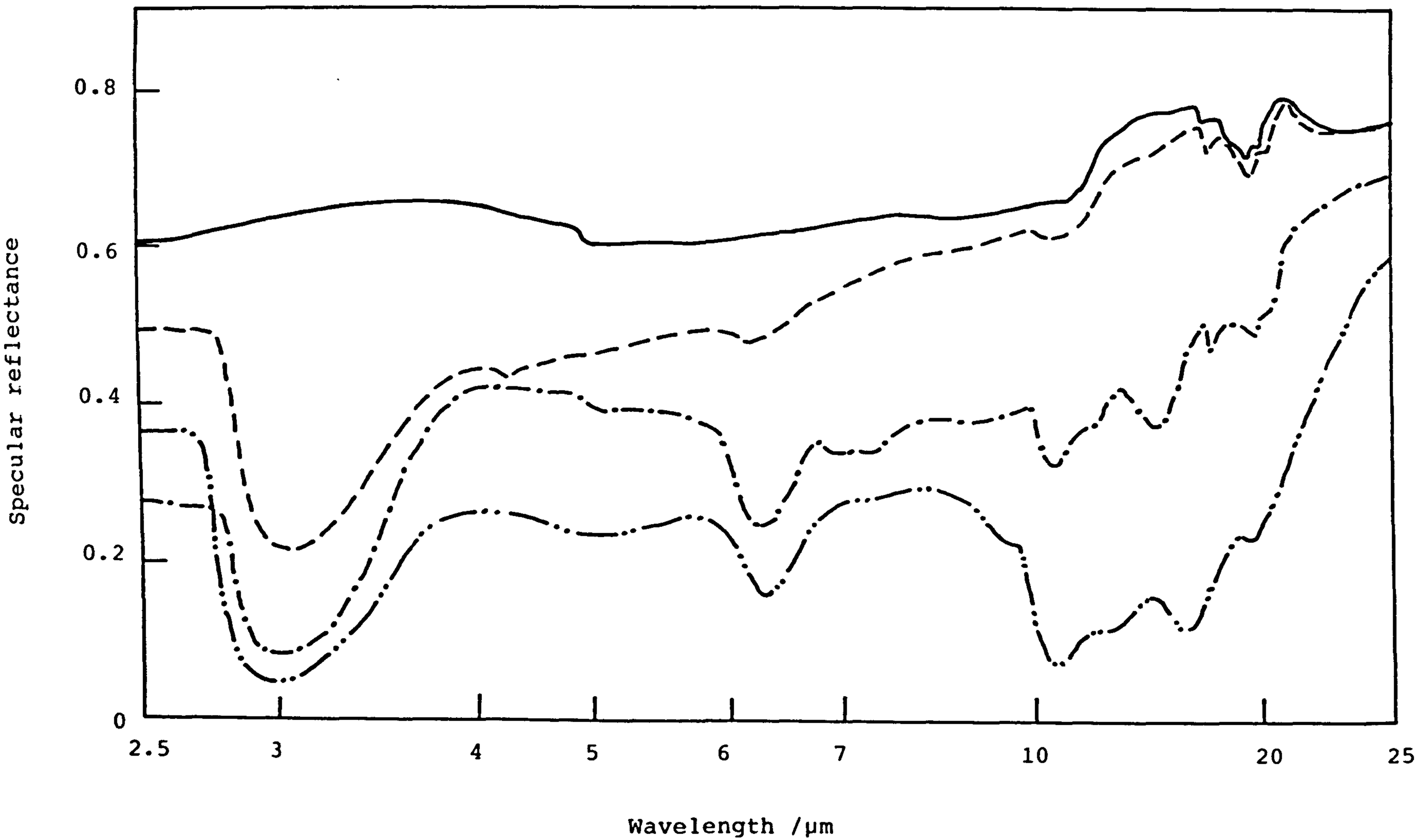

Fig. 3.1.3. Infrared specular reflectance of Mo-black dip coatings on mechanically polished zinc substrates for various coating mass per unit area.
(---) 0.046 mg/cm^2, (-·--·-) 0.12 mg/cm^2, (-···-···-) 0.21 mg/cm^2
(———) aluminium mirror as reference.

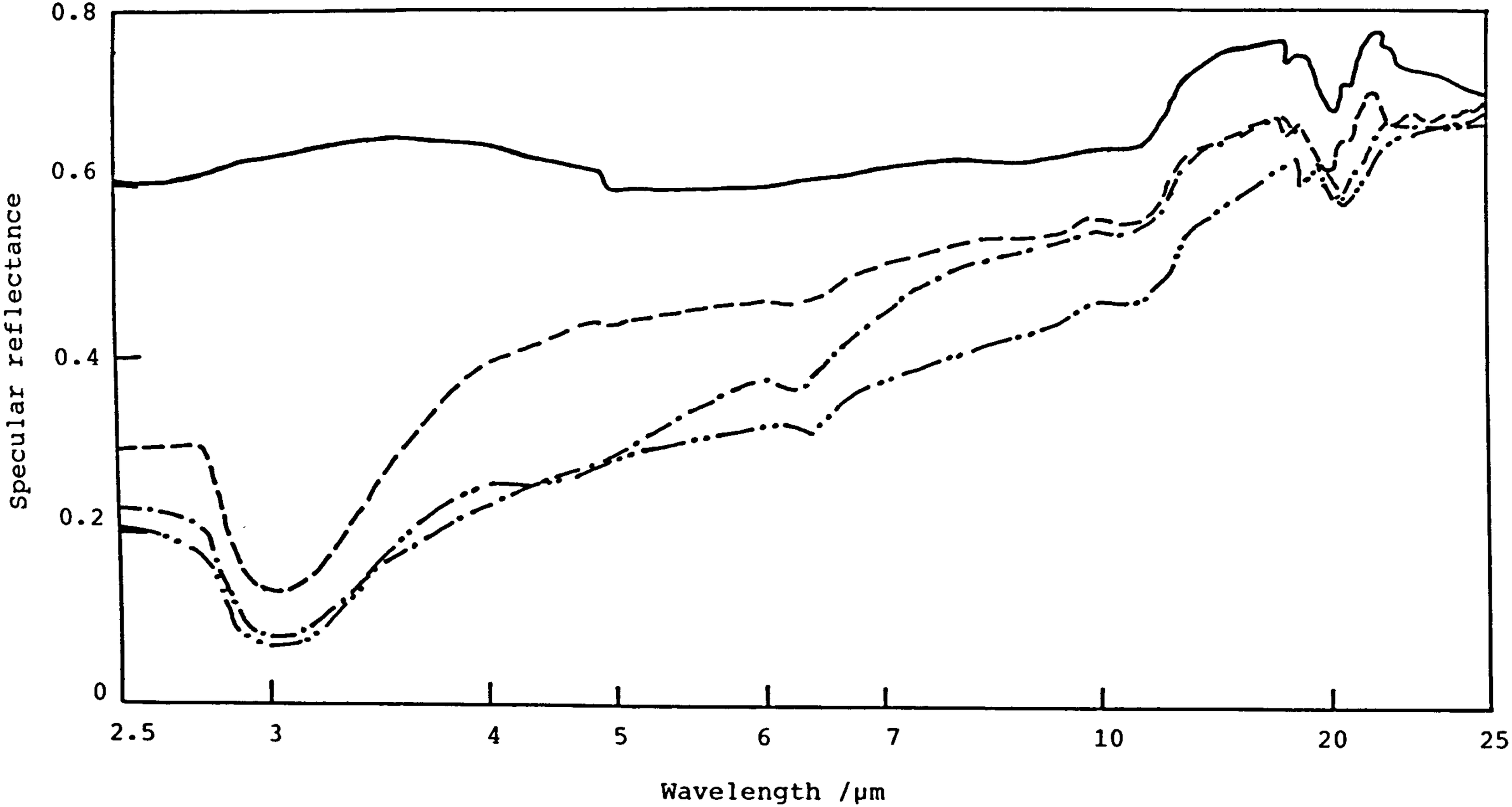

Fig. 3.1.4 (a) Infrared specular reflectance of Mo-black dip coatings on etched zinc substrates for various coating mass per unit area.
(----) 0.039mg/cm², (-·-·-) 0.059mg/cm², (-··-··-) 0.085 mg/cm²
(———) aluminium mirror as reference.

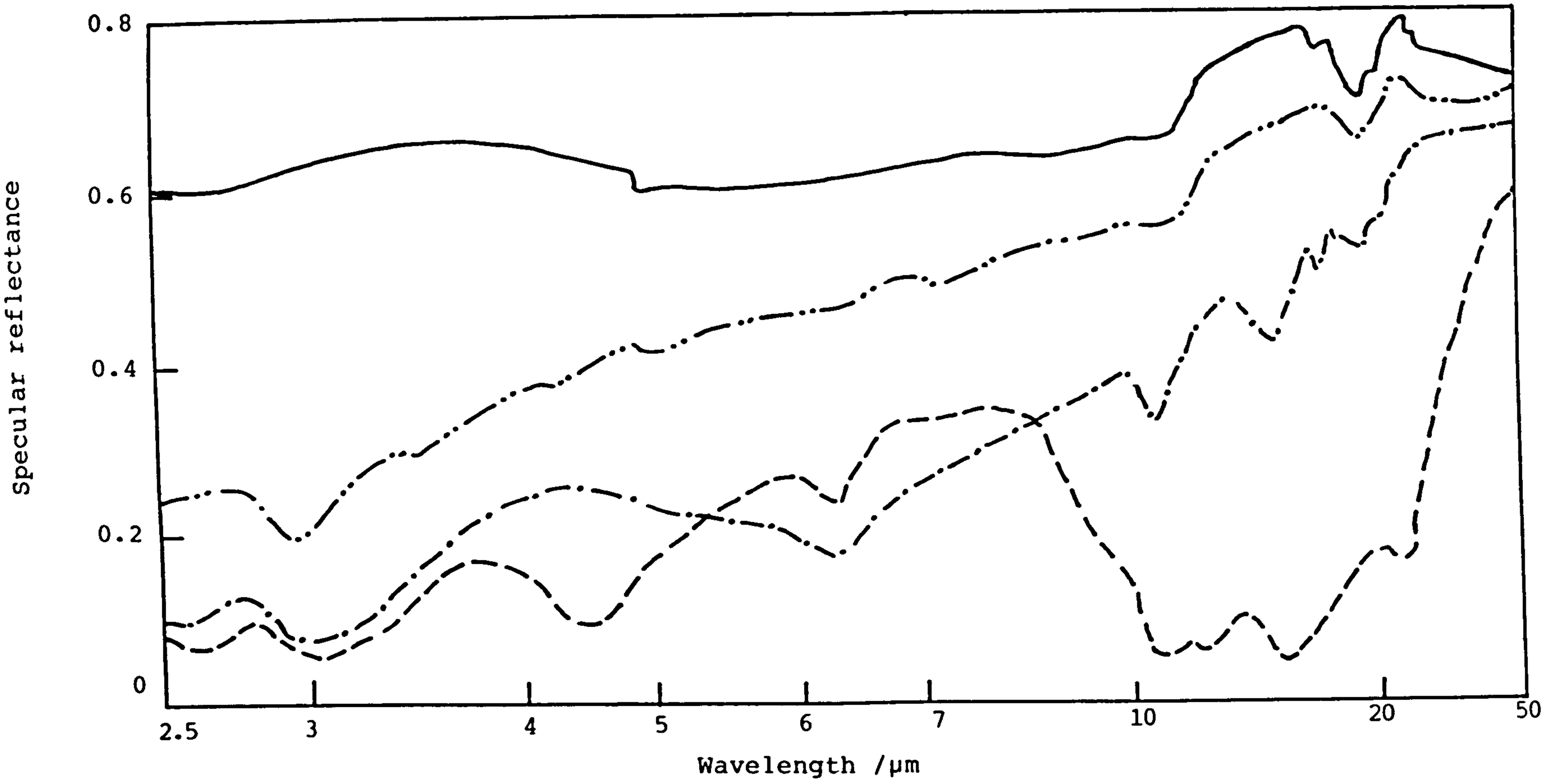

Fig. 3.1.4 (b) Infrared specular reflectance of Mo-black dip coatings on etched zinc substrates for various coating mass per unit area.
(—·—·—) 0.14 mg/cm^2, (----) 0.23 mg/cm^2, (—··—··—) etched zinc substrate,
(———) aluminium mirror as reference.

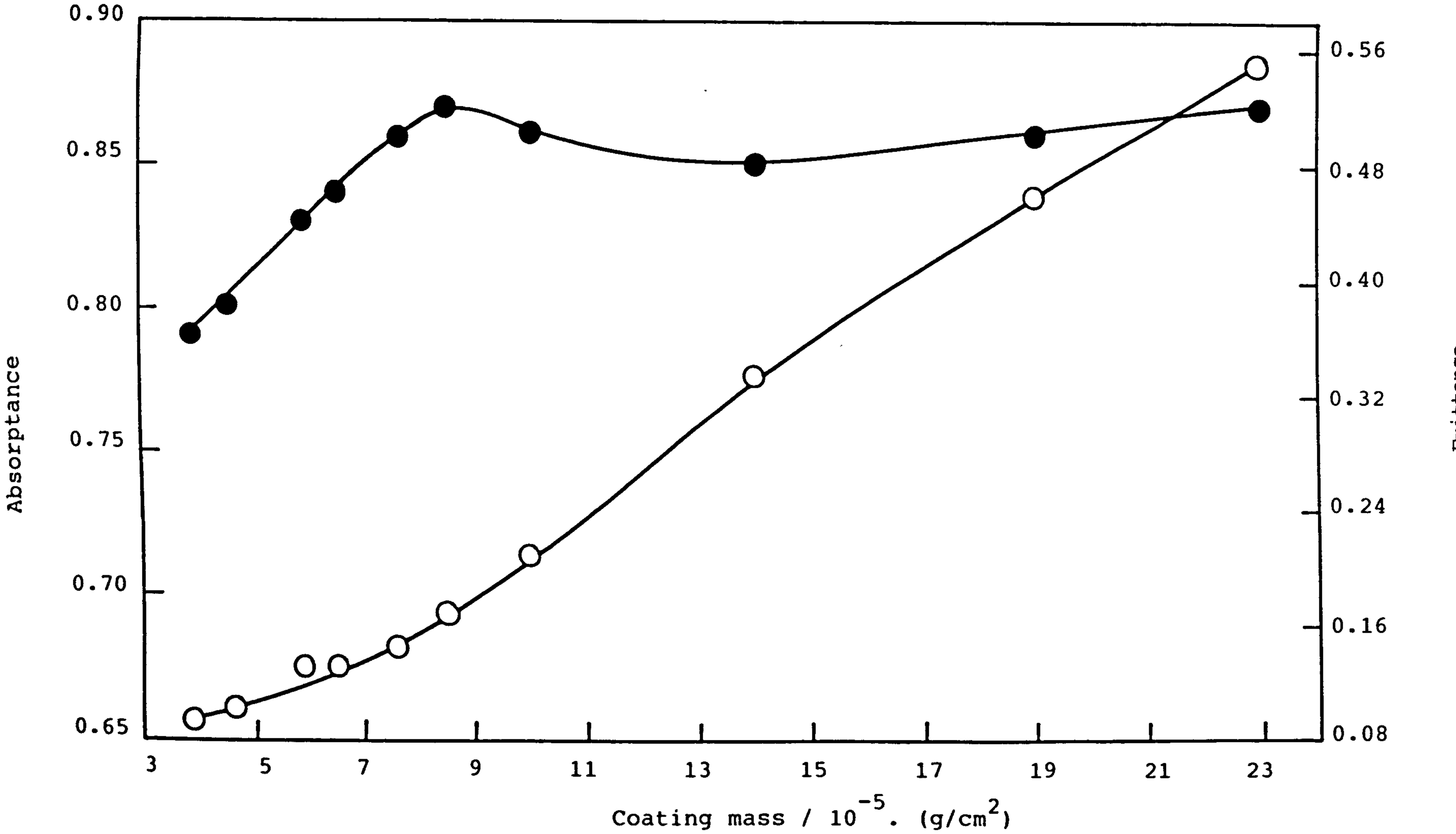

Fig. 3.1.5 (a) Variation of absorptance α_s(●) and emittance ε_{th}(○) with coating mass per unit area of Mo-black dip coatings on etched zinc substrates.

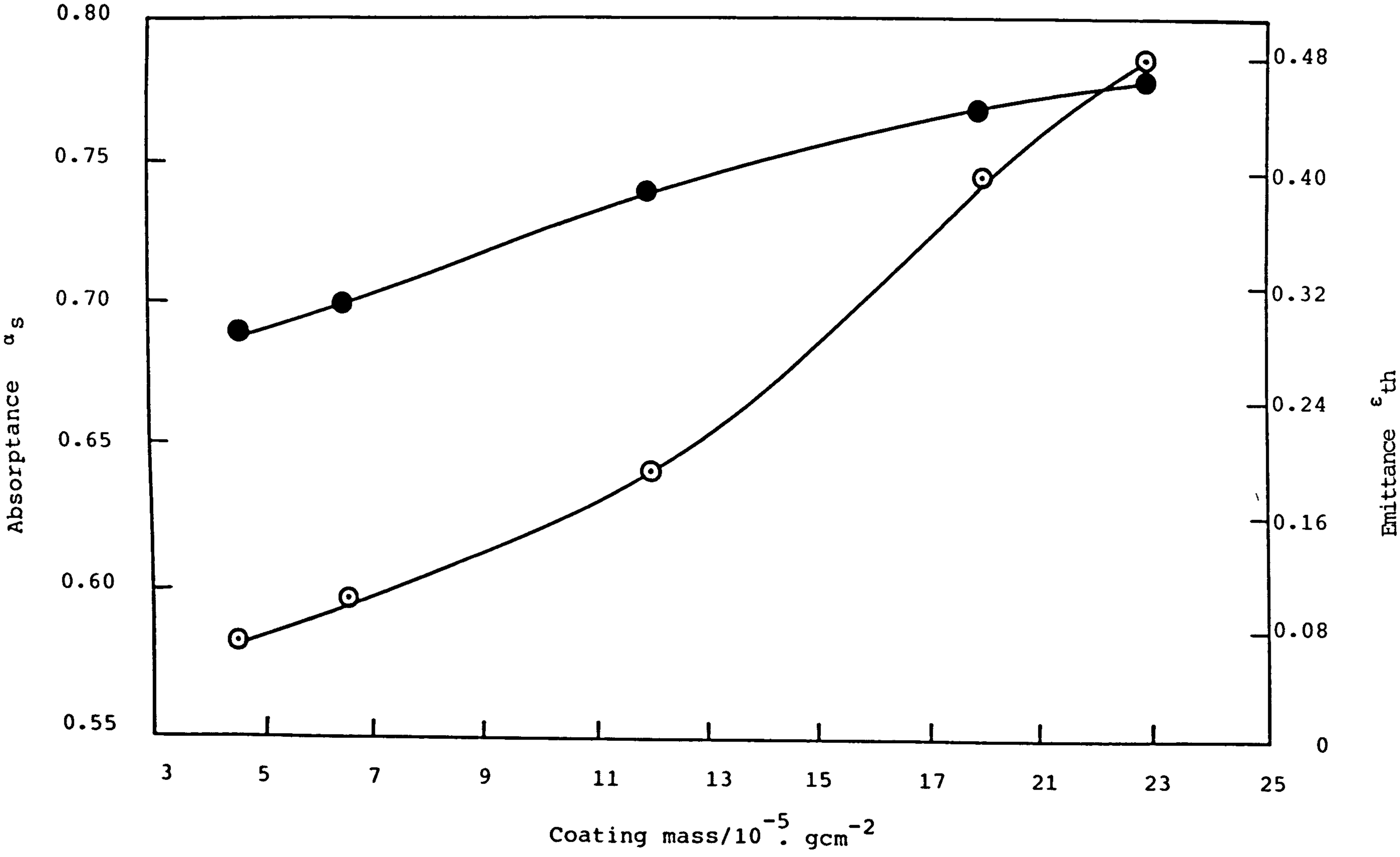

Fig. 3.1.5(b). Variation of absorptance α_s(●) and emittance ε_{th} (O) with coating mass per unit area of Mo-black dip coatings on mechanically polished zinc substrates.

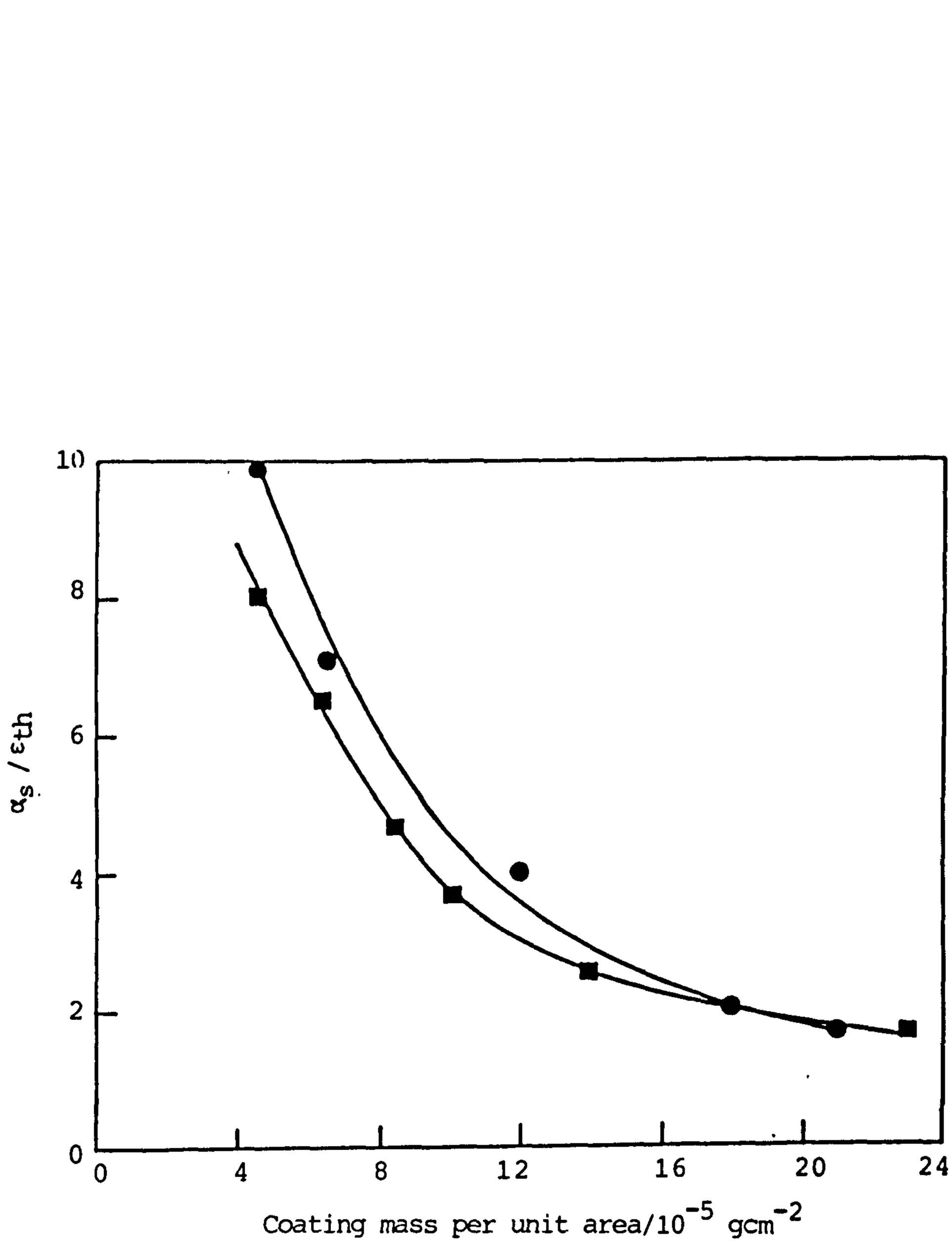

Fig.3.1.5(c) Variation of selectivity factor $\alpha_s/\varepsilon_{th}$ with coating mass per unit area for Mo-black dip coatings on etched (■) and unetched (●) zinc substrates

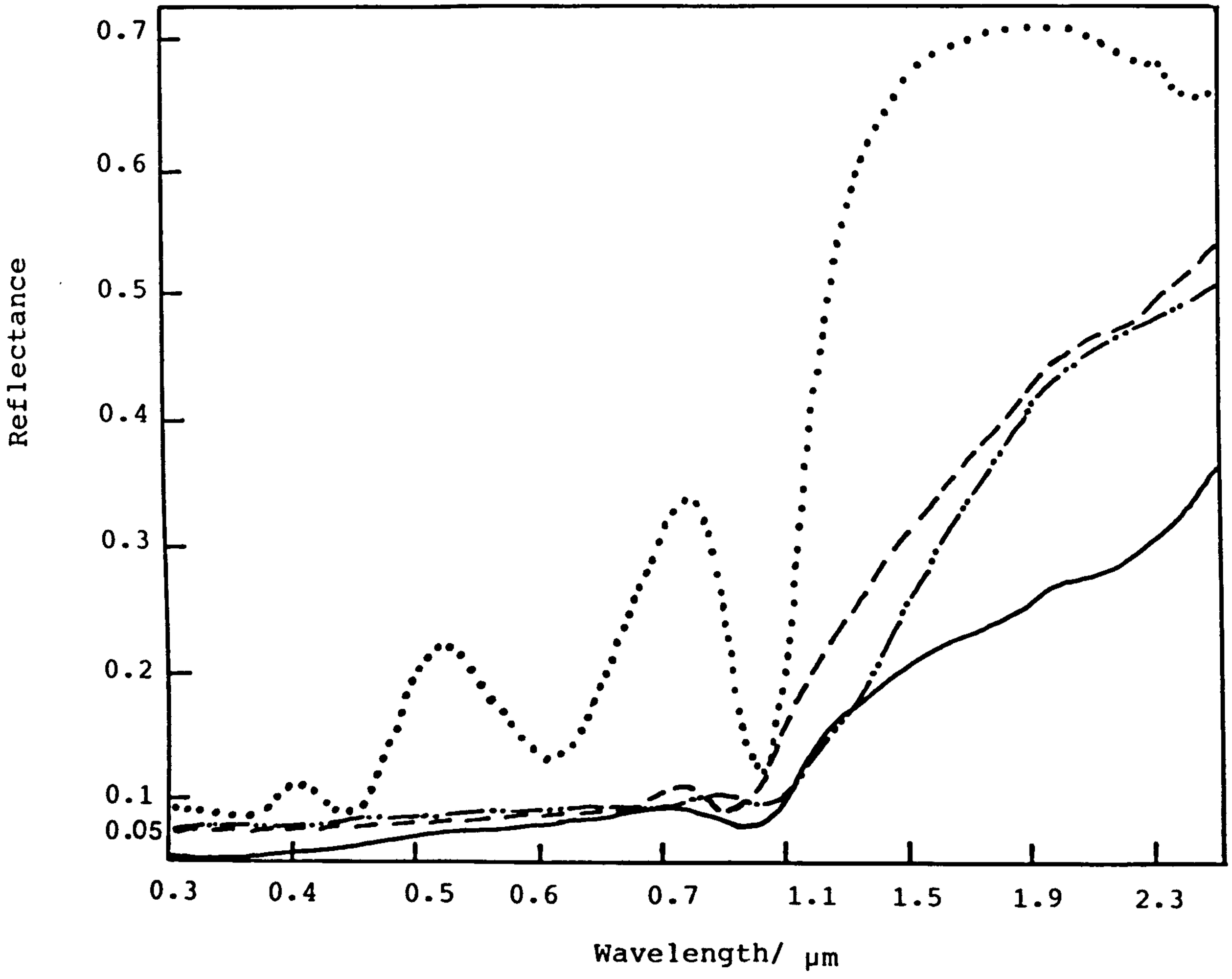

Fig. 3.1.6. Spectral total reflectance of Mo-black dip coatings on zinc substrates with different substrate pretreatments. unetched substrates (.....), etched with 20% HNO_3 (-----), 30% HNO_3 (_._._._), 50% HNO_3 (———).

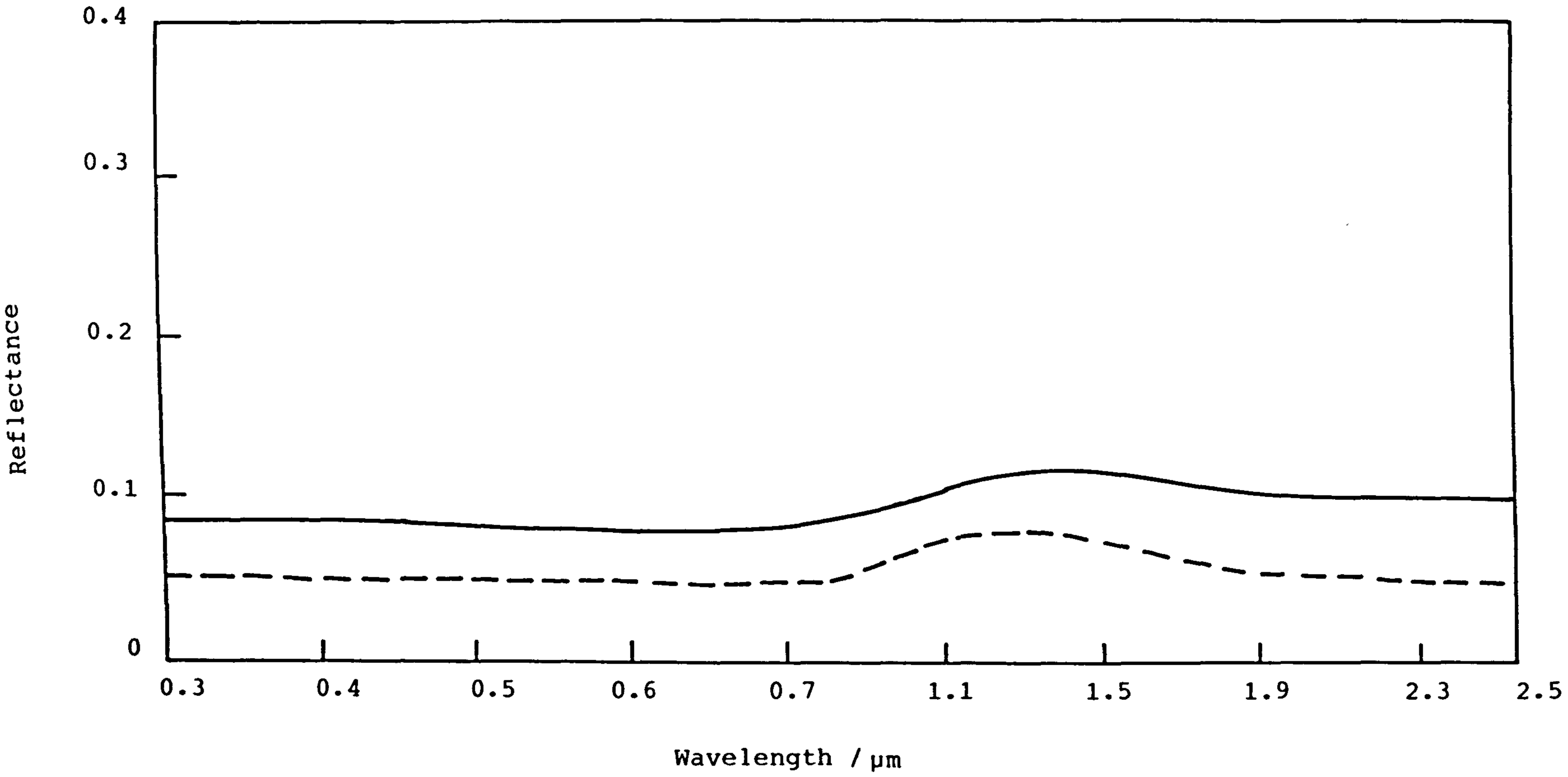

Fig 3.1.7 Spectral reflectance spectra for Mo-black dip coatings on cobalt (NC) substrates.

(---) α_S = 0.94, ε_{th} = 0.28 (Cobalt plated without addition agent)

(——) α_S = 0.91, ε_{th} = 0.10 (Cobalt plated with addition agent)

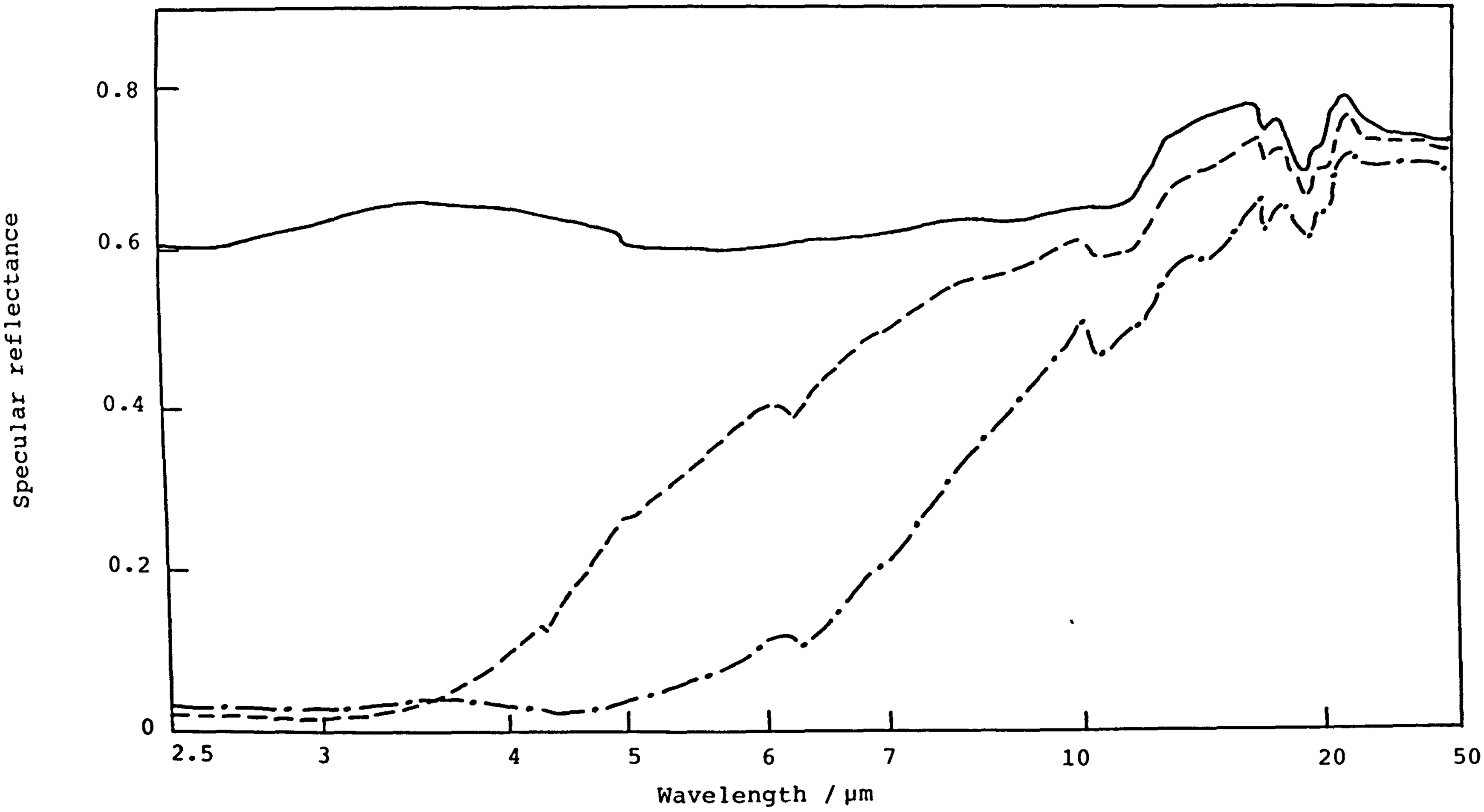

Fig 3.1.8 Specular reflectance spectra in the IR region of the Mo-black dip coatings on cobalt (NC)substrates plated with addition agent (----) and without addition agent (-·-·-), (———) aluminium mirror as reference.

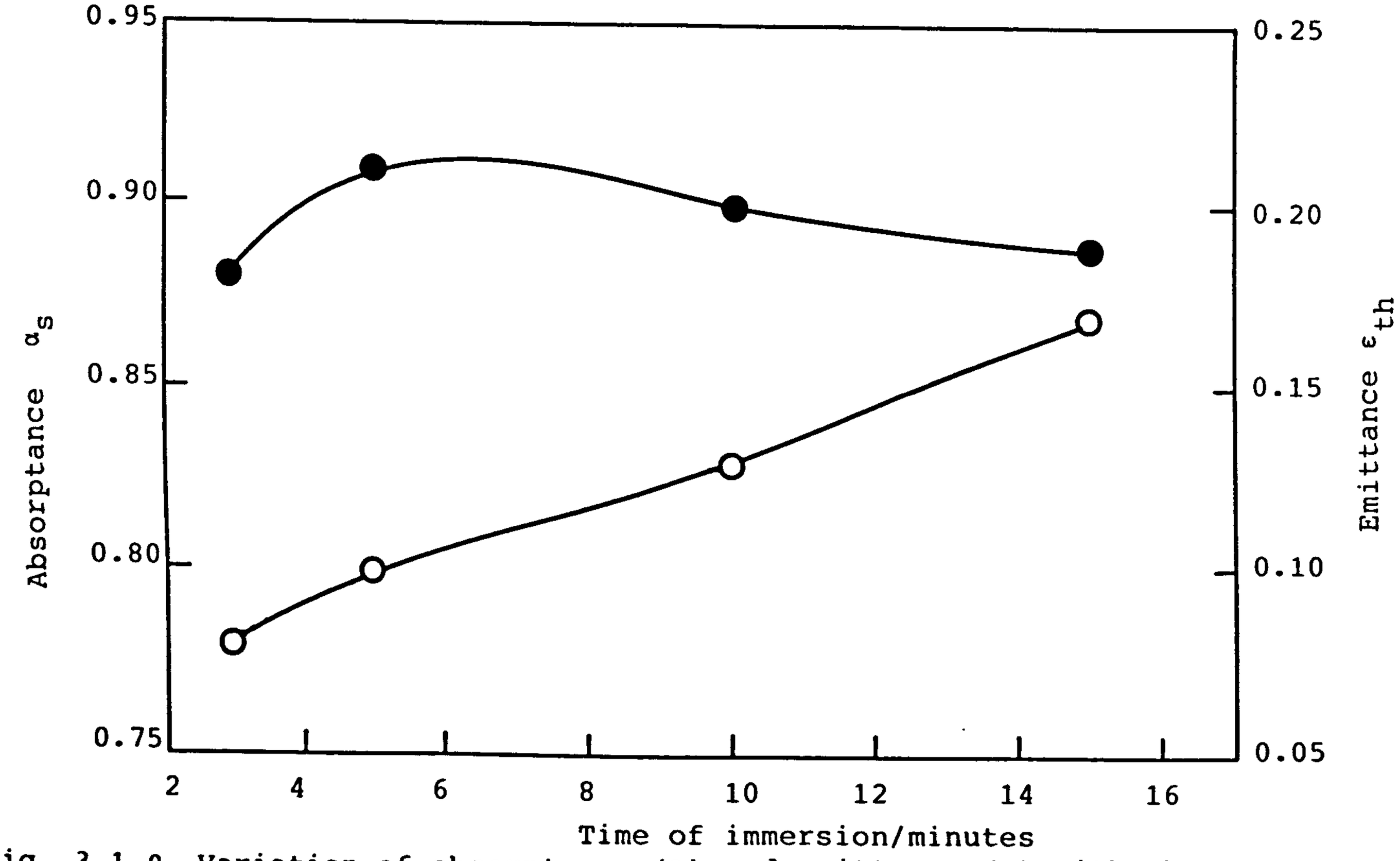

Fig. 3.1.9 Variation of absorptance (●) and emittance (○) with the dipping time of Mo-black coating on cobalt (NC) substrates formed at 60°C.

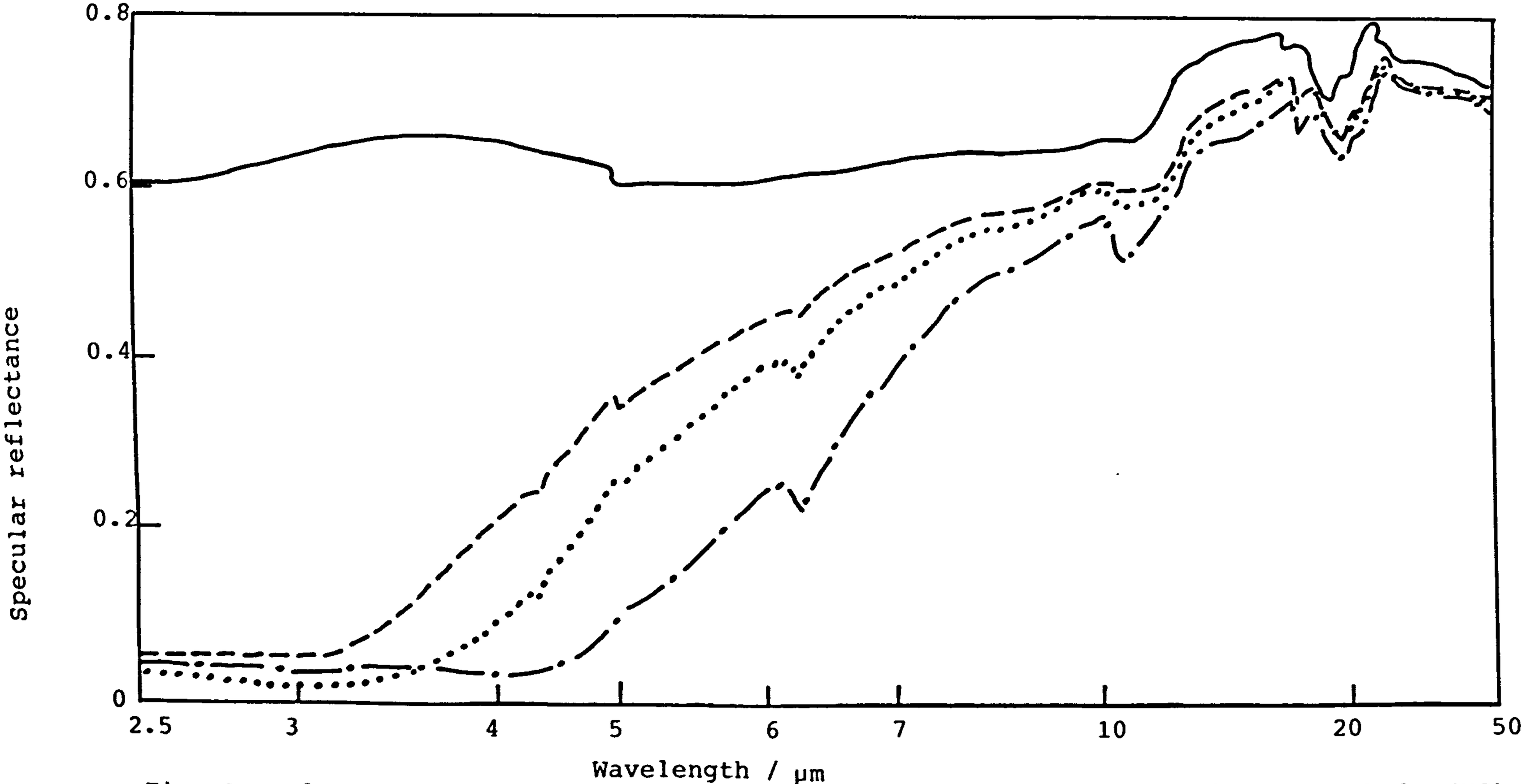

Fig. 3.1.10(a) IR specular reflectance spectra of Mo-black dip coatings on cobalt (NC) substrates (with addition agent) prepared at 60°C for various deposition times. (---) 5 minutes, (.....) 10 minutes, (-·-·-) 15 minutes, (——) aluminium mirror as reference.

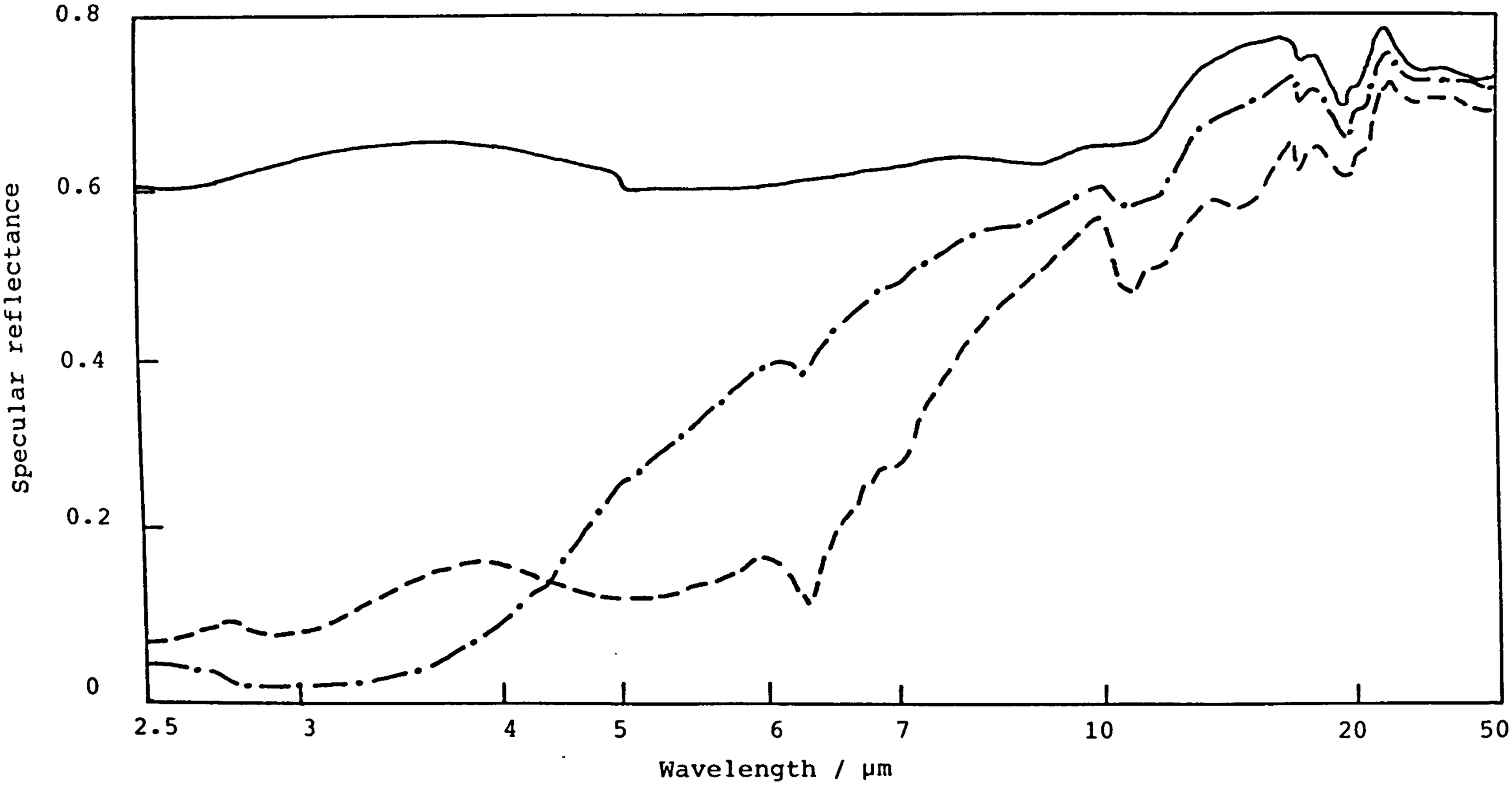

Fig. 3.1.11 IR specular reflectance spectra of Mo-black dip coatings on cobalt (NC) substrates prepared for same deposition time (10 minutes) at two different solution temperature, (—.—.—) 60°C, (— — —) 80°C, (———) aluminium mirror as reference.

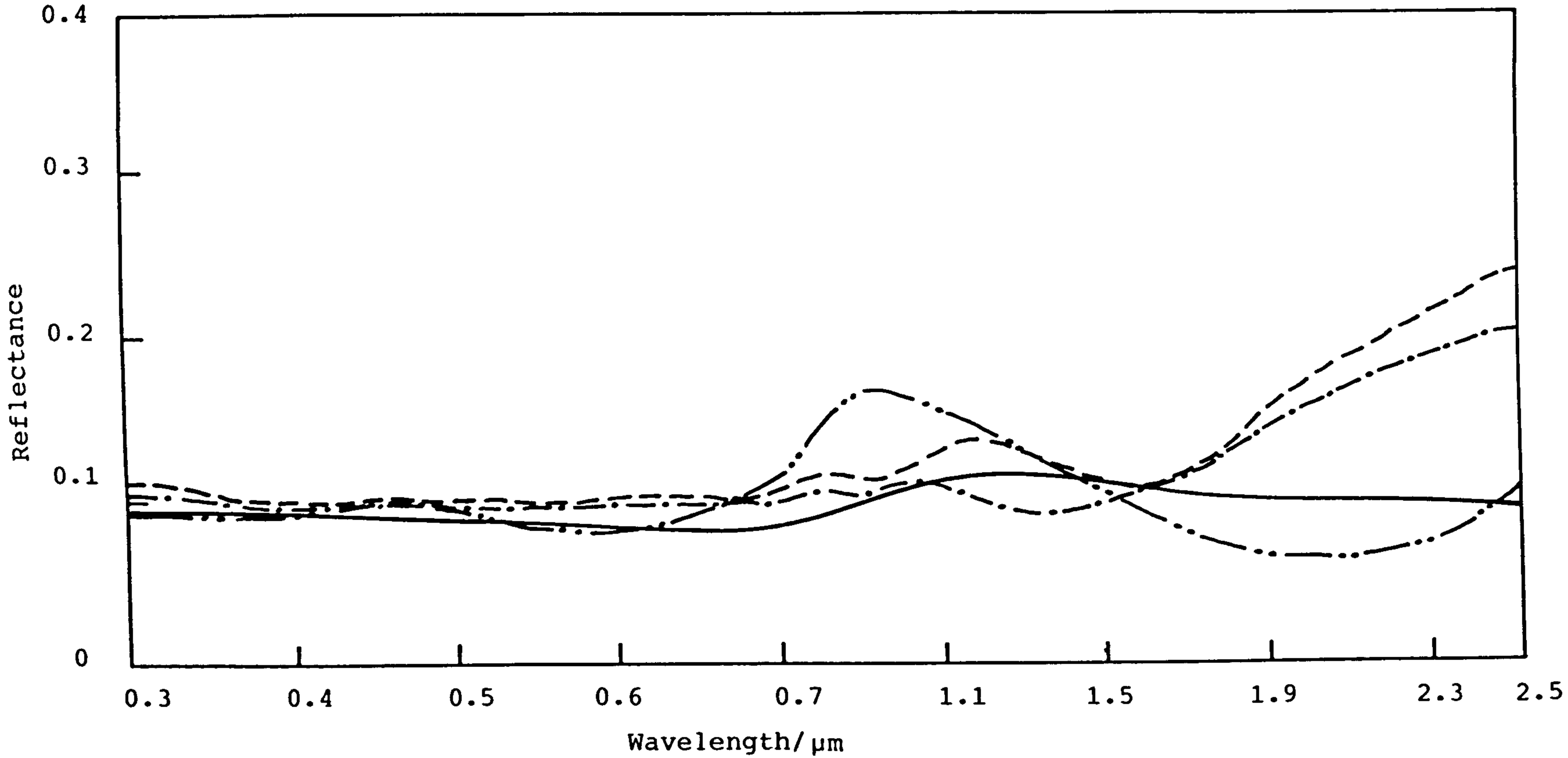

Fig. 3.1.12 Spectral reflectance spectra of Mo-black coatings on cobalt (NC) substrates for various dipping time at 60°C solution temperature (—··—··—) 3 minutes, (————) 5 minutes, (—·—·—) 10 minutes, (– – – –) 15 minutes.

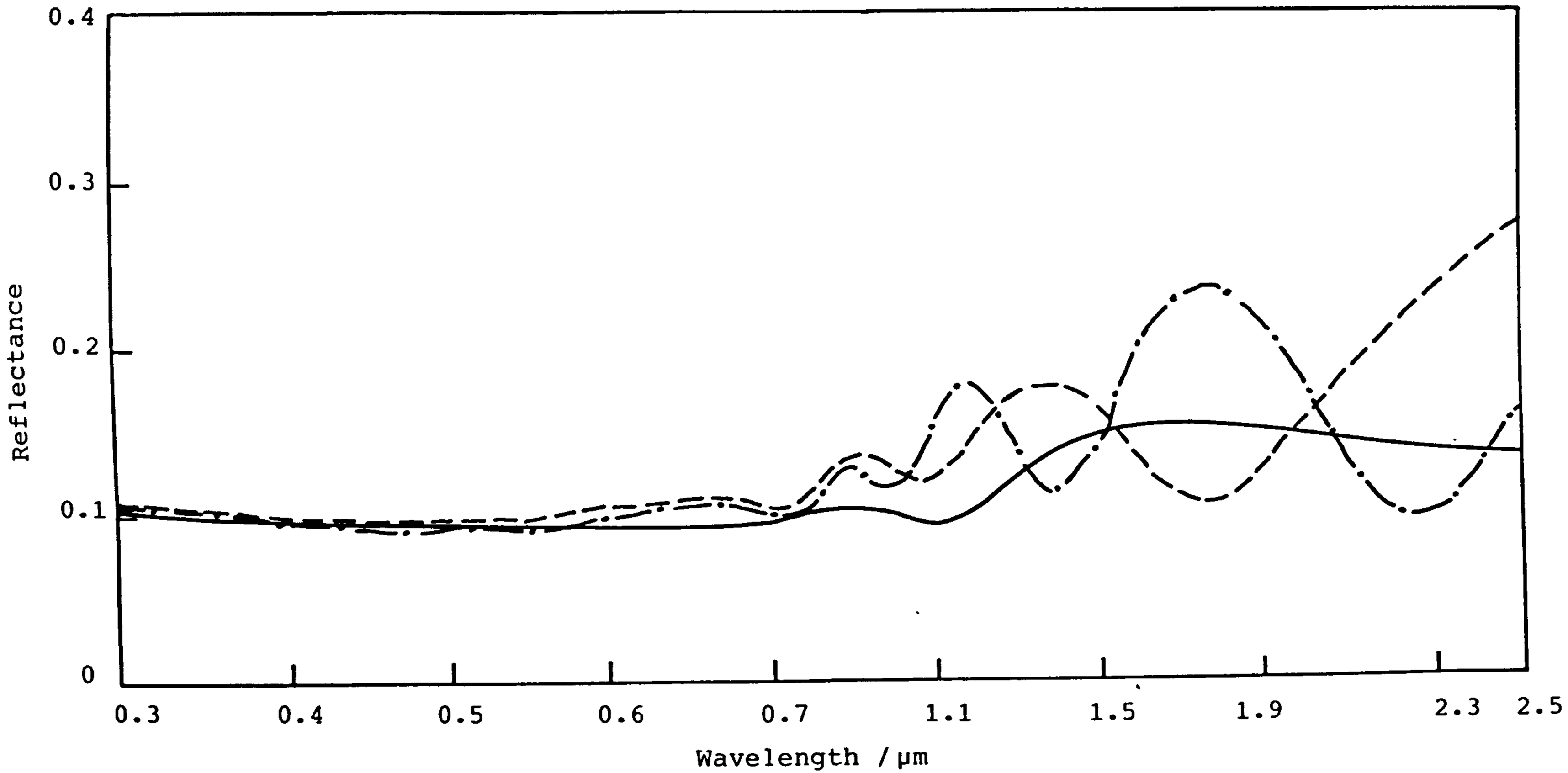

Fig. 3.1.13. Spectral reflectance spectra of Mo-black coatings on cobalt (NC) substrates for various dipping time formed at 80°C
(——) 5 minutes, (– – –) 10 minutes, (—·—·—) 15 minutes.

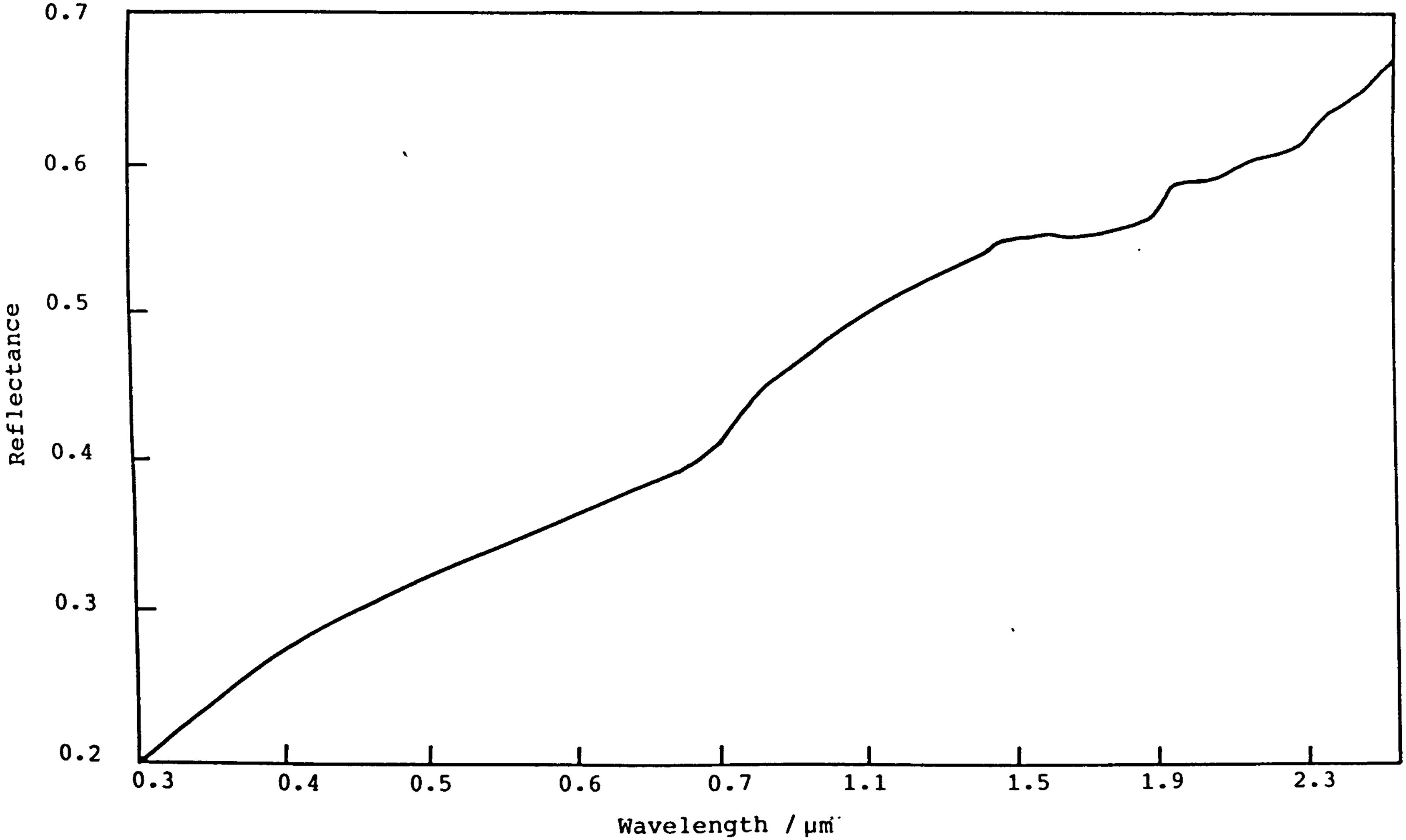

Fig. 3.1.14. Spectral total reflectance of electroplated cobalt deposited on nickel plated copper substrates (with addition agent).

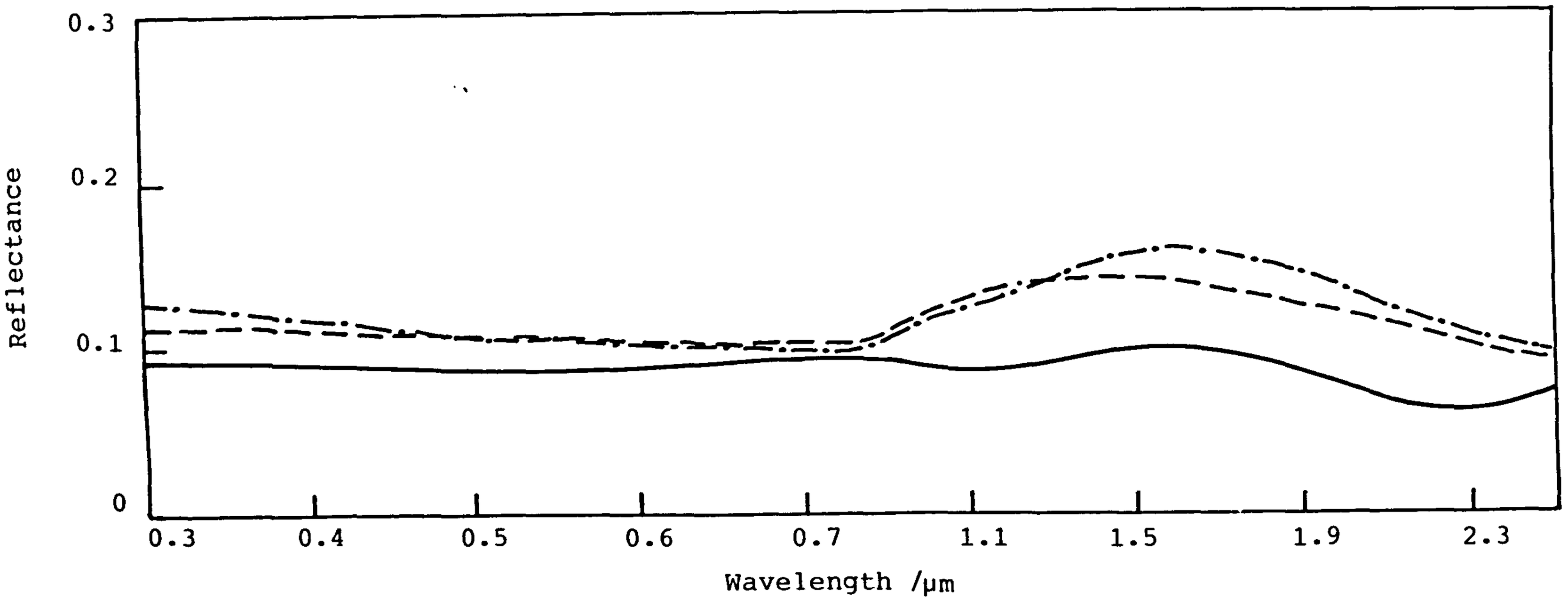

Fig. 3.1.15. Spectral reflectance spectra of Mo-black dip coatings on cobalt (NC) substrates (deposited at comparatively low temperature with low current density) for various dipping time for Mo-black. (——) 5 minutes, (—·—·—) 8 minutes, (— — —) 12 minutes.

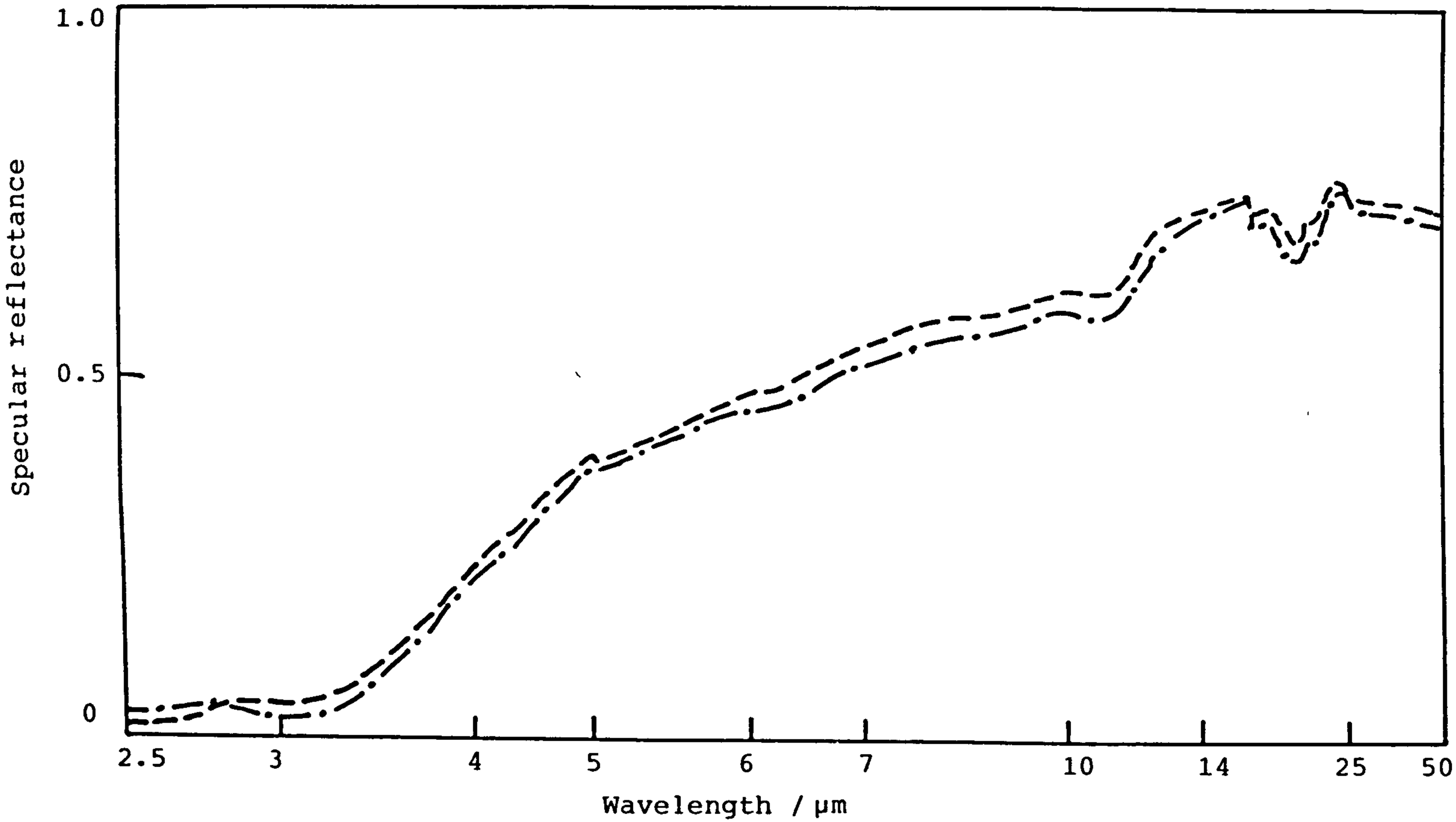

Fig. 3.1.16 IR specular reflectance spectra of Mo-black coatings on cobalt (NC) substrates (prepared at low temperature with low current density. Deposition time of Mo-black (– – –) 5 minutes, (– · – · –) 12 minutes.

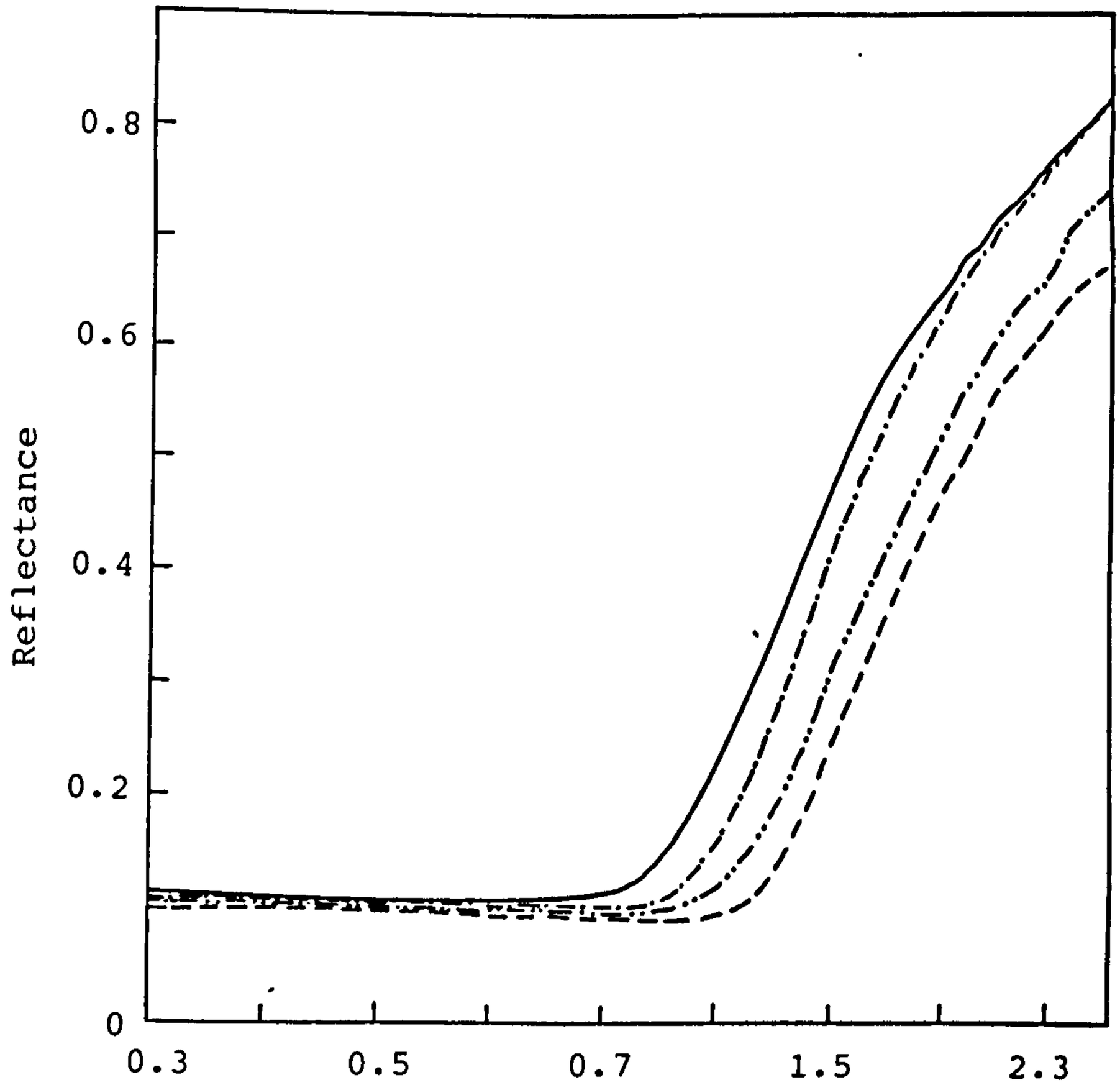

Fig. 3.1.1 7 Spectral total reflectance of electrodeposited Mo-black coatings on aluminium substrates for various coating mass per unit area. (——) 0.70 mg/cm², (-.-.-) 1.18 mg/cm², (-···-···-) 1.64 mg/cm², (----) 2.17 mg/cm².

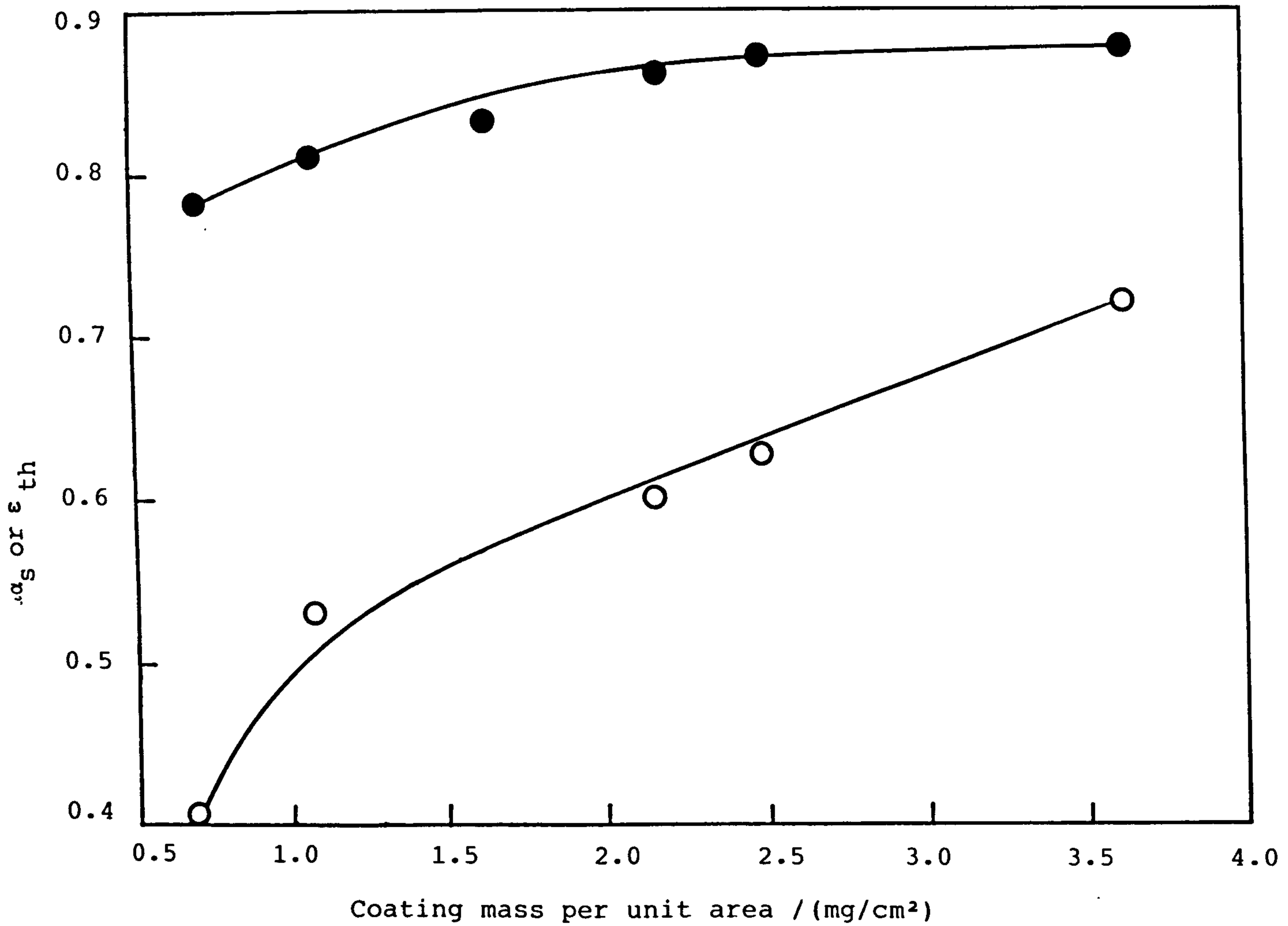

Fig. 3.1.18 Variation of absorptance α_s (●) and emittance ε_{th} (○) with coating mass per unit area for electrodeposited Mo-black coatings on aluminium substrates.

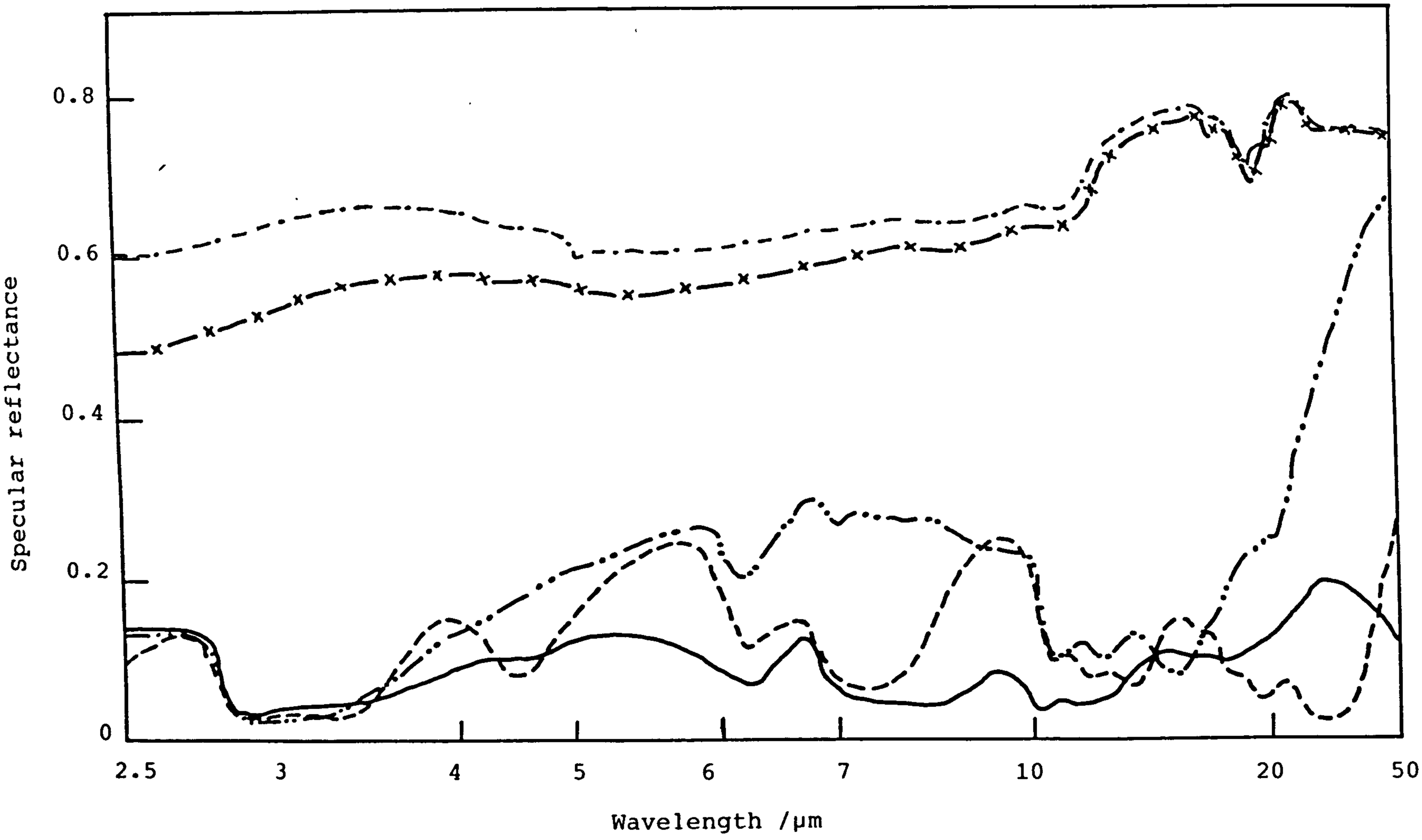

Fig. 3.1.19 Infrared specular reflectance of electrodeposited Mo-black coatings on aluminium substrates for various coating mass per unit area. (-•-•-•) 0.70 mg/cm², (---) 1.18 mg/cm², (——) 2.17 mg/cm², (-×-×-) Al-substrate , (--•--•--) Al-mirror as reference.

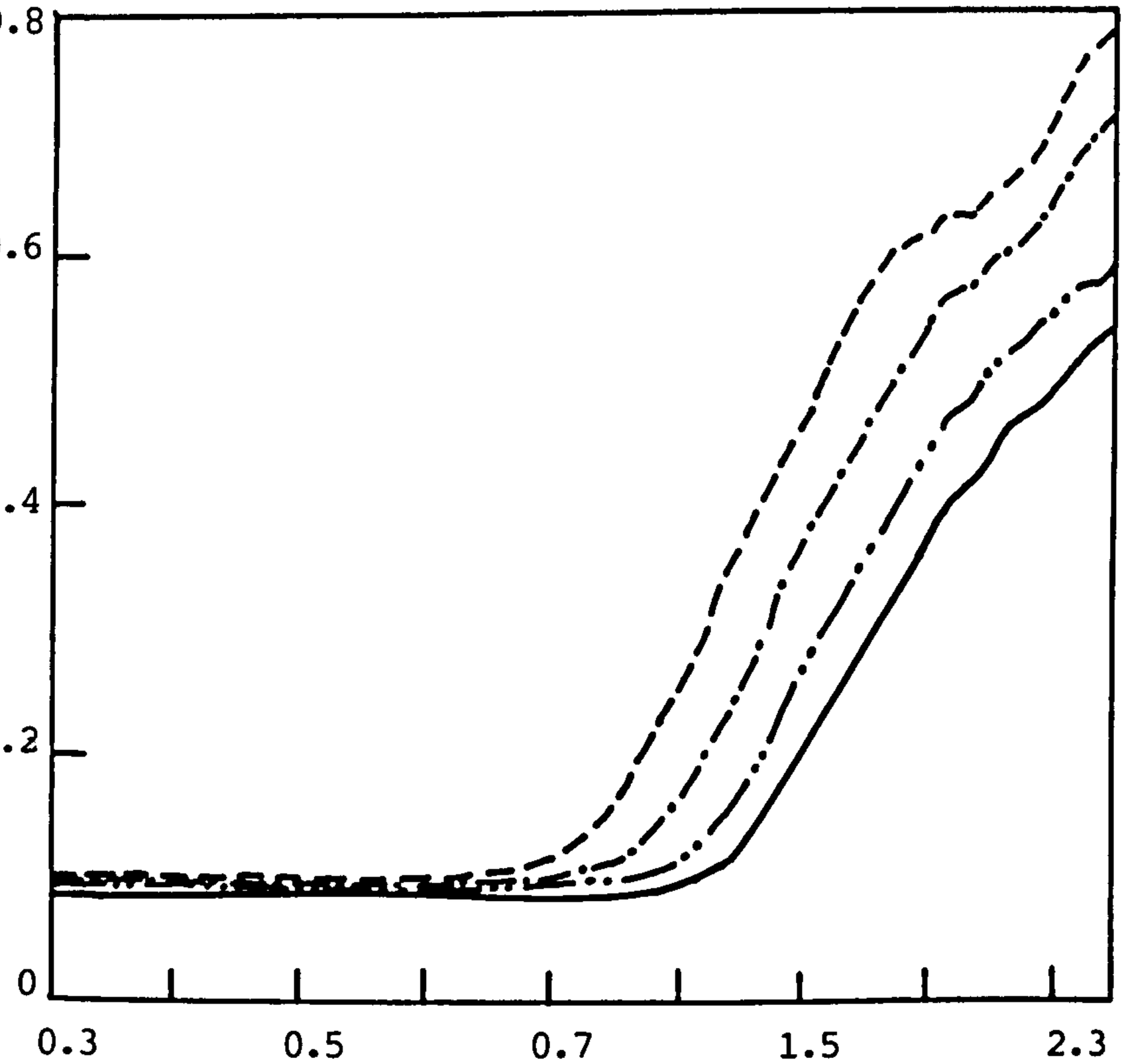

Fig.3.1.20 Spectral total reflectance of electrodeposited Mo-black coatings on aluminium coated rough glass for various thicknesses. (---) 1.5 μm, (- · - · -) 2.0 μm, (-•• -••-) 2.8 μm, (——) 3.6 μm.

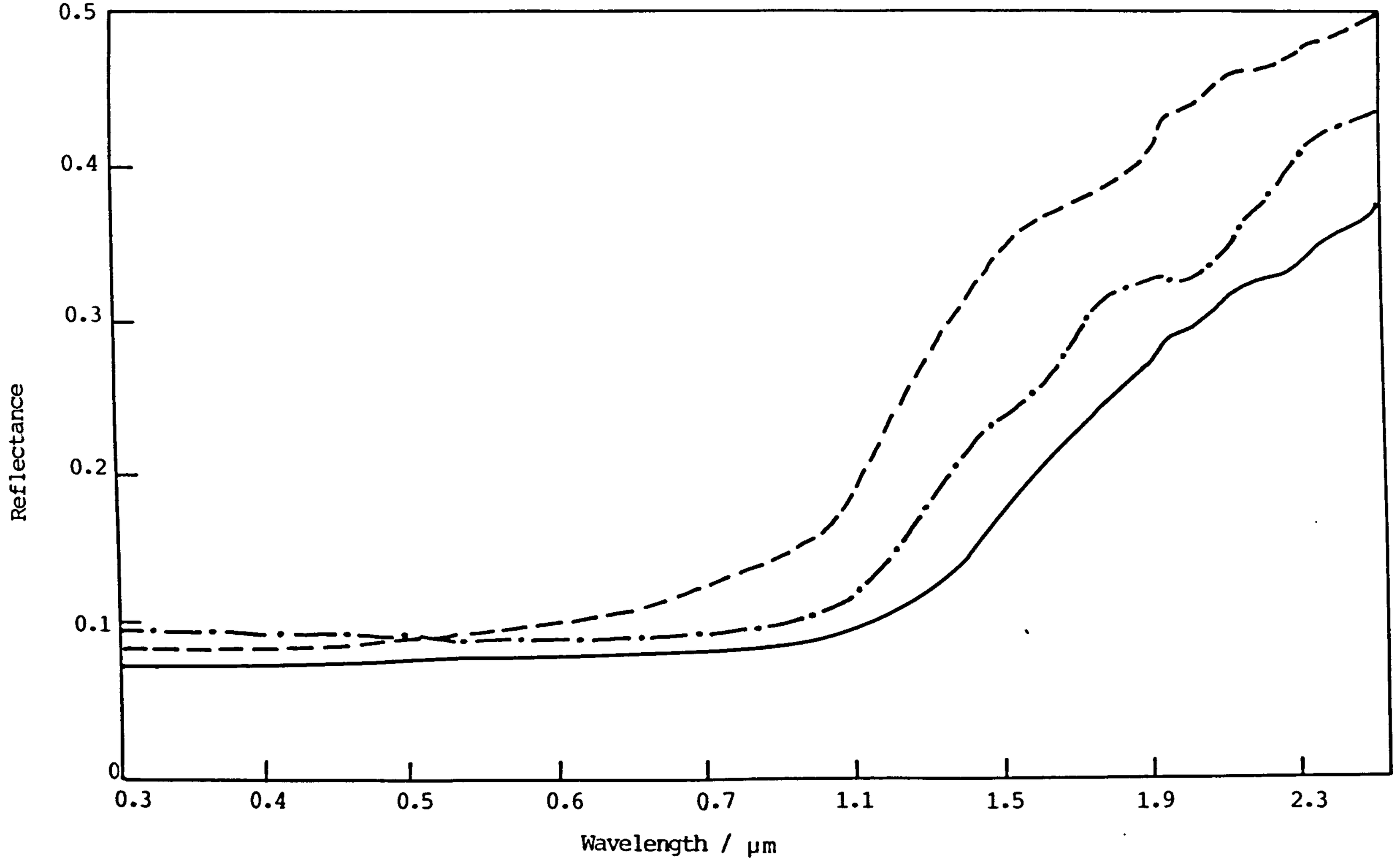

Fig. 3.1.21 Spectral reflectance spectra of Mo-black coatings on galvanised steel substrates of various deposition times. (– –) 2 minutes, (–·––·–) 5 minutes and (———) 10 minutes.

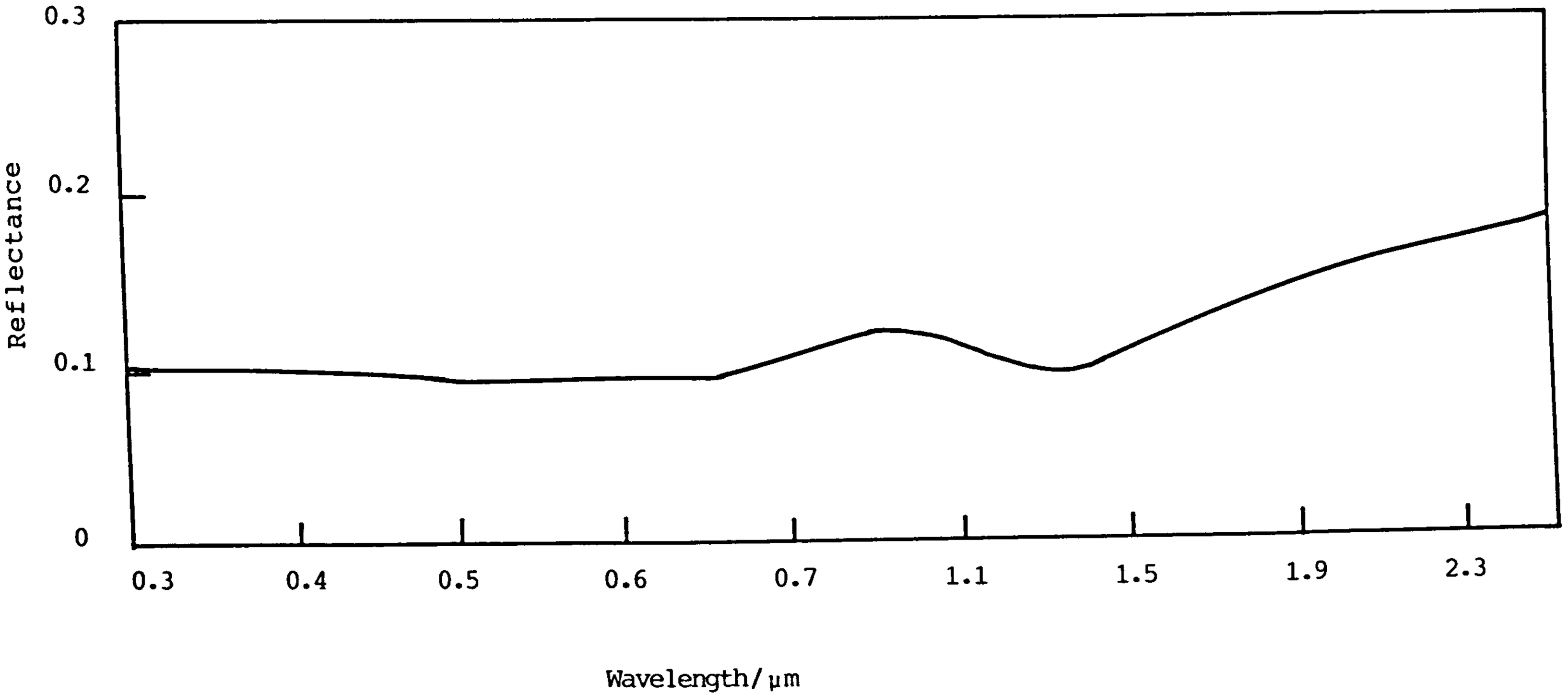

Fig. 3.1.22 Spectral total reflectance spectrum of Mo-black coating on cobalt plated aluminium substrate.

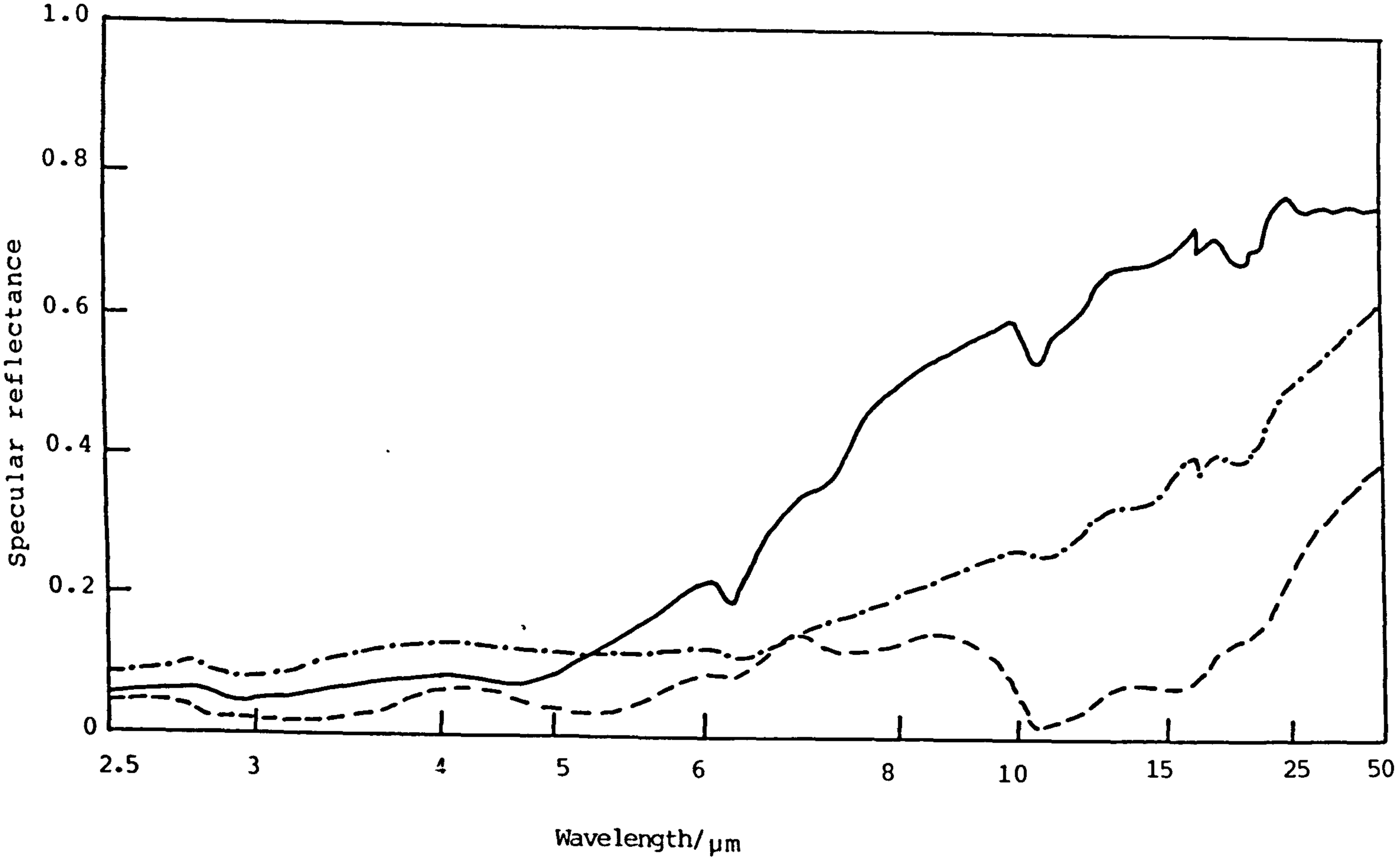

Fig. 3.1.23 IR specular reflectance spectra of Mo-black coatings on (——) cobalt plated aluminium, (—·—·—) galvanised steel and (----) vacuum evaporated aluminium on rough glass substrates.

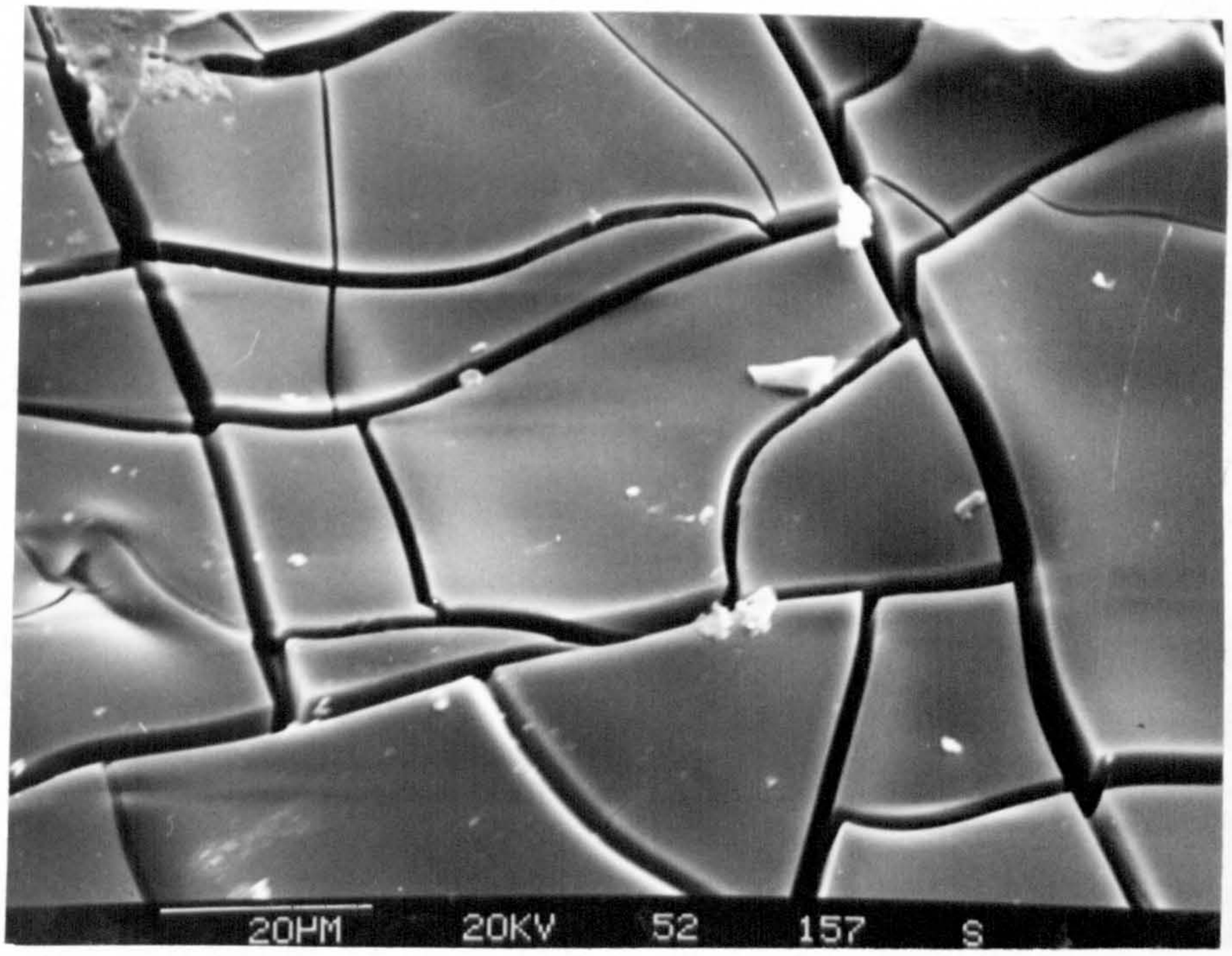

Fig.3.2.1 S.E.M. micrograph of electrodeposited Mo-black coating on aluminium substrate showing a flat platelet structure (coating density~3.9 mg/cm^2). Magnification : 1000X.

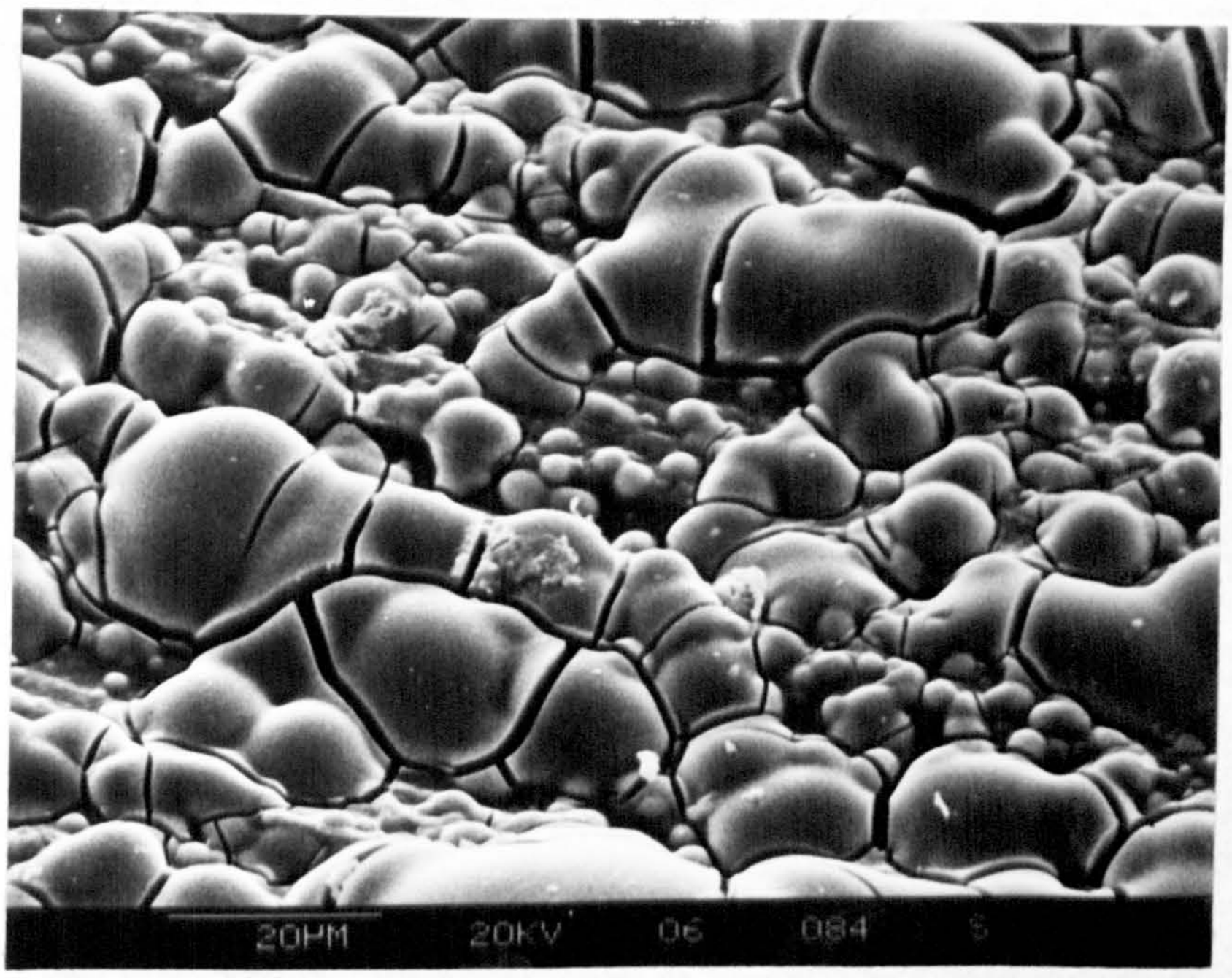

Fig.3.2.2 S.E.M. micrograph of electrodeposited Mo-black coating on aluminium showing different sizes of quasi hemisphere (coating density~1.5 mg/cm^2). Magnification :1000X.

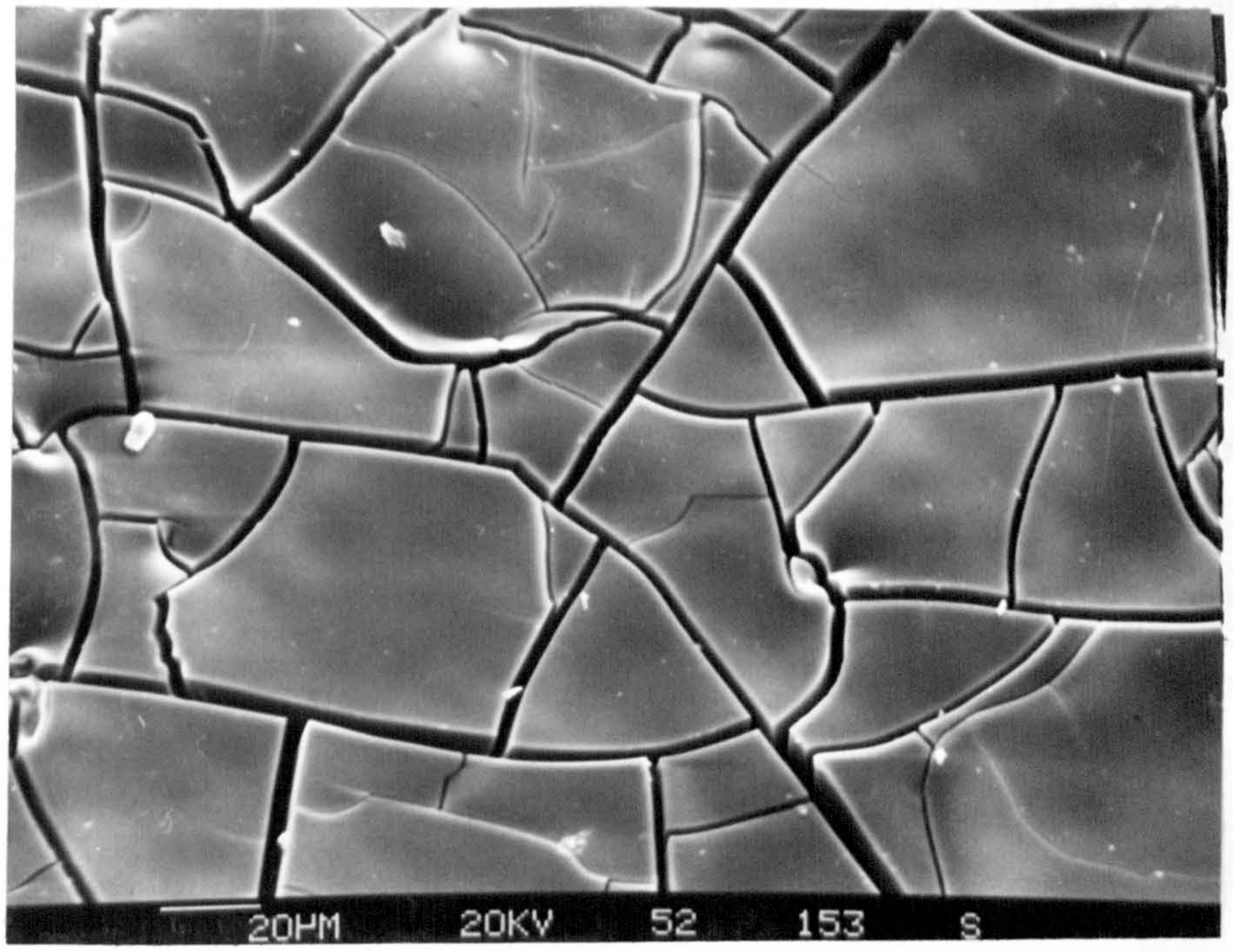

Fig.3.2.3 S.E.M. micrograph of electroplated Mo-black coating on aluminium. (Coating density~3.8 mg/cm^2). Magnification : 500X.

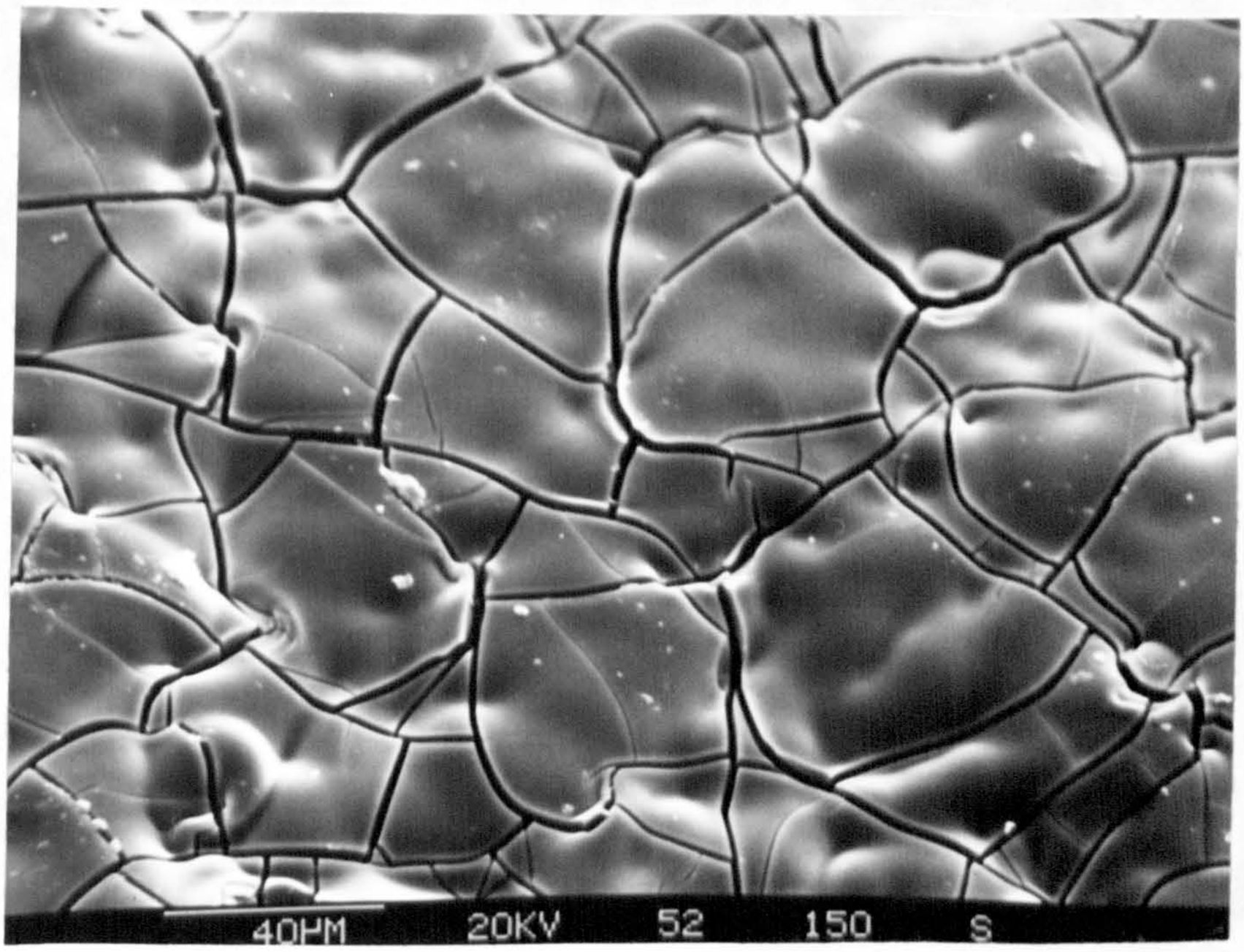

Fig.3.2.4(a) S.E.M. micrograph of electroplated Mo-black coating on aluminium. (Coating density~3.2 mg/cm^2) Magnification: 500X.

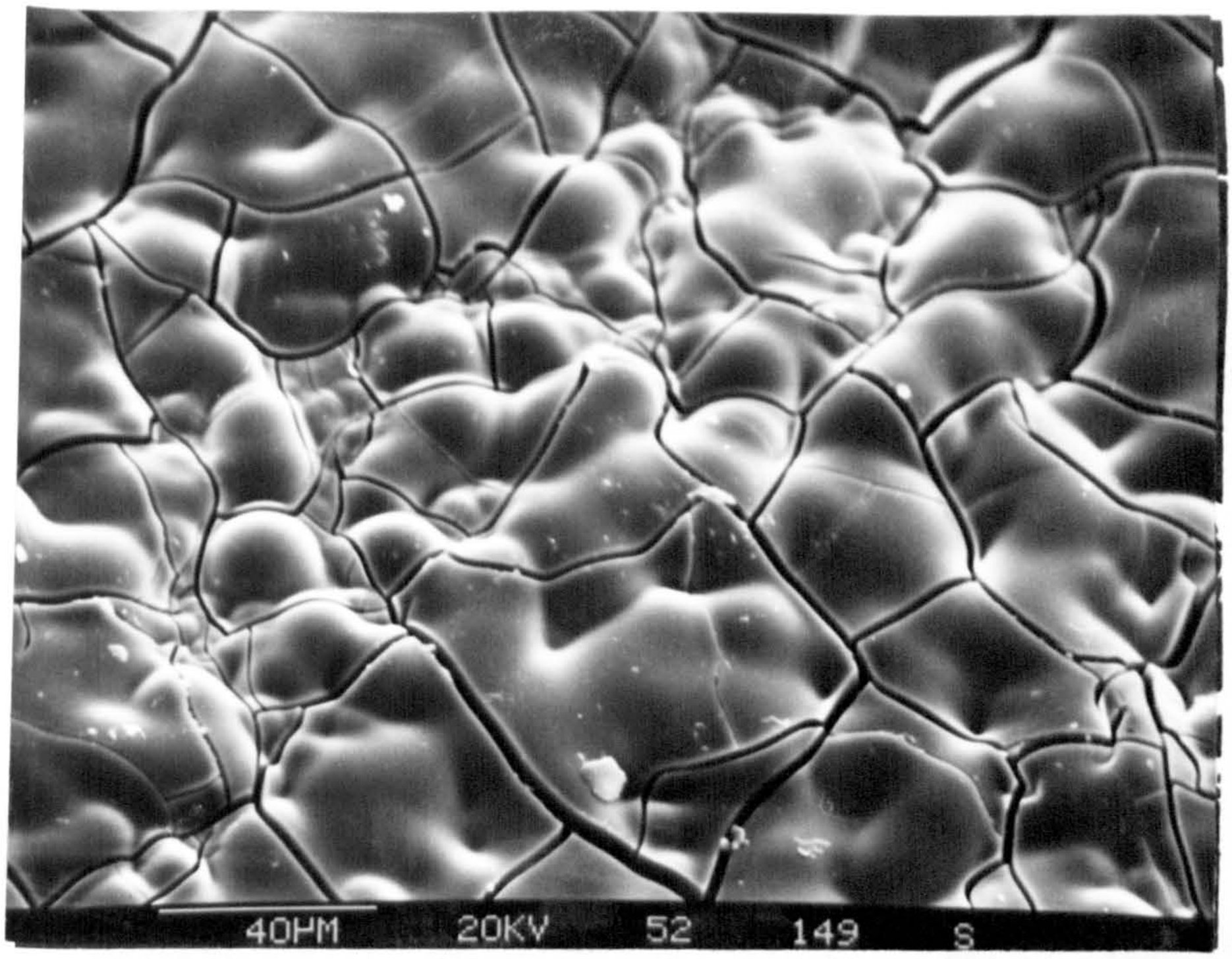

Fig.3.2.4(b) S.E.M. micrograph of the same Mo-black coating (Fig.3.2.4(a) at different area. Magnification: 500X.

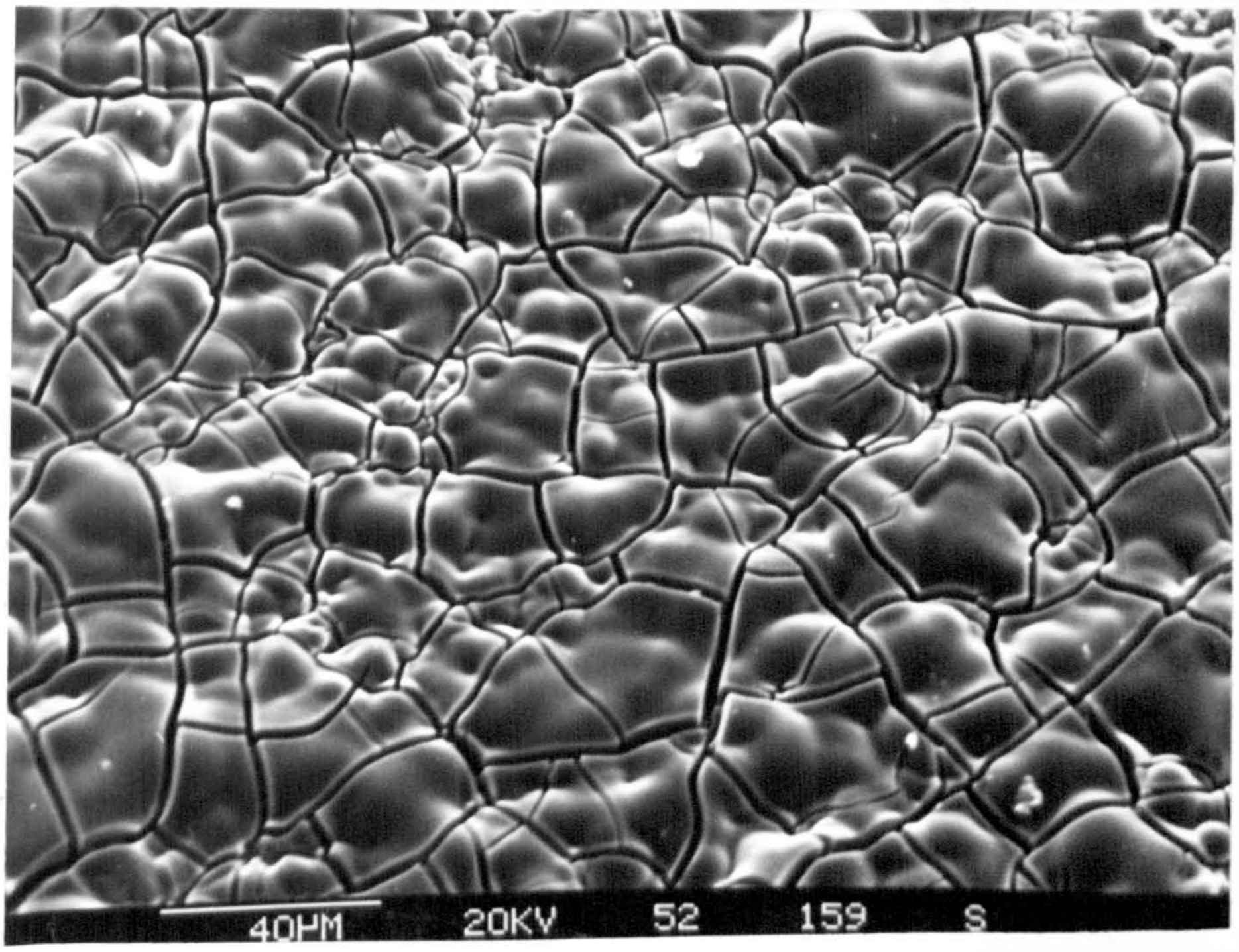

Fig.3.2.5 S.E.M. micrograph of electroplated Mo-black coating on aluminium (coating density~2.5 mg/cm^2). Magnification: 500X.

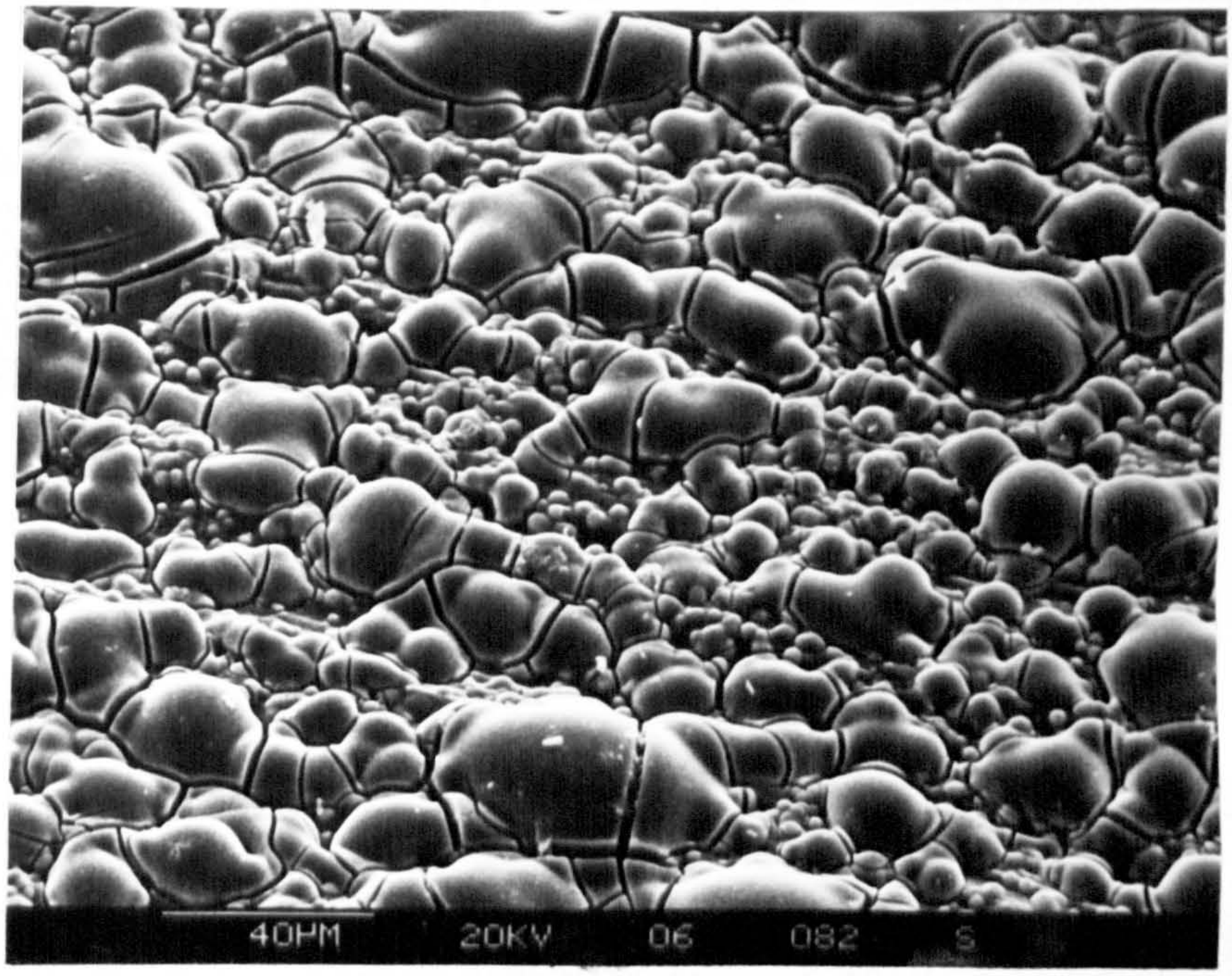

Fig.3.2.6 S.E.M. micrograph of electroplated Mo-black coating on aluminium substrate of coating density~1.5 mg/cm². Magnification: 500X

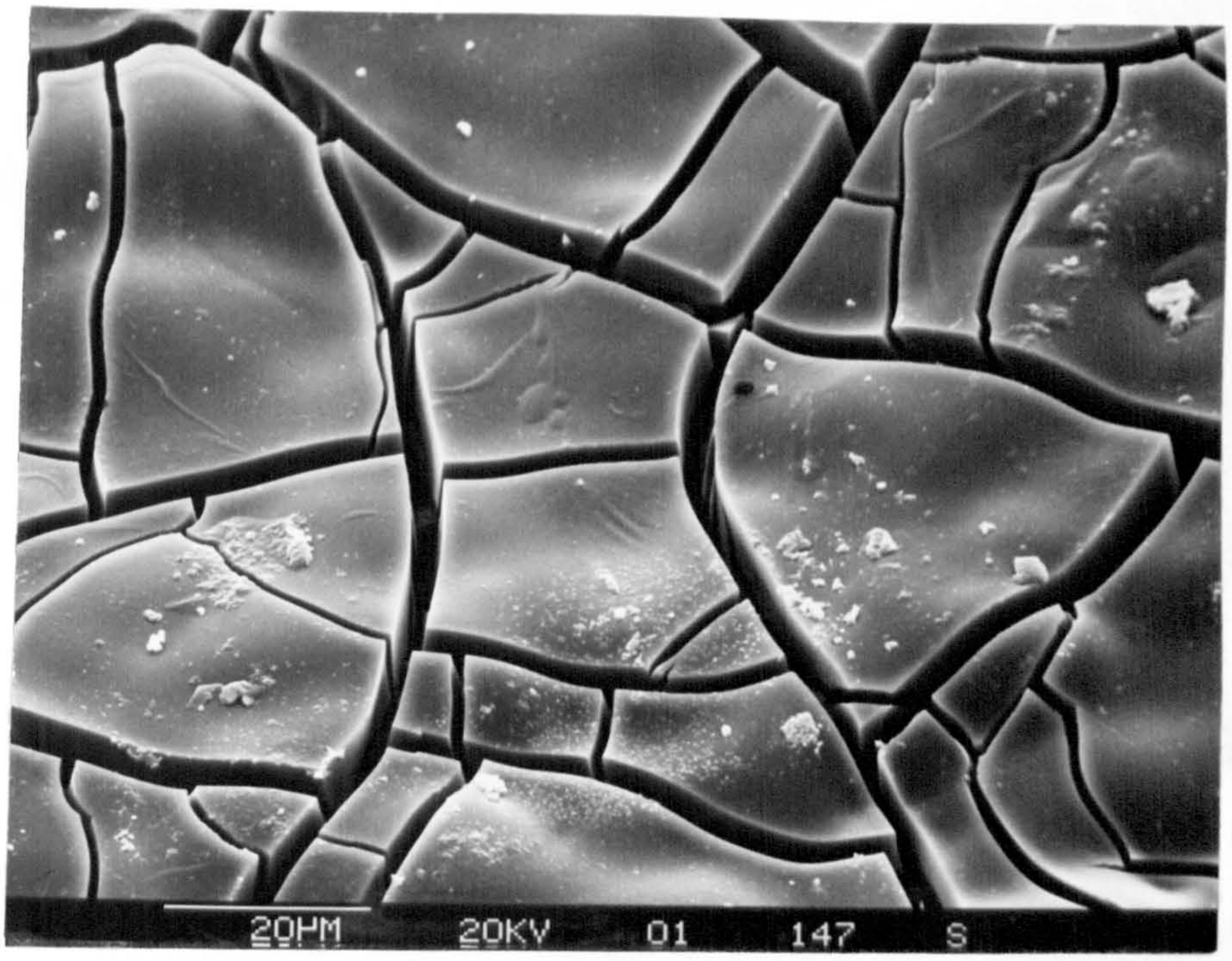

Fig.3.2.7 S.E.M. micrograph of Mo-black coating on aluminium of coating density~2.7 mg/cm² plated with current density of 1.5 mA/cm². Magnification: 1000X.

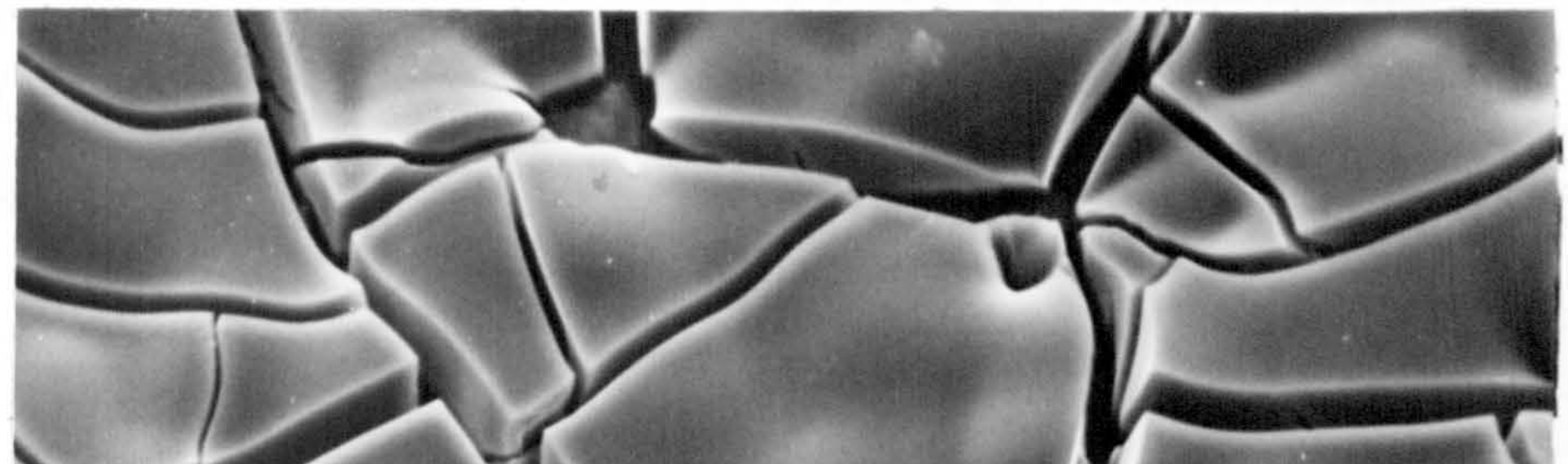

Fig.3.2.8 S.E.M. micrograph of Mo-black coating on aluminium of coating density~2.9 mg/cm², plated with high current density (3.15 mA/cm²). Magnification: 1000X

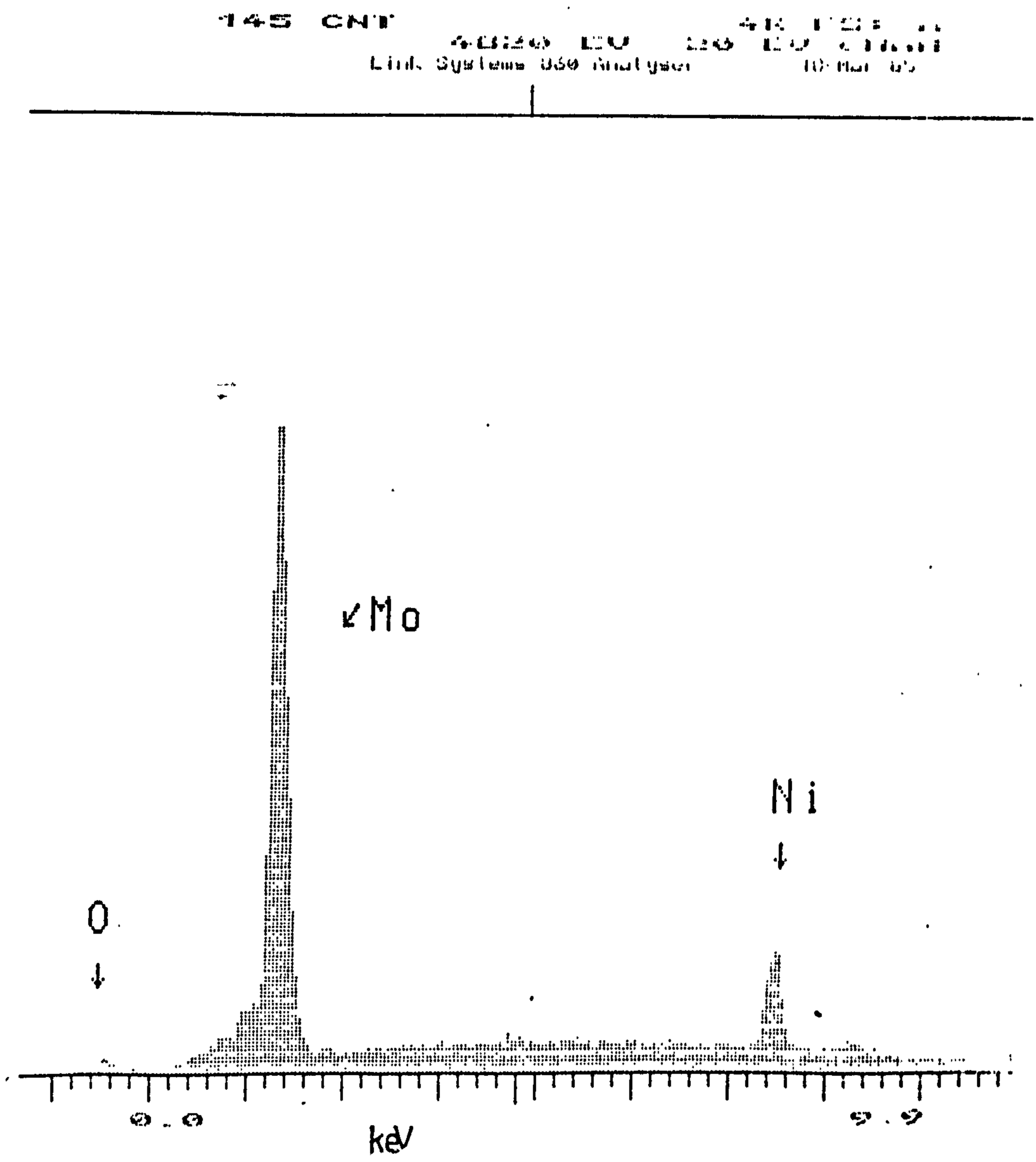

Fig.3.2.9 EDX spectrum from the surface of Mo-black coating of Fig.3.2.7, plated with low current density (1.5 mA/cm²).

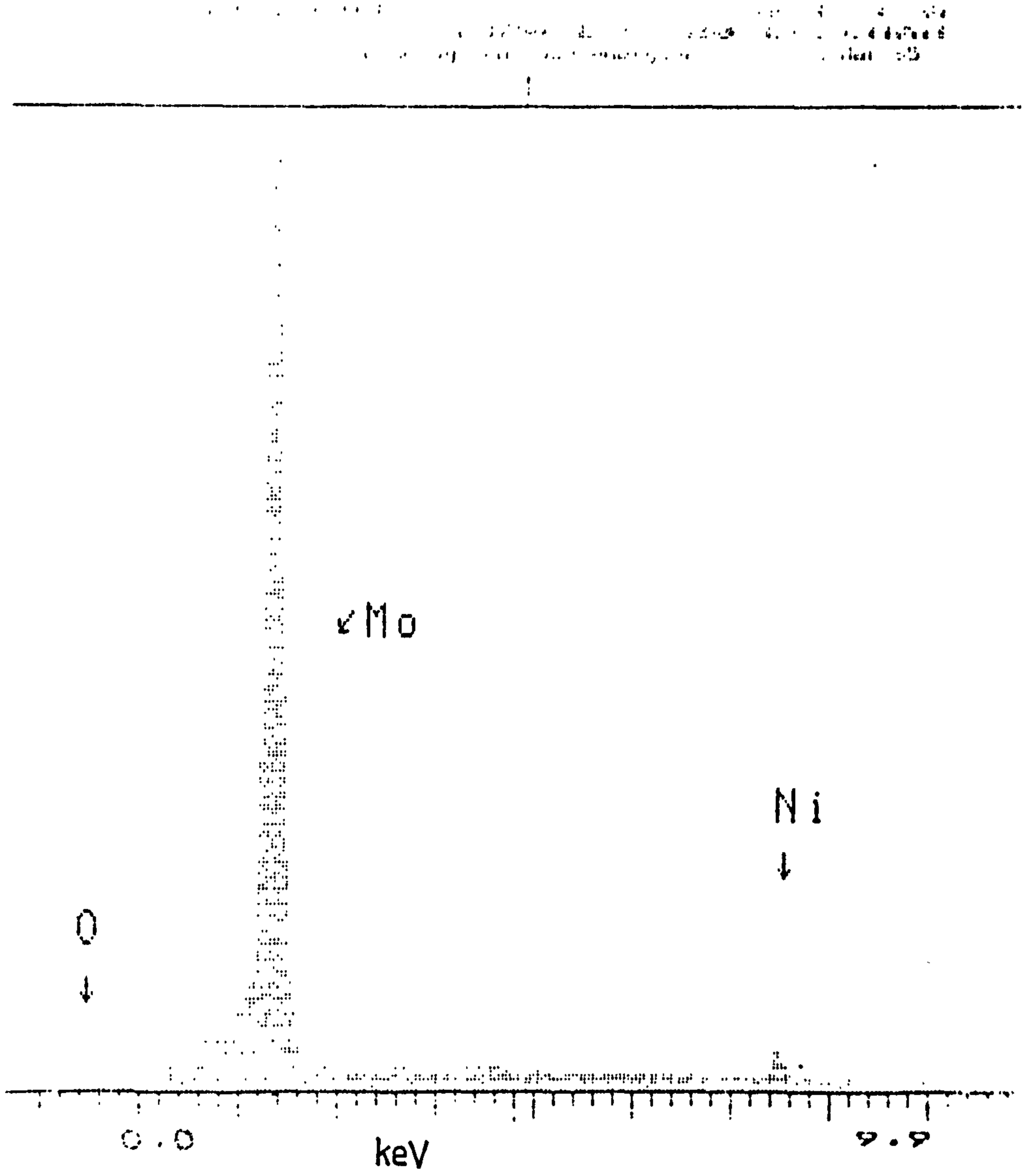

Fig.3.2.10 EDX spectrum from the surface of Mo-black coating of Fig.3.2.8 on aluminium plated with high current density (3.15 mA/cm²).

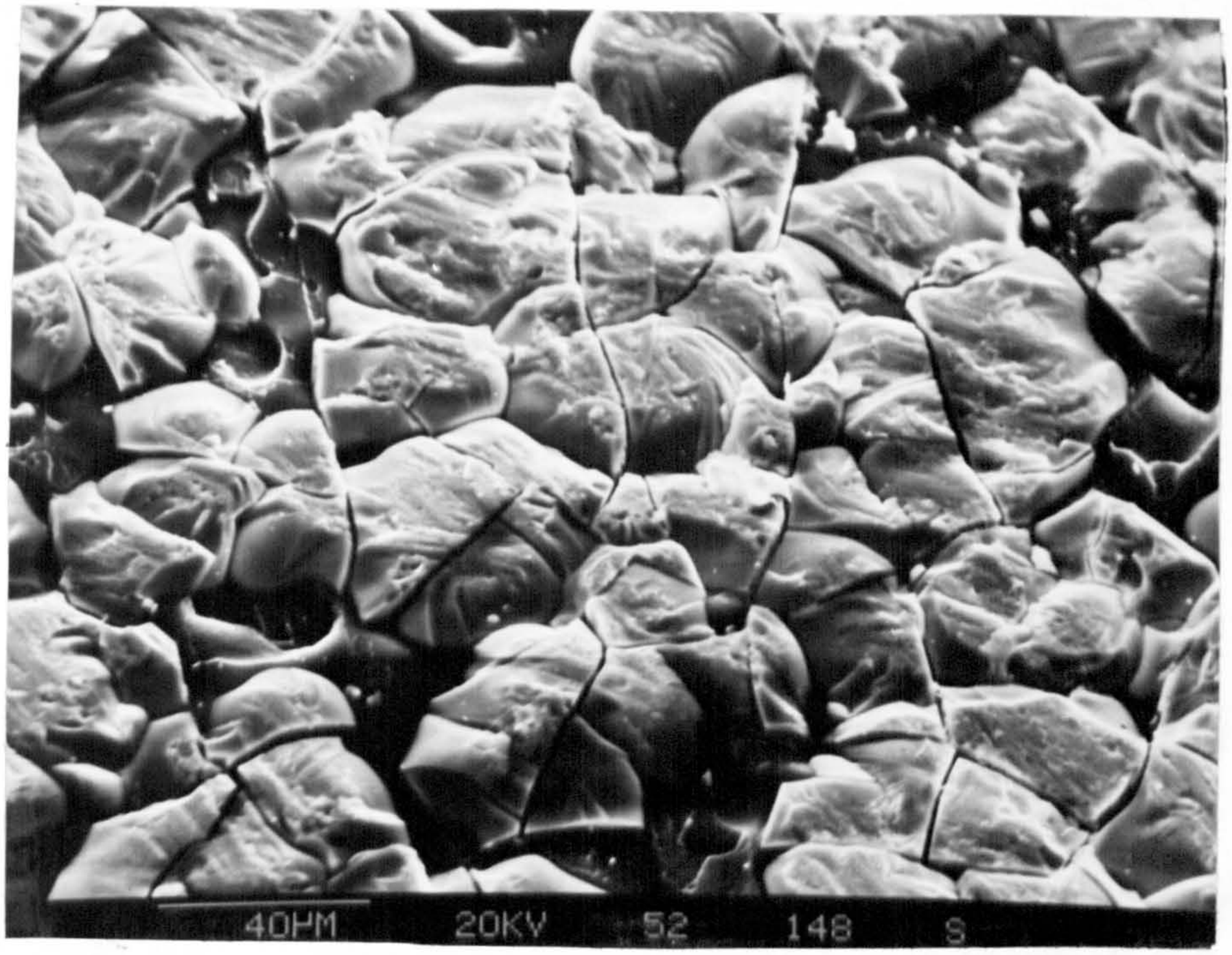

(a)

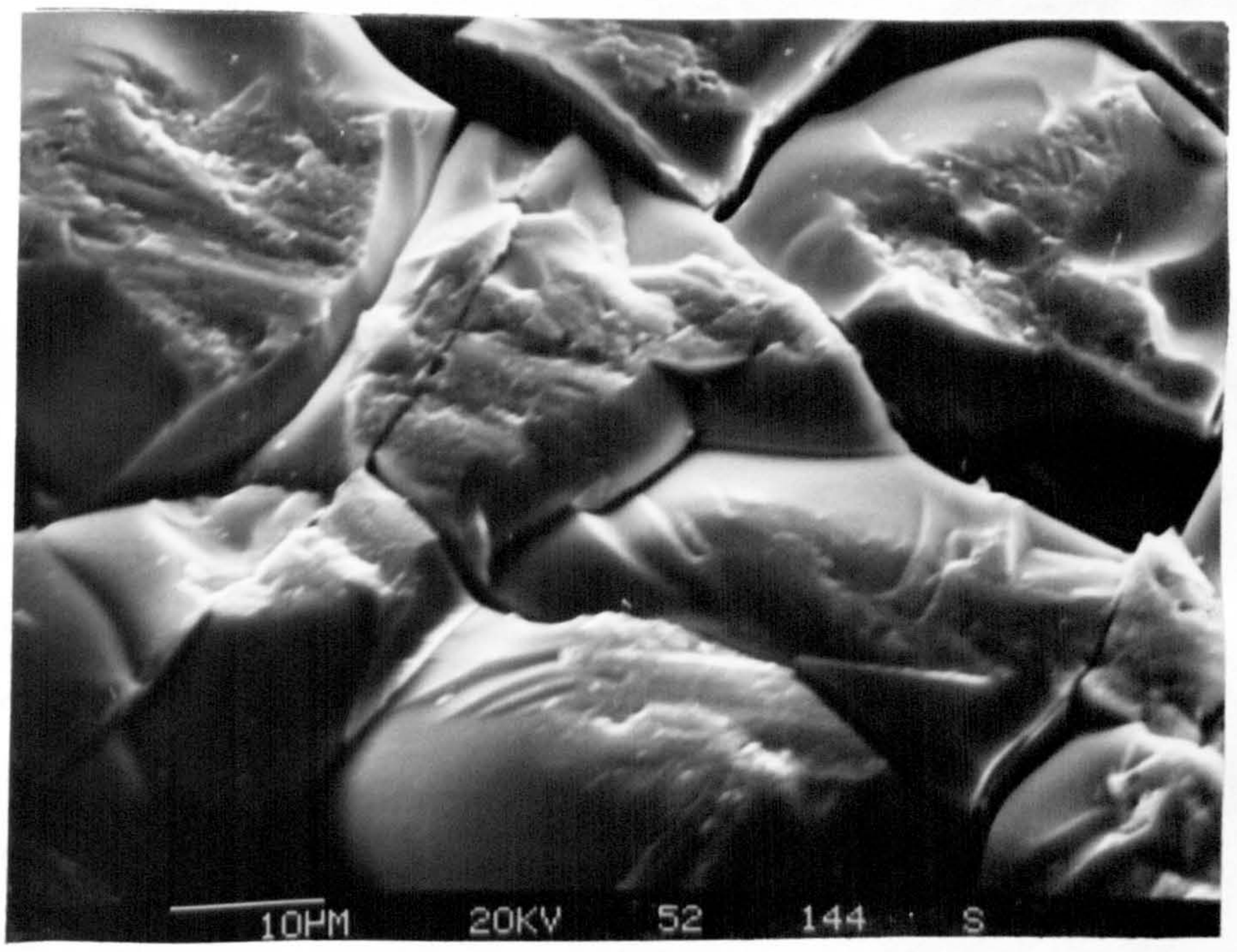

(b)

Fig.3.2.11 S.E.M. micrograph of electroplated Mo-black coating interface as removed from the aluminium substrate. (a) Magnification: 500X, (b) Magnification: 1500X.

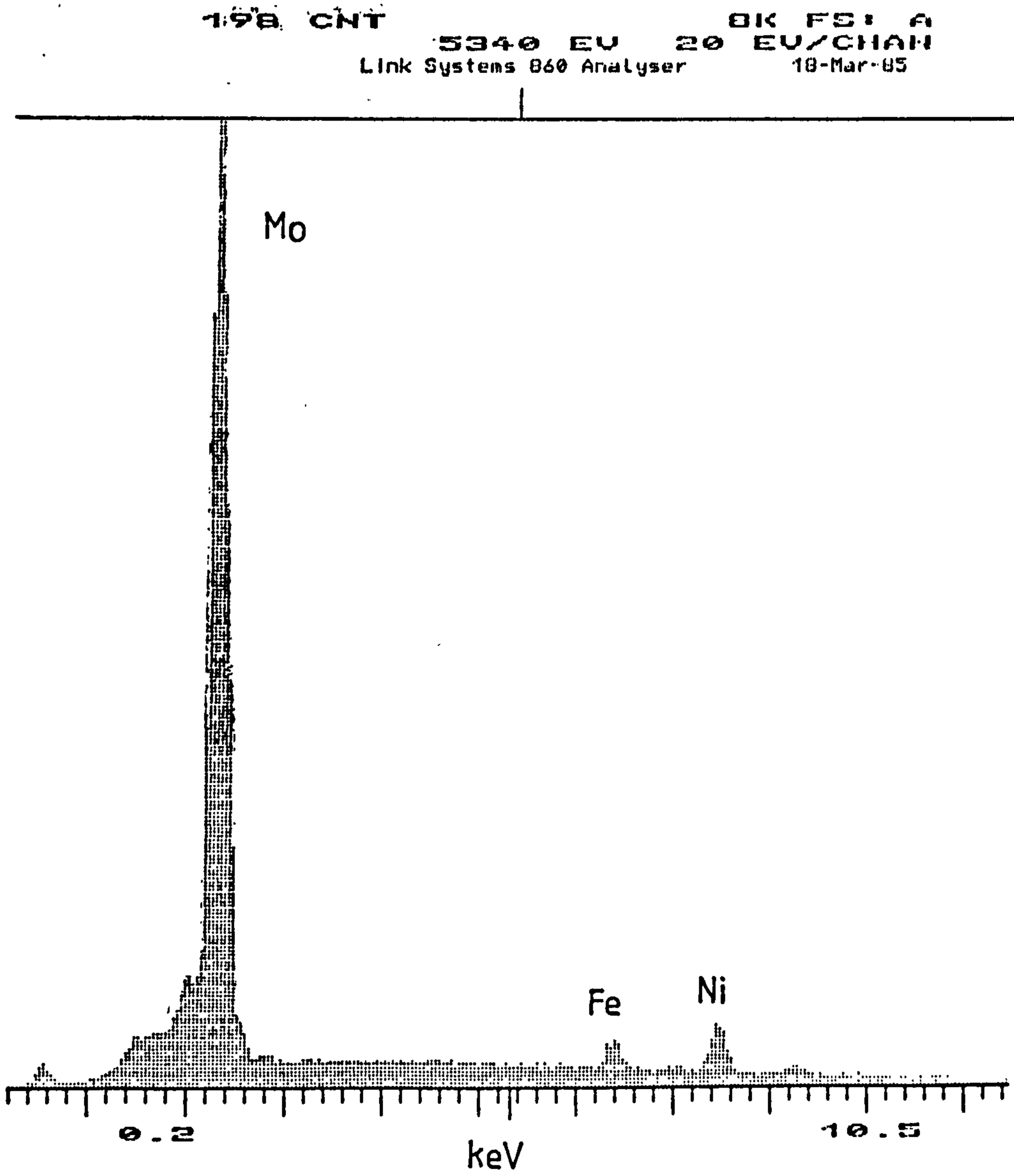

Fig.3.2.12 EDX spectrum from the electrodeposited Mo-black coating to aluminium interface.

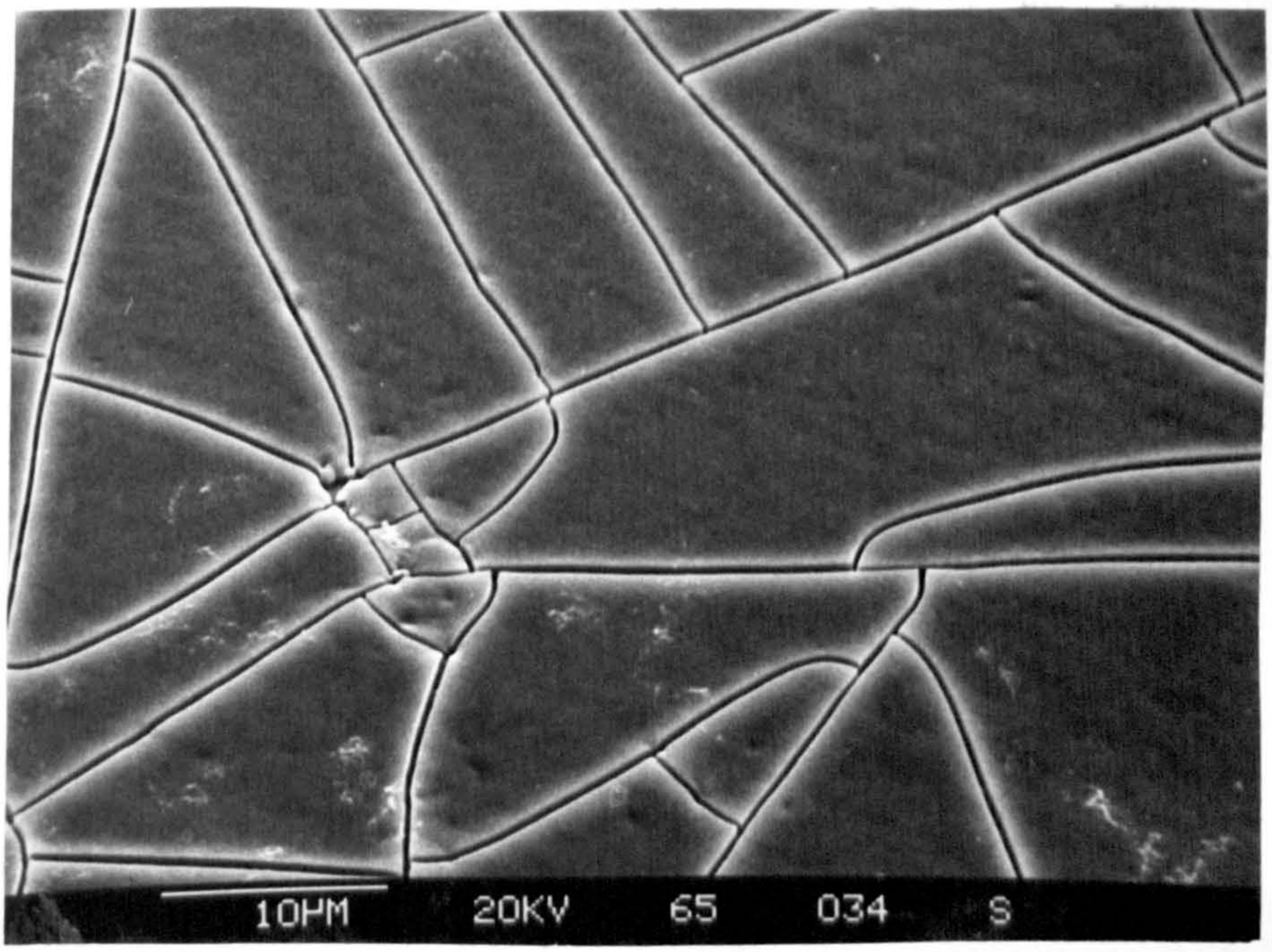

Fig.3.2.13 S.E.M. micrograph of a Mo-black dip coating on mechanically polished zinc showing large numbers of flat platelets. Magnification: 2000X.

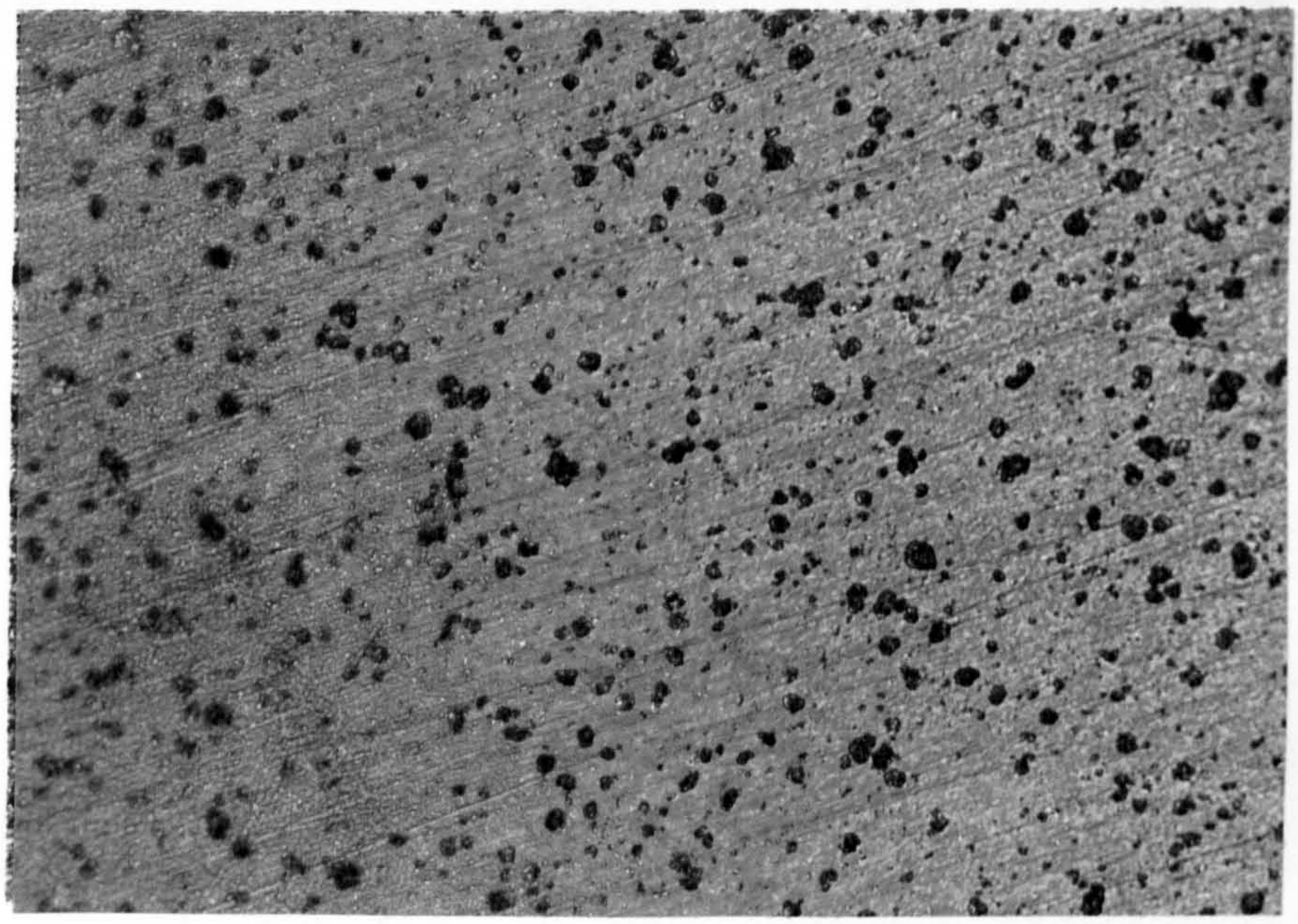

Fig.3.2.14 Optical microscopic photograph of Mo-black dip coating on zinc in wet condition: showing no crack. Deposition time = 6 seconds. Magnification: 100X.

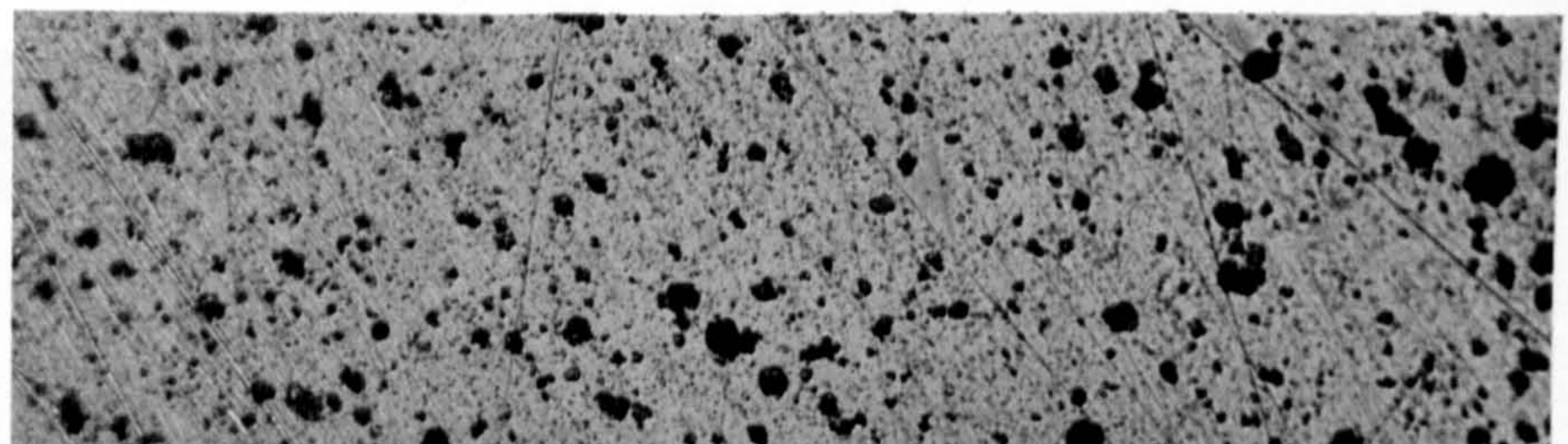

Fig.3.2.15 Optical microscopic photograph of Mo-black dip coating on zinc in wet condition showing no crack. Deposition time = 10 seconds. Magnification: 100X.

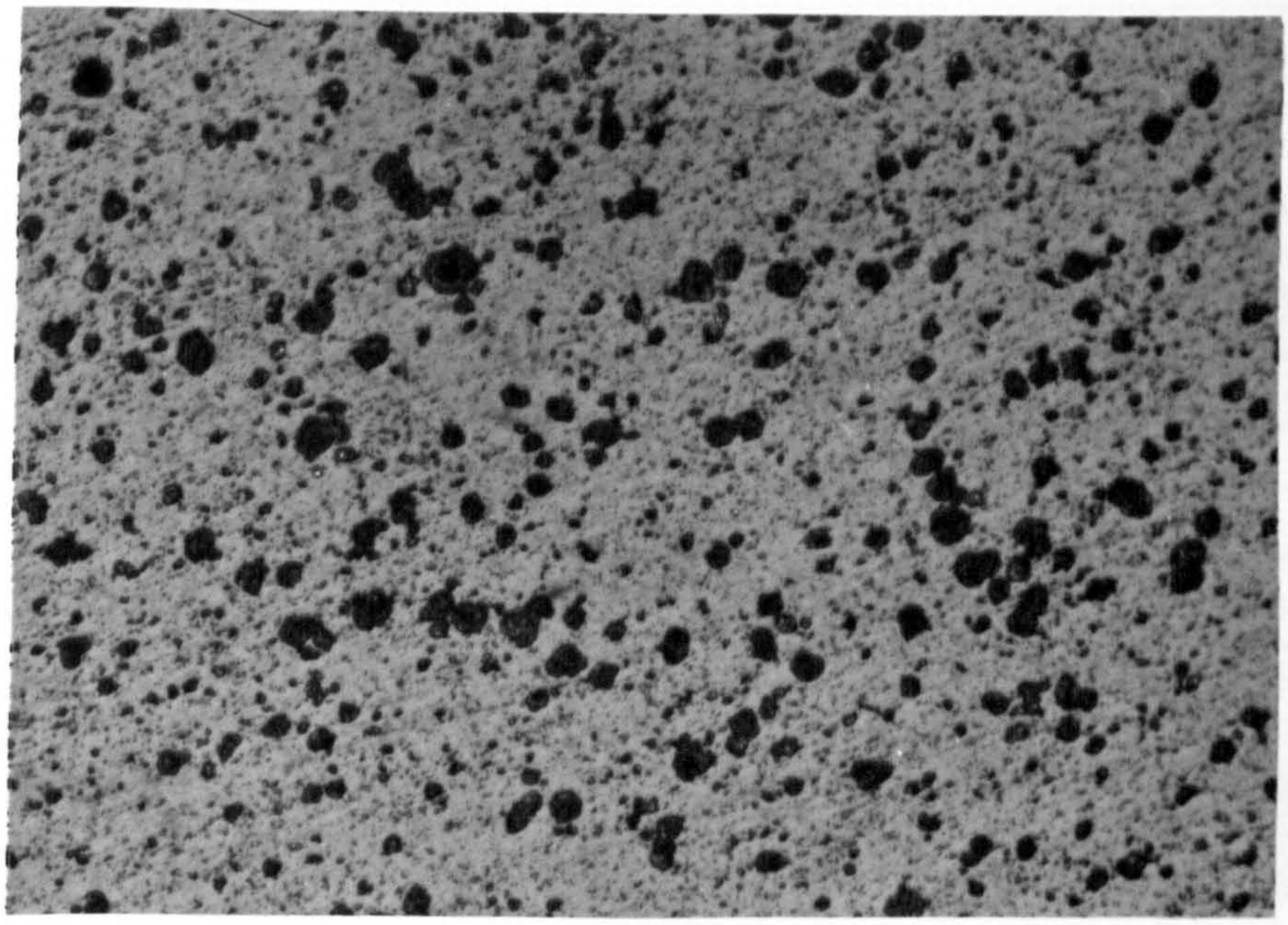

Fig.3.2.16 Optical microscopic photograph of Mo-black dip coating on zinc in wet condition showing no crack. Deposition time = 20 seconds. Magnification: 100X.

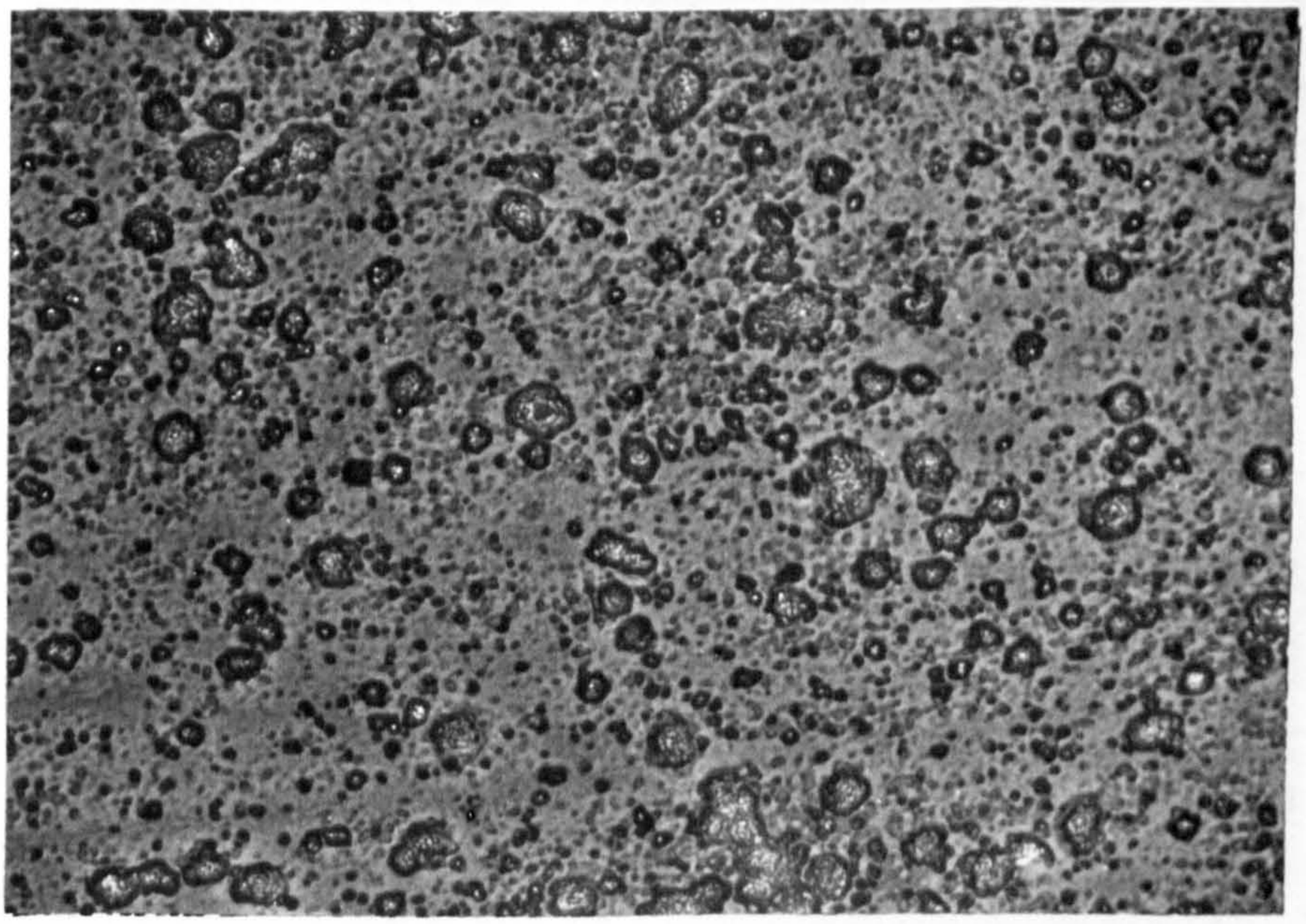

Fig.3.2.17 Optical microscopic photograph of Mo-black dip coating on zinc in wet condition showing no crack. Deposition time = 60 seconds. Magnification: 100X.

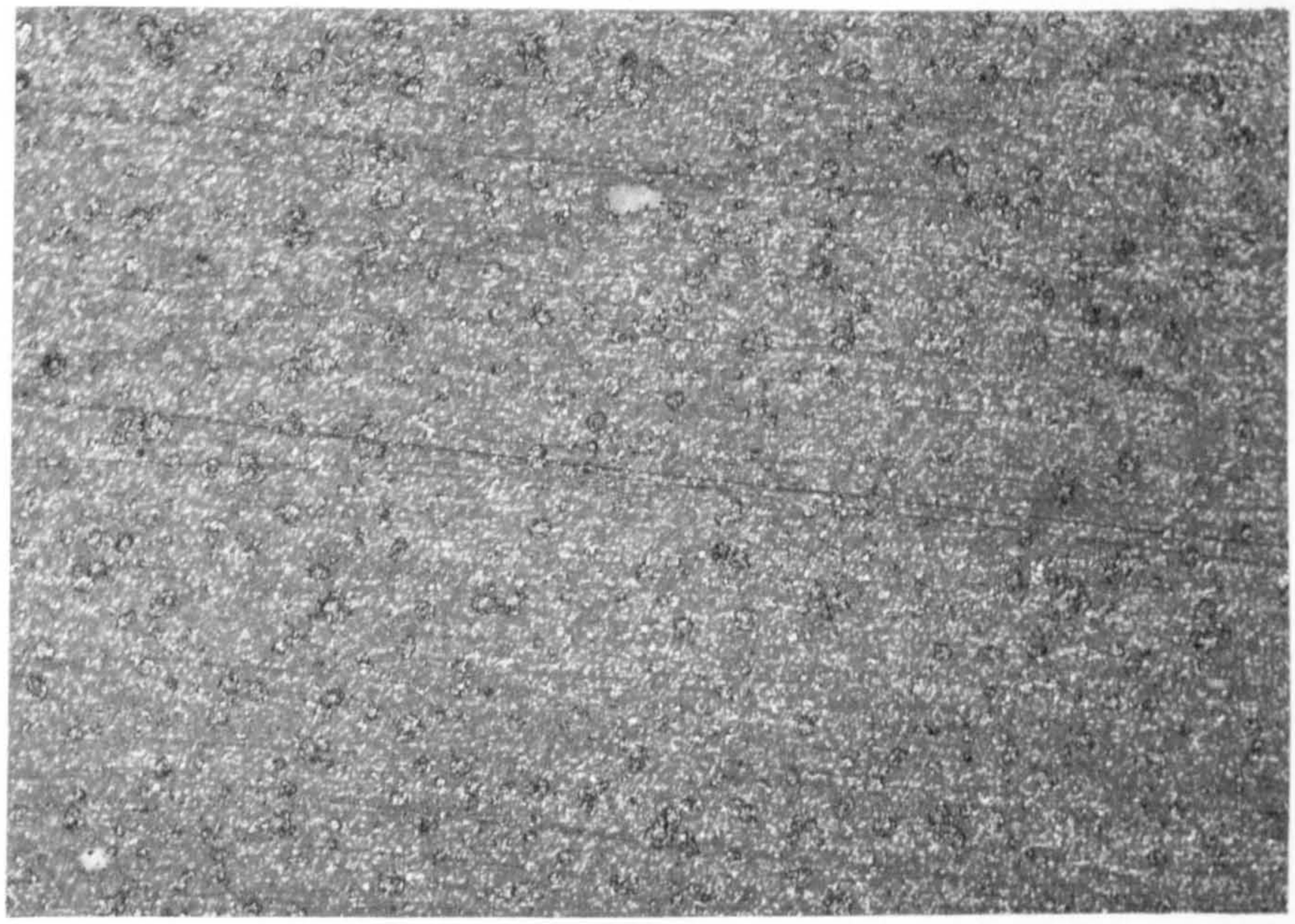

Fig.3.2.18 Optical microscopic photograph of Mo-black dip coating of Fig.3.2.14 in dry condition. No crack in the surface. Magnification: 100X.

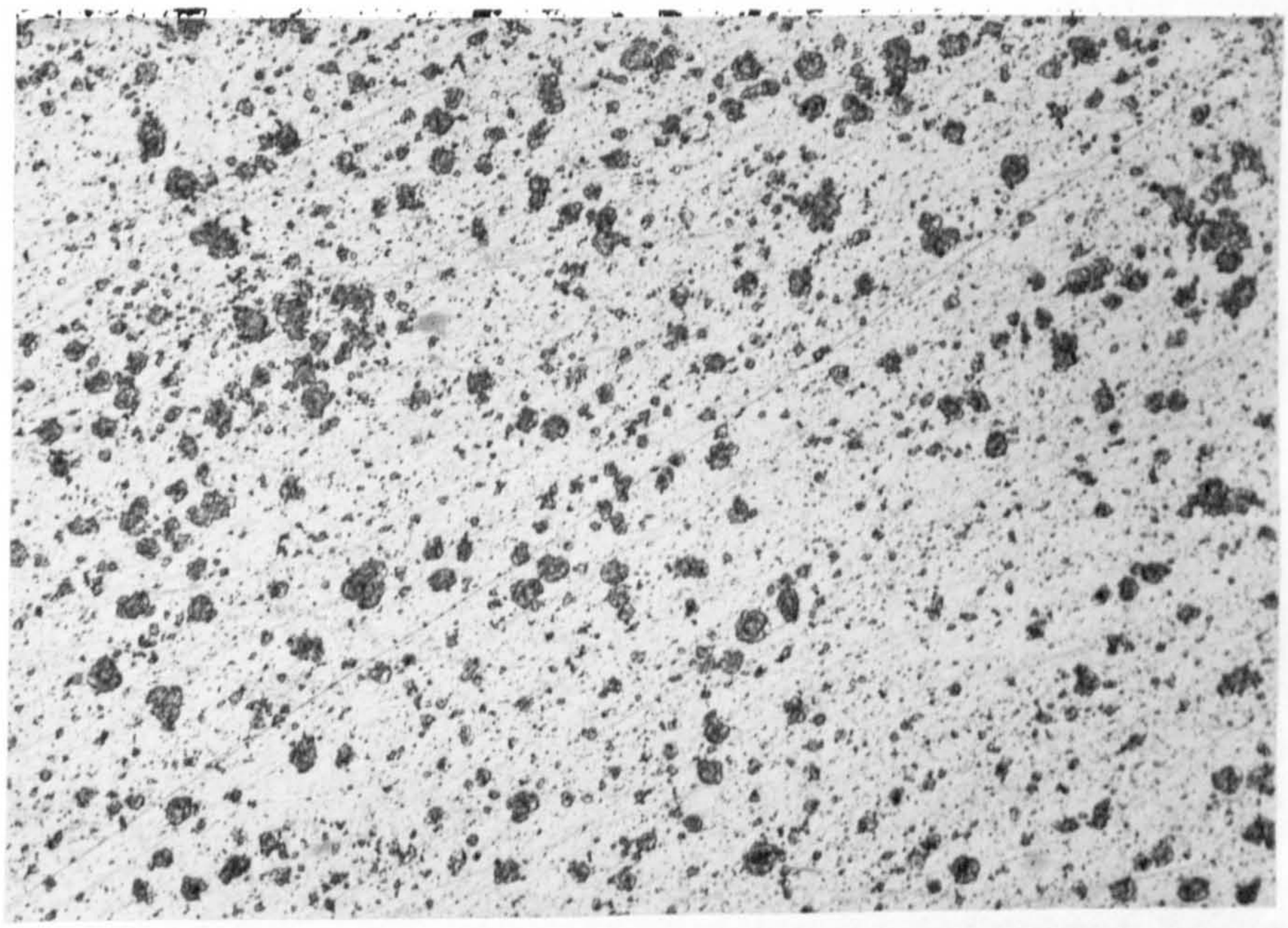

Fig.3.2.19 Optical microscopic photograph of Mo-black dip coating of Fig.3.2.15 in dry condition showing no crack. Magnification: 100X.

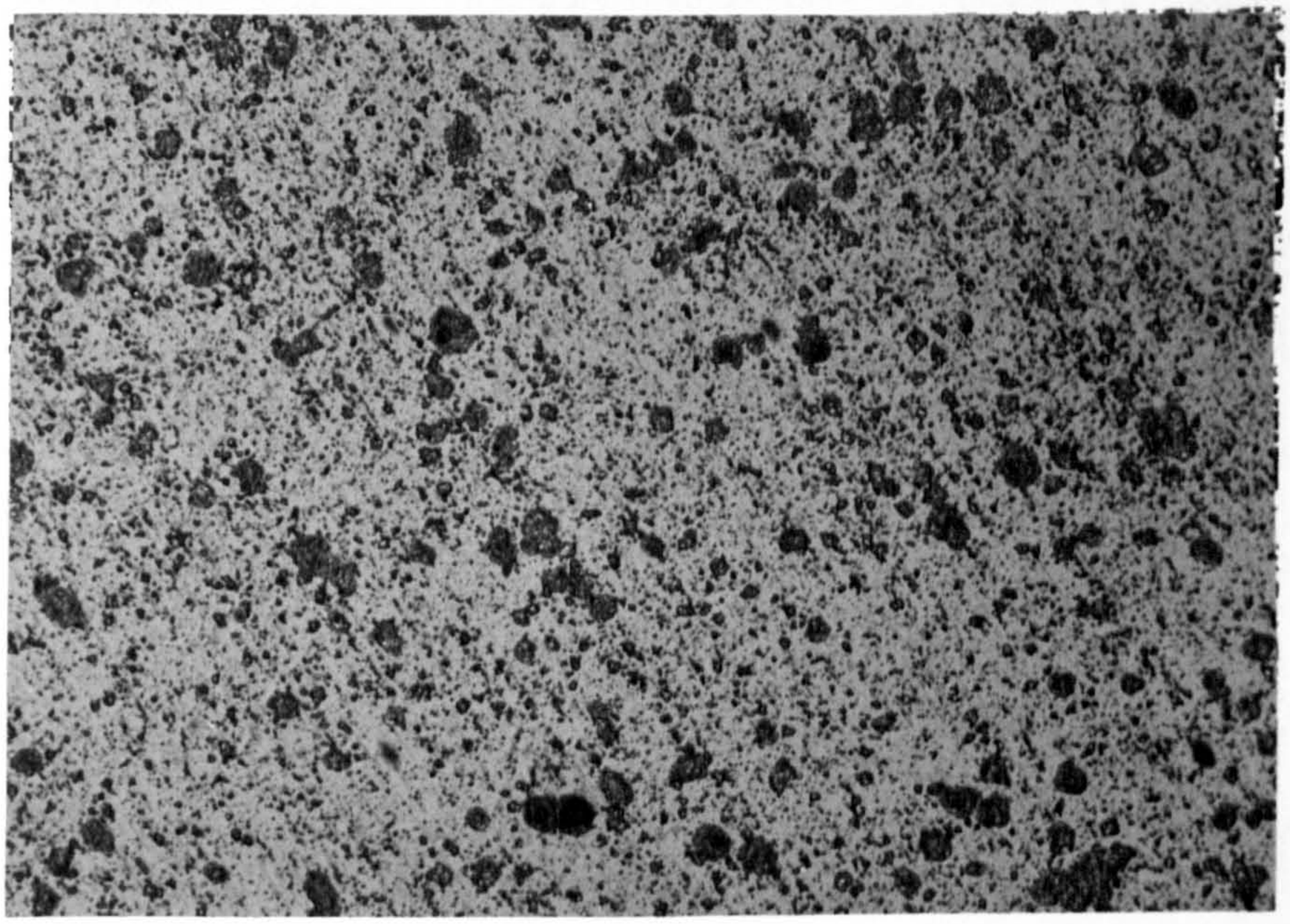

Fig.3.2.20 Optical microscopic phtograph of Mo-black dip coating of Fig.3.2.16 in dry condition showing no crack.
Magnification: 100X.

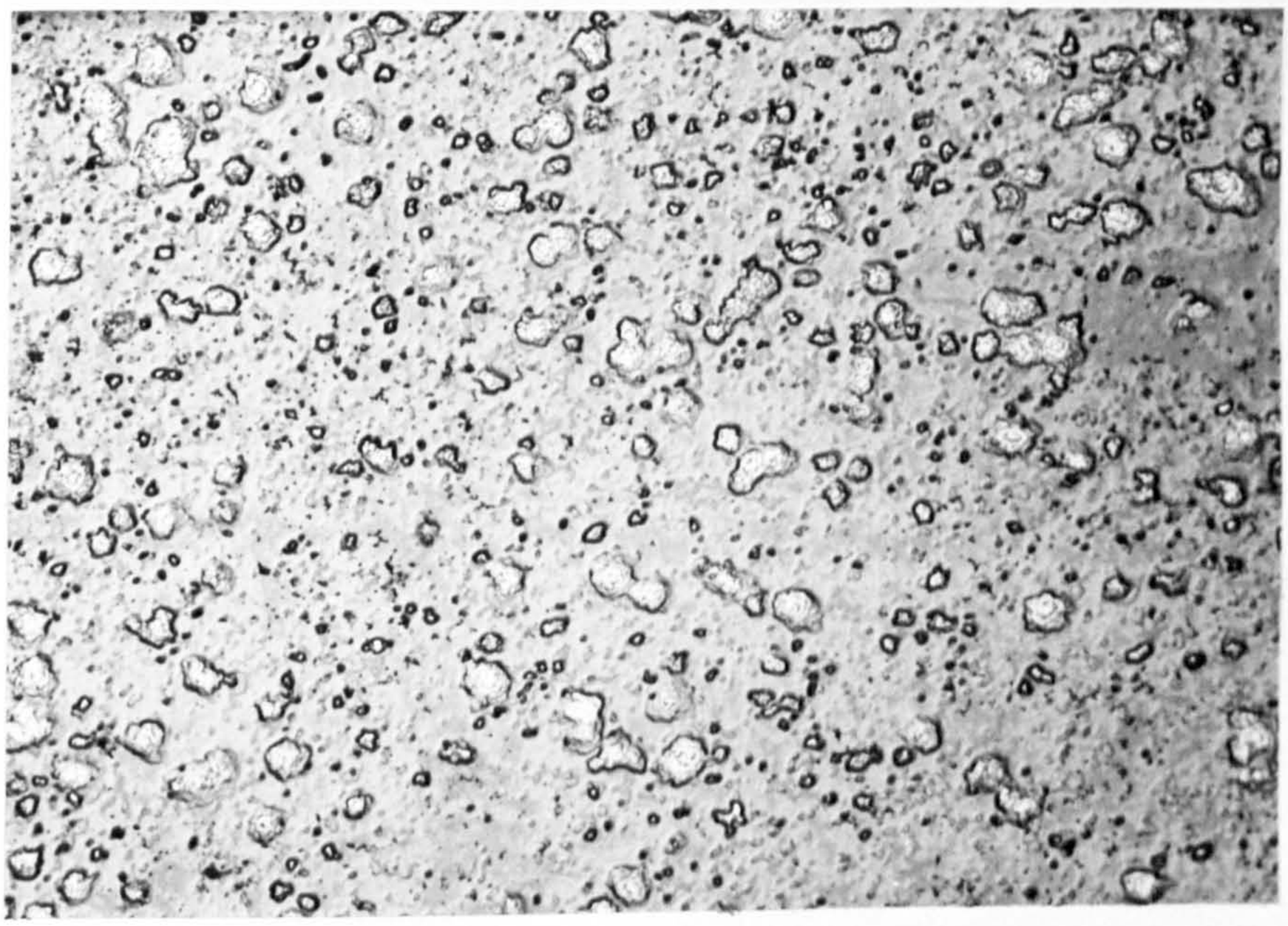

Fig.3.2.21 Optical microscopic photograph of Mo-black dip coating of Fig.3.2.17, in dry condition showing no crack.
Magnification: 100X.

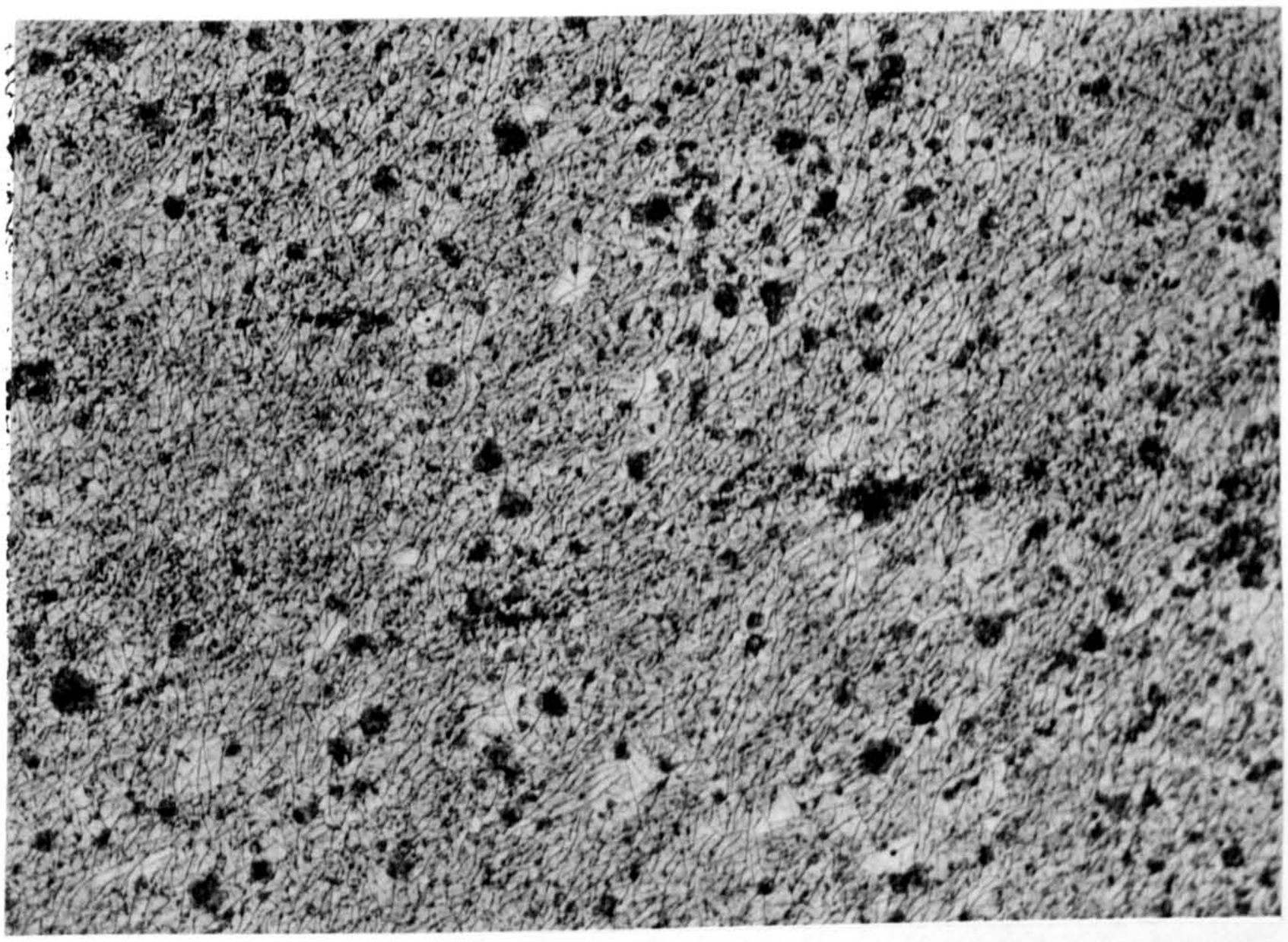

Fig.3.2.22 Optical microscopic photograph of Mo-black dip coating on zinc of Fig.3.2.15 after applying hot air, showing large numbers of cracks. Magnification: 100X.

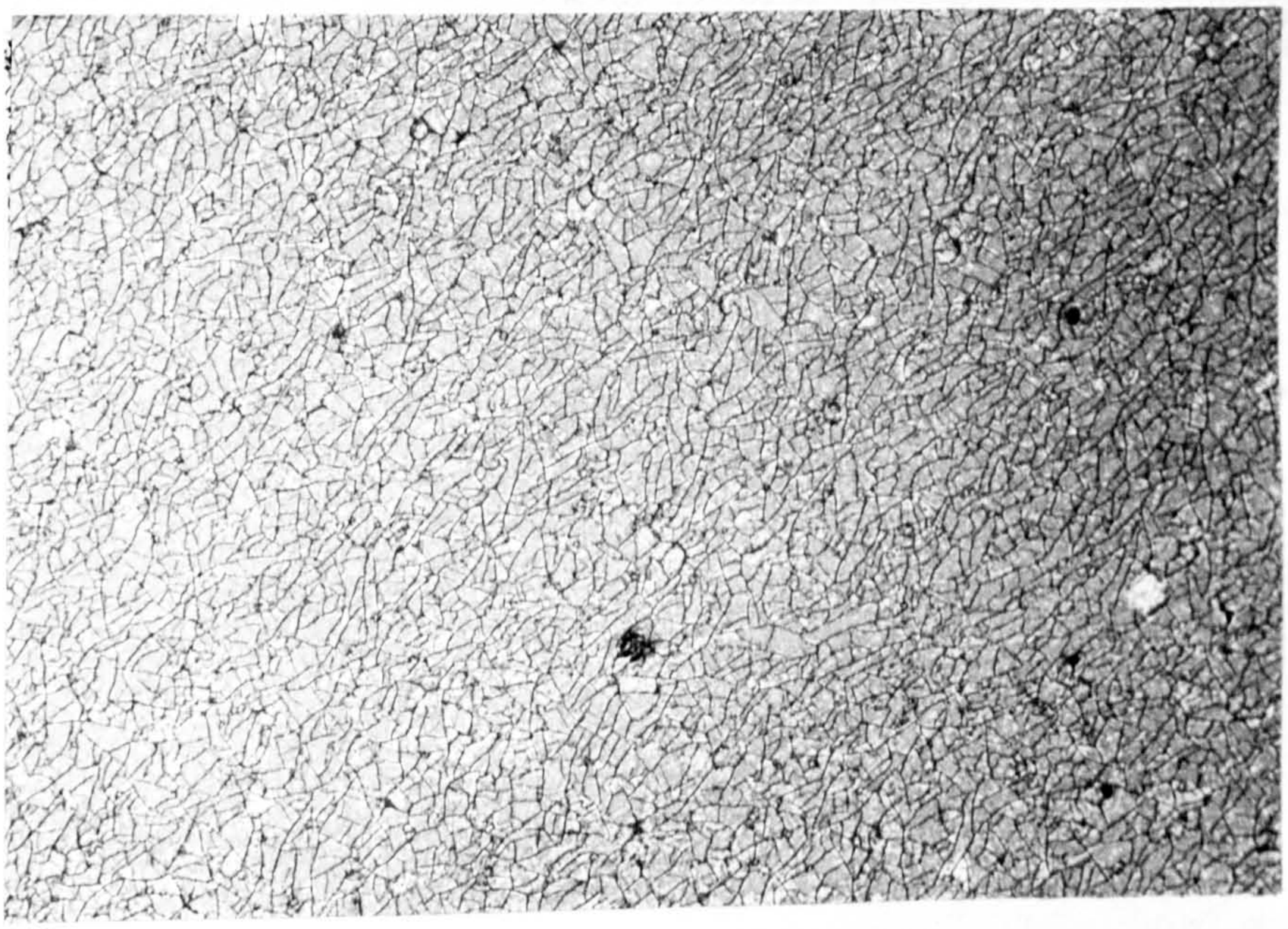

Fig.3.2.23 Optical microscopic photograph of Mo-black dip coating of Fig.3.2.16 after applying hot air showing large numbers of cracks. Magnification: 100X.

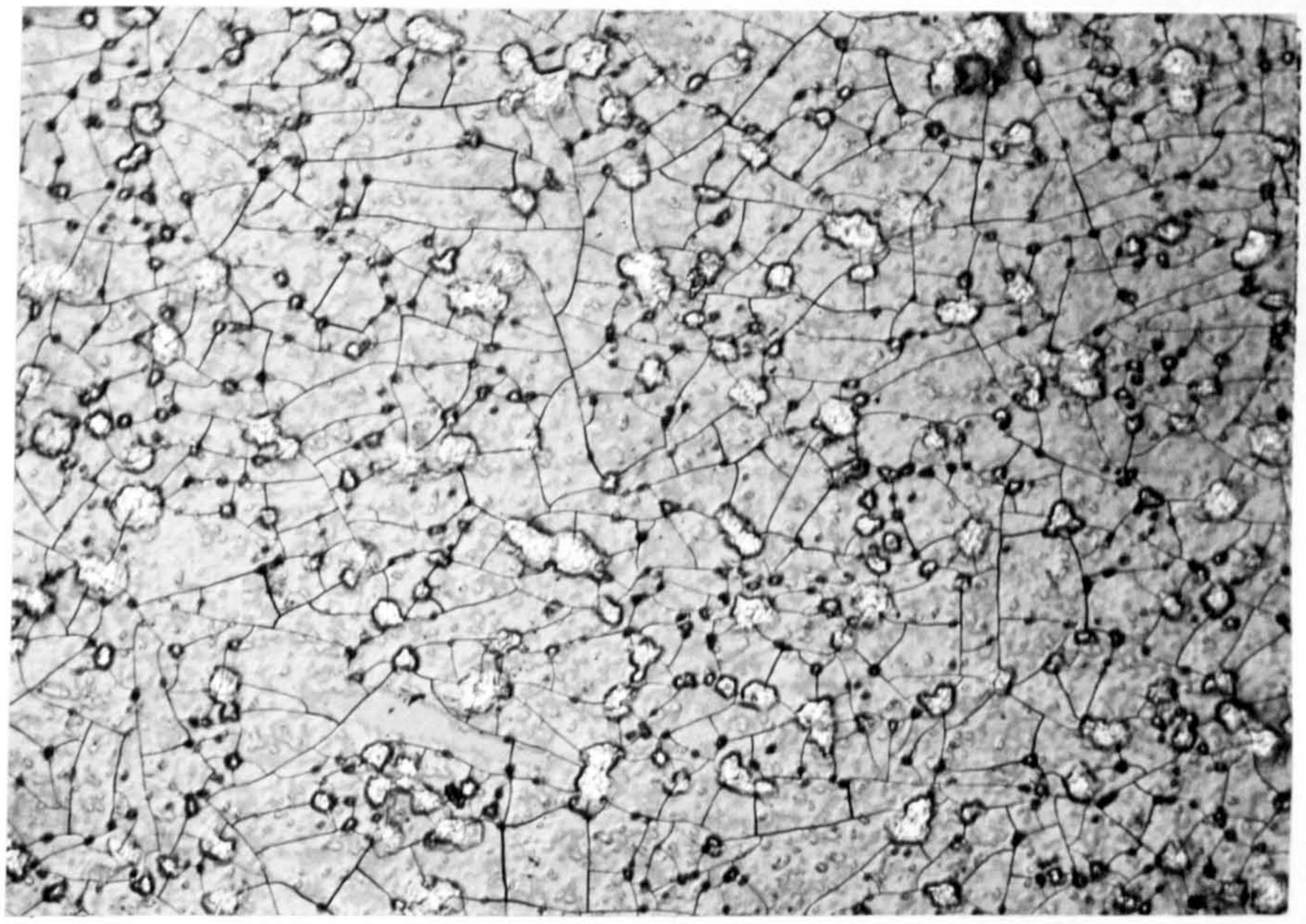

Fig.3.2.24 Optical microscopic photograph of Mo-black dip coating of Fig.3.2.17 after applying hot air, showing large numbers of cracks. Magnification: 100X.

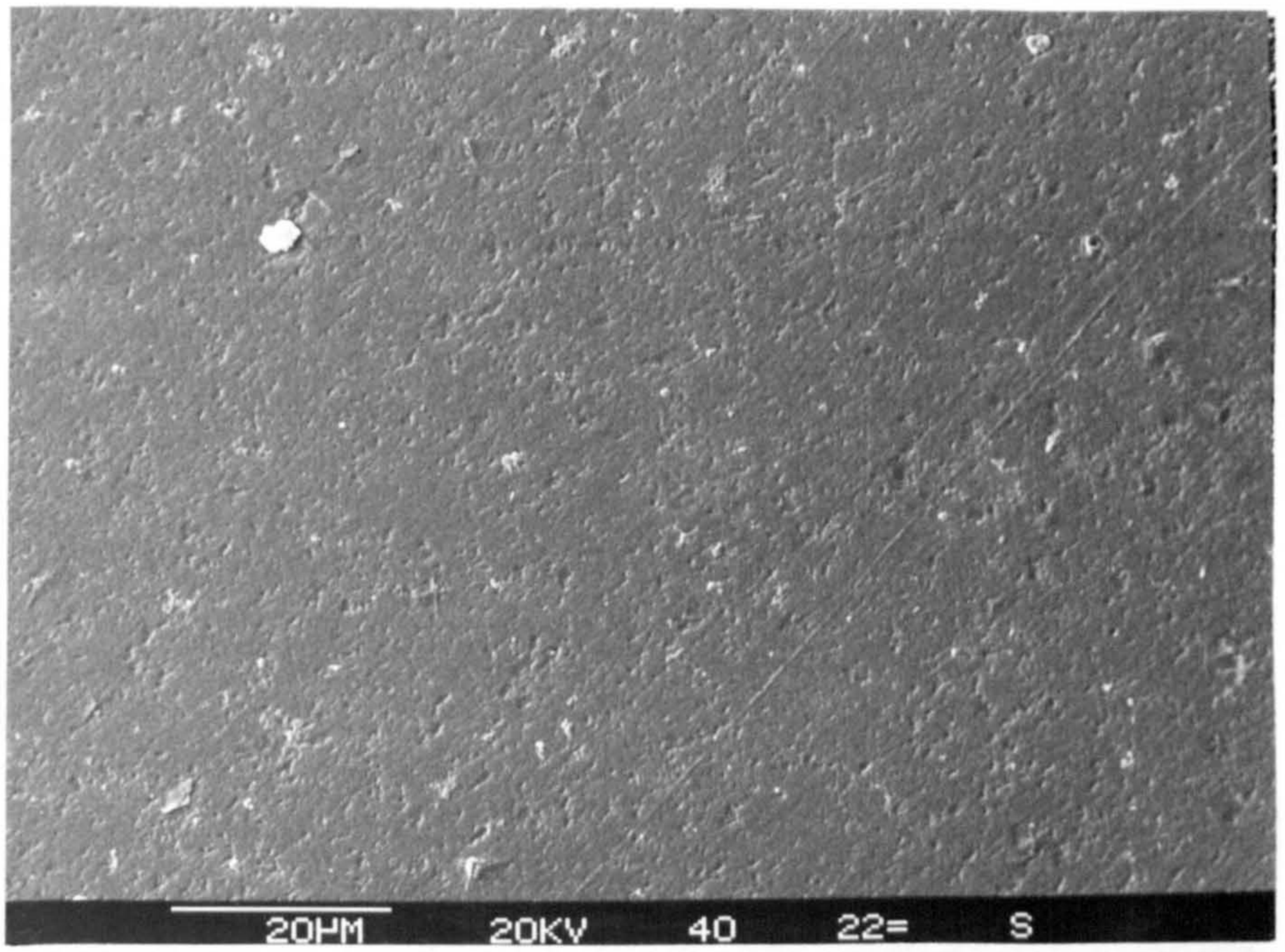

(a)

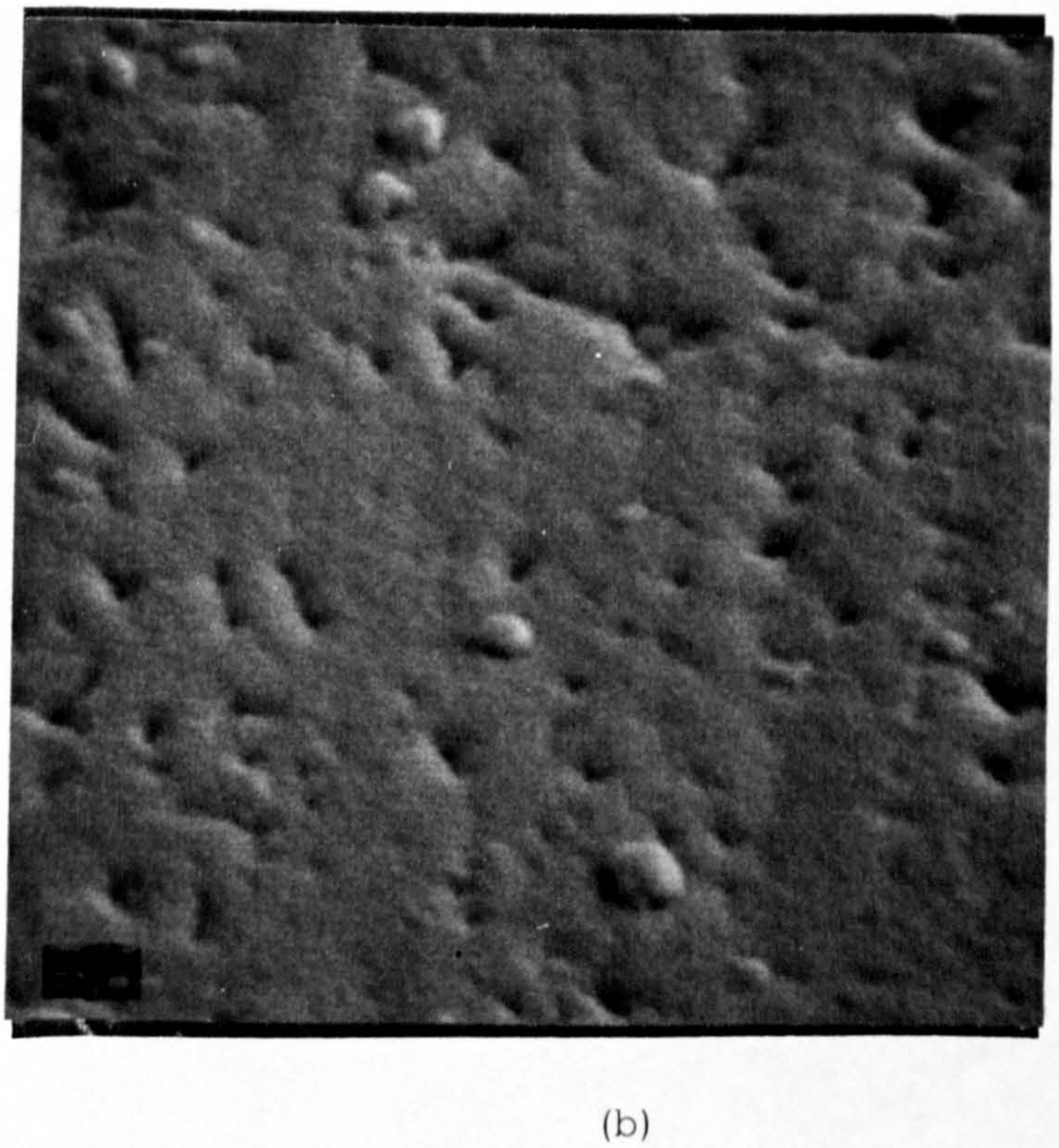

(b)

Fig.3.2.25 S.E.M. micrograph of a thin-Mo-black dip coating on zinc of deposition time 5 seconds.
(a) Magnification: 1000X, (b) Magnification: 16000X.

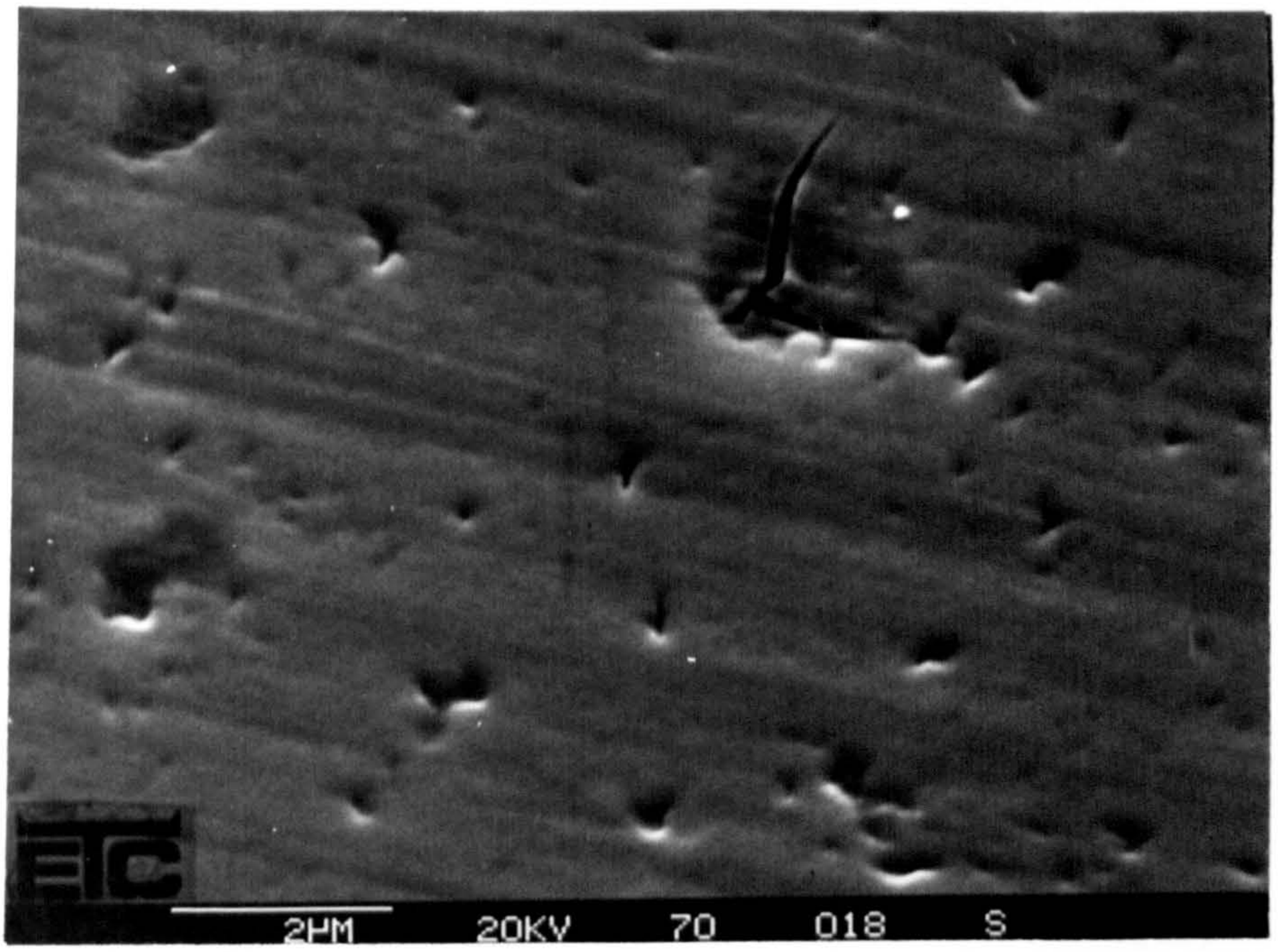

Fig.3.2.26(a) S.E.M. micrograph of a Mo-black dip coating on zinc of deposition time 8 seconds showing one crack. Magnification: 10 000X.

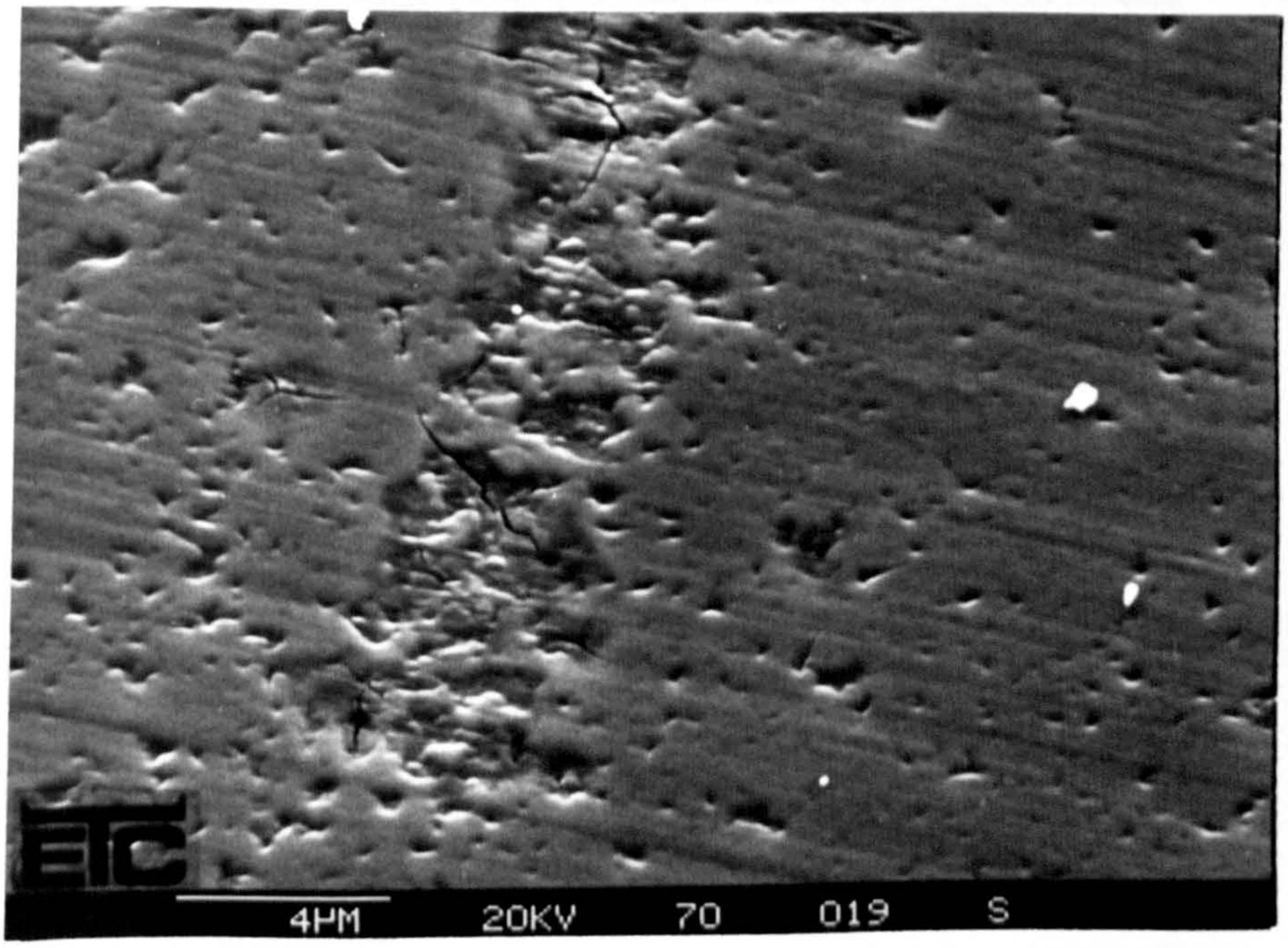

Fig.3.2.26(b) S.E.M. micrograph of the same coating (Fig.3.2.26a) at another area showing few cracks. Magnification: 5000X.

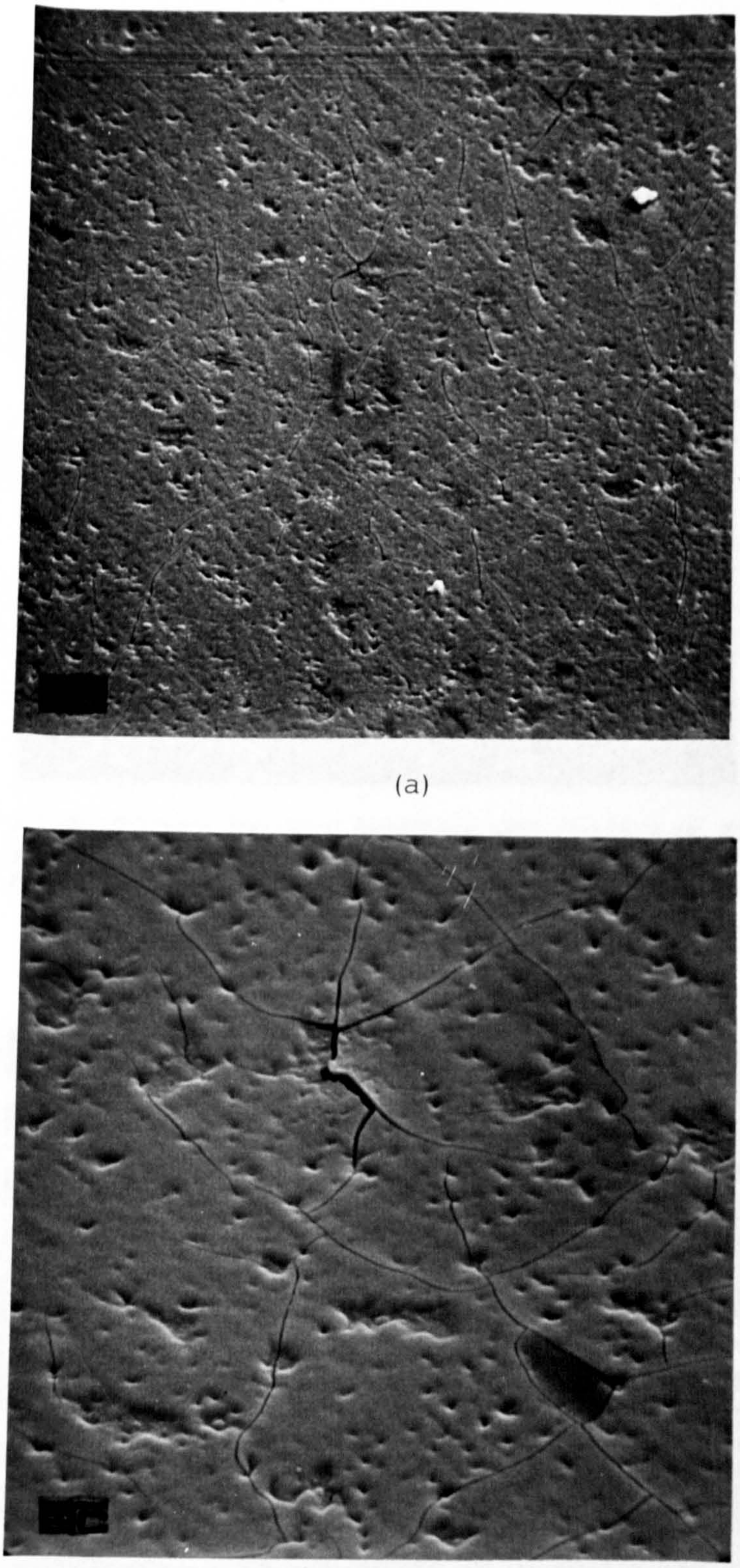

(a)

(b)

Fig.3.2.27 S.E.M micrograph of a Mo-black dip coating on zinc of deposition time 10 seconds showing thin cracks on the surface
(a) Magnification: 2000X, (b) Magnification 5000X.

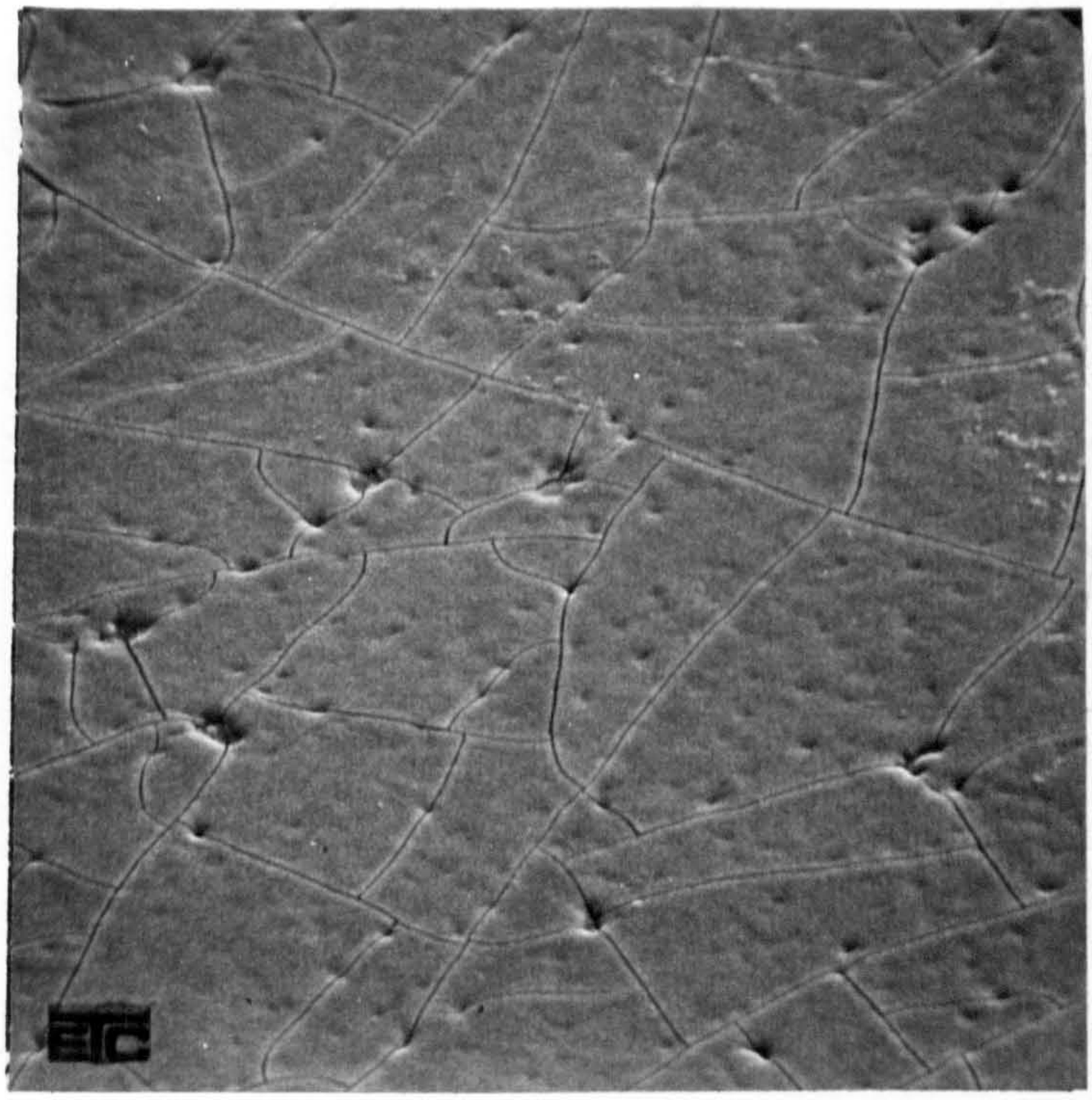

Fig.3.2.28 S.E.M. micrograph of a Mo-black dip coating on zinc substrate of deposition time 50 seconds.
Magnification: 2000X.

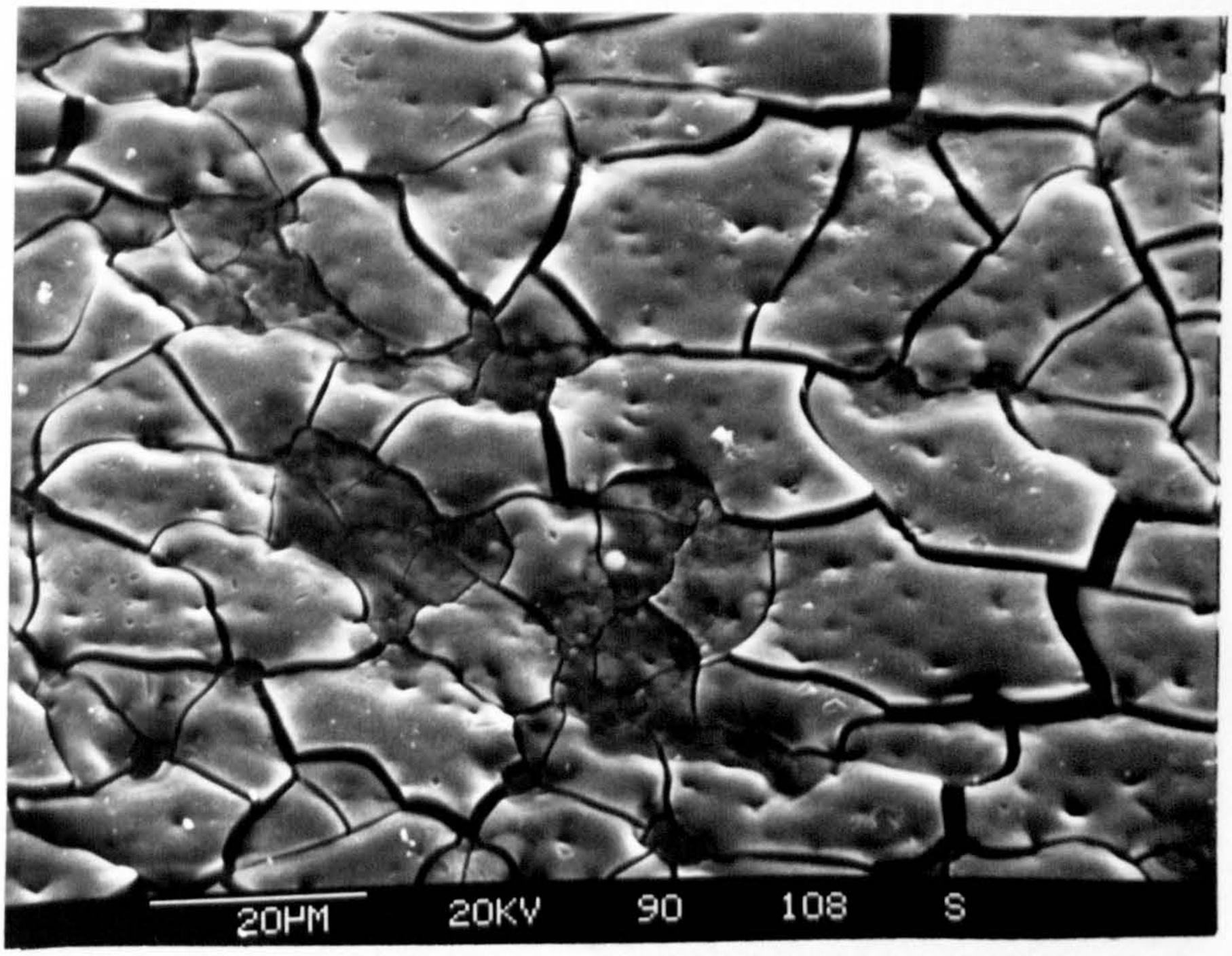

Fig.3.2.29 S.E.M. micrograph of thick Mo-black dip coating on zinc. Deposition time = 120 seconds.
Magnification: 1000X.

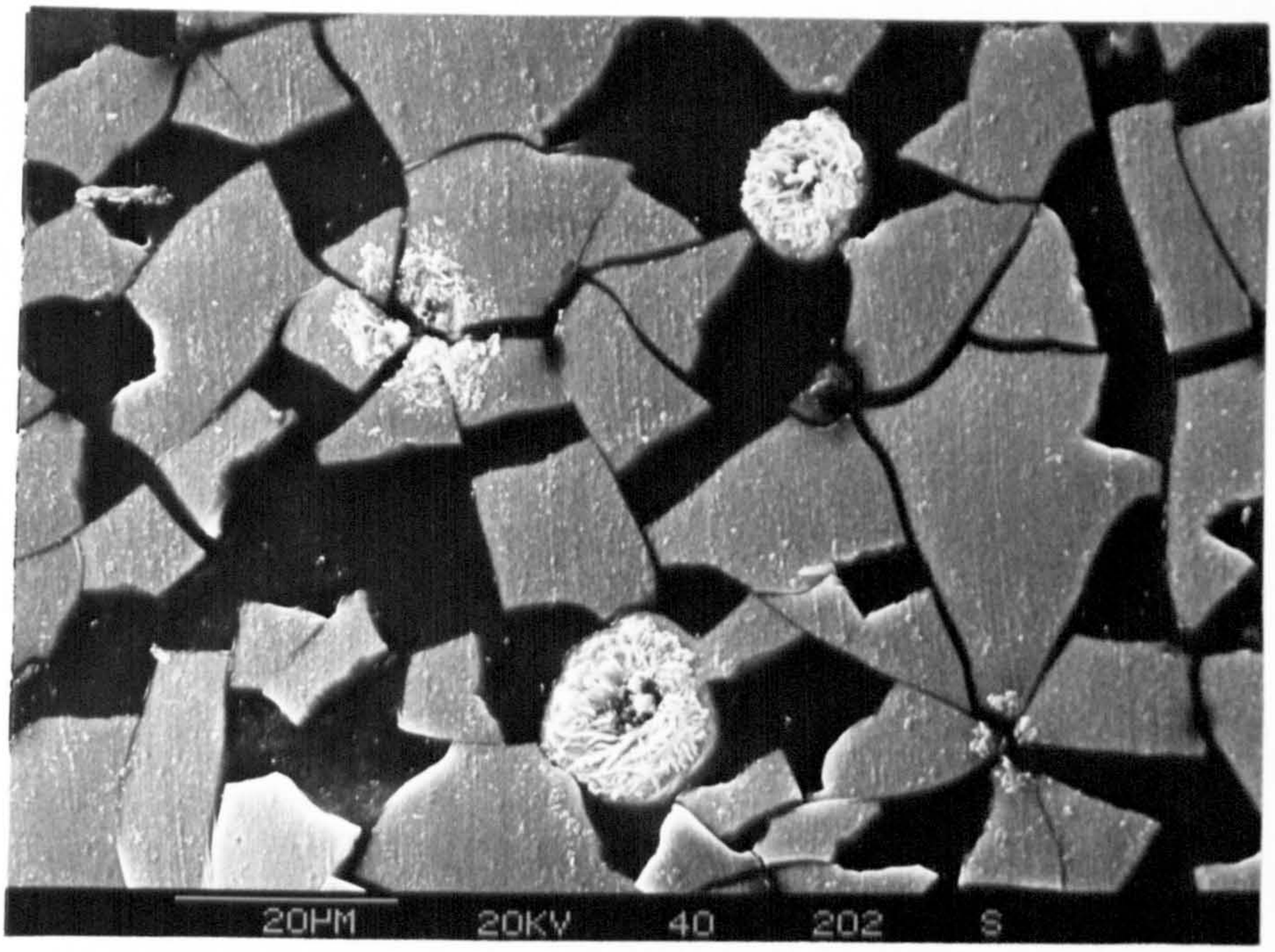

Fig.3.3.30 Underneath surface of the Mo-black dip coating on zinc showing smooth interface of the fragments.
Magnification: 1000X.

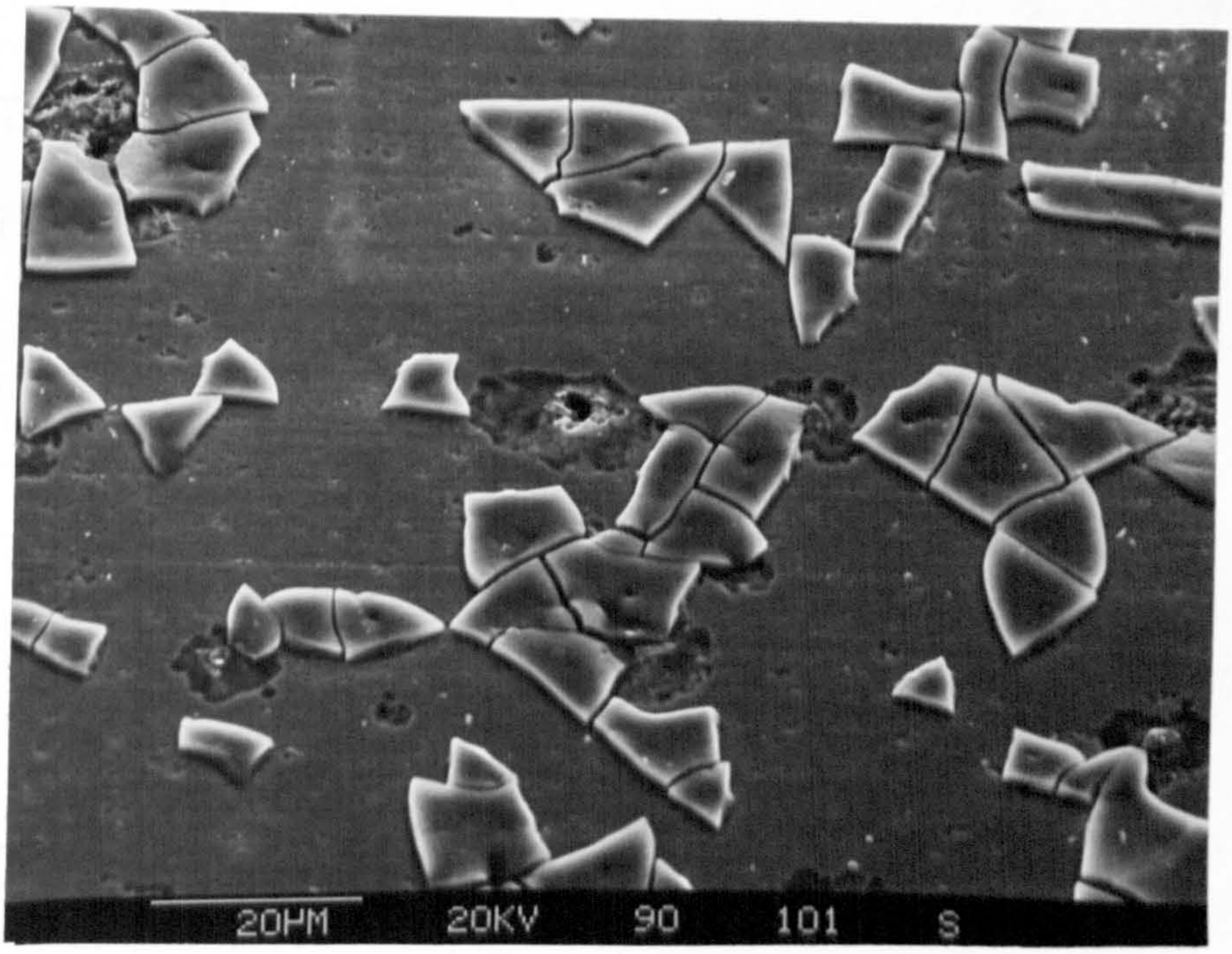

Fig.3.2.31 S.E.M. micrograph of a Mo-black coating on zinc after peeling some fragments with adhesive tape showing some damaged area on the substrate.
Magnification: 1000X.

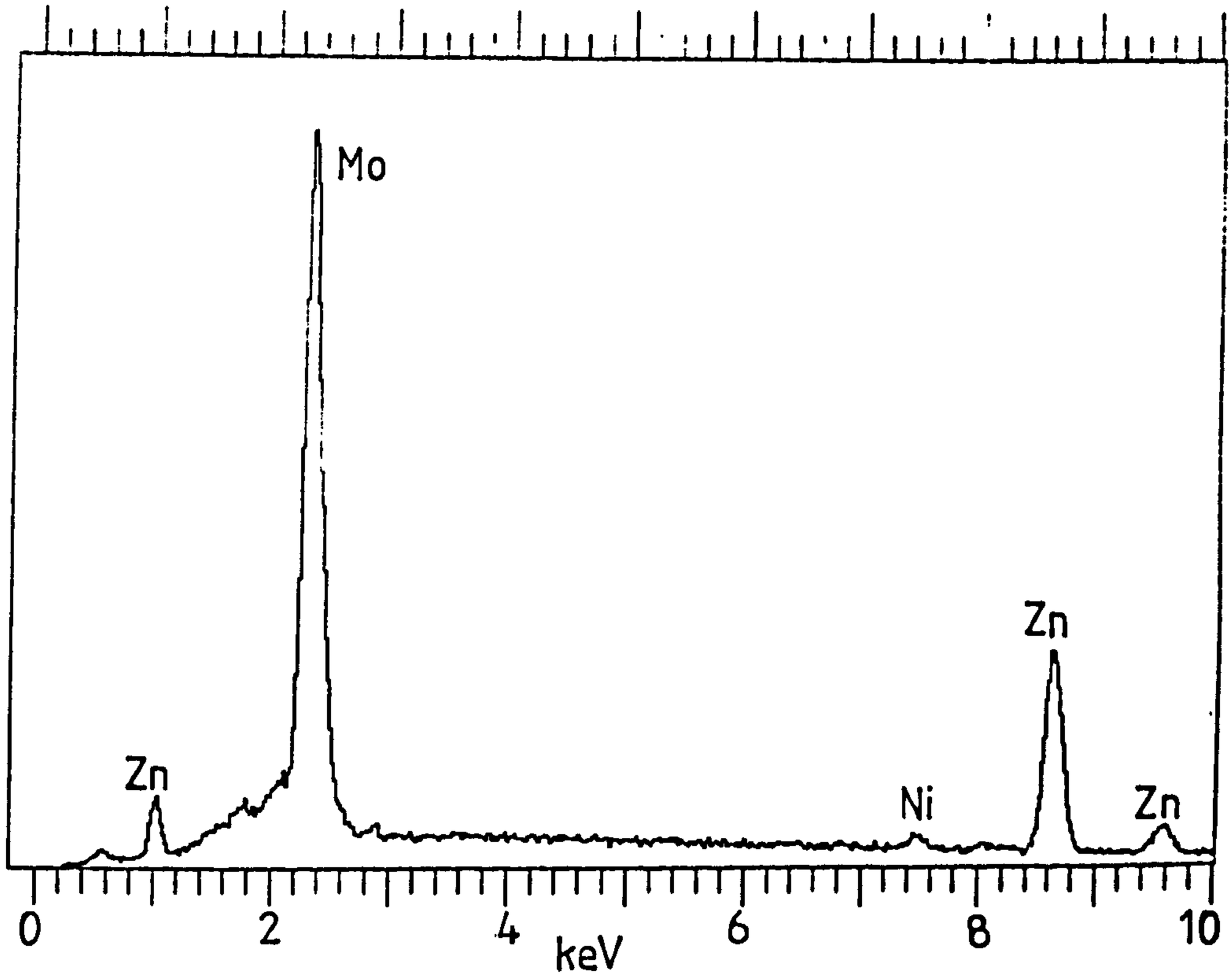

Fig.3.2.32 EDX spectrum of a Mo-black dip coating on mechanically polished zinc substrate.

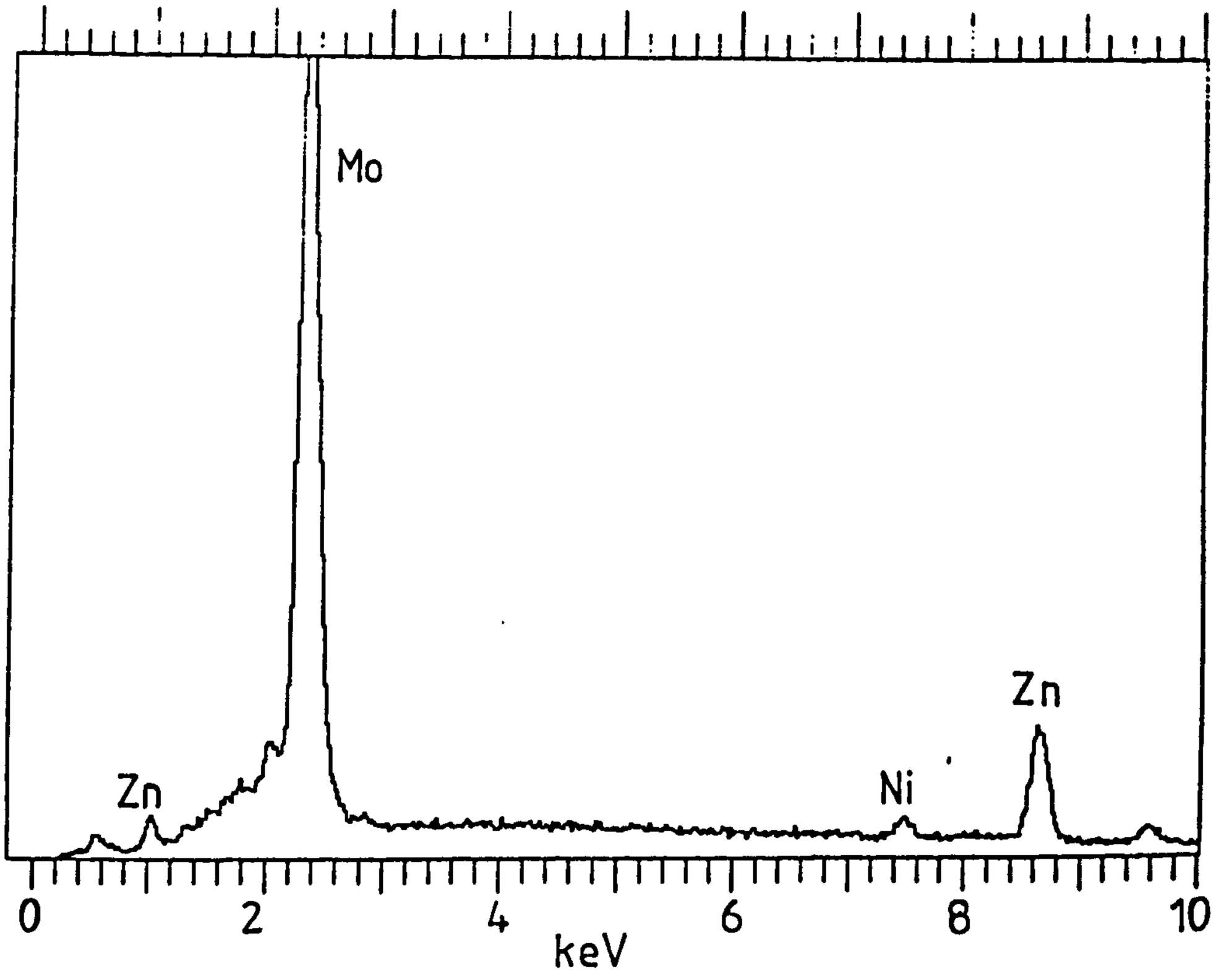

Fig.3.2.33 EDX spectrum from the underneath surface of Mo-black dip coating on zinc substrate.

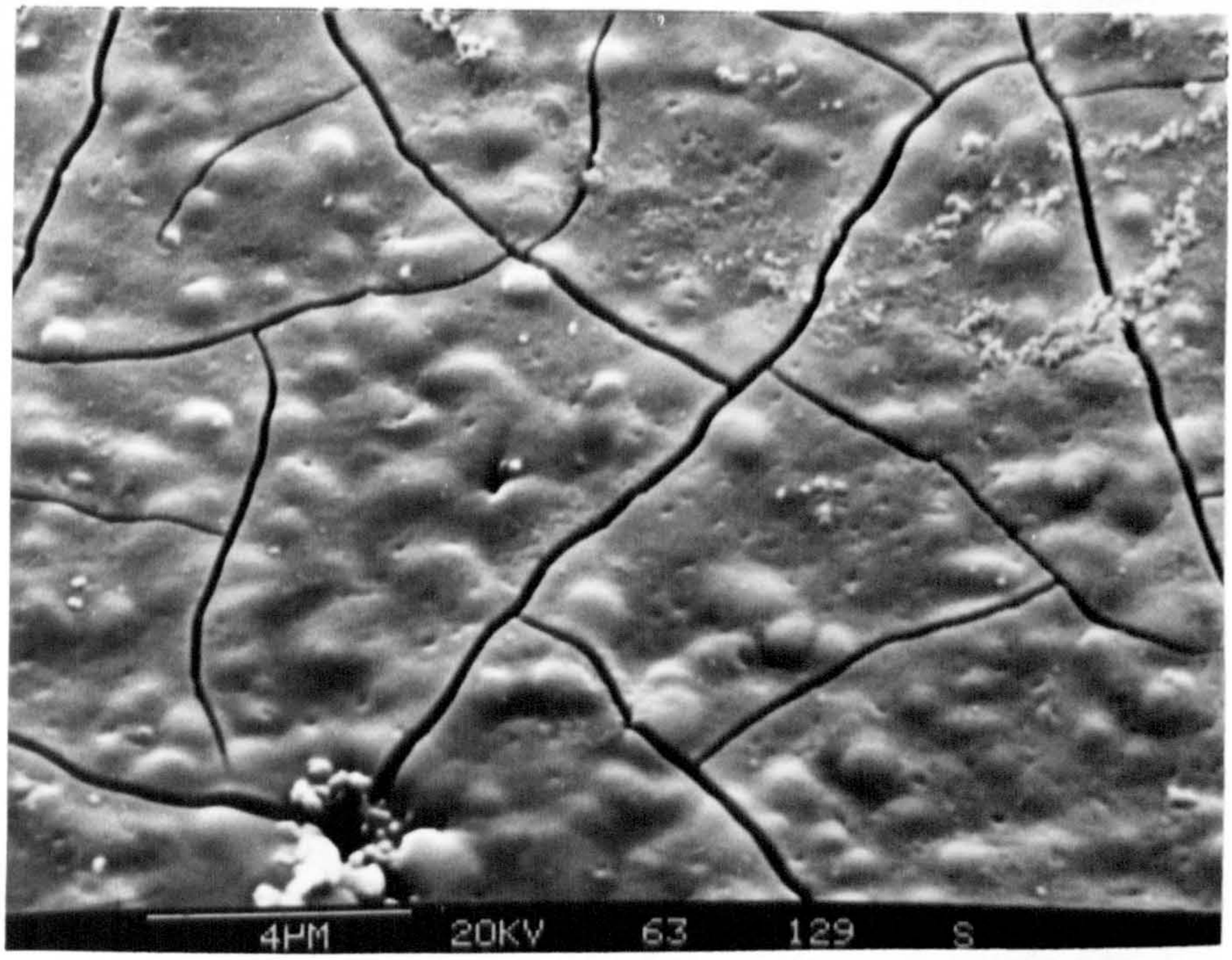

Fig.3.2.34 S.E.M. micrograph of a Mo-black dip coating on an etched zinc substrate (5% HNO_3). Magnification: 6000X.

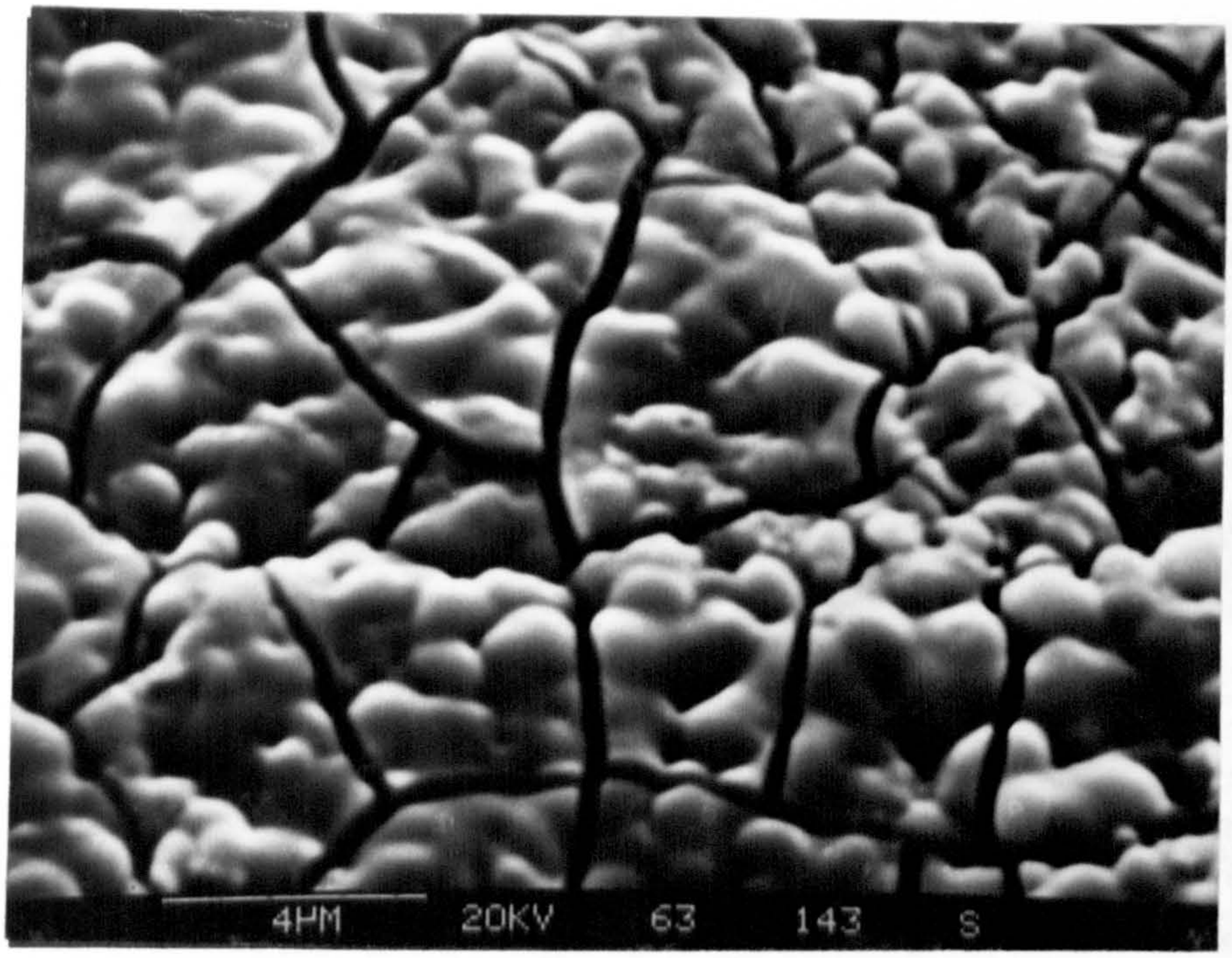

Fig.3.2.35 S.E.M. micrograph of a Mo-black dip coating on etched zinc substrate (10%HNO_3). Magnification: 6000X.

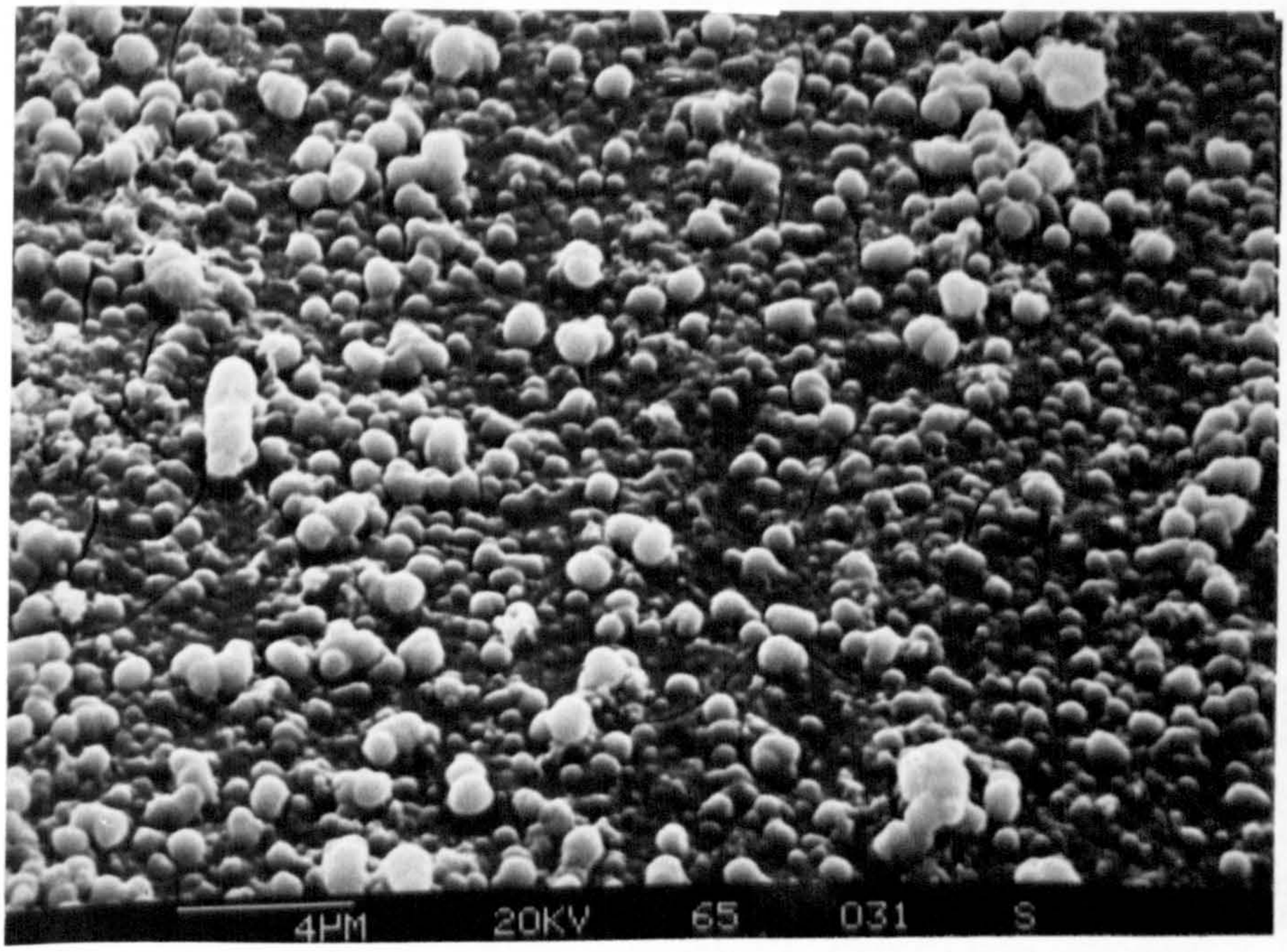

Fig.3.2.36 S.E.M. micrograph of a Mo-black dip coating on an etched zinc substrate (20% HNO_3, 5 seconds etching). Magnification: 4000X.

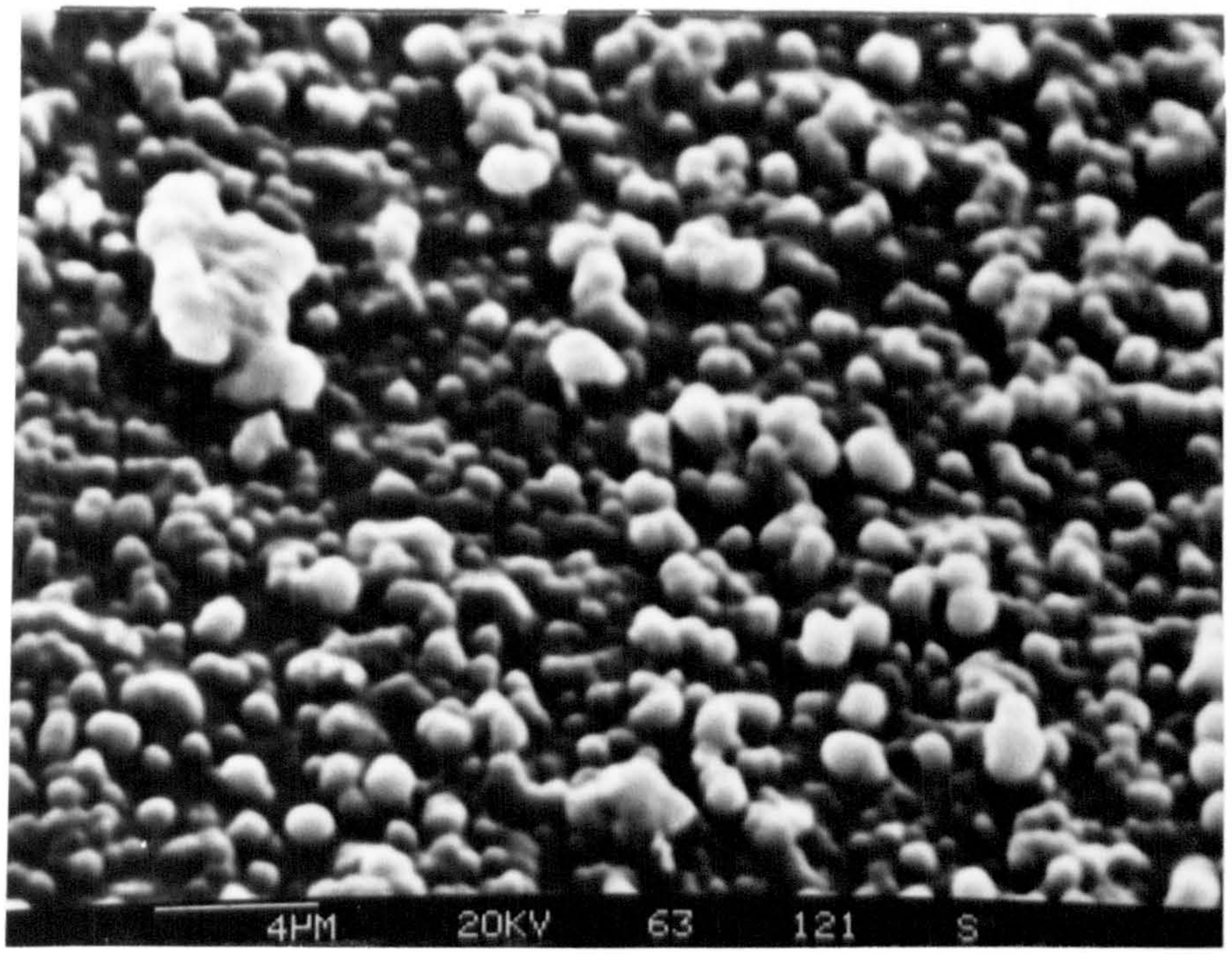

Fig.3.2.37 S.E.M. micrograph of a Mo-black dip coating on an etched zinc substrate. (20%HNO_3, 10 seconds etching time). Magnification: 4000X.

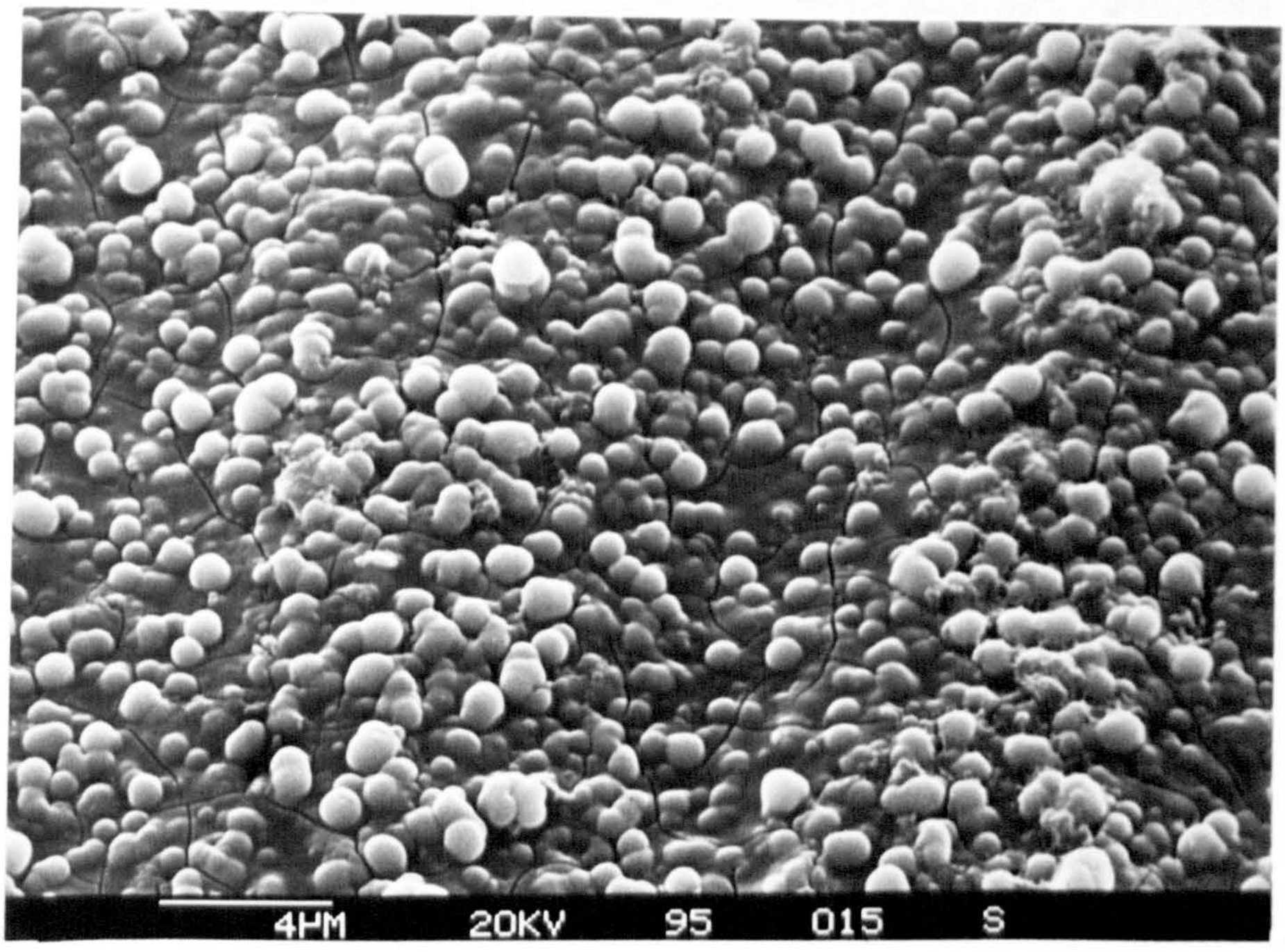

Fig.3.2.38 S.E.M. micrograph of a Mo-black dip cotaing on an etched zinc substrate. (30%HNO_3, 4 seconds etching time). Magnification: 4000X.

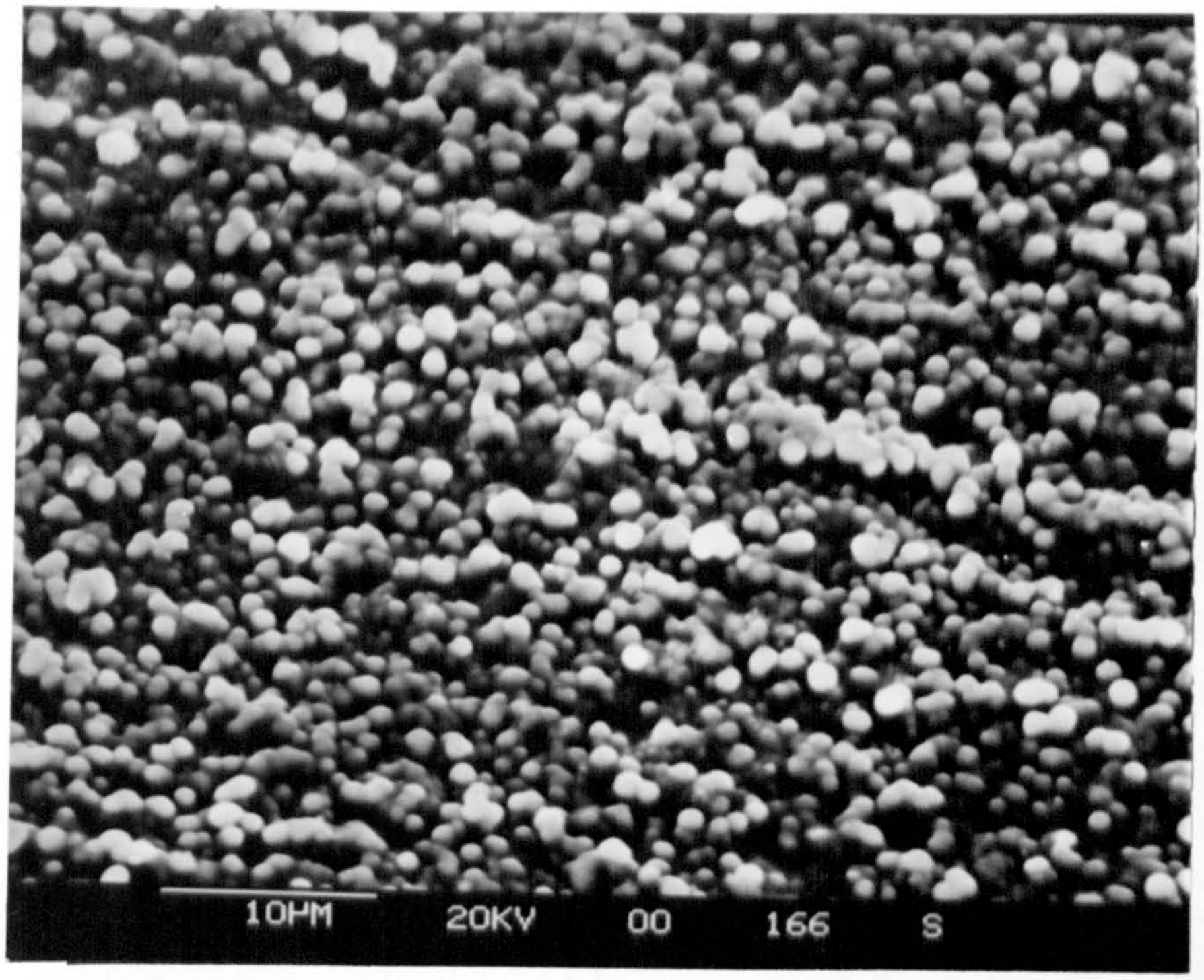

(a)

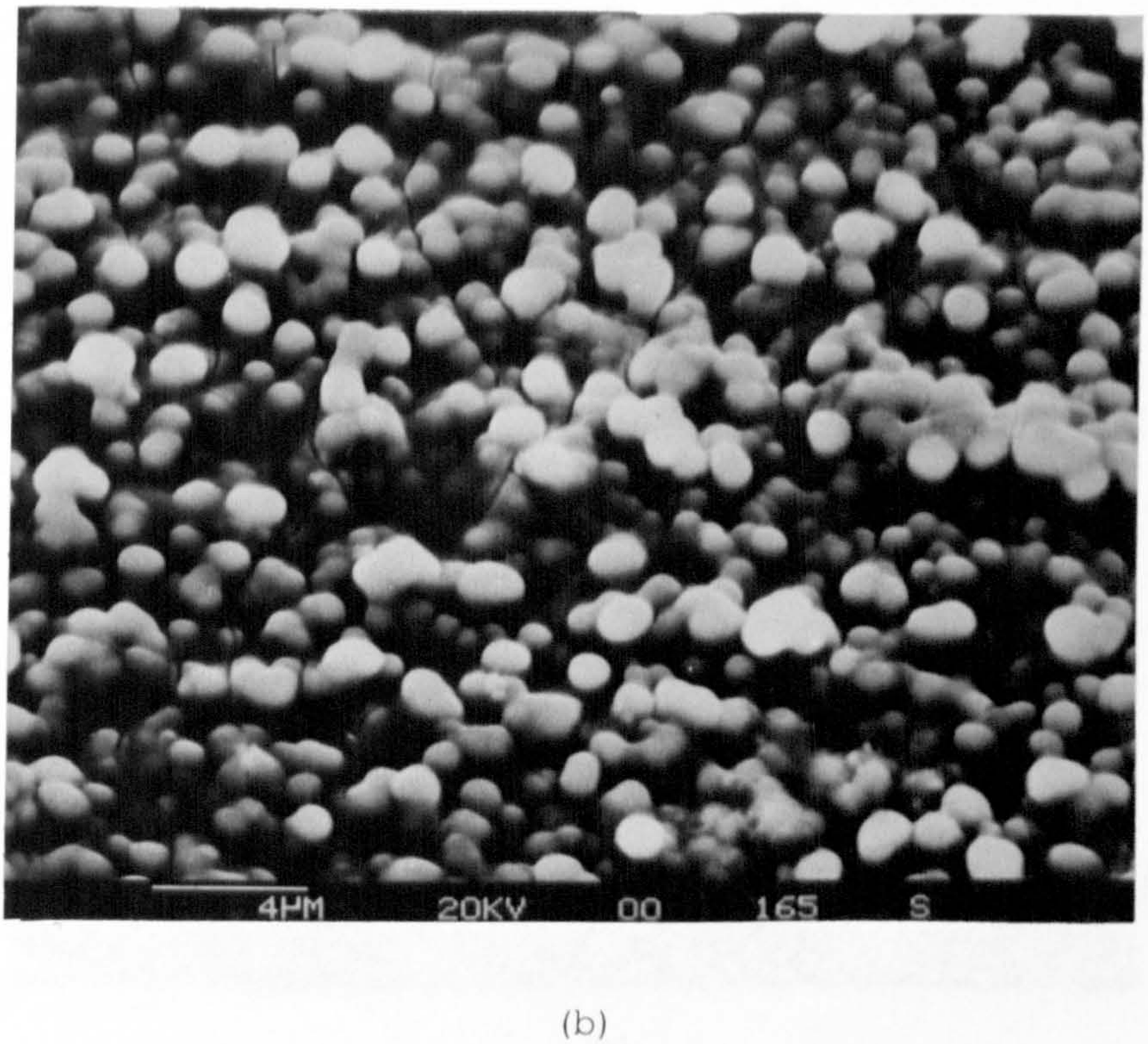

(b)

Fig.3.2.39 S.E.M. micrograph of a Mo-black dip coating on an etched zinc substrate (30%HNO_3, 8 seconds etching time). (a) Magnification: 2000X, (b) Magnification: 4000X.

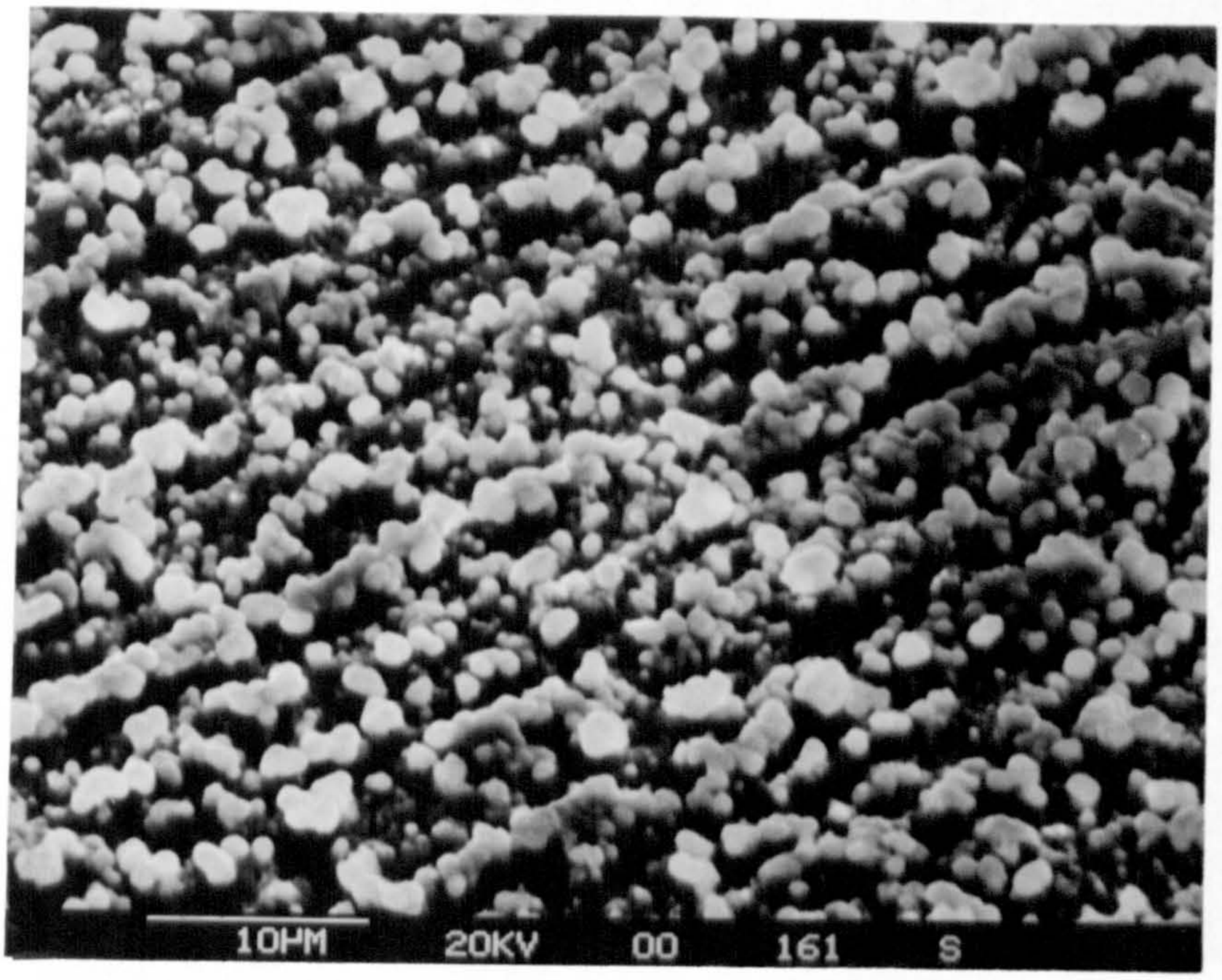

(a)

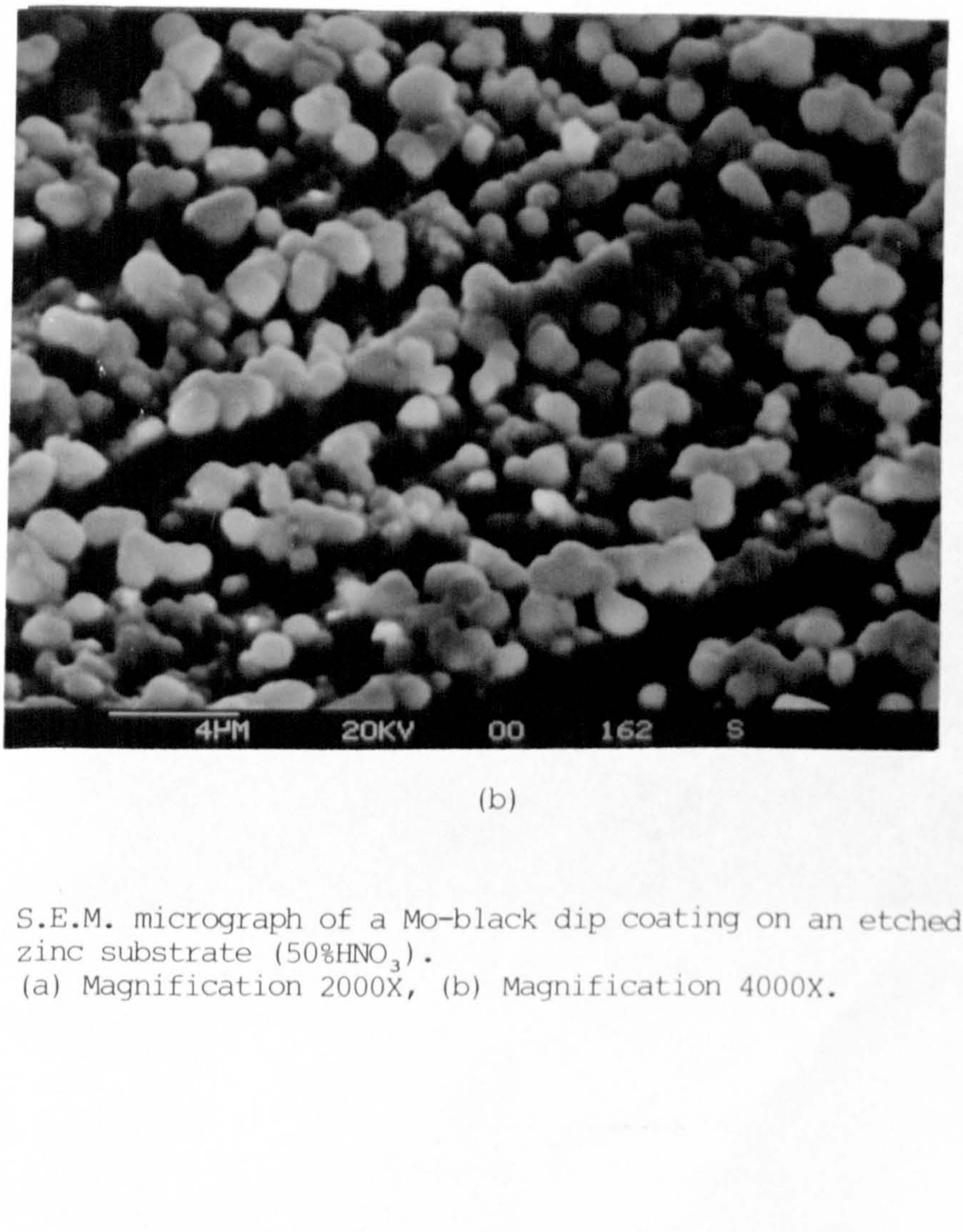

(b)

Fig.3.2.40 S.E.M. micrograph of a Mo-black dip coating on an etched zinc substrate (50%HNO_3).
(a) Magnification 2000X, (b) Magnification 4000X.

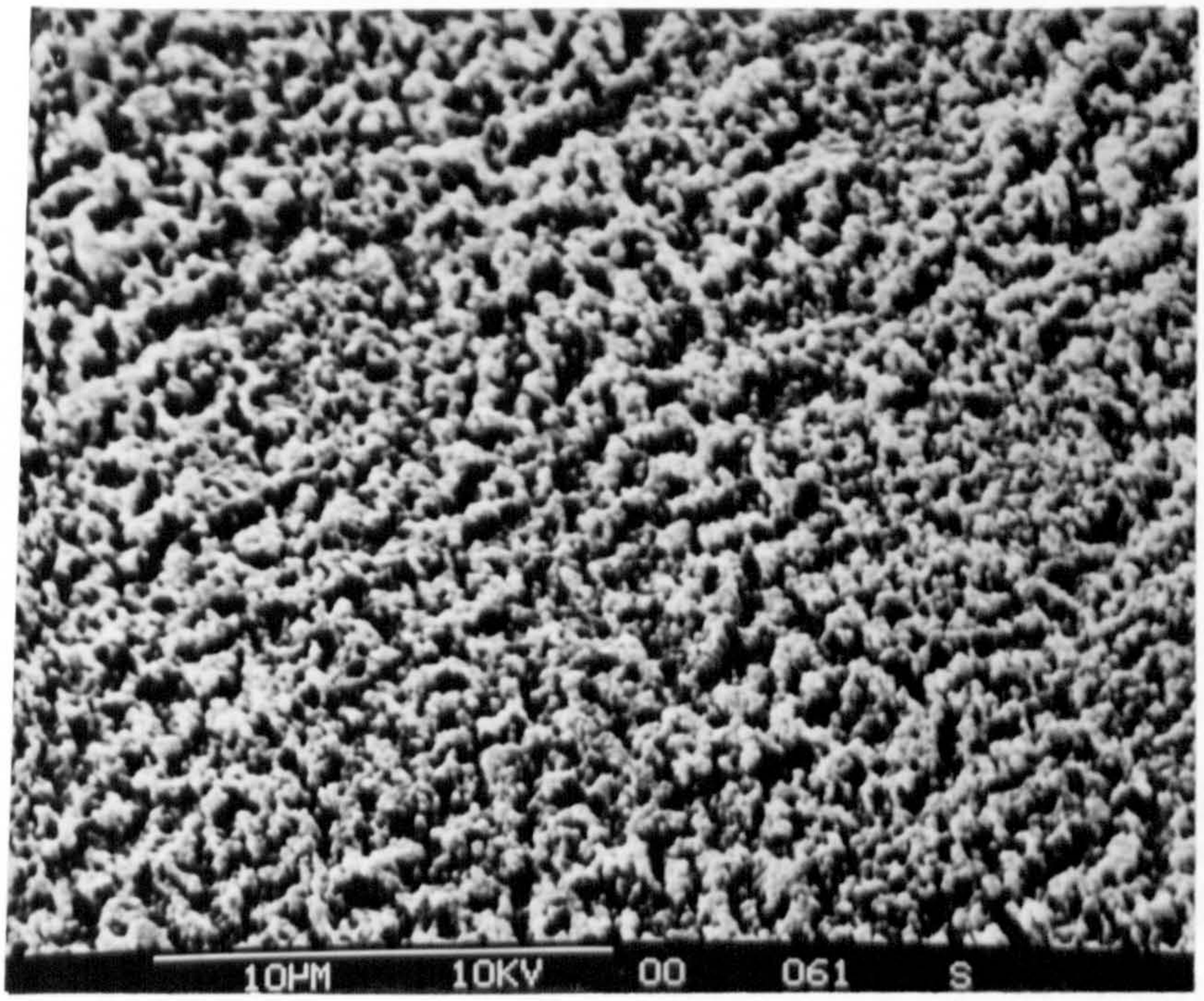

Fig.3.2.41 S.E.M. micrograph of a zinc substrate after etching with 30%HNO_3. Magnification: 4000X.

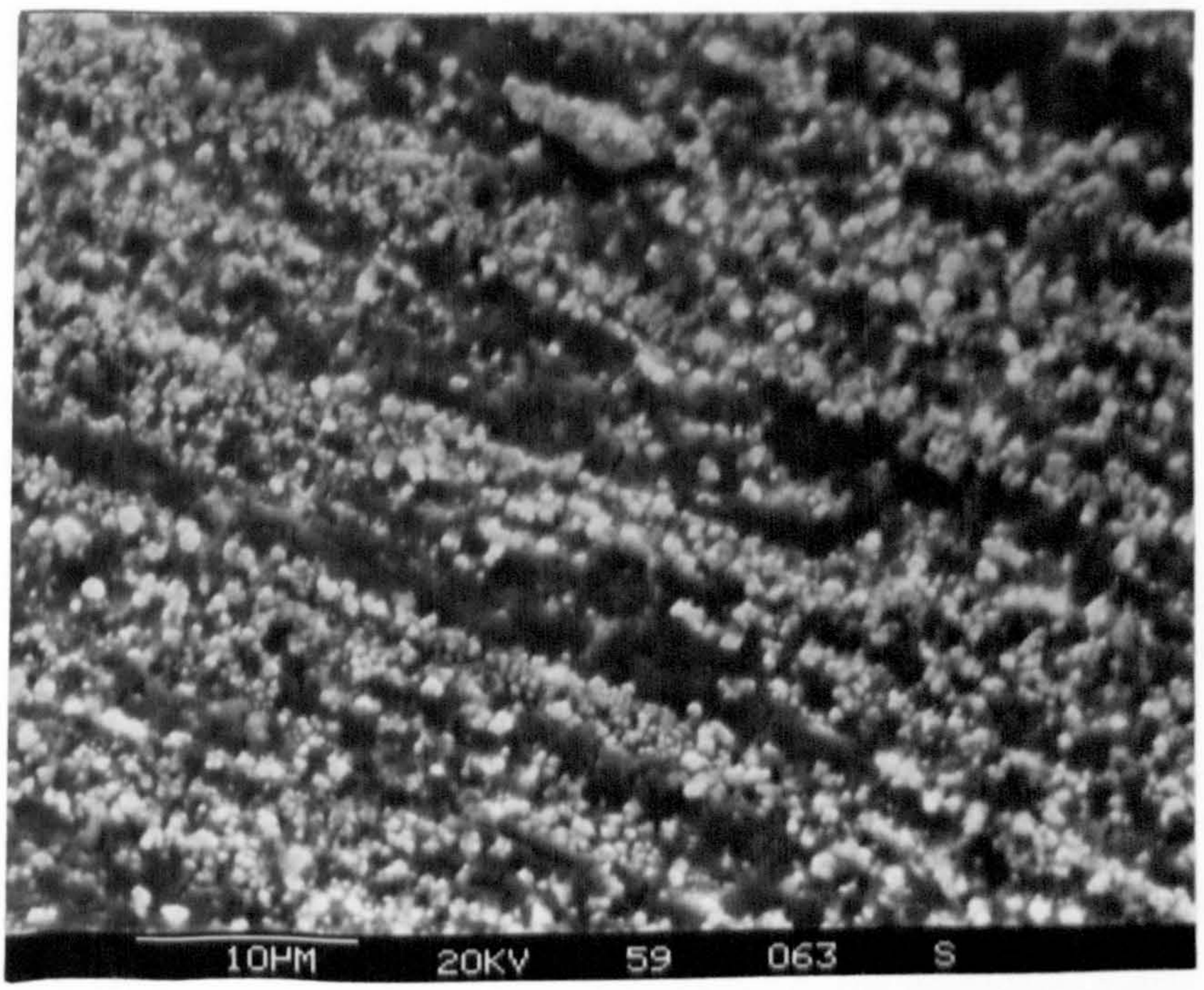

Fig.3.2.42 S.E.M. micrograph of a zinc substrate after etching with a 50%HNO_3. Magnification: 2000X.

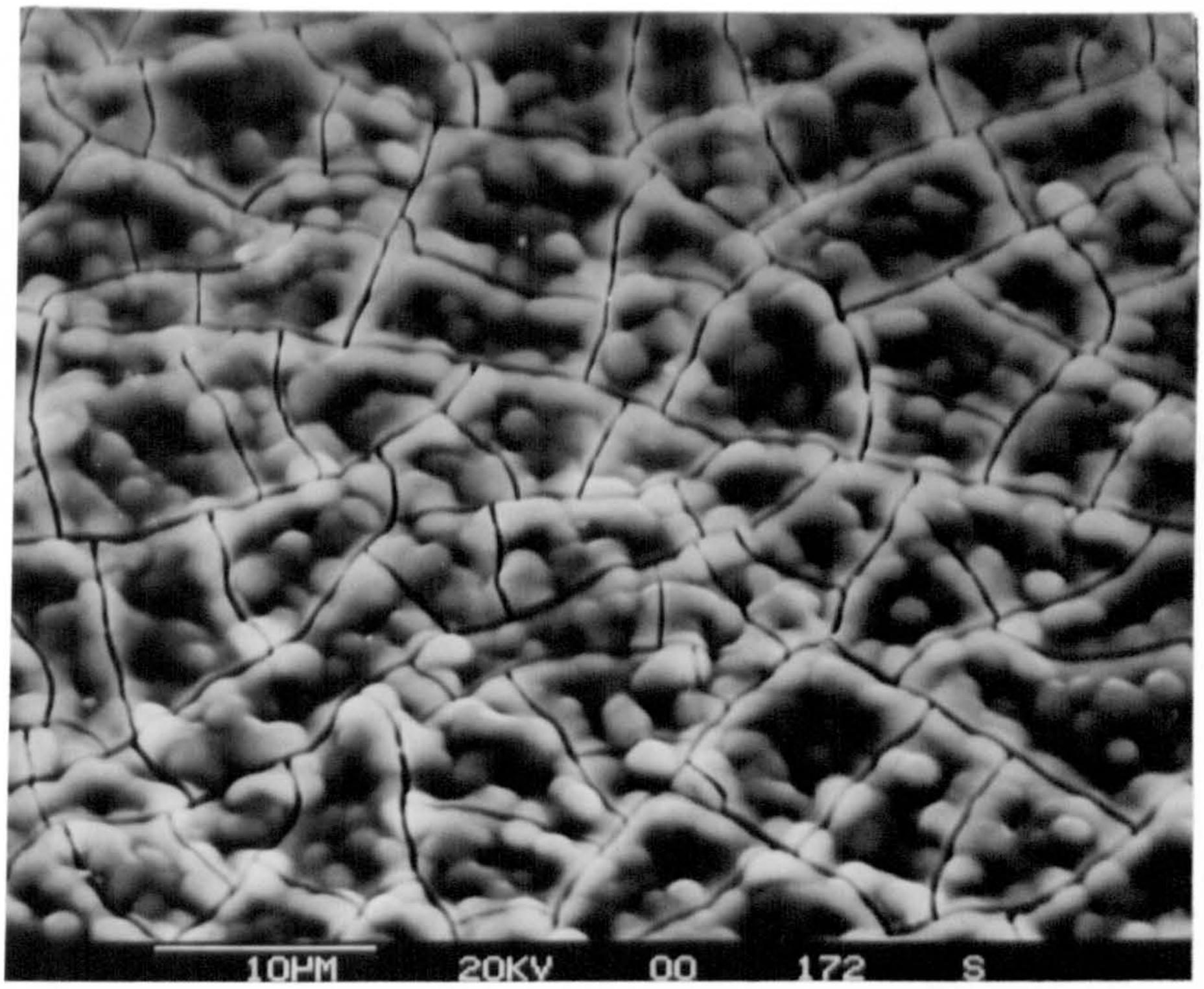

Fig.3.2.43 S.E.M. micrograph of a thick Mo-black coating on etched zinc showing less prominent nodules (deposition time : 2 minutes). Magnification: 2000x.

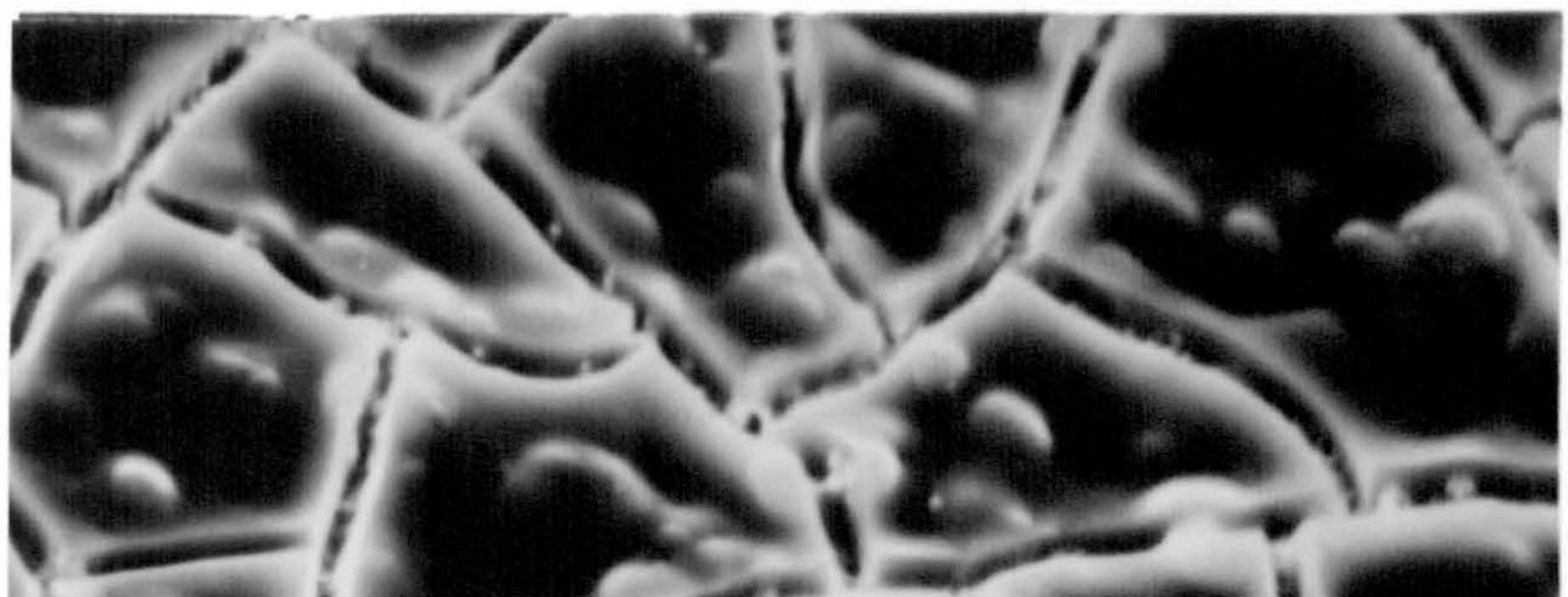

Fig.3.2.44 S.E.M. micrograph of a thick Mo-black coating on etched zinc substrate showing comparatively smooth surface (deposition time = 5 minutes). Magnification: 4000X.

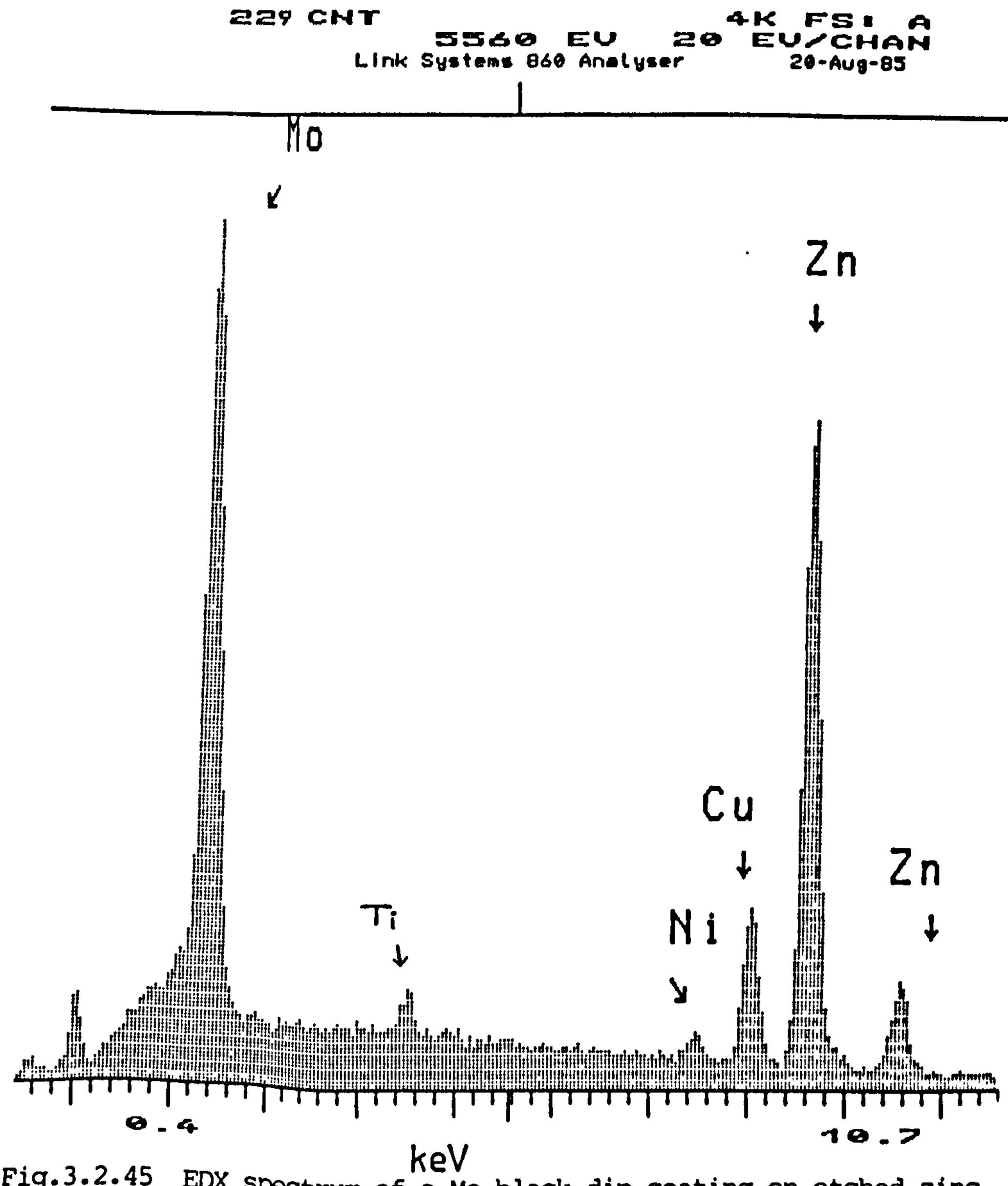

Fig.3.2.45 EDX spectrum of a Mo-black dip coating on etched zinc substrate of coating density~4.5×10^{-5} g/cm².

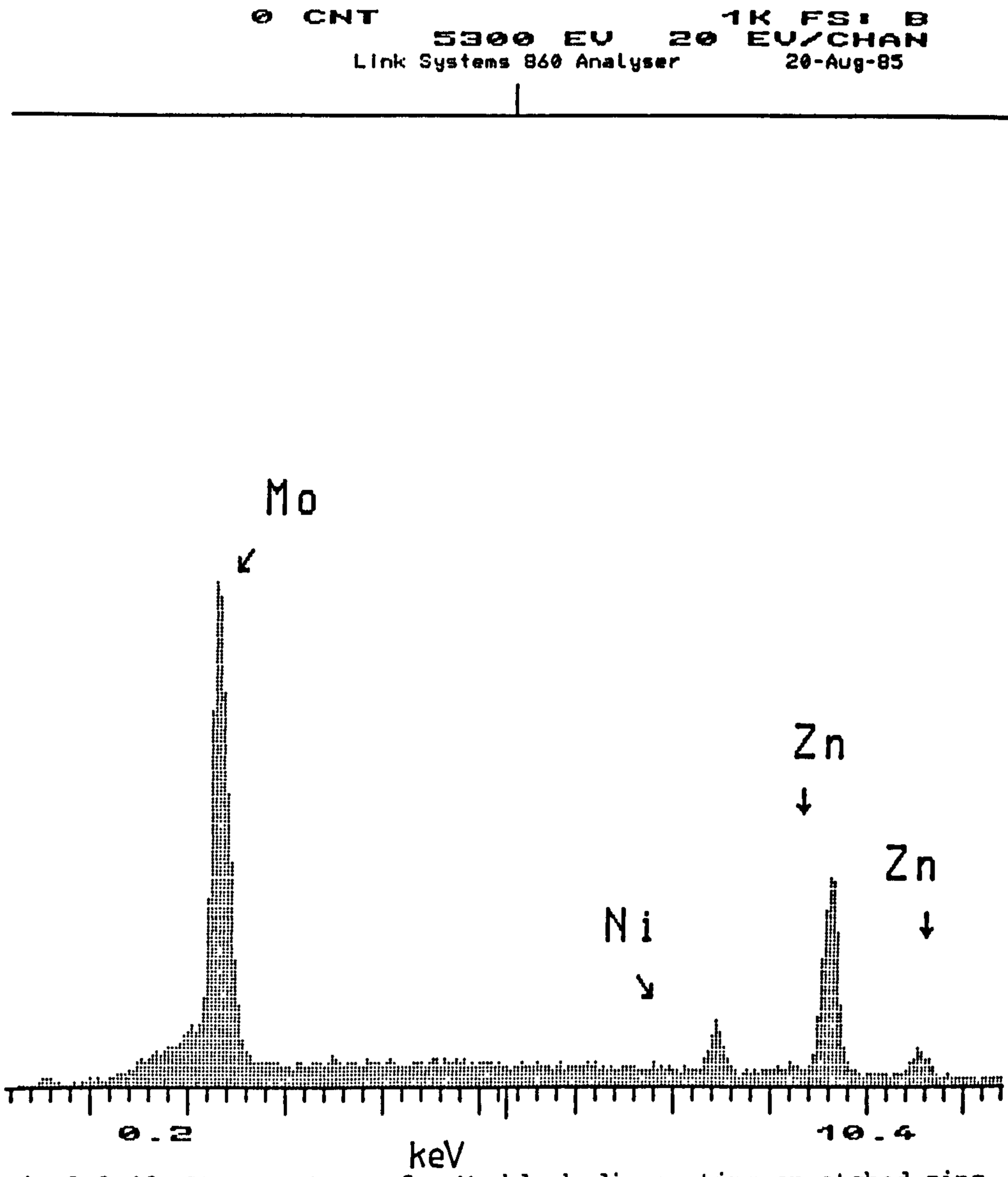

Fig.3.2.46 EDX spectrum of a Mo-black dip coating on etched zinc substrate of coating density~2.01 X 10^{-4} g/cm^2.

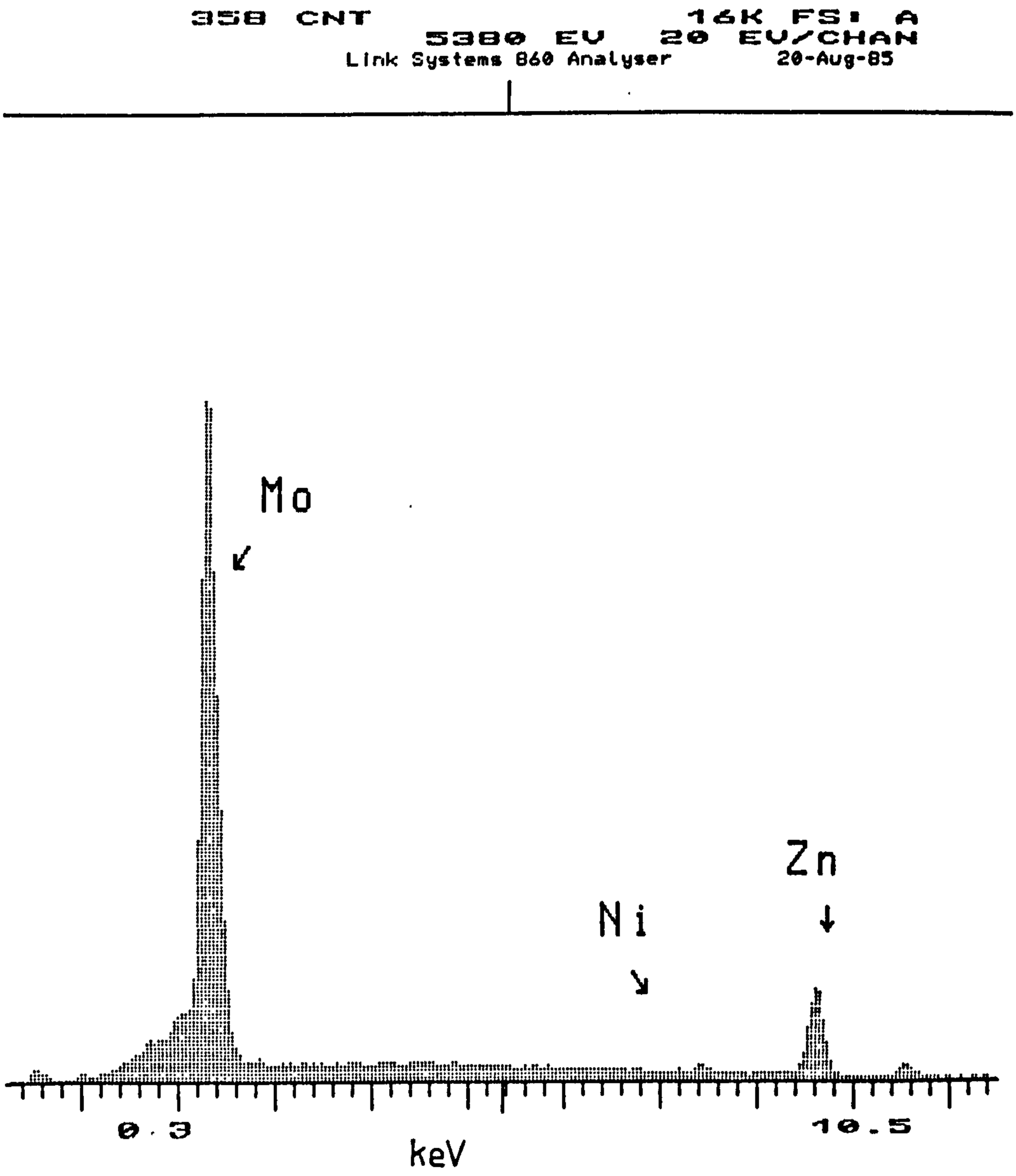

Fig.3.2.47 EDX spectrum of a Mo-black dip coating on etched zinc substrate of coating density~2.9 X 10^{-4} g/cm².

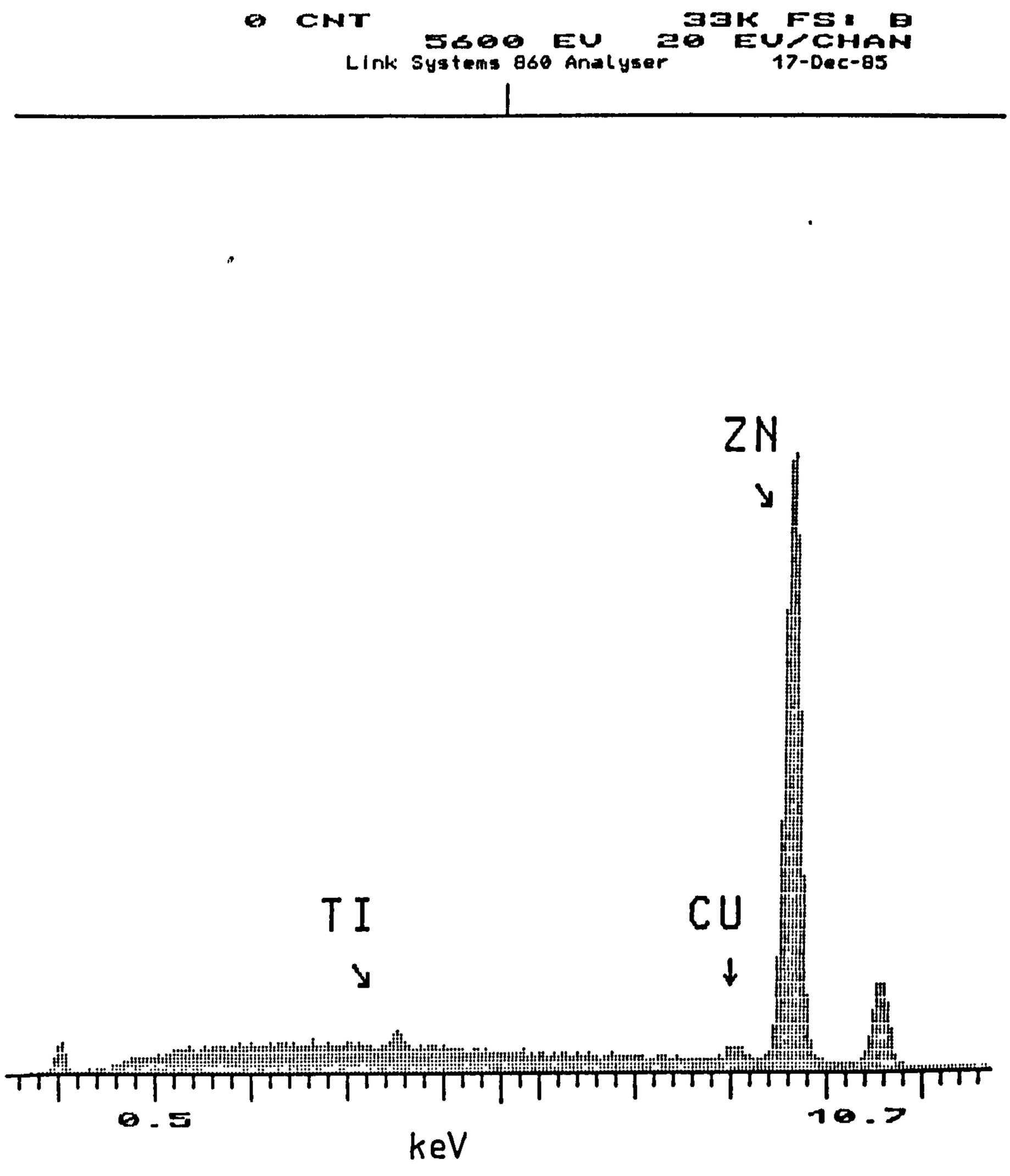

Fig.3.2.48 EDX spectrum of an etched zinc substrate.

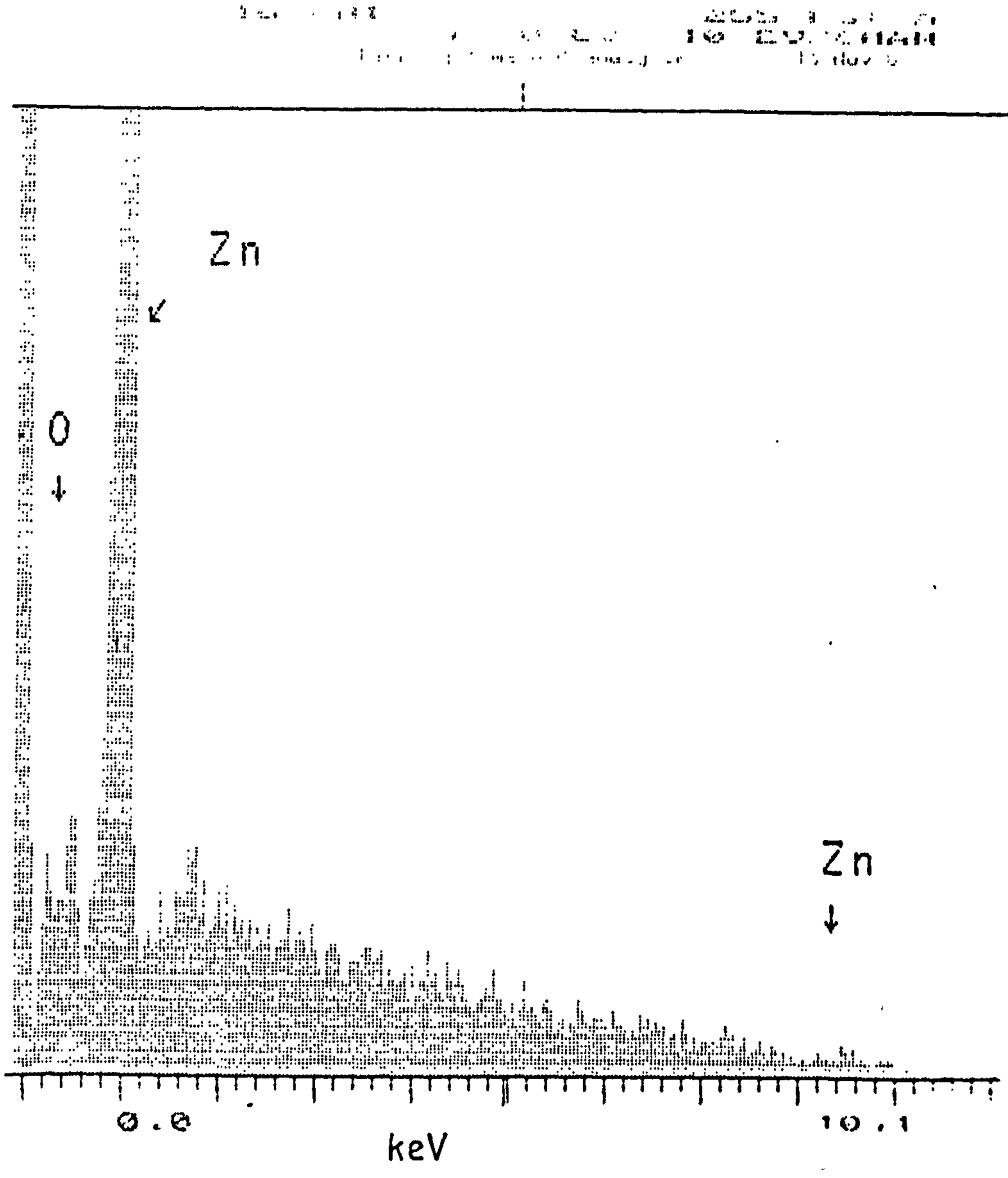

Fig.3.2.49 EDX spectrum of an unetched zinc substrate.

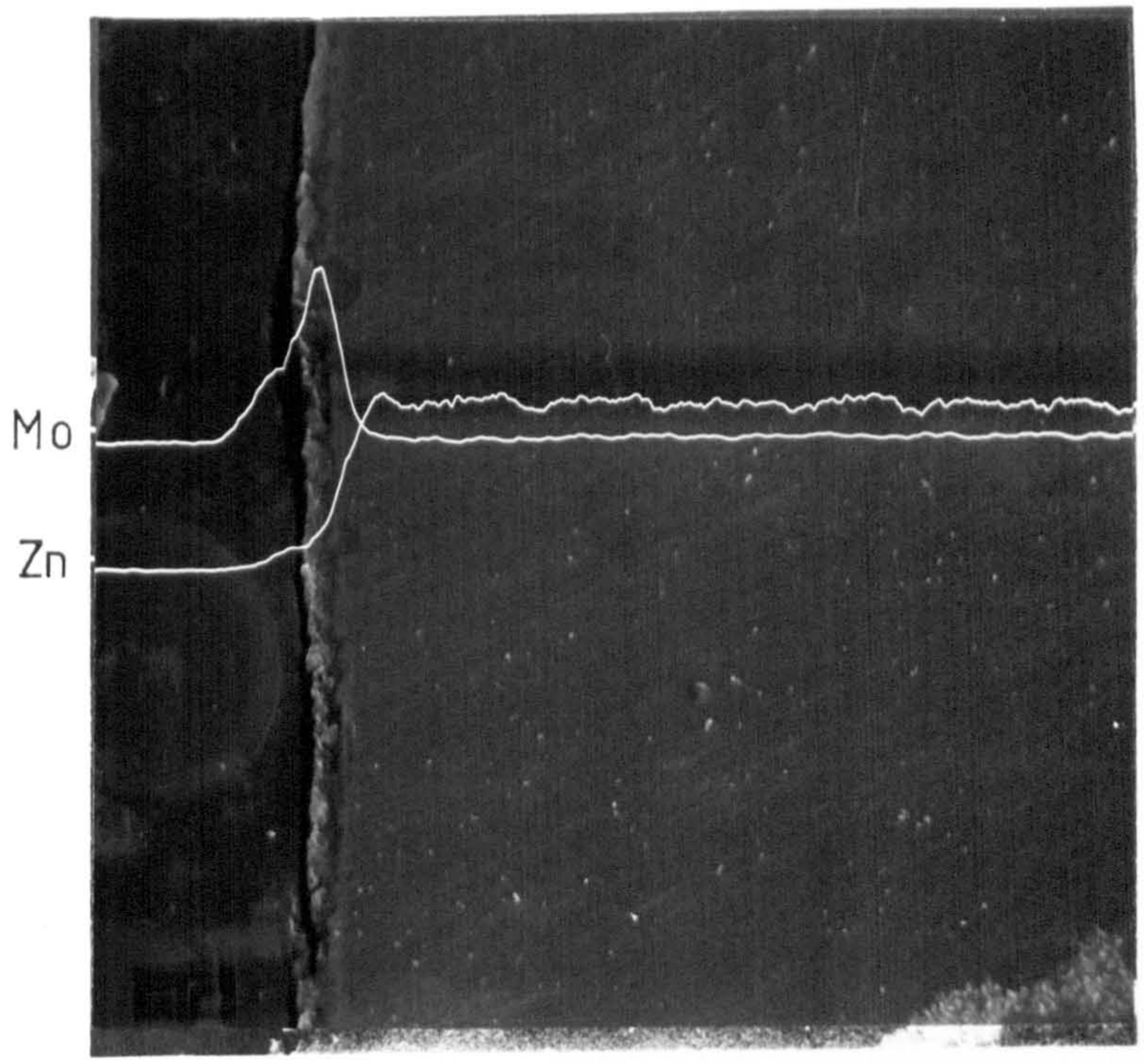

Fig.3.2.50 The Mo and Zn X-ray line scans of the metallographic cross-section of a Mo-black dip coating on etched zinc substrate. Magnification: 1000X.

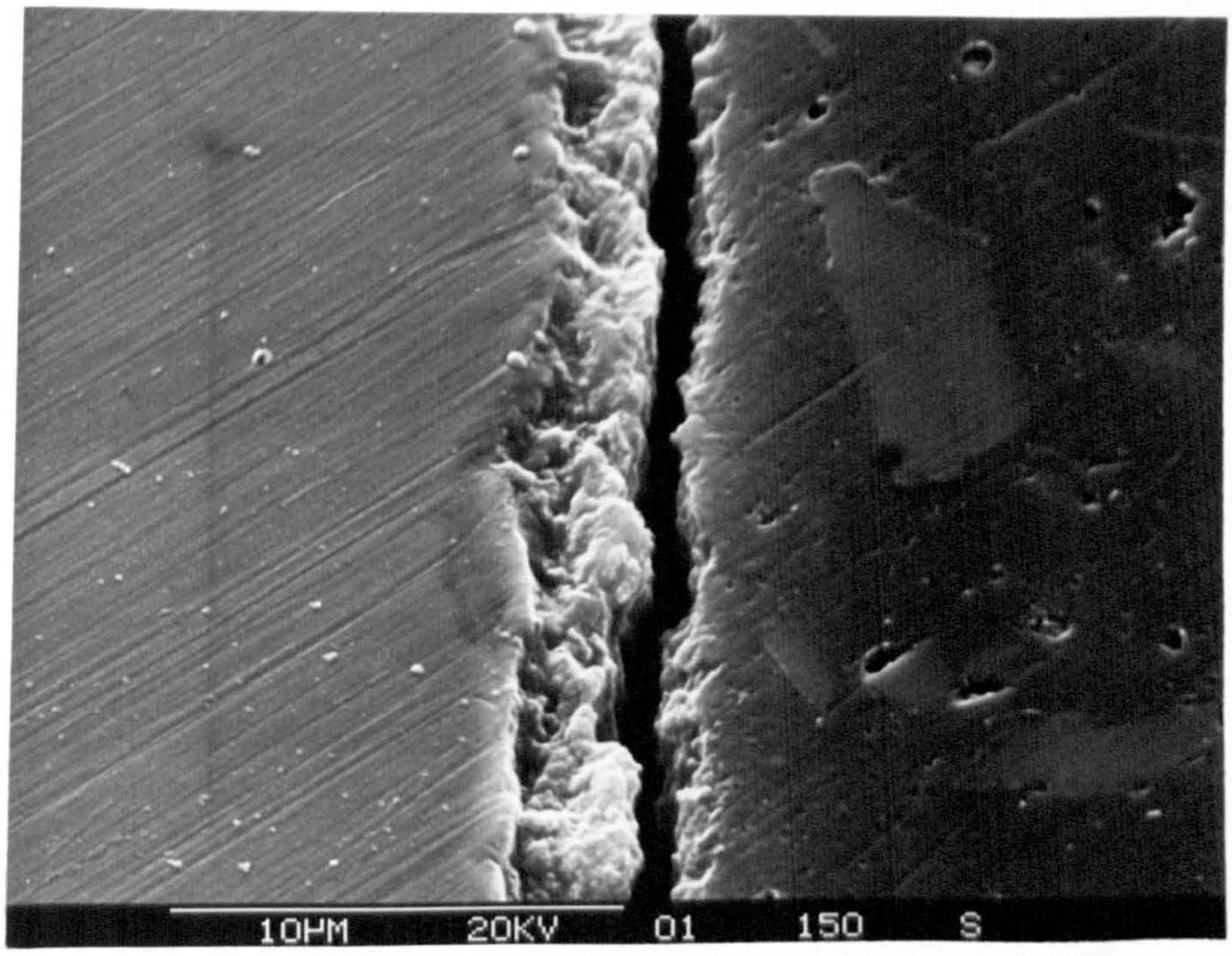

Fig.3.2.51 S.E.M. micrograph of the metallographic section of Fig.3.2.50 at higher magnification. Magnification: 4000X.

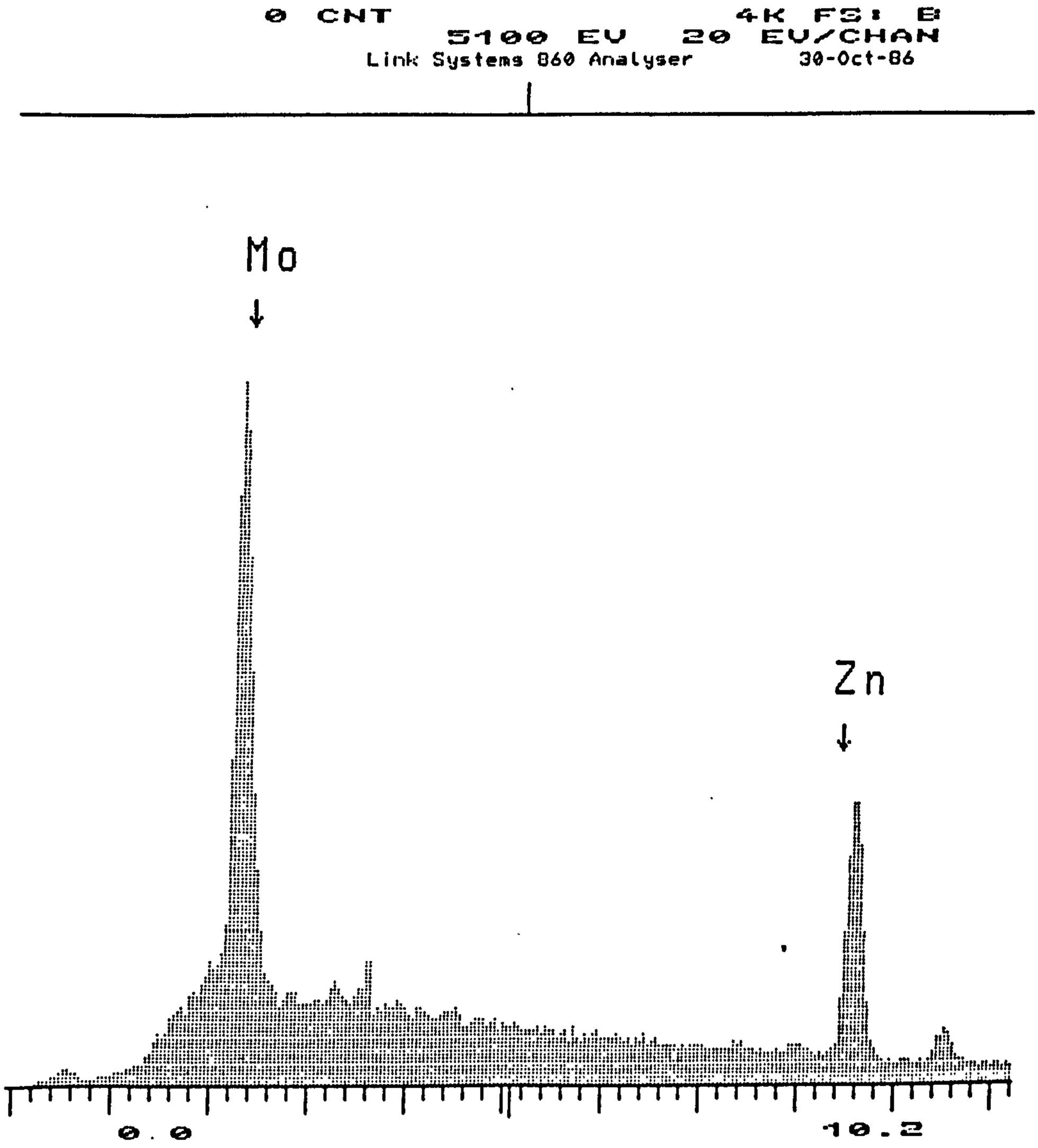

Fig.3.2.52 EDX spectrum obtained from the cross-section of the Mo-black coating of Fig.3.2.51.

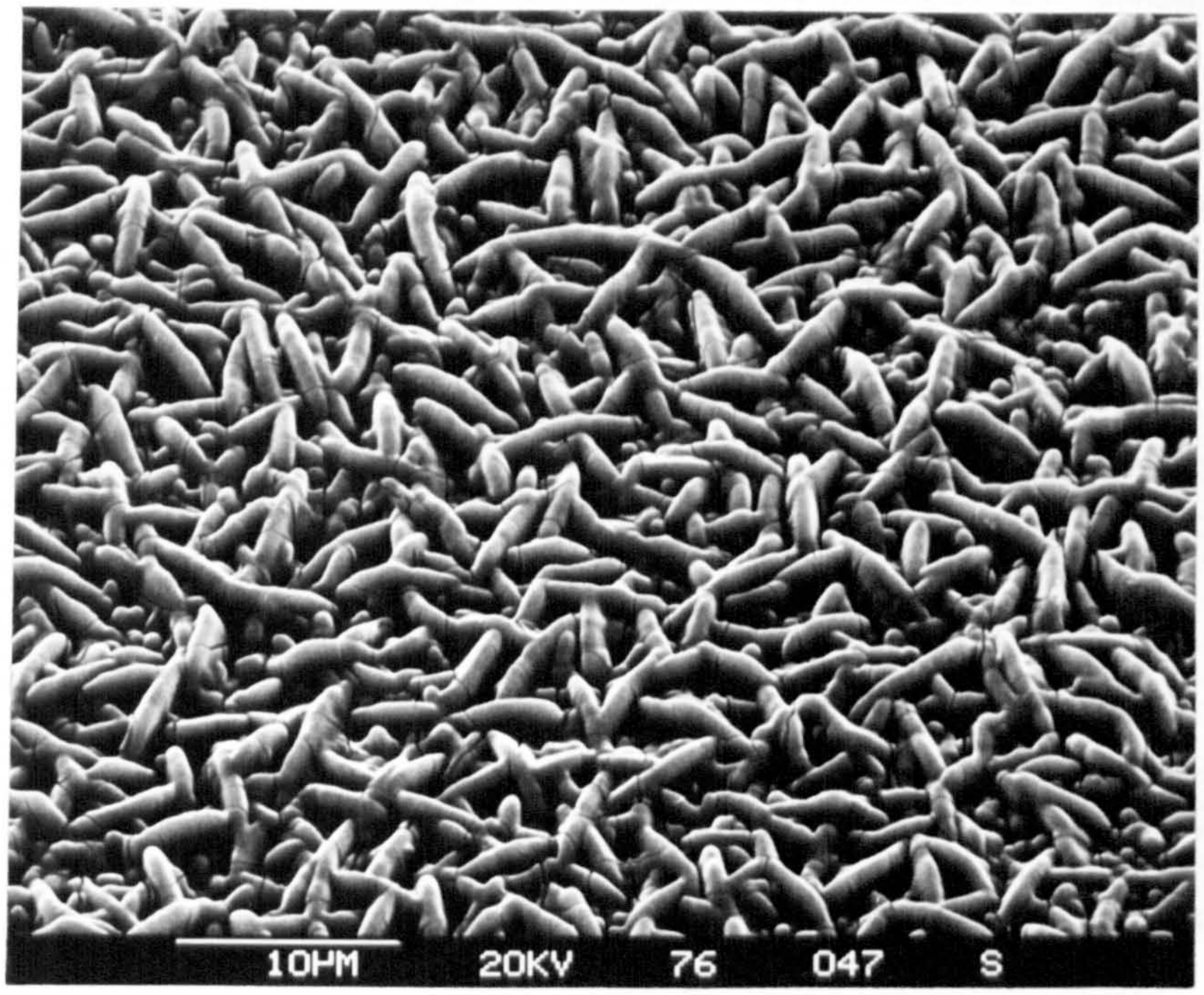

(a)

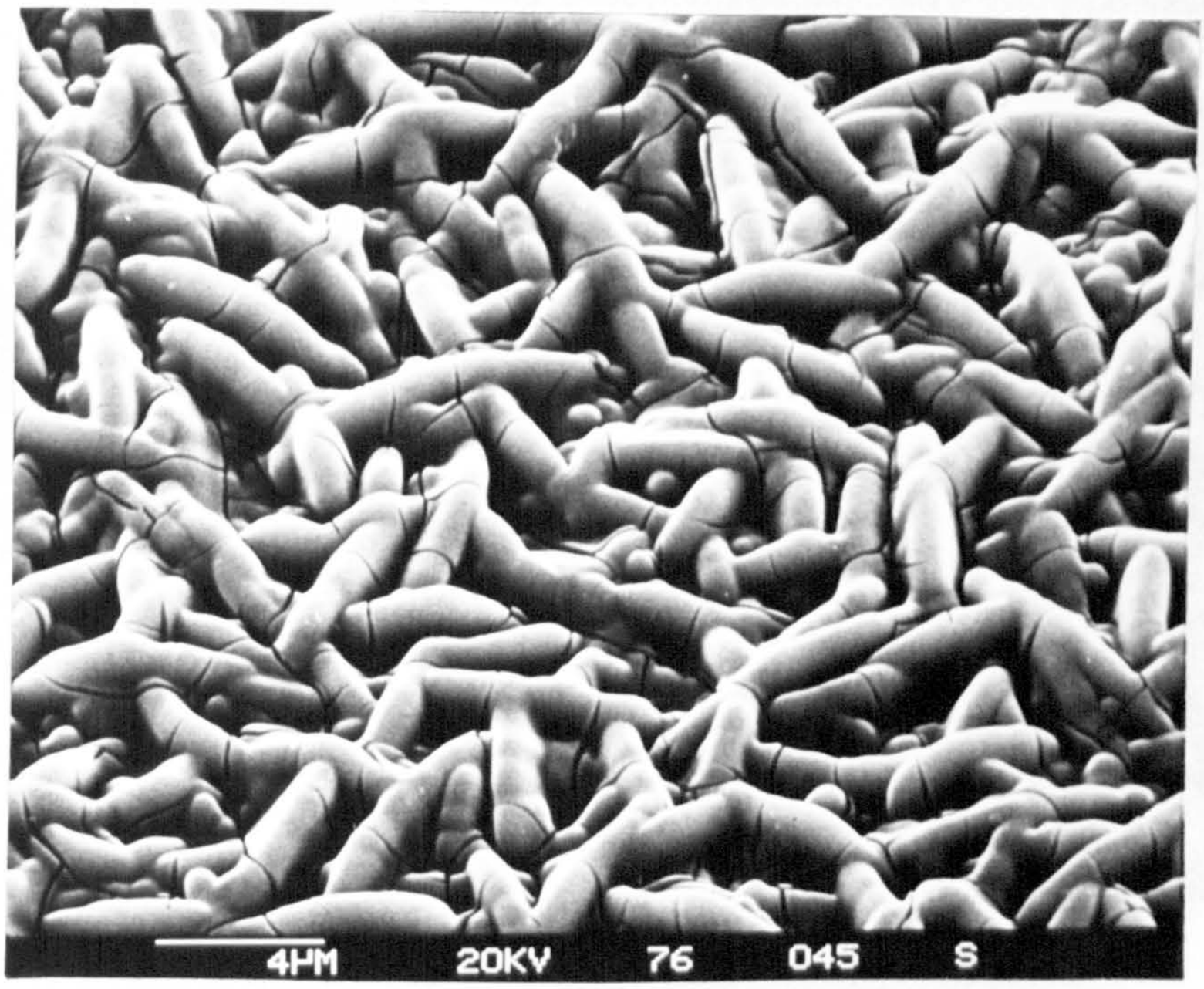

(b)

Fig.3.2.53 S.E.M. micrograph of a Mo-black dip coating on a cobalt (NC) substrate showing a limb-like structure. For this surface $\alpha_s = 0.94$, $\varepsilon_{th} = 0.28$.
(a) Magnification: 2000X, (b) Magnification: 4000X.

(a)

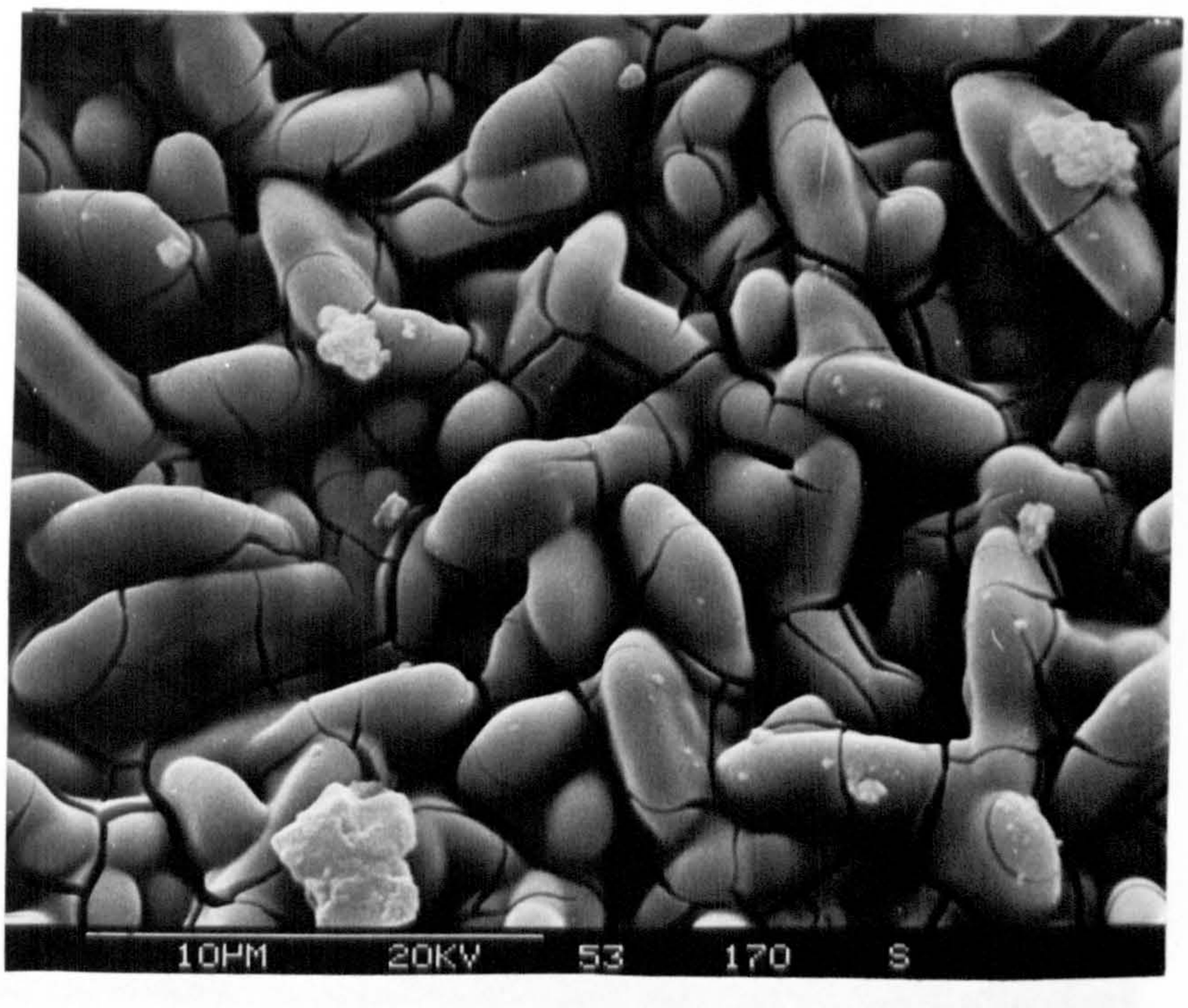

(b)

Fig.3.2.54 S.E.M. micrograph of a Mo-black dip coating on a cobalt (NC) substrate. For this surface $\alpha_s = 0.92$, $\varepsilon_{th} = 0.3$.
(a) Magnification: 2000X, (b) Magnification: 40000X.

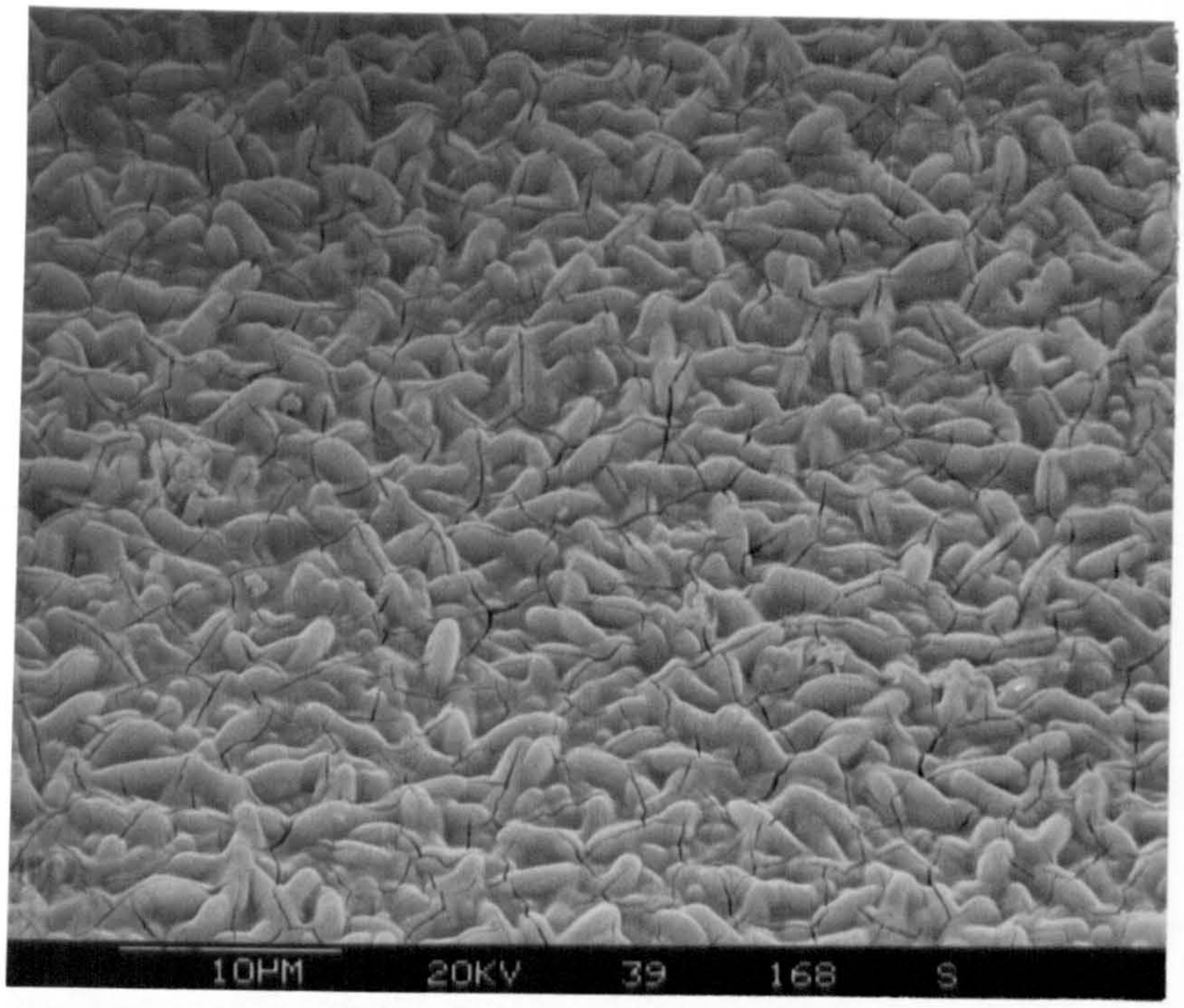

(a)

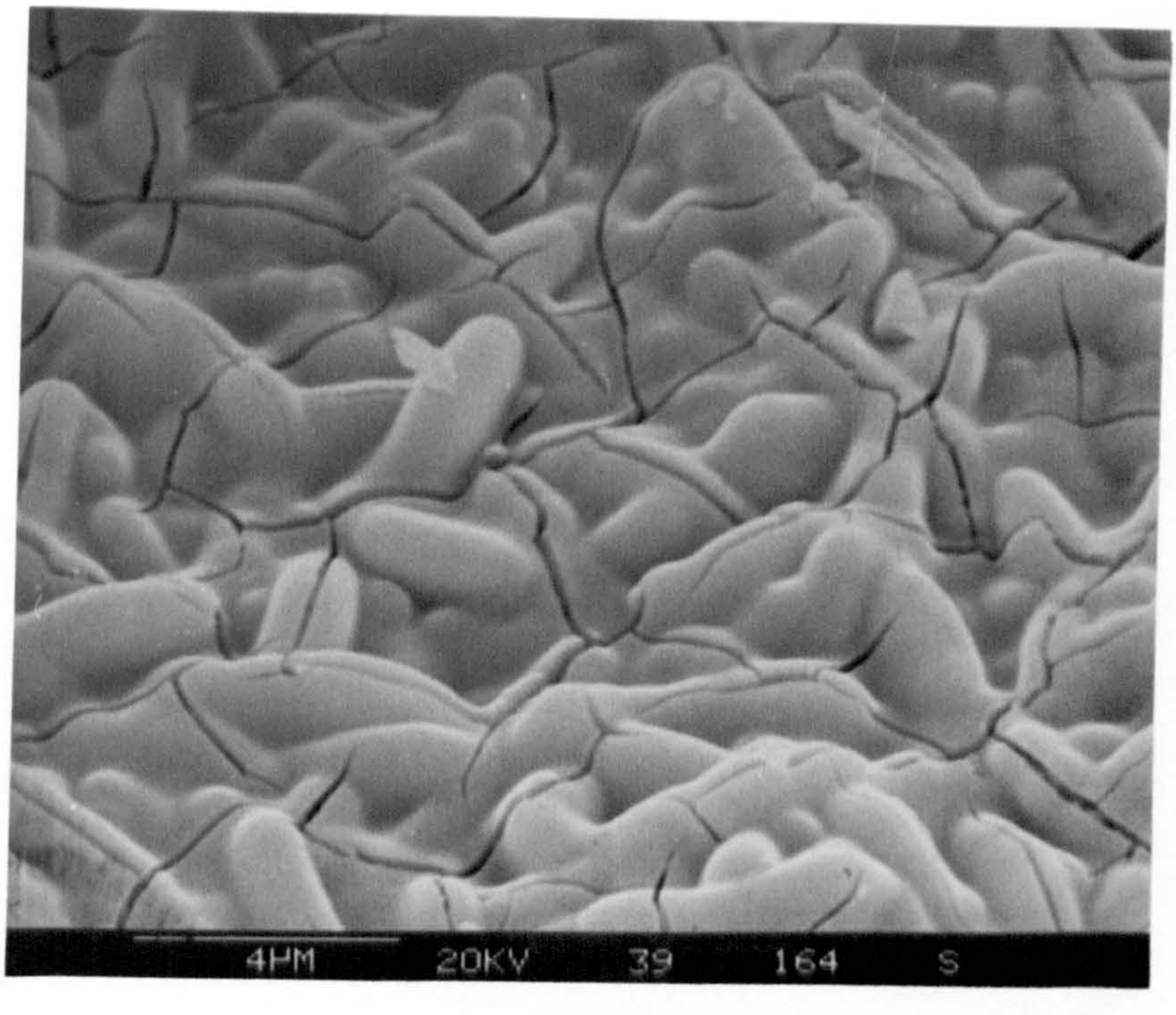

(b)

Fig.3.2.55 S.E.M. micrograph of a Mo-black dip coating on a cobalt (NC) substrate. For this surface $\alpha_s = 0.90$, $\varepsilon_{th} = 0.25$.
(a) Magnification: 2000X, (b) Magnfication: 4000X.

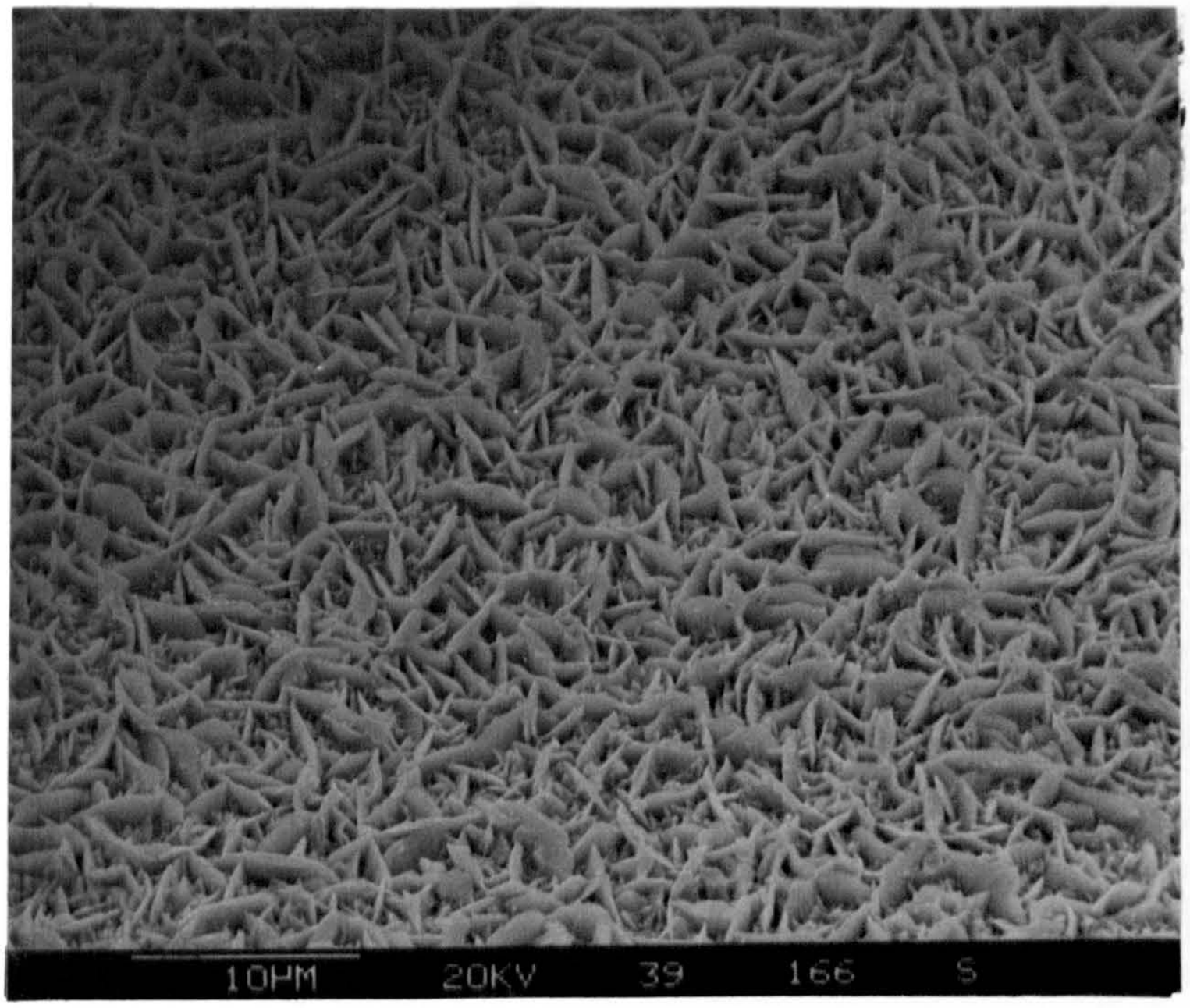

(a)

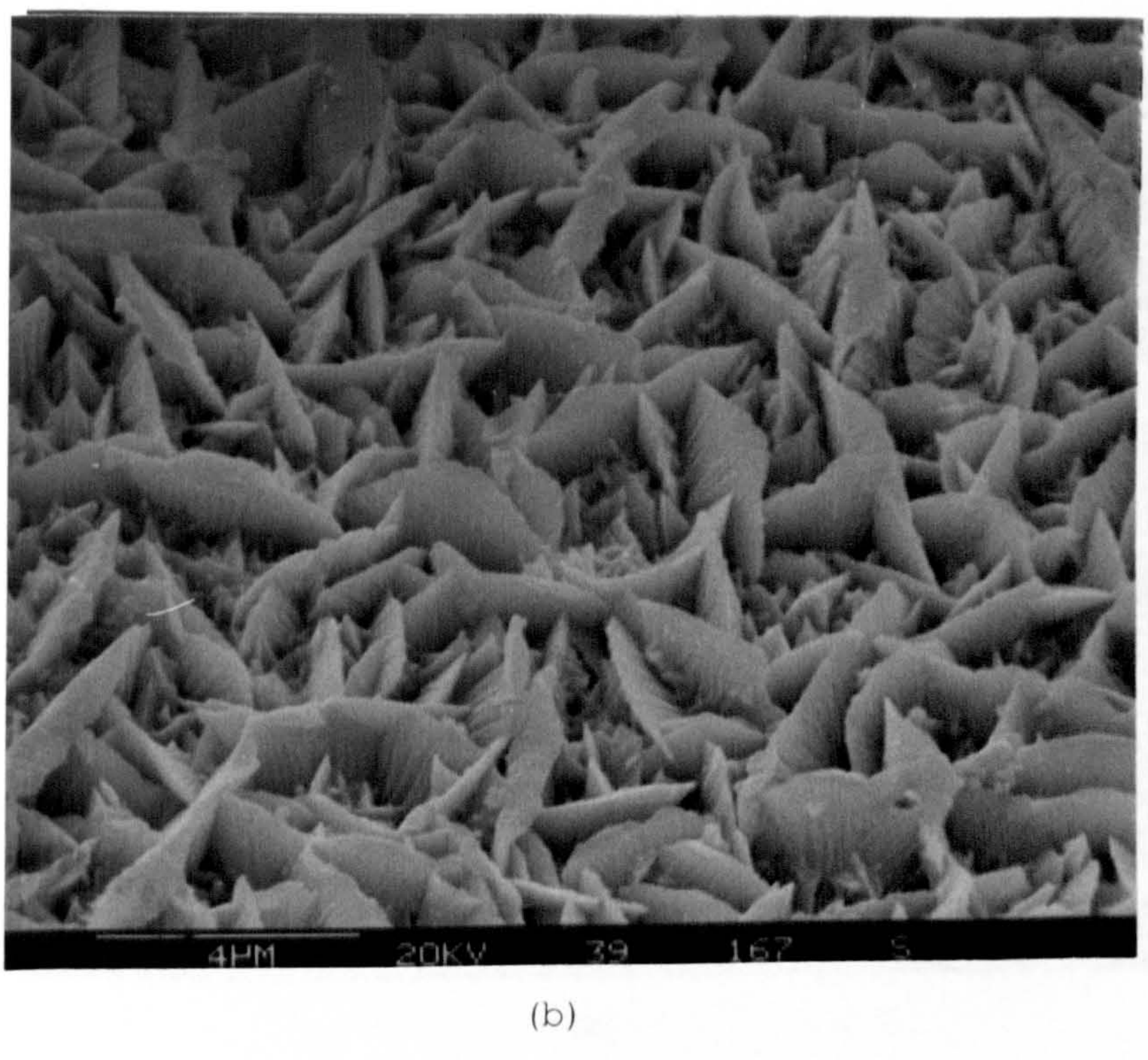

(b)

Fig.3.2.56 S.E.M. micrograph of an electroplated cobalt substrate (on nickel plated copper) plated at 60°C with 30 mA/cm² current density for 5 minutes.
(a) Magnfication 2000X, (b) Magnification 6000X.

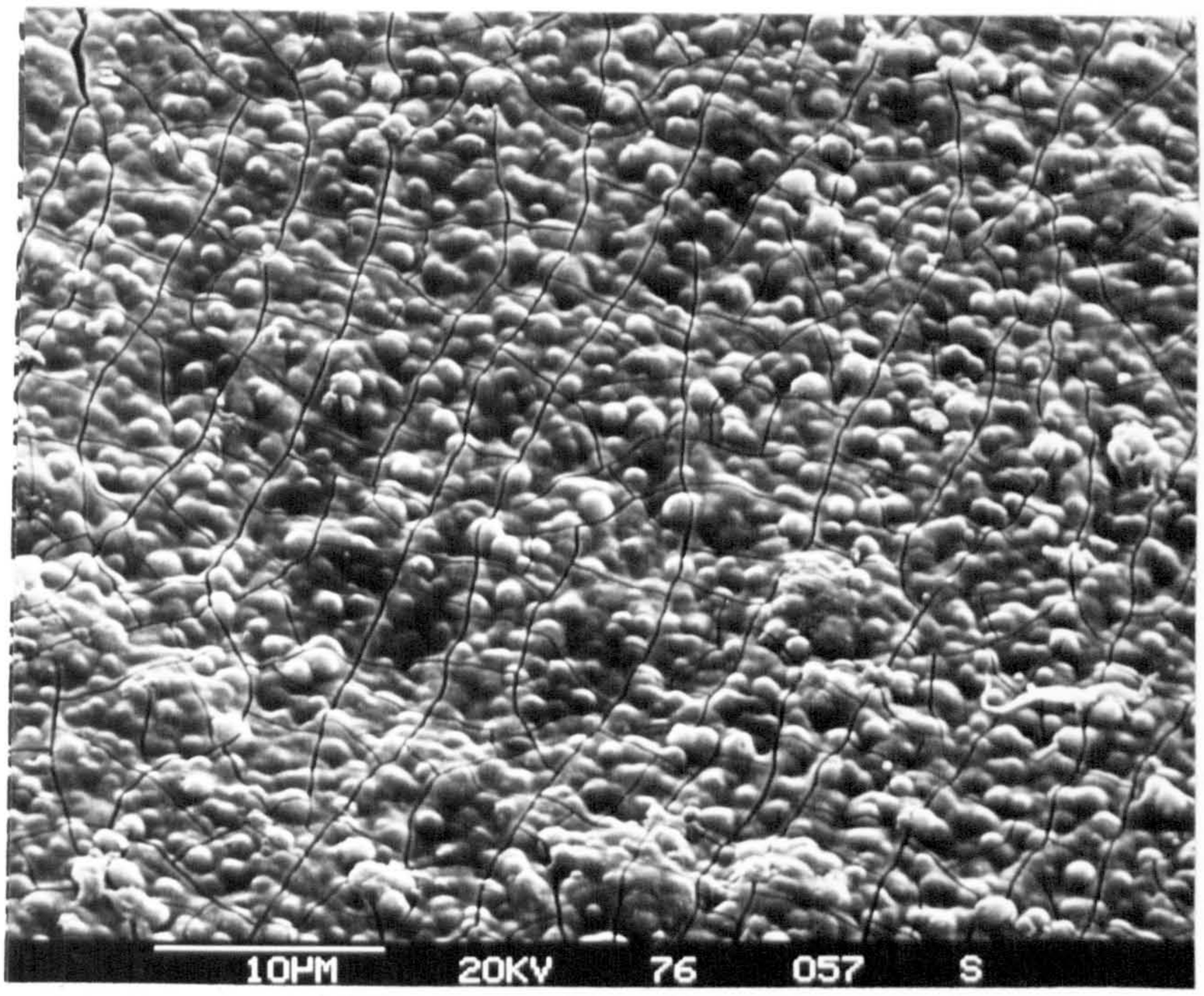

(a)

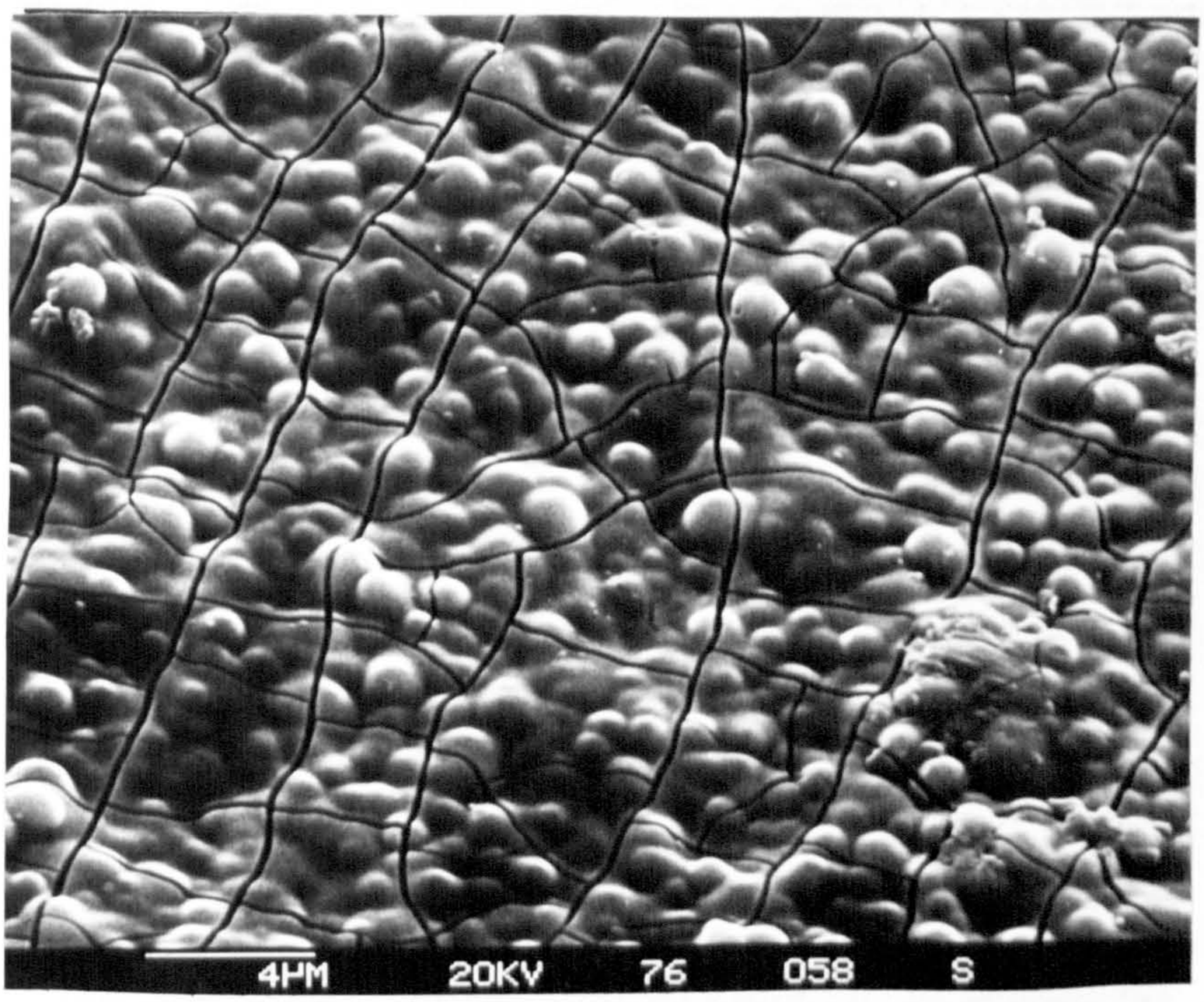

(b)

Fig.3.2.57 S.E.M. micrograph of a Mo-black dip coating on cobalt (NC) substrate (with addition agent) showing large number of nodules. For this surface $\alpha_S = 0.90$, $\varepsilon_{th} = 0.12$.
(a) Magnification: 2000X, (b) Magnification: 4000X.

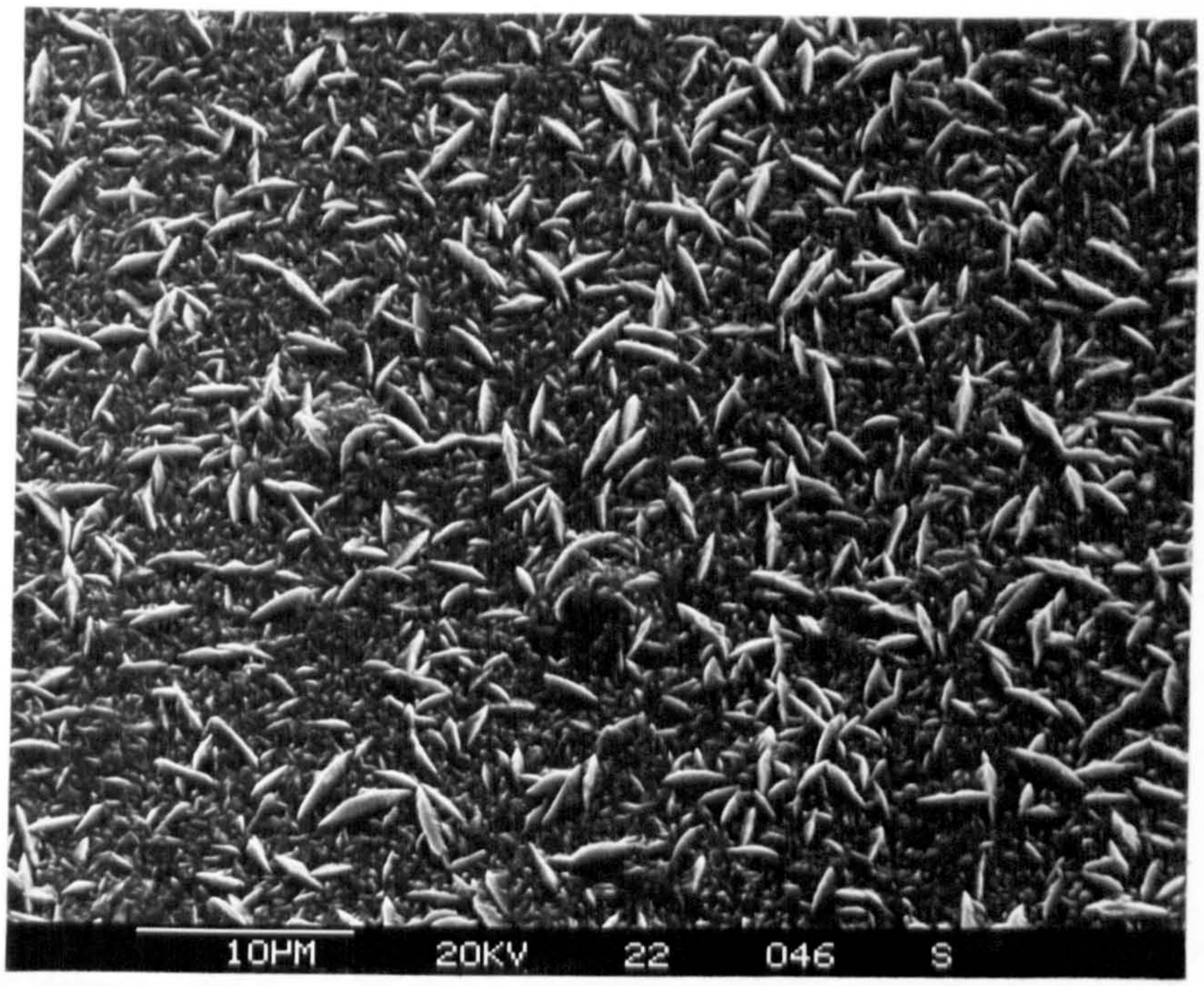

(a)

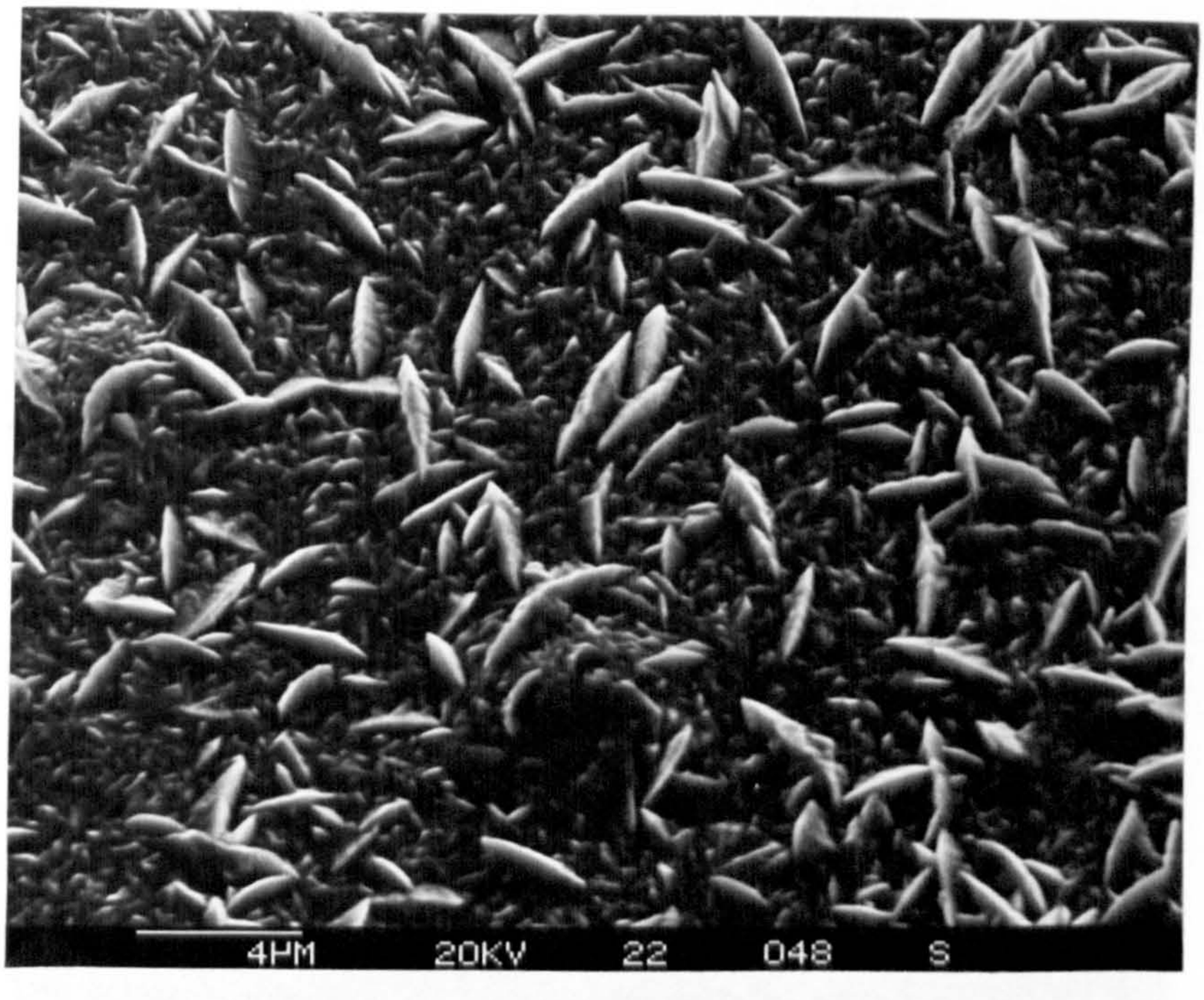

(b)

Fig.3.2.58 S.E.M. micrograph of a cobalt surface plated with addition agent at a temperature of 60°C with 40 mA/cm² current density for 6 minutes.
(a) Magnification: 2000X, (b) Magnification: 4000X.

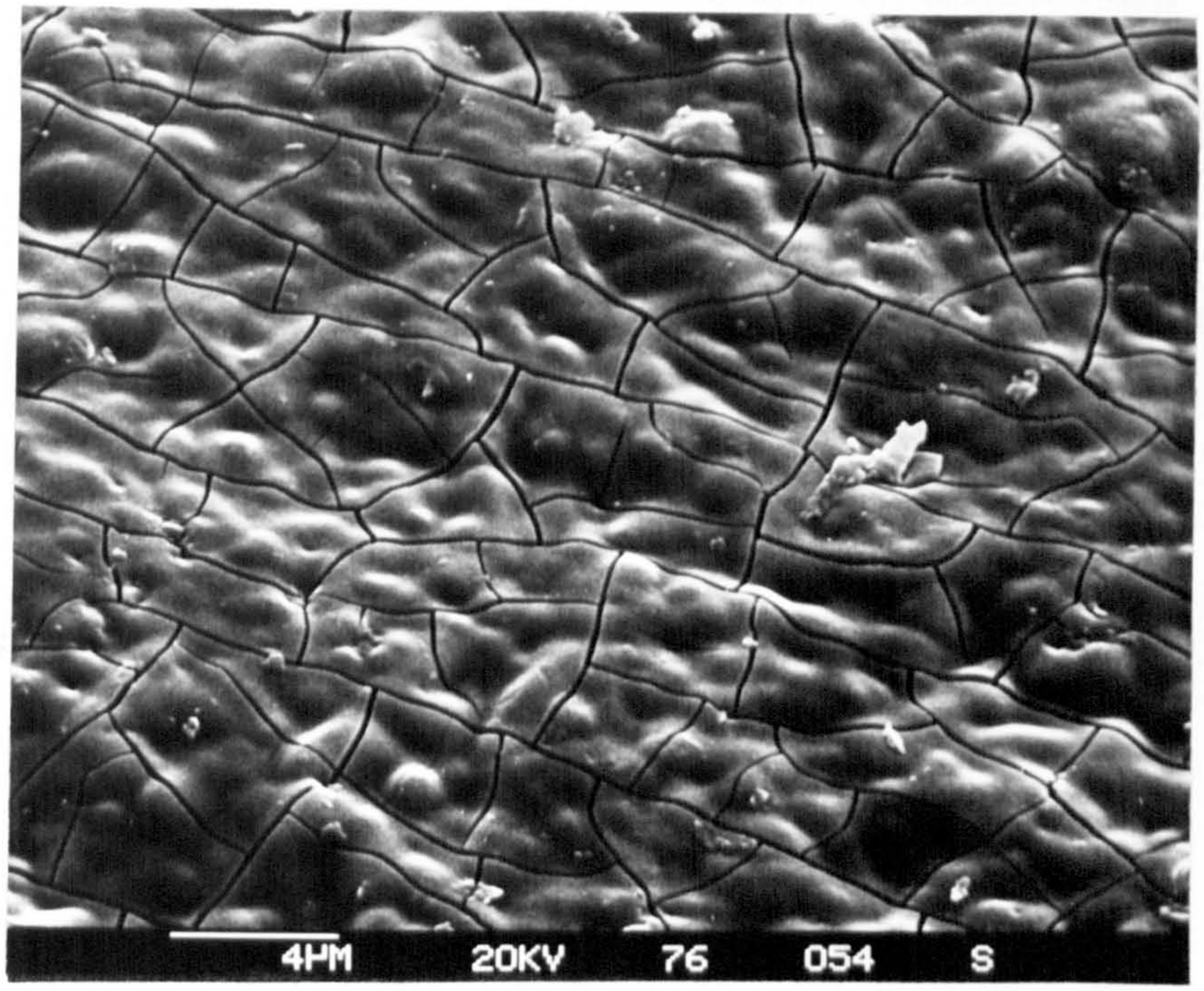

Fig.3.3.59 S.E.M. micrograph of a Mo-black dip coating on cobalt (NC) substrate (with addition agent). For this surface σ_s = 0.89, ε_{th} = 0.17. Magnification: 4000X.

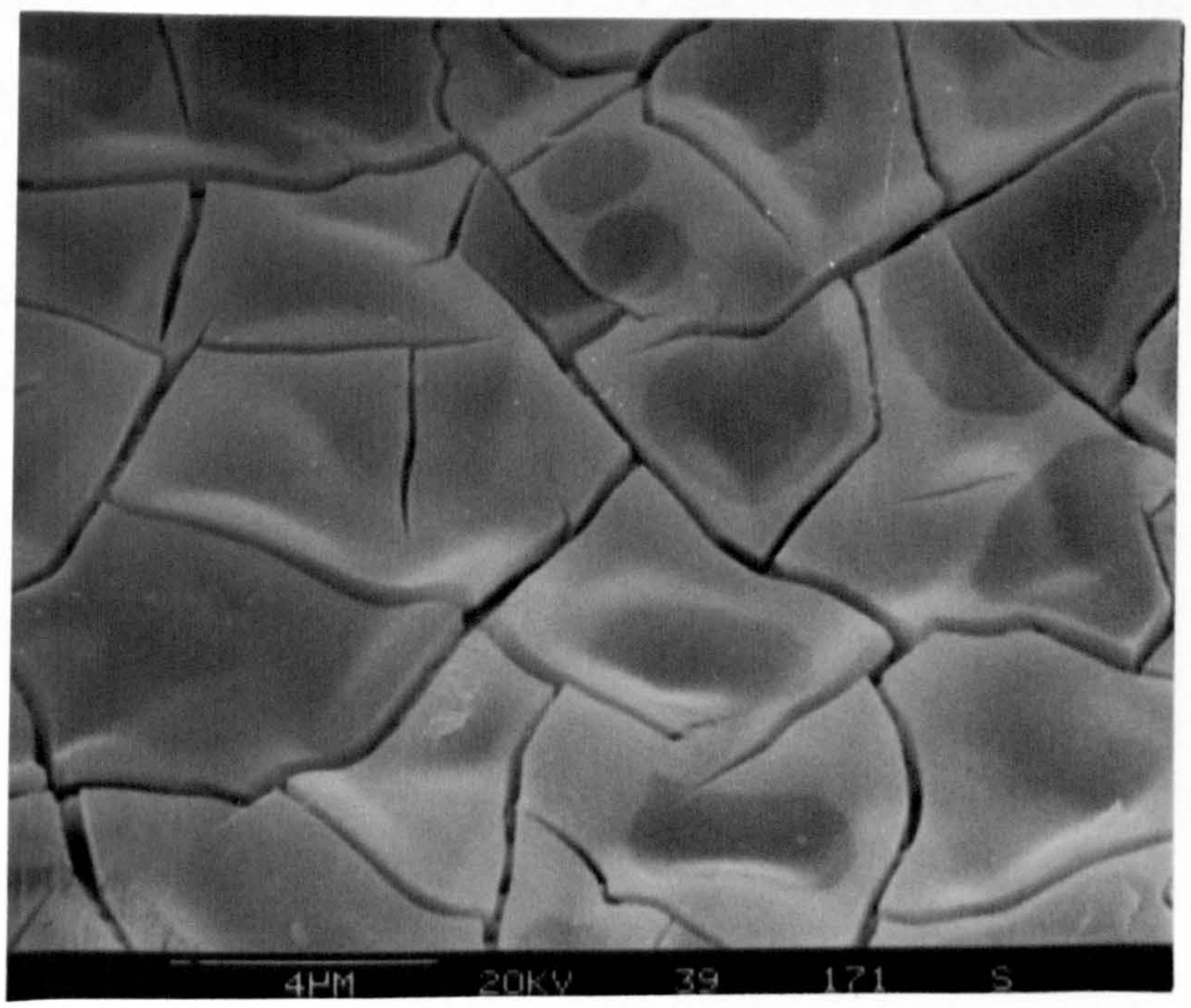

Fig.3.2.60 S.E.M. micrograph of a Mo-black coating prepared at a temperature of 80°C on cobalt (NC) substrate. For this surface α_s = 0.87, ε_{th} = 0.21. Magnification: 4000X.

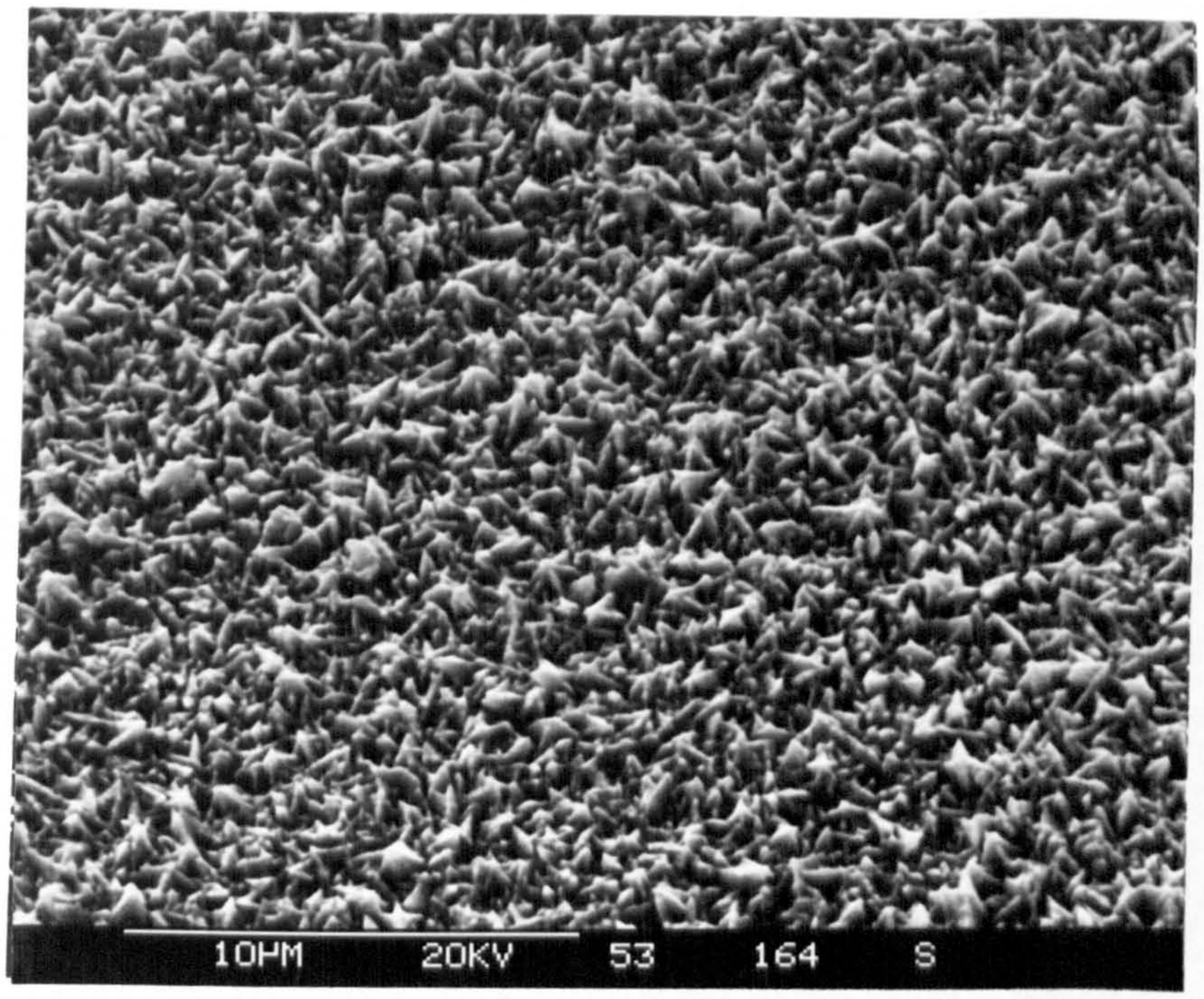

(a)

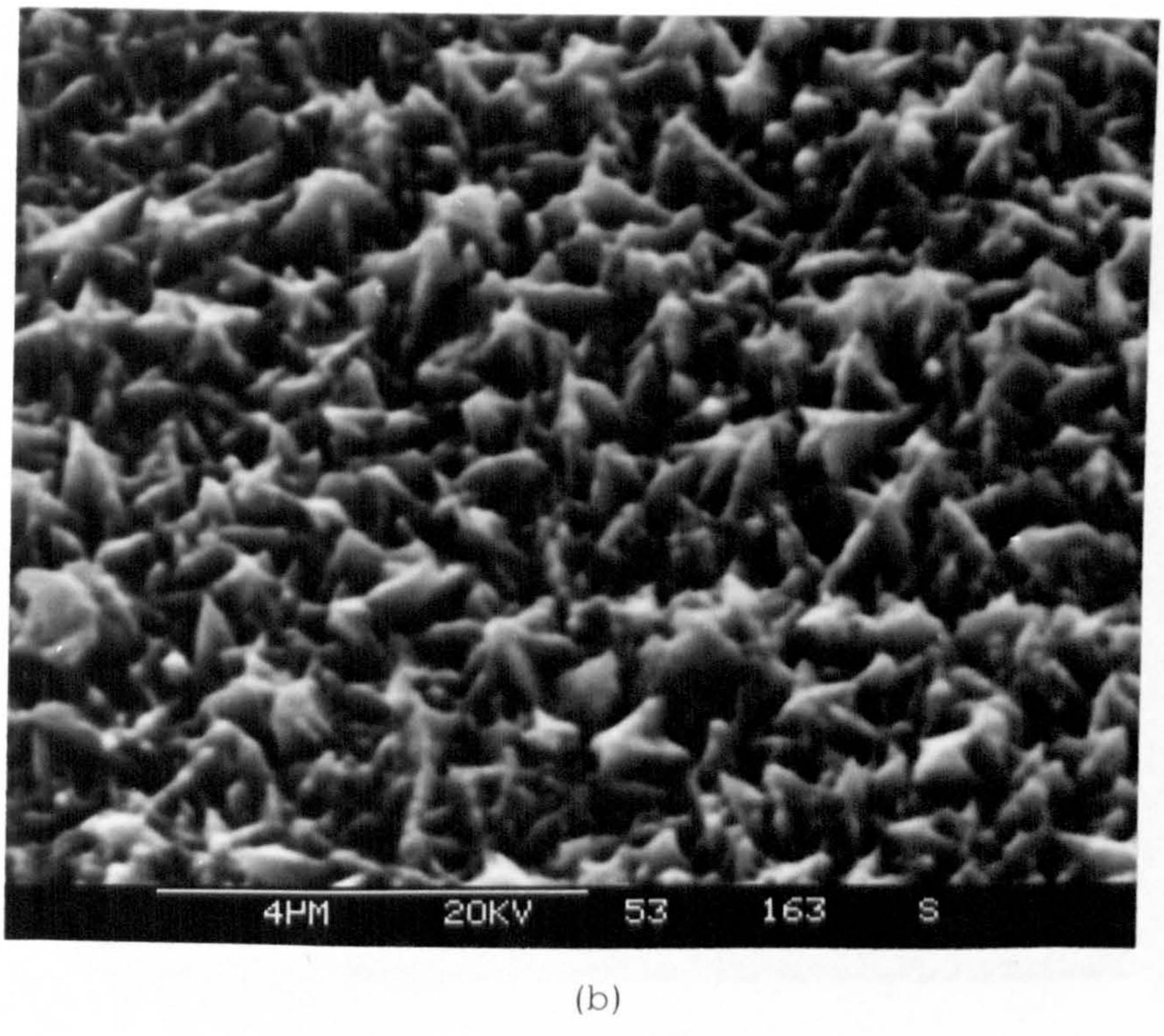

(b)

Fig.3.2.61 S.E.M. micrograph of a cobalt surface plated at 45°C with 25 mA/cm² current density for 4 minutes on nickel plated copper.
(a) Magnification: 4000X, (b) Magnification:10 000X.

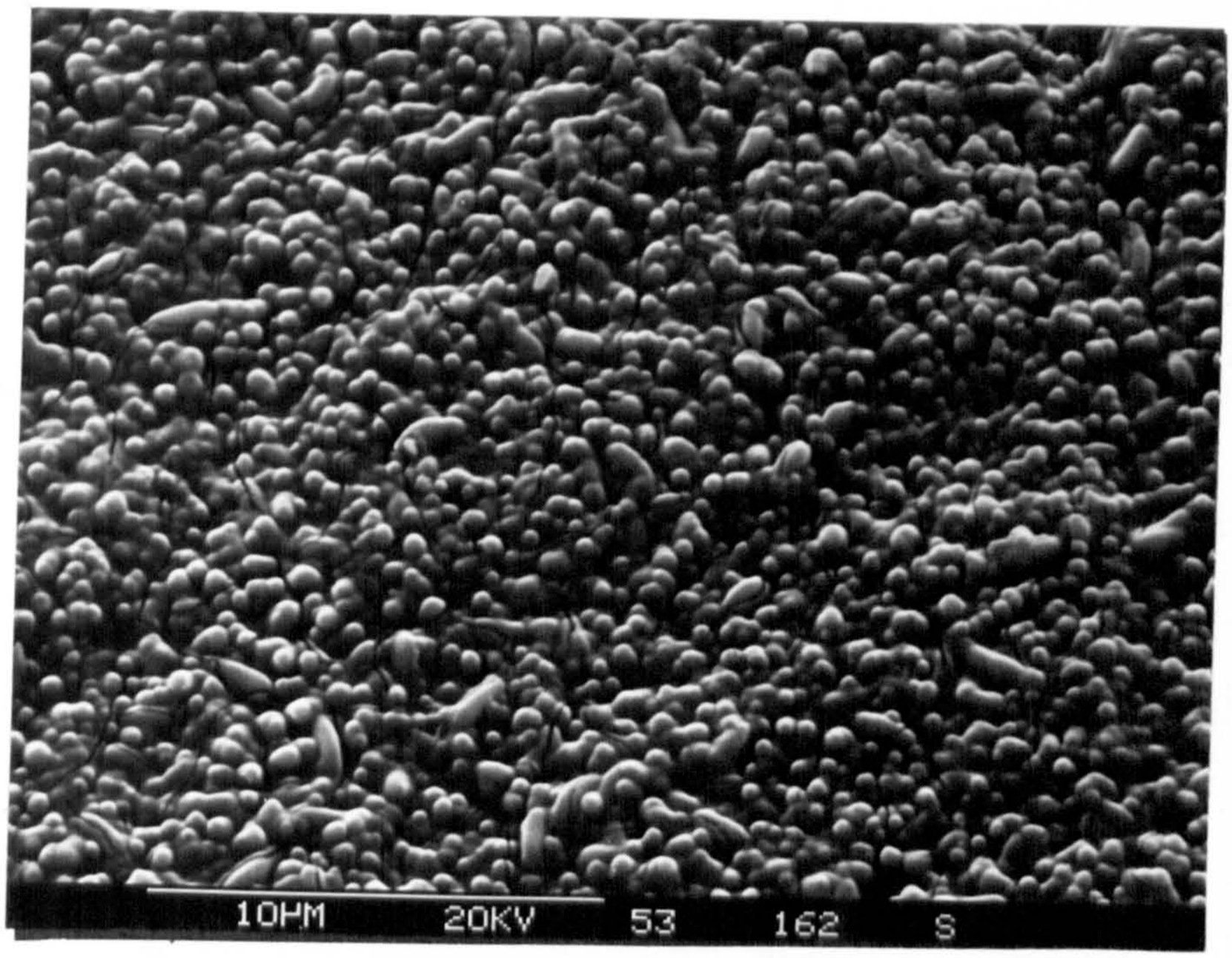

(a)

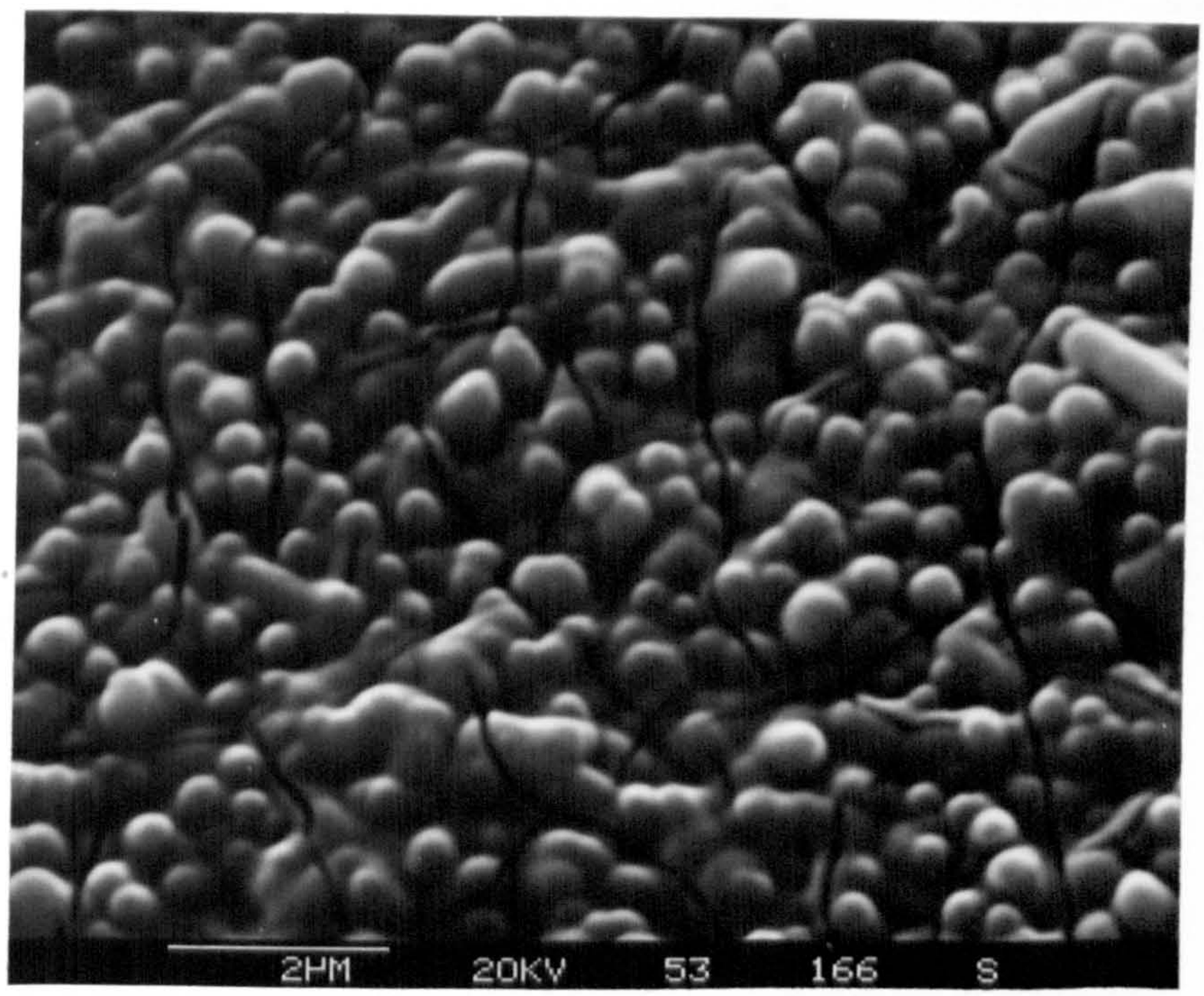

(b)

Fig.3.2.62 S.E.M. micrograph of a Mo-black dip coating on cobalt (NC) substrate. For this surface α_s = 0. 91, ε_{th} = 0.09 (a) Magnification: 2000X, (b) Magnification: 10000X.

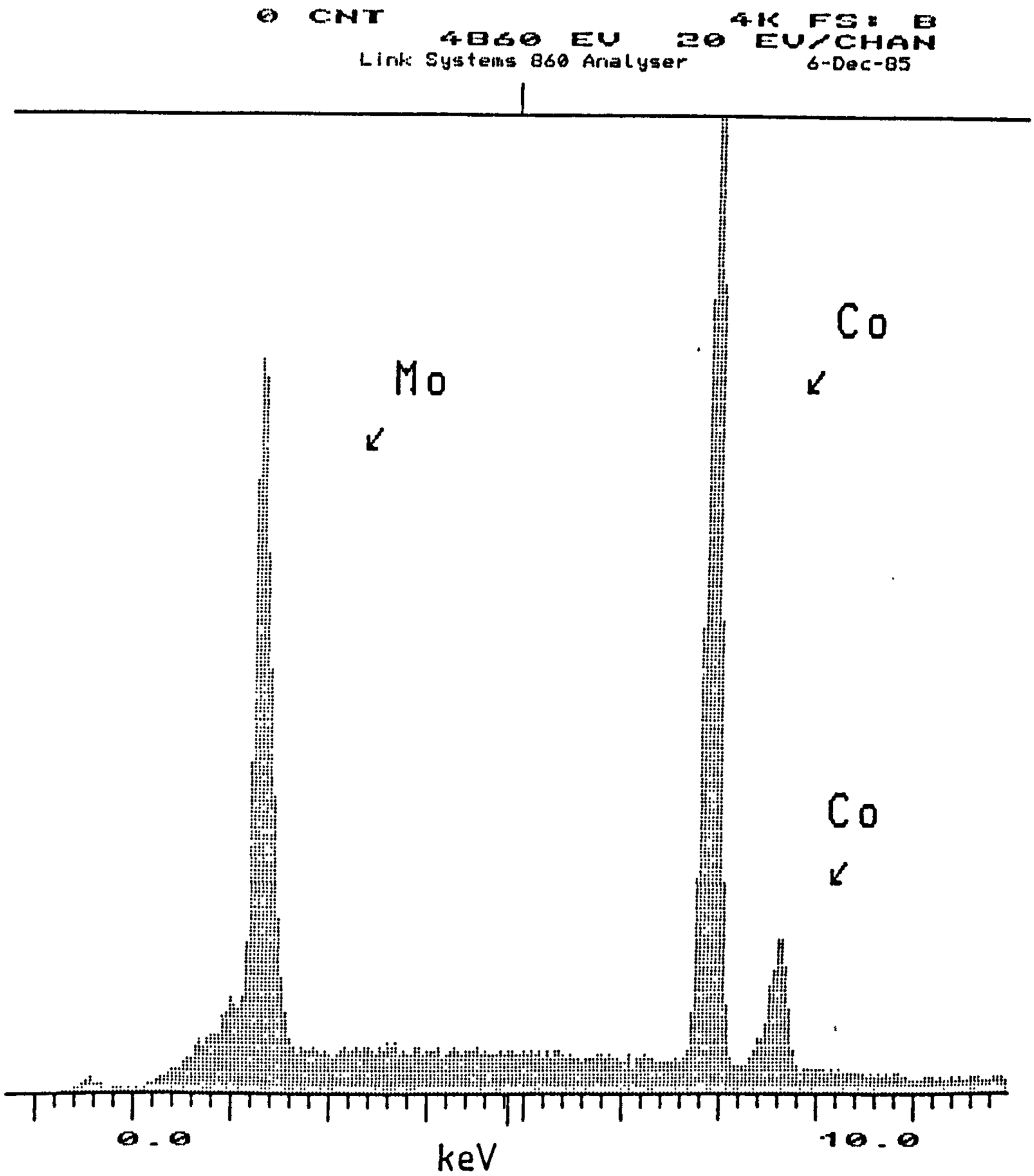

Fig.3.2.63 EDX spectrum of a Mo-black dip coating on cobalt (NC) substrate. Deposition time = 15 minutes.

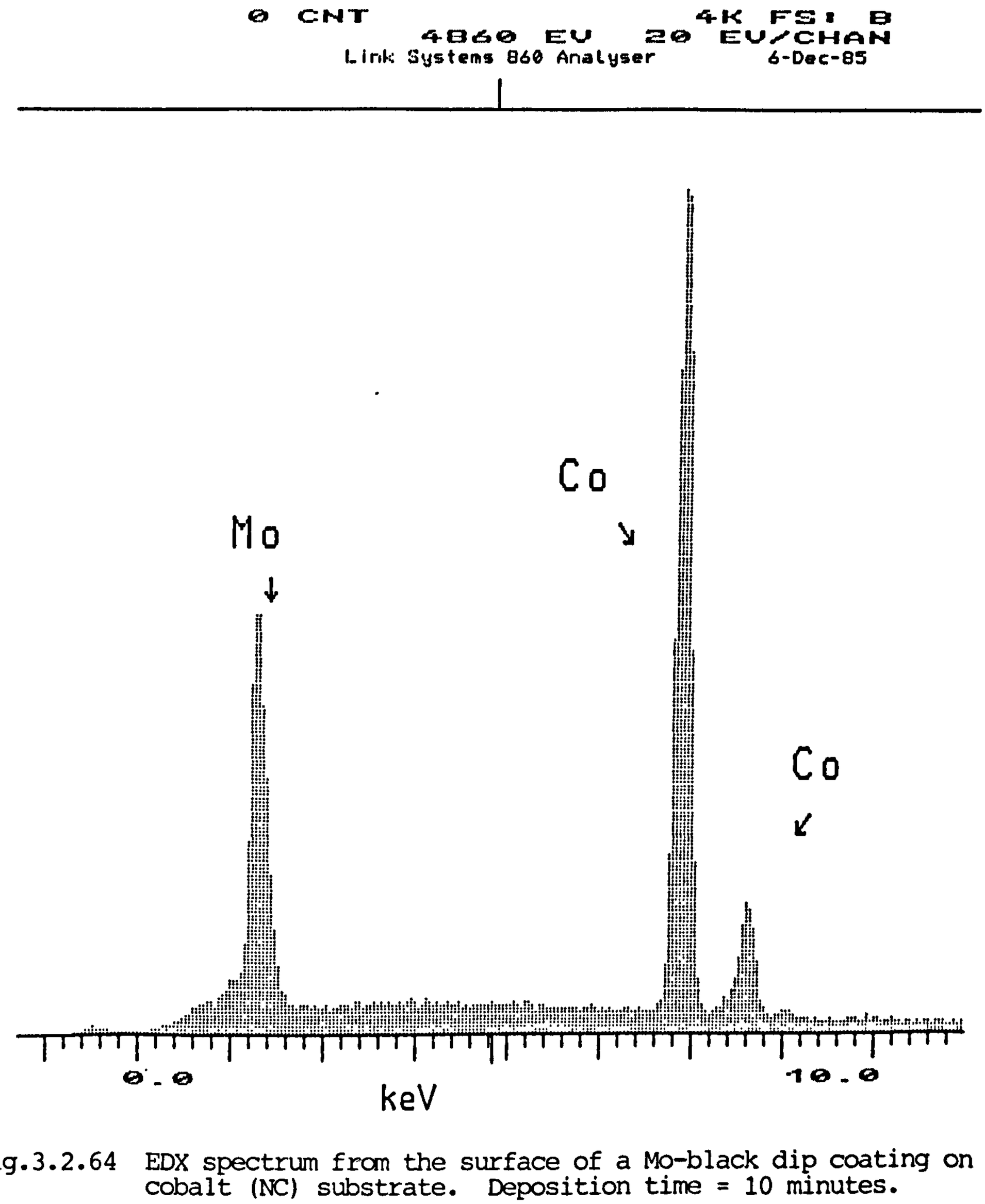

Fig.3.2.64 EDX spectrum from the surface of a Mo-black dip coating on cobalt (NC) substrate. Deposition time = 10 minutes.

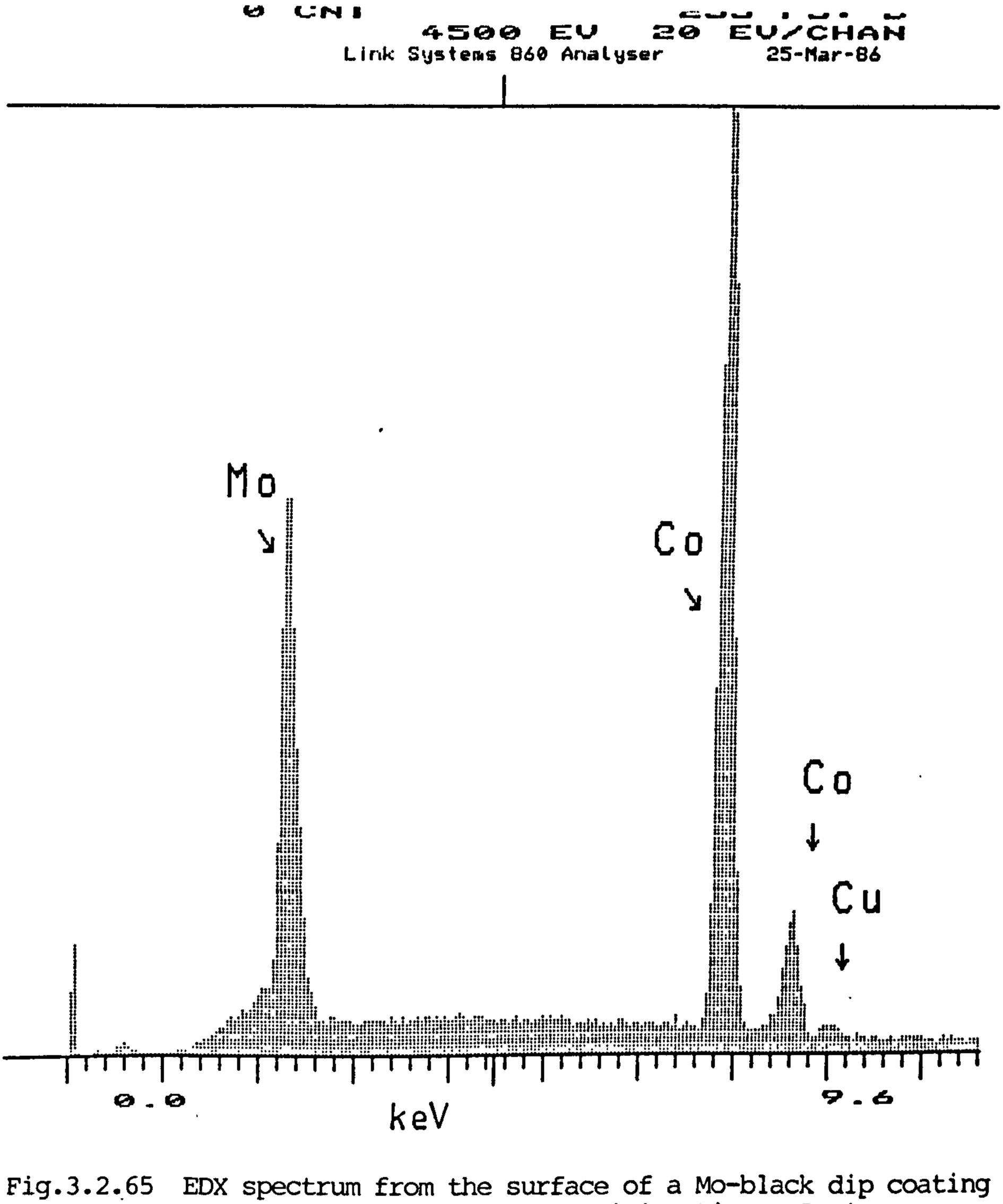

Fig.3.2.65 EDX spectrum from the surface of a Mo-black dip coating on cobalt (NC) substrate. Deposition time = 5 minutes.

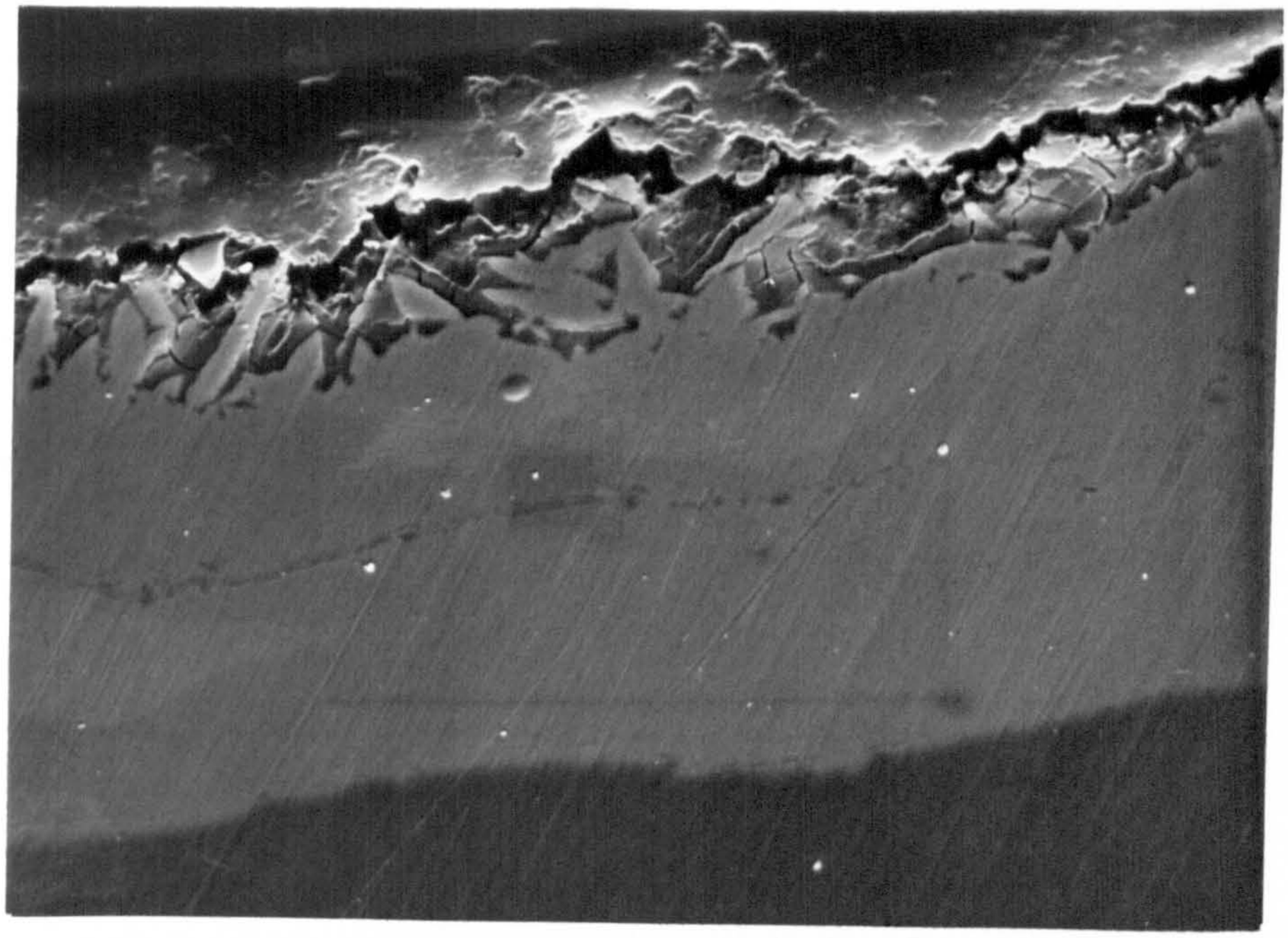

Fig.3.2.66 S.E.M. micrograph of the metallographic cross-section of a Mo-black coating on cobalt (NC) substrate.
Magnification: 2000X.

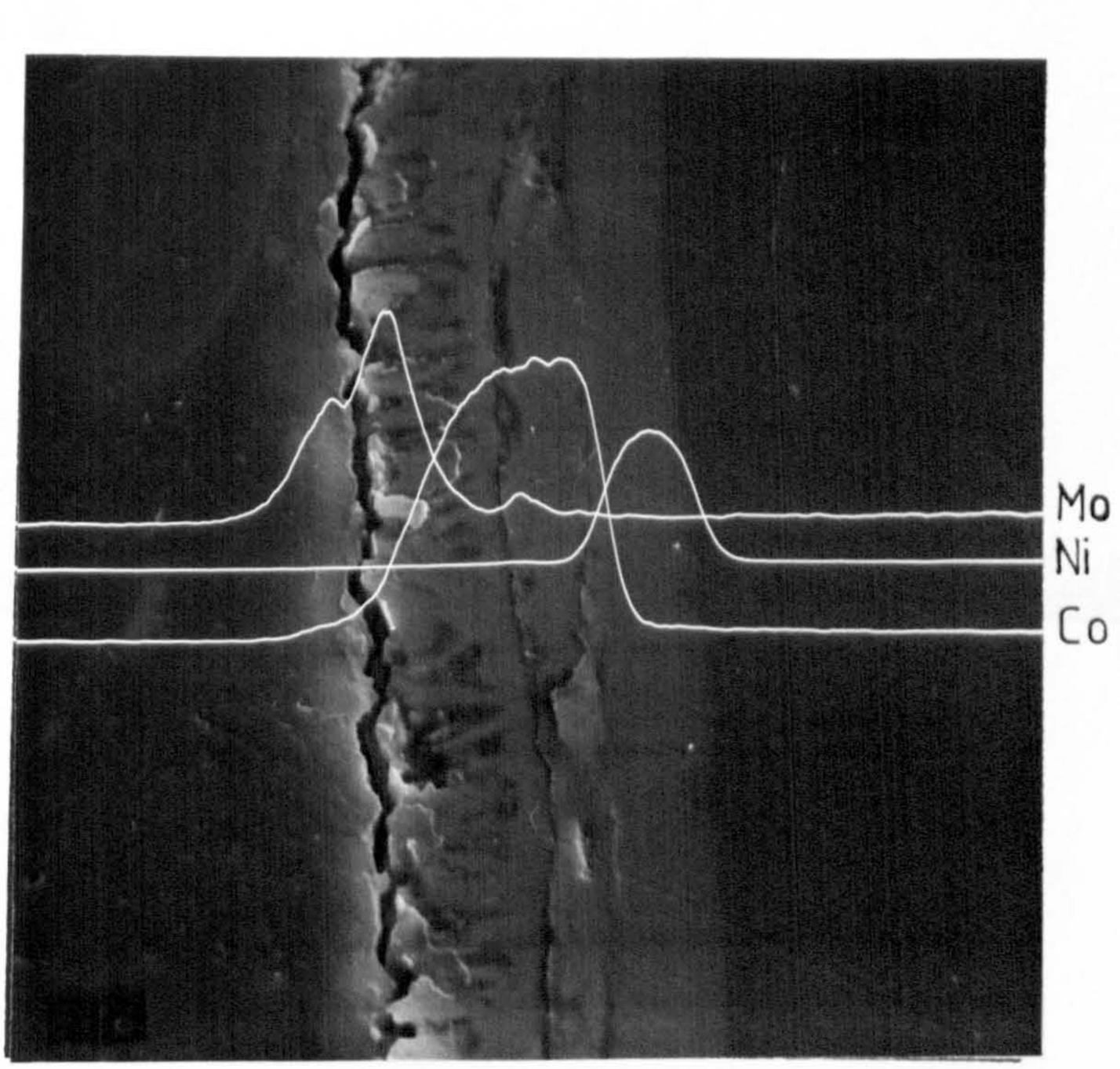

Fig.3.2.67 The Mo, Co and Ni X-ray line scans of the metallographic cross-section of Mo-black coating on cobalt (NC) substrate
Magnification: 1000X.

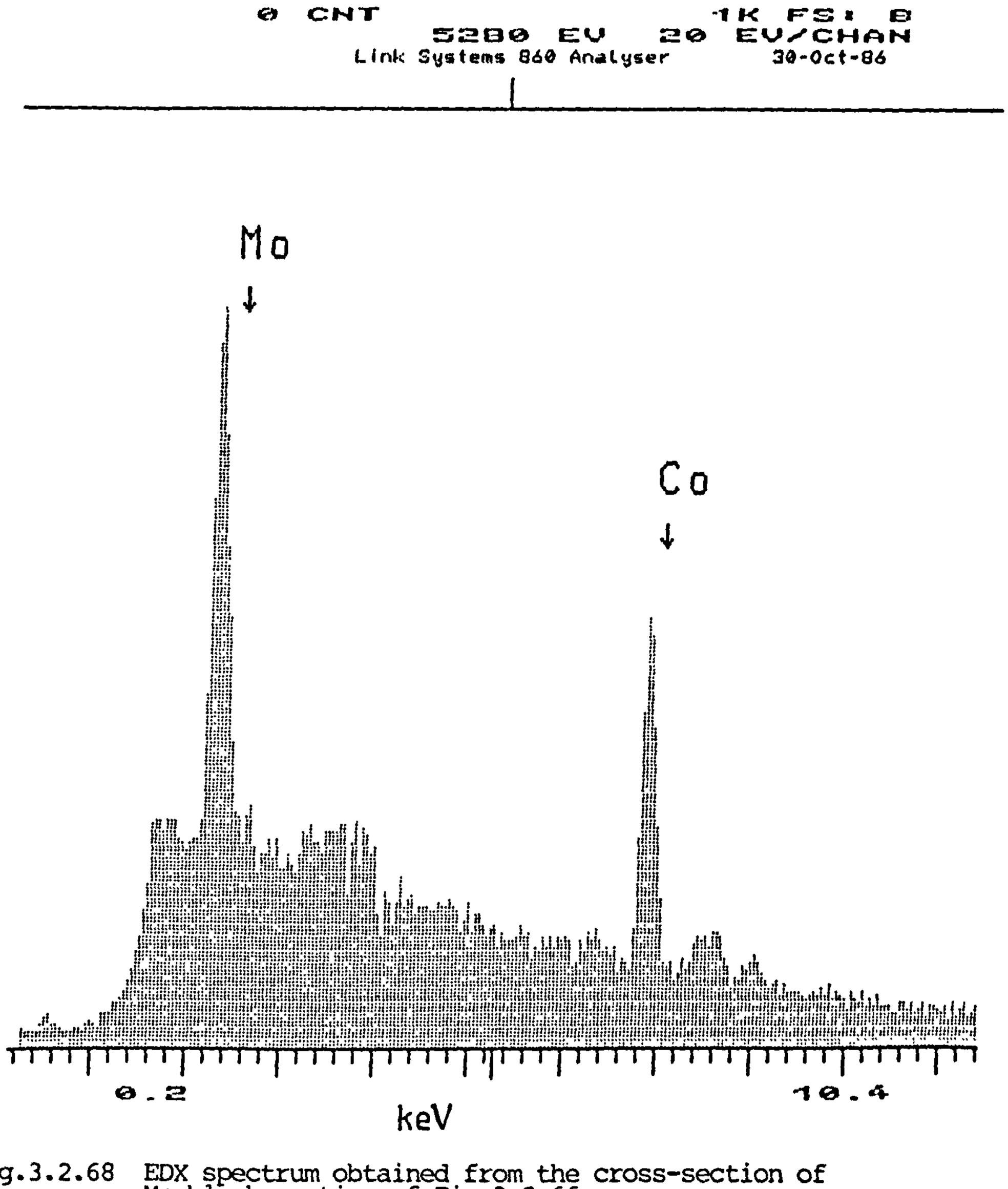

Fig.3.2.68 EDX spectrum obtained from the cross-section of Mo-black coating of Fig.3.2.66.

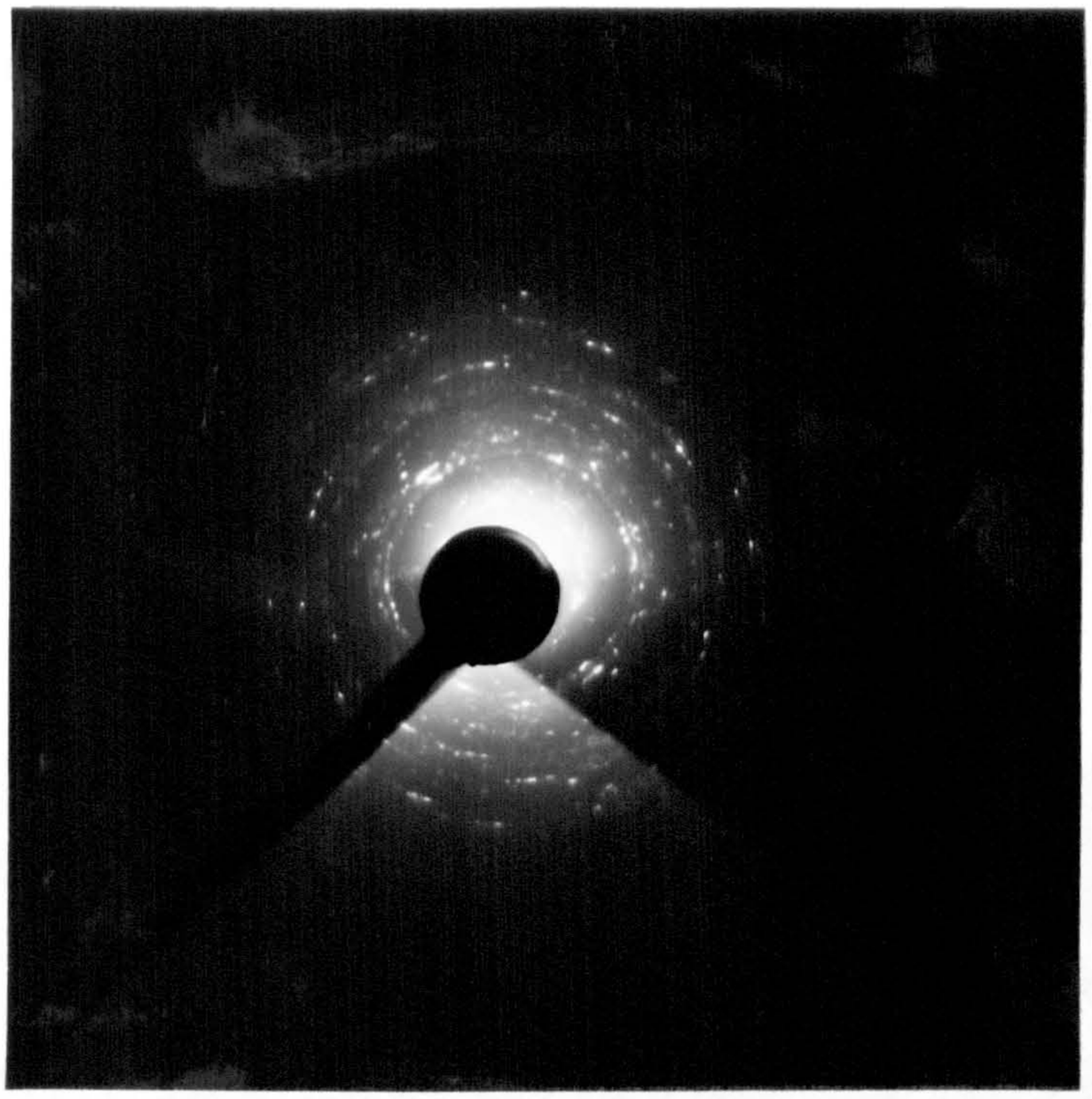

Fig.3.3.1 Reflection electron diffraction pattern of a Mo-black dip-coating on an etched zinc substrate.

Fig.3.3.2 Reflection electron diffraction pattern of a Mo-black dip coating on an etched zinc substrate after heating in air at 400 °C for 4 hours.

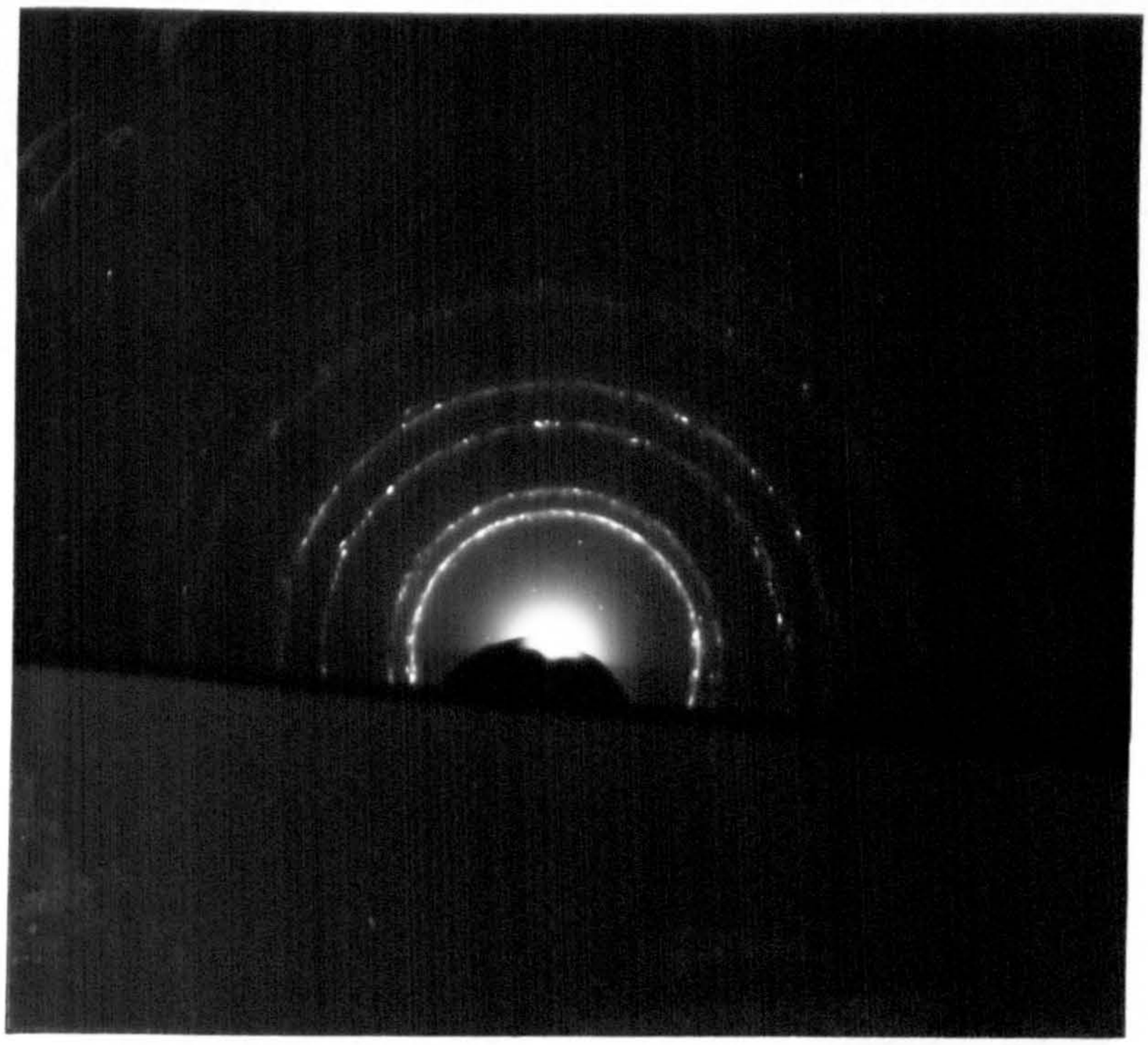

Fig.3.3.3 Reflection electron diffraction pattern of a Mo-black coating on a cobalt (NC) substrate.

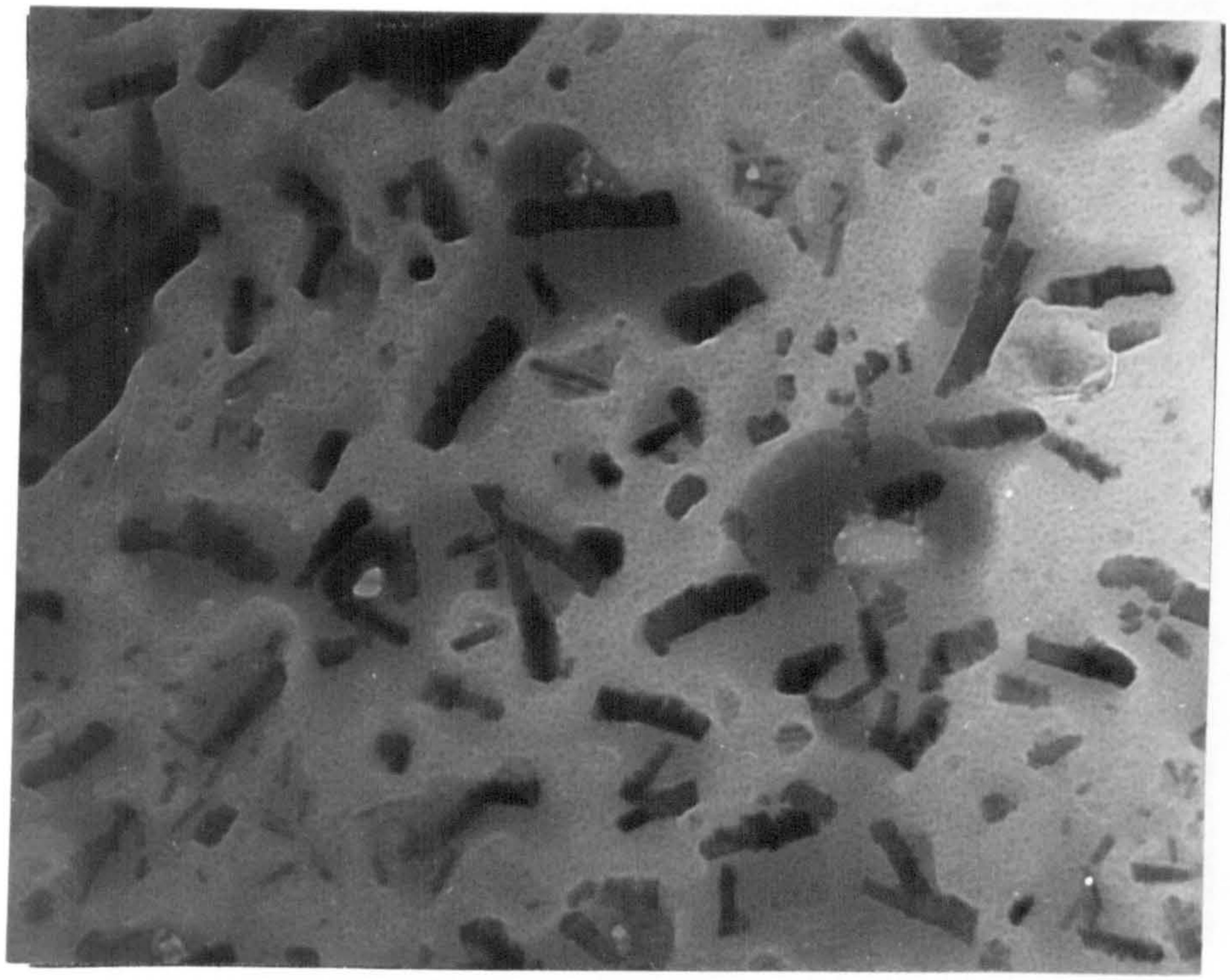

Fig.3.3.4(a) T.E.M. micrograph of an electro plated Mo-black coating from an aluminium substrate. Magnification: 76000X.

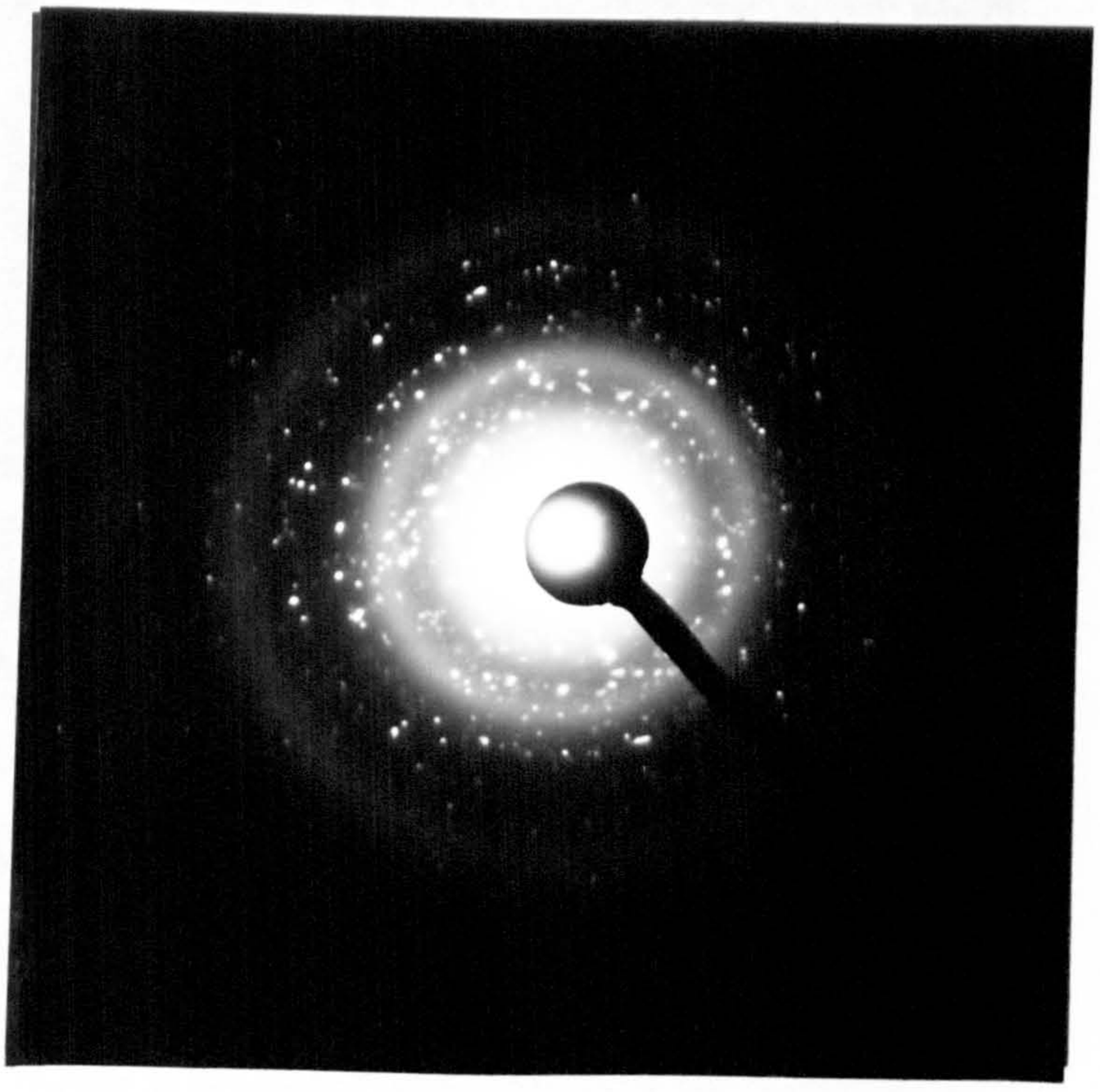

Fig.3.3.4(b) Corresponding electron diffraction pattern of Fig.3.3.4(a).

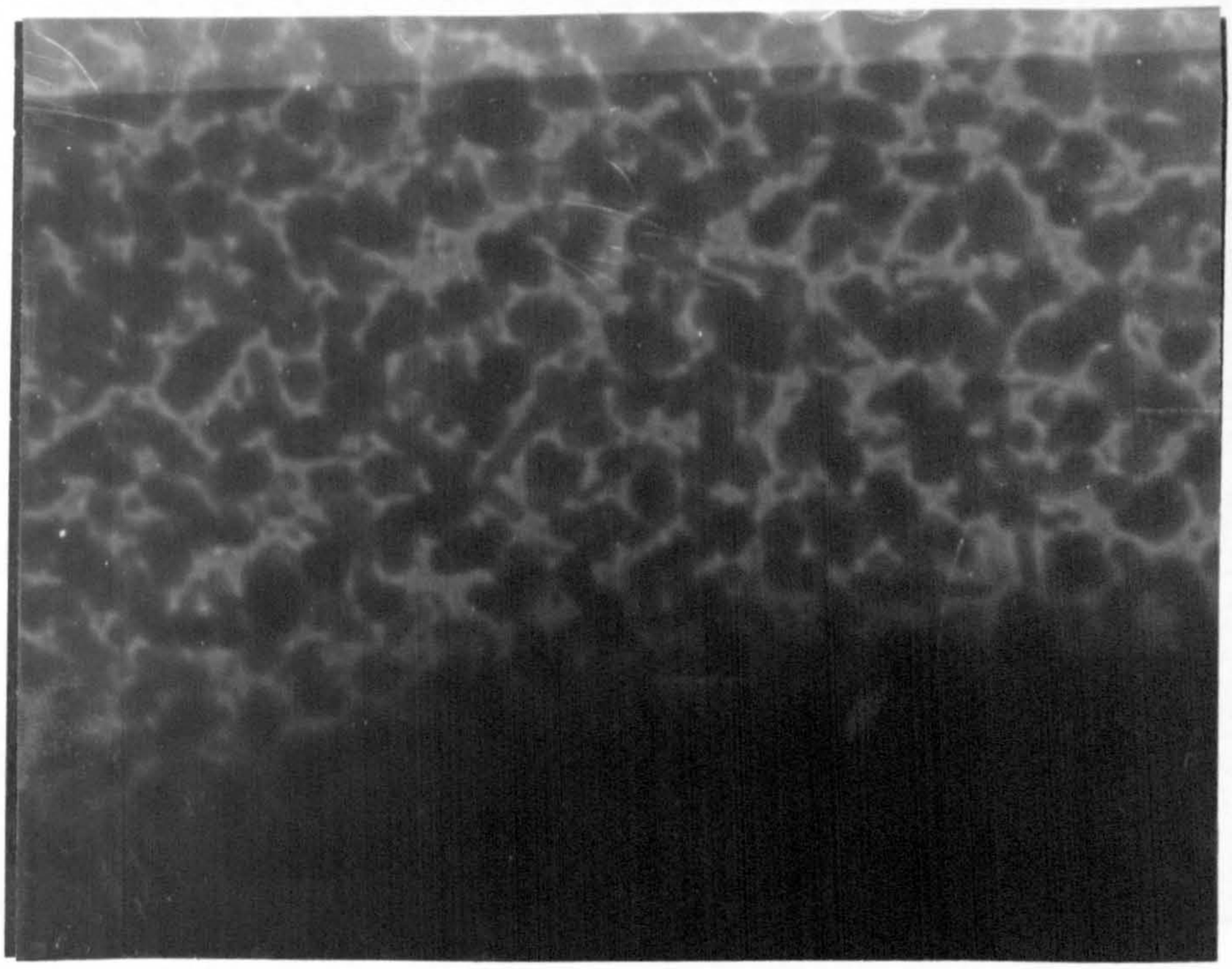

Fig.3.3.5(a) T.E.M. micrograph of an electroplated Mo-black coating prepared on copper substrate at room temperature. Magnification: 76000X.

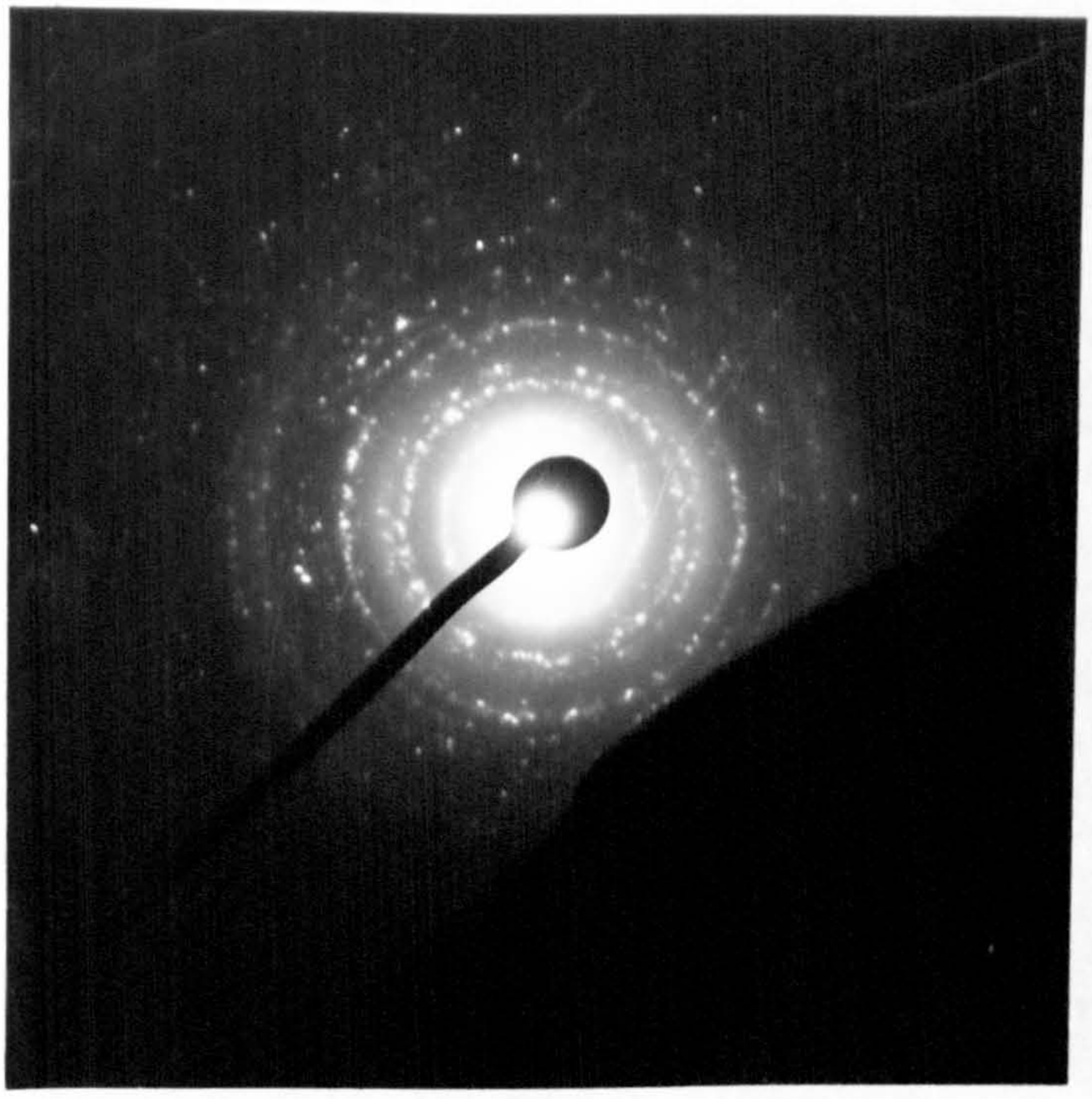

Fig.3.3.5(b) Corresponding electron diffraction pattern of Fig.3.3.5(a).

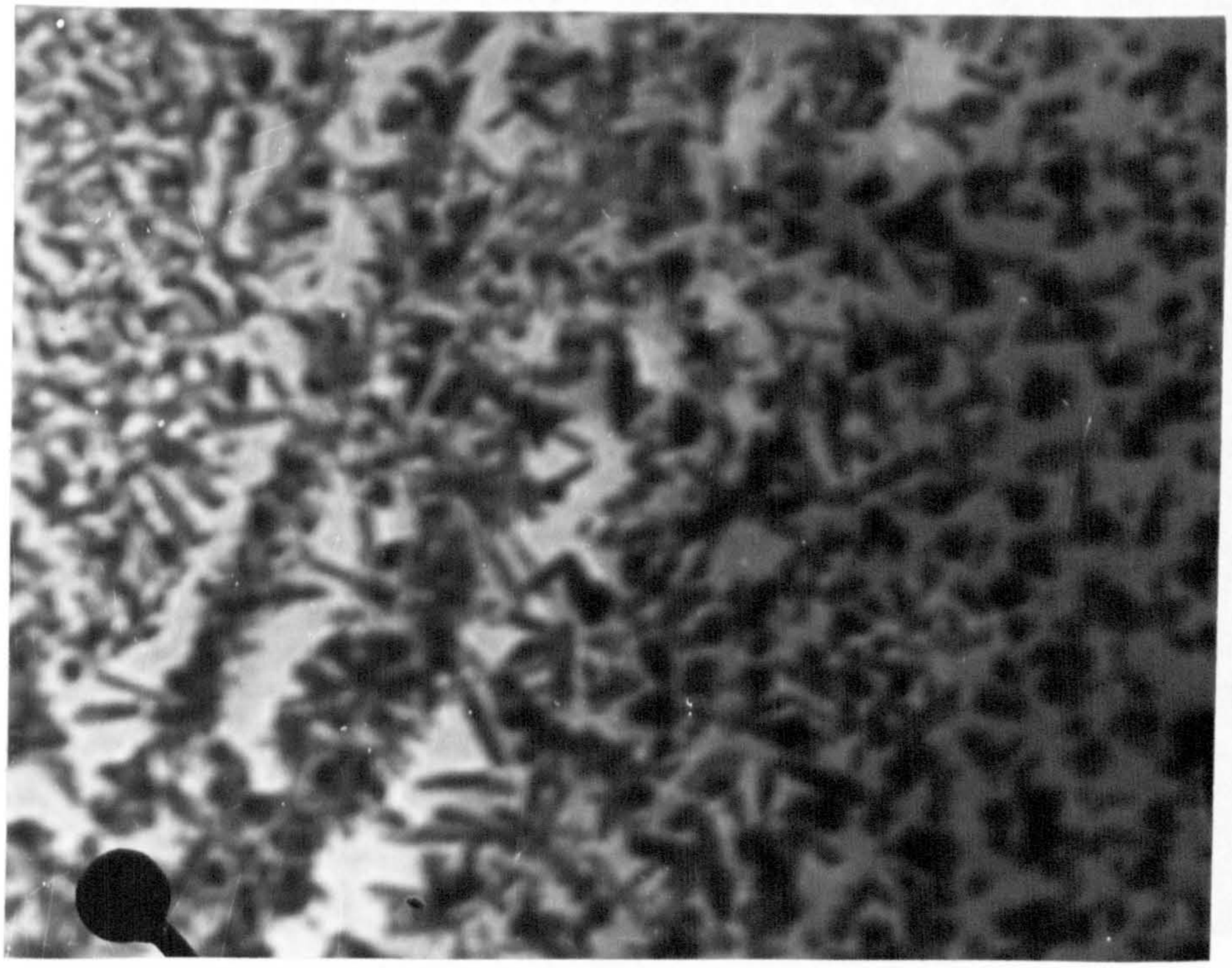

Fig.3.3.6(a) T.E.M. micrograph of the same sample (Fig.3.3.5) after holding at -160° for 2.5 hours.
Magnification: 76000X.

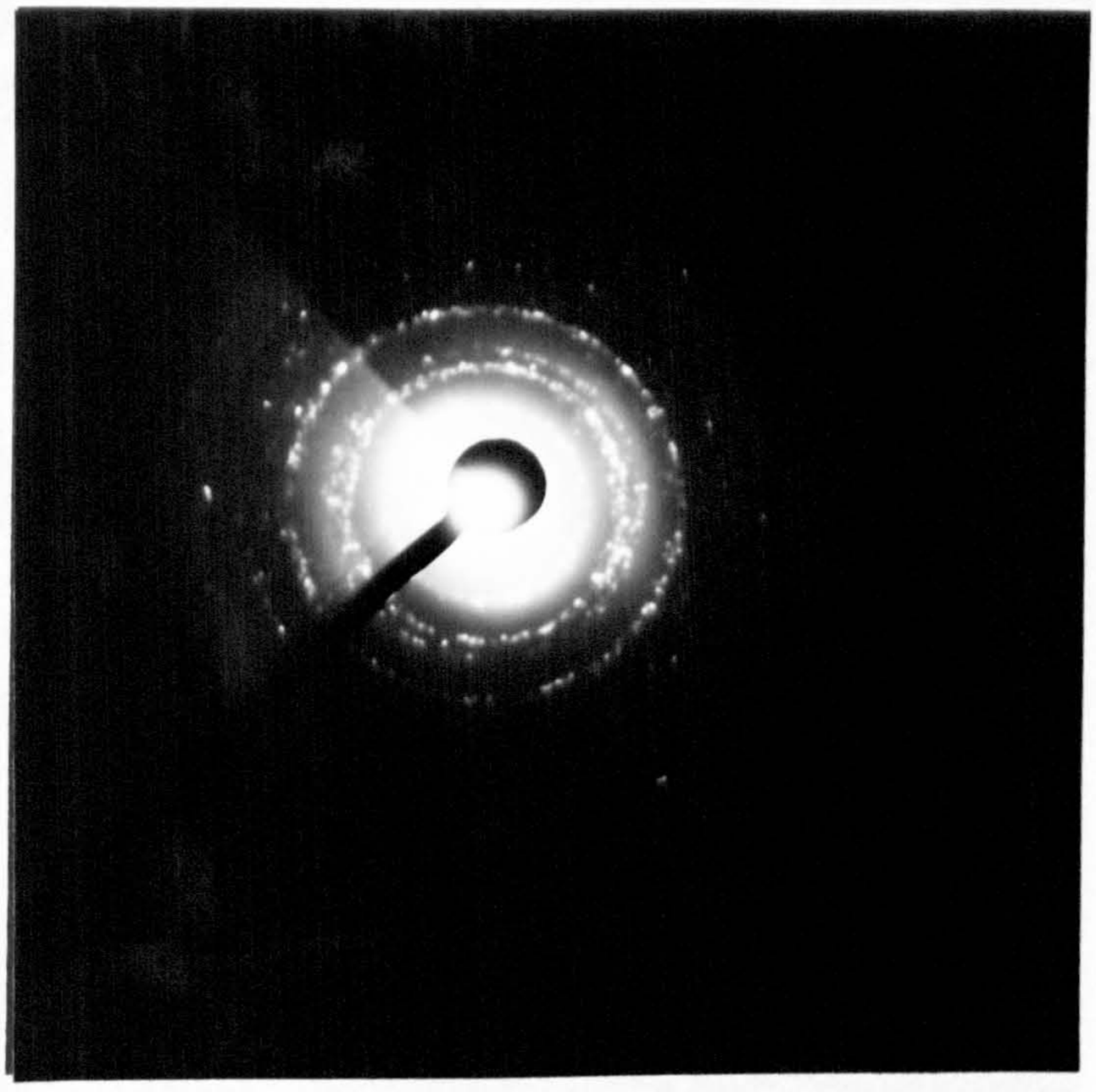

Fig.3.3.6(b) Corresponding electron diffraction pattern of Fig.3.3.6(a).

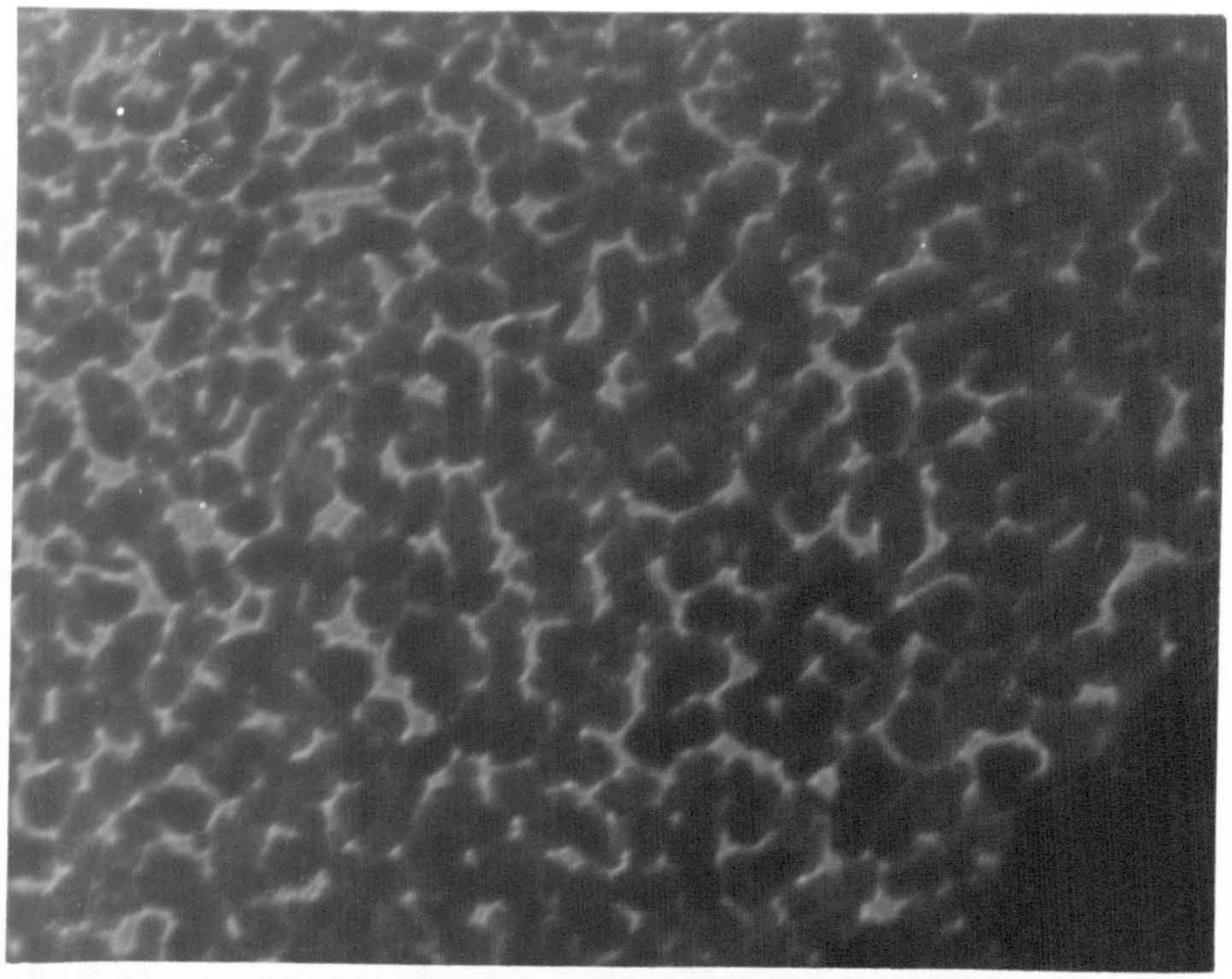

Fig.3.3.7(a) T.E.M. micrograph of the same coating (Fig.3.3.6) at room temperature after holding at -160°C for 2.5 hours. Magnification: 76000X.

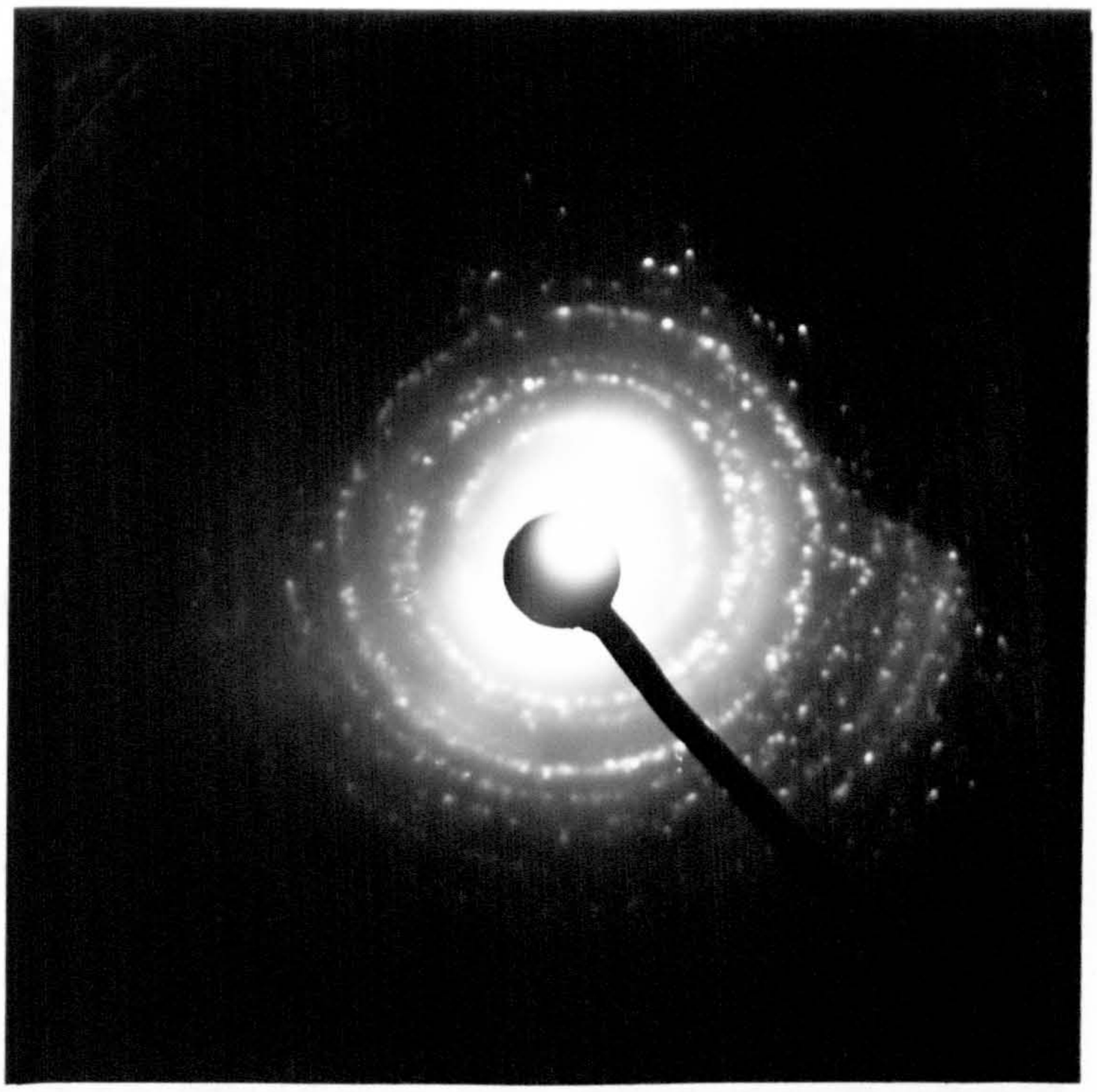

Fig.3.3.7(b) Corresponding electron diffraction pattern of Fig.3.3.7(a).

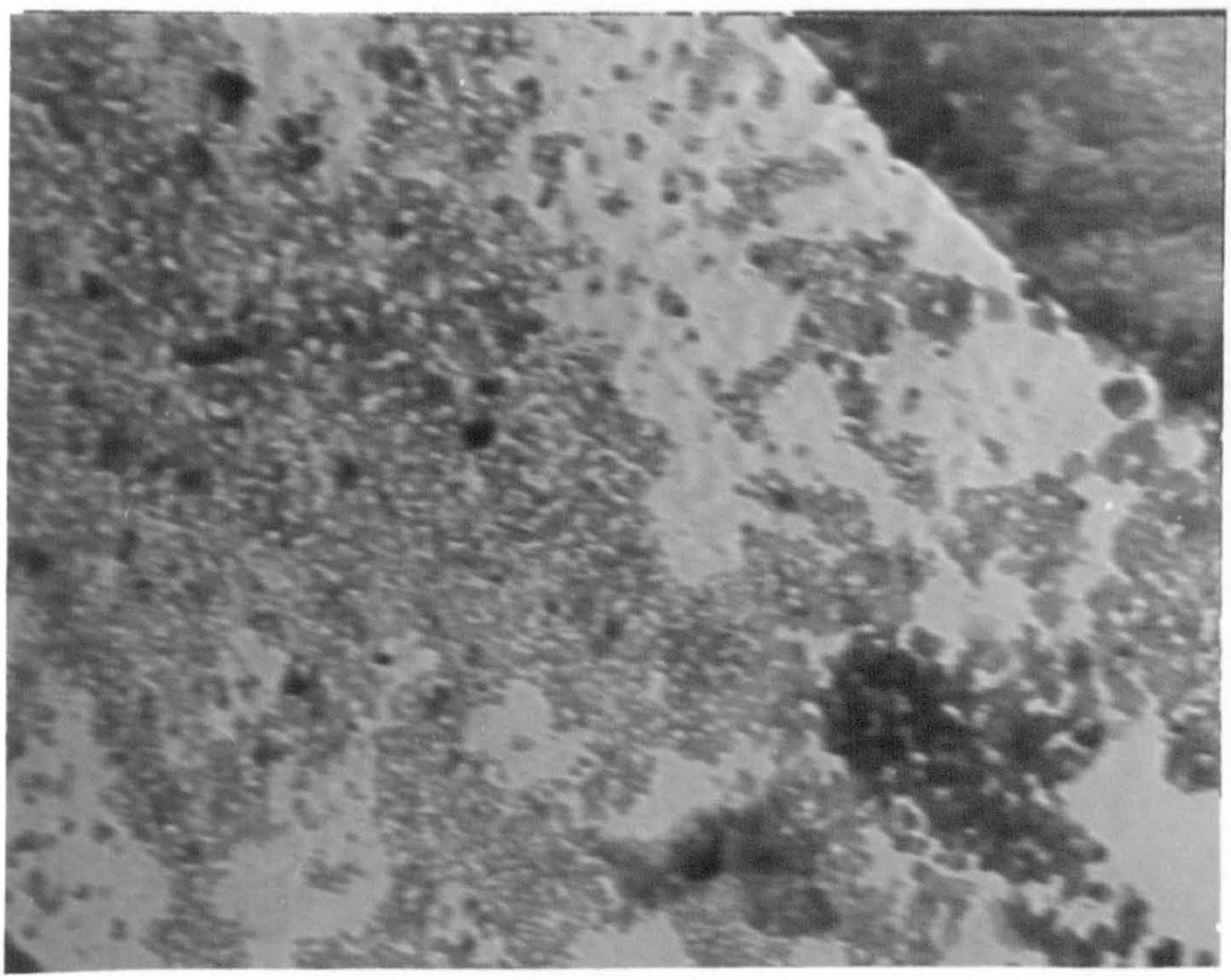

Fig.3.3.8(a) T.E.M. micrograph of an electroplated Mo-black coating prepared on copper substrate (as prepared). Magnification: 76000X.

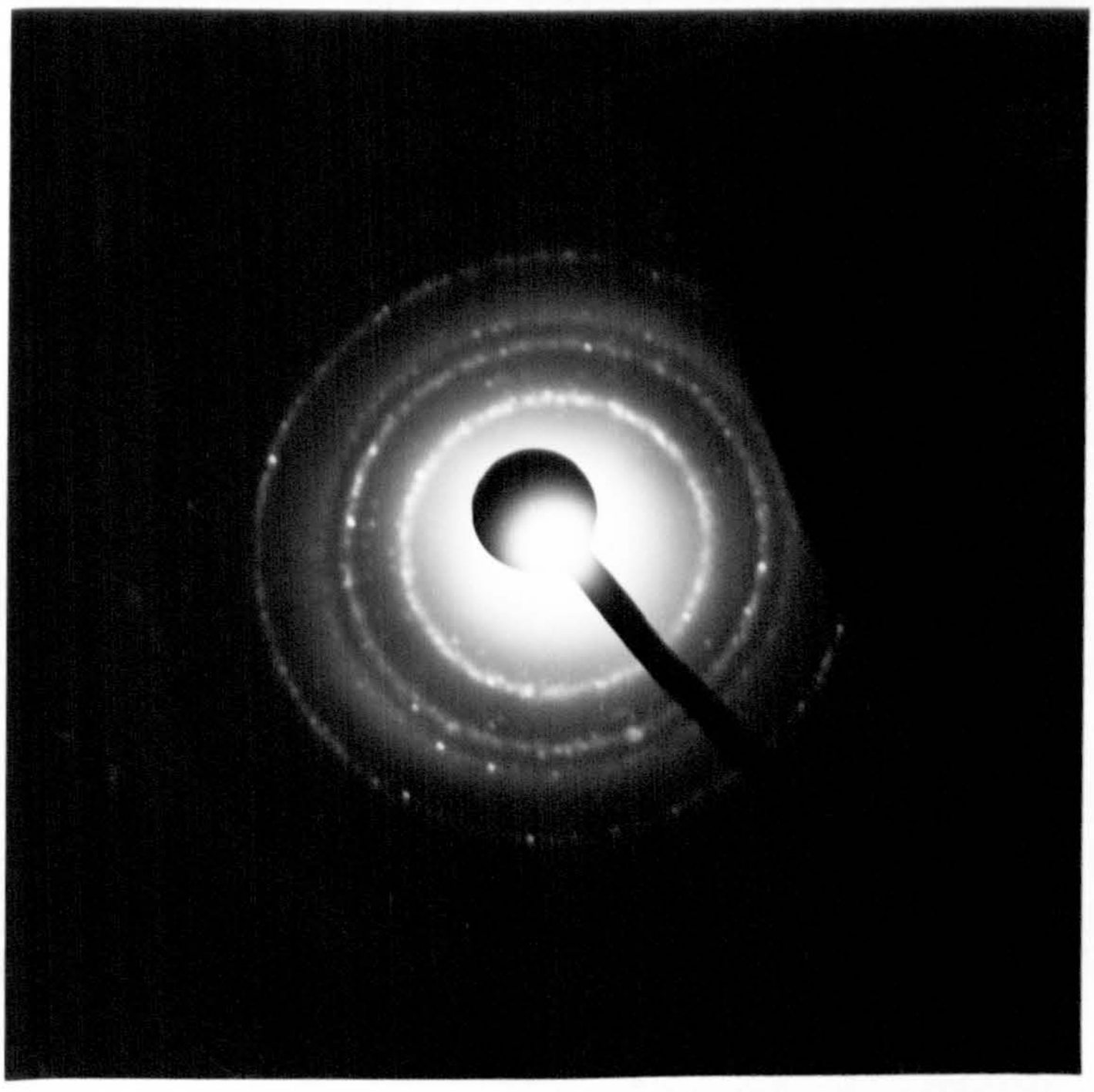

Fig.3.3.8(b) Corresponding electron diffraction pattern of Fig.3.3.8(a).

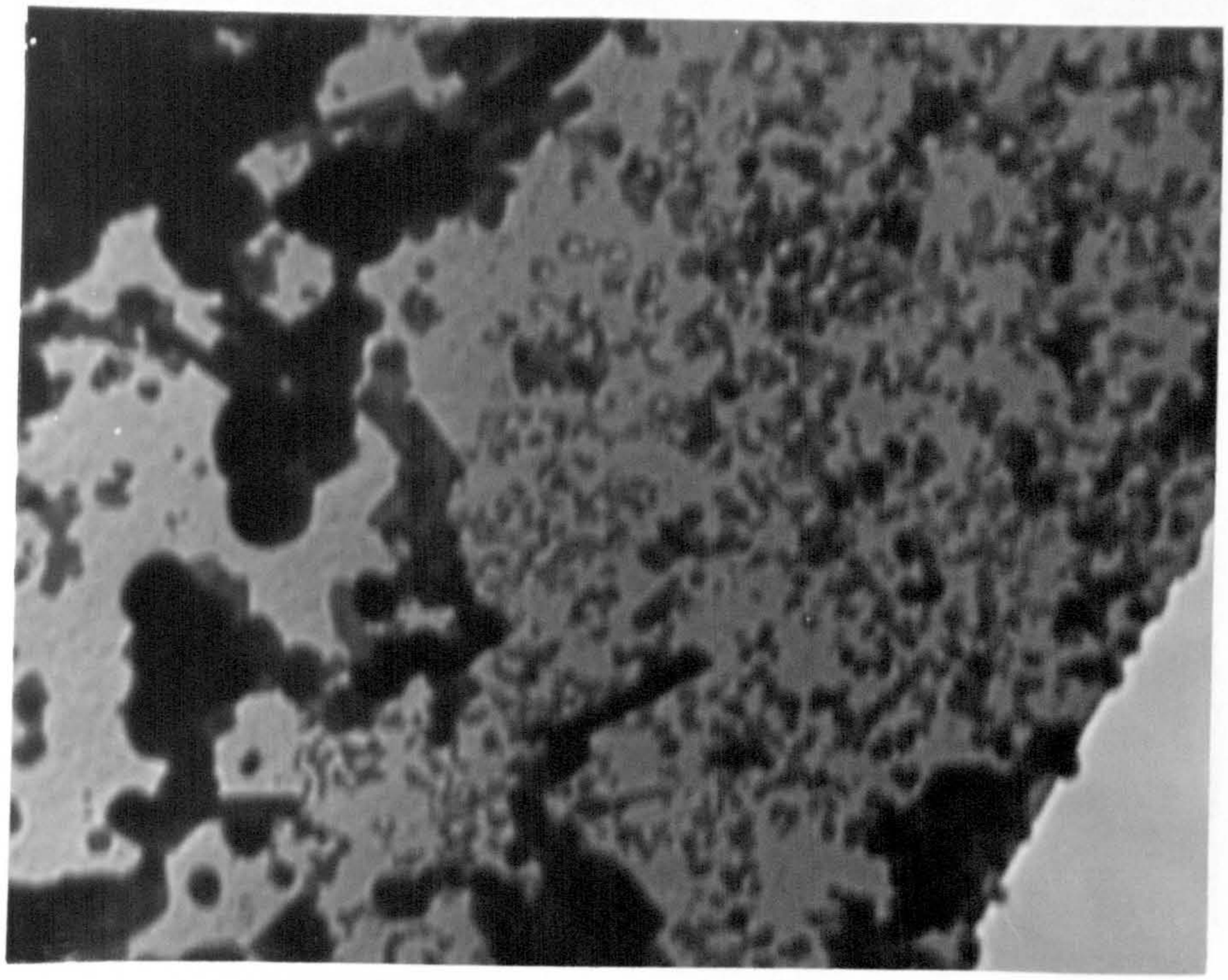

Fig.3.3.9(a) T.E.M. micrograph of the same sample of Fig.3.3.8 at 200°C after annealing for 65 minutes. Magnification: 76000X.

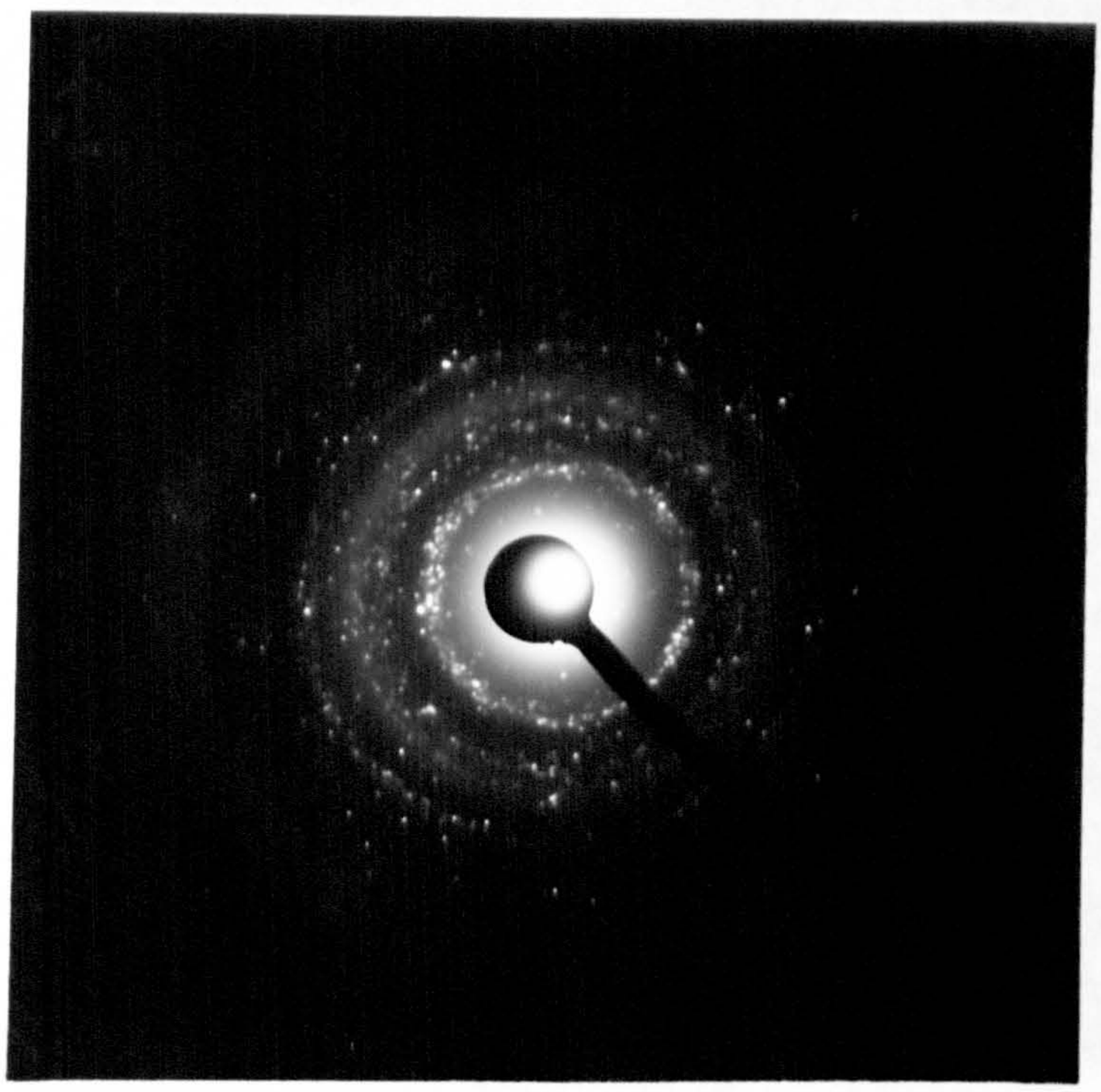

Fig.3.3.9(b) Corresponding electron diffraction pattern of Fig.3.3.9(a).

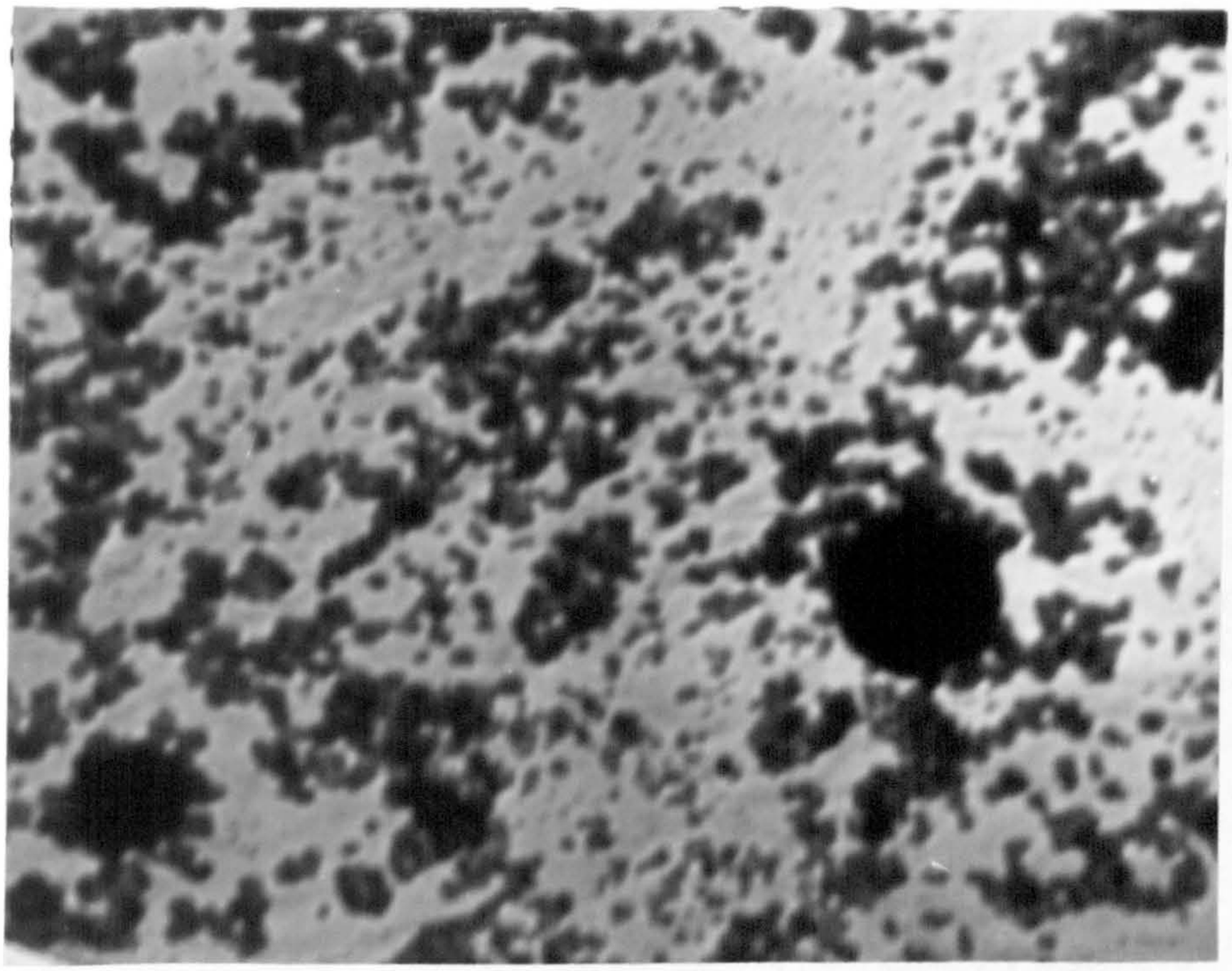

Fig.3.3.10(a) T.E.M. micrograph of the same sample (Fig.3.3.8) at 320°C after annealing for 65 minutes. Magnification: 76000X.

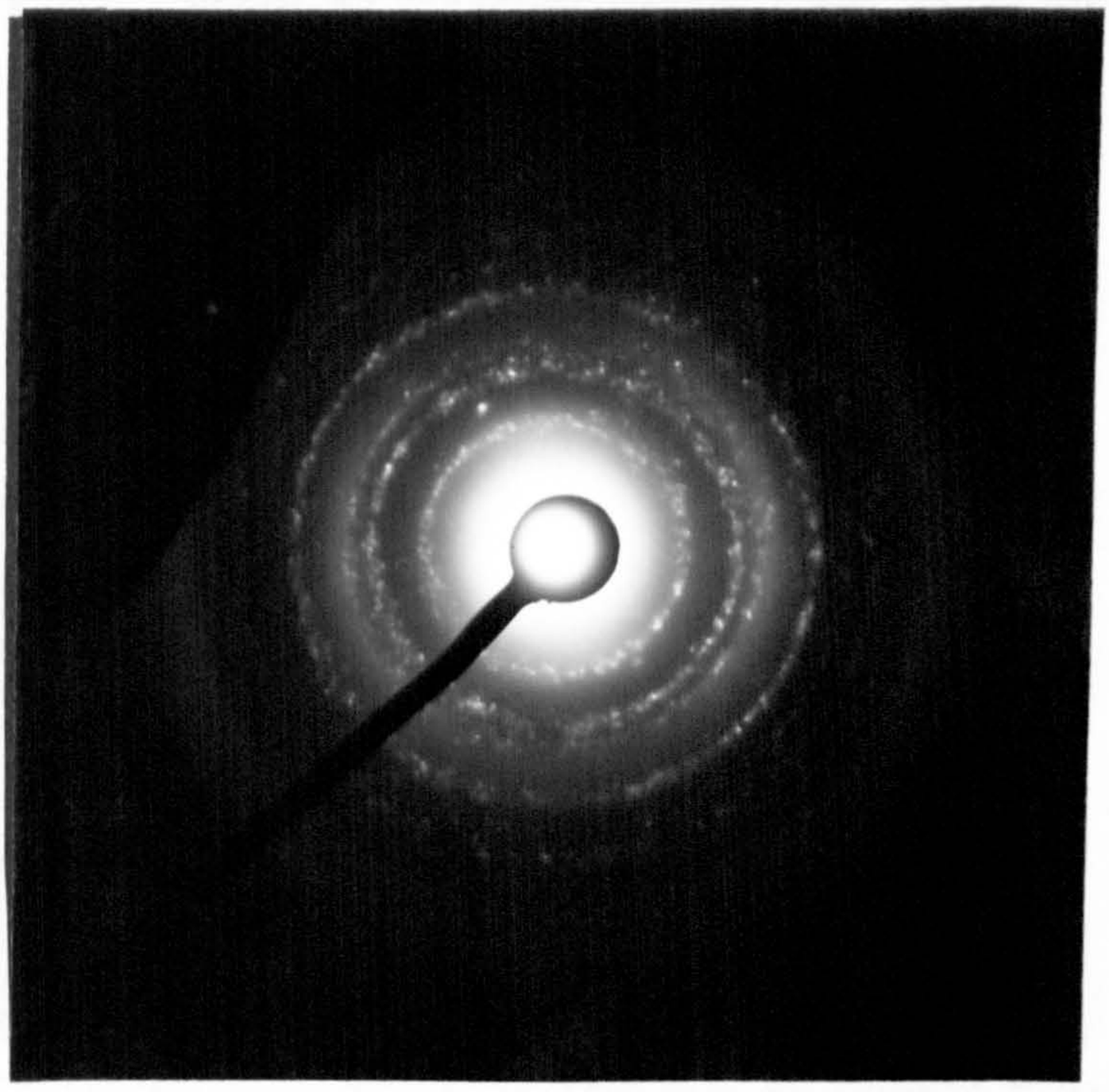

Fig.3.3.10(b) Corresponding electron diffraction pattern of Fig.3.3.10(a).

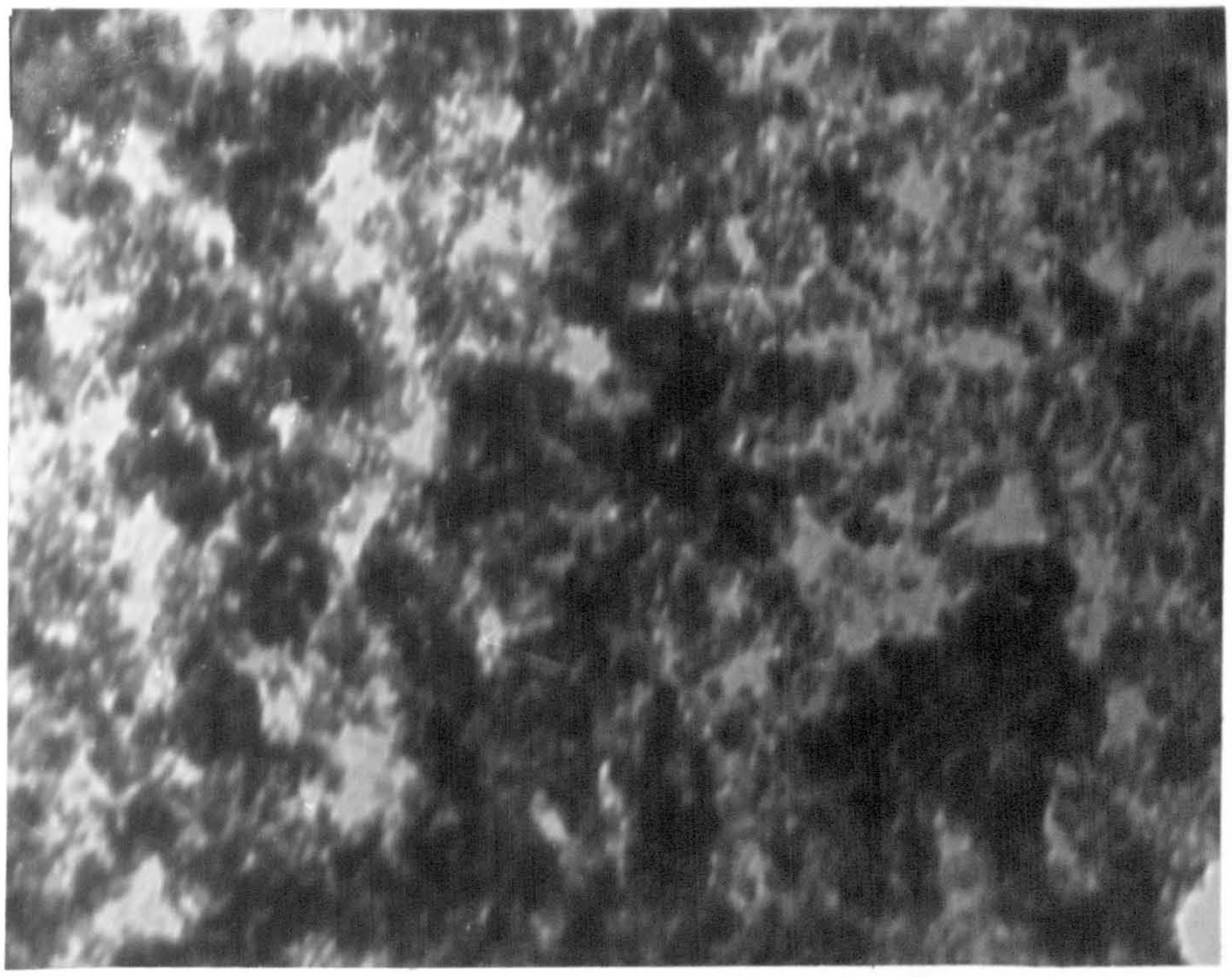

Fig.3.3.11(a) T.E.M. micrograph of the same sample (Fig.3.3.8) at room temperature after annealing at 320°C for 2 hours. Magnification: 76000X.

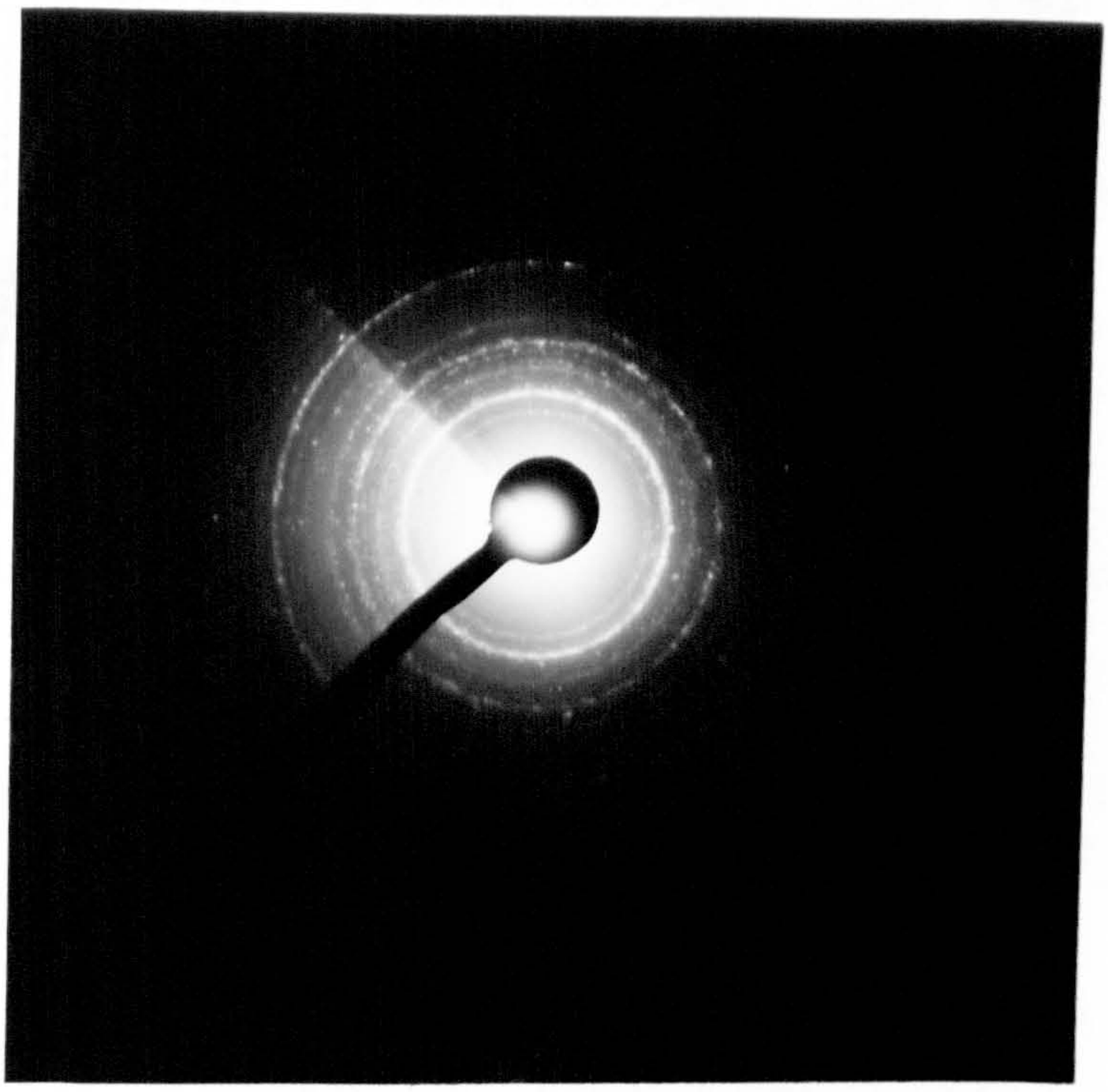

Fig.3.3.11(b) Corresponding electron diffraction pattern of Fig.3.3.11(a).

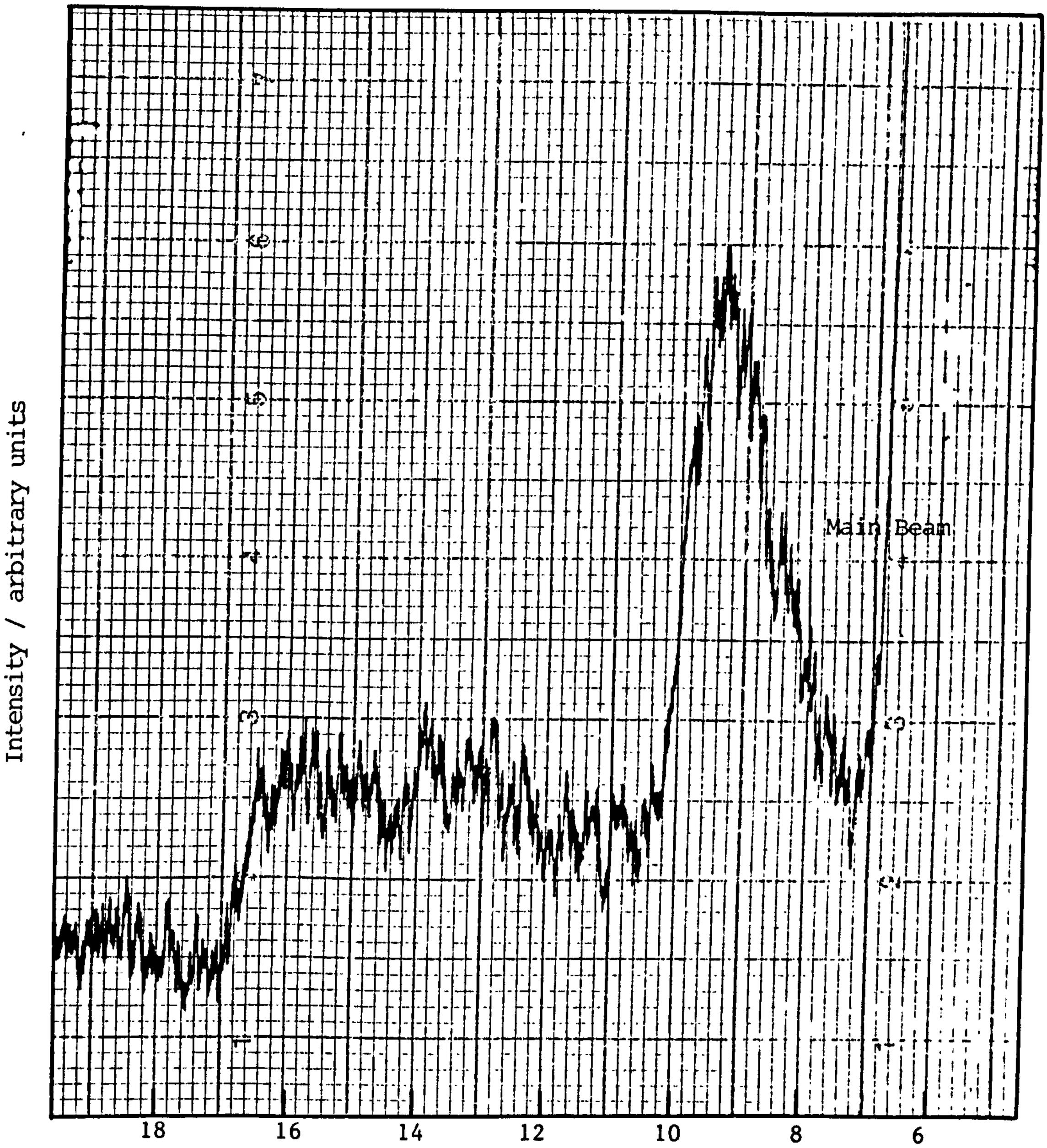

Fig.3.4.1 X-ray diffraction pattern of Mo-black coating on aluminium substrate using Co $K\alpha$ radiation. (λ = 0.179 nm)

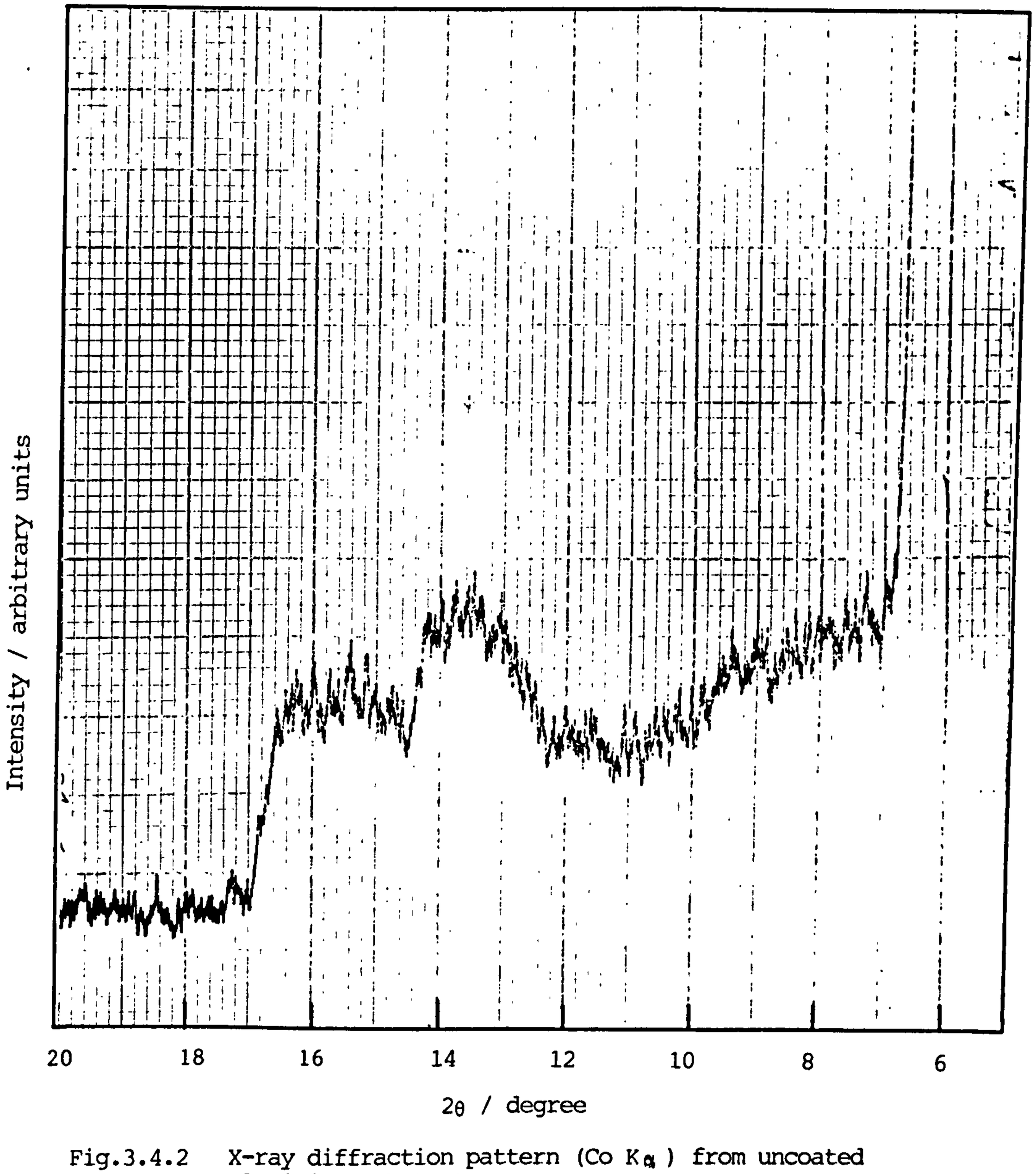

Fig.3.4.2 X-ray diffraction pattern (Co K_α) from uncoated aluminium substrate.

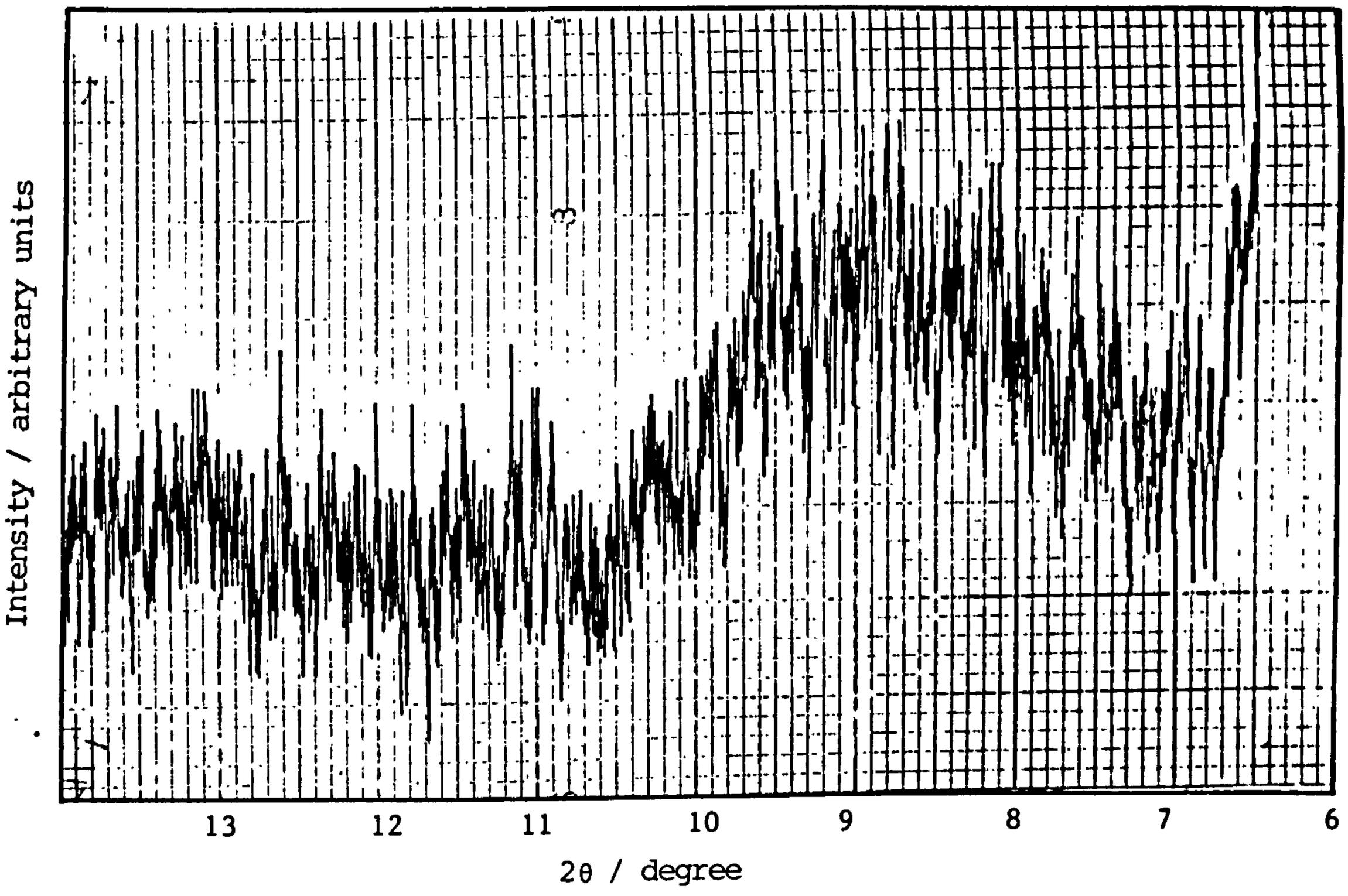

Fig.3.4.3 X-ray diffraction pattern from Mo-black dip coating on zinc substrate.

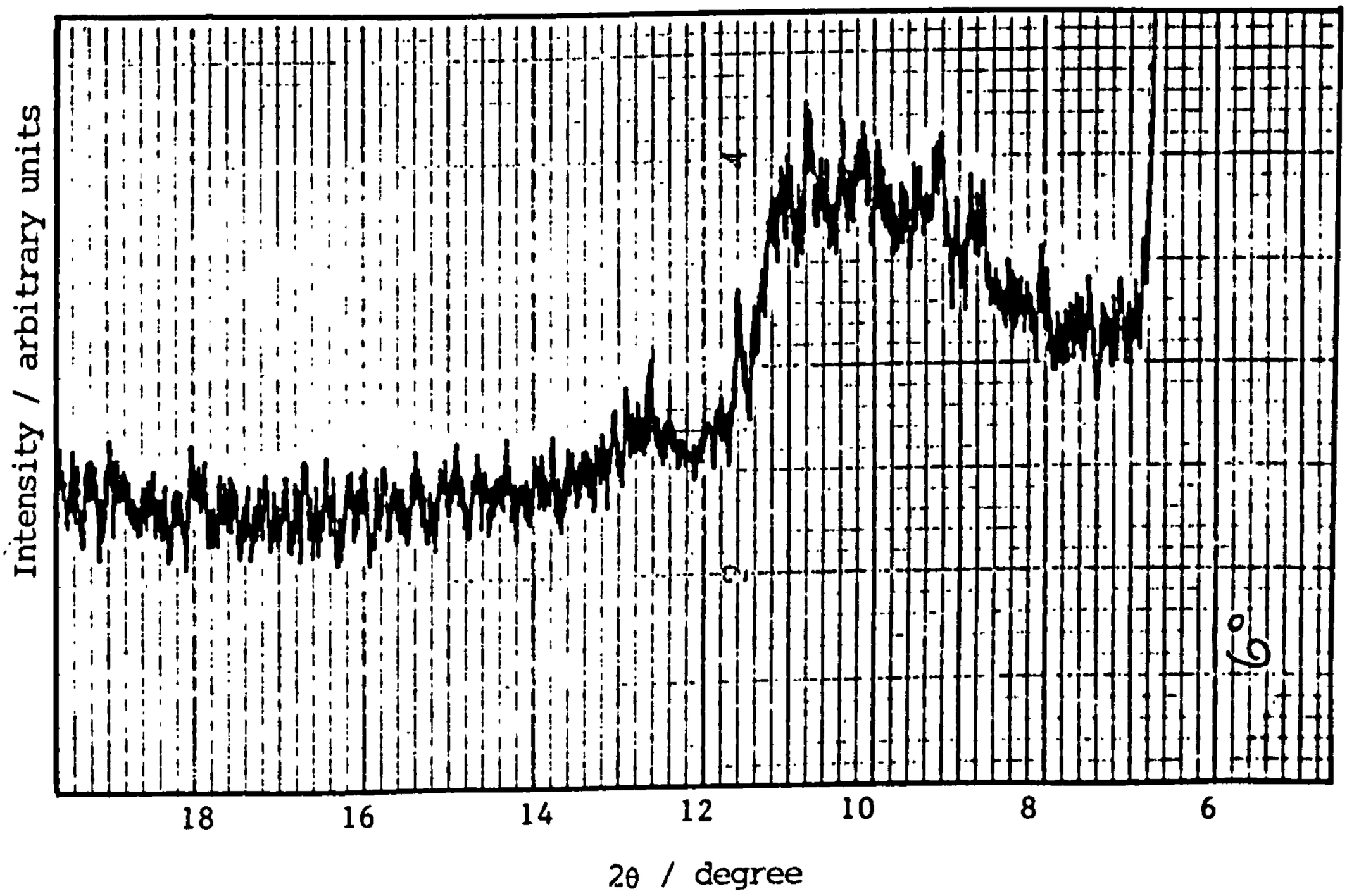

Fig.3.4.4 X-ray diffraction pattern from Mo-black dip coating on cobalt (NC) substrate.

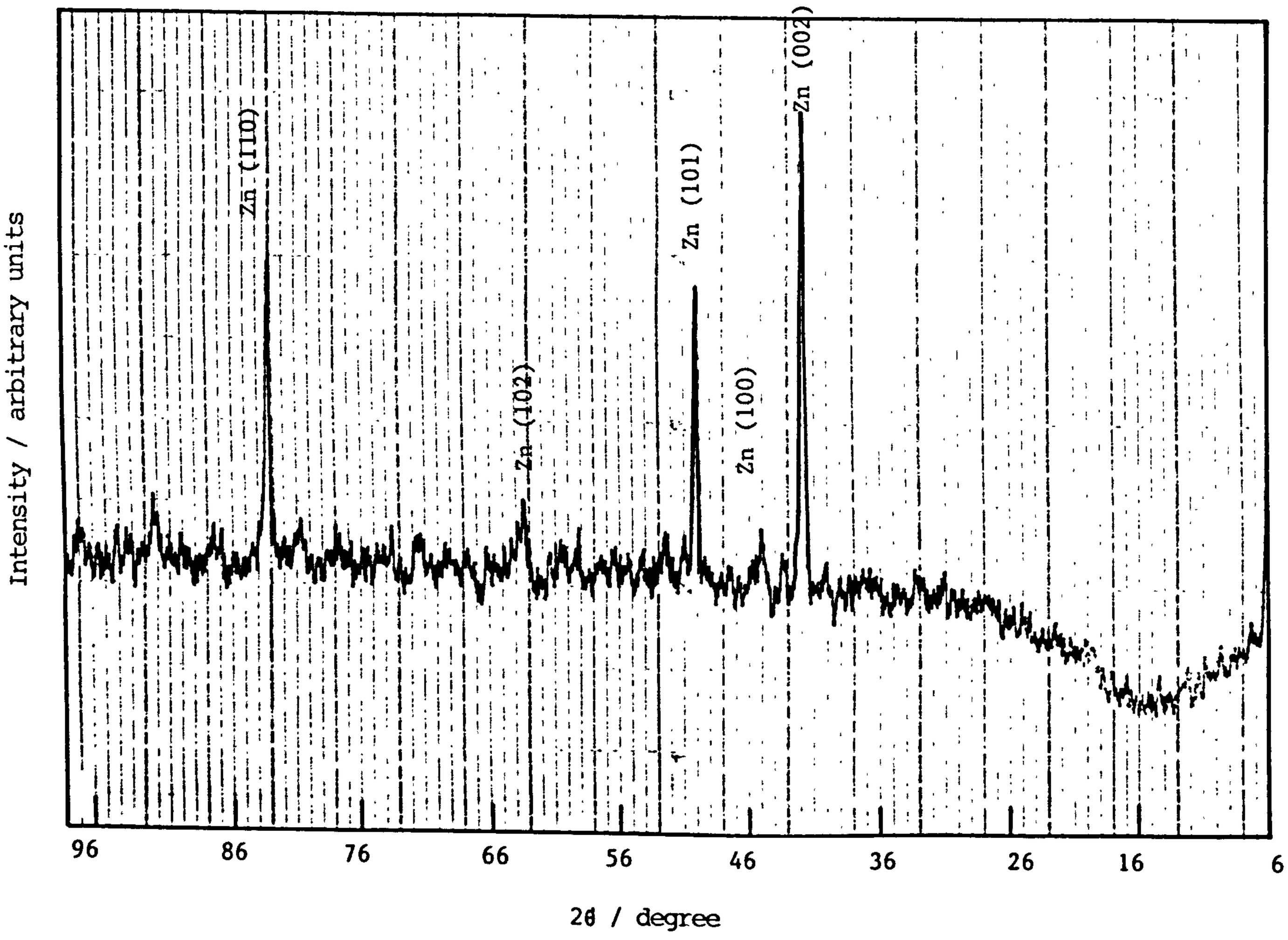

Fig.3.4.5 X-ray diffraction pattern from Mo-black dip coating on etched zinc substrate.

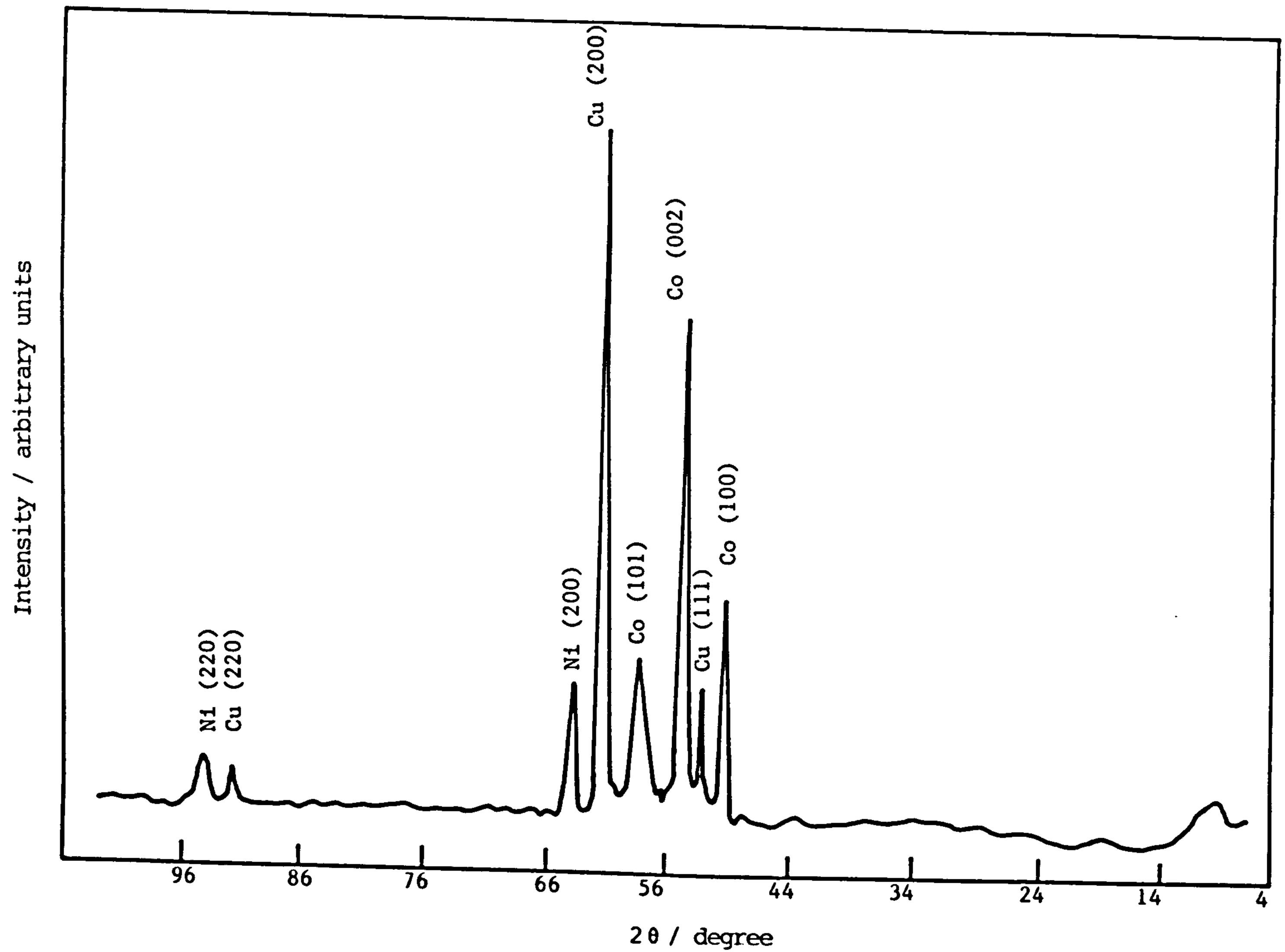

Fig.3.4.6 X-ray diffraction pattern from Mo-black coating on cobalt (NC) substrate.

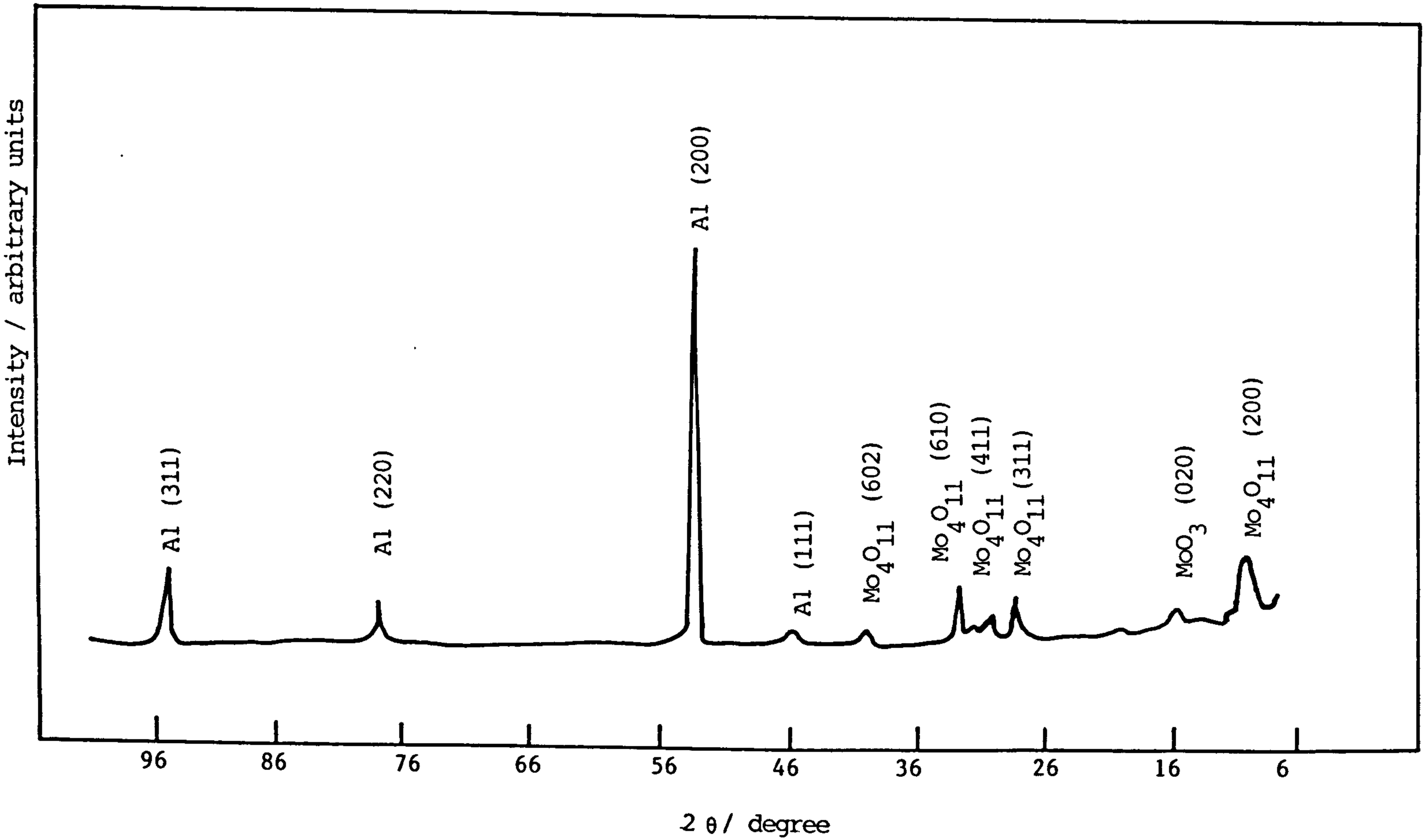

Fig.3.4.7 X-ray diffraction pattern (Co K_α) from electrodeposited Mo-black coating on aluminium substrate after heating in air at 400°C for 8 hours.

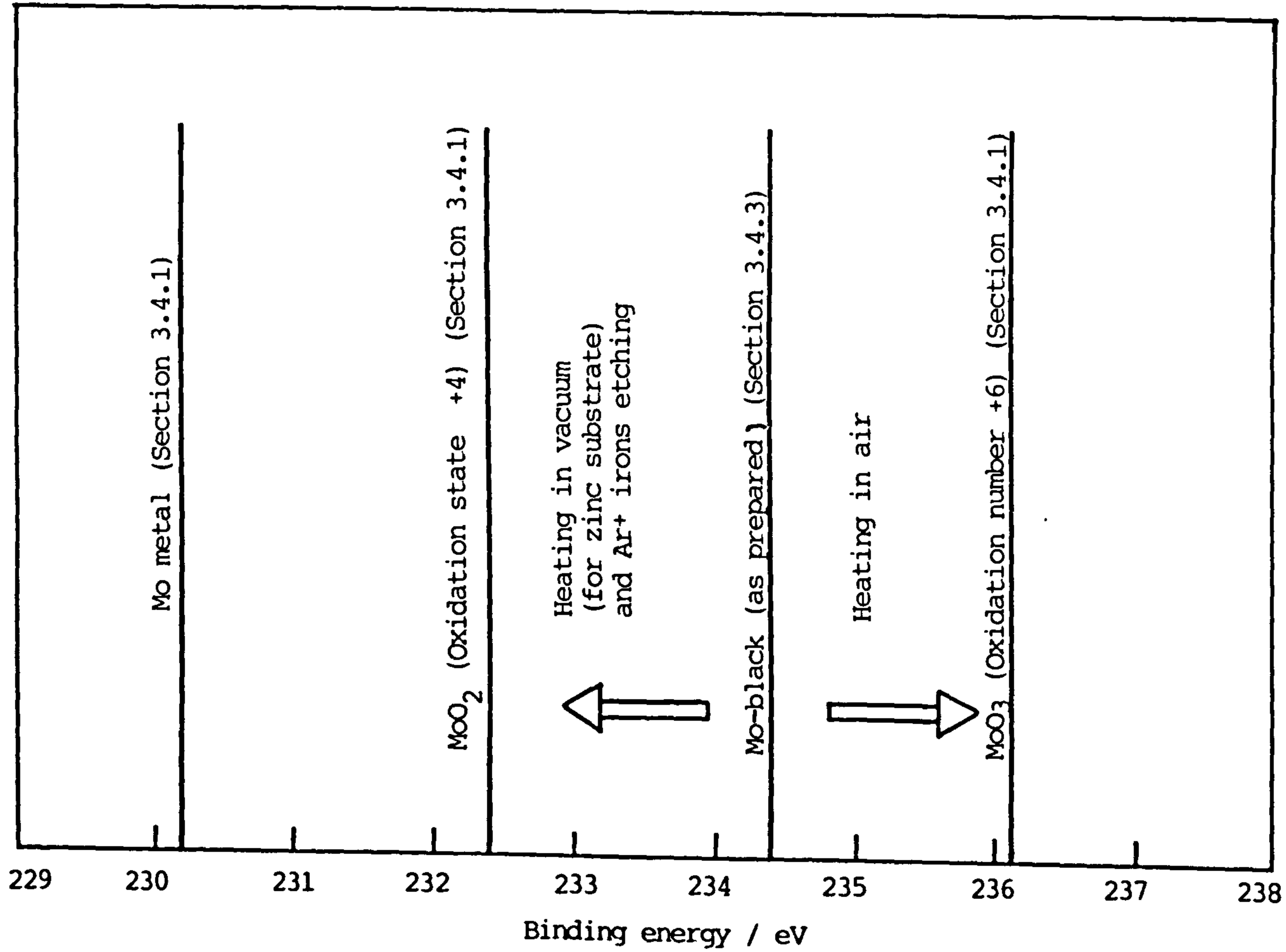

Fig.3.5.0 Schematic diagram showing the relative position of the Mo $3d_{3/2}$ XPS peaks for Mo-metal, MoO_2, MoO_3 and Mo-black coatings after various treatments

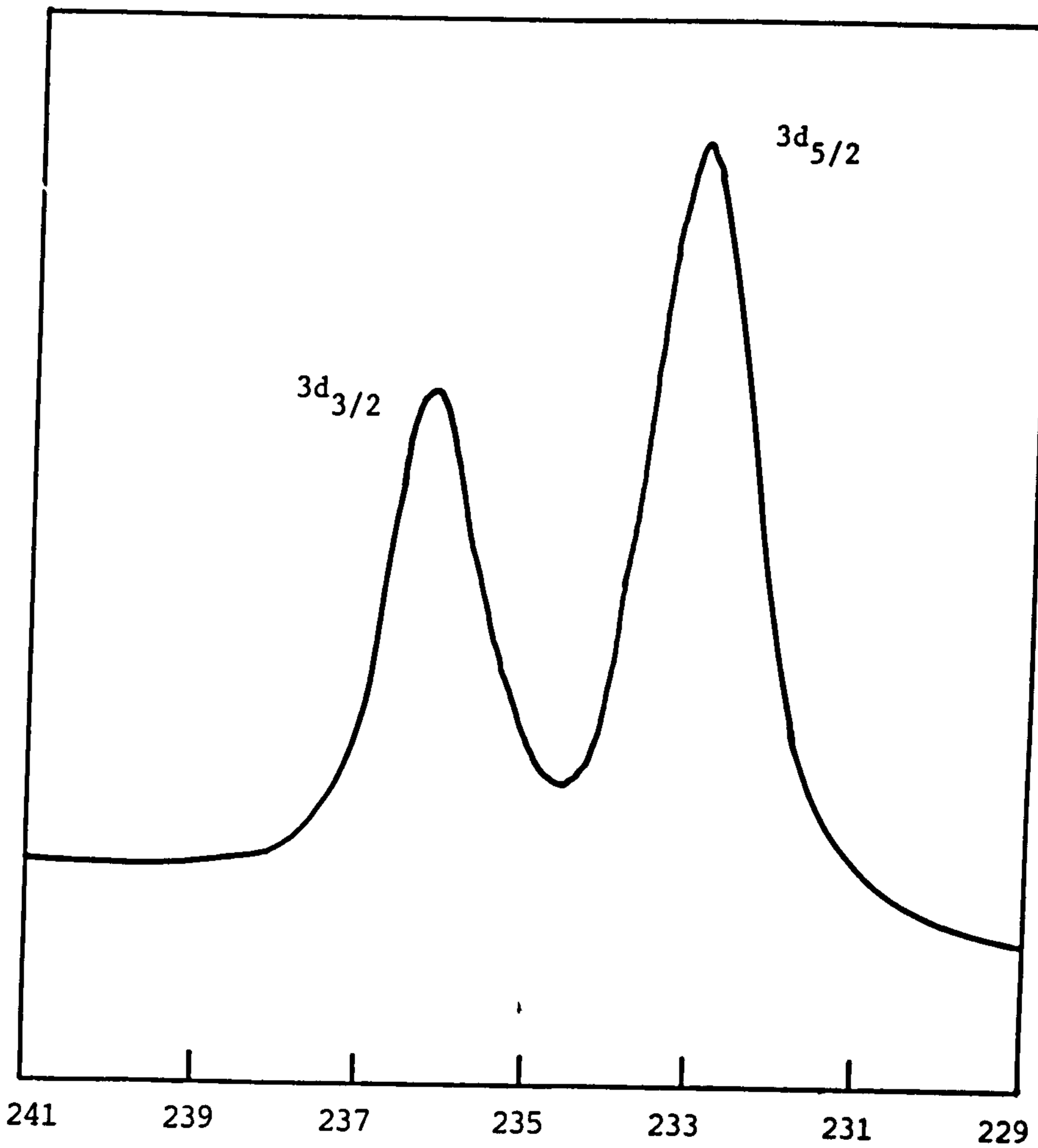

Fig.3.5.1 Narrow scan spectrum of Mo 3d doublet of MoO_3

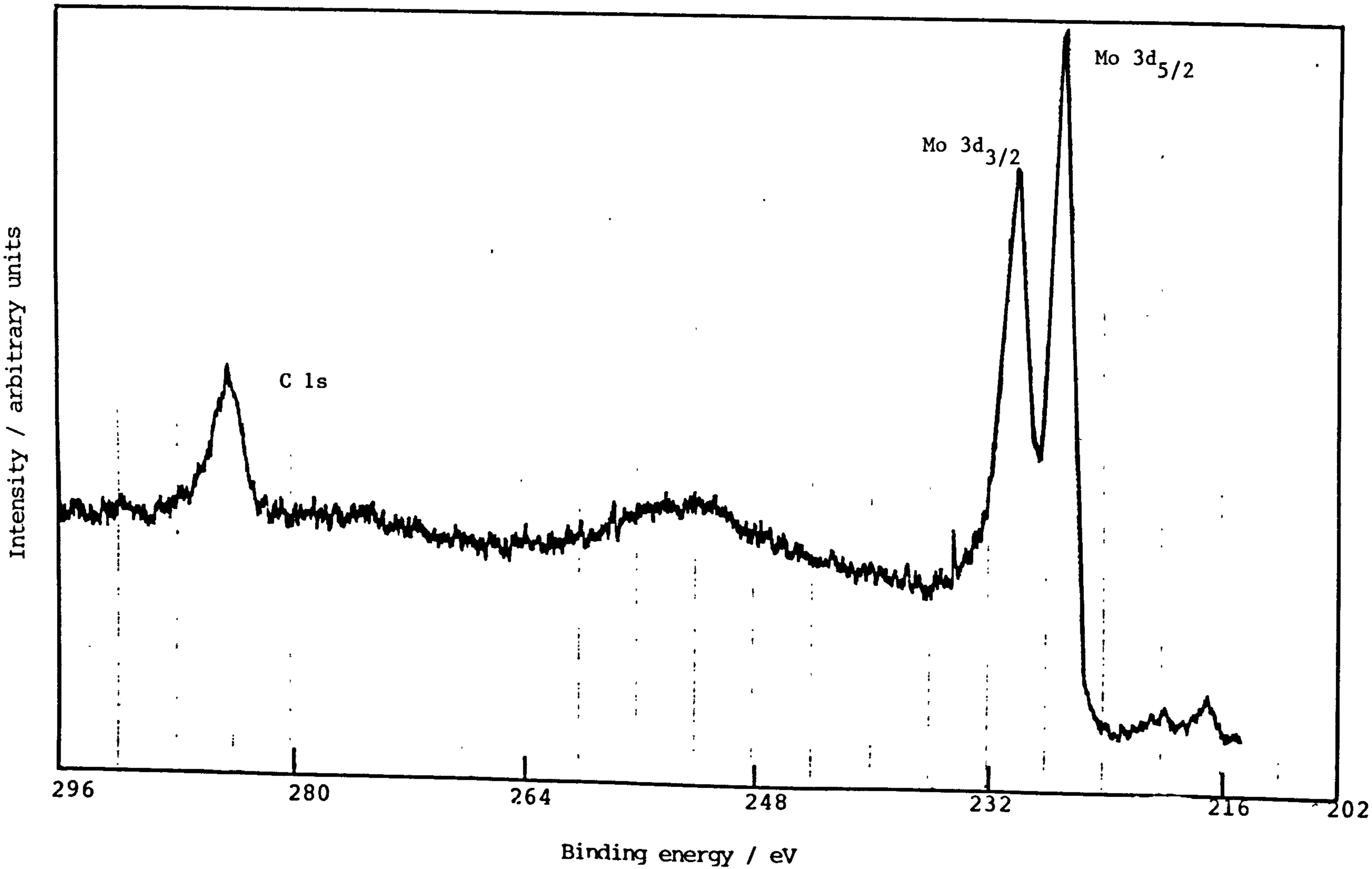

Fig.3.5.2 X-ray photoelectron spectrum of Mo 3d doublet and C 1s obtained from Mo-metal foil.

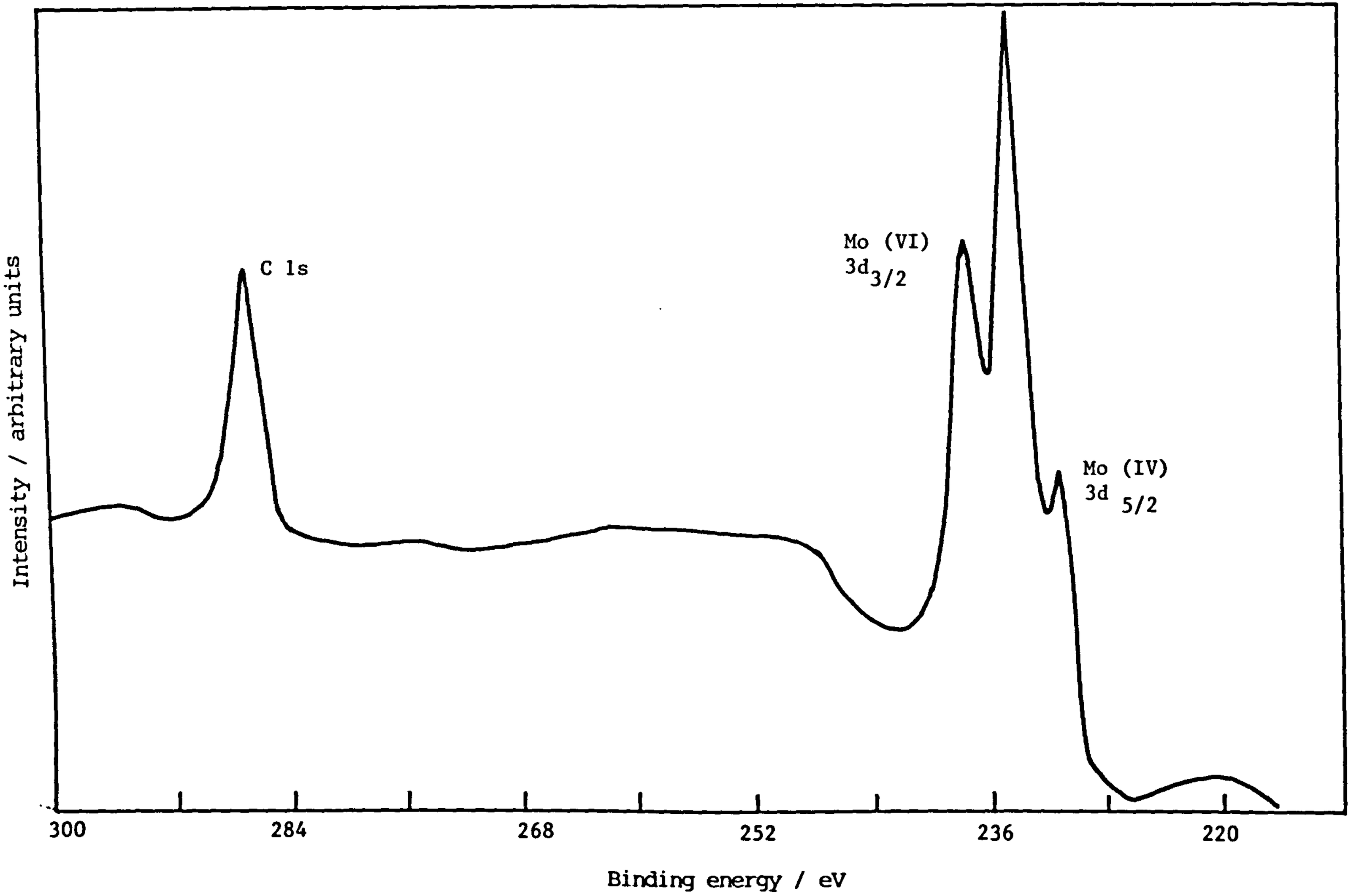

Fig.3.5.3 Photoelectron spectrum of Mo 3d doublet and C 1s peak obtained from MoO_2 powder.

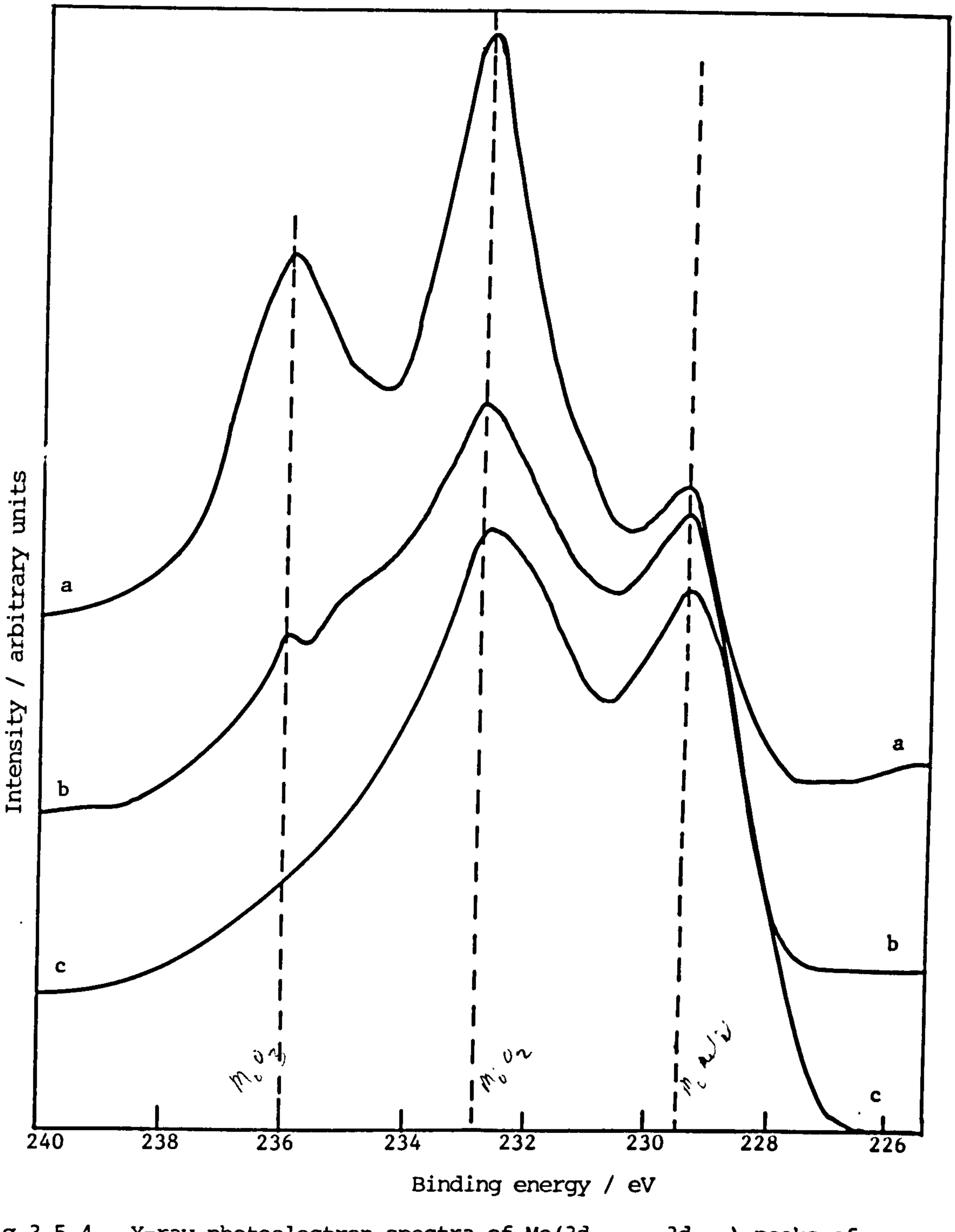

Fig.3.5.4 X-ray photoelectron spectra of Mo($3d_{3/2}$ - $3d_{5/2}$) peaks of MoO_2 powder;

(a) before exposure to Ar^+ ions,
(b) after exposure to Ar^+ ions for 10 minutes,
(c) after exposure to Ar^+ ions for 30 minutes.

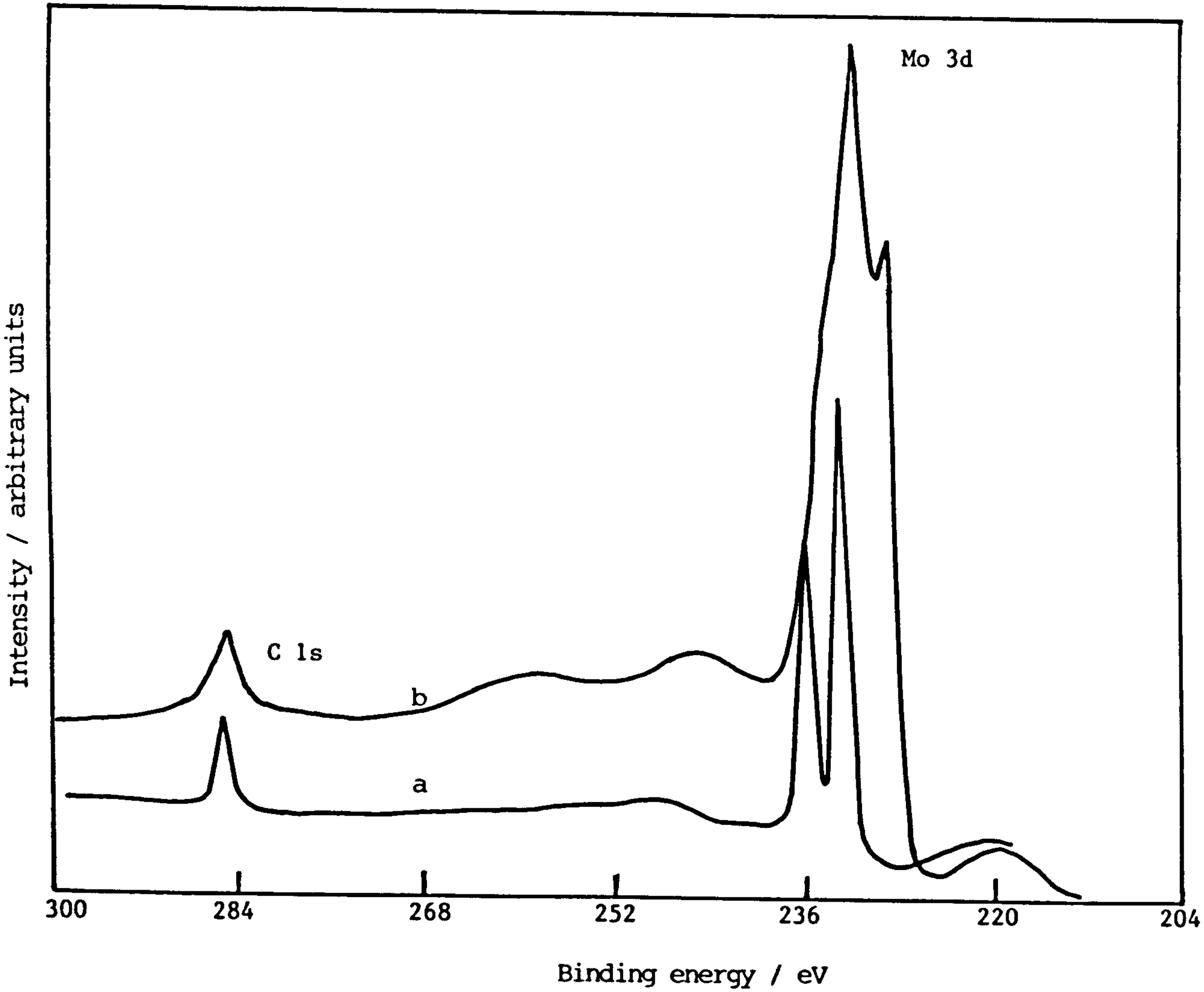

Fig.3.5.5 X-ray photoelectron spectrum of Mo3d doublet and C 1s obtained from MoO_3 powder; (a) before etching, (b) after etching with Ar^+ ions for 10 minutes.

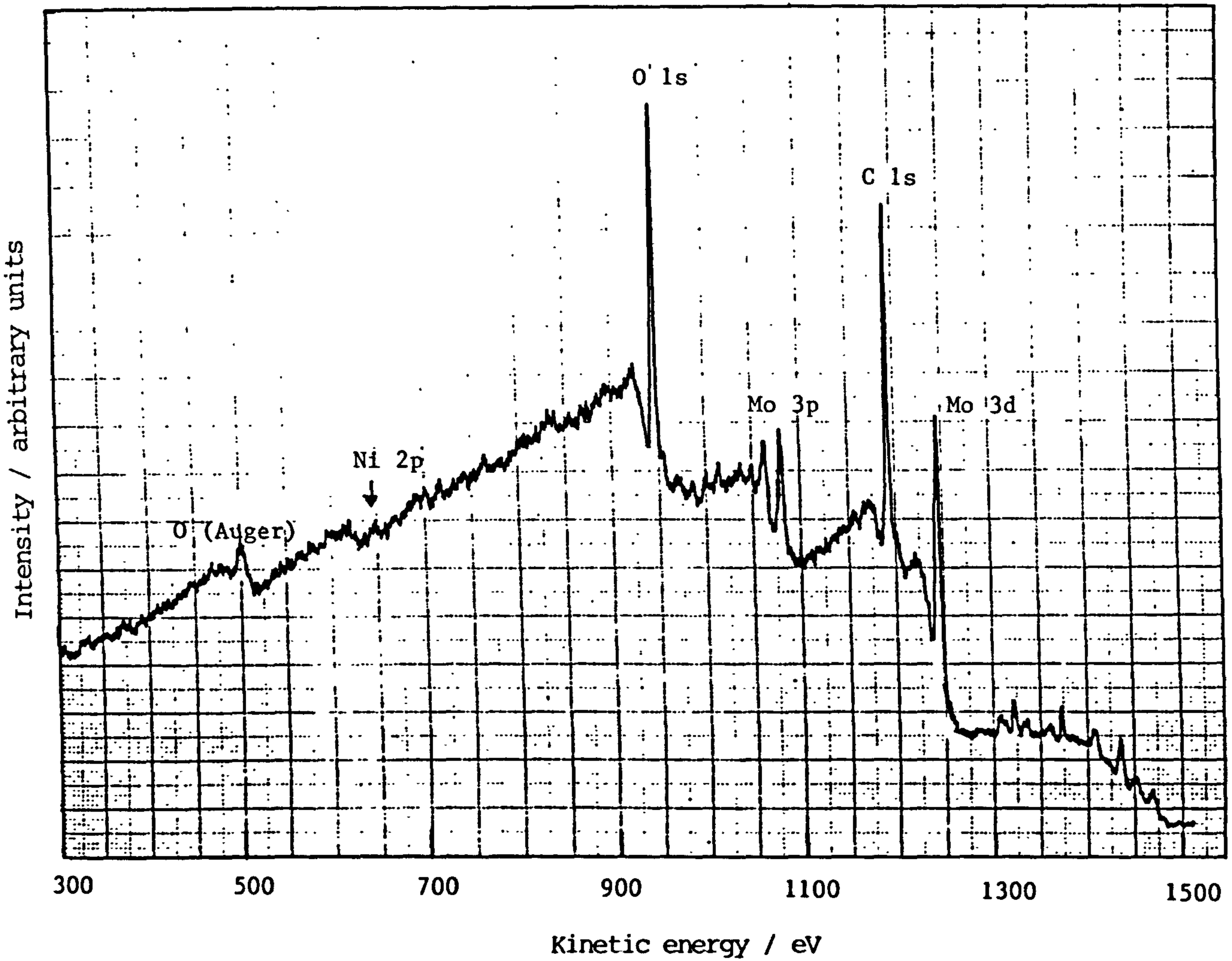

Fig.3.5.6 Survey scan spectrum of Mo-black coating on aluminium substrate.

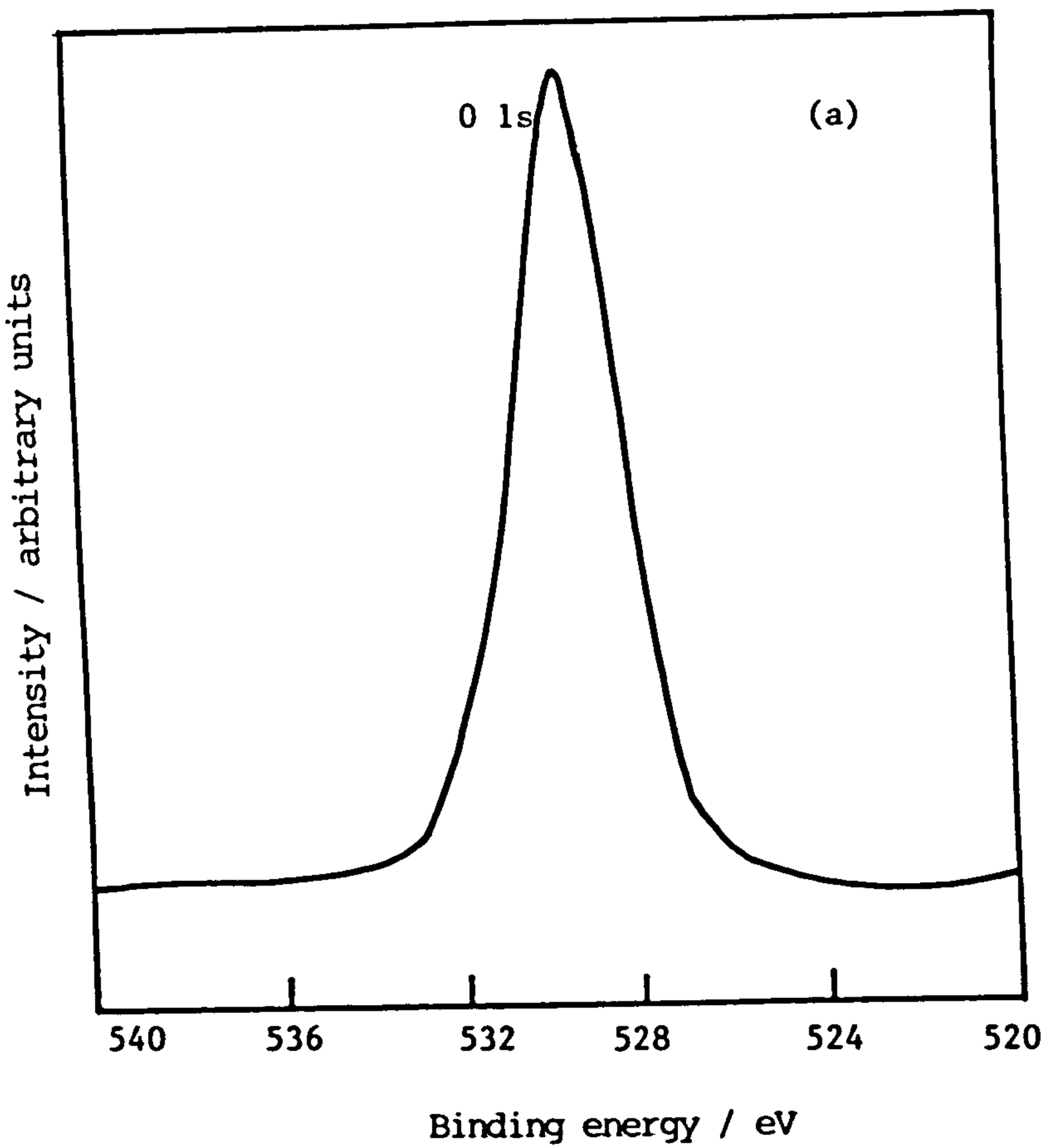

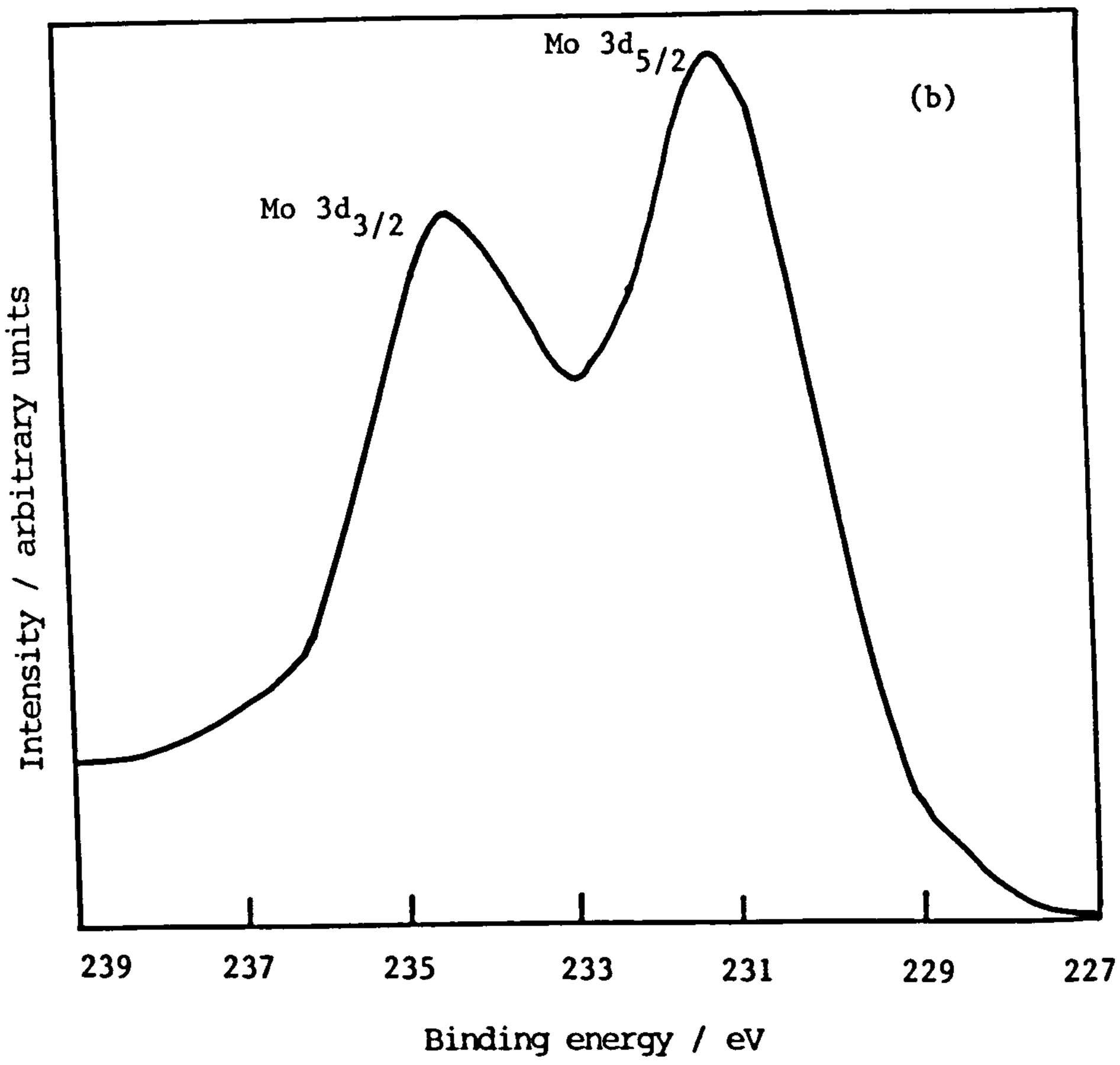

Fig.3.5.7 Narrow scan spectra of (a) 0 1s peak and (b) Mo 3d doublet obtained from Mo-black coating on an aluminium substrate.

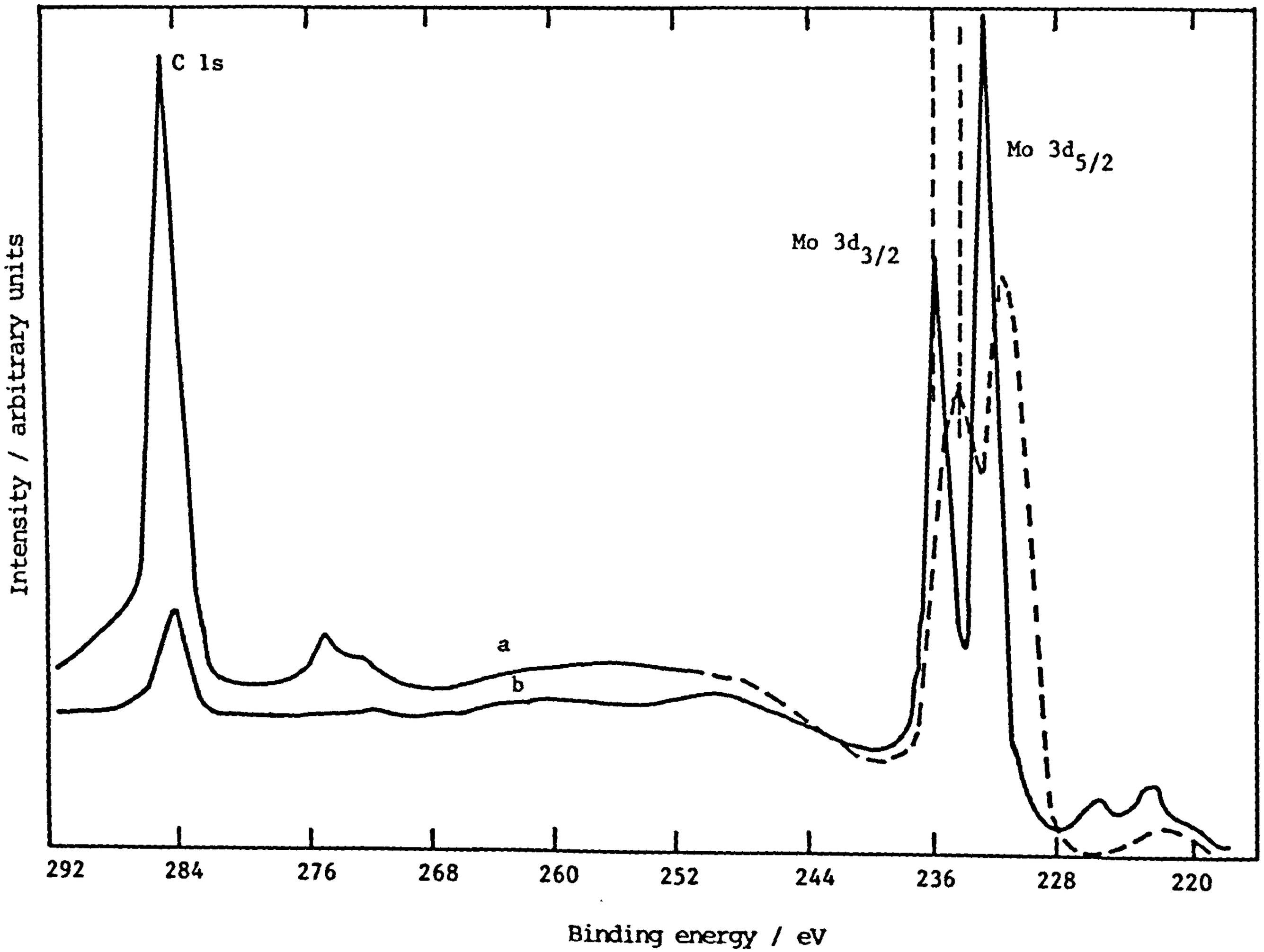

Fig.3.5.8 X-ray photoelectron spectra of Mo 3d doublet and C 1s;

(a) Mo-black coating
(b) MoO_3 powder

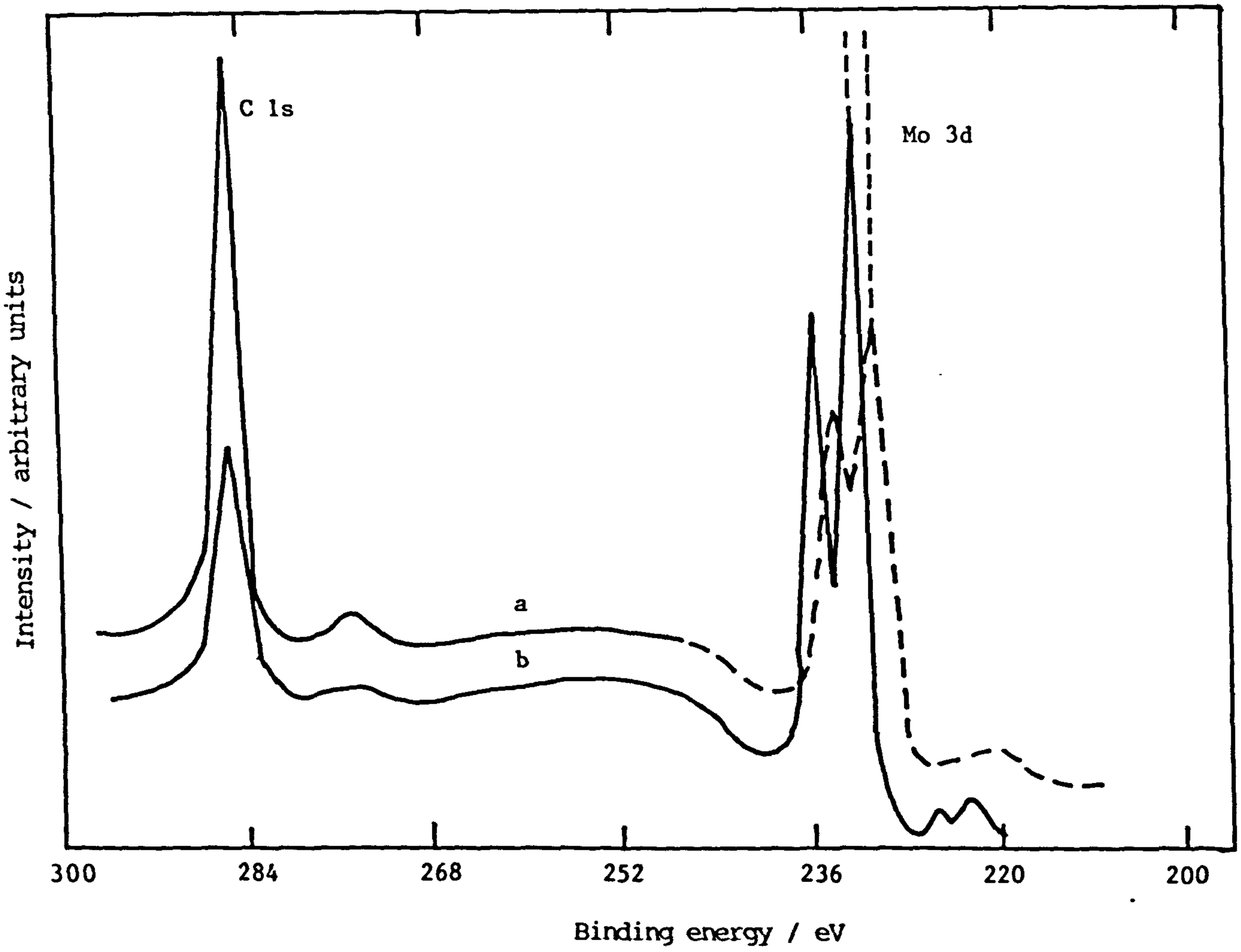

Fig.3.5.9 X-ray photoelectron spectra of Mo 3d doublet and C 1s obtained from Mo-black coating on aluminium substrate; (a) as-prepared, (b) after heating in air at 400°C for 2 hours.

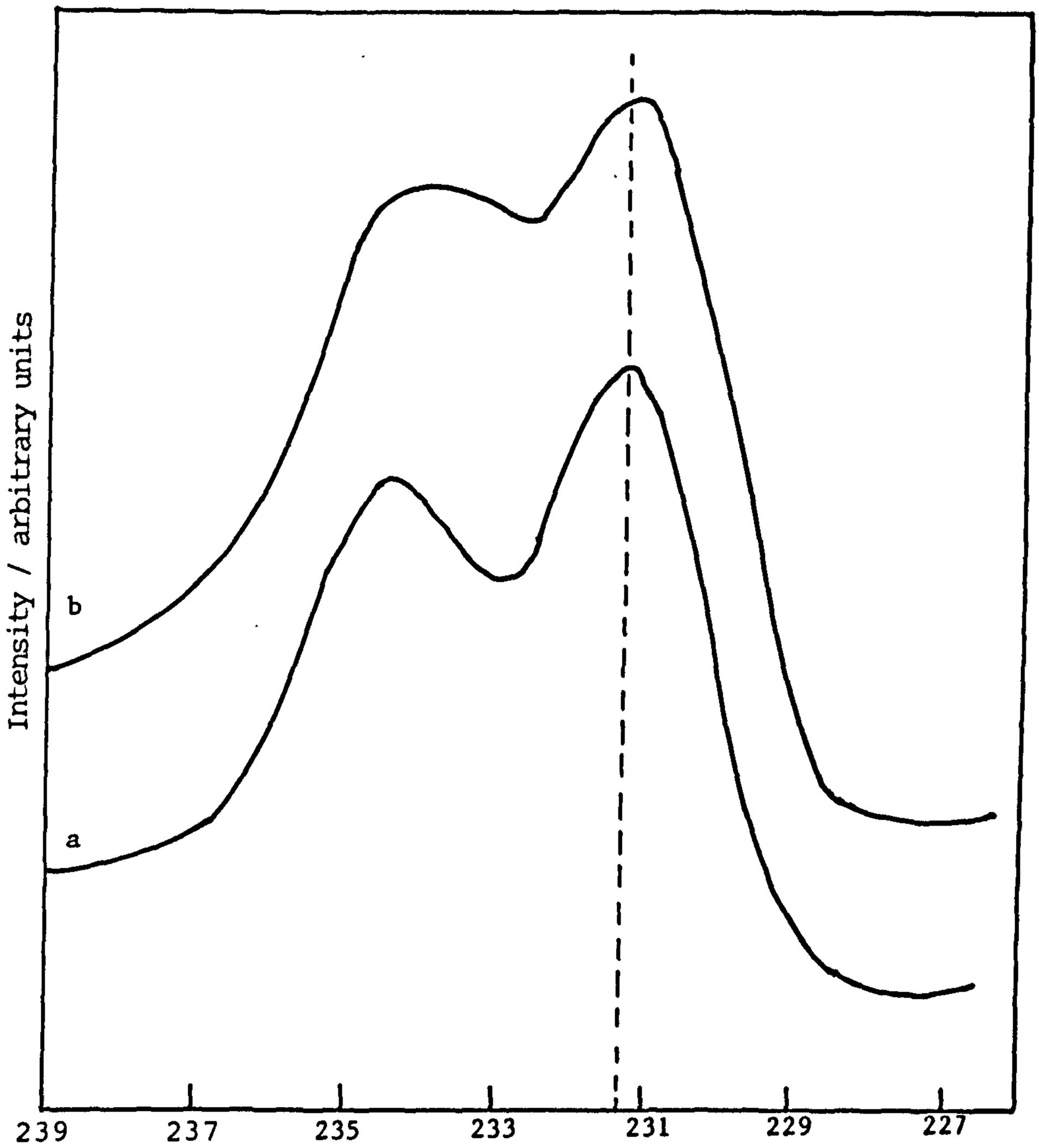

Fig.3.5.10 X-ray photoelectron spectra of Mo 3d doublet of Mo-black coating on aluminium substrate;
(a) before heat treatment,
(b) after heating inside the spectrometer at a temperature of 450°C for 2 hours.

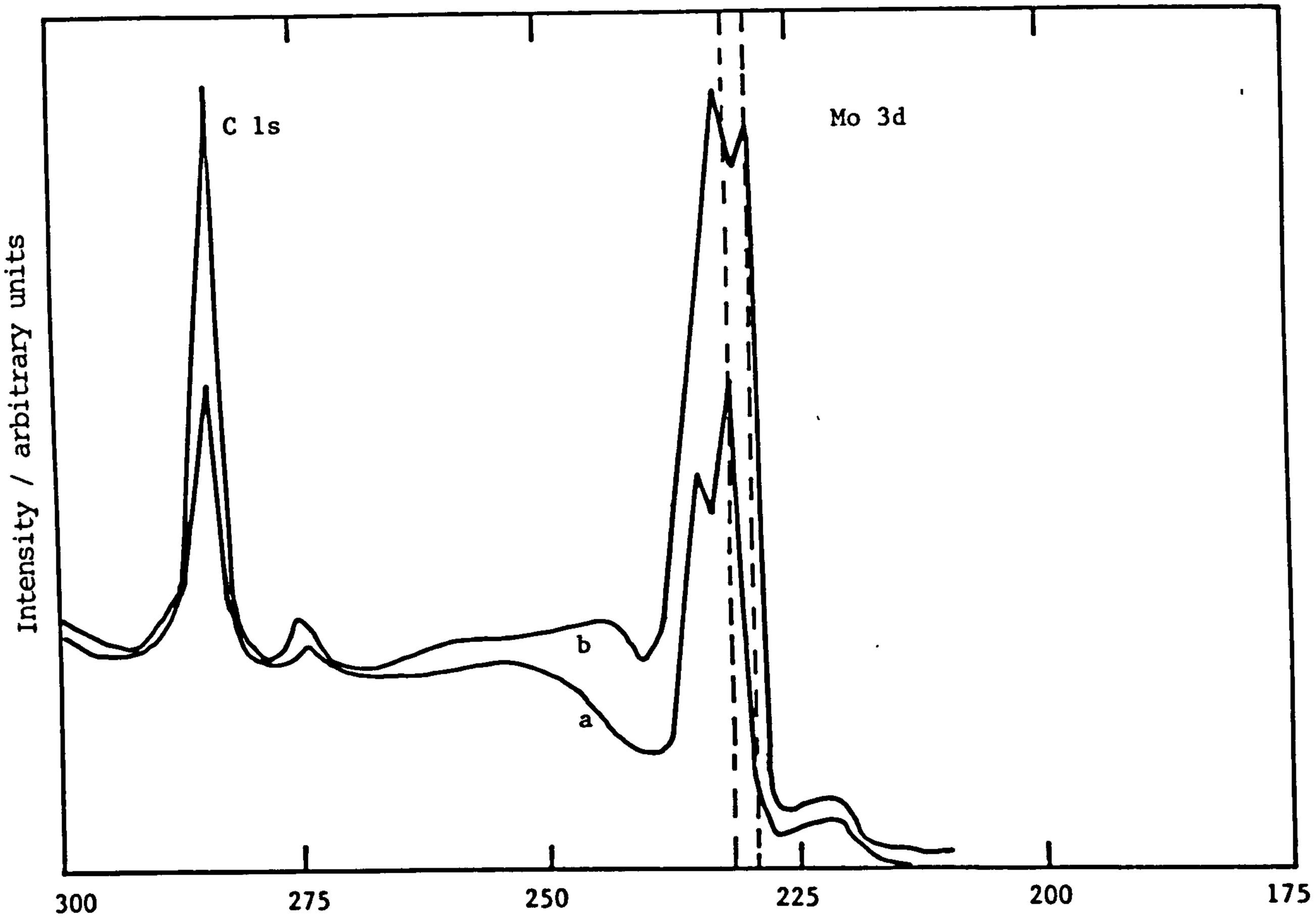

Fig.3.5.11 X-ray photoelectron spectra of Mo 3d doublet and C 1s obtained from Mo-black coating on aluminium substrate;
(a) as prepared,
(b) after etching with Ar^+ for 10 minutes.

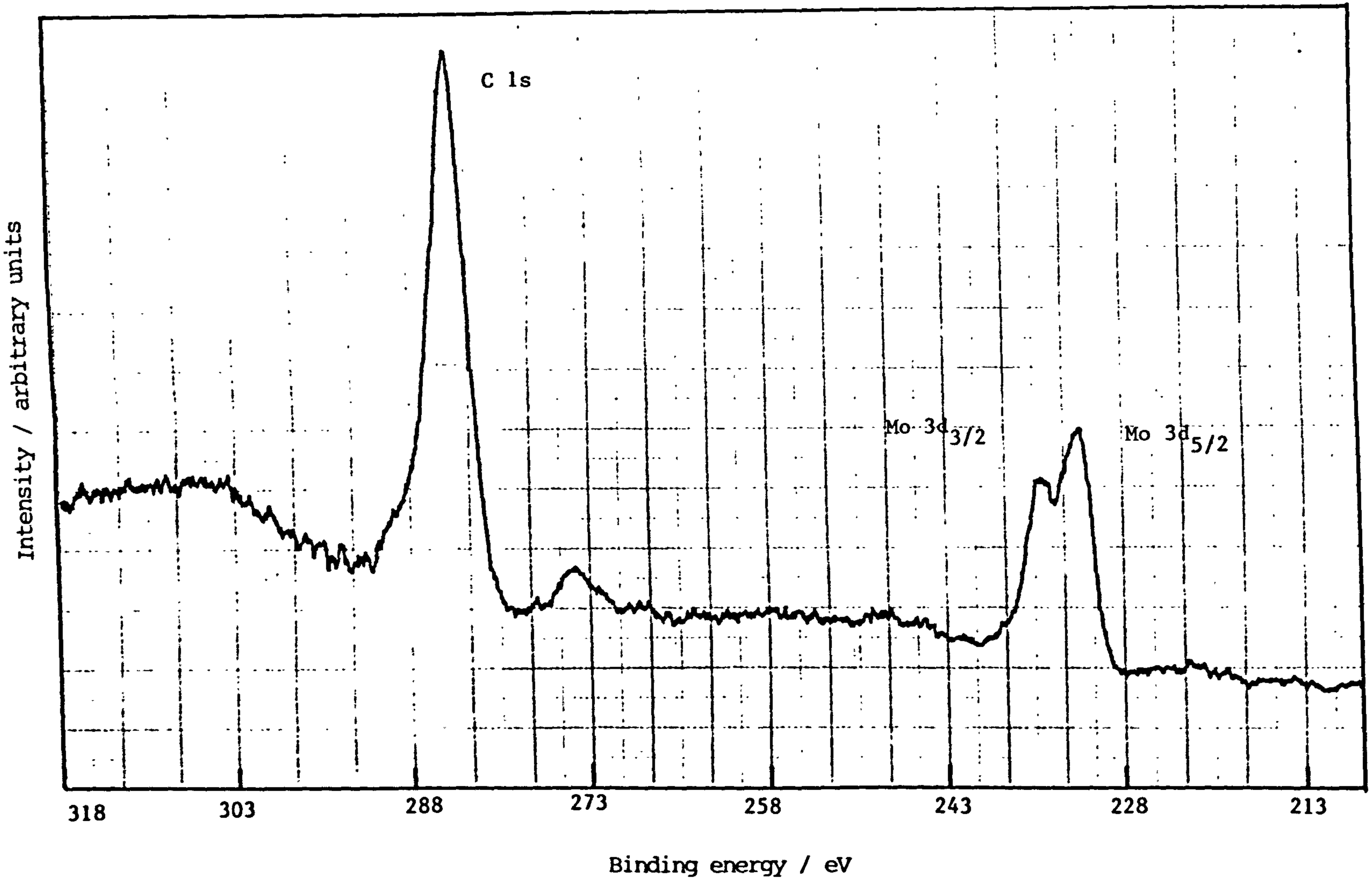

Fig.3.5.12 X-ray photoelectron spectra of Mo 3d doublet and C 1s obtained from the interface of the Mo-black coating on Aluminium.

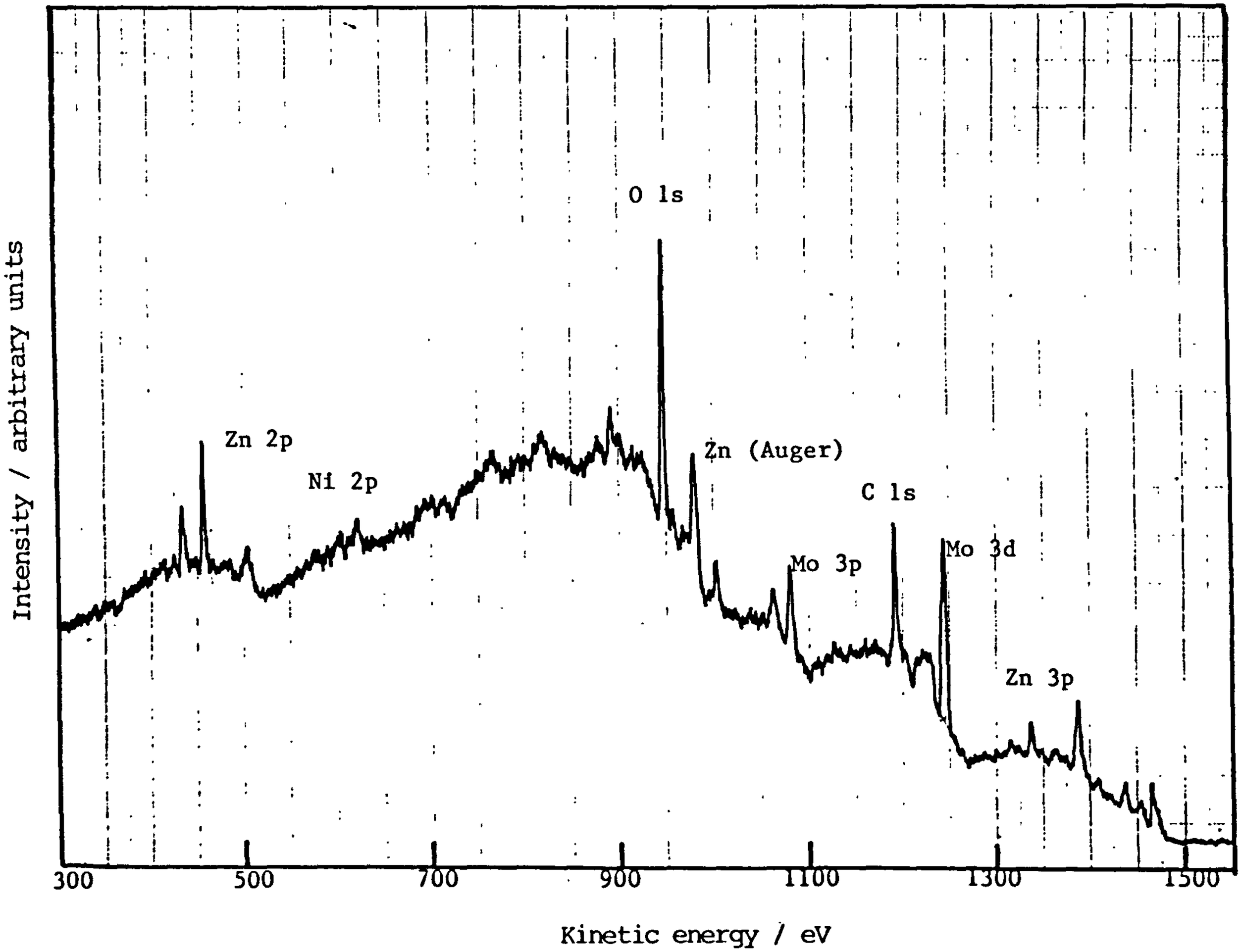

Fig.3.5.13(a) A typical survey scan spectrum of a Mo-black dip coating on zinc substrate. (take off angle = 70°).

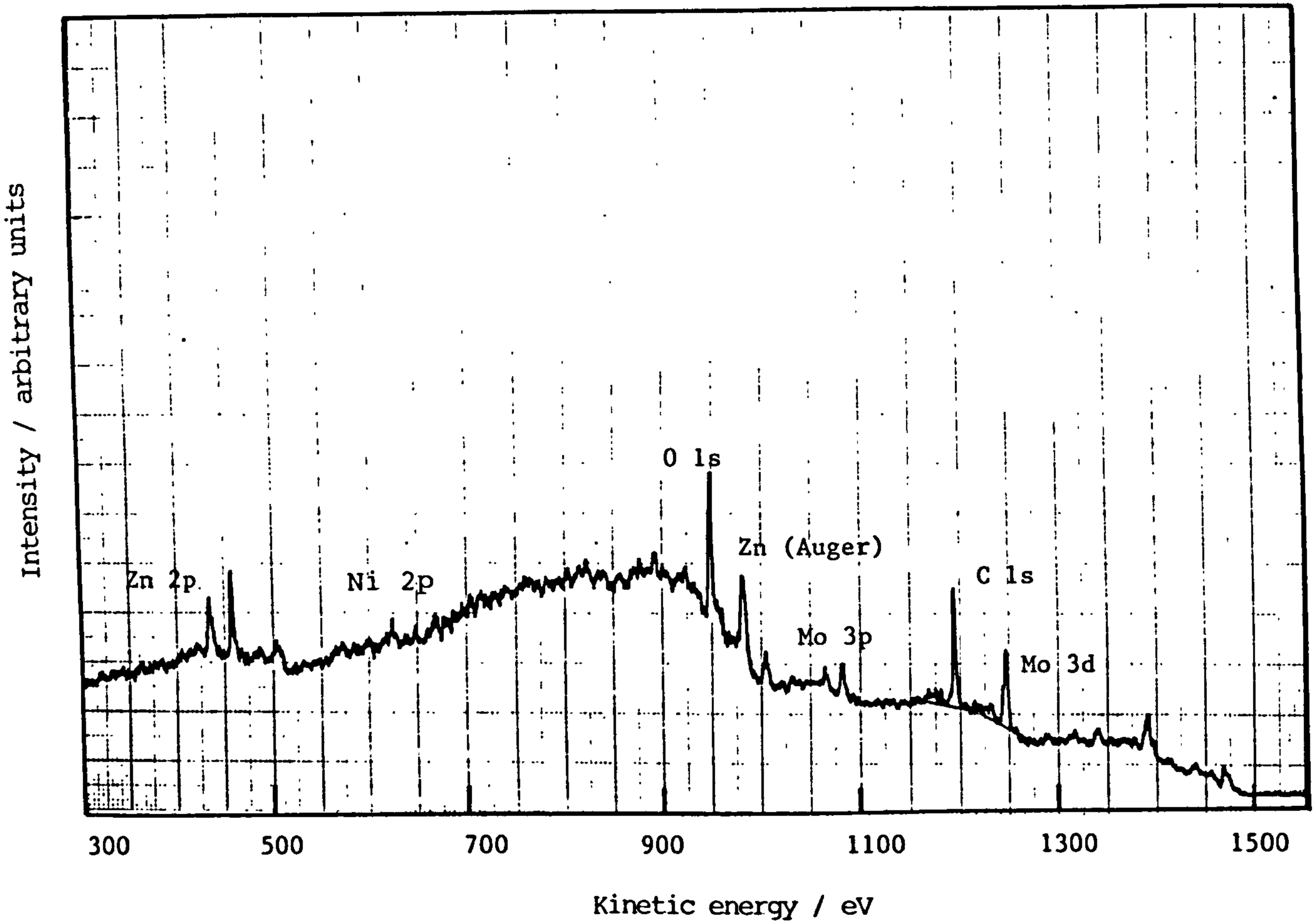

Fig.3.5.13(b) Survey scan spectrum of the same coating (Fig.3.4.13.a) at take off angle = 20°.

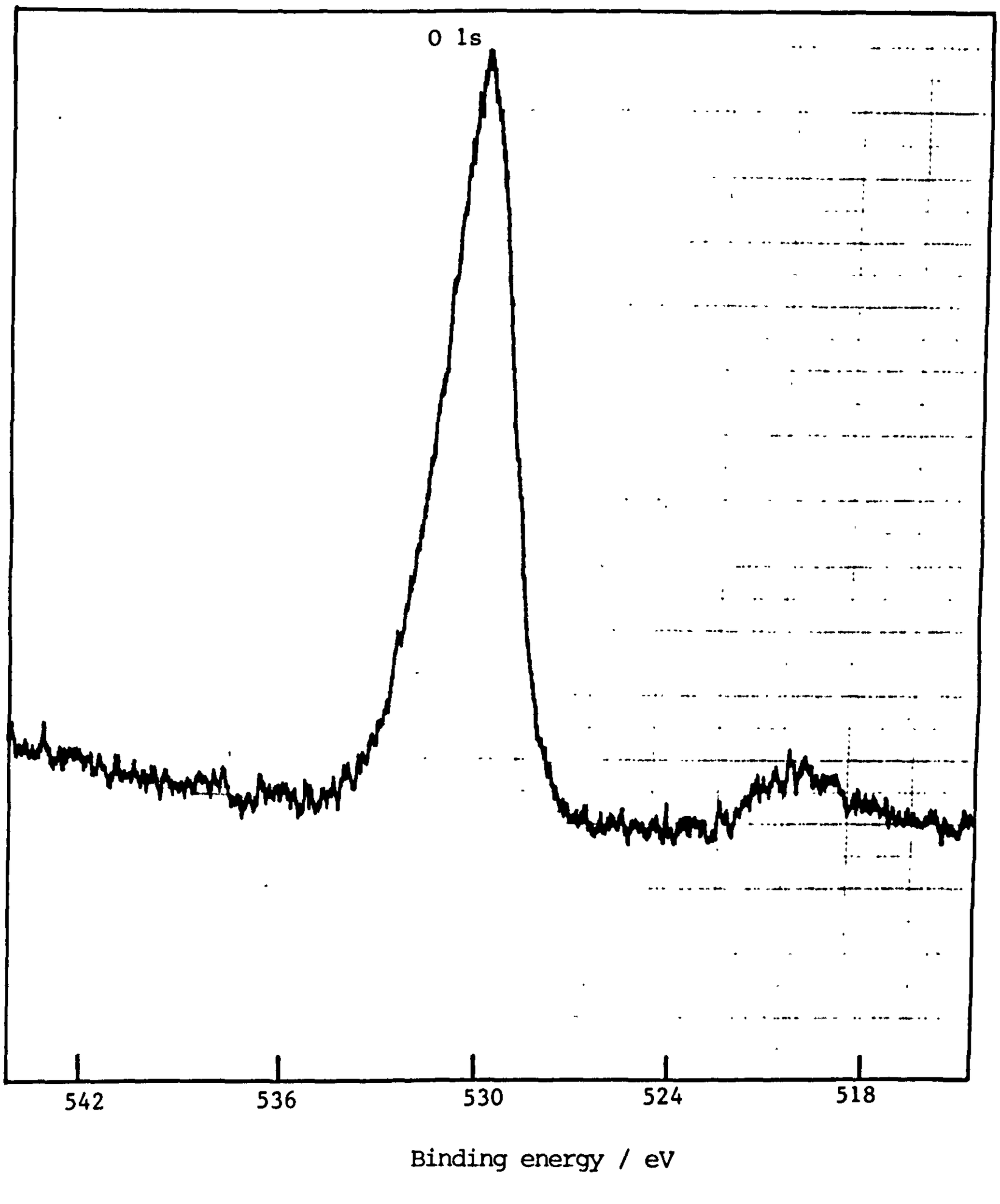

Fig.3.5.14 Narrow scan spectrum of O 1s obtained from Mo-black dip coating on zinc substrate.

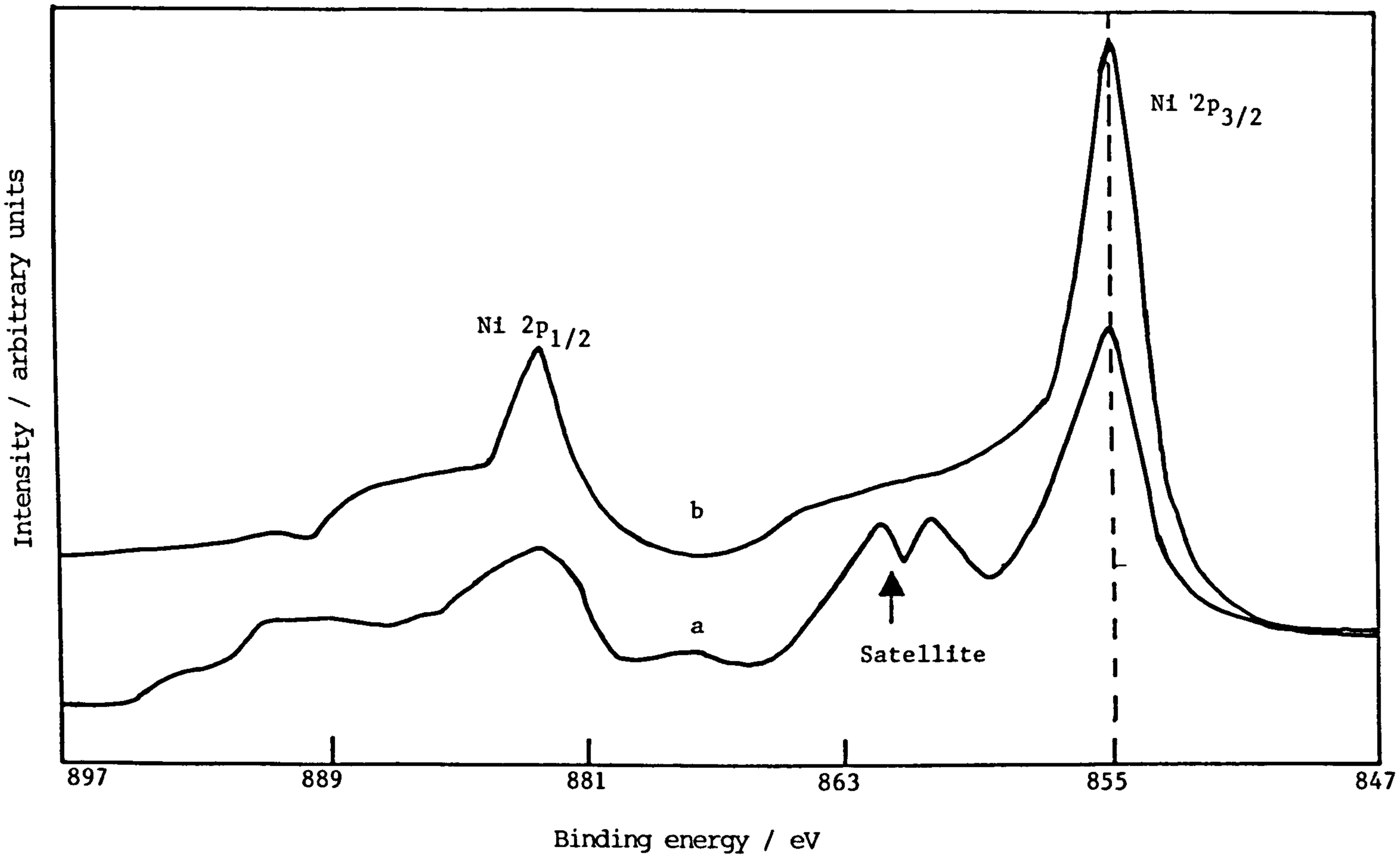

Fig.3.5.15 Narrow scan spectra of Ni 2p from Mo-black dip coating on zinc substrate;
(a) before etching,
(b) after etching with Ar^+ ions for 30 minutes.

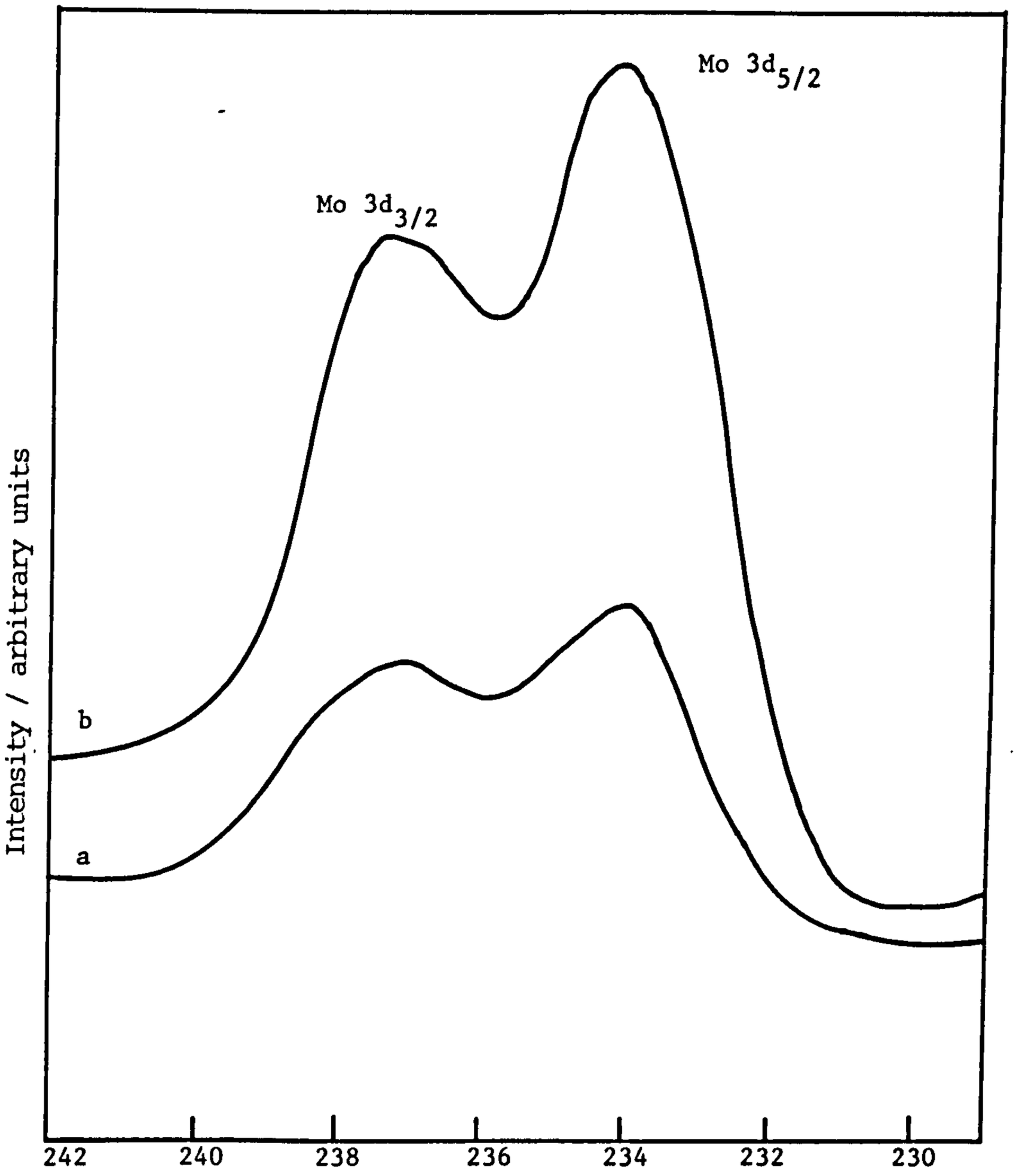

Fig.3.5.16 Narrow scan spectra of Mo 3d doublet from Mo-black dip coatings
(a) on unetched zinc,
(b) on etched zinc.

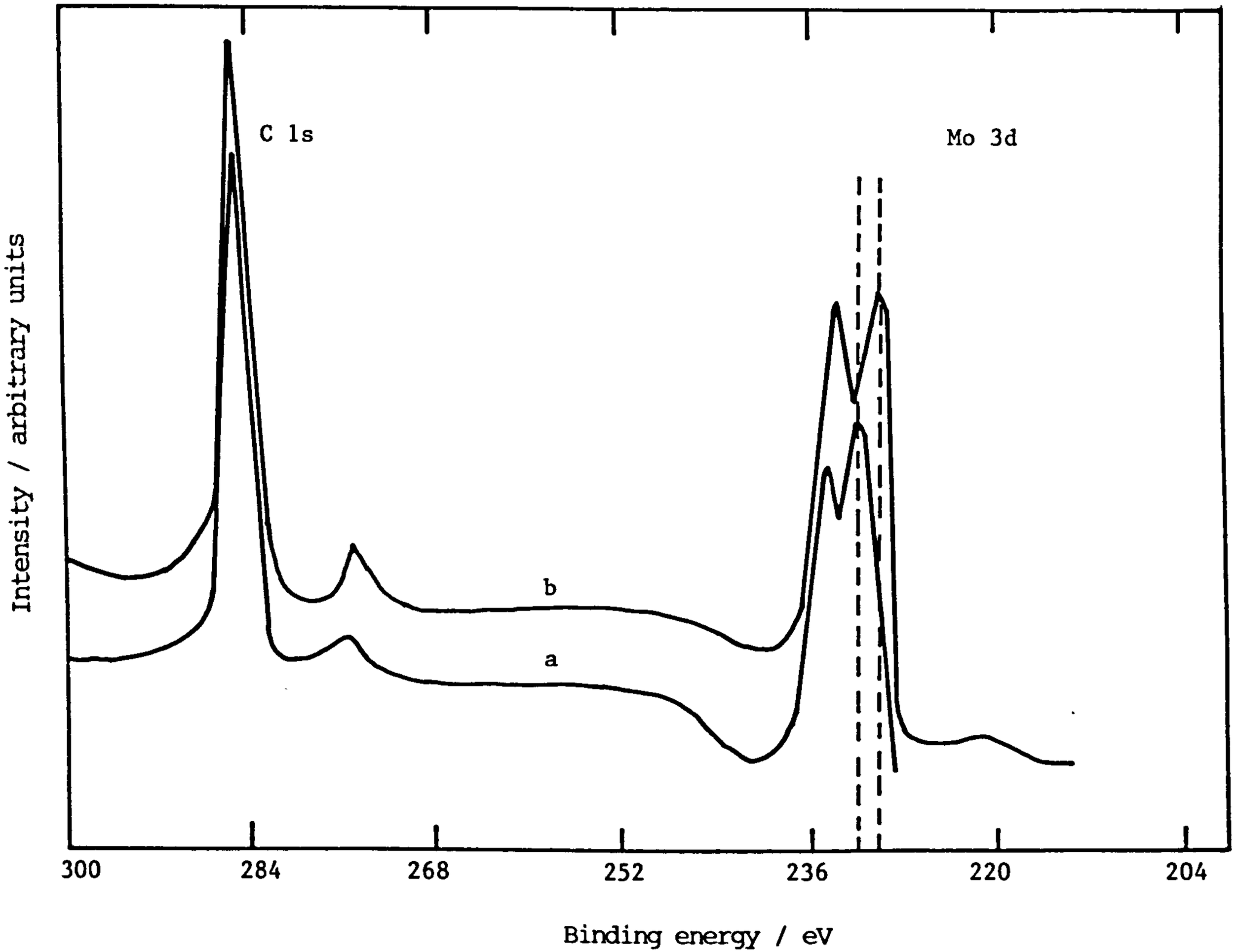

Fig.3.5.17 X-ray photoelectron spectra of Mo 3d doublet and C 1s for Mo-black coating on unetched zinc substrate;
(a) as prepared,
(b) after heating at 300°C for 1.5 hours inside the spectrometer.

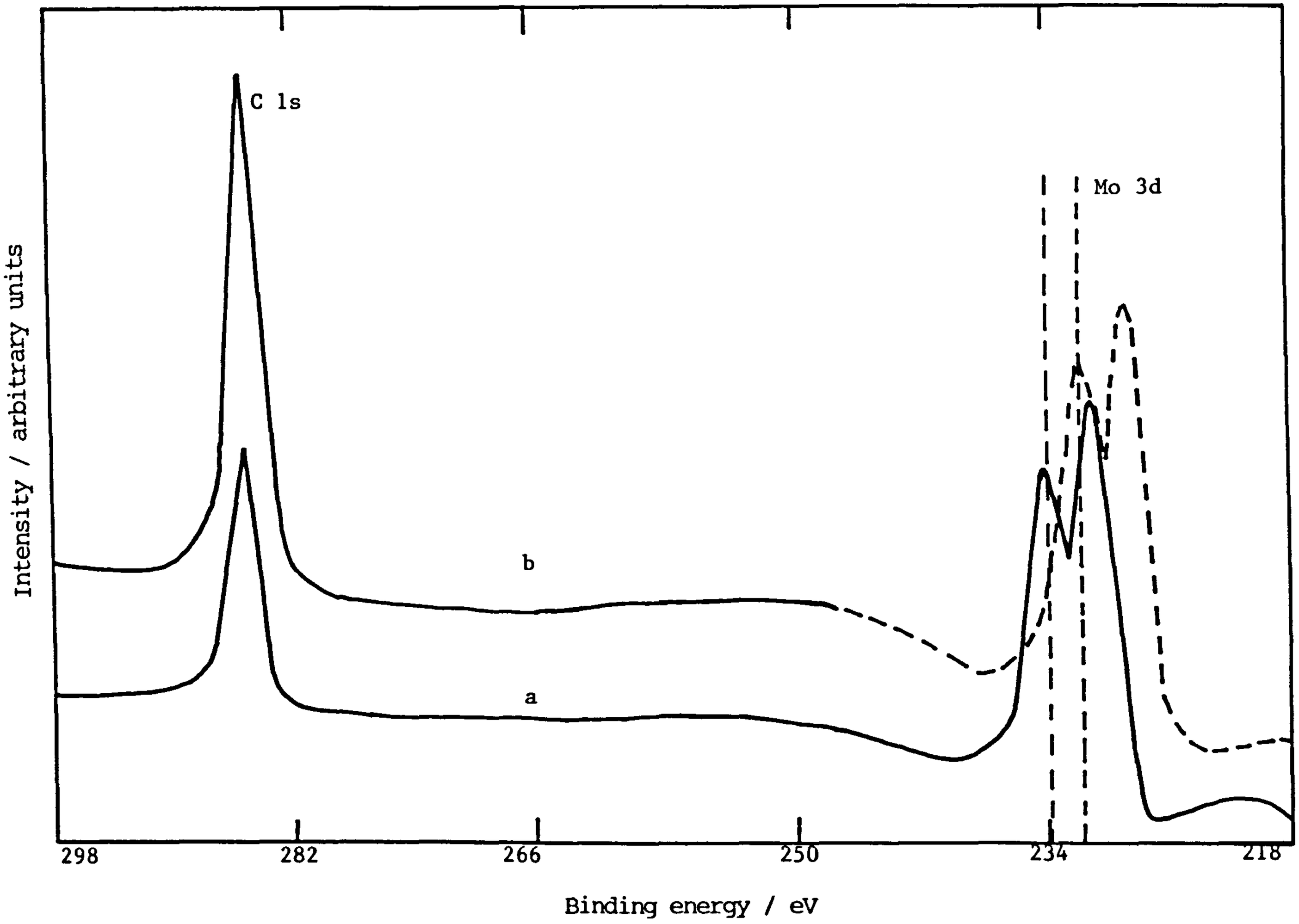

Fig.3.5.18 X-ray photoelectron spectra of Mo 3d doublet of a Mo-black dip coating on etched zinc;
(a) as-prepared,
(b) after heating in vacuum at 300°C for 3 hours.

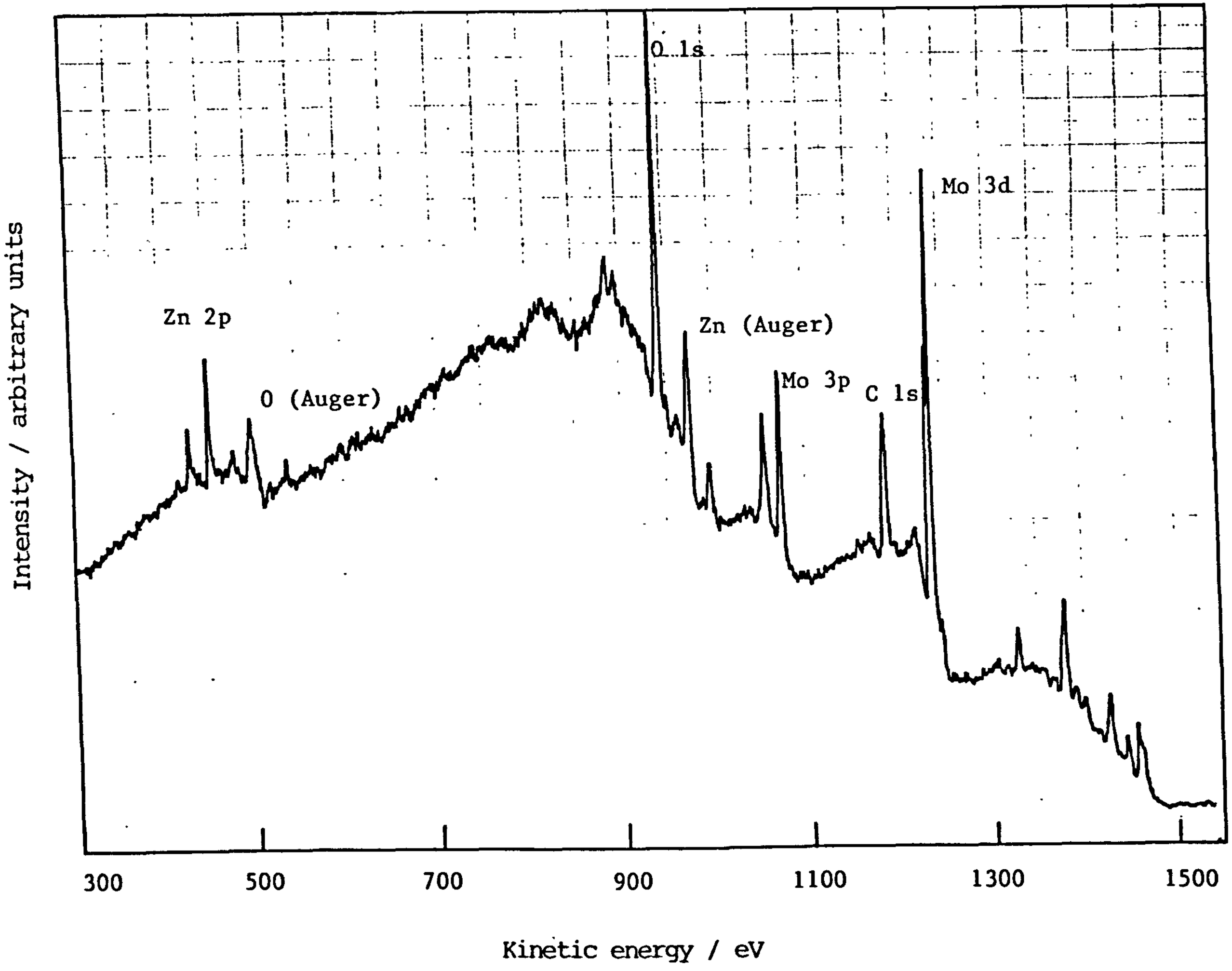

Fig.3.5.19 Survey scan spectrum obtained from Mo-black dip coating on zinc substrate after heating in air at a temperature of 390°C for 2 hours.

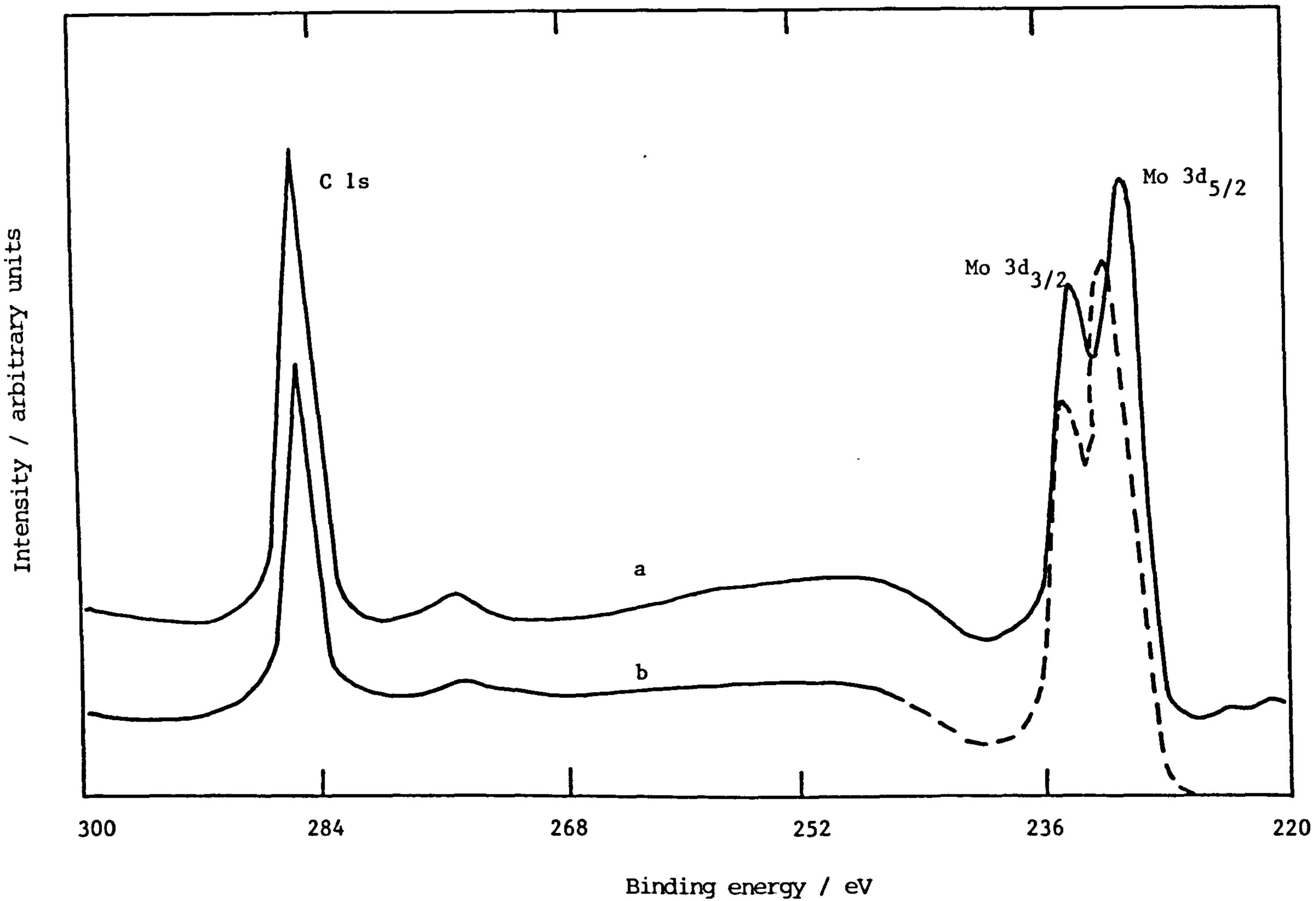

Fig.3.5.20 X-ray photoelectron spectra of Mo 3d doublet and C 1s peak for a Mo-black dip coating on etched zinc; (a) as-prepared, (b) after heating in air at 200°C for 2 hours.

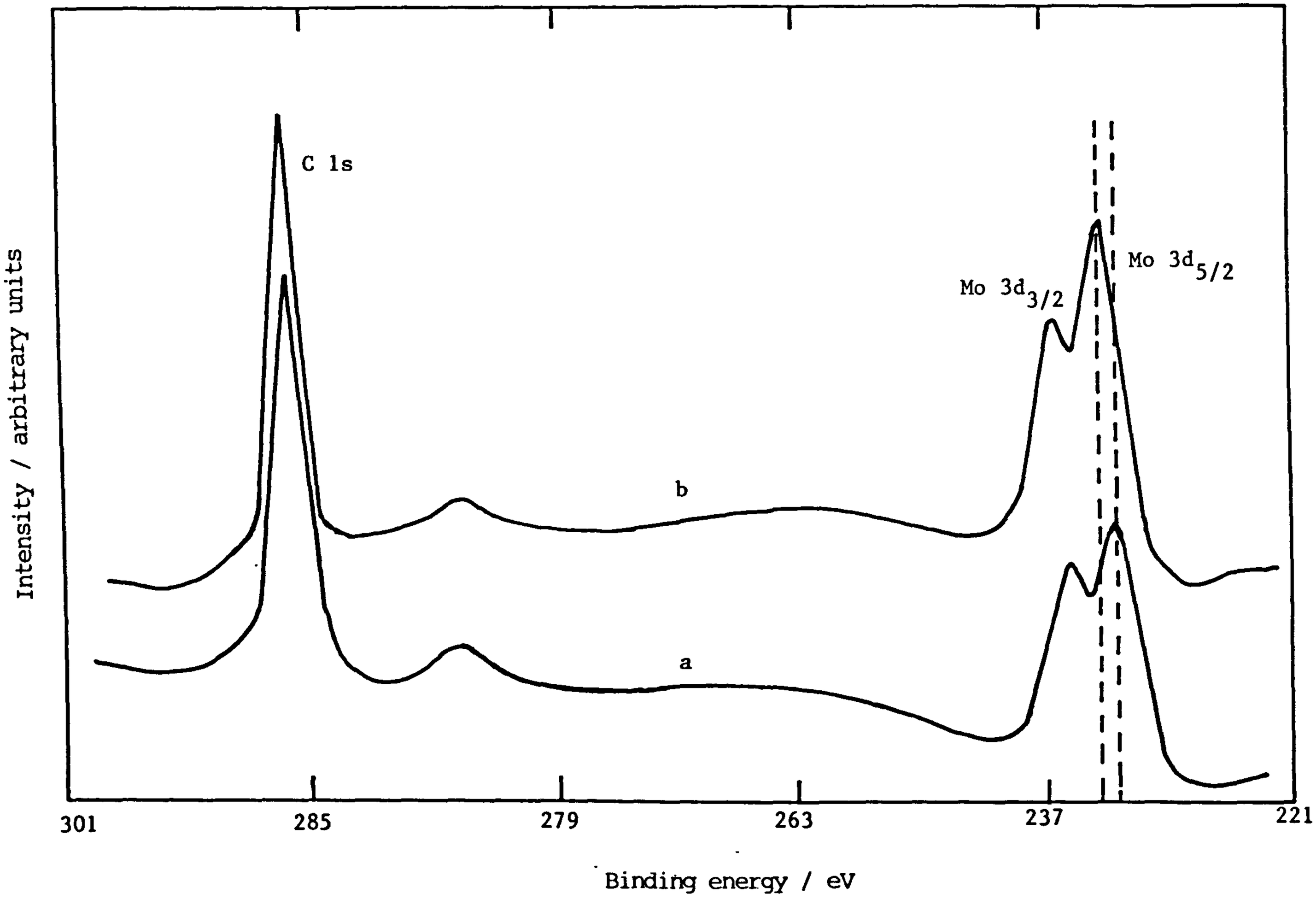

Fig.3.5.21 X-ray photoelectron spectra of Mo 3d doublet and C 1s peak for a Mo-black coating on unetched zinc; a) as-prepared, b) after heating in air at 200°C for 2 hours.

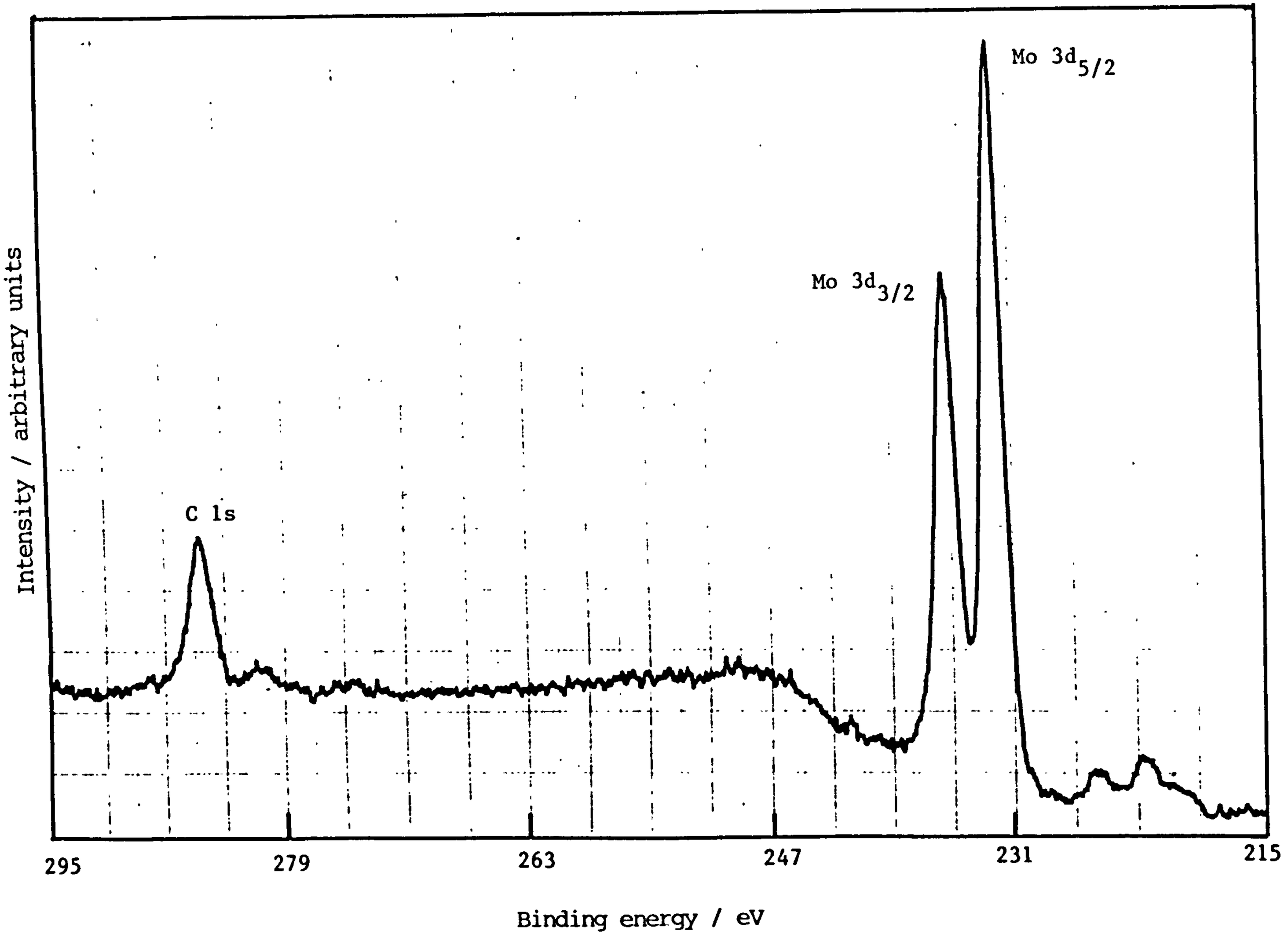

Fig.3.5.22 X-ray photoelectron spectrum of Mo 3d doublet obtained from Mo-black dip coating on etched zinc after heating in air at a temperature of 390°C for 2 hours.

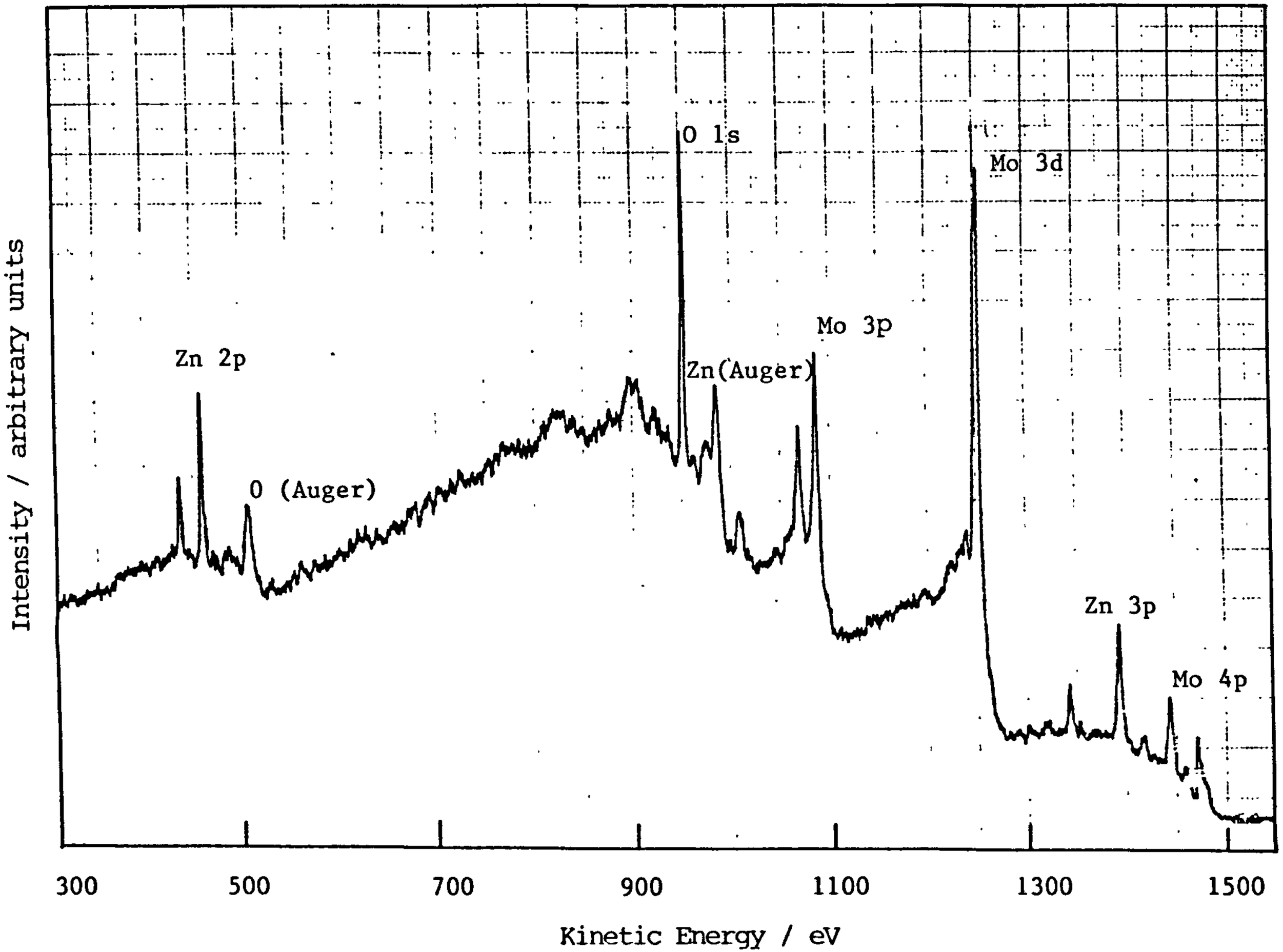

Fig.3.5.23 Survey scan spectrum of a Mo-black dip coating on etched zinc substrate after etching with Ar^+ ions for 200 minutes.

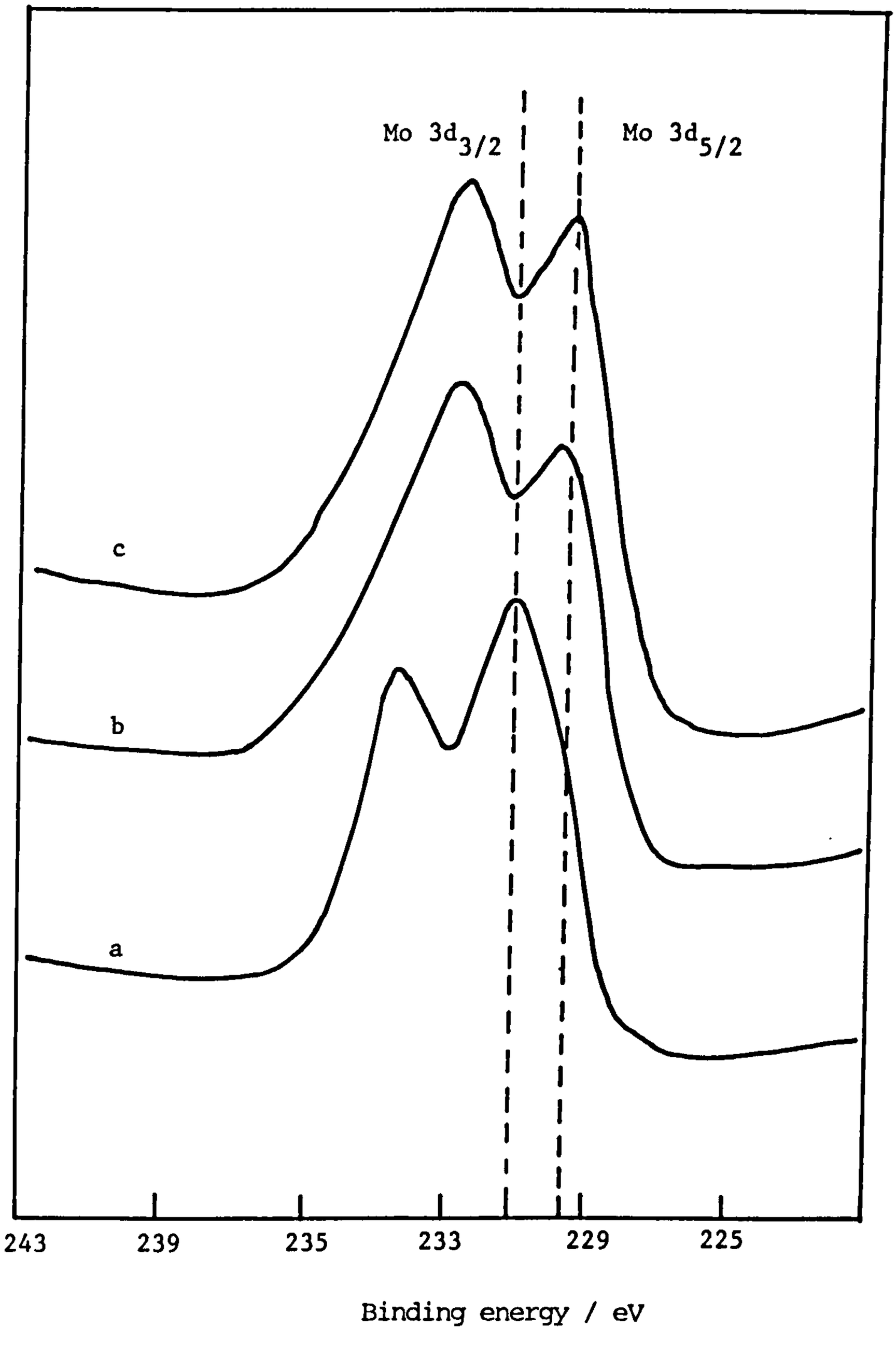

Fig.3.5.24 Narrow scan spectra of Mo 3d doublet of a Mo-black dip coating on zinc;
(a) as prepared,
(b) after etching with Ar^+ ions for 10 minutes,
(c) after etching with Ar^+ ions for 165 minutes.

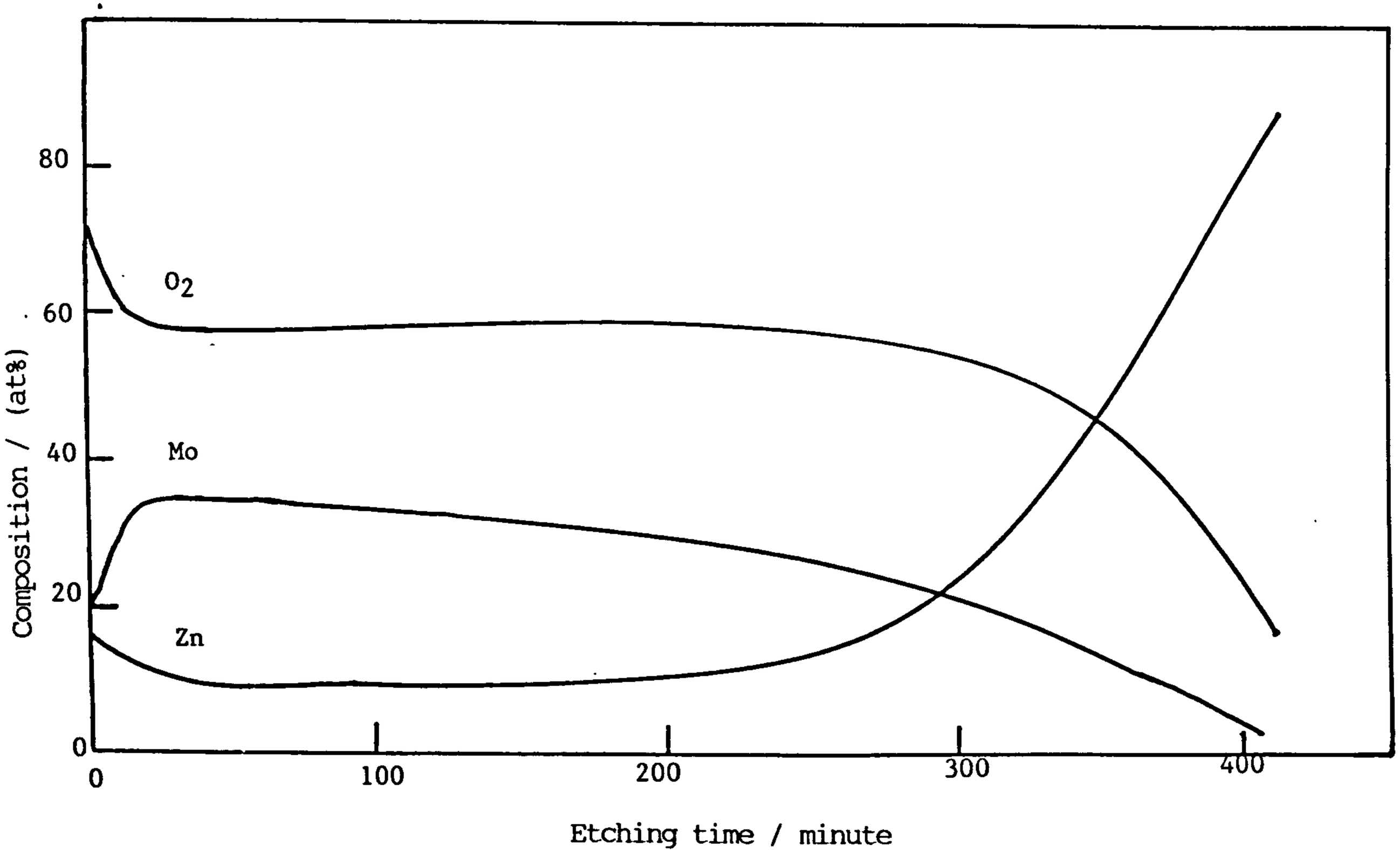

Fig.3.5.25 XPS depth profile of a Mo-black dip coating on zinc substrate.

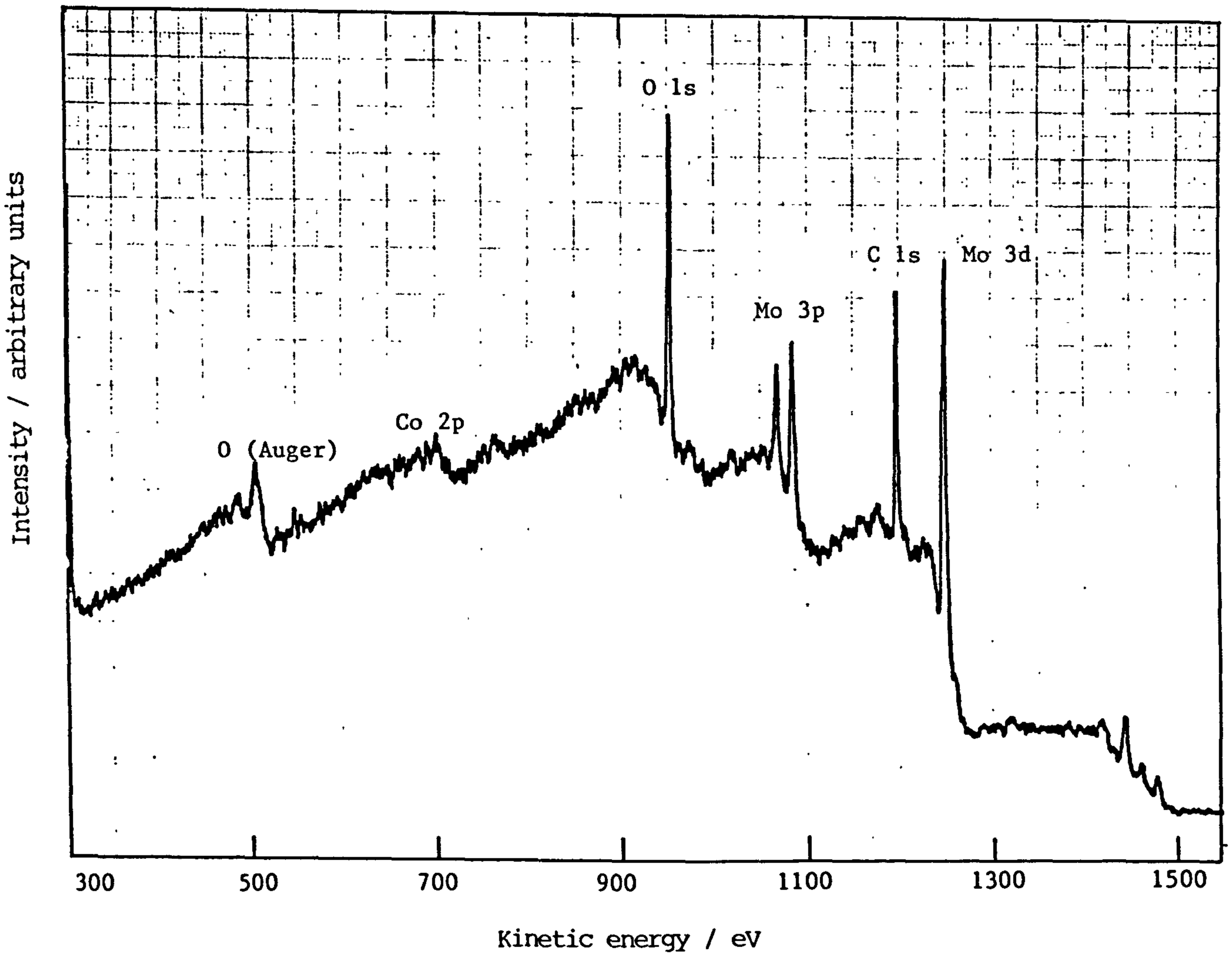

Fig.3.5.26 Survey scan spectrum of Mo-black dip coating on cobalt (NC) substrate.

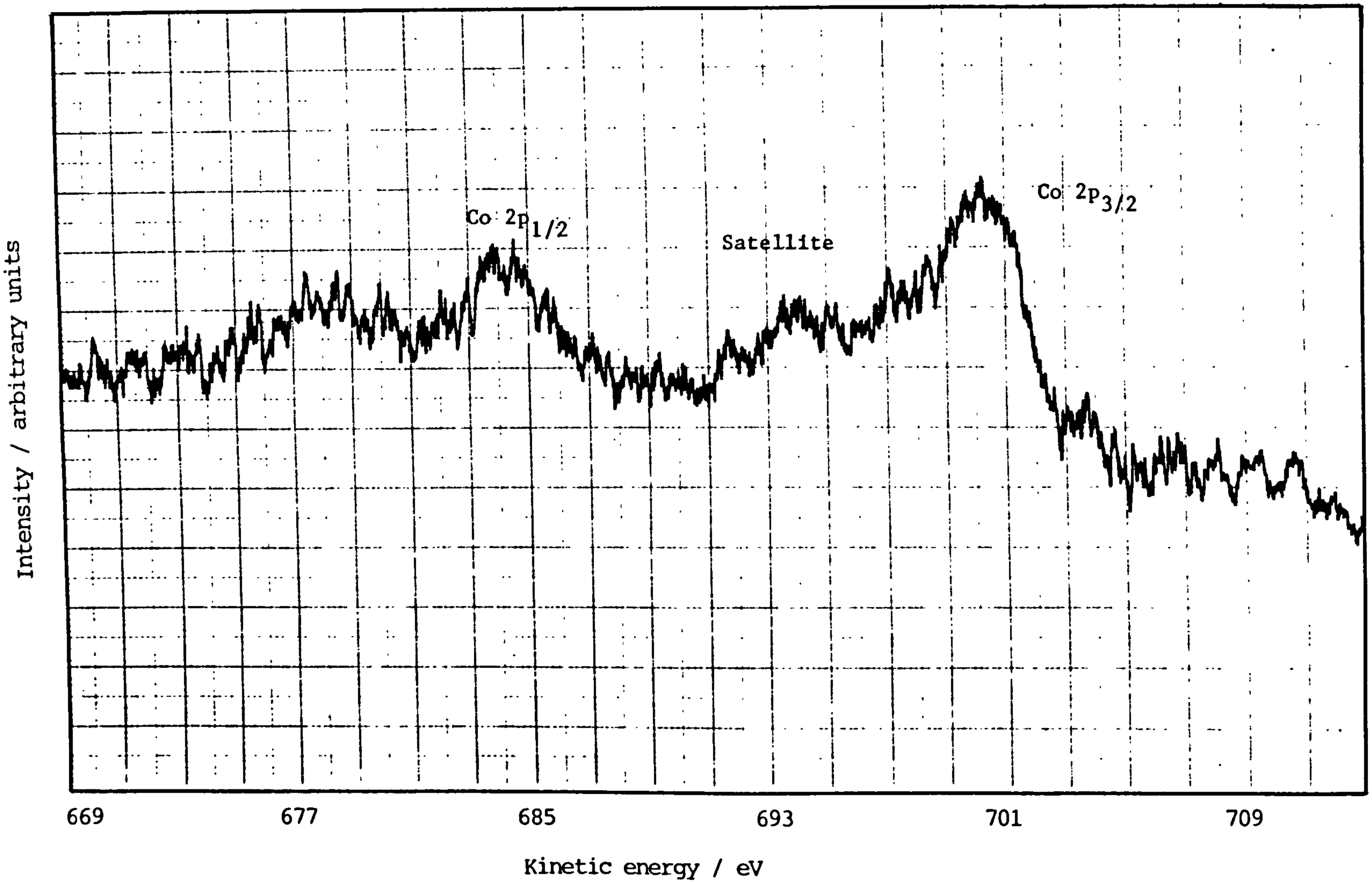

Fig.3.5.27 Narrow scan spectrum of Co 2p obtained from Mo-black dip coating on cobalt (NC) substrate.

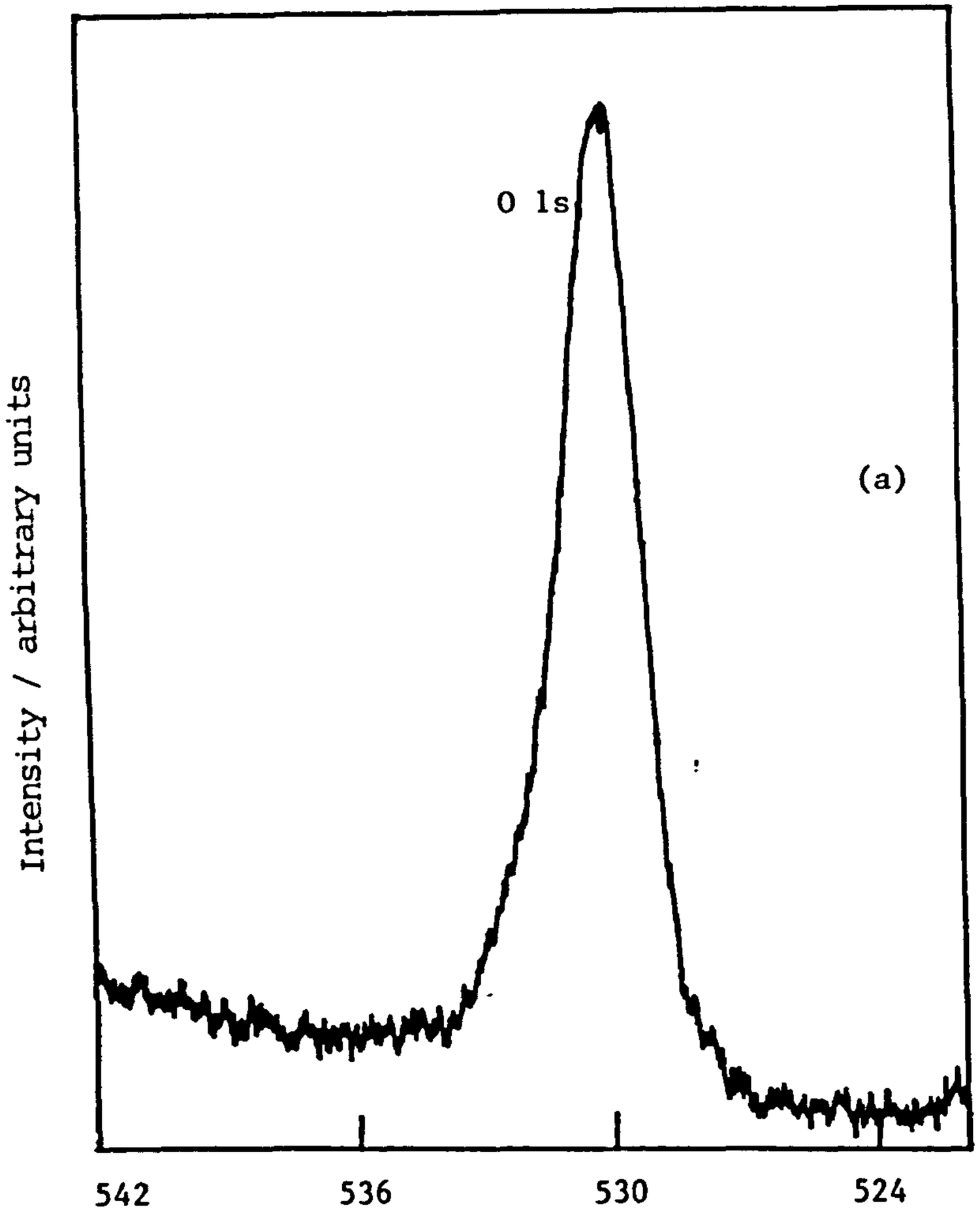

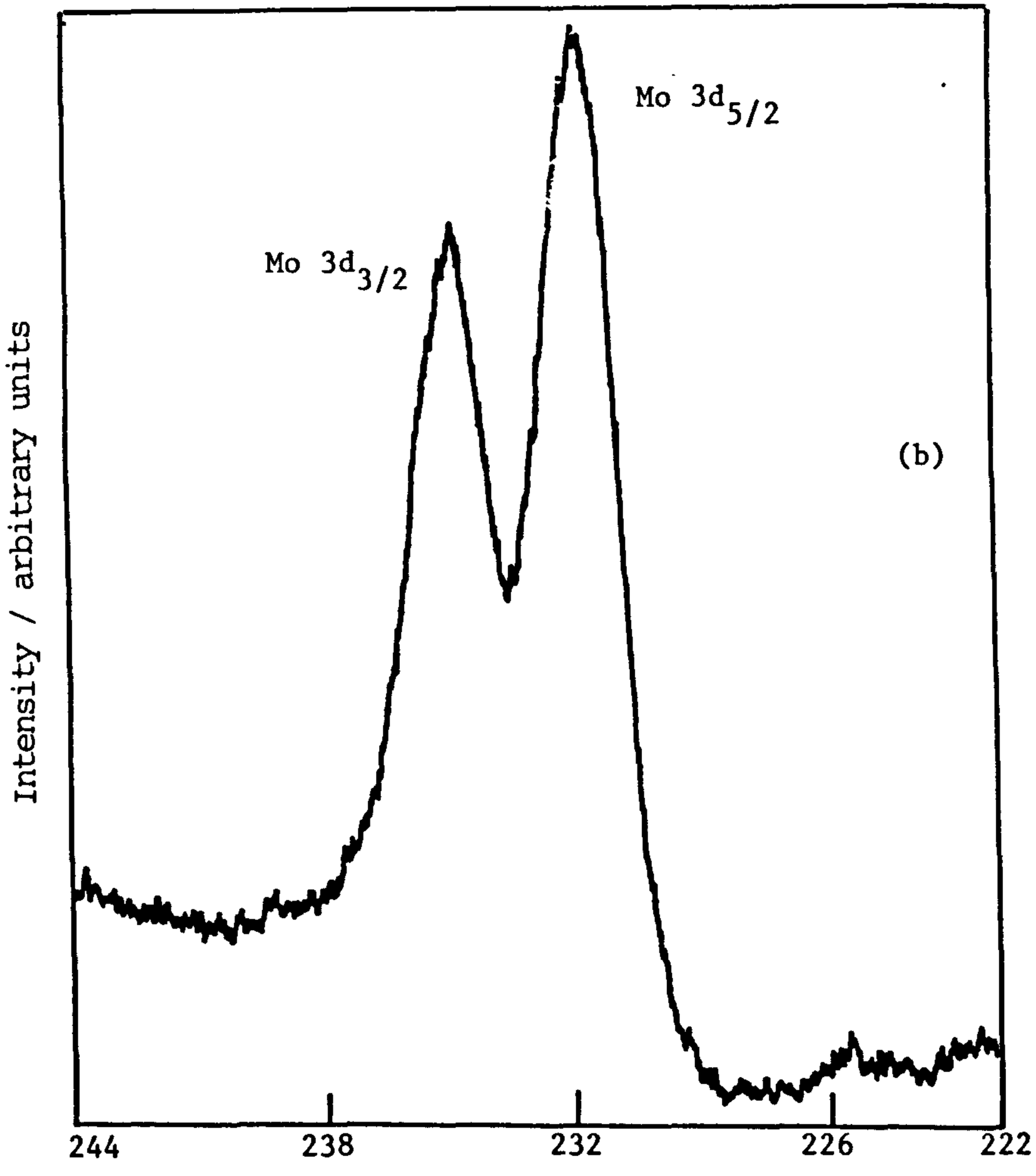

Fig.3.5.28 Narrow scan spectra of O 1s (a) and Mo 3d doublet (b) obtained from Mo-black dip coating on cobalt (NC) substrate.

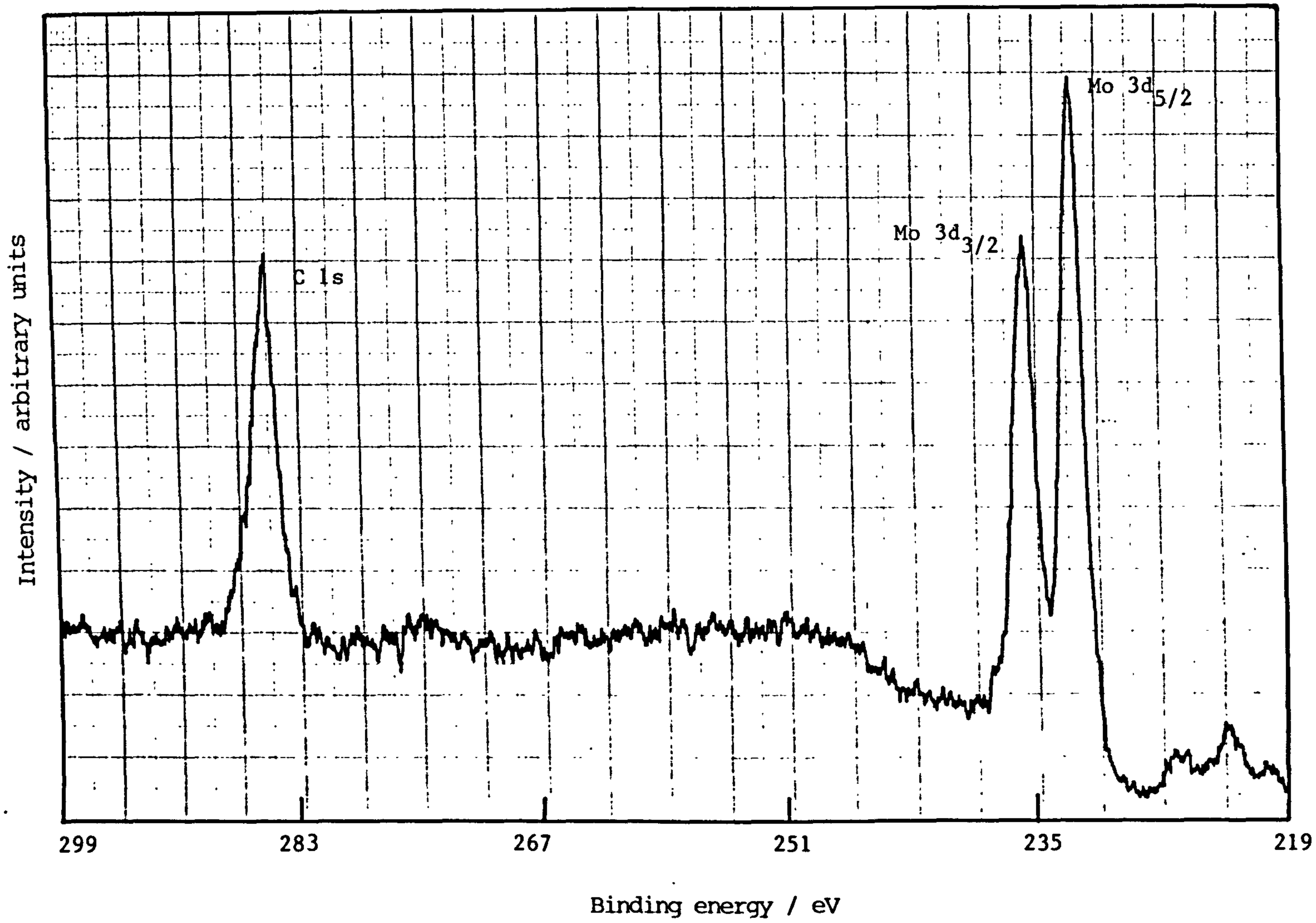

Fig.3.5.29 X-ray photoelectron spectrum of Mo 3d doublet for Mo-black dip coating on cobalt (NC) substrate after heating in air at 400°C for 2 hours, including C 1s peak.

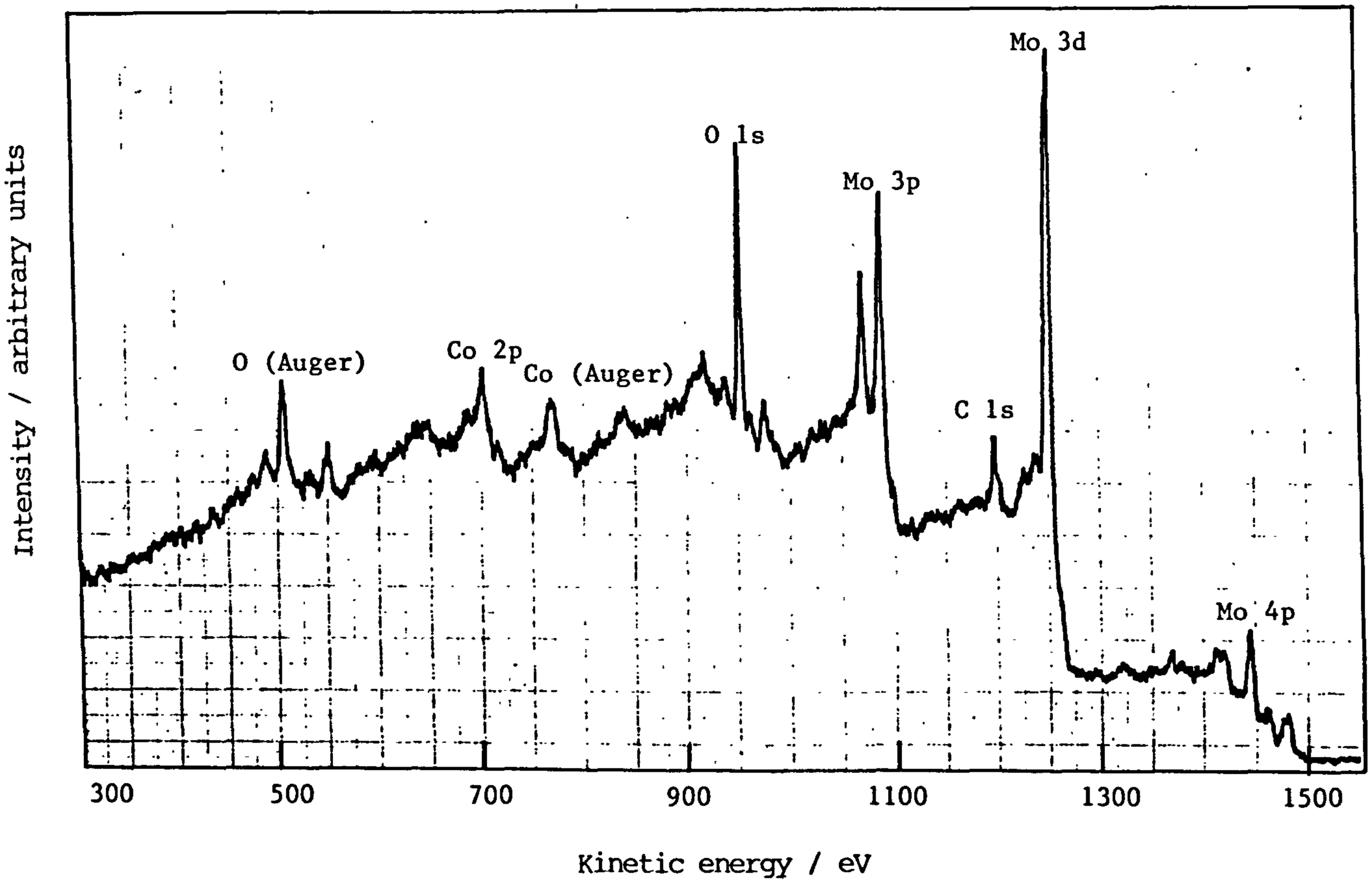

Fig.3.5.30 Survey scan spectrum of a Mo-black dip coating on cobalt (NC) substrate after etching with Ar^+ ions for 70 minutes.

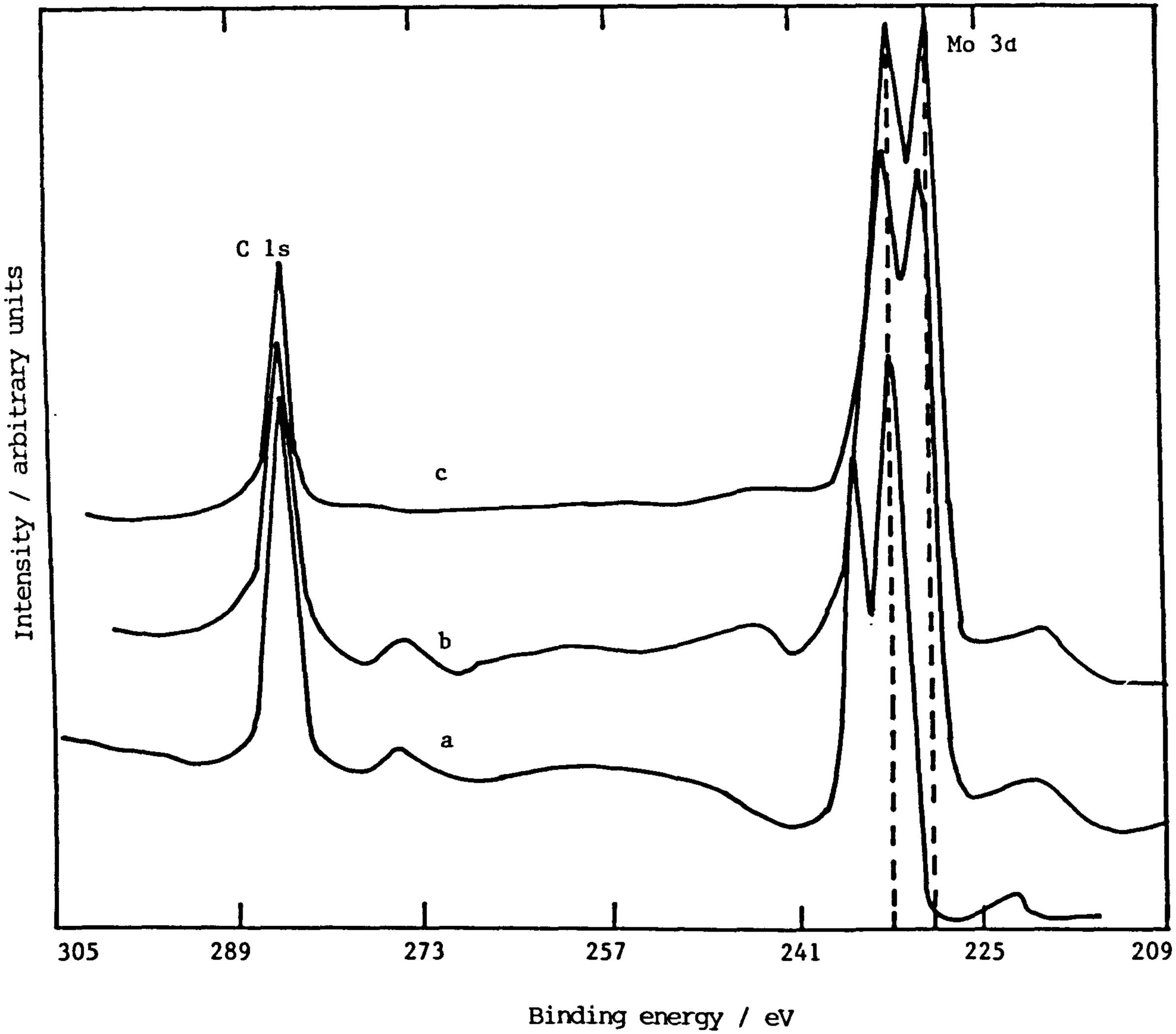

Fig.3.5.31 X-ray photoelectron spectra of Mo 3d doublet obtained from Mo-black dip coating on Cobalt (NC) substrate; (a) as-prepared, (b) after etching 10 minutes, (c) after etching 70 minutes with Ar^+.

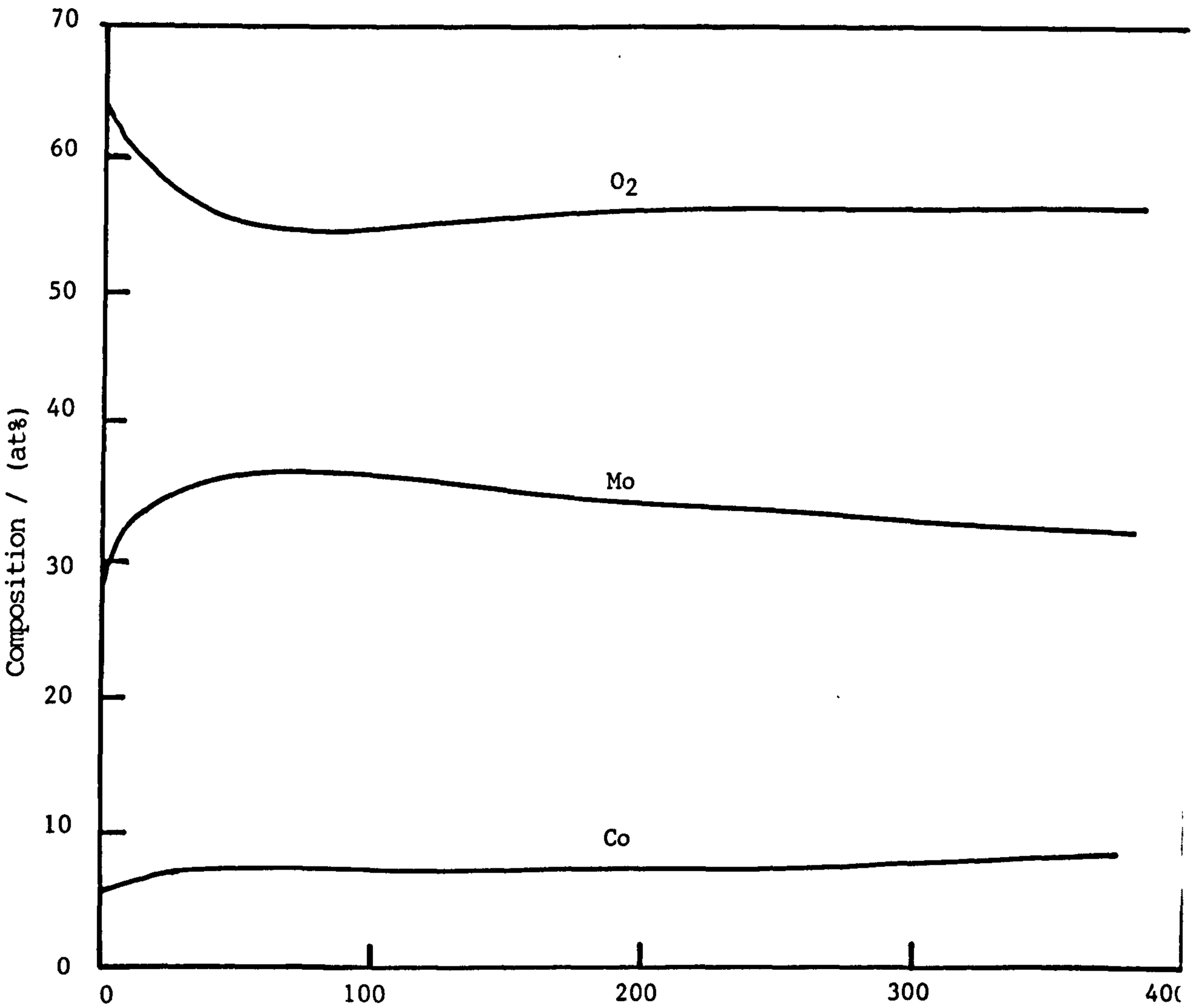

Fig.3.5.32 XPS depth profile of a Mo-black dip coating on cobalt (NC) substrate.

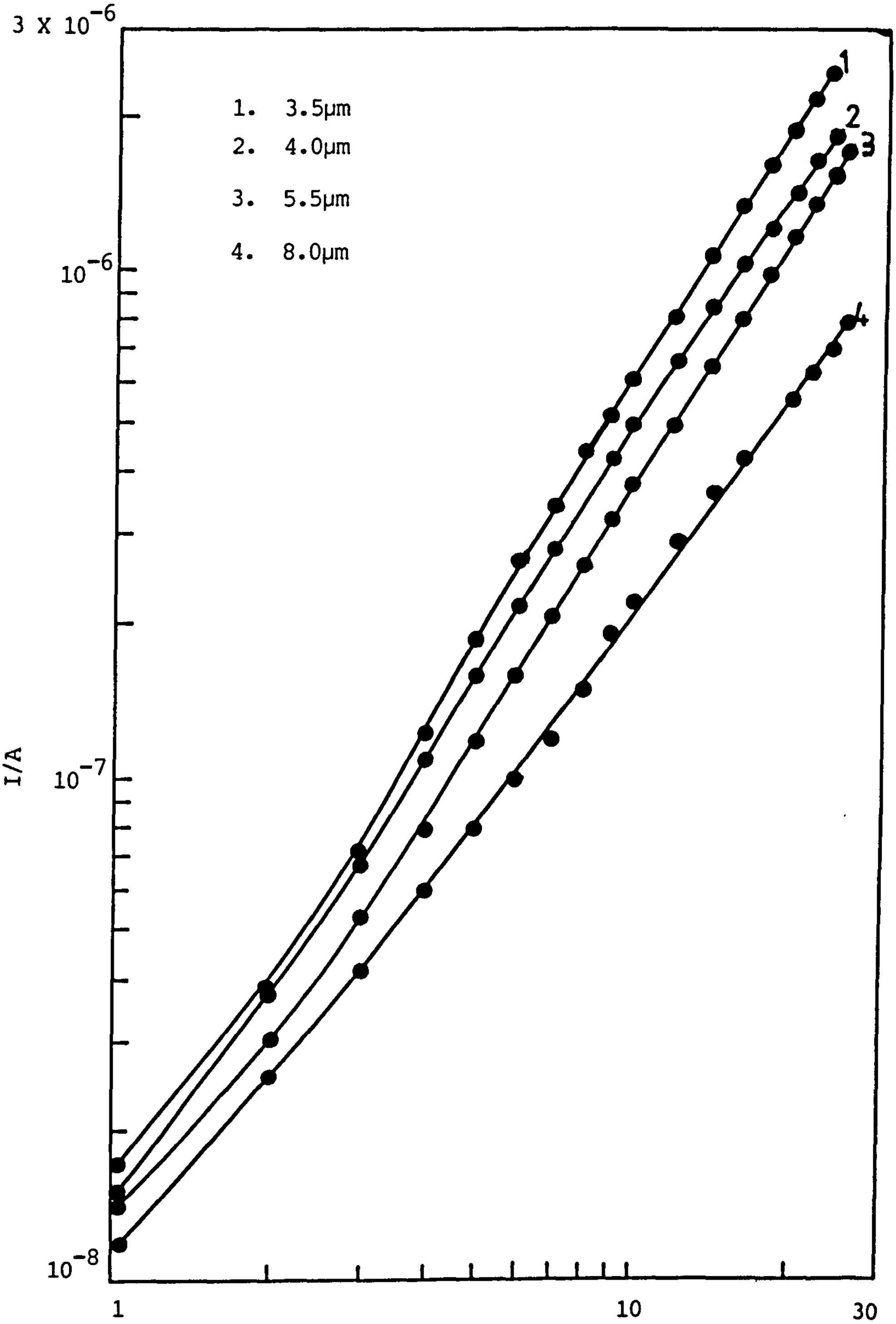

Fig.3.6.1 I-V characteristics for Mo-black coatings at room temperature for various thicknesses.

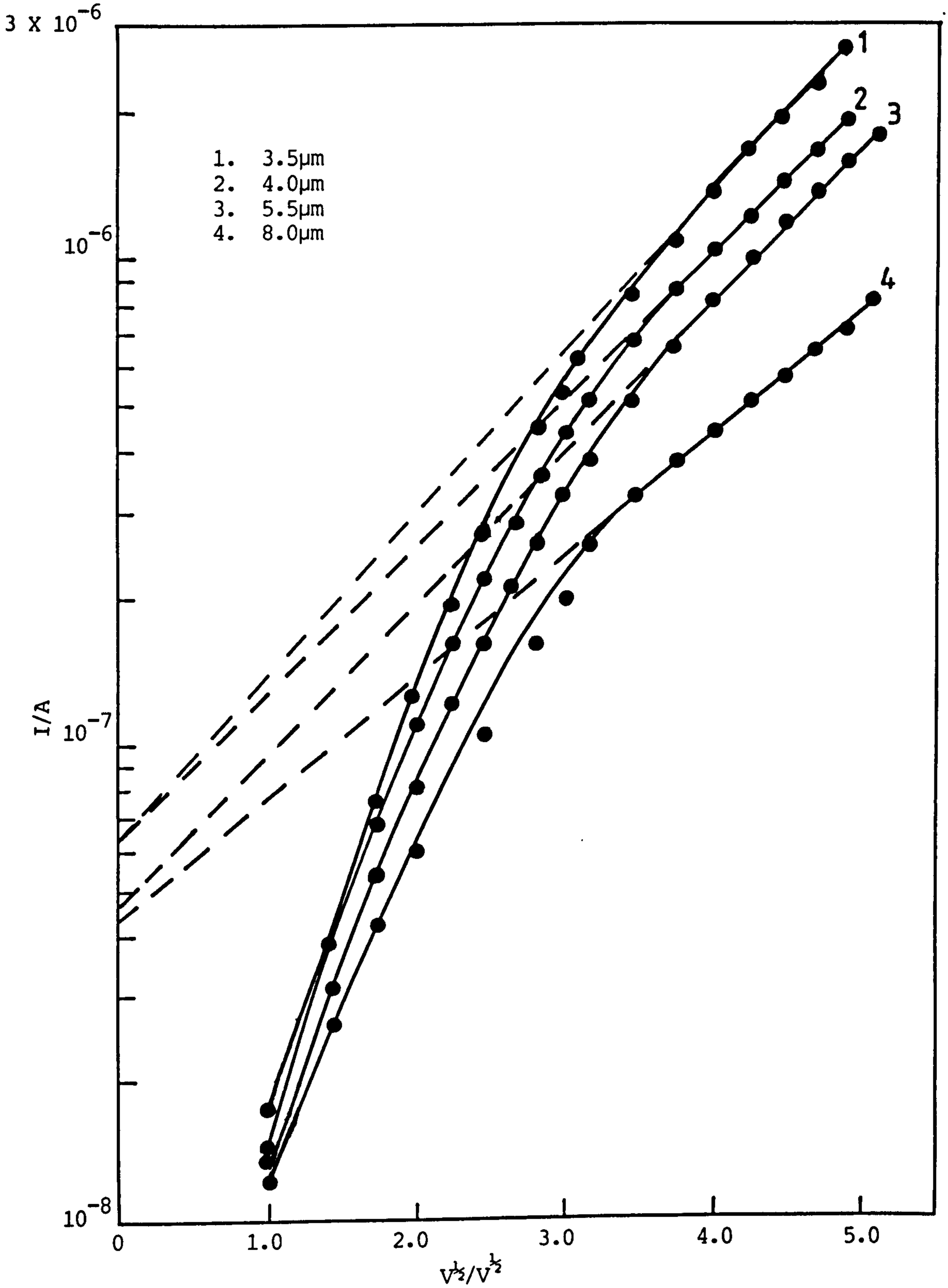

Fig.3.6.2 Plots of LogI as a function of $V^{\frac{1}{2}}$ for Mo-black coatings at room temperature for four different coating thicknesses.

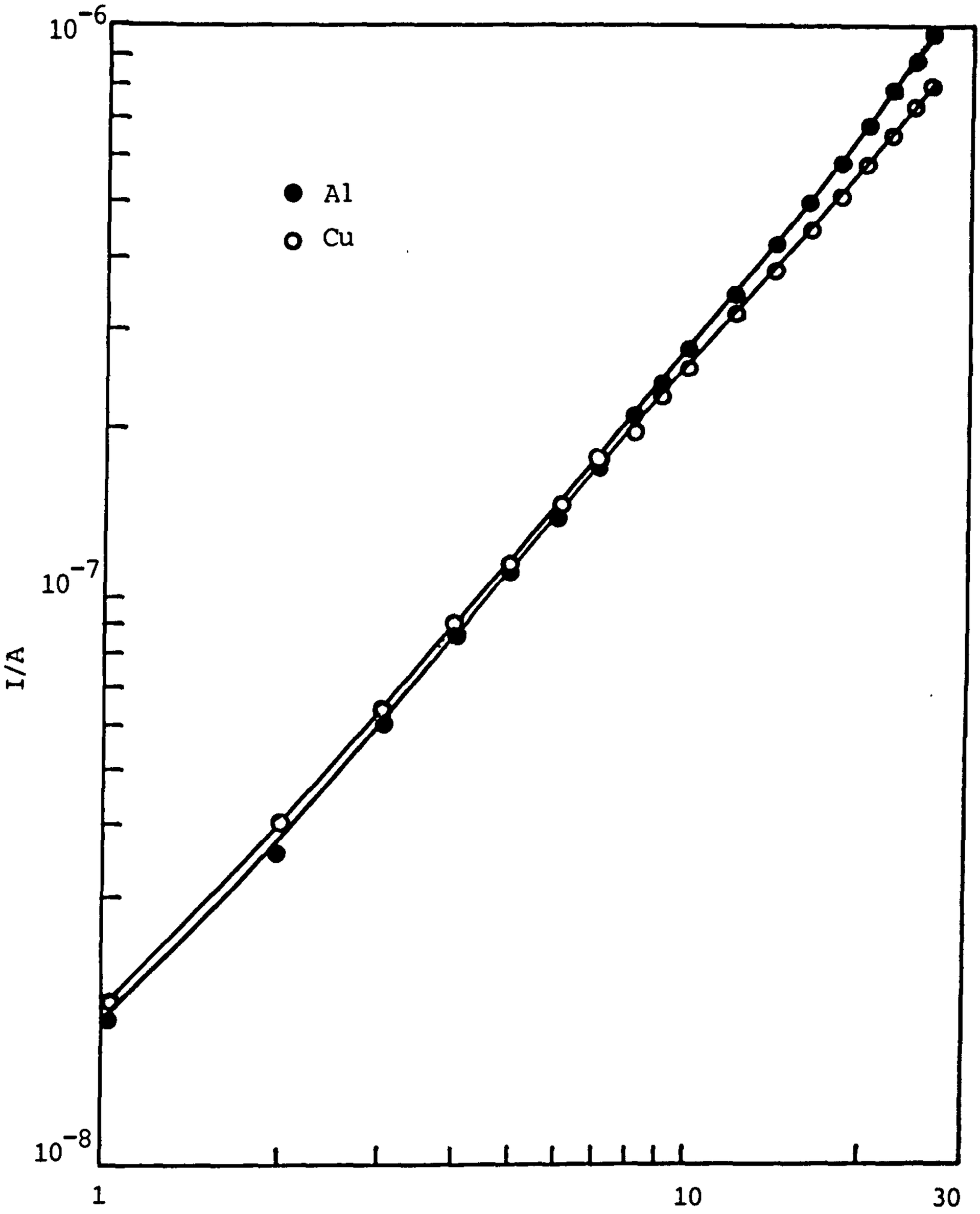

Fig.3.6.3 I-V characteristics at room temperature of Mo-black coatings of given thickness for two different pairs of electrode materials.

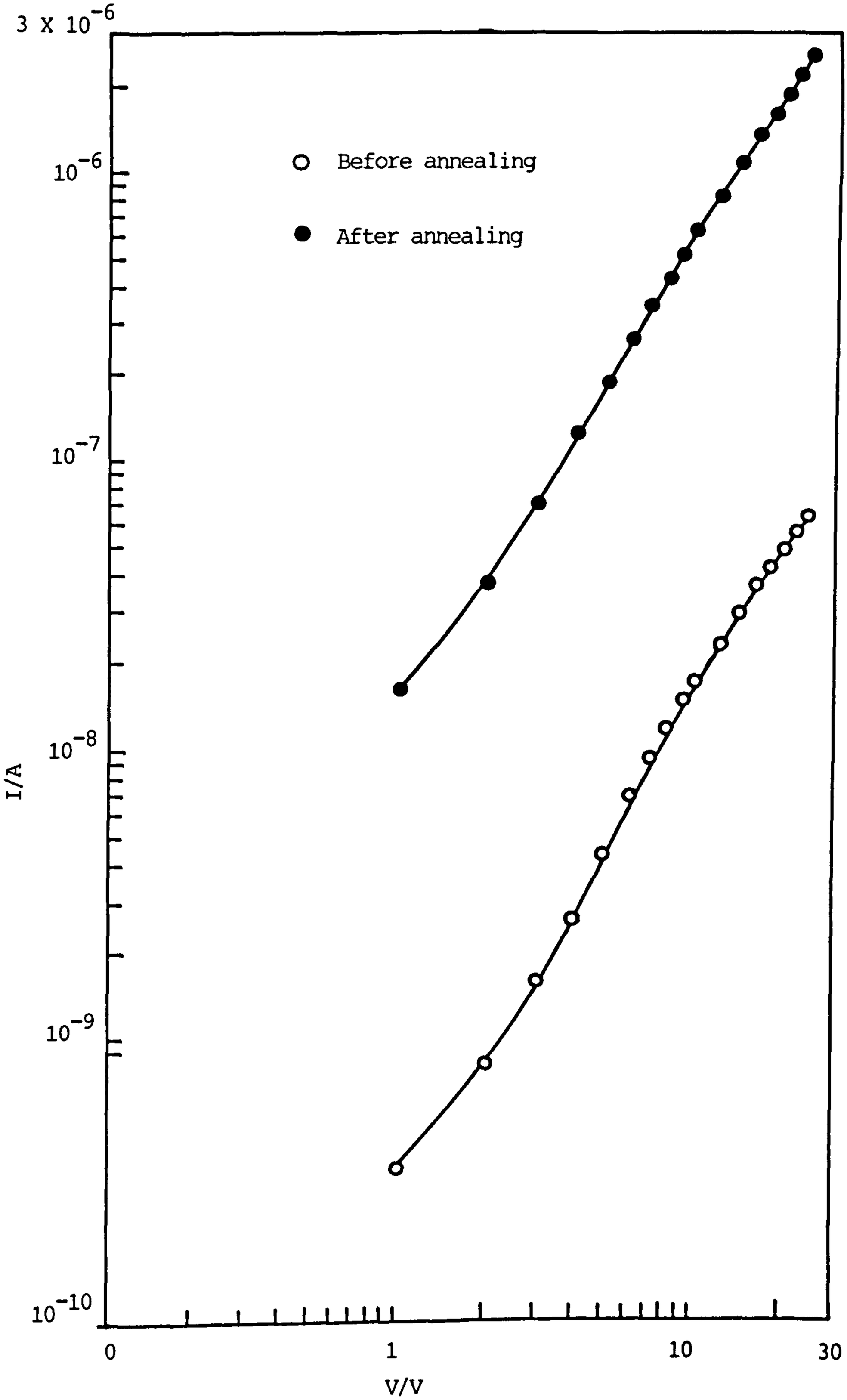

Fig.3.6.4 Effect of annealing on I-V characteristics of a Mo-black coating.

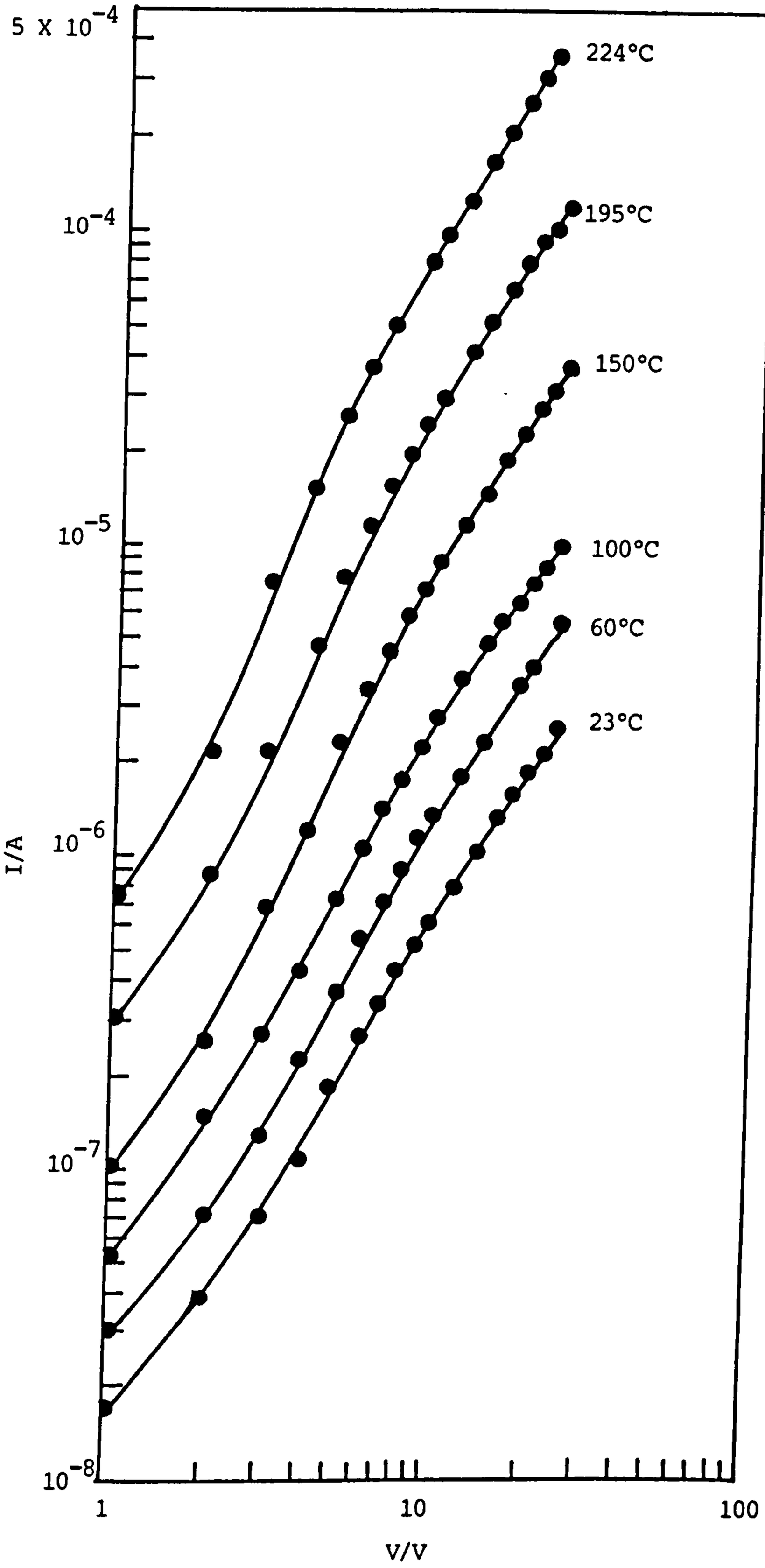

Fig.3.6.5.a I-V characteristics for Mo-black coating (of thickness~3.5μm) at different temperatures.

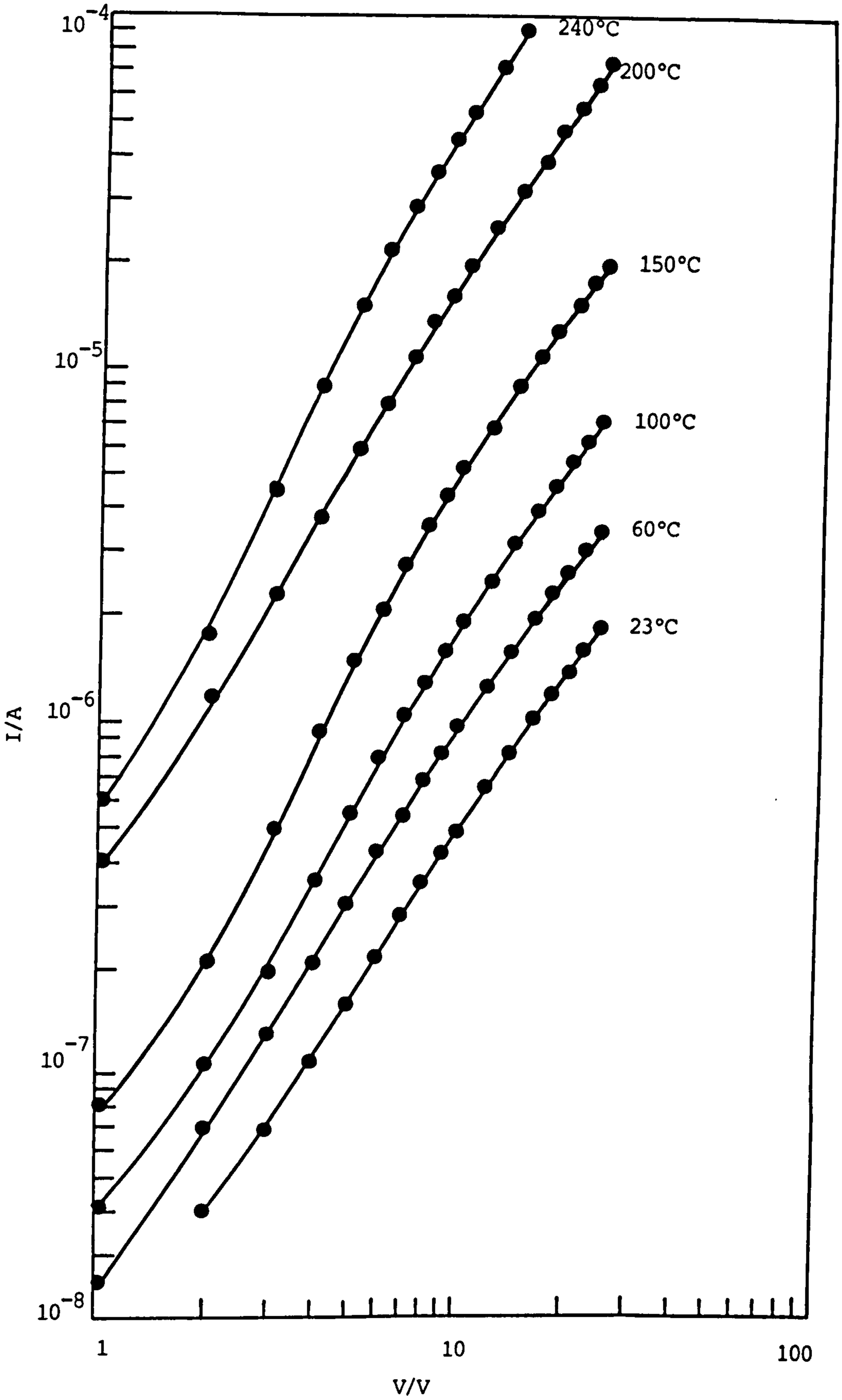

Fig.3.6.5.b. I-V characteristics for Mo-black coating (of thickness~ 5.5μm) at different temperatures.

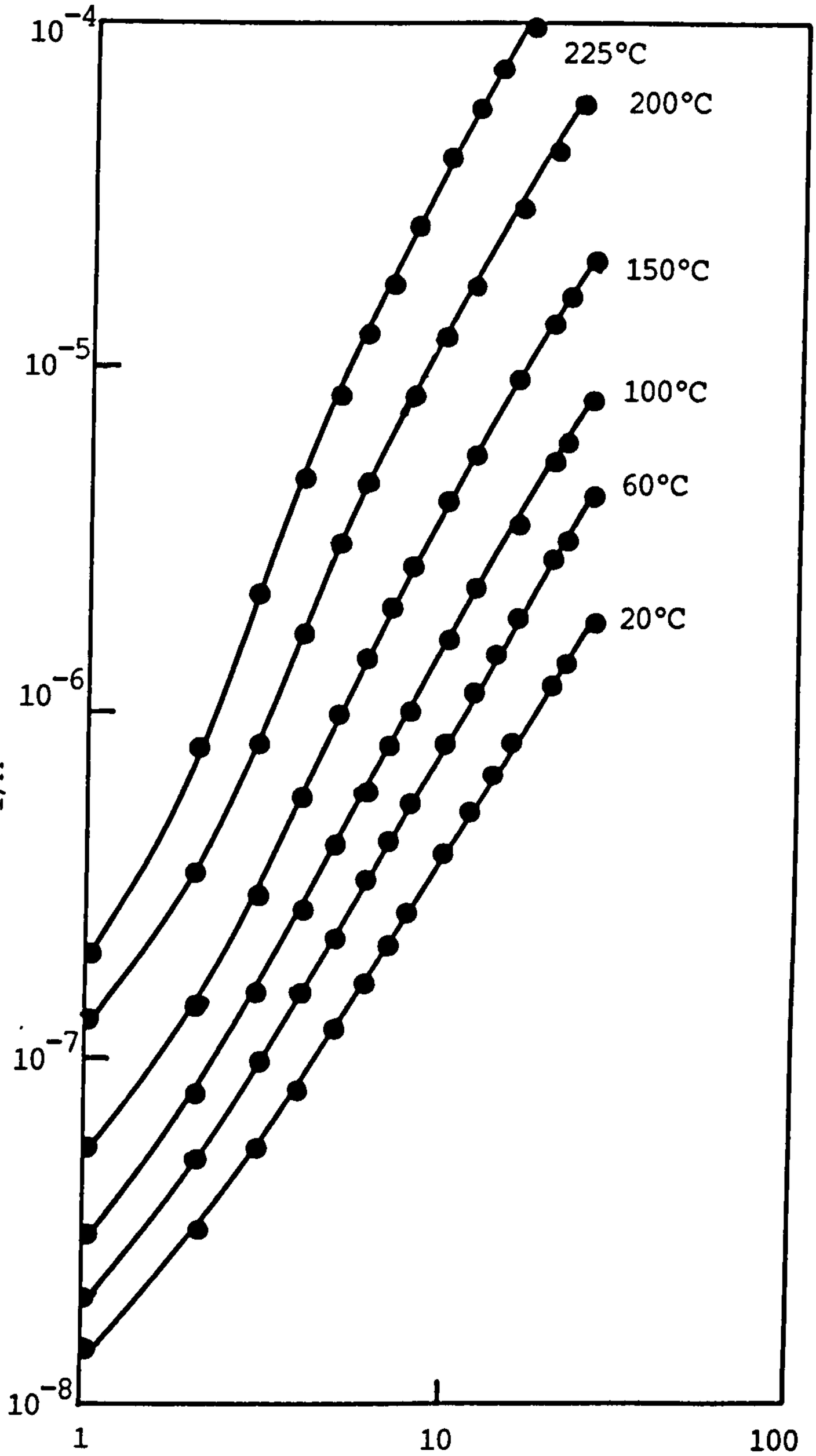

Fig.3.6.5.c I-V characteristics for Mo-black coating (of thickness~5.5μm) at different temperatures.

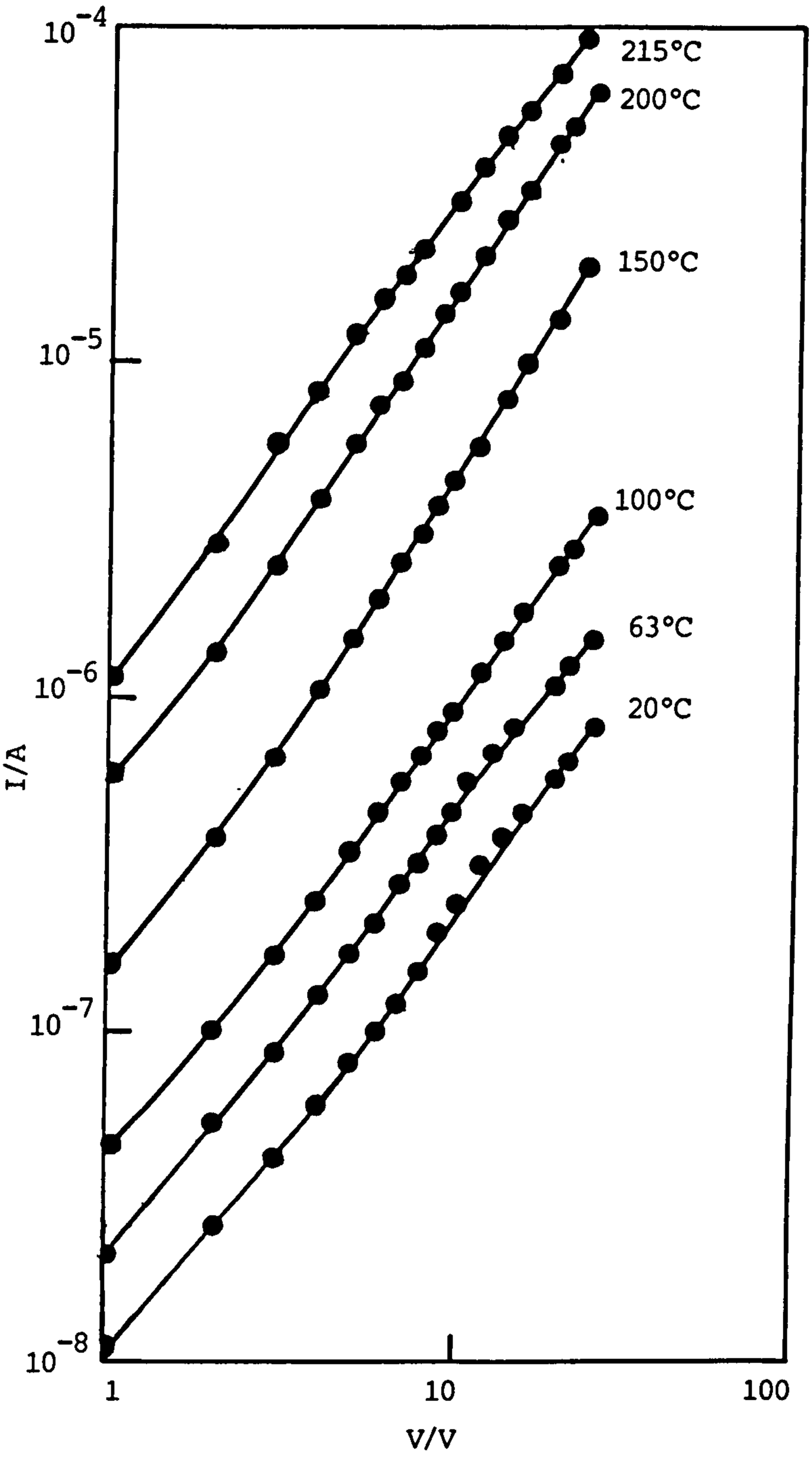

Fig.3.6.5.d I-V characteristics for Mo-black coating (of thickness ~ 8.0μm) at different temperatures.

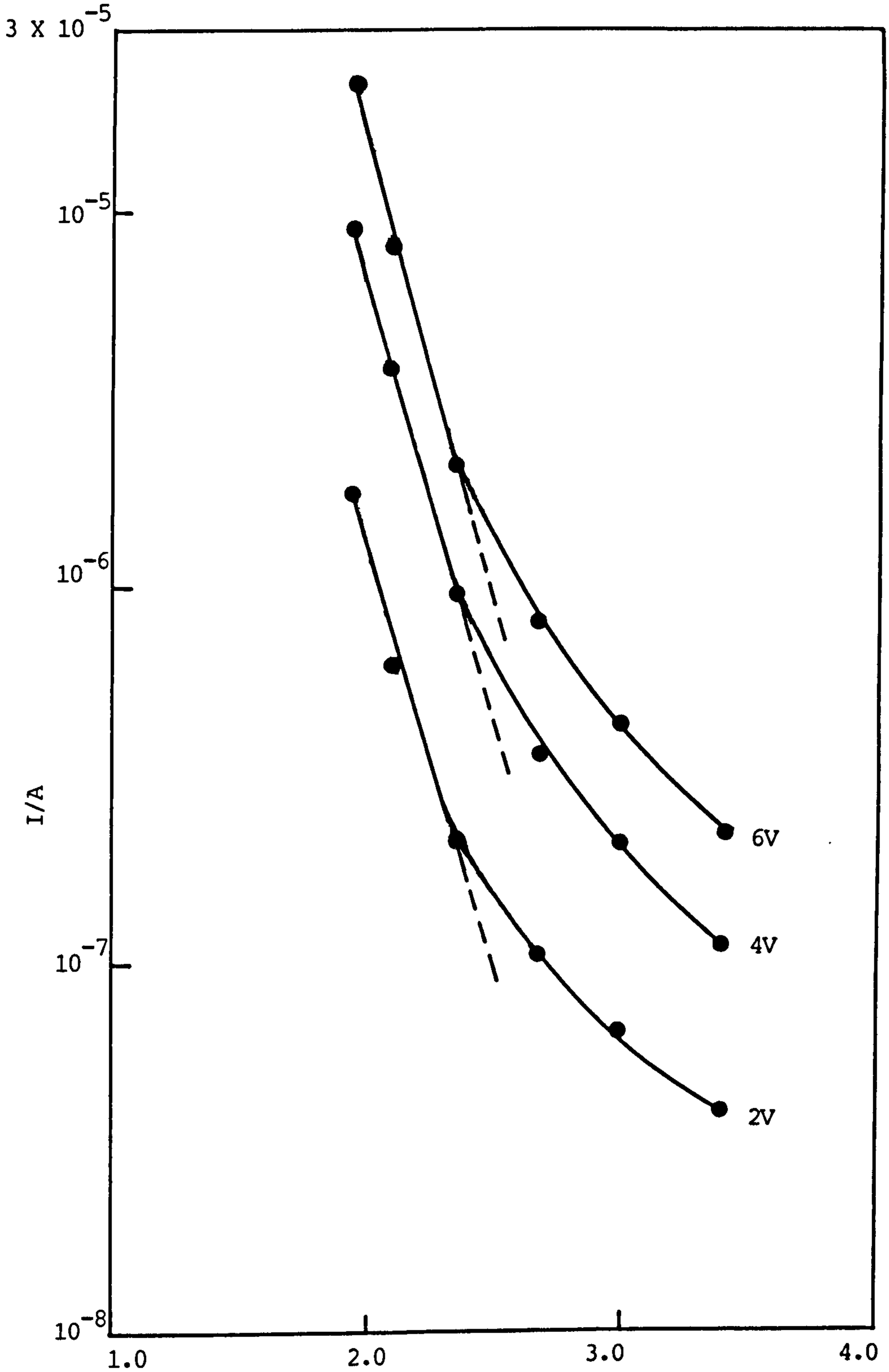

Fig.3.6.6.a Plots of LogI as a function of 1/T for the data in Fig.3.6.5.a at three fixed bias voltages.

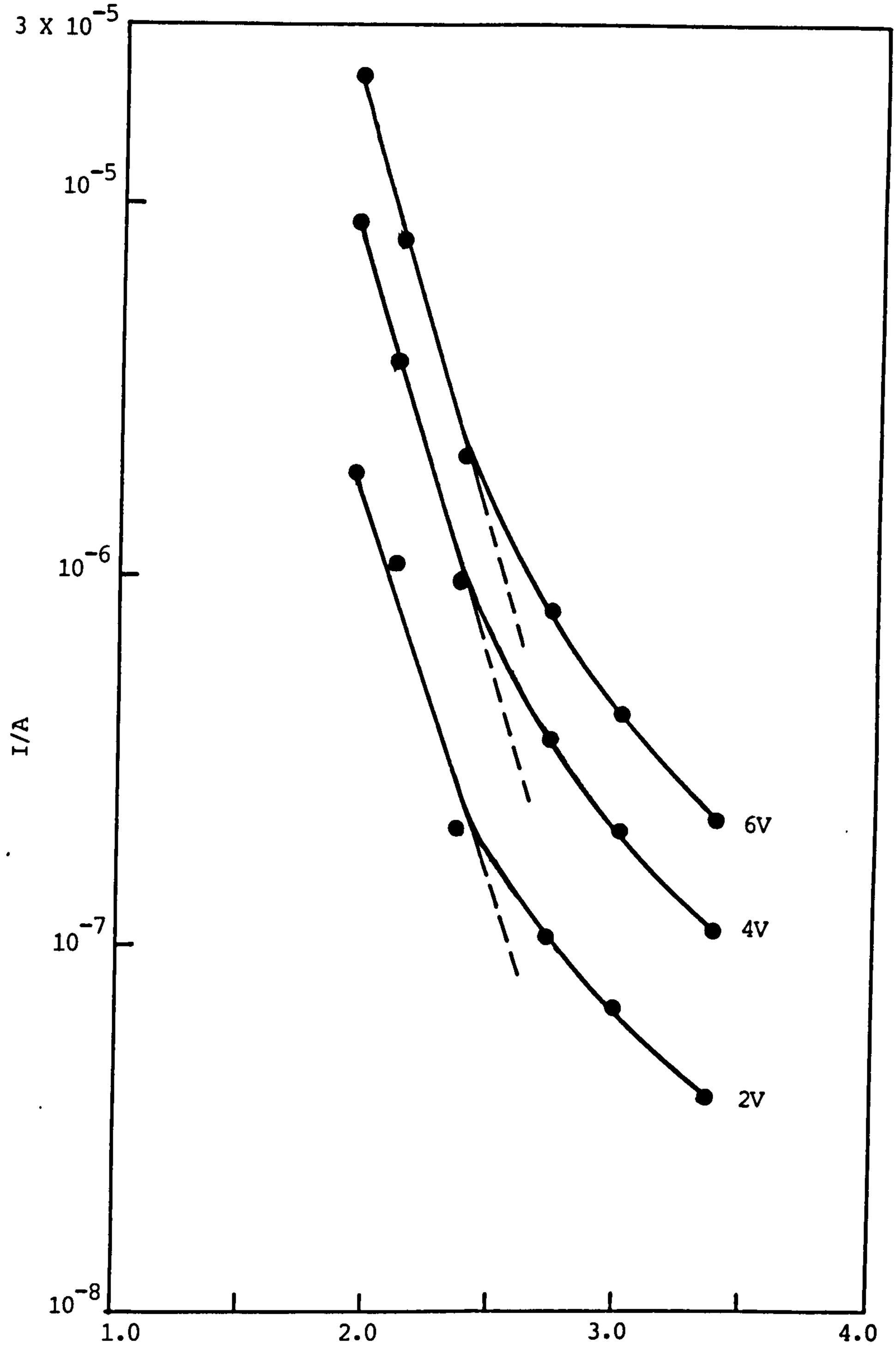

Fig.3.6.6.b Plots of LogI as a function of 1/T for the data in Fig.3.6.5.b at three fixed bias voltages.

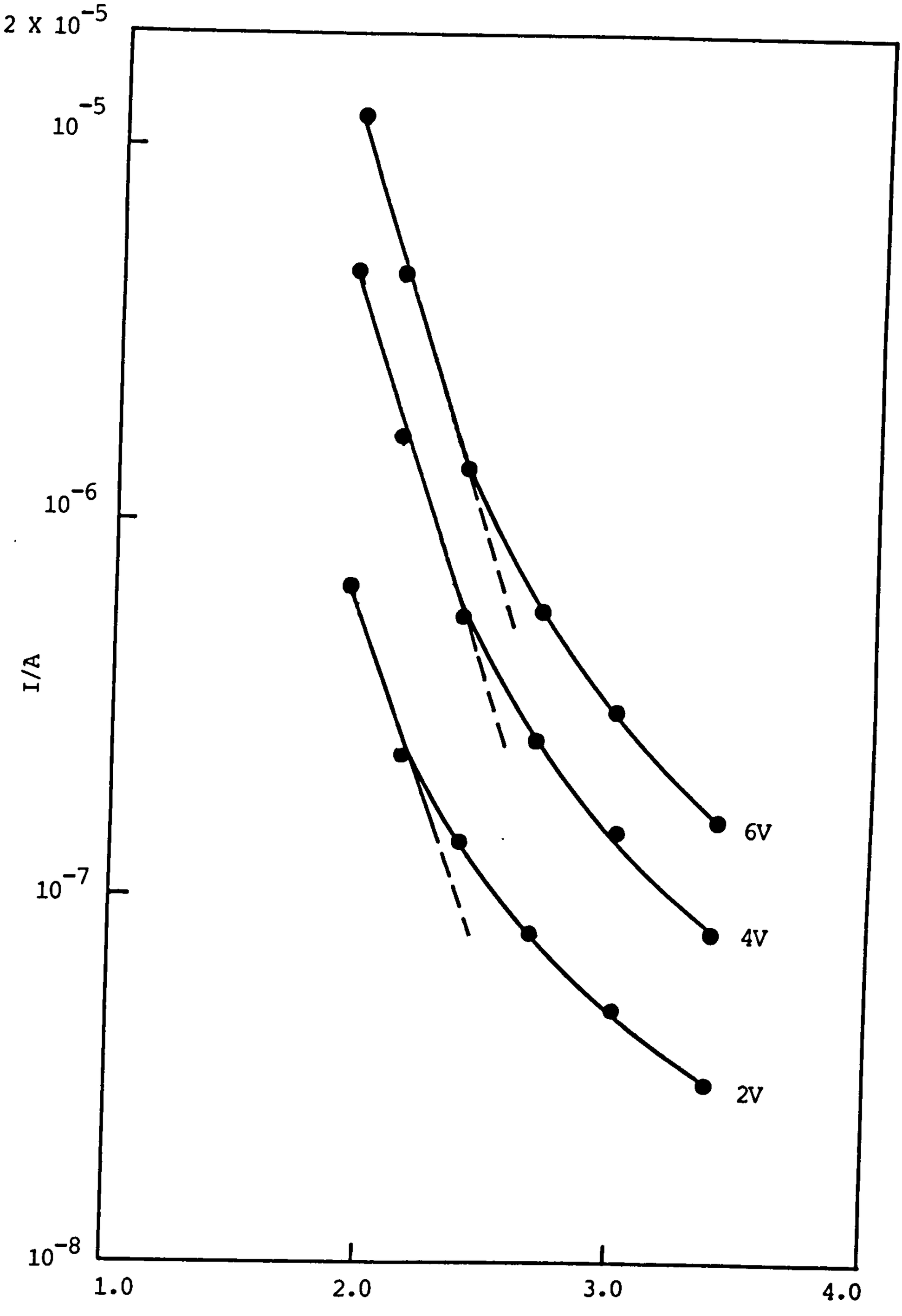

Fig.3.6.6.c. Plots of LogI as a function of 1/T for the data in Fig.3.6.5.c. at three fixed bias voltages.

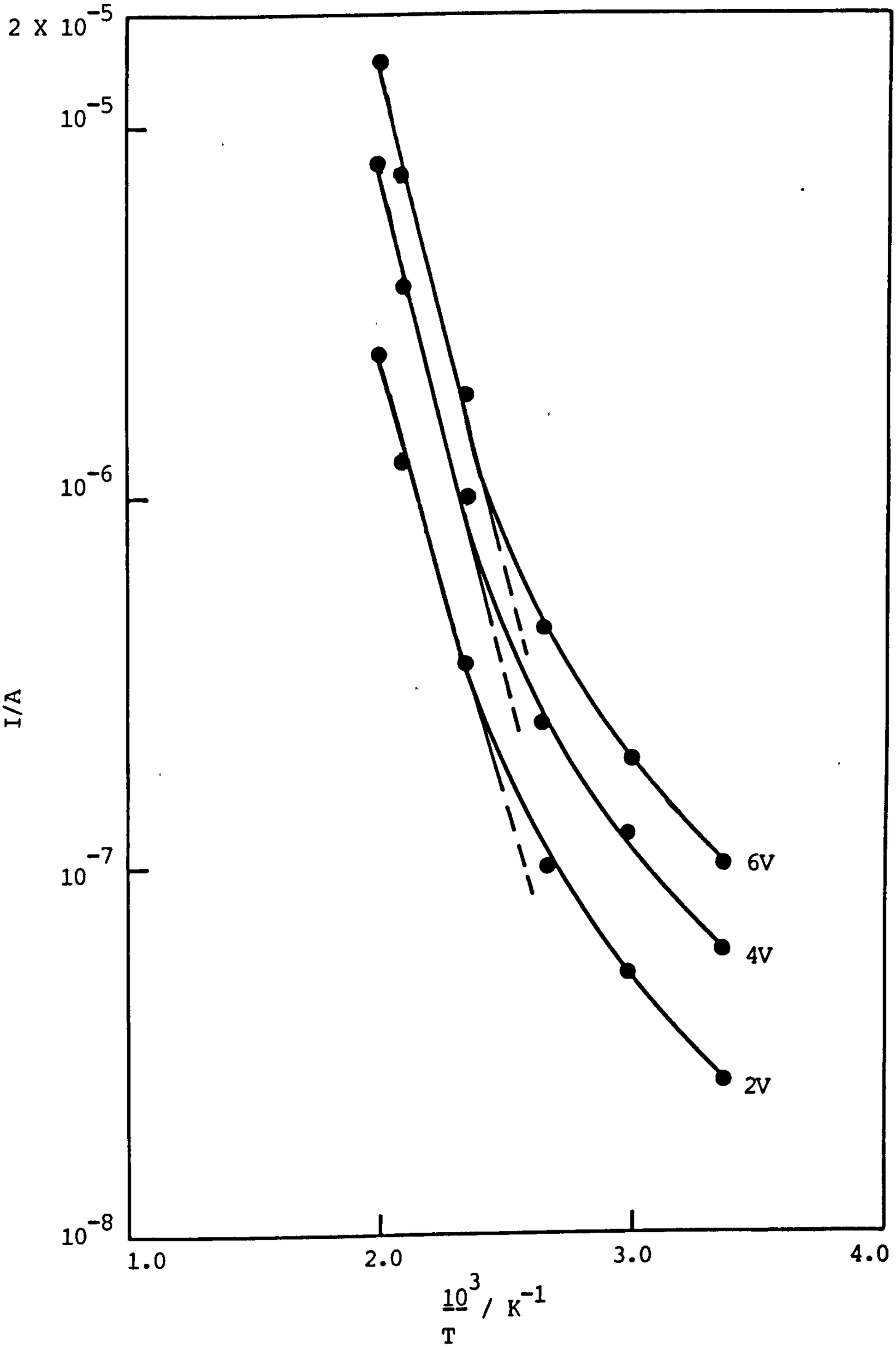

Fig.3.6.6.d. Plots of LogI as a function of 1/T for the data in Fig.3.6.5.d at three fixed bias voltages.

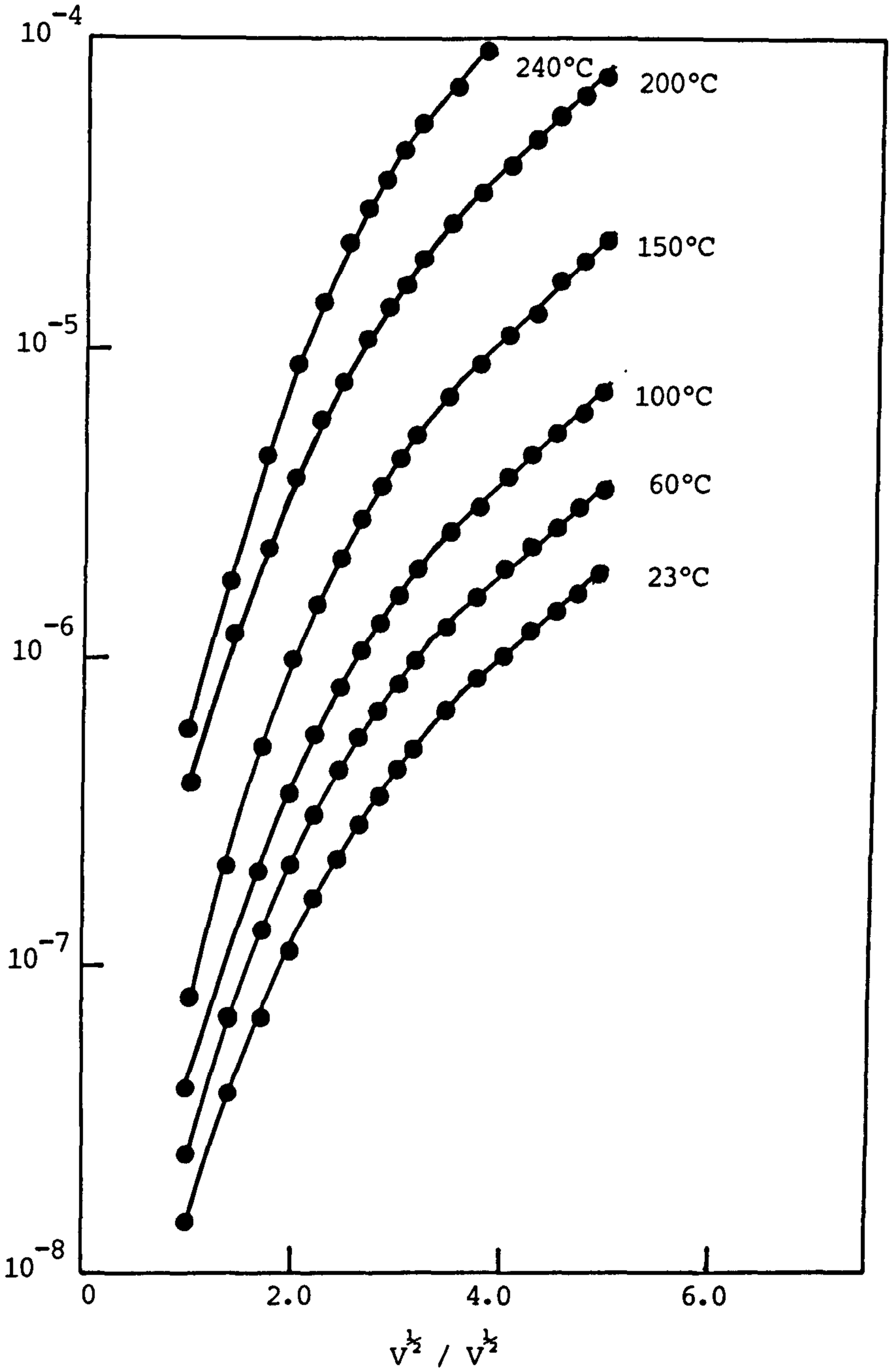

Fig.3.6.7.a Plots of LogI as a function of $V^{\frac{1}{2}}$ for Mo-black coating of thickness ~ 4μm at different temperatures.

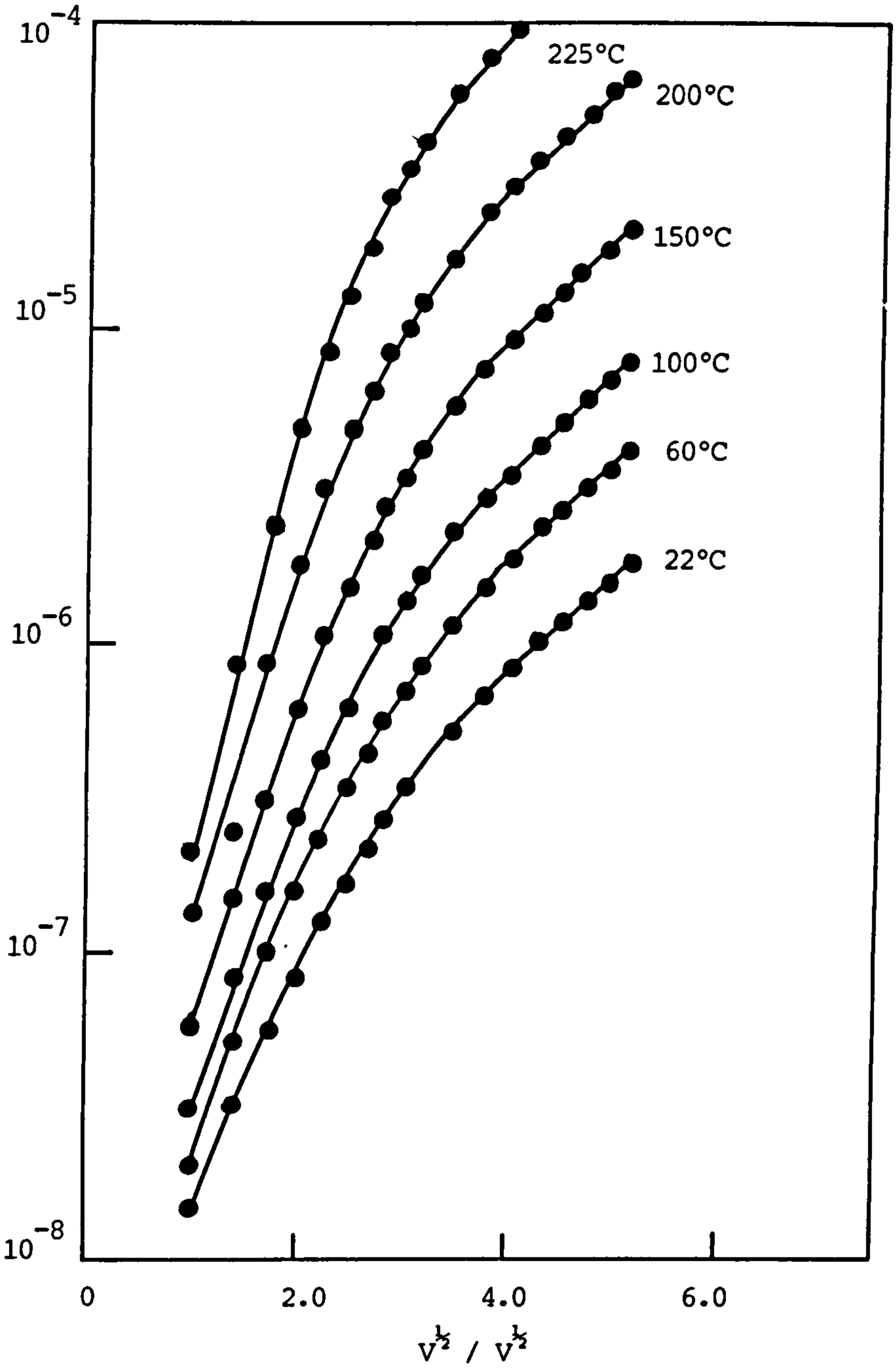

Fig.3.6.7.b. Plots of LogI as a function of $V^{\frac{1}{2}}$ for Mo-black coating of thickness ~ 5.5μm at different temperatures.

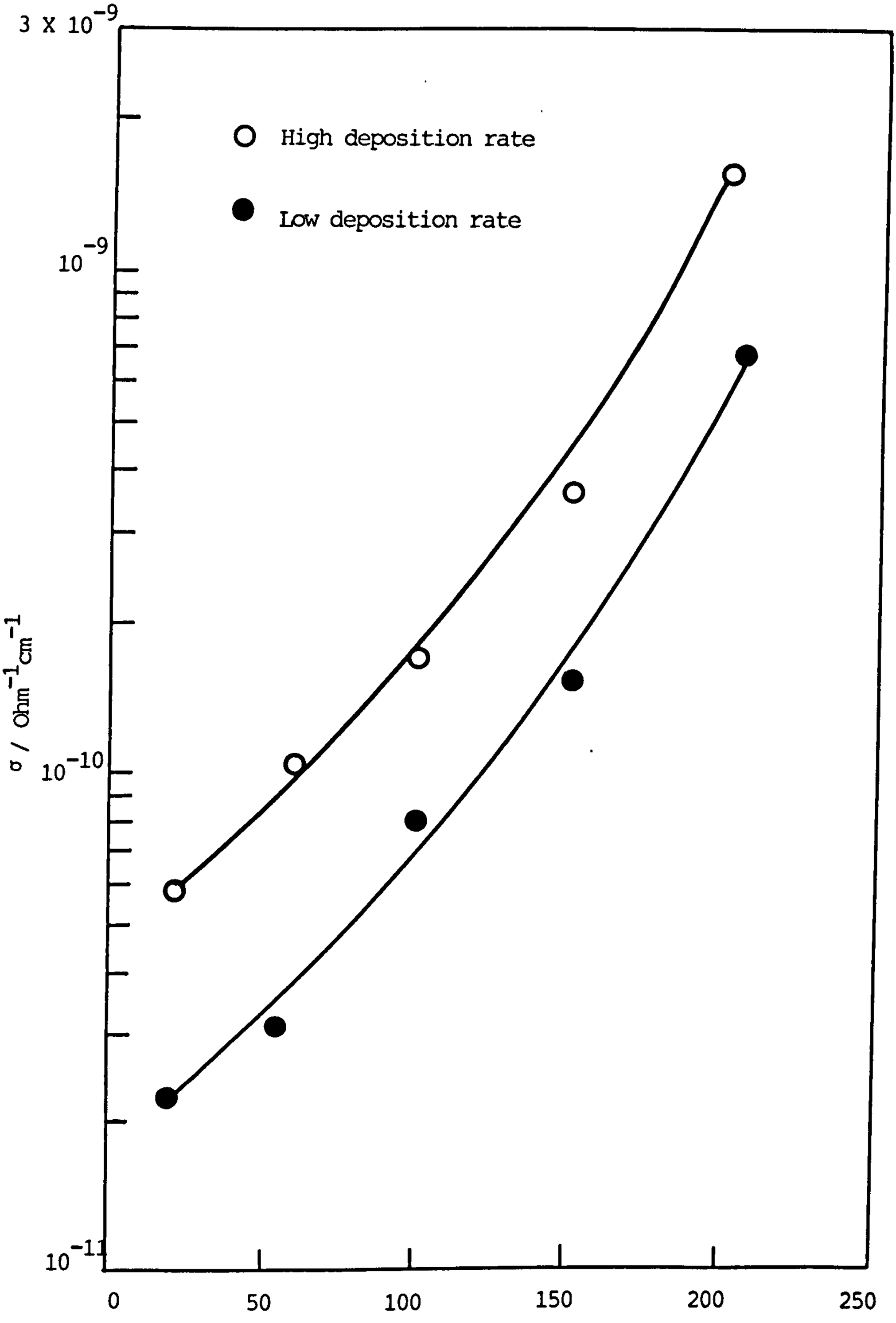

Fig.3.6.8 Effect of deposition rate on the conductivity of Mo-black coatings.

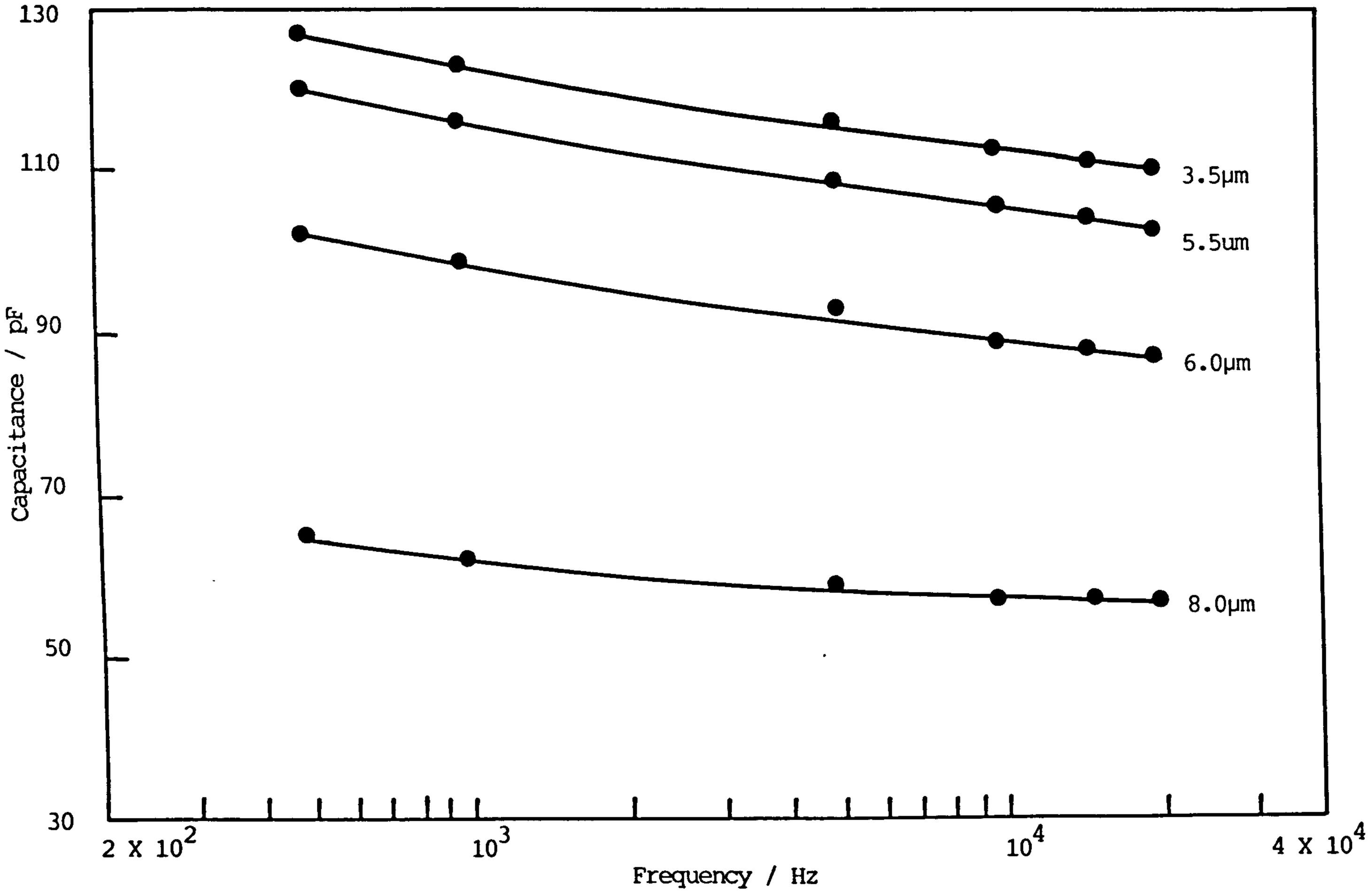

Fig.3.6.9 Variation of capacitance with frequency for Mo-black coatings of various thicknesses.

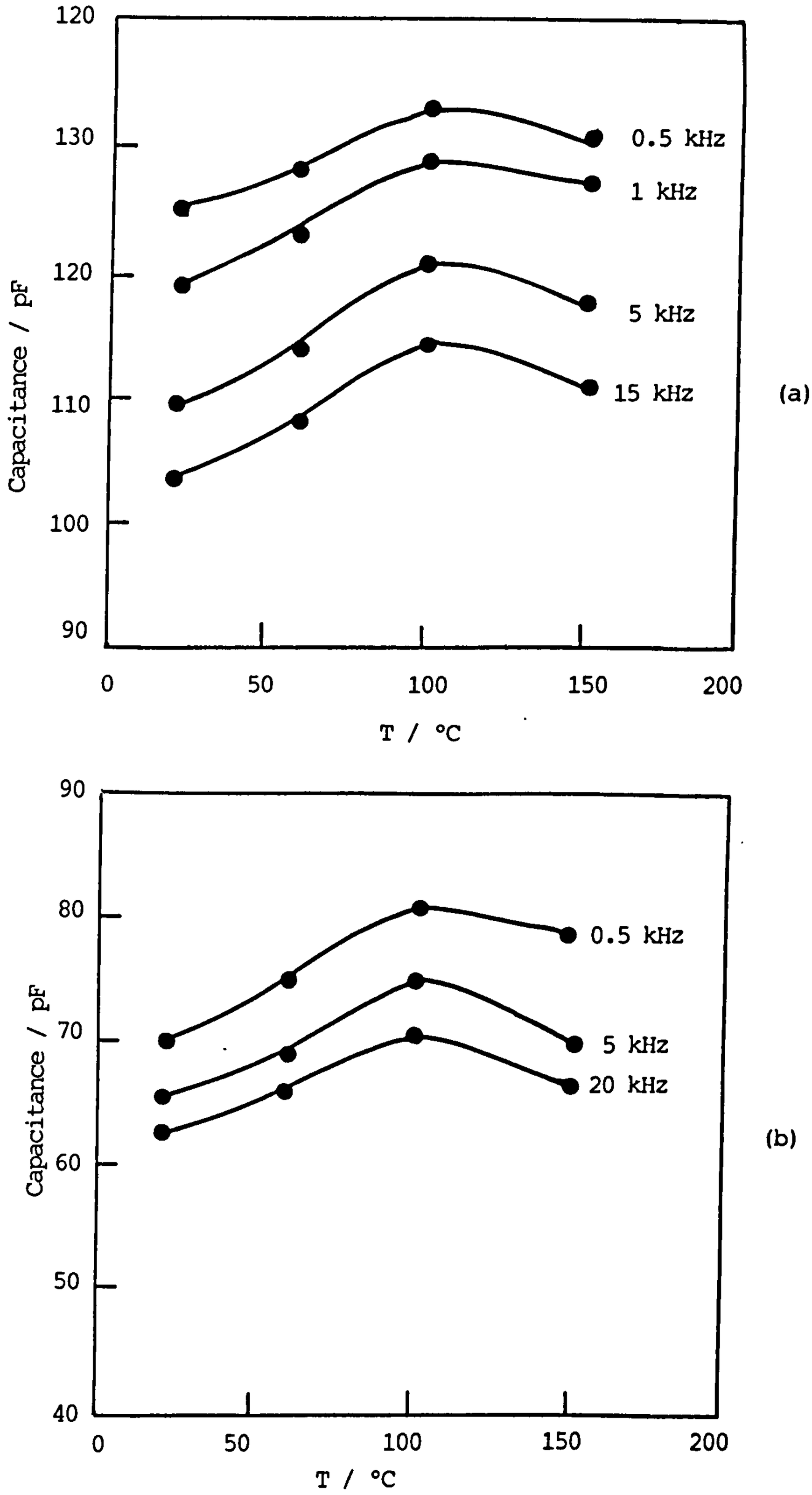

Fig.3.6.10 Variation of capacitance with temperature at different frequencies for Mo-black coatings.
(a) coating thickness ~ 4 μm
(b) coating thickness ~ 7 μm.

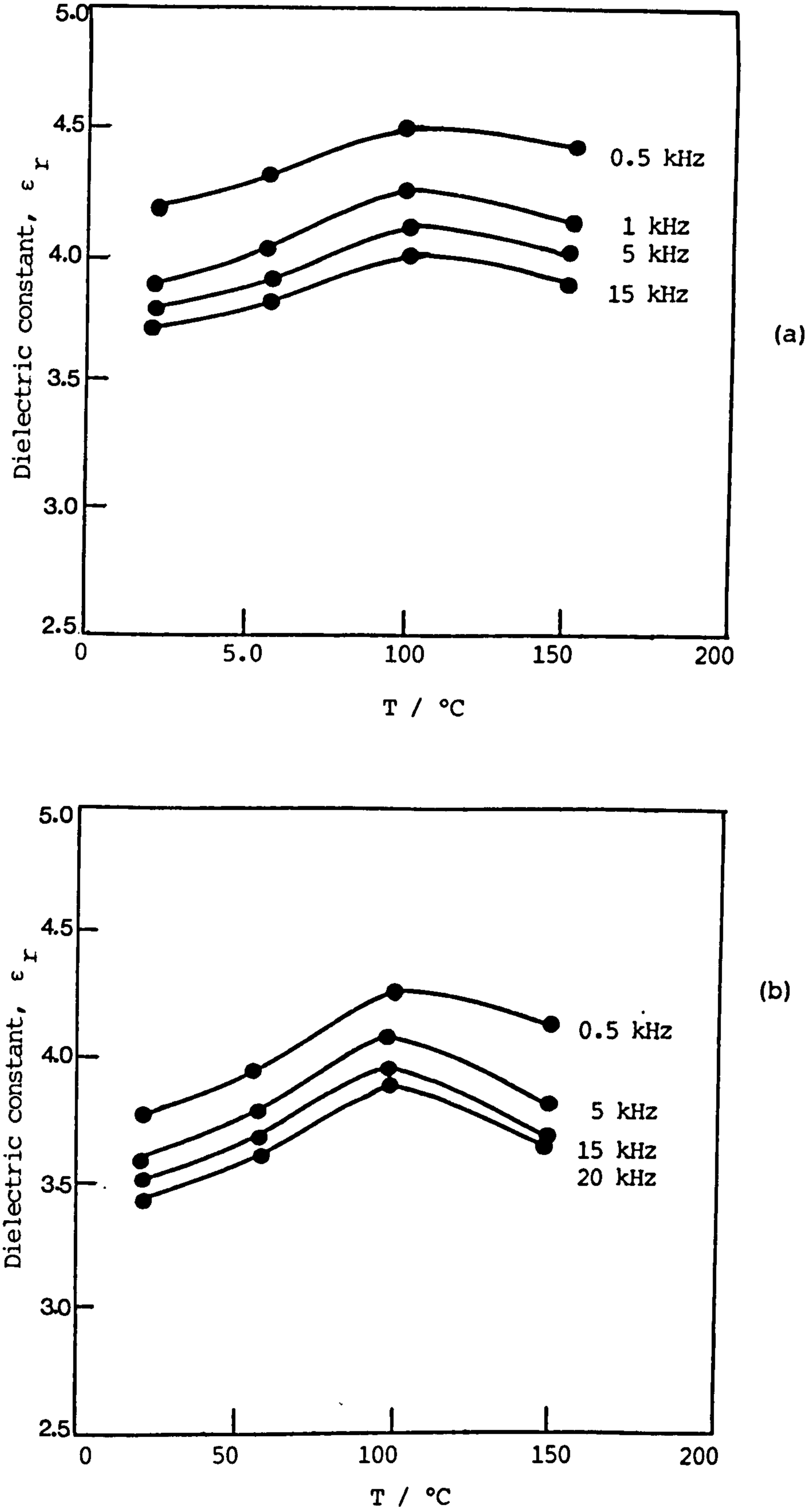

Fig.3.6.11 Variation of relative dielectric constant ε_r with temperature at different fixed frequencies for Mo-black coatings.
(a) coating thickness~4 μm
(b) coating thickness~7 μm

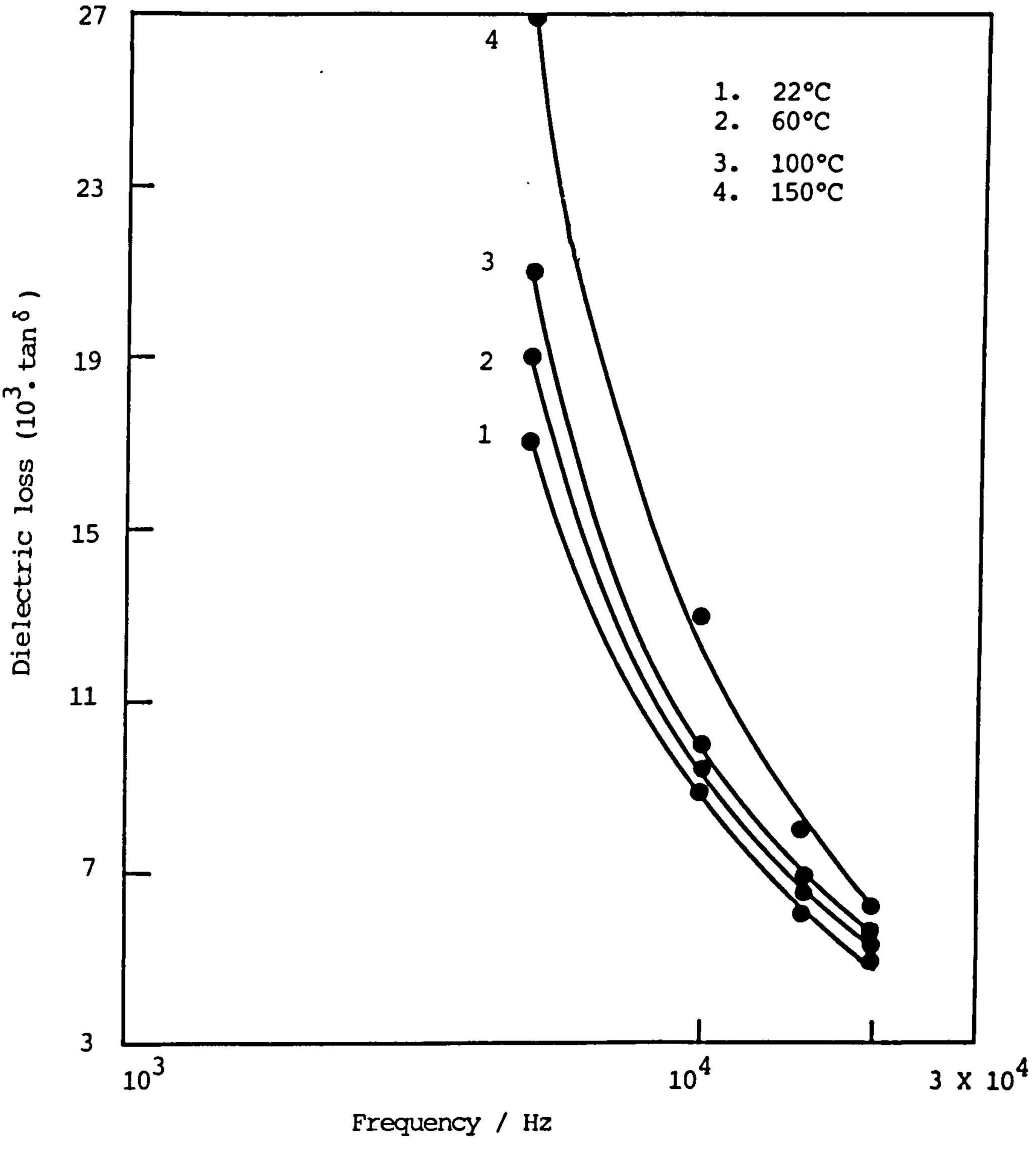

Figure 3.6.12 Plots of dielectric loss tan δ as a function of frequency for Mo-black coating of thickness ~ 4 μm at different temperatures.

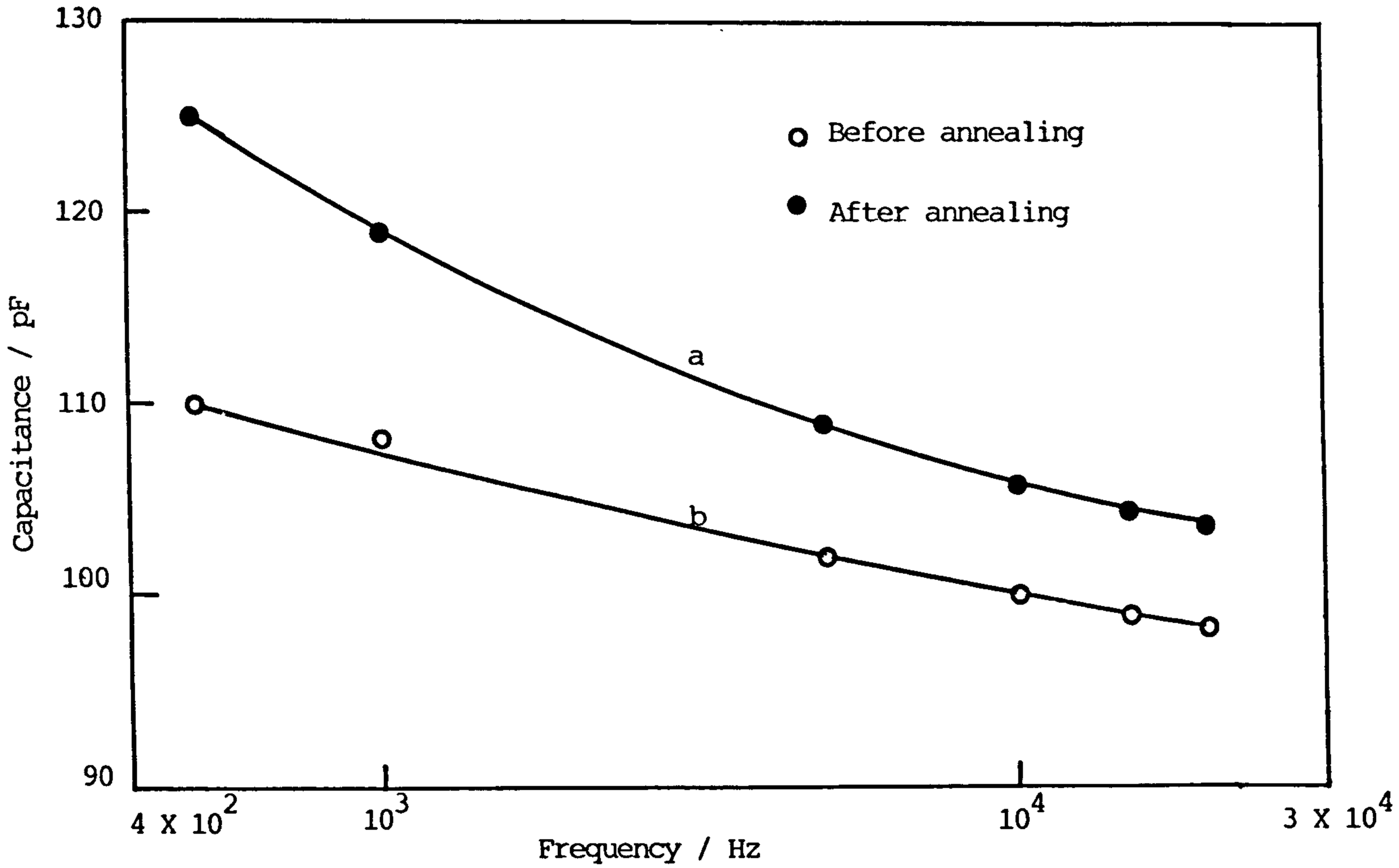

Fig.3.6.13 Effect of annealing on capacitance of Mo-black coating of thickness ~4 μm.

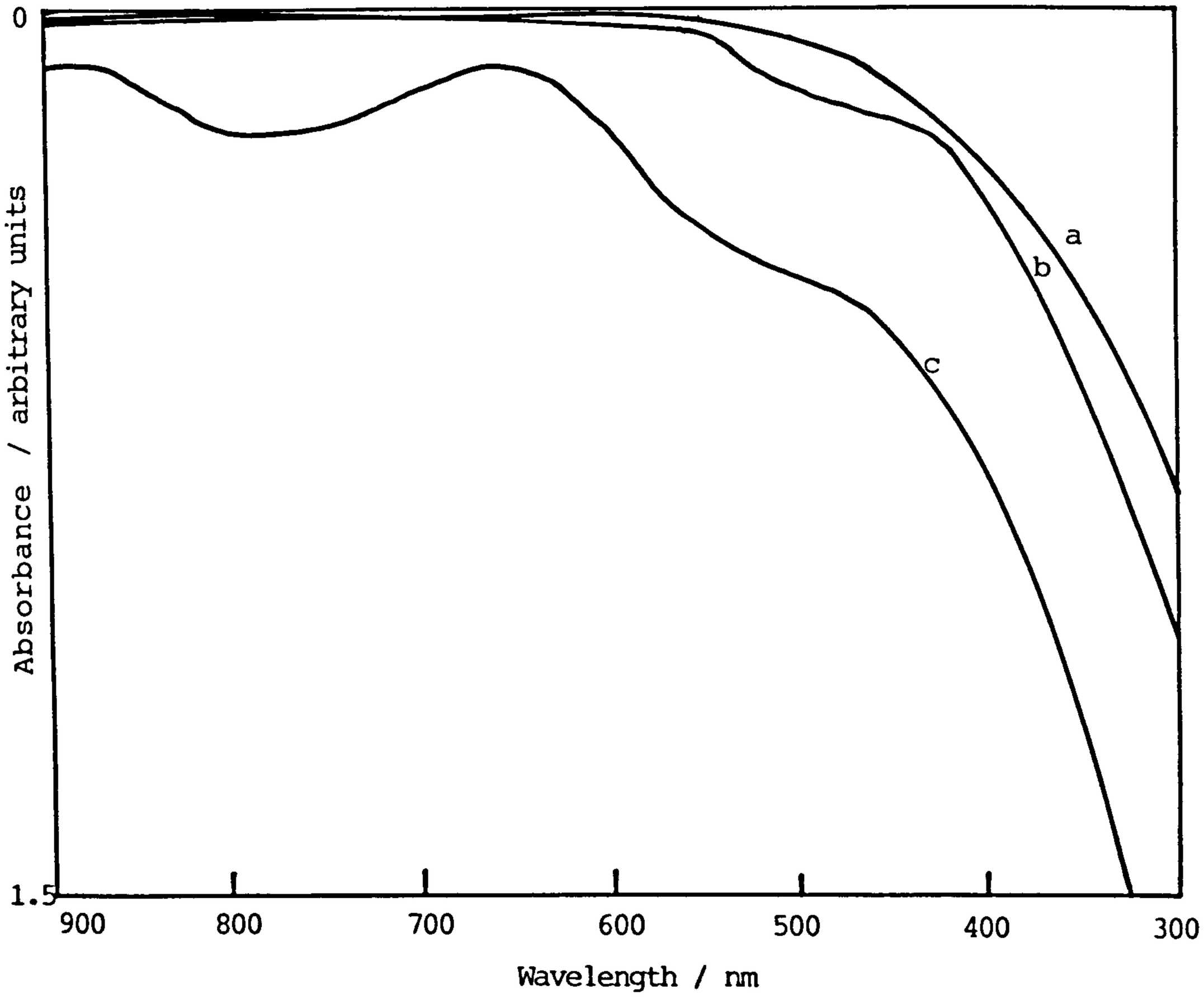

Fig.3.7.1 Absorbance spectra as a function of wavelength for Mo-black coating of different thicknesses prepared at low current density of about 1.4 mA/cm^2: (a) 210 nm, (b) 230 nm, (c) 500 nm.

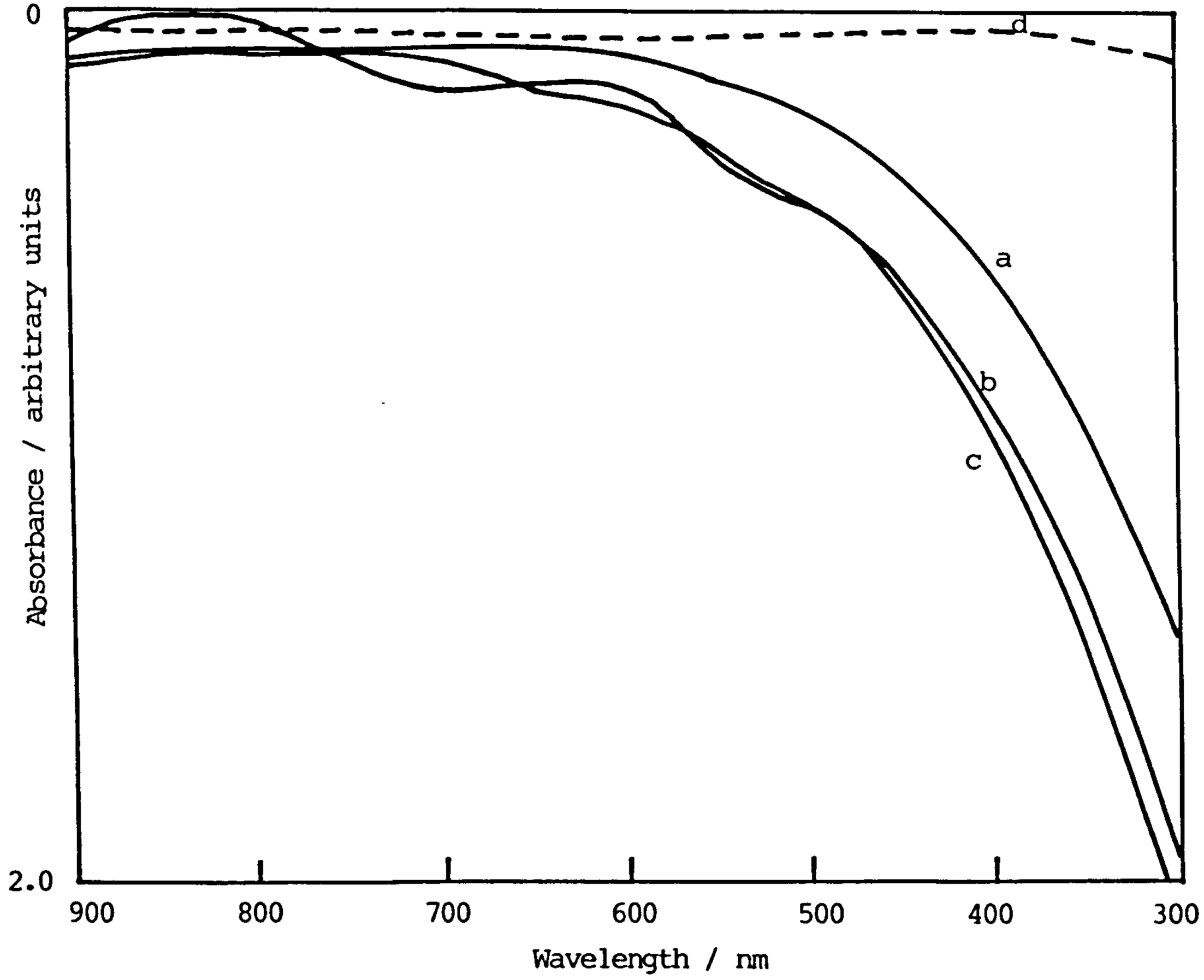

Fig.3.7.2 Absorbance spectra as a function of wavelength for Mo-black coating of different thicknesses prepared at high current density of about $2.8 mA/cm^2$: (a) 300 nm, (b) 370 nm, (c) 400 nm, (d) aluminium/glass substrate.

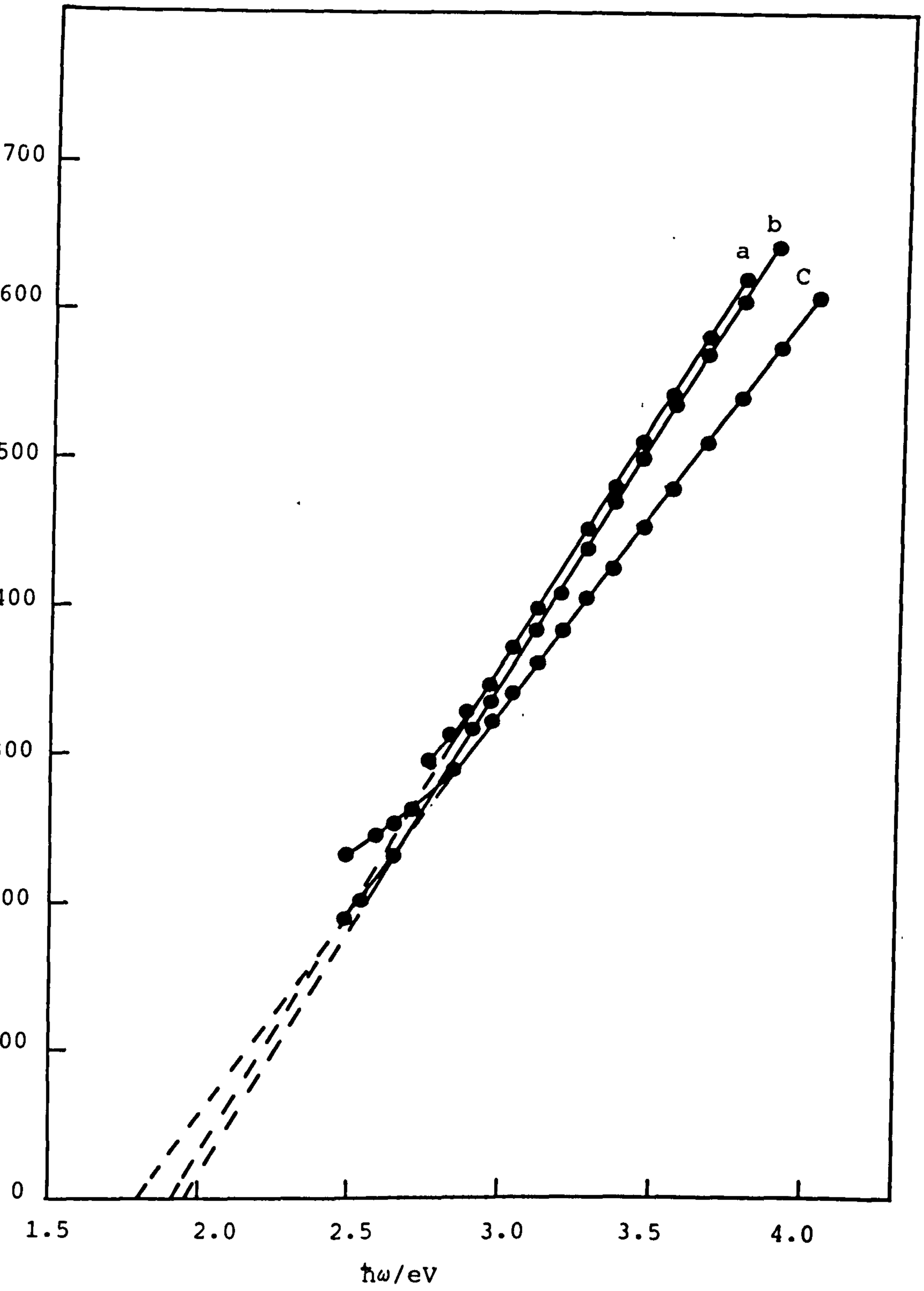

Fig. 3.7.3. $(\alpha\hbar\omega)^{\frac{1}{2}}$ as a function of $\hbar\omega$ for the data of Fig.3.7.1. (a) 210 nm, (b) 230 nm, (c) 500 nm.

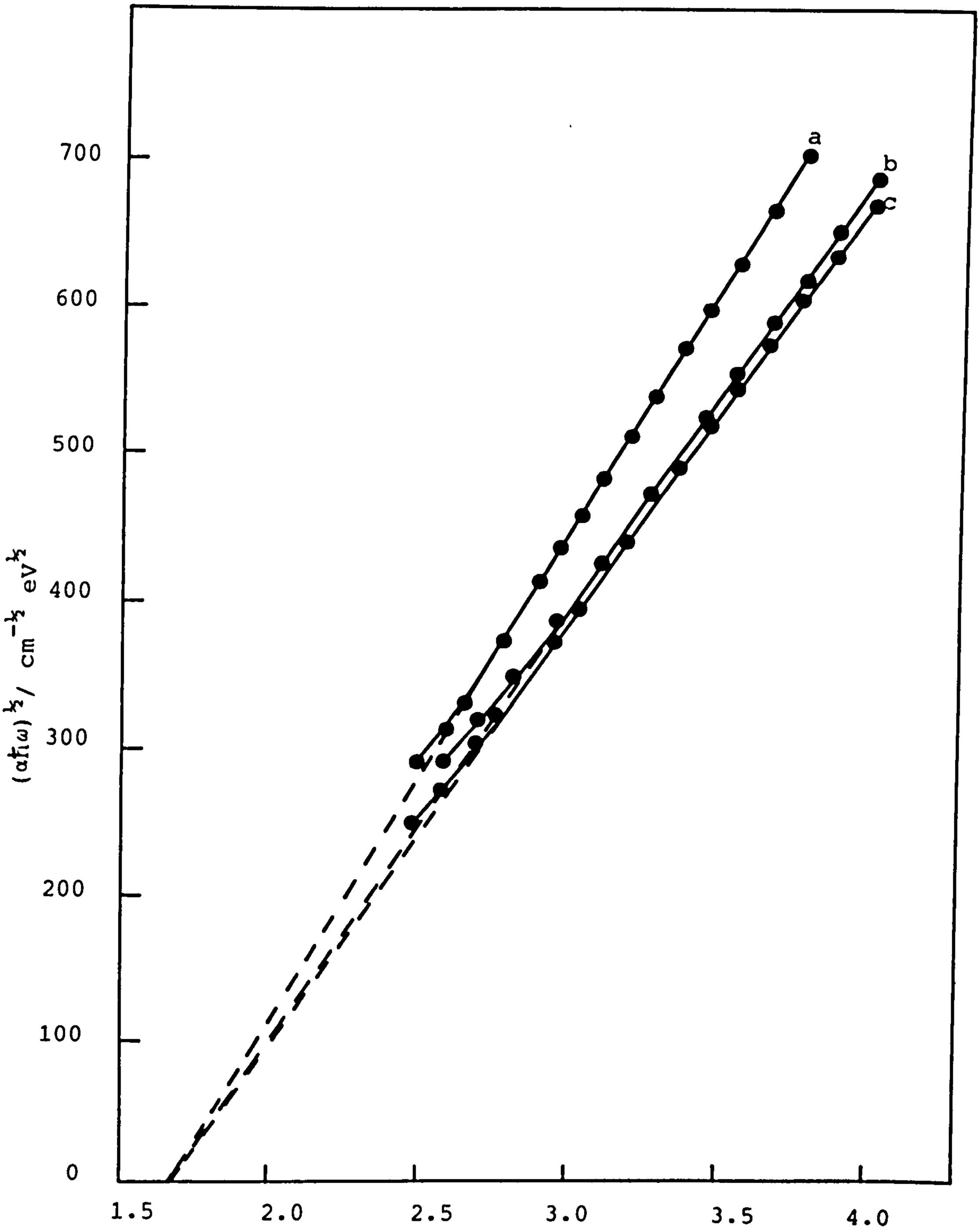

Fig. 3.7.4. $(\alpha\hbar\omega)^{\frac{1}{2}}$ as a function of photon energy $\hbar\omega$ for the data of Fig 3.7.2. (a) 300 nm, (b) 370 nm, (c) 400 nm.

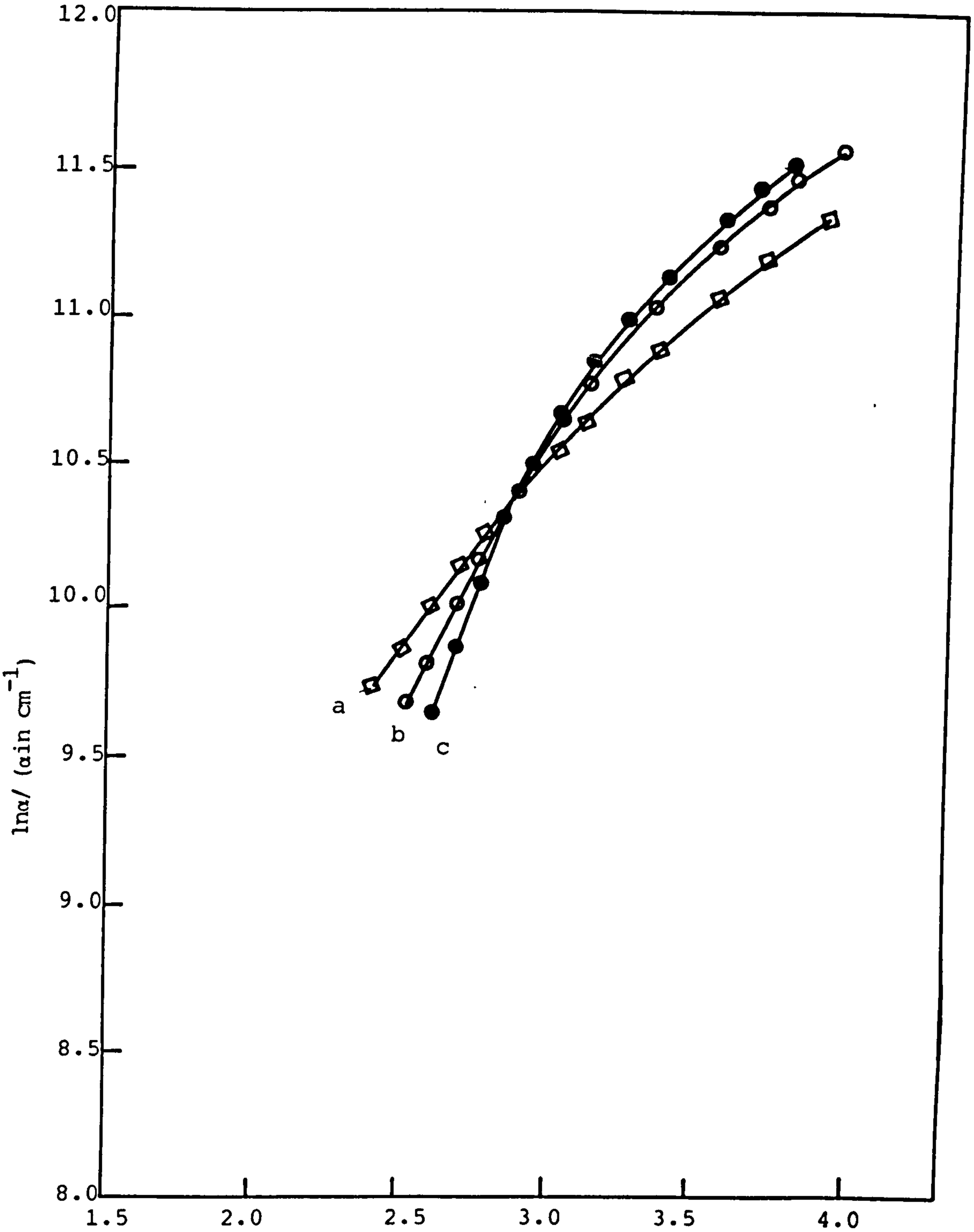

Fig. 3.7.5. Data of Fig.3.7.1. replotted in accordance with the Urbach rule. (a) 210nm, (b) 230nm, (c) 500nm.

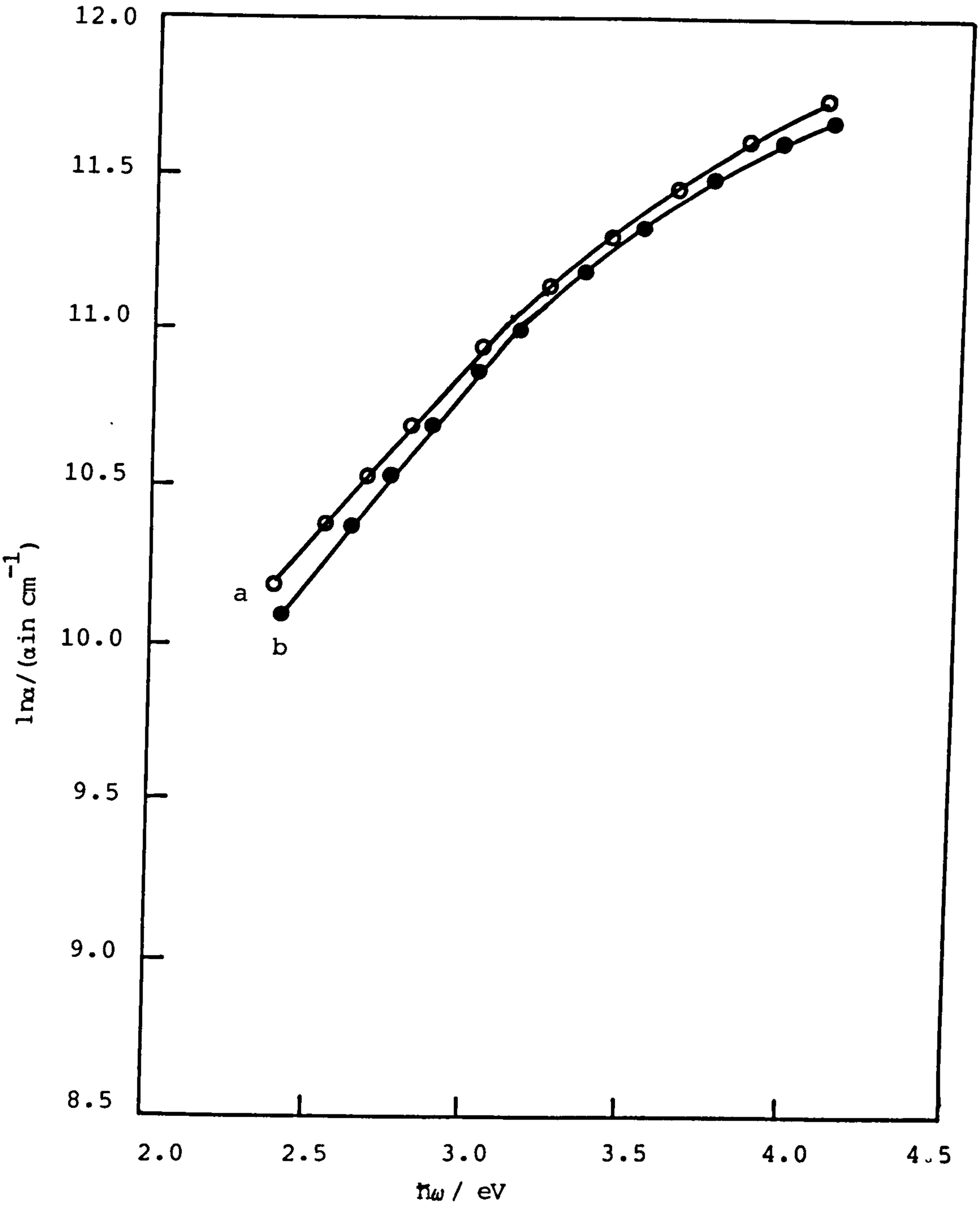

Fig. 3.7.6. Data of Fig. 3.7.2. replotted in accordance with the Urbach rule. (a) 300 nm, (b) 370 nm.

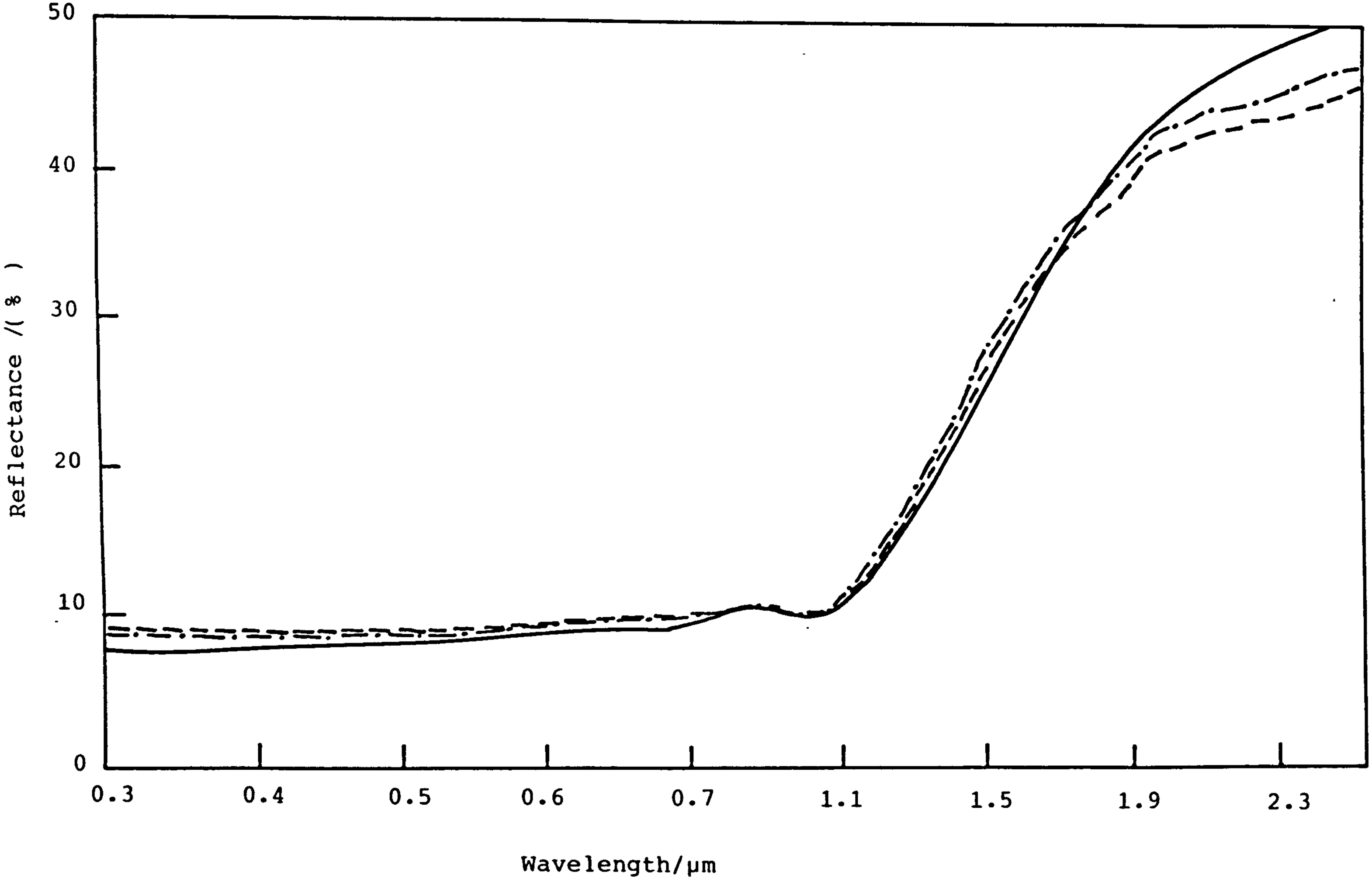

Fig. 4.1 (a) Spectral reflectance of Mo-black dip coating on etched zincsubstrate before and after heating in air at 100°C; (——) as prepared, (-·-·) 8 hours, (----) 24 hours.

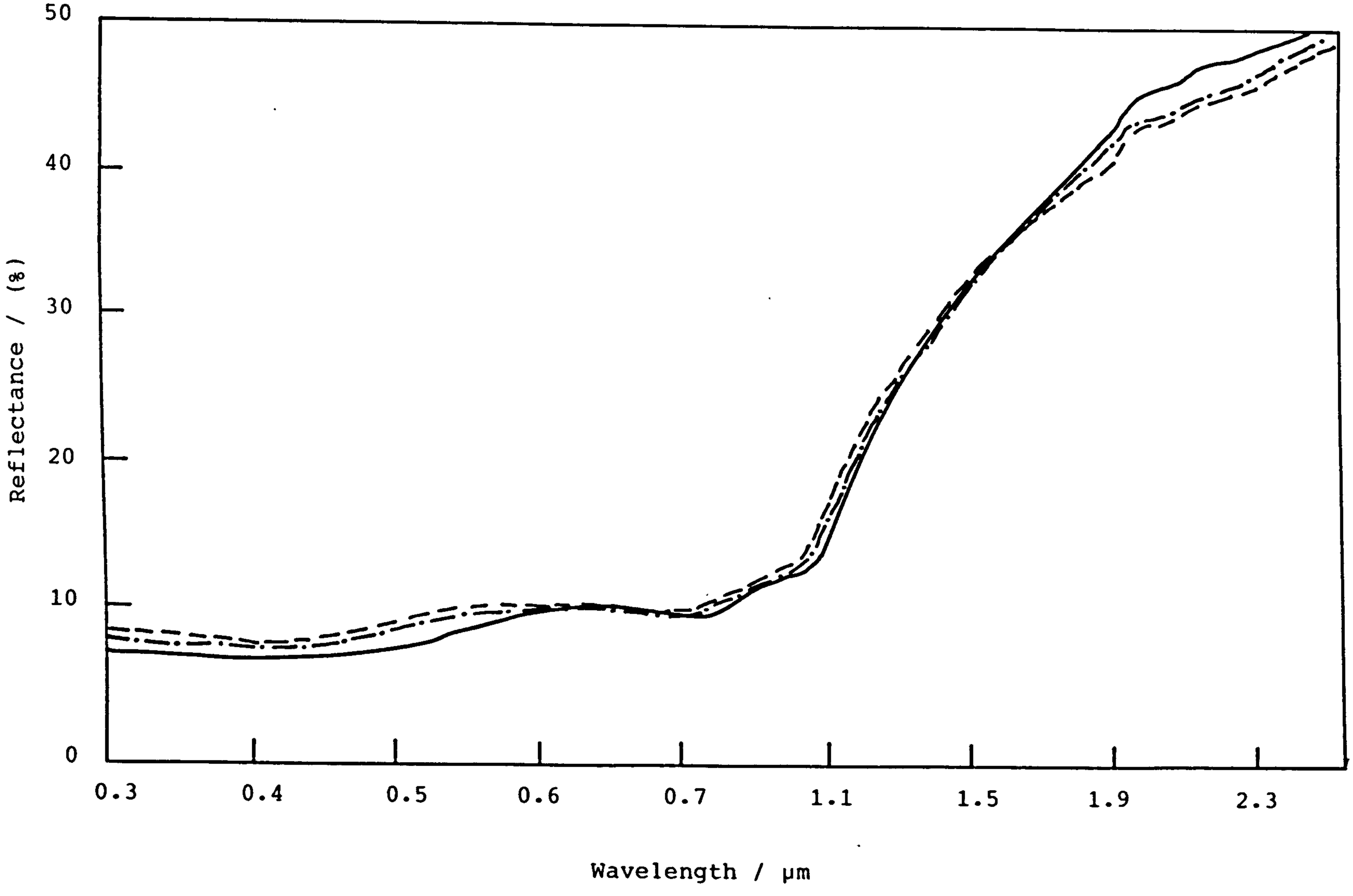

Fig. 4.1.b. Spectral reflectance of Mo-black dip coating on etched zinc before and after heating in air at 150°C; (——) as prepared, (-·-·) 8 hours, (----) 24 hours.

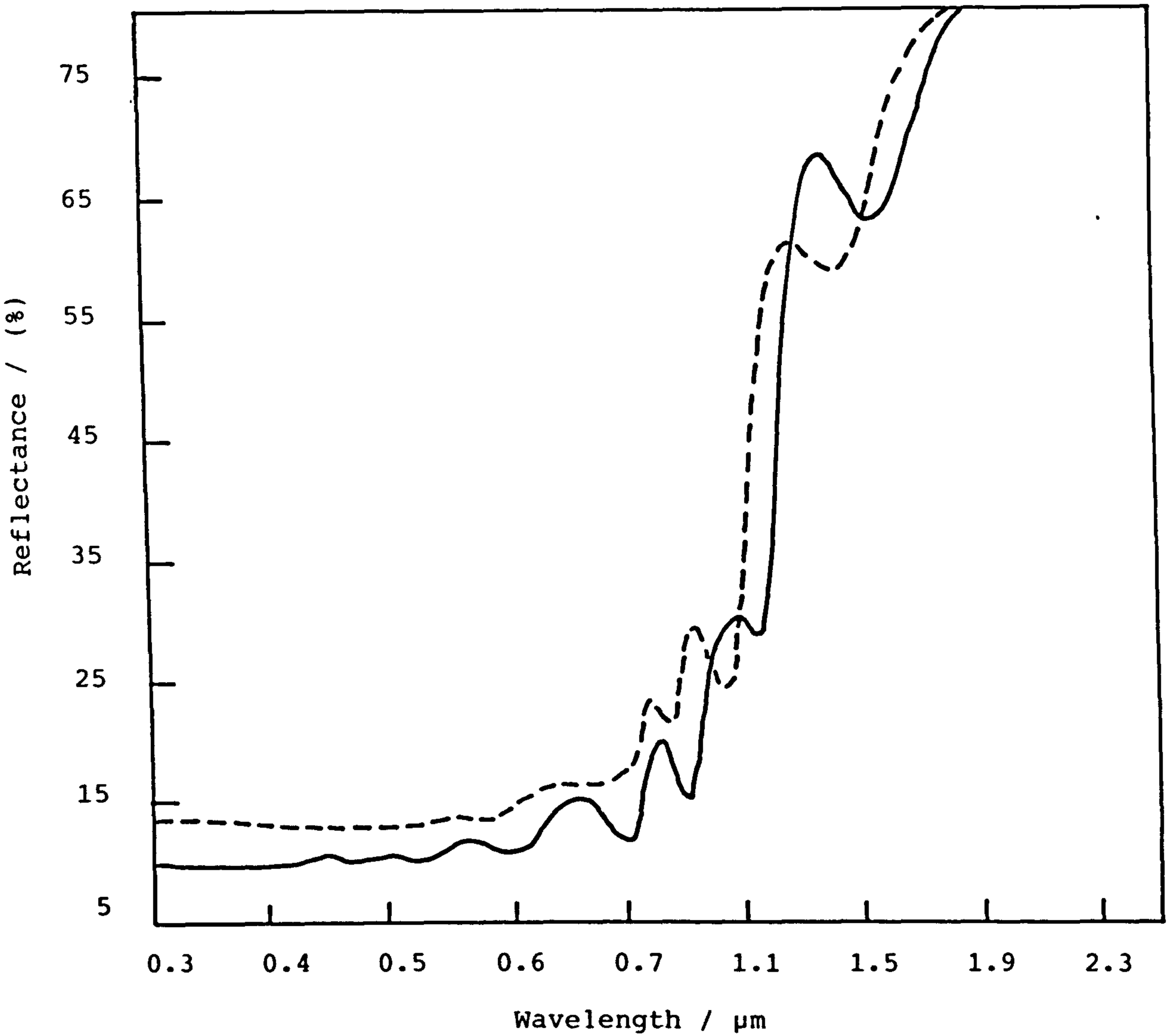

Fig. 4.2. Spectral reflectance of Mo-black dip coating on unetched zinc substrate before heating (——) and after heating (----) at 150°C for 8 hours.

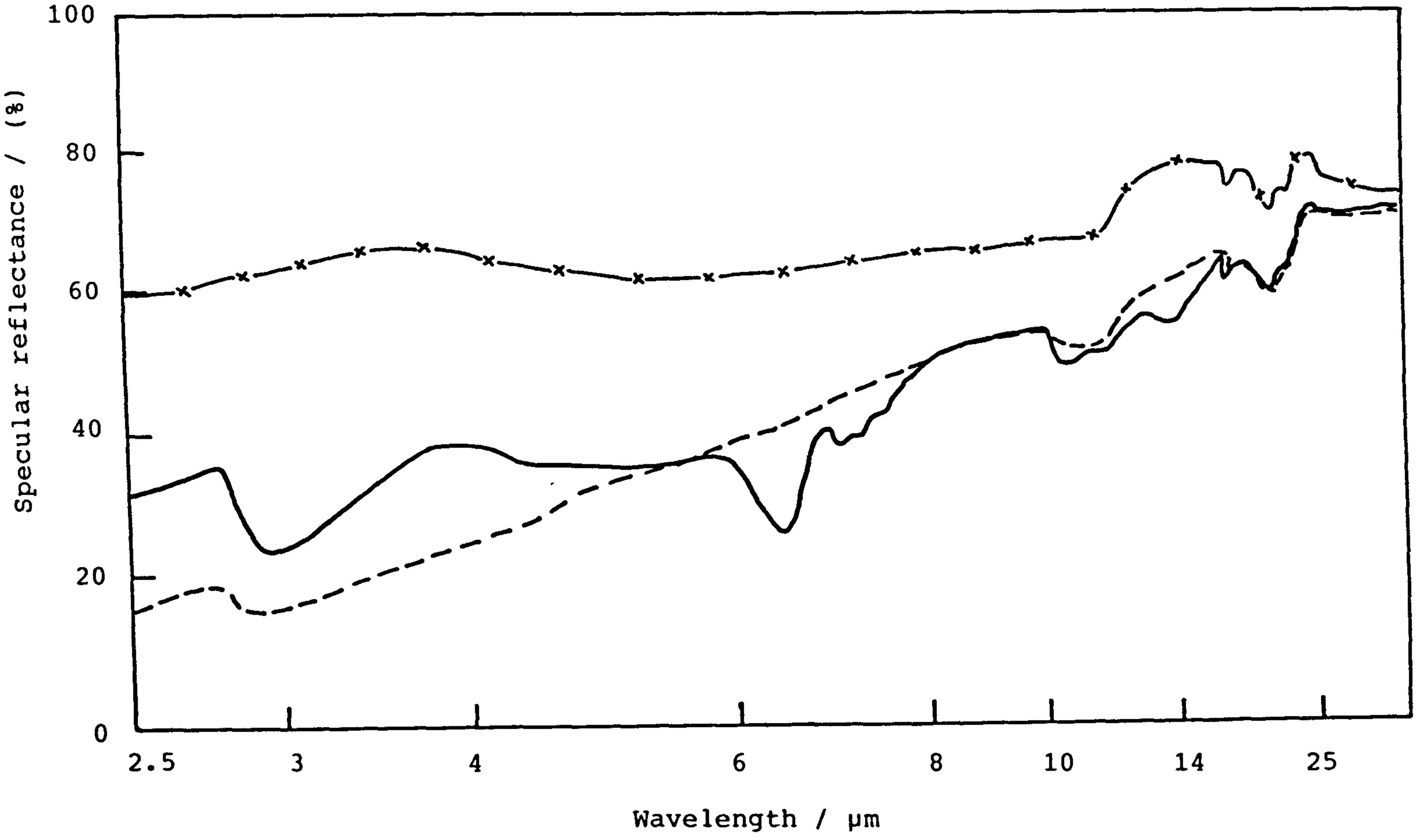

Fig. 4.3. Specular reflectance of a Mo-black dip coating on etched zinc before heating (——) and after heating at 100°C for 24 hours (---), reference Al-mirror (-×-×-)

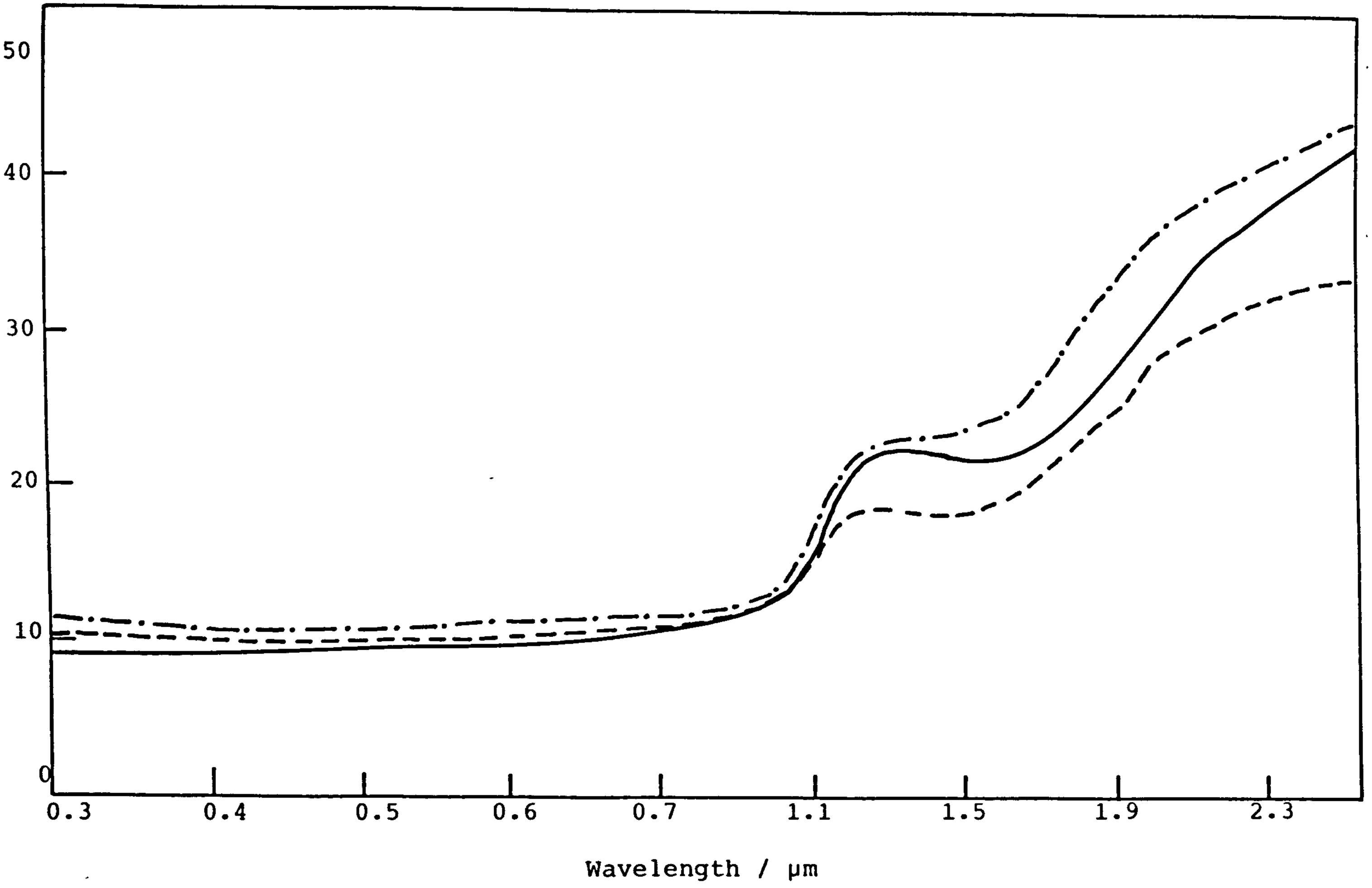

Fig. 4.4. Spectral reflectance of Mo-black dip coating on etched zinc before and after heating in air at 200°C; (——) as prepared, (----) 8 hours, (-·-·-) 16 hours.

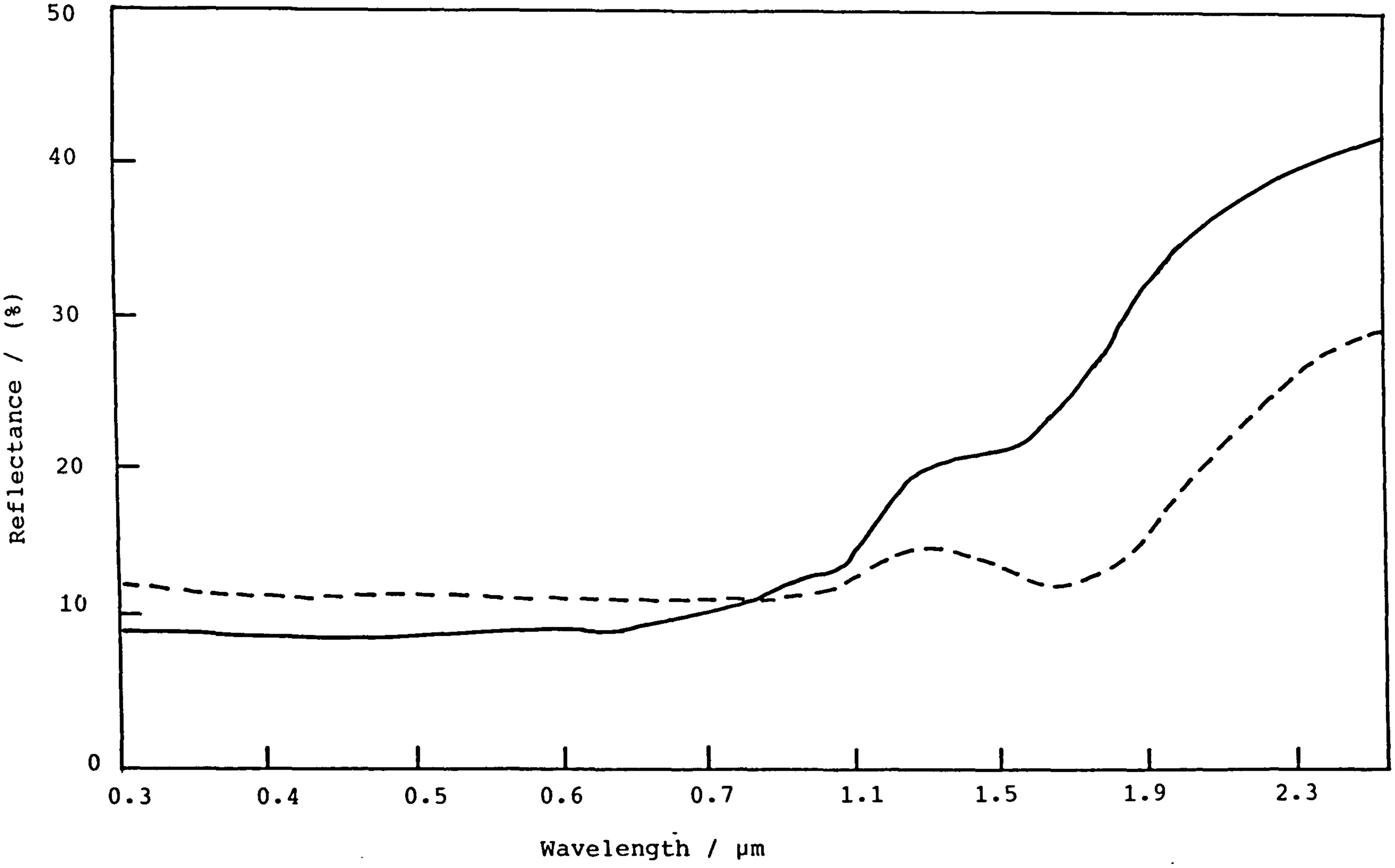

Fig. 4.5. Spectral reflectance of a Mo-black coating on etched zinc substrate before heating (——) and after heating in air at 300°C for 4 hours (---).

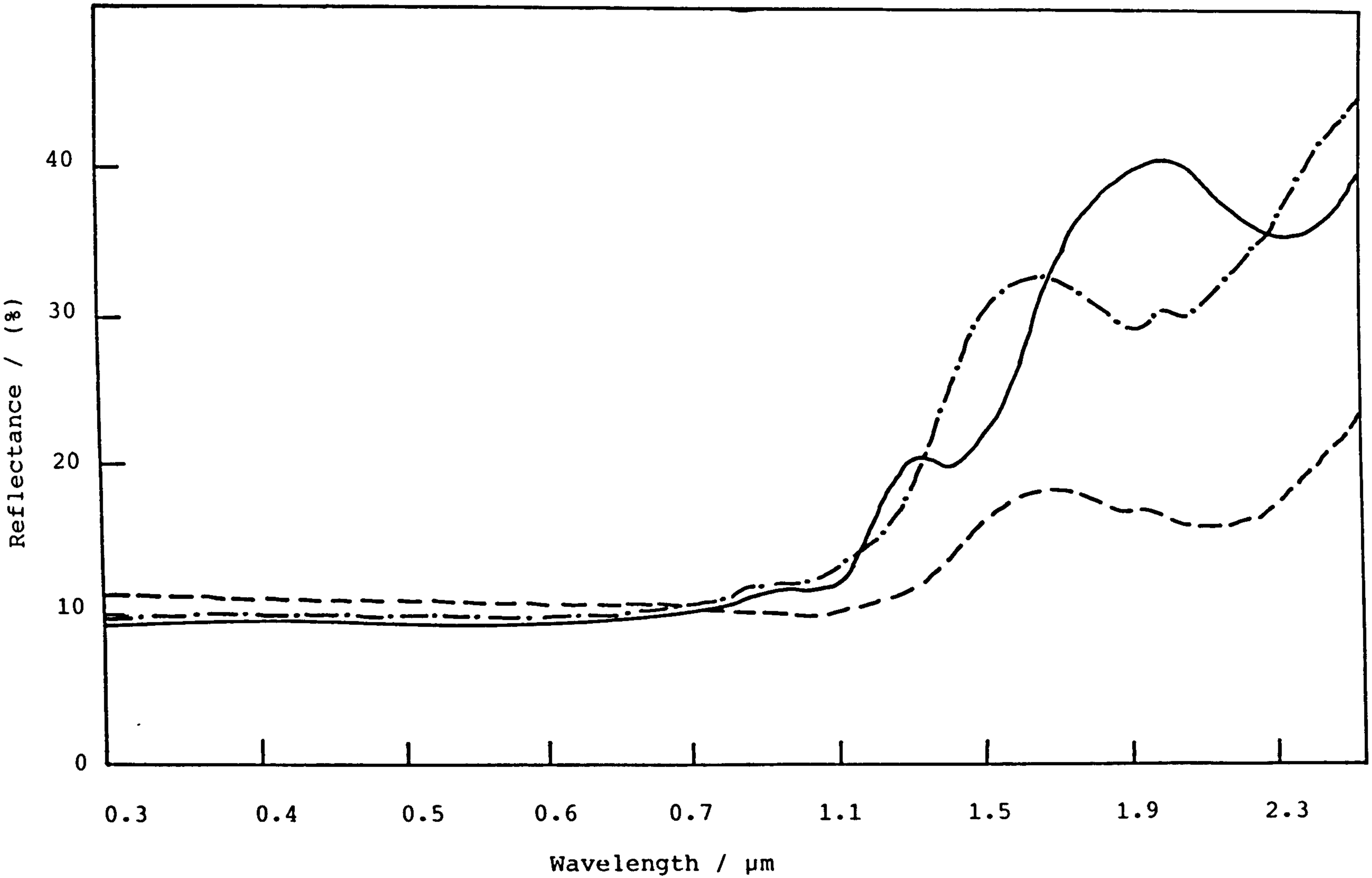

Fig. 4.6. Spectral reflectance of Mo-black coating on etched zinc substrate before heating (——) and after heating in air; 8 hours at 200°C (-·-·), 3 hours at 300°C (---).

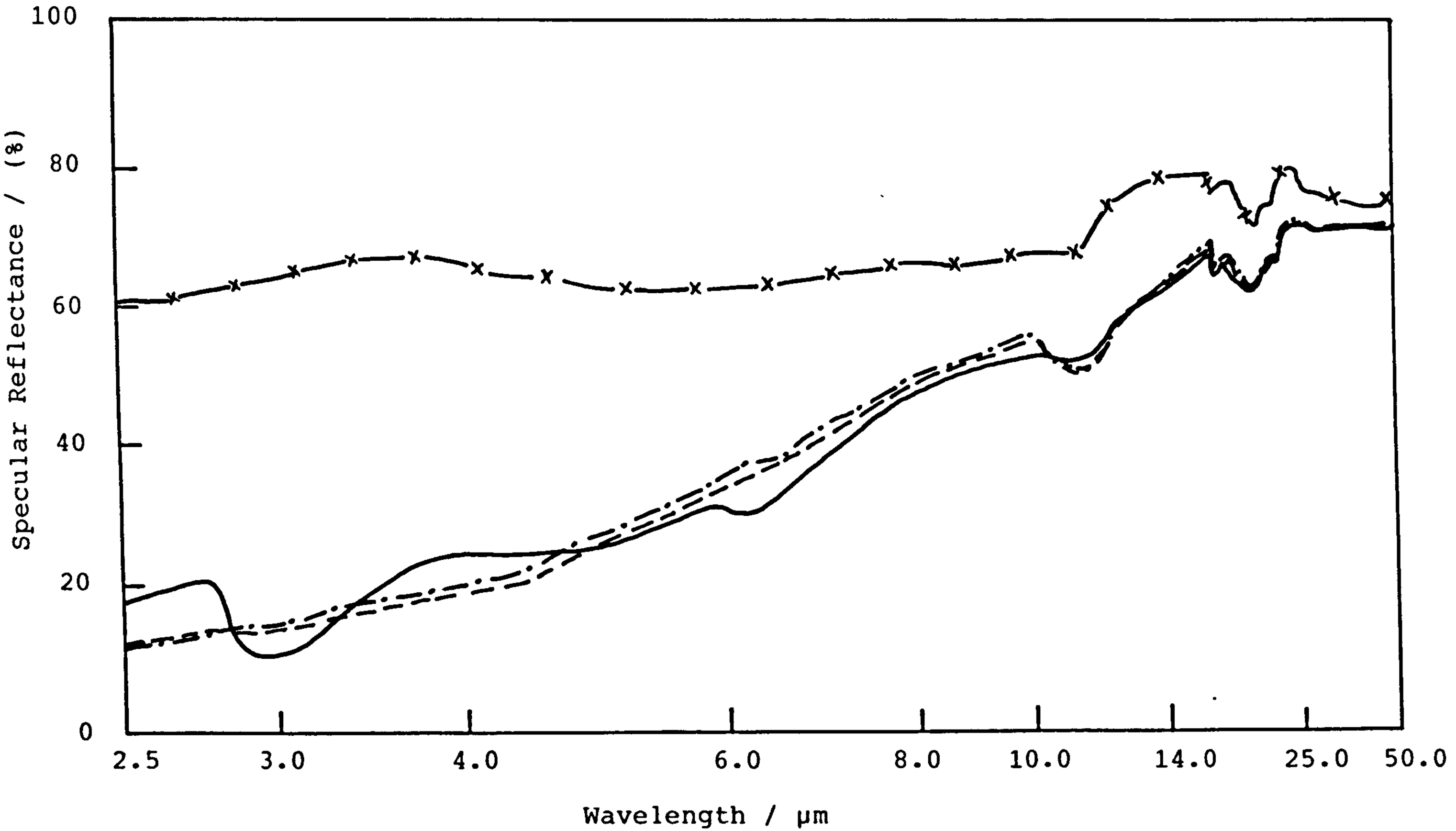

Fig. 4.7. Specular reflectance of a Mo-black coating on etched zinc; (——) as prepared, (-·-·-) 8 hours at 200°C, (----) 4 hours at 300°C, (——x——) Baseline.

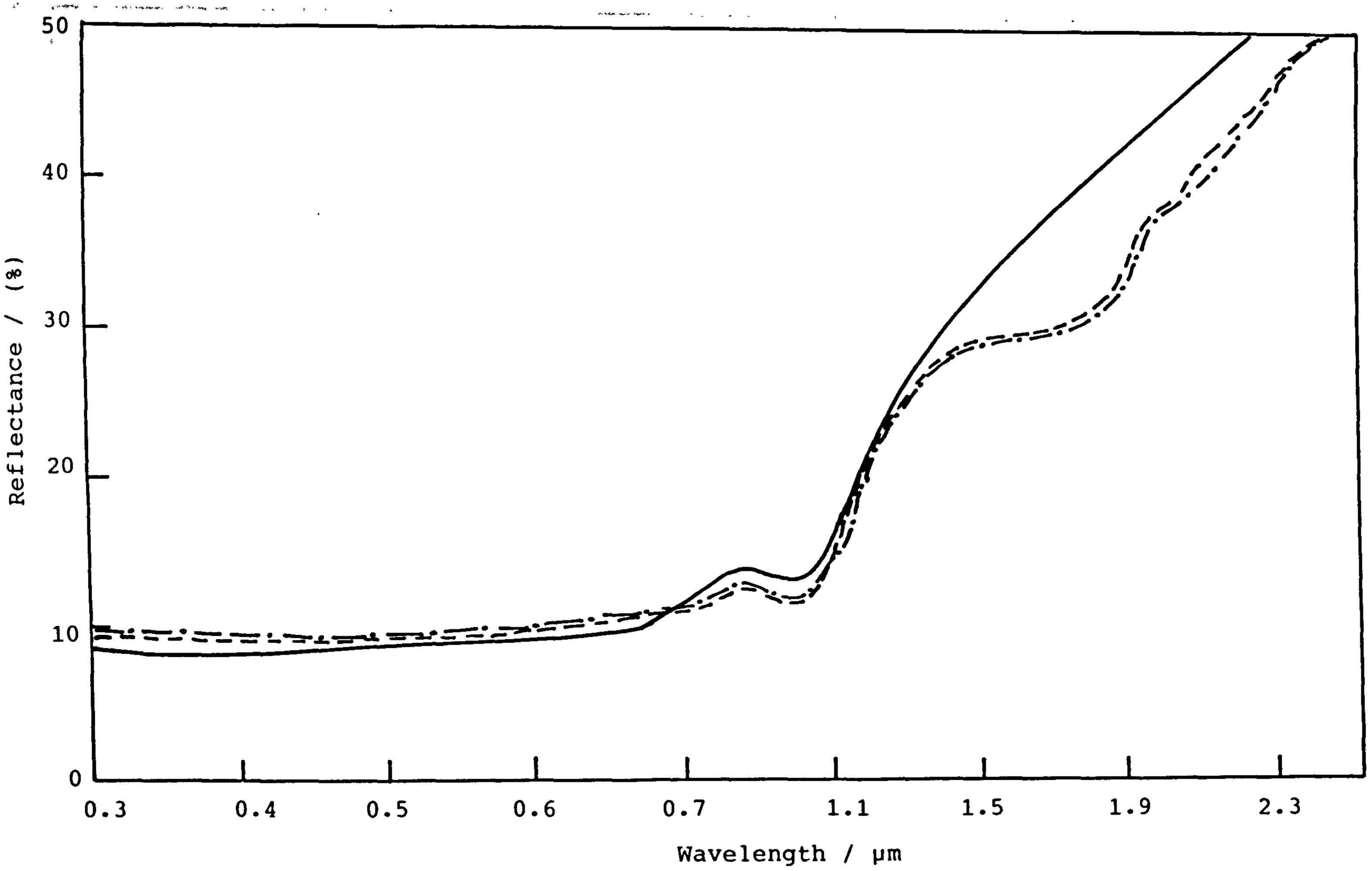

Fig. 4.8. Spectral reflectance of Mo-black coating on etched zinc before heating (——) and after heating in vacuum at 100°C for 8 hours (---) and 24 hours (-·-·).

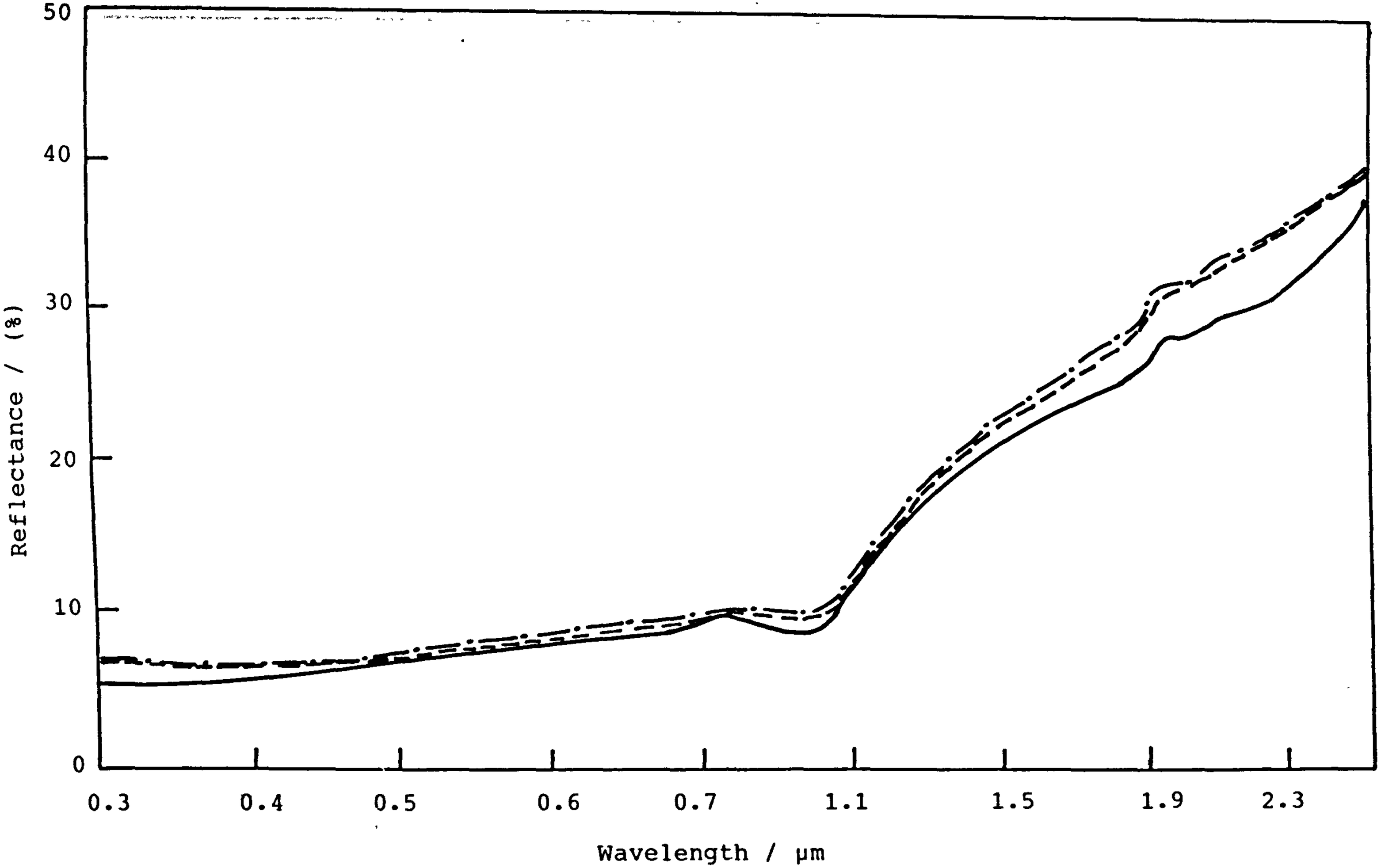

Fig. 4.9. Spectral reflectance of a Mo-black coating on etched zinc (with 50% HNO_3) before heating (—), after heating in vacuum at 100°C for 8 hours (-·-·-·) and 24 hours (----).

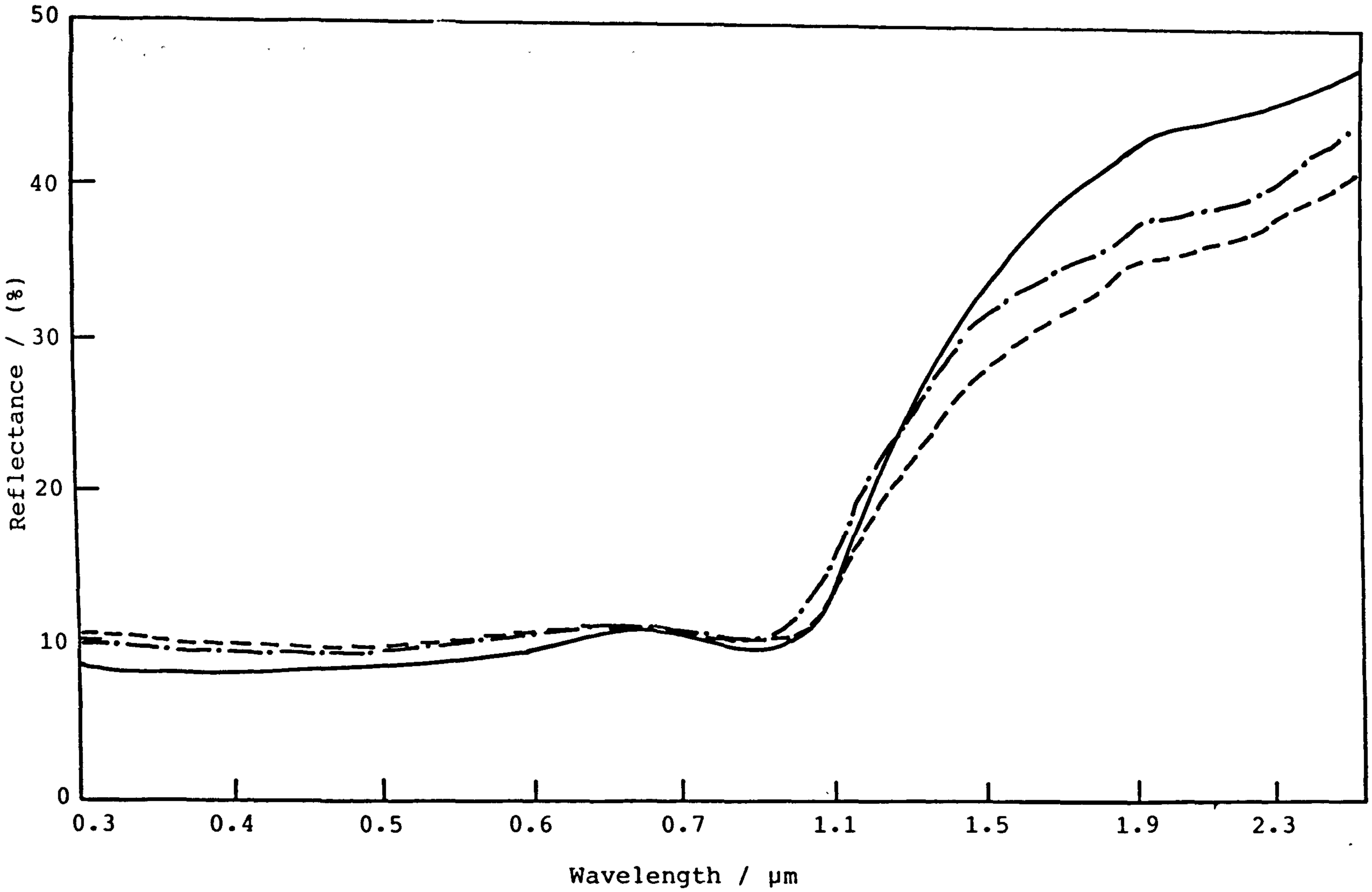

Fig. 4.10. Spectral reflectance of Mo-black coating on etched zinc before heating (—), after heating in vacuum at 200°C for 8 hours (-·-·-) and 16 hours (---).

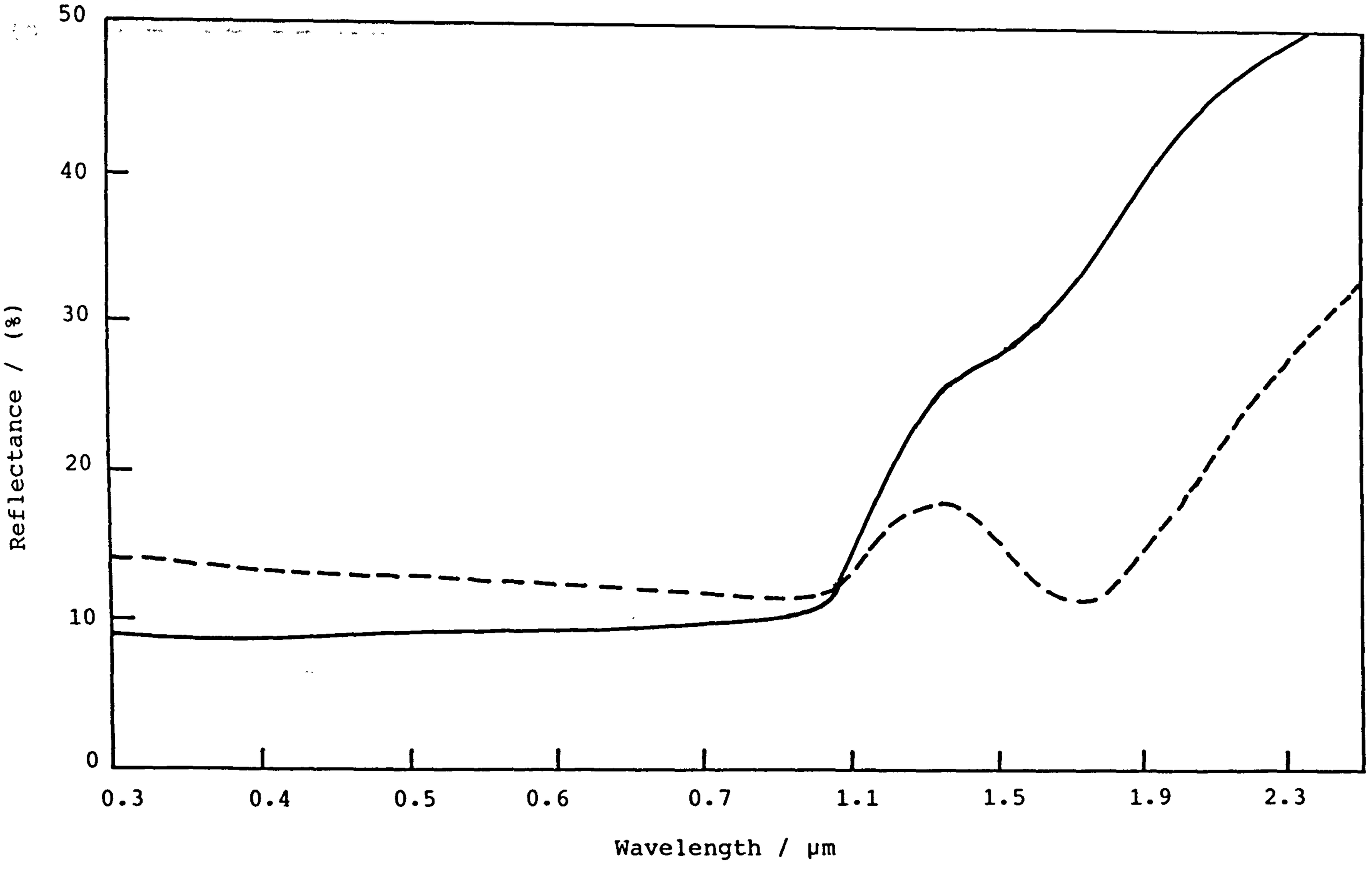

Fig. 4.11. Spectral reflectance of Mo-black coating on etched zinc before heating (——) and after heating in vacuum at 325°C for 4 hours (----).

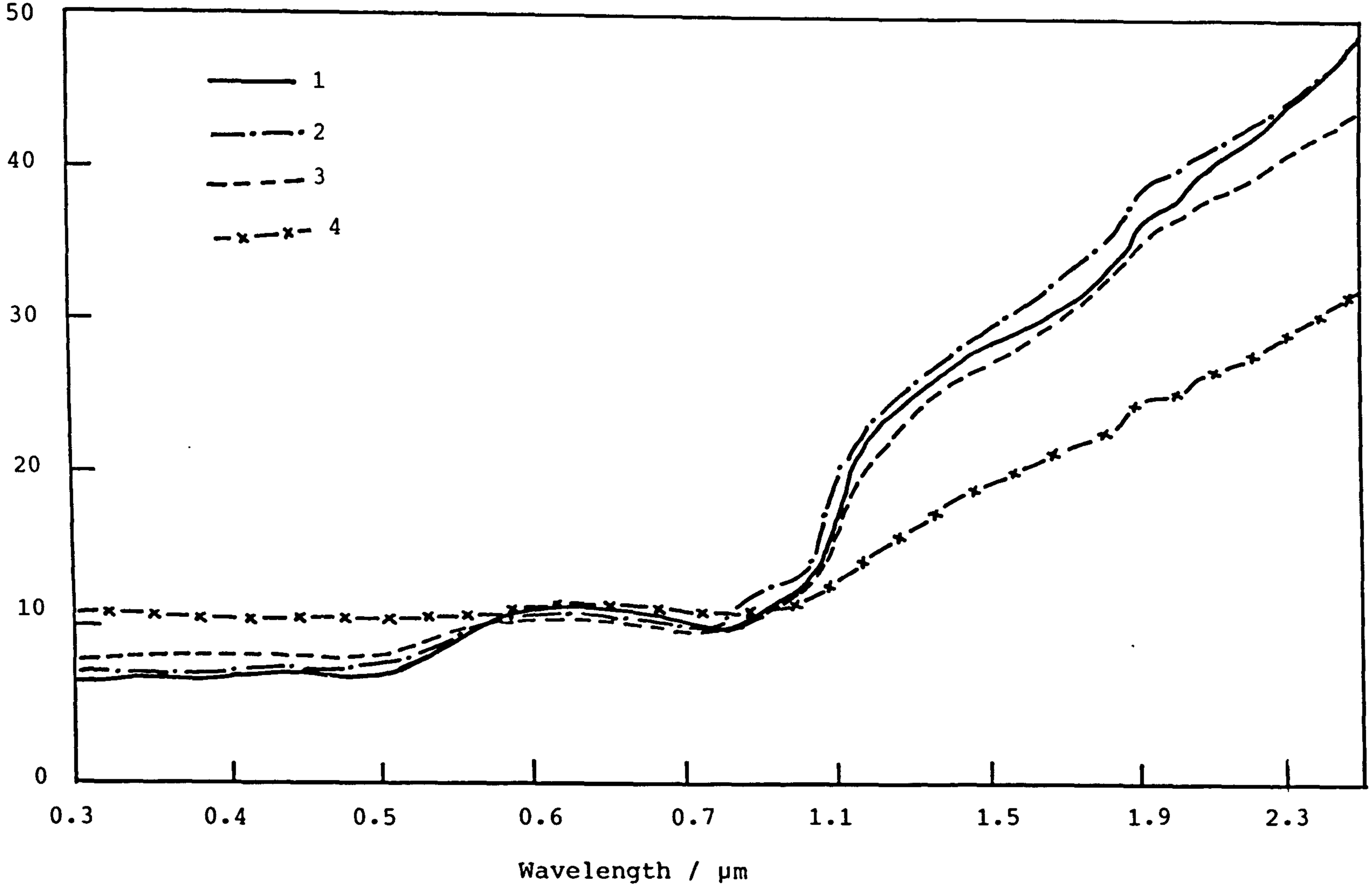

Fig. 4.12. Spectral reflectance of Mo-black coating on etched zinc after heat treating in vacuum at different temperatures. The curve numbers correspond to the sample numbers in Table 4.4.

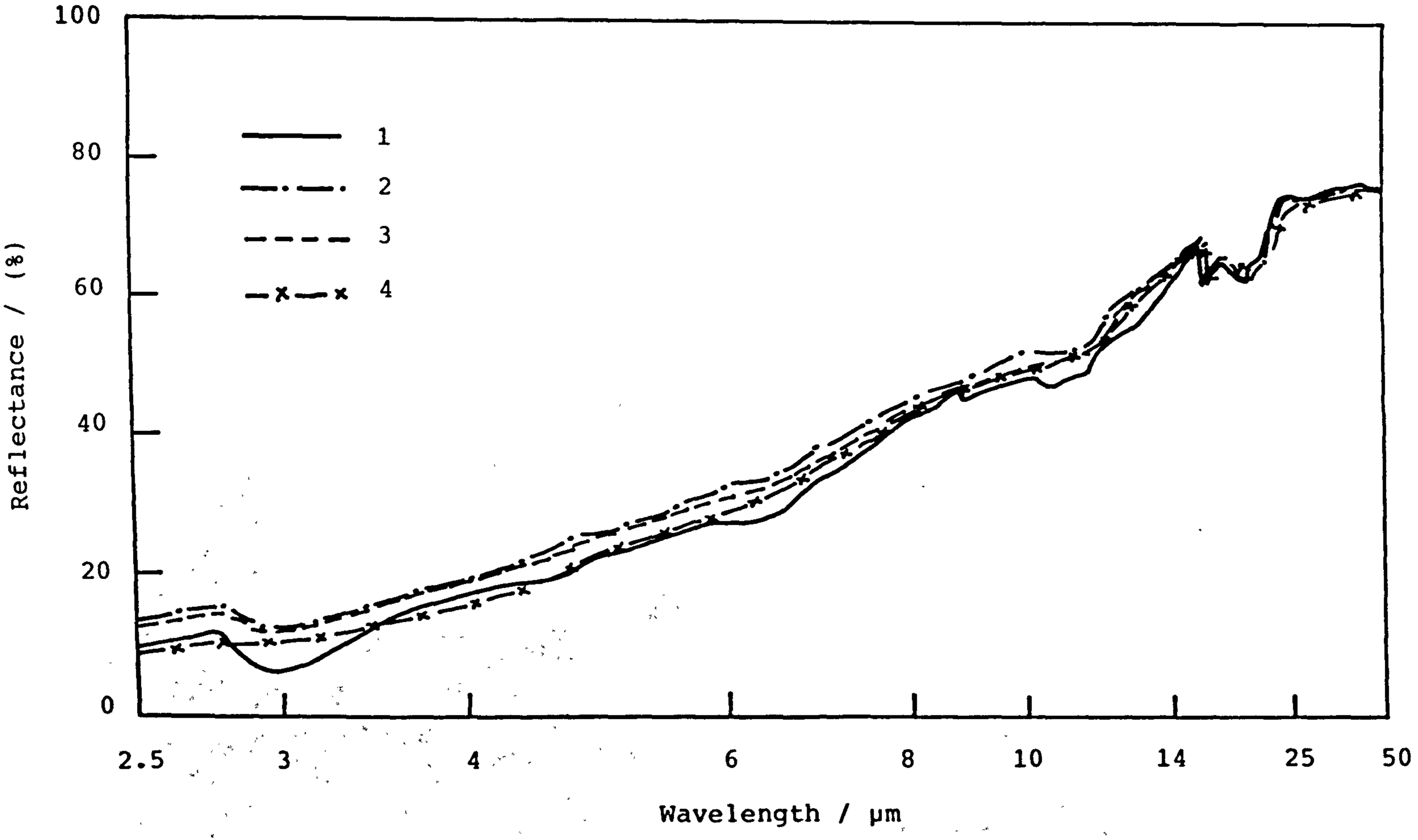

Fig. 4.13. Specular reflectance of the coating in Fig. 4.12. in the IR region. The curve numbers correspond to the sample numbers in Table 4.4.

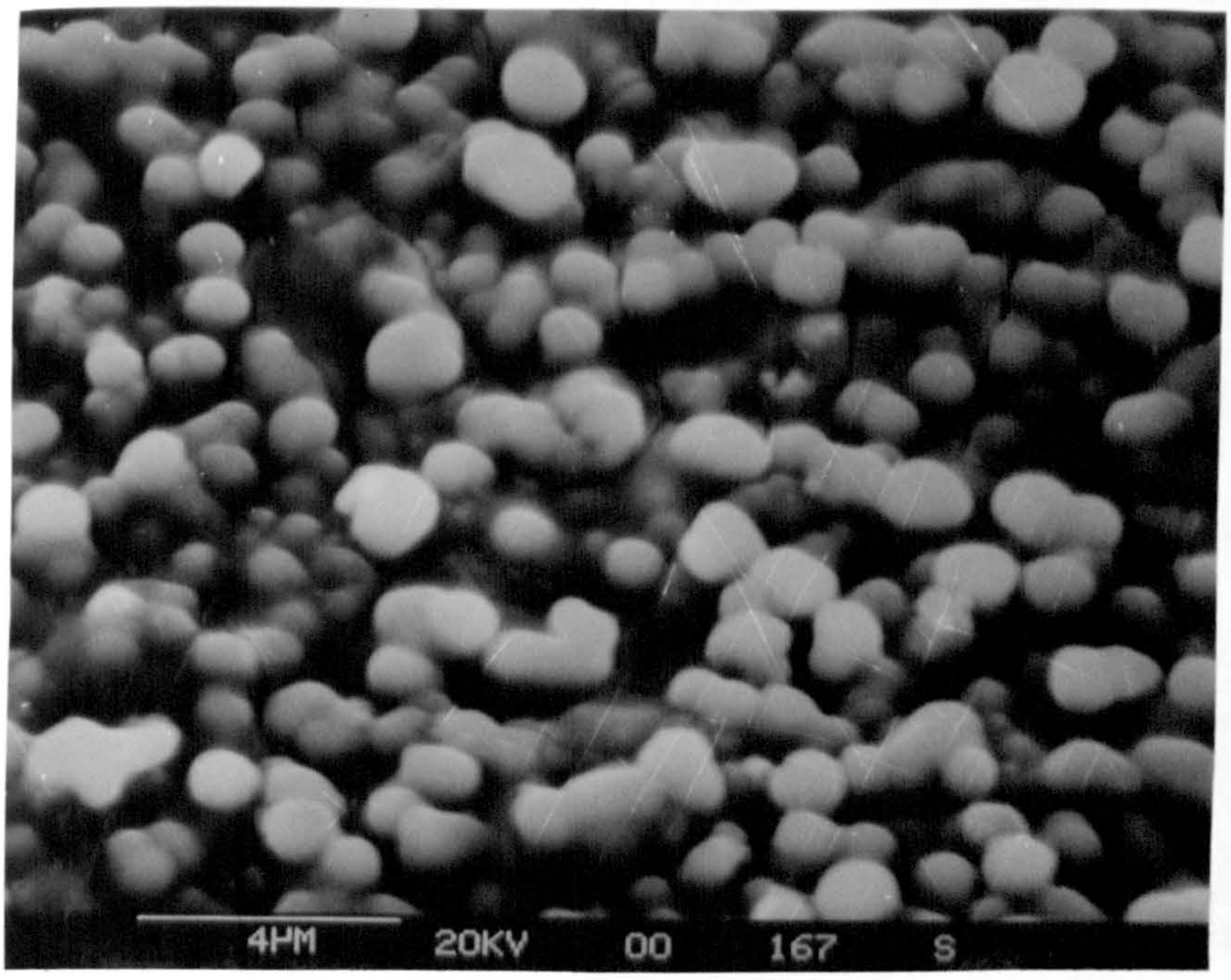

Fig. 4.14 SEM micrograph of a Mo-black dip coating on etched zinc substrate Magnification : 6000 x

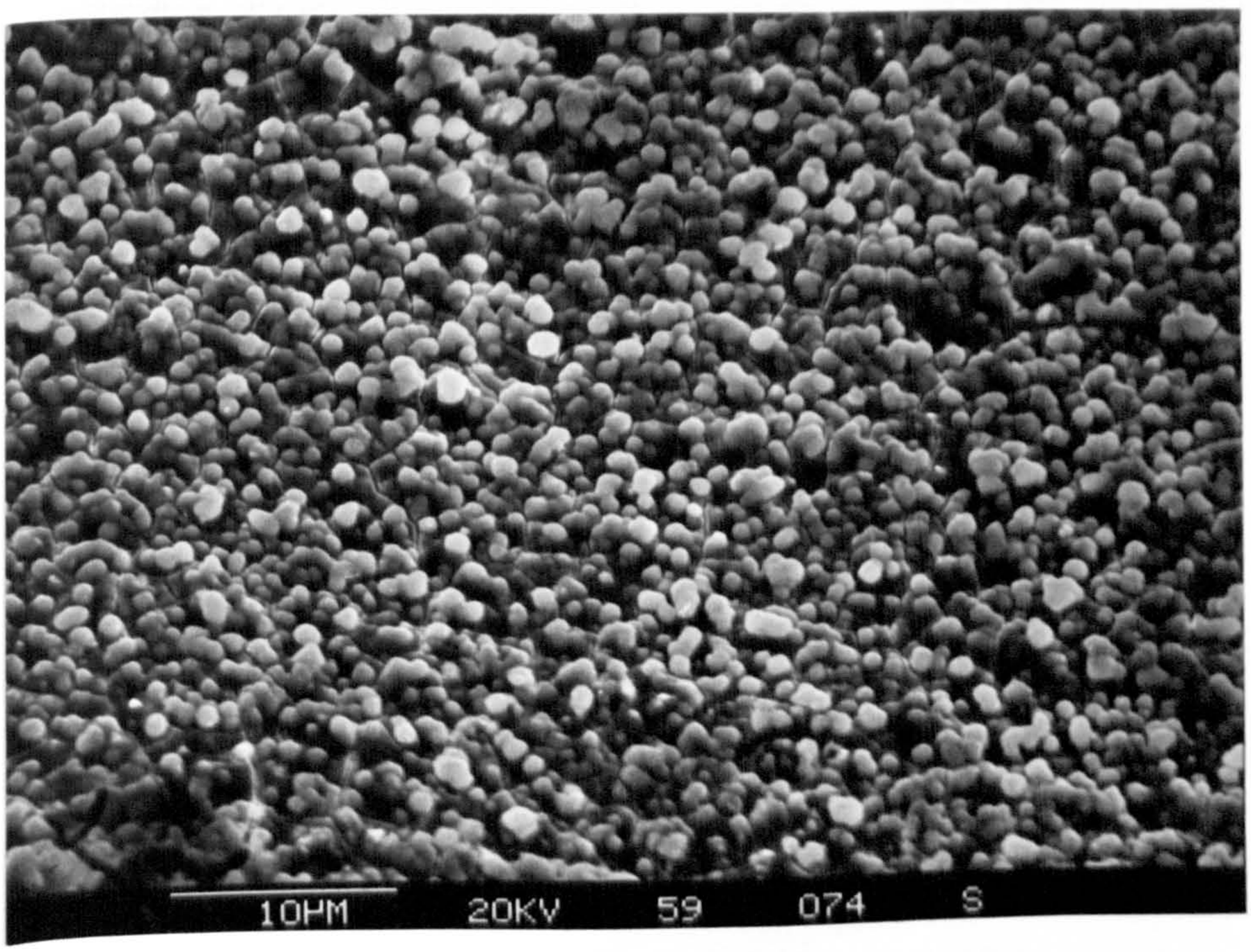

Fig. 4.15 SEM micrograph of the same coating as in Fig 4.14. after heat treatment in air at 100°C for 24 hours.

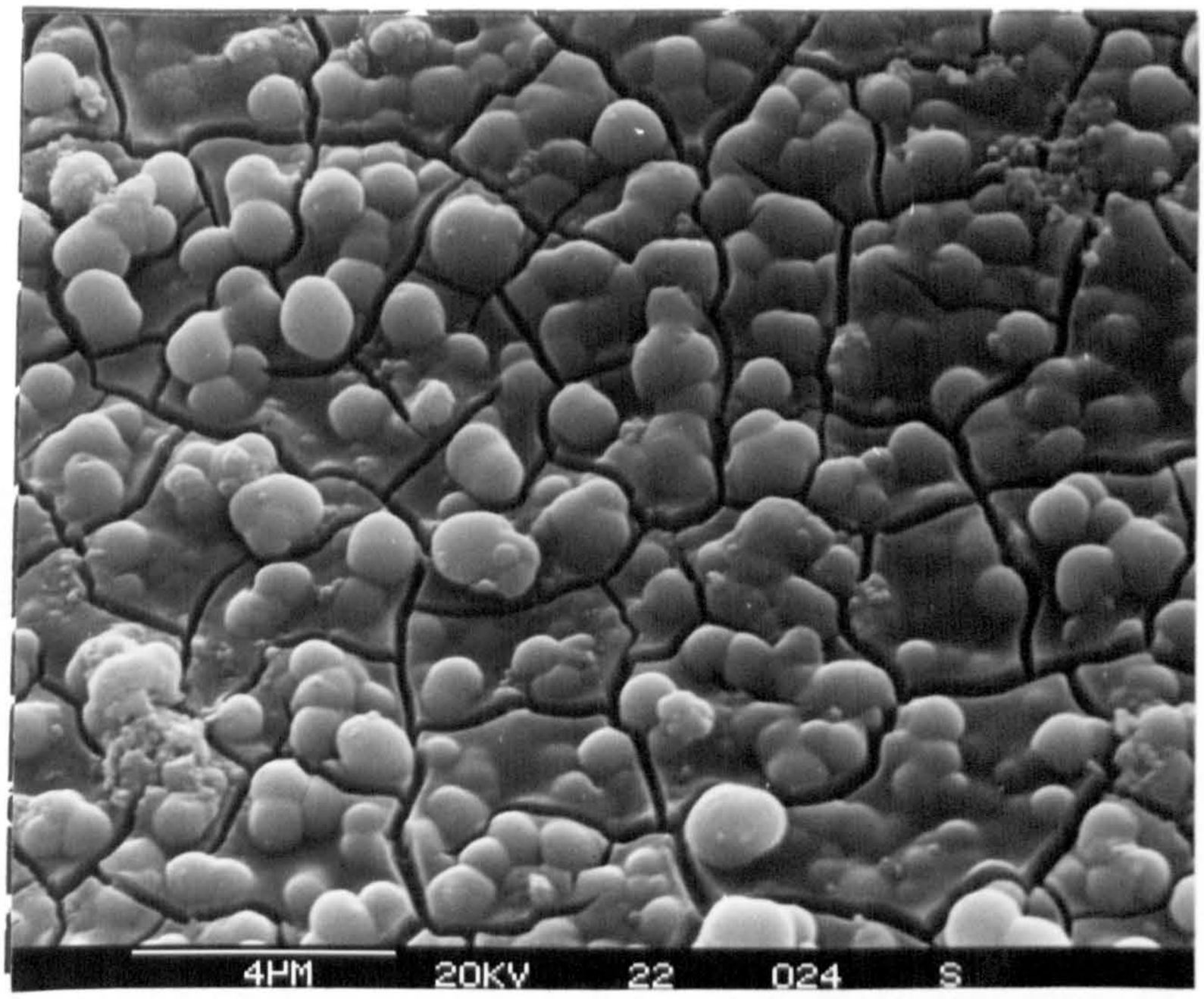

Fig. 4.16 SEM micrograph of the same coating as in Fig. 4.14. after heat treatment in air at 200°C for 4 hours.
Magnification : 6000 x

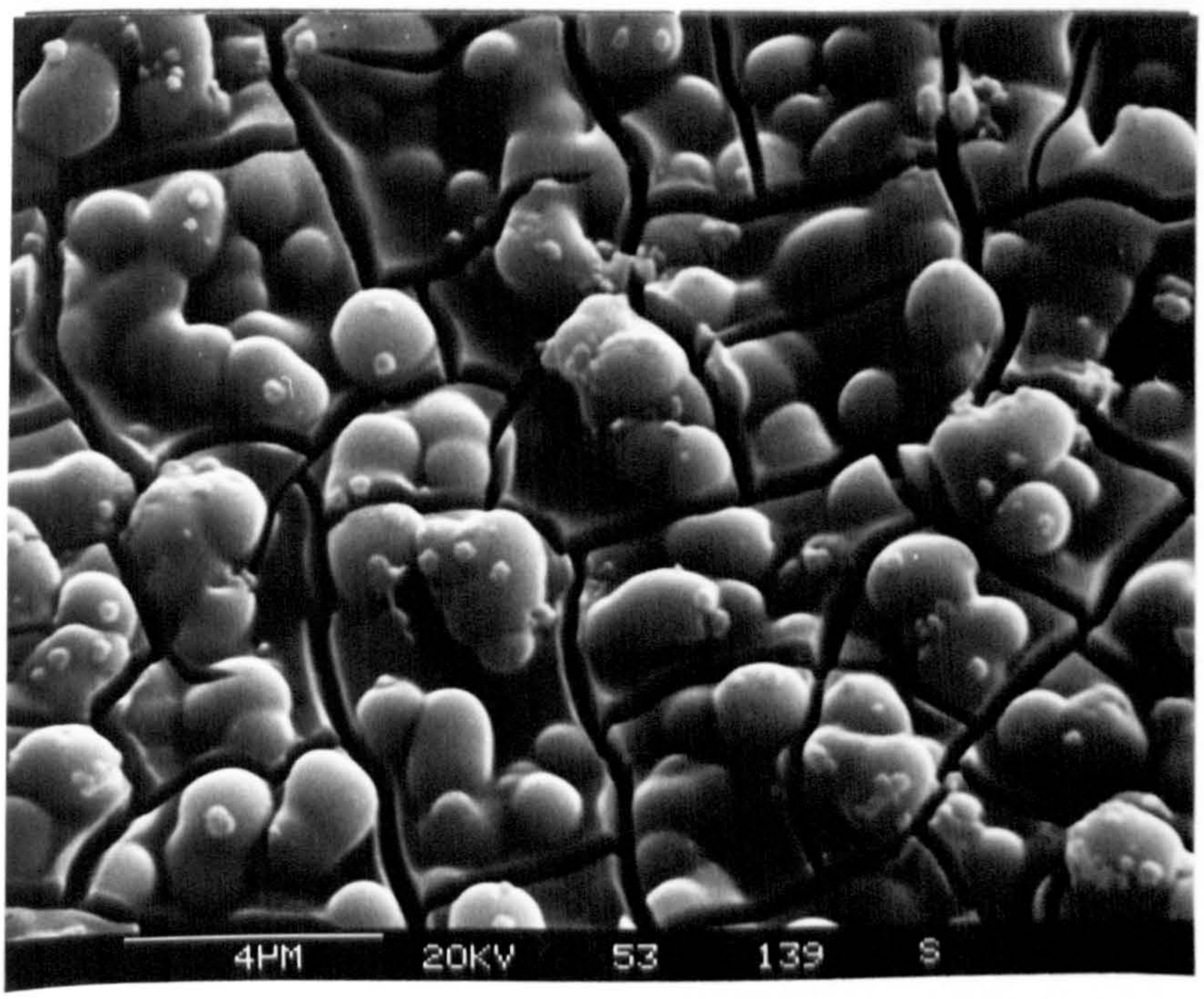

Fig. 4.17 SEM micrograph of the same coating as in Fig. 4.14. after heat treatment in air at 300°C for 4 hours.
Magnification : 6000 x

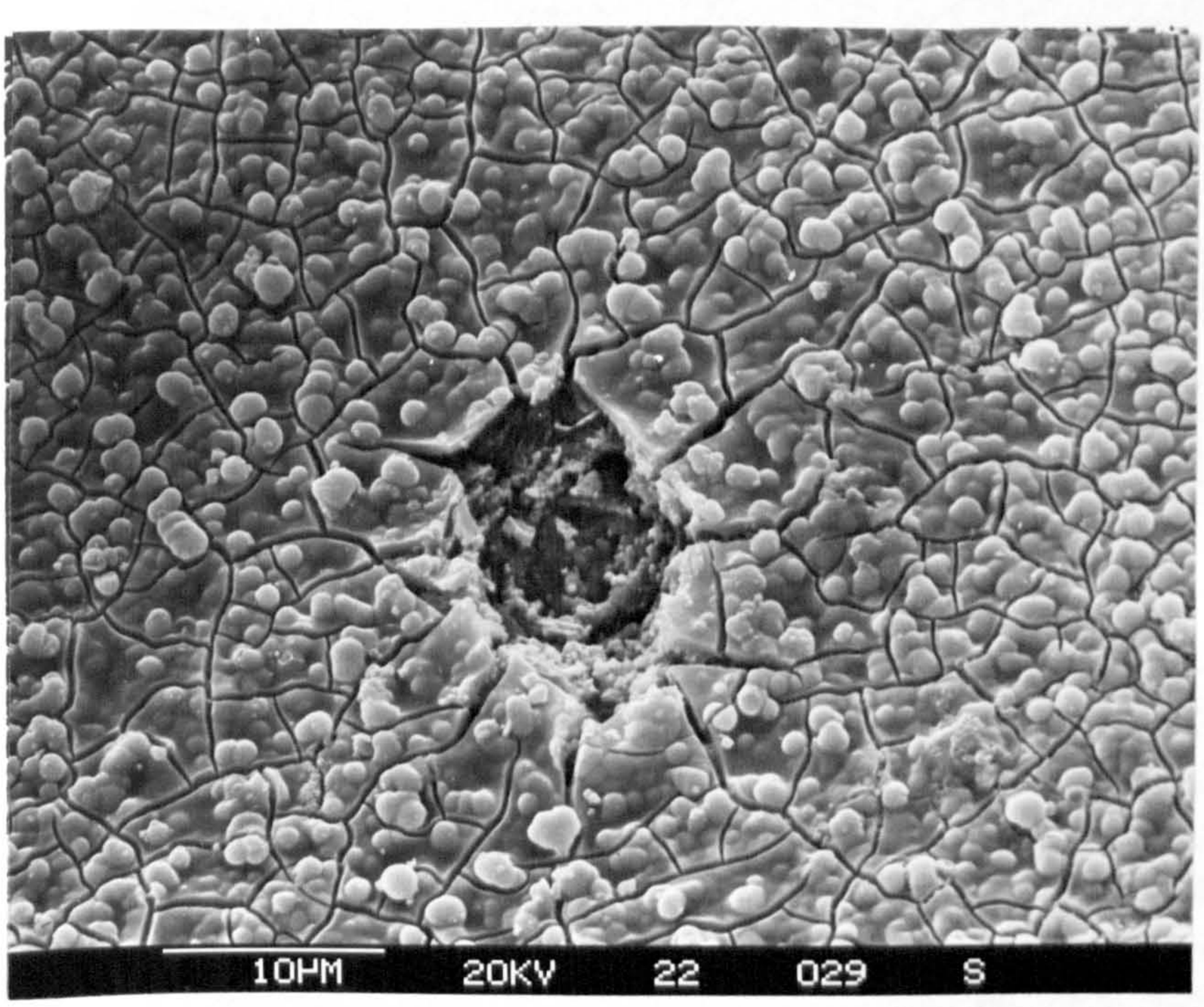

Fig. 4.18 SEM micrograph of a Mo-black dip coating on etched zinc after heat treatment in air at 300°C.
Magnification : 2000 x

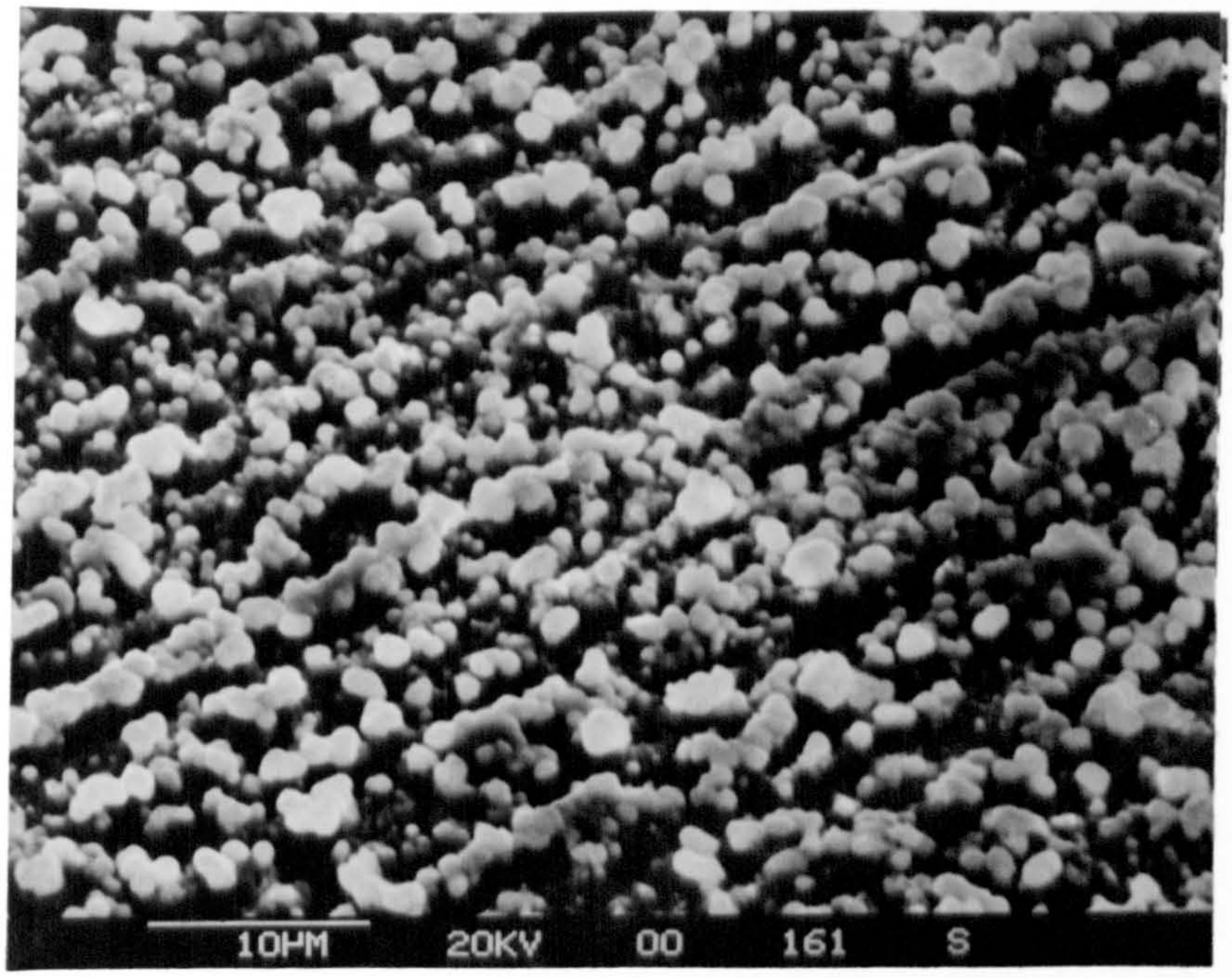

(a)

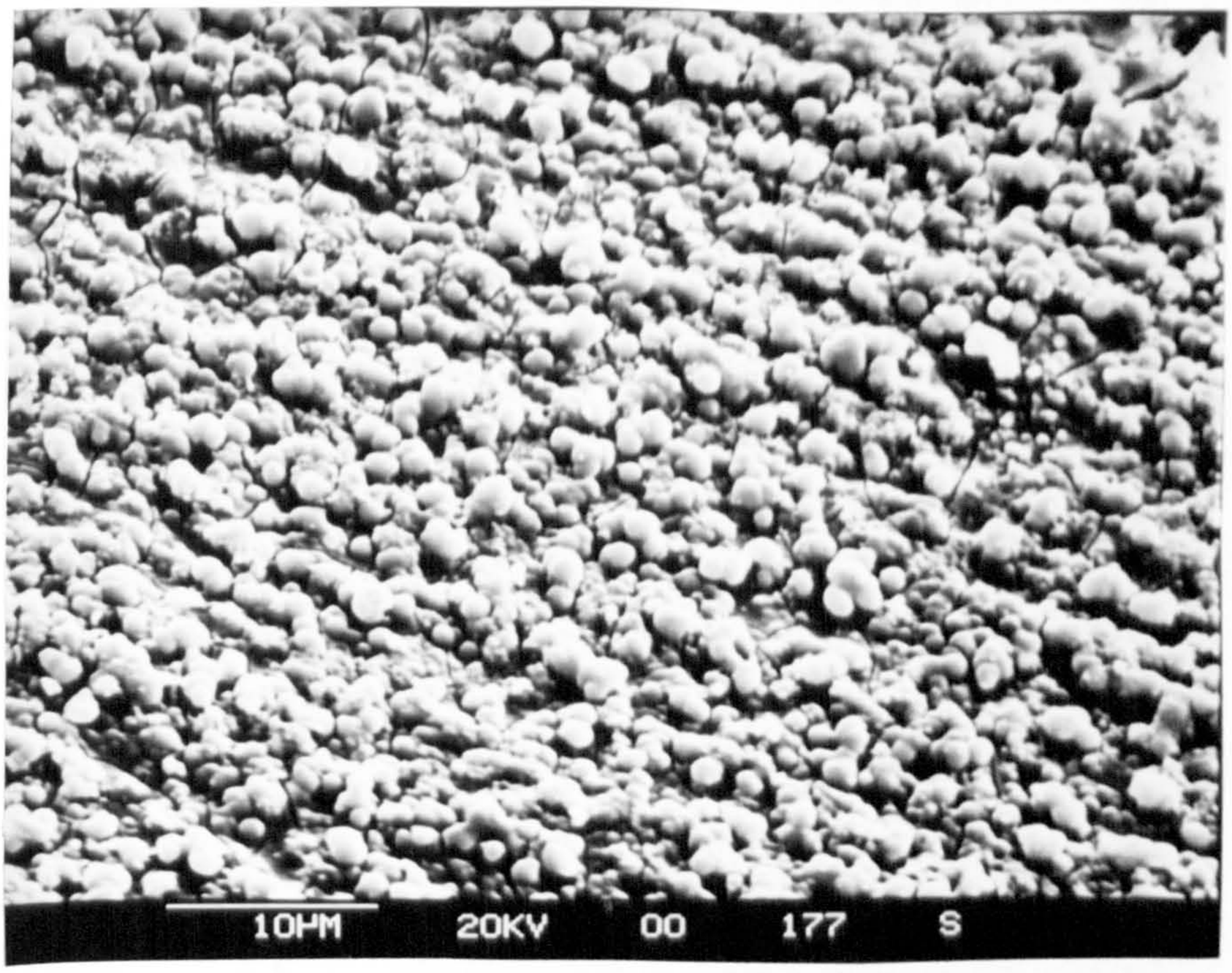

(b)

Fig. 4.19. SEM micrograph of Mo-black dip coating on etched zinc substrate (50% HNO_3) : (a) As prepared (b) After heat treatment in vacuum at 150°C for 8 hours. Magnification : 2000 x

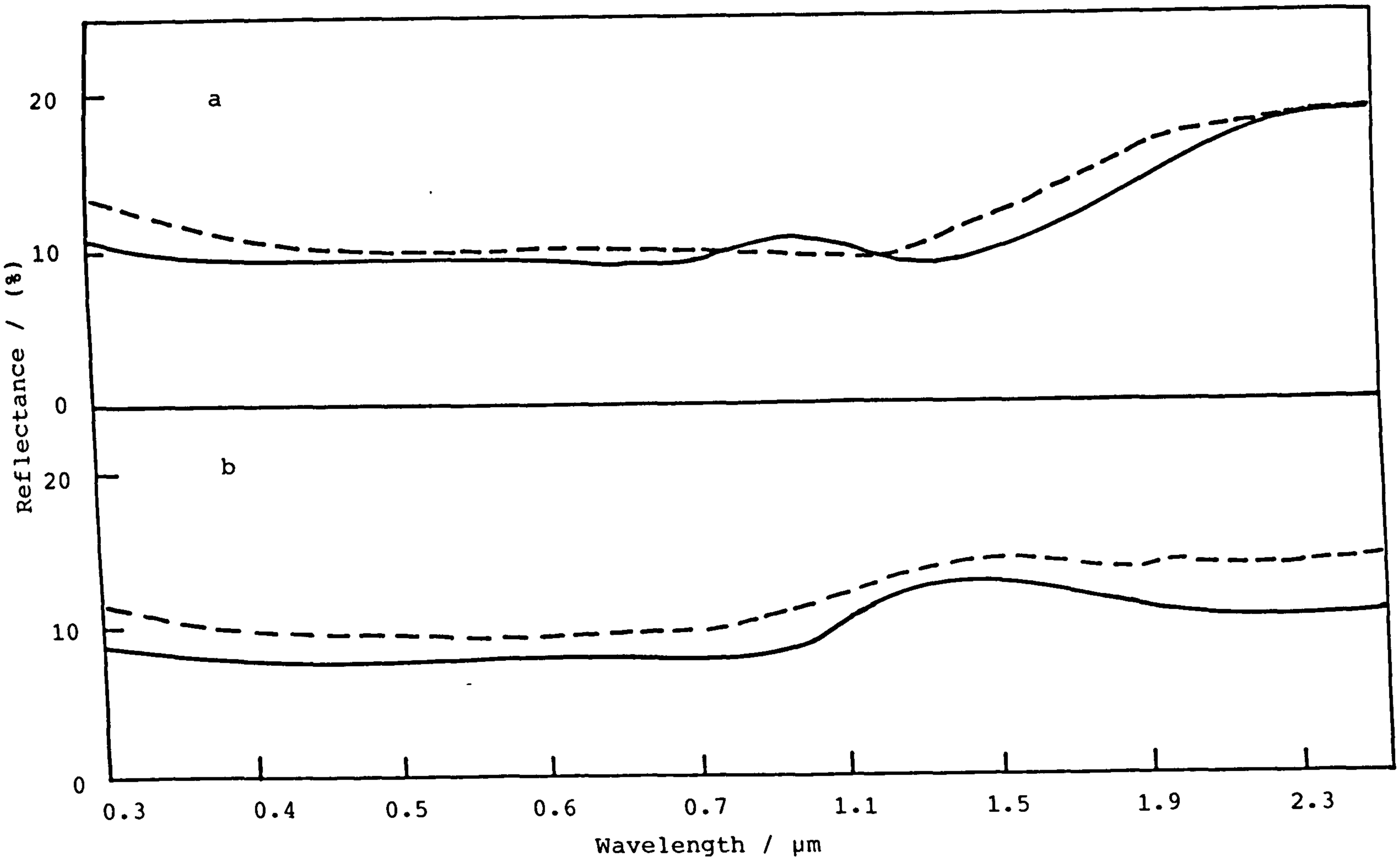

Fig. 4.20. Spectral reflectance of a Mo-black dip coating on a cobalt (NC) substrate (a) with addition agent (b) without addition agent; (—) as prepared, (----) after heating air at 200°C for 5 hours.

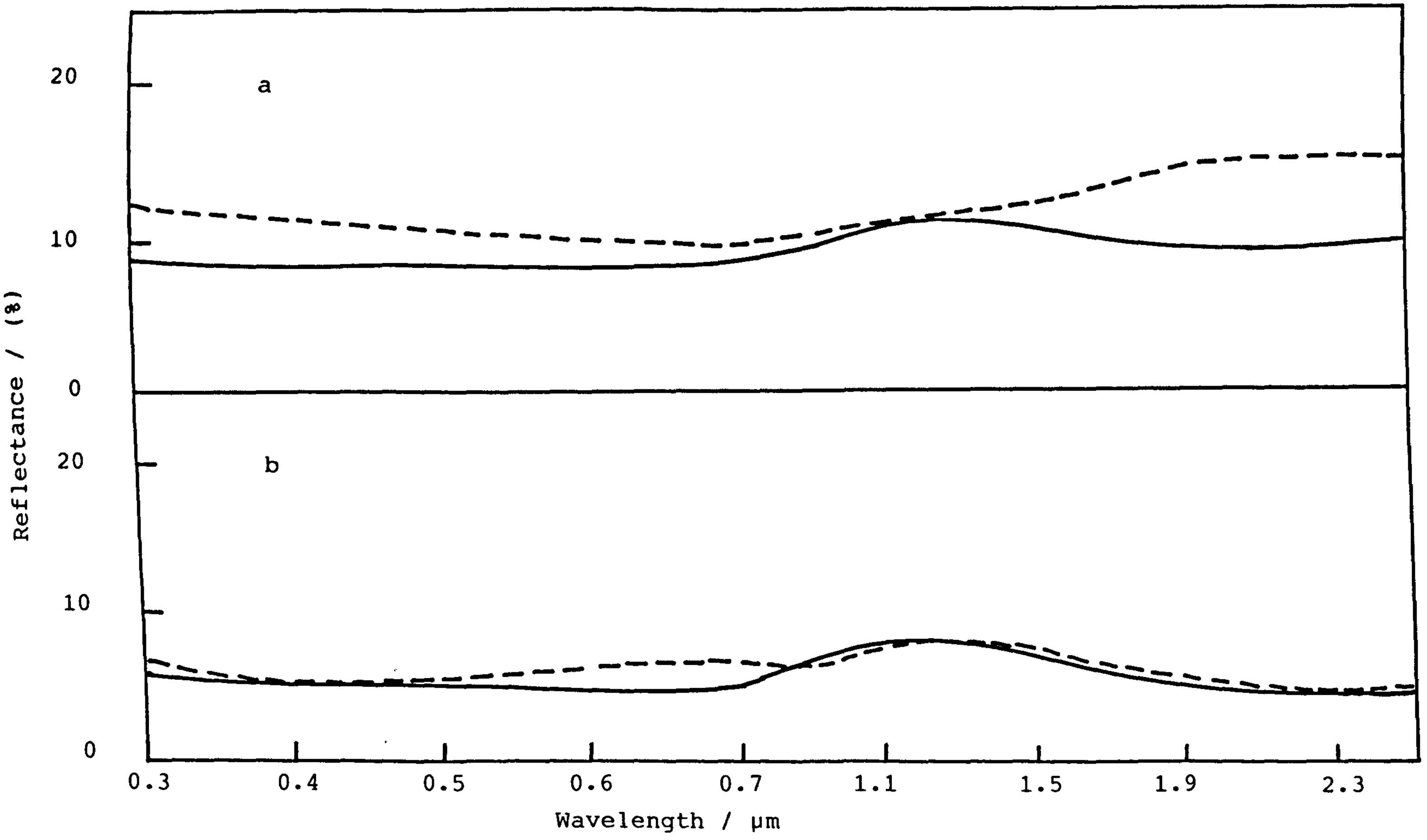

Fig. 4.21 Spectral reflectance of a Mo-black coating on cobalt (NC) substrate (a) with addition agent (b) without addition agent; (——) as prepared, (-----) after heat treatment in air at 300°C for 5 hours.

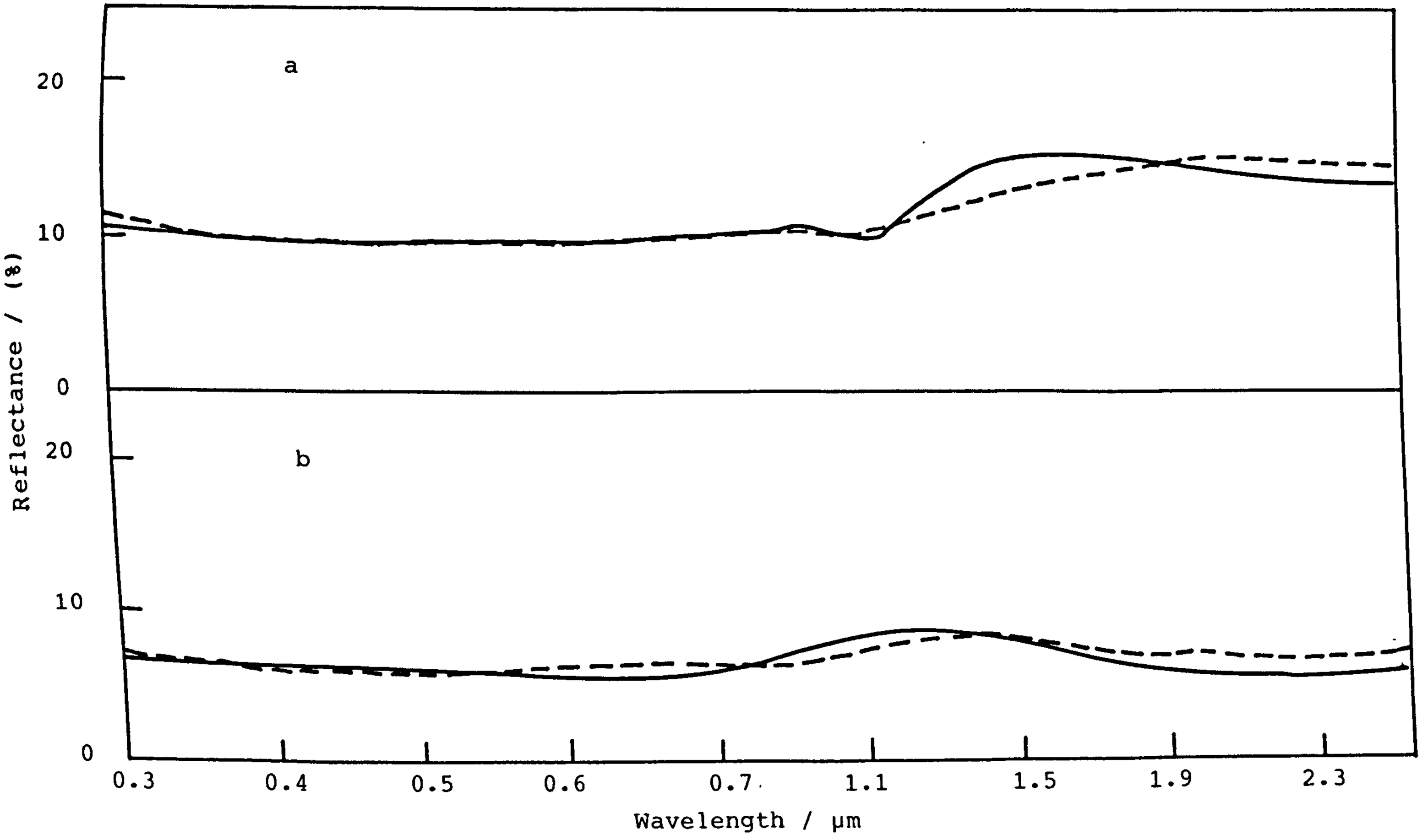

Fig. 4.22. Spectral reflectance of Mo-black dip coatings on cobalt (NC) substrates (a) with addition agent (b) without addition agent; (____) as prepared, (----) after heating in air at 400°C for 2 hours.

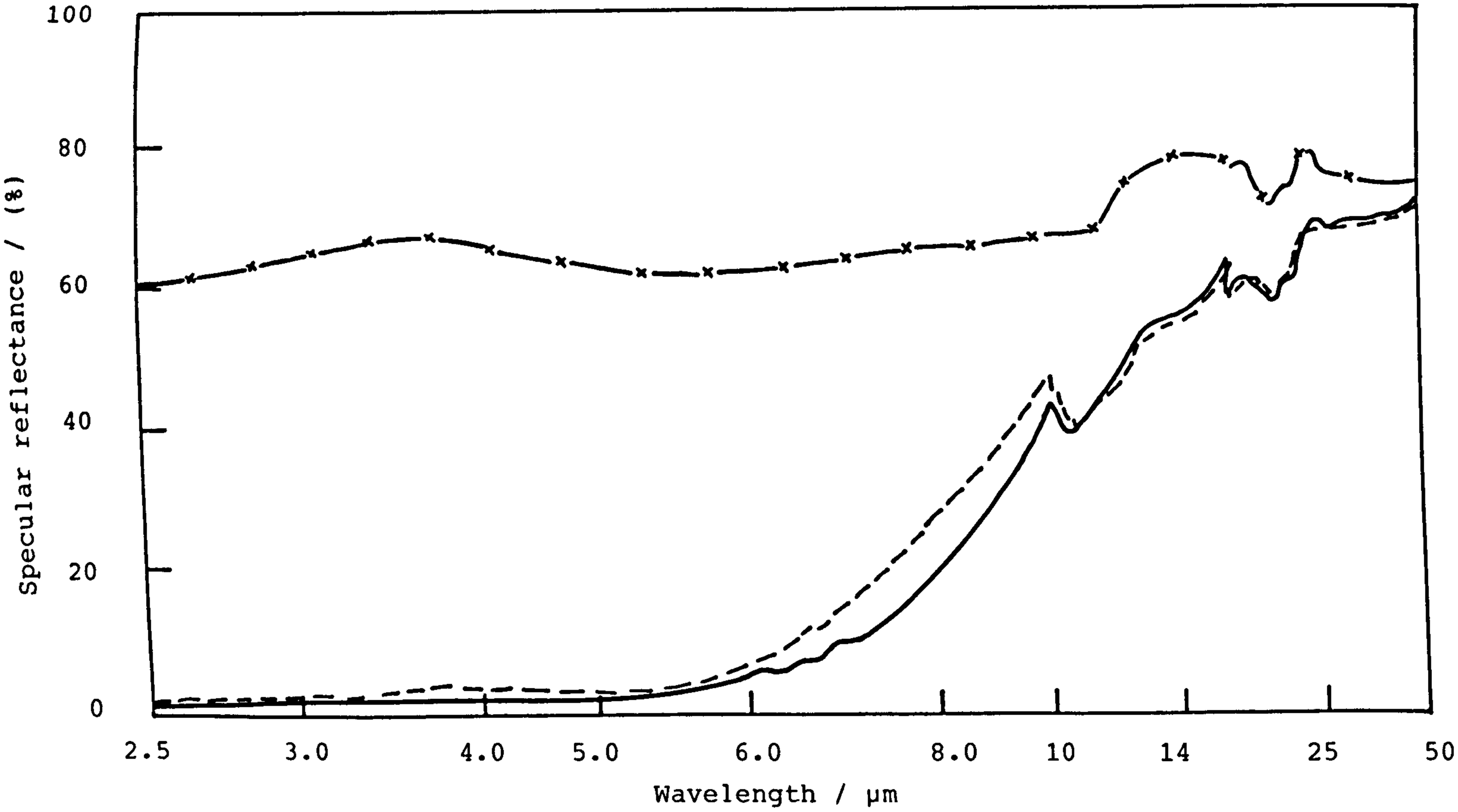

Fig. 4.23. Specular reflectance of a Mo-black coating on cobalt (NC) substrate (without addition agent); before heat treatment (——) and after heat treatment at 400°C for 2 hours (---), reference Al-mirror (-×-×-).

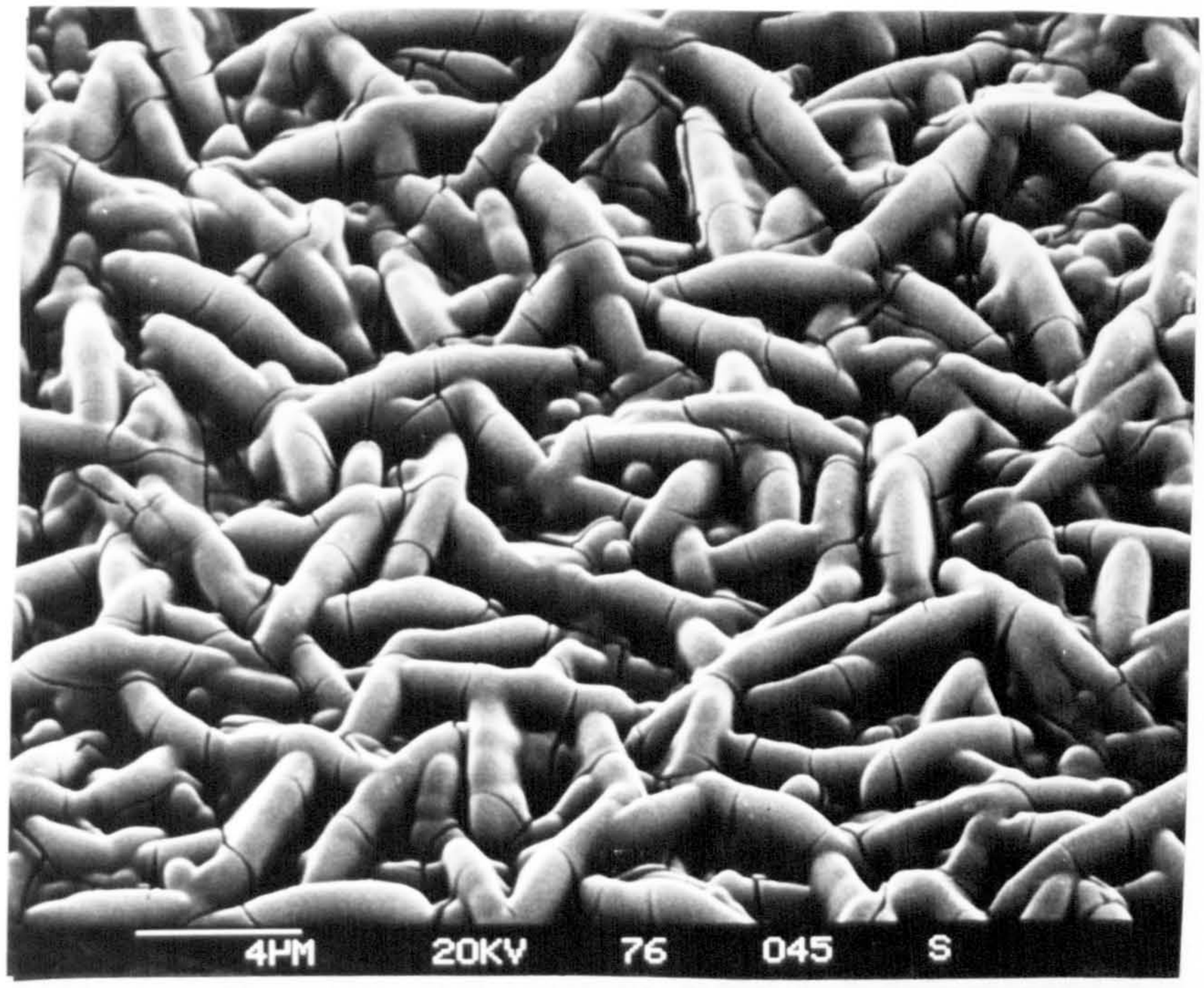

(a)

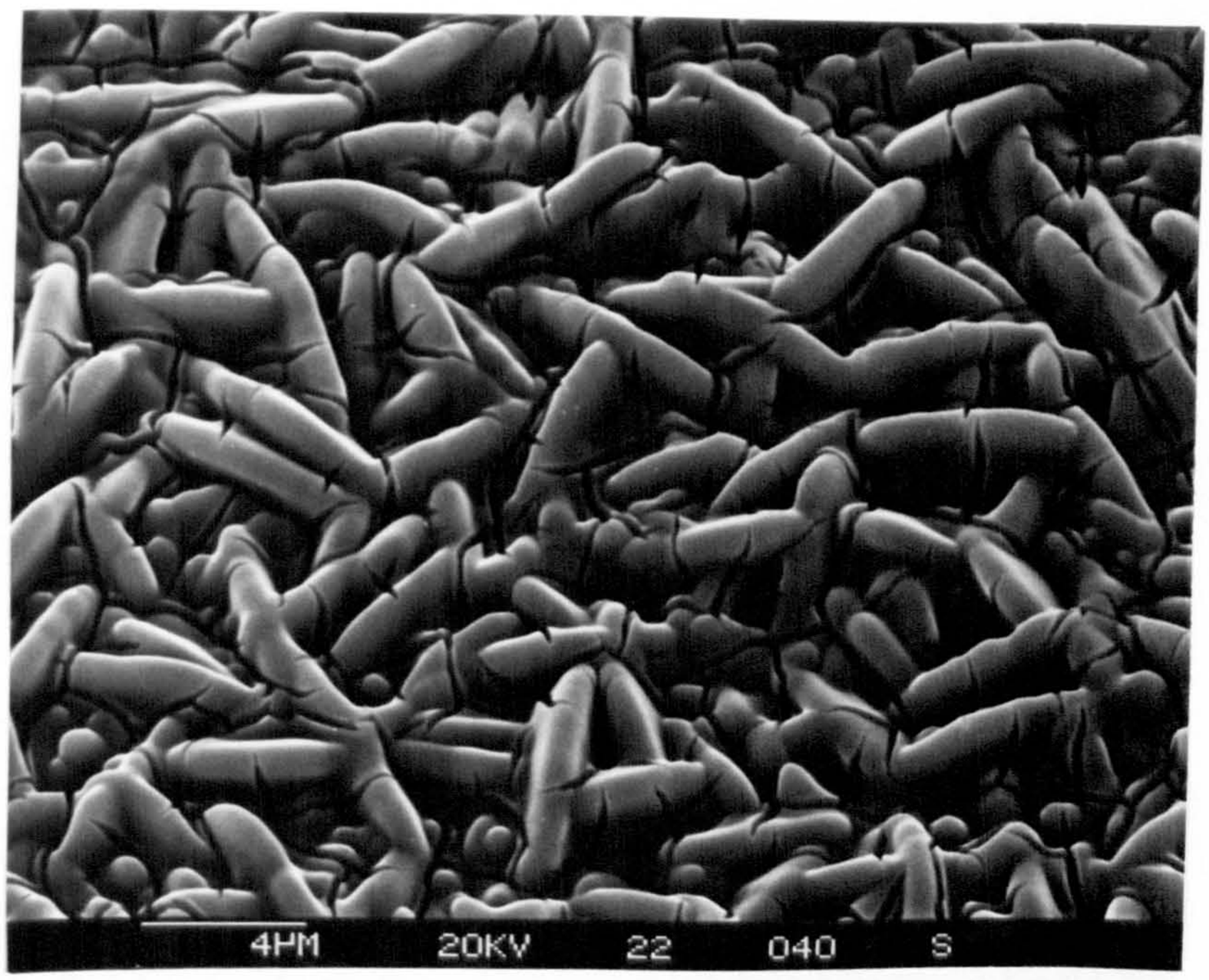

(b)

Fig. 4.25. SEM micrograph of a Mo-black dip coating on cobalt (NC) substrate plated without addition agent (a) As prepared (b) After heat treatment at 300°C for 5 hours Magnification : 4000 x

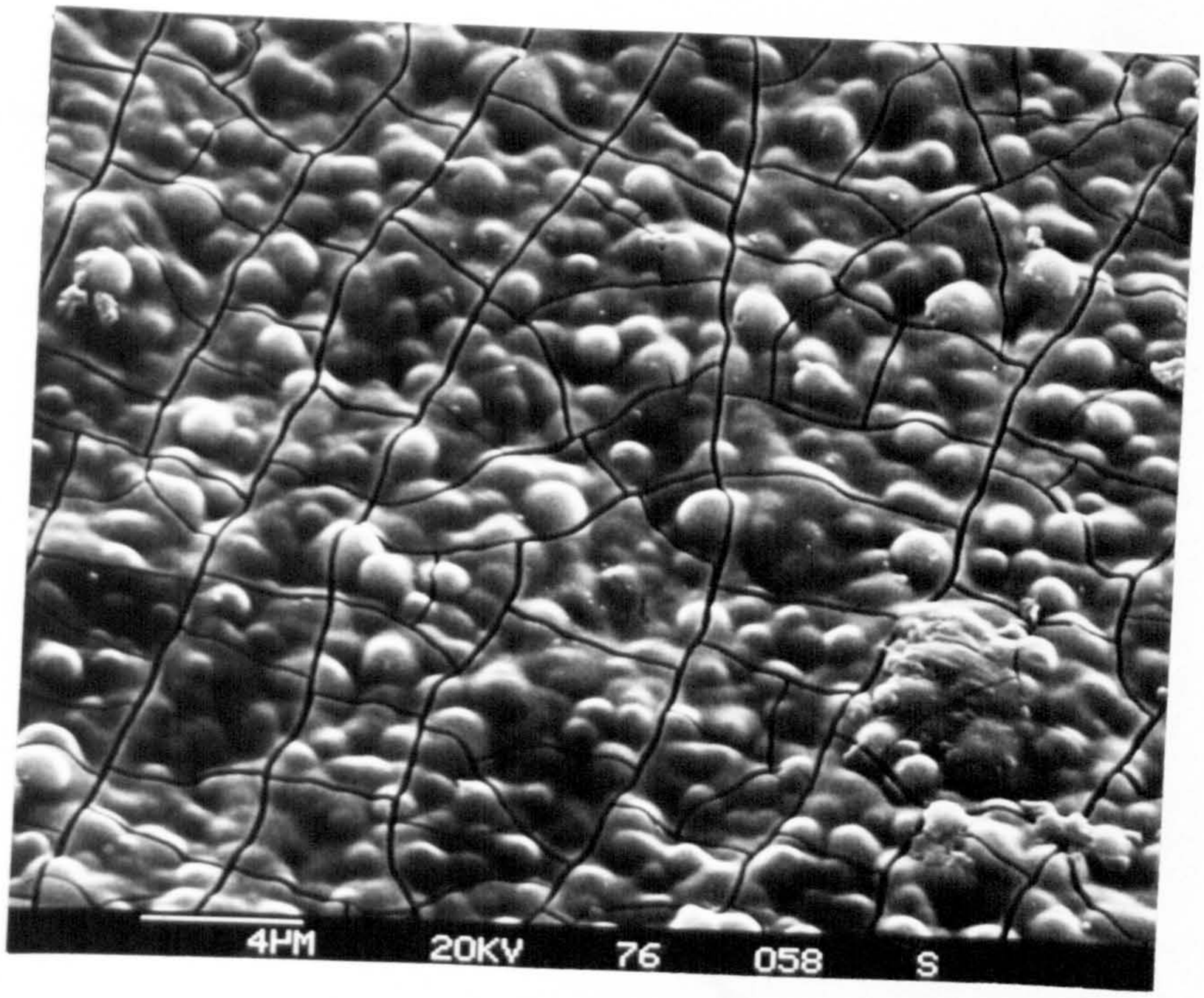

(a)

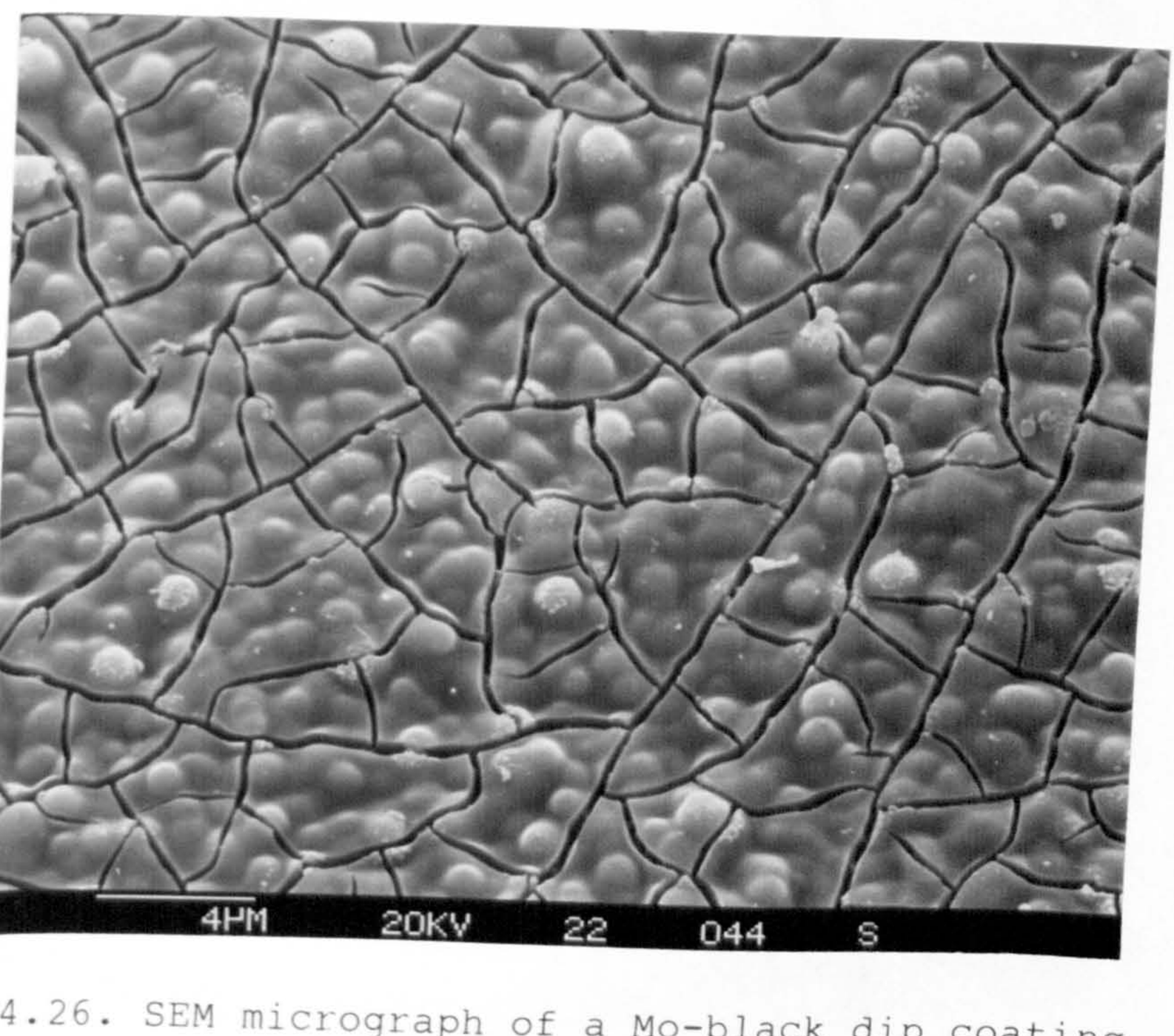

(b)

Fig. 4.26. SEM micrograph of a Mo-black dip coating on a cobaly (NC) substrate plated with addition agent. (a) As prepared. (b) After heat treatment at 300°C for 5 hours
Magnification : 4000 x

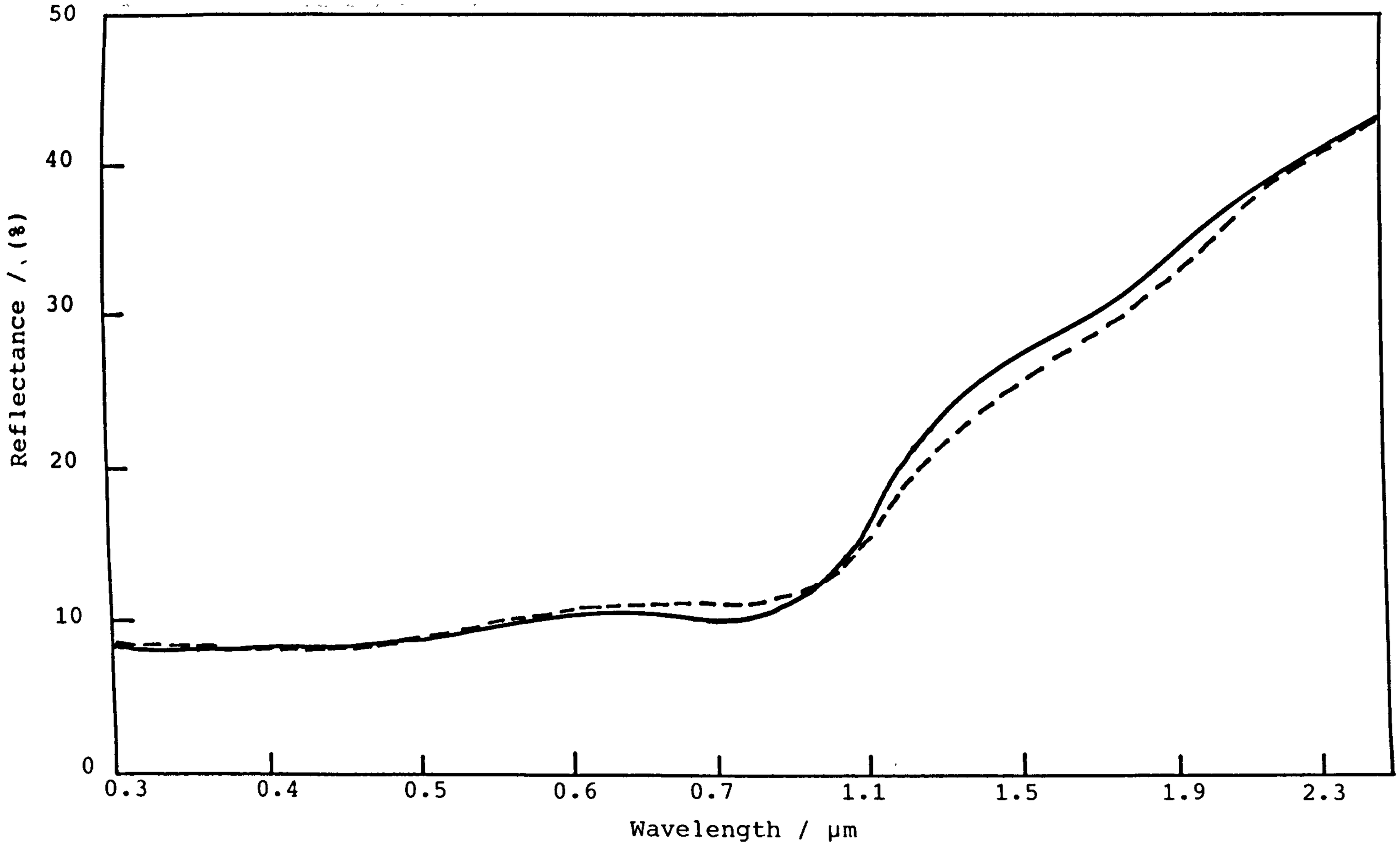

Fig. 4.27. Spectral reflectance spectra of a Mo-black coating on etched zinc; as prepared (___), after outdoor ageing for 5 months (----).

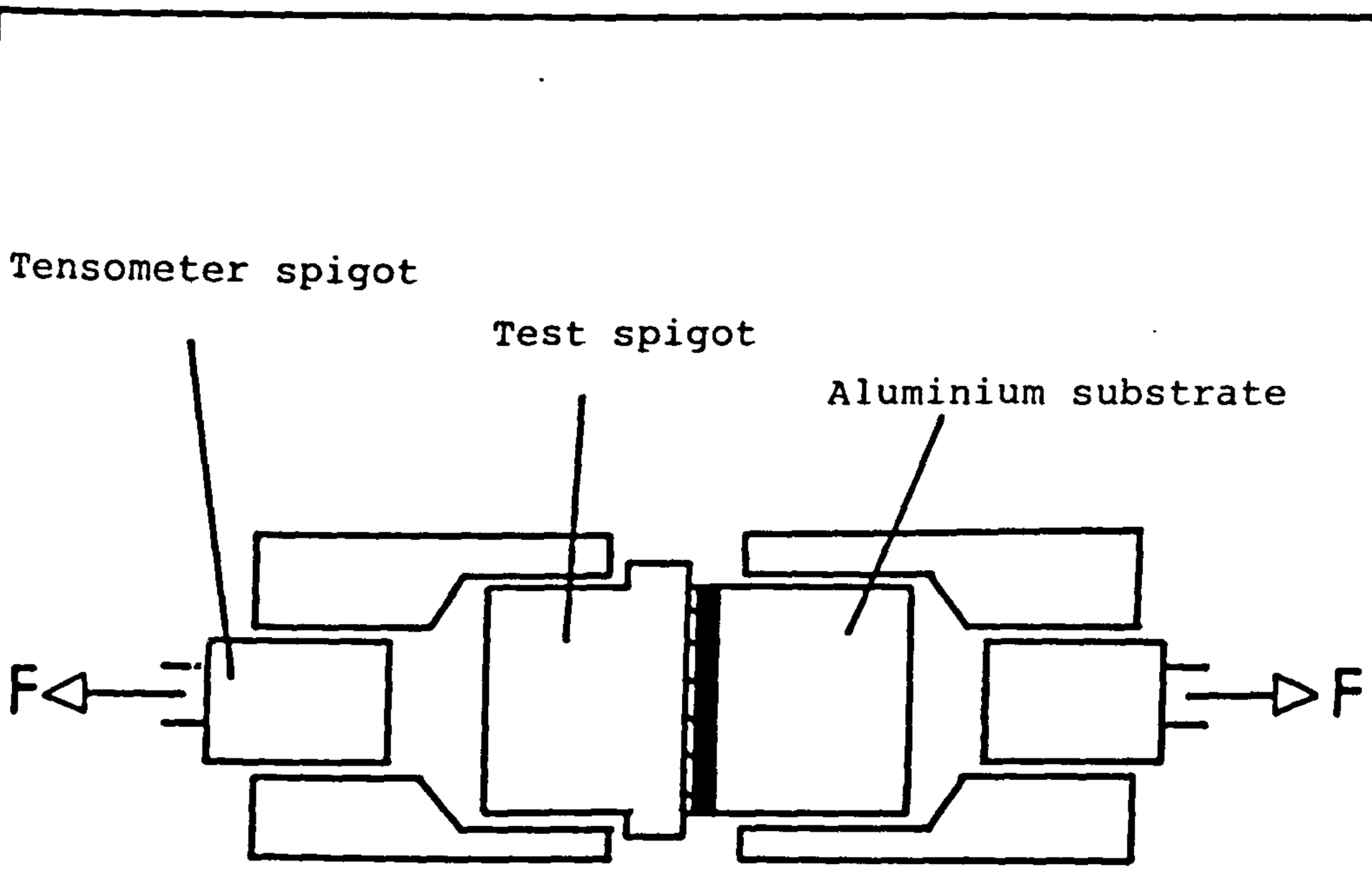

(a)

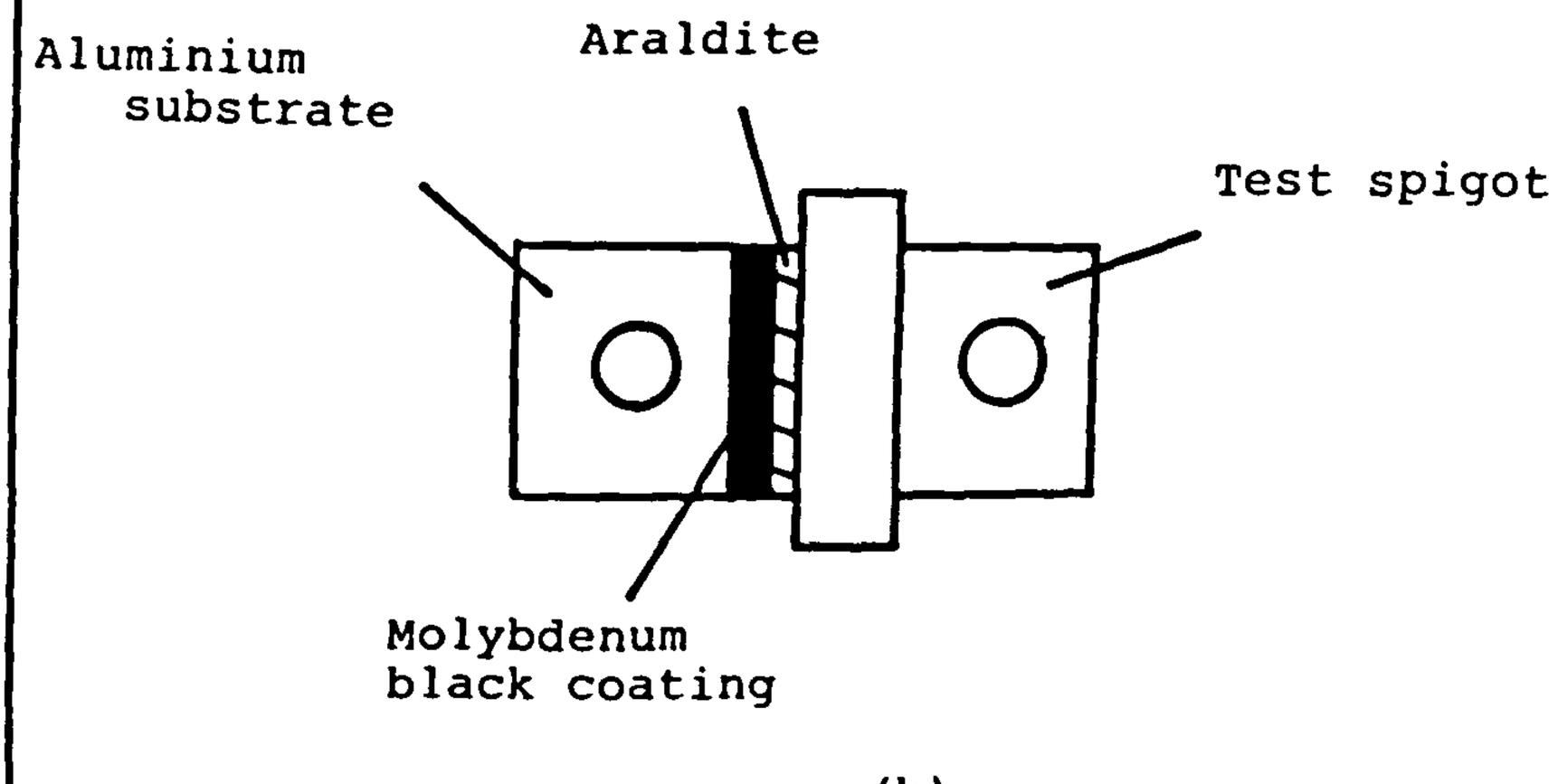

(b)

Fig. 4.28 (a) Schematic diagram of adhesion testing arrangement using tensometer.

(b) Mo-coated substrate adhered to test spigot.

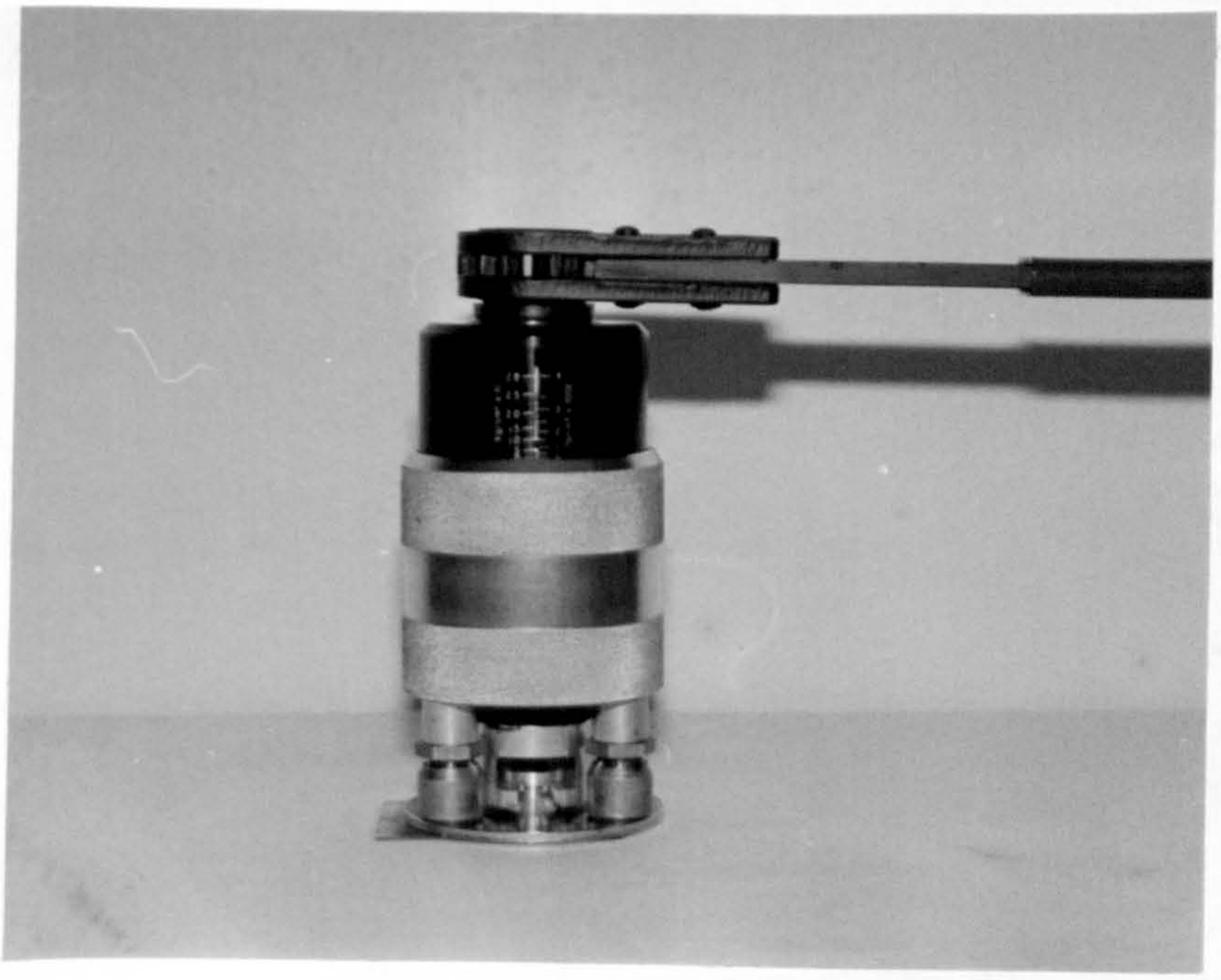

Fig.4.29 Photograph of Elcometer (model 106) adhesion tester

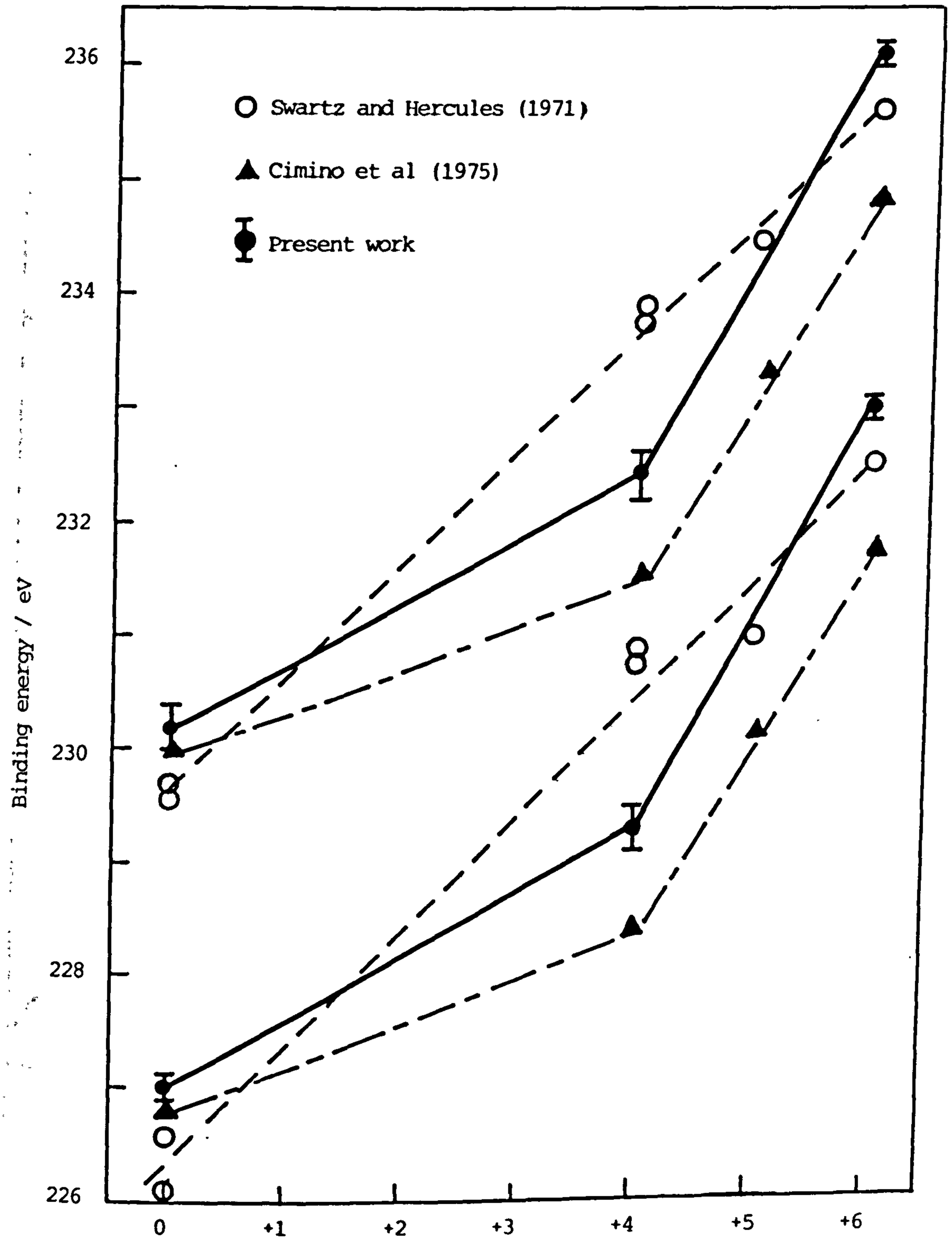

Fig.5.1. Molybdenum ($3d_{3/2}$ - $3d_{5/2}$) binding energies as a function of oxidation state.

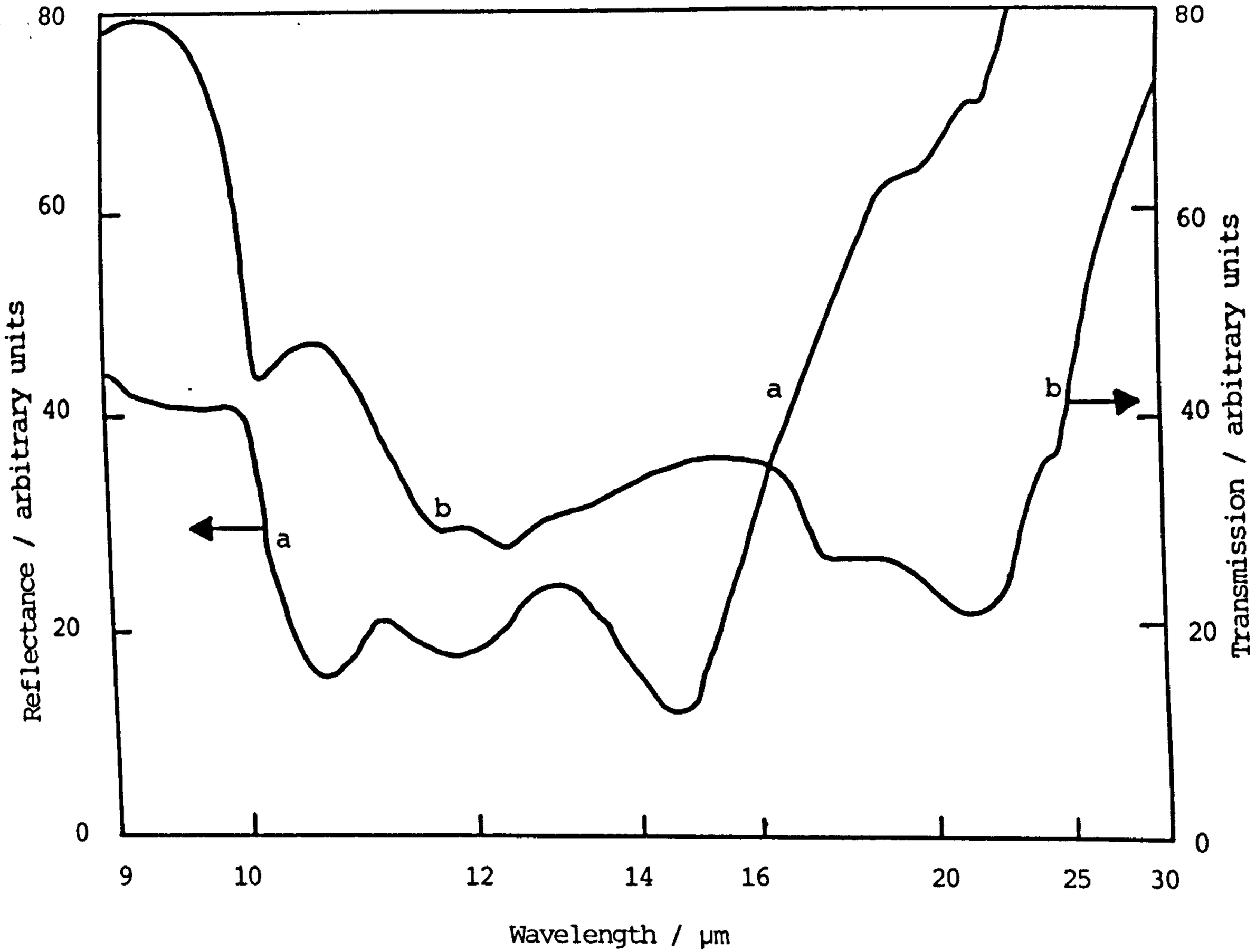

Fig.5.2. Reflectance and transmission spectra for Mo-black coating (a) and MoO_3 powder (b).

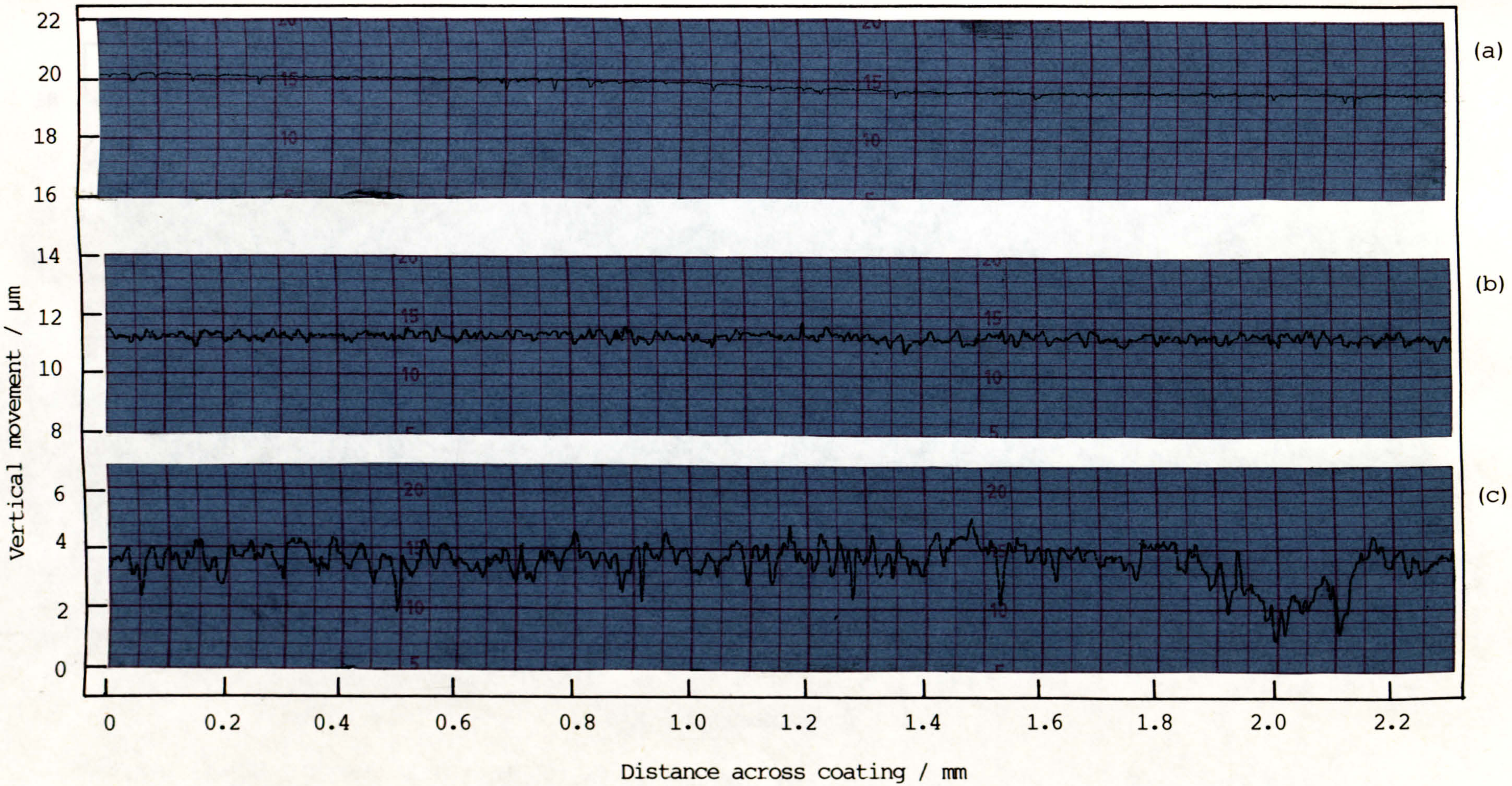

Fig.5.3. Surface profile scans obtained using Talysurf instrument of Mo-black dip coating on zinc substrate (a) Polished zinc (0.5µ finish), (b) Polished zinc (6.0µ finish), (c) Etched zinc (30% HNO_3)

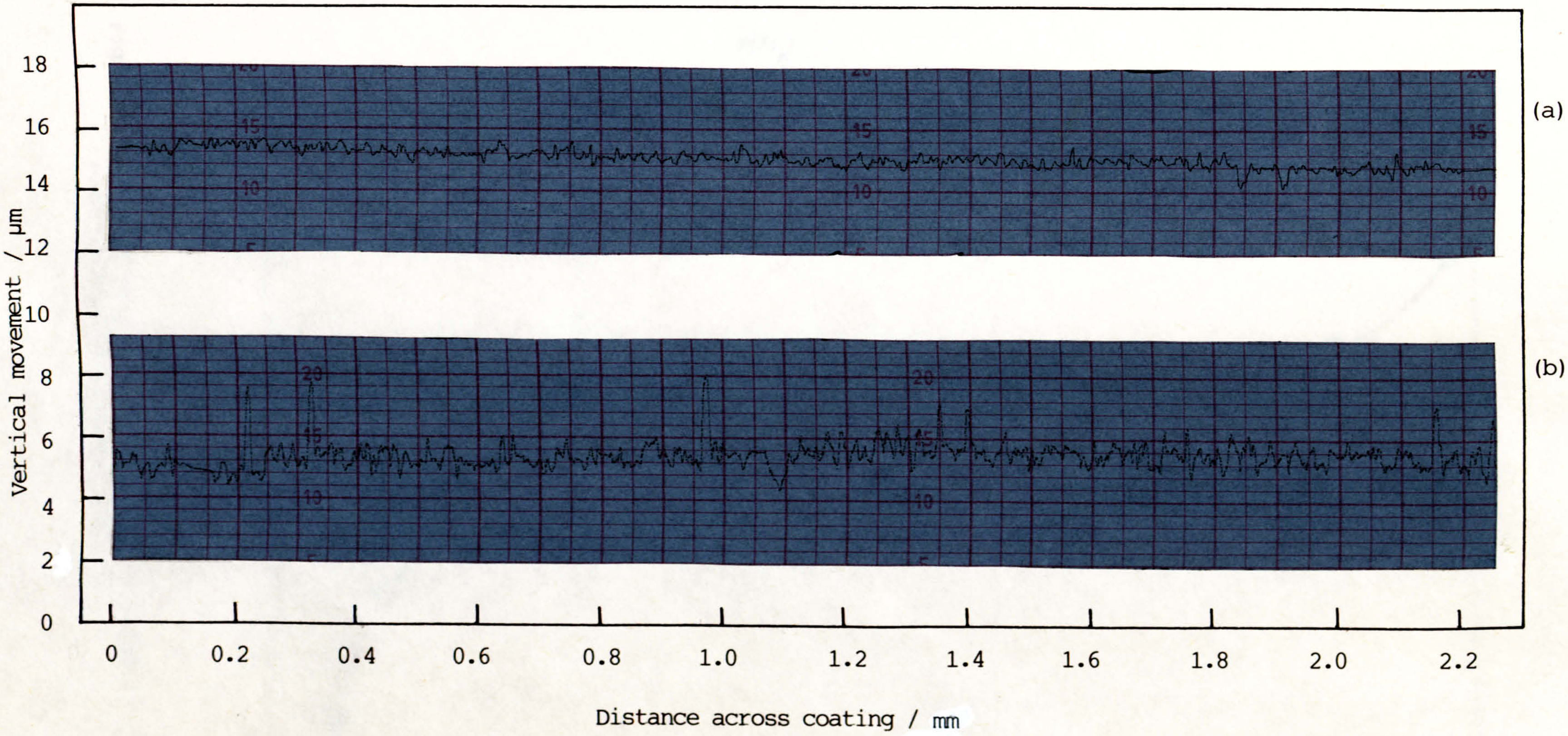

Fig.5.4 Surface profile scans obtained using Talysurf instrument of Mo-black dip coating on cobalt (NC) substrate. (a) With addition agent, (b) Without addition agent.

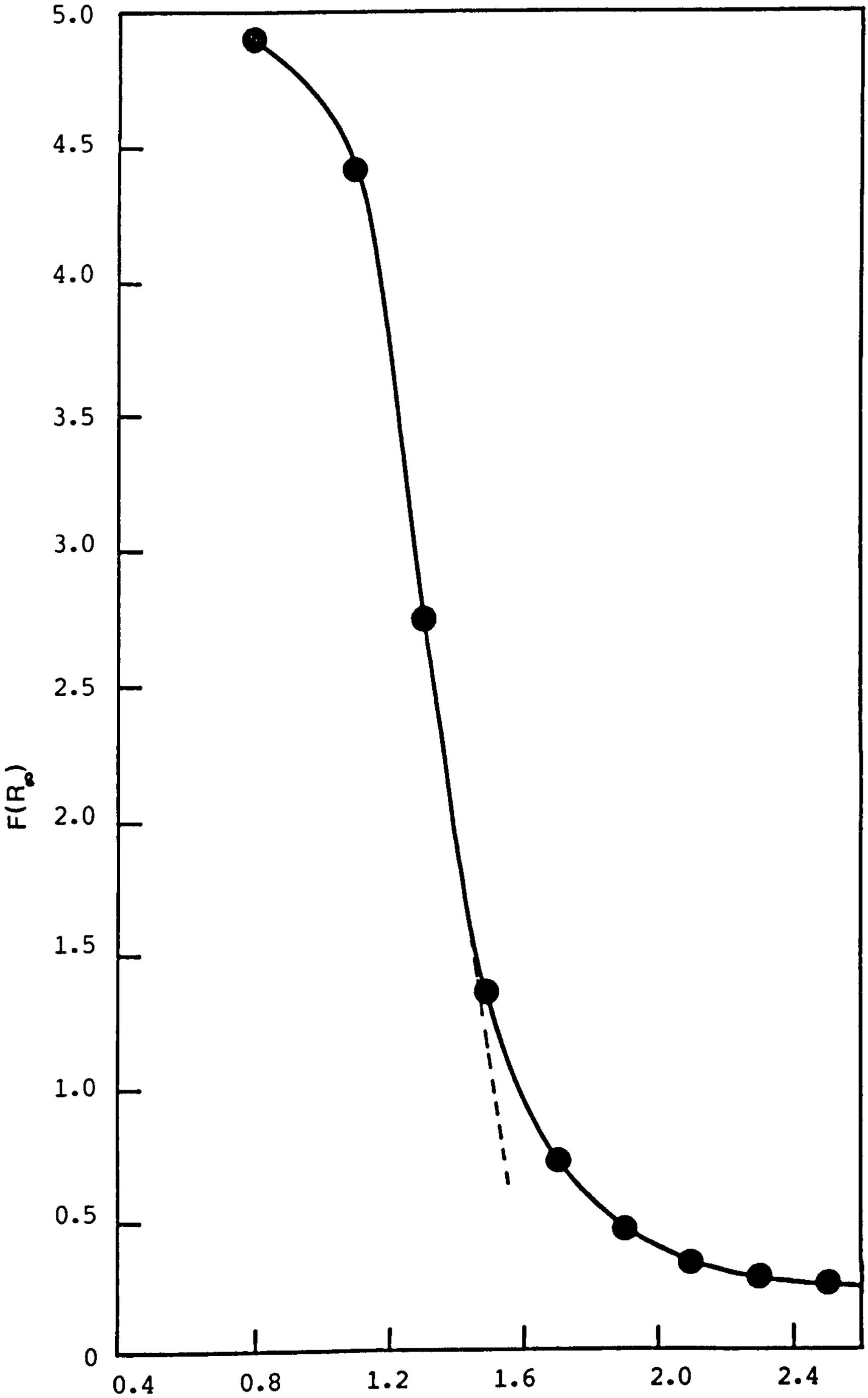

Fig.5.5. Plots of $F(R_\infty)$ as a function of wavelength λ of an electrodeposited Mo-black coating.

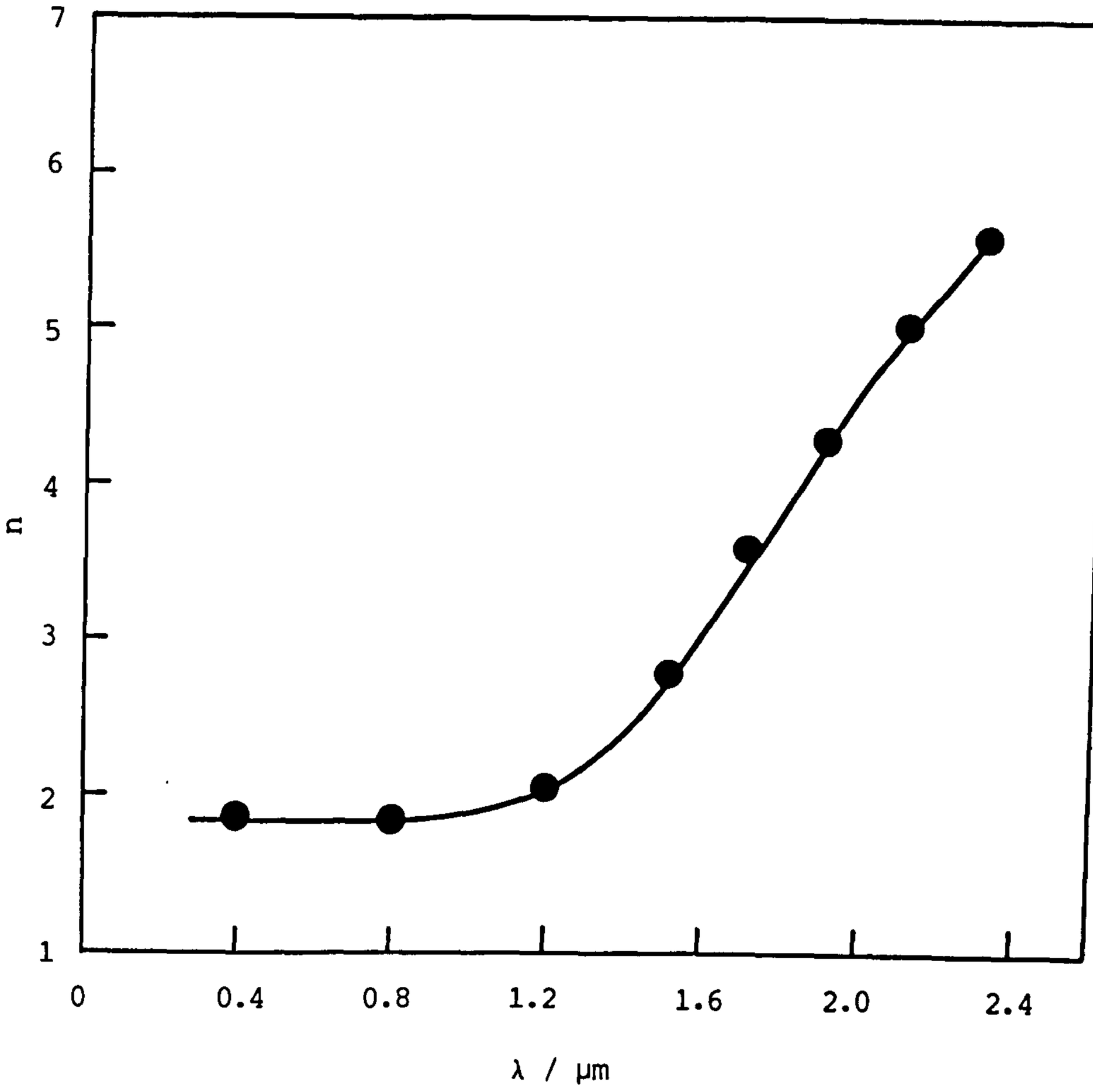

Fig.5.6. Variation of refraction index n of electrodeposited Mo-black coating with wavelength. Thickness-6μm.

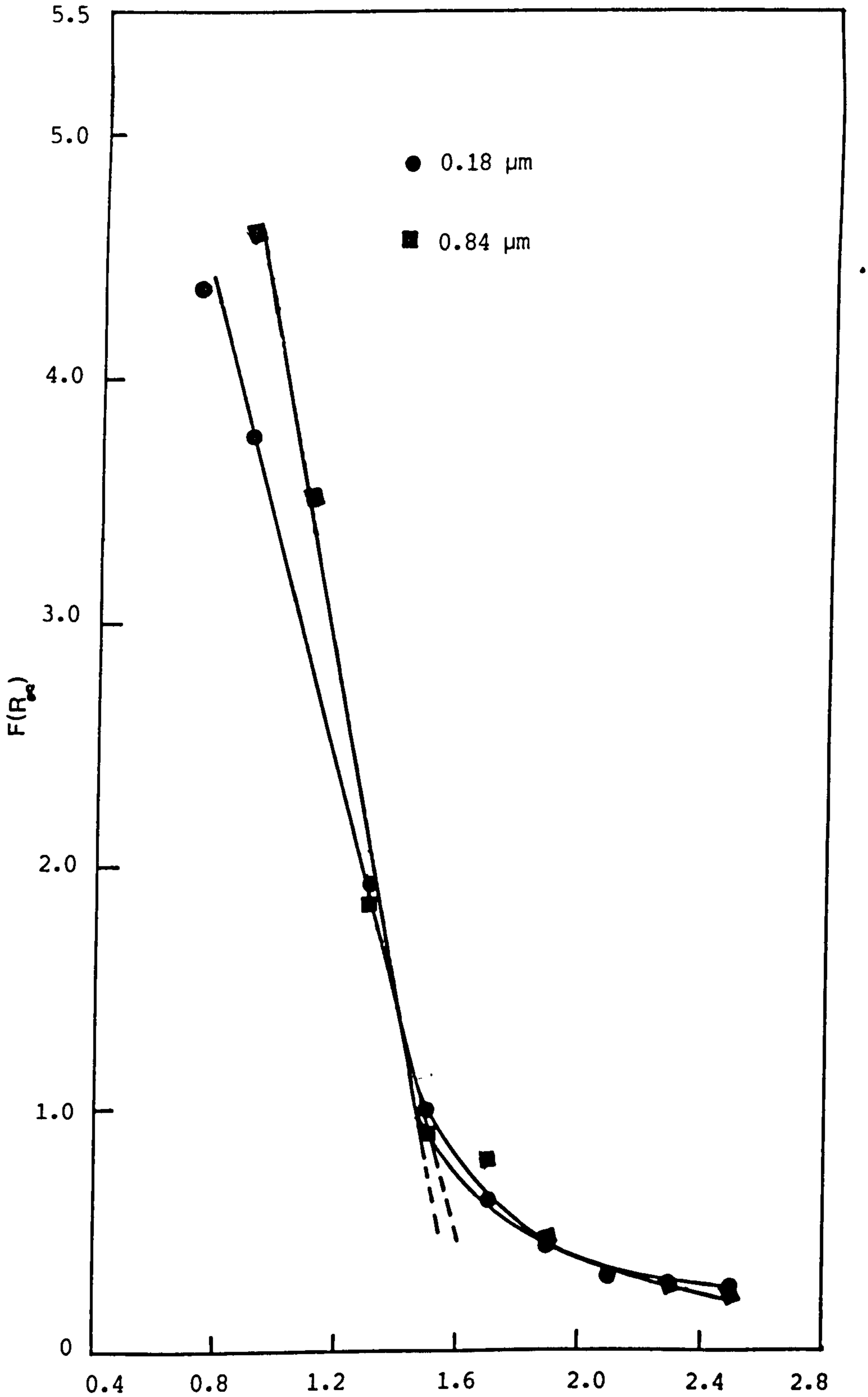

Fig.5.7. Plots of Kubelka-Munk function $F(R_\infty)$ as a function of wavelength λ for Mo-black dip coating on etched zinc substrate.

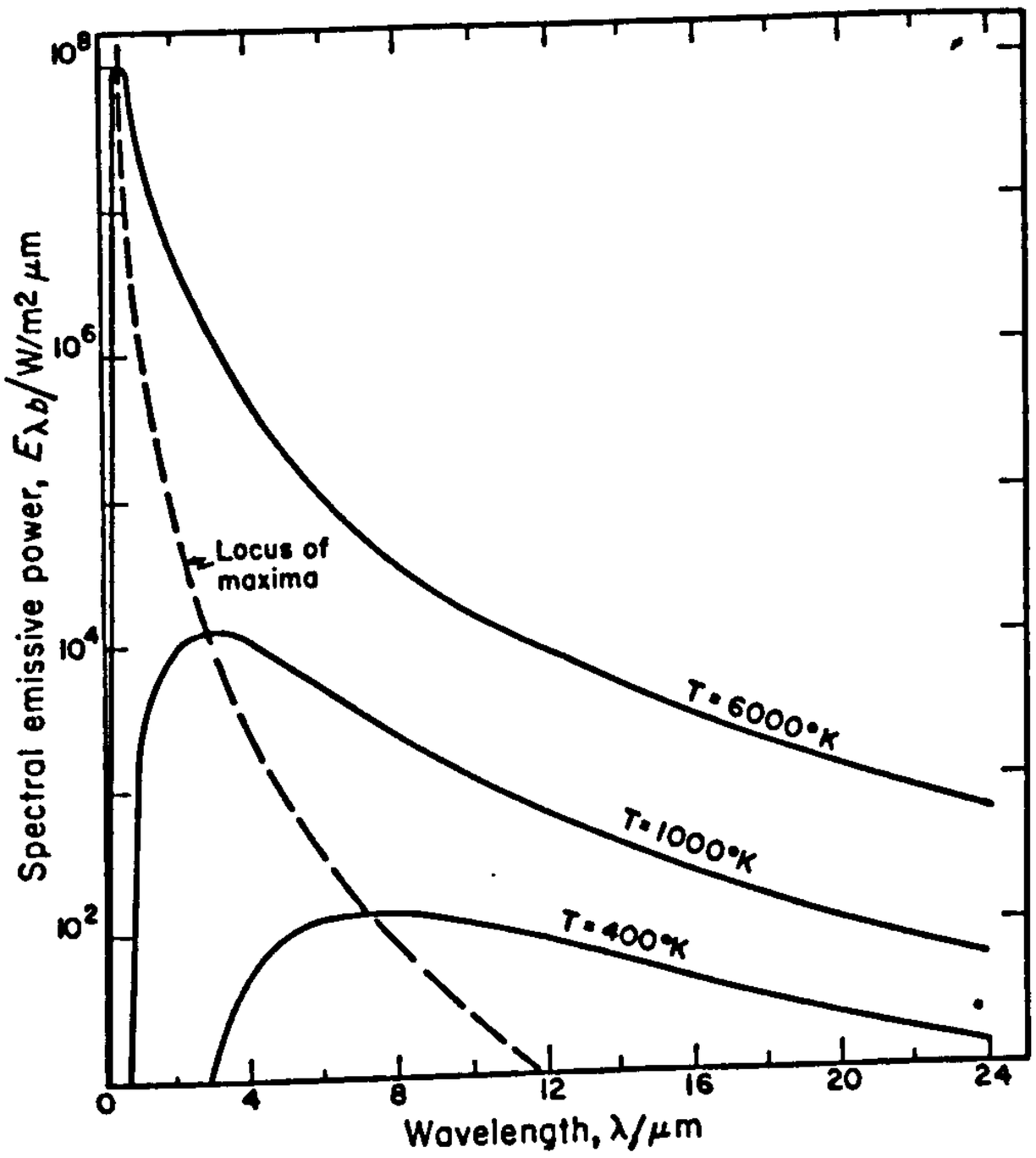

Fig.A.1. Spectral distribution of blackbody radiation.

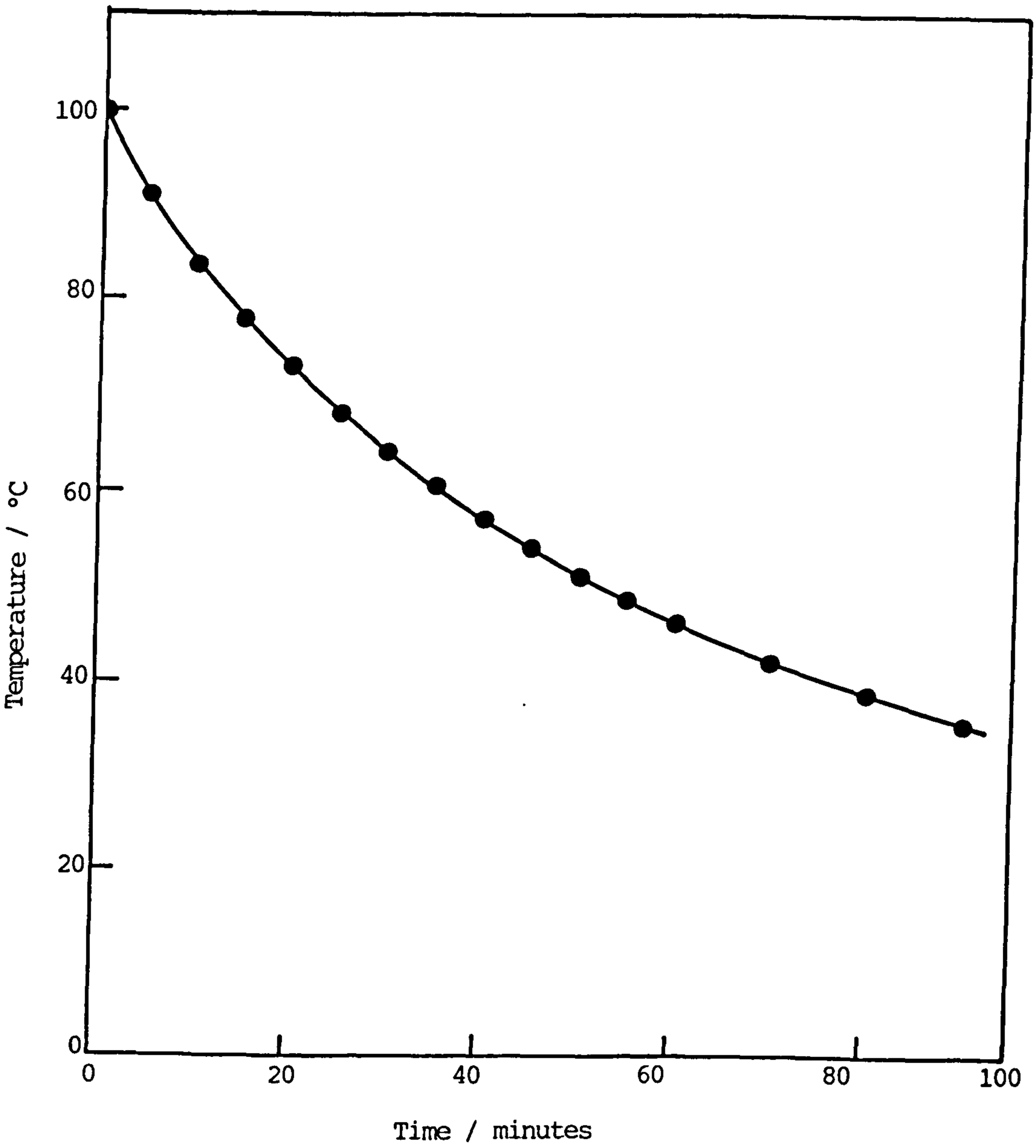

Fig.C.1. Temperature variation with time for shiny aluminium during cooling in vacuum.

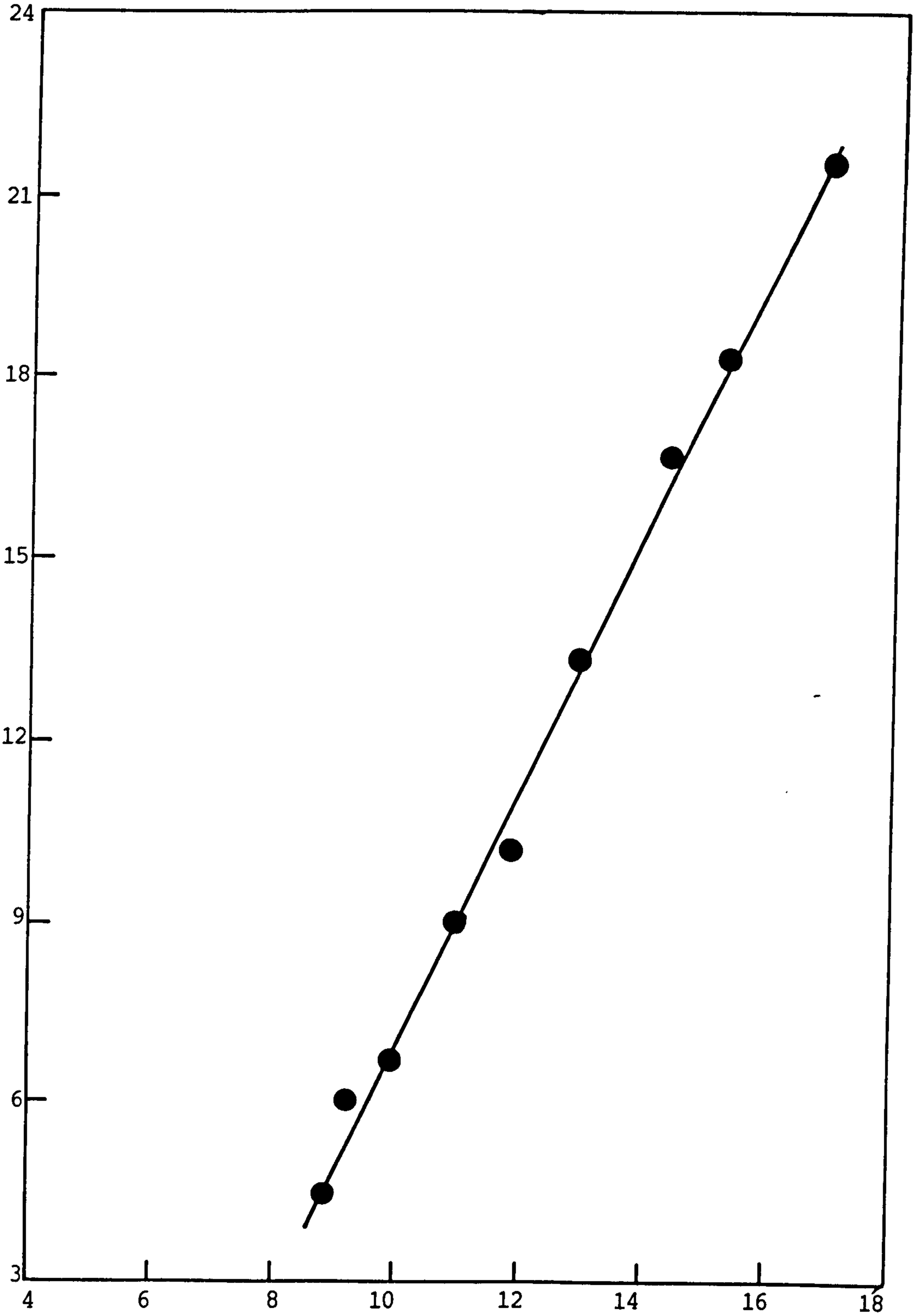

Fig.C.2. Plots of dT/dt as a function of T^4 for shiny aluminium specimen.

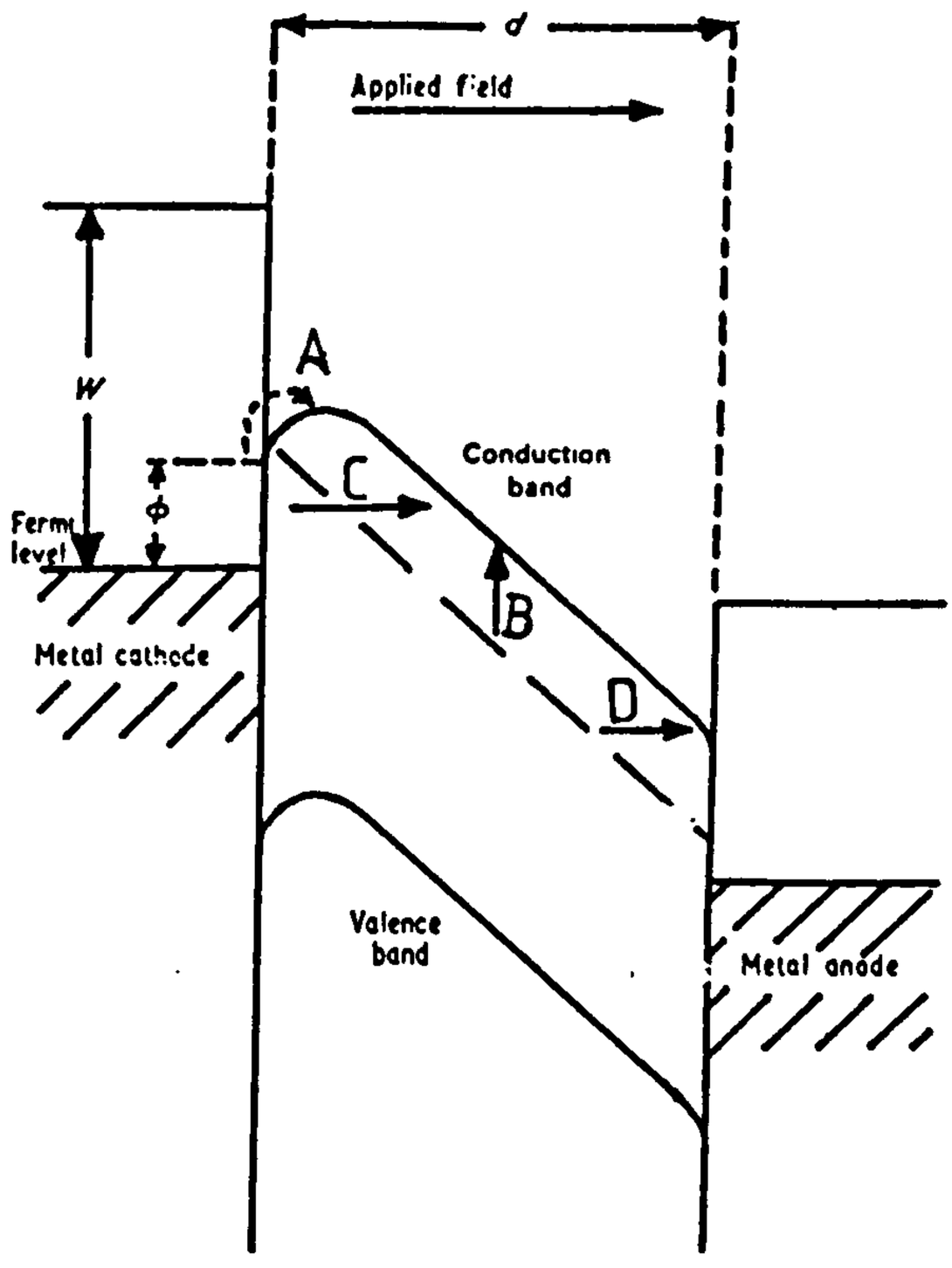

Fig. E.1. The energy band diagram of an MIM structure showing the possible conduction processes under high field conditions.

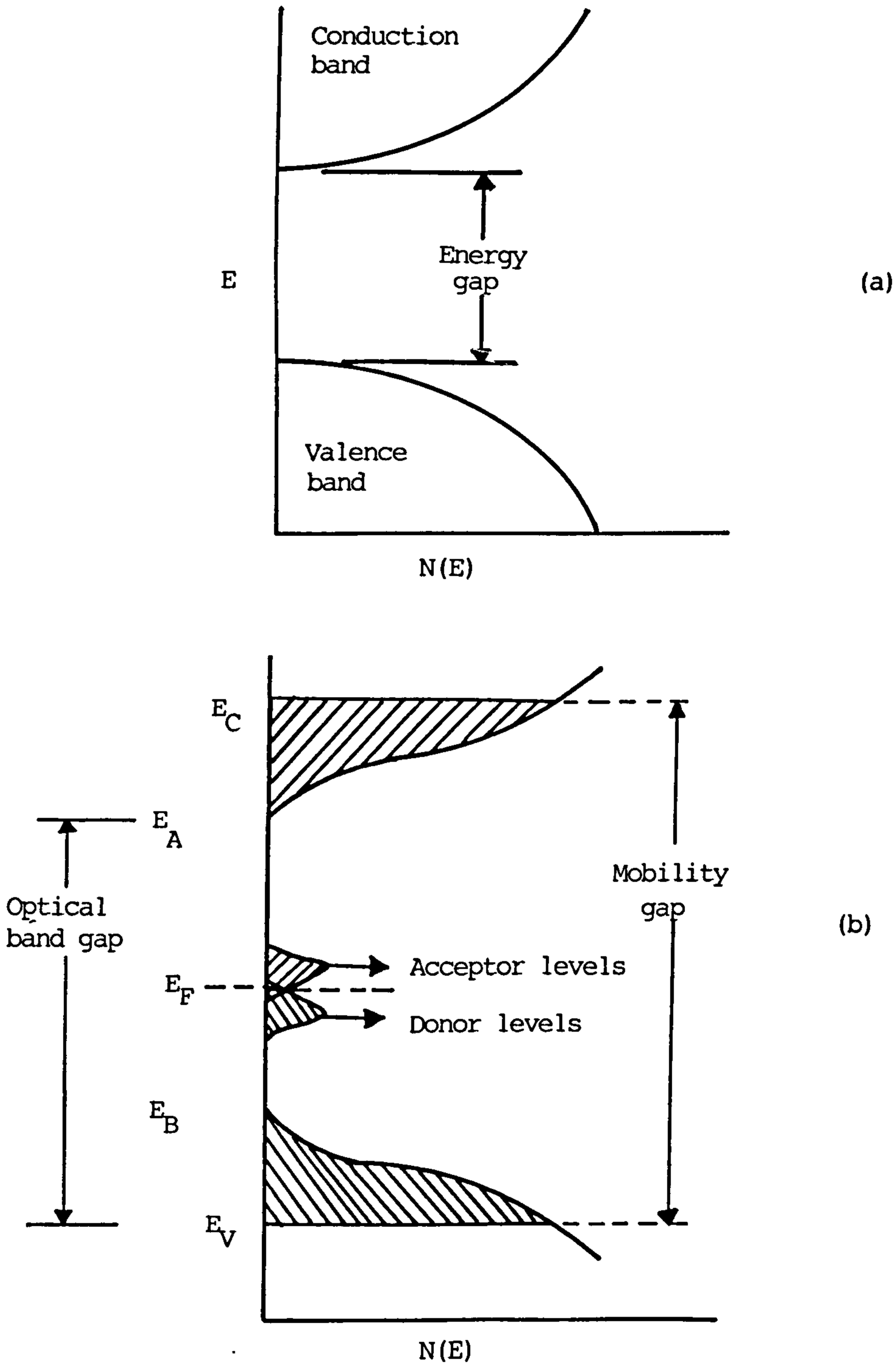

Fig.F.1. Density of slates N(E) as a function of energy for
(a) crystalline material
(b) non-crystalline material.